

UC San Diego

UC San Diego Electronic Theses and Dissertations

Title

Lead-Halide Perovskite for Visible-Light Photocatalytic Ring-Forming Reactions

Permalink

<https://escholarship.org/uc/item/0kc9h4ds>

Author

Lin, Yixiong

Publication Date

2023

Peer reviewed|Thesis/dissertation

UNIVERSITY OF CALIFORNIA SAN DIEGO
SAN DIEGO STATE UNIVERSITY

Lead-Halide Perovskite for Visible-Light Photocatalytic Ring-Forming Reactions

A Dissertation submitted in partial satisfaction of the requirements
for the degree Doctor of Philosophy

in

Chemistry

by

Yixiong Lin

Committee in charge:

University of California San Diego

Professor David Fenning
Professor Haim Weizman

San Diego State University

Professor Yong Yan, Chair
Professor Thomas Cole
Professor Jing Gu

2023

Copyright

Yixiong Lin, 2023

All rights reserved.

The Dissertation of Yixiong Lin is approved, and it is acceptable in quality and form for publication on microfilm and electronically.

Chair

University of California San Diego

San Diego State University

2023

DEDICATION

This dissertation is dedicated to my dear grandma, Xiufang Zhang.

And to my loving family members.

TABLE OF CONTENTS

DISSERTATION APPROVAL PAGE	iii
DEDICATION	iv
TABLE OF CONTENTS.....	v
LIST OF FIGURES	ix
LIST OF SCHEMES.....	xiii
LIST OF TABLES.....	xvi
LIST OF ABBREVIATIONS	xvii
ACKNOWLEDGEMENTS	xxi
VITA.....	xxiii
ABSTRACT OF THE DISSERTATION	xxv
Chapter 1 Introduction.....	1
1.1 Background Introduction	1
1.2 General Mechanism of Visible-Light-Driven Homogeneous Photocatalysis.....	2
1.3 Representative Examples of Photocatalytic Ring-Forming Reactions	4
1.3.1 Photocatalytic [4+2] Cycloaddition	4
1.3.2 Photocatalytic Redox-Based [2+2] Cycloaddition.....	6
1.3.3 Photocatalytic Energy-Transfer-Based [2+2] Cycloaddition.....	7
1.3.4 Photocatalytic Radical Cascade Cyclization	8
1.3.5 Photocatalytic Ring-Opening Cyclization.....	9
1.4 Visible-Light-Driven Heterogeneous Photocatalysis.....	10
1.4.1 General Mechanism of Visible-Light-Driven Heterogeneous Photocatalysis	11
1.4.2 Heterogeneous Photocatalysis for Ring-Forming Reactions	12
1.4.2a Titanium Oxide (TiO ₂) for Photocatalytic Ring-Forming Reactions	12
1.4.2b Cadmium Chalcogenide (CdSe, CdS) for Photocatalytic Ring-Forming Reactions	18
1.4.2c Carbon Nitride (CN) for Photocatalytic Ring-Forming Reactions.....	23
1.4.2d Conjugated Microporous Polymers and Covalent Organic Frameworks for Photocatalytic Ring-Forming Reactions	32
1.4.3 Conclusion.....	38
1.5 Lead-Halide Perovskite Nanocrystals as a Potential Candidate for Ring-Forming Reactions	39

1.5.1 Metal-Halide Perovskite as an Emerging Photovoltaic Material	39
1.5.2 APbX ₃ Lead-Halide Perovskite Nanocrystals	39
1.5.3 LHP NCs as Potential Heterogeneous Photocatalysts.....	40
1.5.4 Our Previous Work on Employing LHP NCs for Photocatalytic Organic Transformation	42
1.6 Objectives of the Thesis	45
1.7 Reference	48
Chapter 2 Lead-Halide Perovskite Nanocrystals for Photocatalytic Redox-Neutral Syntheses of Pyrrole and Pyrazole Derivatives	57
2.1 Chapter Summary	57
2.2 Introduction	57
2.3 Results and Discussion.....	60
2.3.1 NCs-Photocatalyzed Synthesis of Pyrrole Derivatives	60
2.3.2 NCs-Photocatalyzed Synthesis of Pyrazole Derivatives	64
2.4 Chapter Conclusion	68
2.5 Experimental Section	69
2.5.1 General Information	69
2.5.2 Preparation of CsPbBr ₃ NCs Photocatalyst.....	70
2.5.3 Preparation of Starting Materials	71
2.5.4 Photocatalytic Synthesis of Products	76
2.5.5 Cyclic Voltammetry (CV) Data	87
2.5.6 Photoluminescence (PL) Quenching Study.....	88
2.5.7 Radical Trapping Experiments.....	89
2.6 Acknowledgements	92
2.7 Reference	92
Chapter 3 Triplet Energy Transfer from Lead Halide Perovskite for Highly Selective Photocatalytic [2+2] Cycloaddition	94
3.1 Chapter Summary	94
3.2 Introduction	94
3.3 Results and Discussion.....	97
3.3.1 Screening of Triplet Energy Acceptor	97
3.3.2 Studies of the Surface Binding	99

3.3.3 TET-Induced [2+2] Cycloaddition Reactions	100
3.3.4 TET Dynamics	104
3.3.5 DFT Studies.....	108
3.4 Chapter Conclusions	112
3.5 Experimental Section	112
3.5.1 General Information	112
3.5.2 Preparation of Perovskite Photocatalysts	114
3.5.3 Preparation of Substrates.....	116
3.5.4 Condition Exploration for Perovskite-Photocatalyzed [2+2] Cycloaddition	123
3.5.5 Photocatalytic Synthesis of Products	126
3.5.6 HPLC Analysis on the Reaction Mixture of Cycloaddition of 7a.....	134
3.5.7 Photoluminescence (PL) Quenching Study.....	135
3.5.8 Time-Dependent NMR Study	141
3.5.9 Investigation of Surface Binding.....	145
3.5.10 Catalyst Stability and Recyclability	148
3.5.11 UV-Vis Spectra of Substrate and PL Spectra of CsPbBr ₃ NCs	152
3.5.12 Transient Absorption (TA) Spectroscopy Experiment Setup	153
3.5.13 DFT Calculations	153
3.6 Acknowledgements	155
3.7 Reference	155
Chapter 4 CsPbBr₃ Perovskite Nanocrystals for Photocatalytic [3+2] Cycloaddition.....	160
4.1 Chapter Summary	160
4.2 Introduction	161
4.3 Results and Discussion.....	162
4.3.1 Bromine Radicals	162
4.3.2 Photocatalytic Design.....	164
4.3.3 Reaction Development	165
4.3.4 Reaction Scope.....	166
4.3.5 Mechanistic Investigation	169
4.3.6 Catalyst Recycling.....	172
4.3.7 More Applications.....	173
4.4 Conclusion	174
4.5 Experimental Section	175
4.5.1 General Information	175
4.5.2 Condition Exploration	177

4.5.3 Preparation of CsPbBr ₃ NCs Photocatalyst.....	178
4.5.4 Preparation of Starting Materials	179
4.5.5 Photocatalytic Synthesis of Products	187
4.5.6 Bromine Radical Trapping Experiment	209
4.5.7 Proposed Mechanism for the Hydrogen Atom Transfer	210
4.5.8 CsPbBr ₃ Nanocrystals Catalyst Recycling Experiment	211
4.5.9 Gram-scale Synthesis of Benzyl Bromide from Toluene.....	212
4.5.10 Analysis of Side Products from [3+2] Cycloaddition	214
4.5.11 Photoluminescence (PL) Measurements of CsPbBr ₃ NCs in DBM.....	215
4.5.12 Cyclic Voltammetry Data.....	216
4.6 Acknowledgements	217
4.7 Reference	217
Chapter 5 Summary and Outlook.....	222
5.1 Dissertation Summary	222
5.2 Future Directions and Outlook.....	224
5.2.1 Charge-Transfer-Based [2+2] Cycloaddition.....	224
5.2.2 Synthesis of Bioisosteres of <i>meta</i> -Substituted Benzenes via Br Radical-Mediated Ring-Opening [3+2] Cycloaddition	224
5.2.3 Outlook.....	225
5.3 Reference	226
Appendix A. DFT Geometries	227
Cartesian coordinates for structures of computation shown in Section 3.5.13:.....	227
Appendix B. NMR Spectra.....	239
NMR spectra for compounds in Chapter 2:	239
NMR spectra for compounds in Chapter 3:	257
NMR spectra for compounds in Chapter 4:	272

LIST OF FIGURES

Figure 1.1 General pathways of homogeneous photocatalysis. Under visible light irradiation, photocatalyst (PC) first gets to its excited state (PC*) by promoting one electron from HOMO to LUMO. Then the resulting PC* participates in substrate activation via a reductive quenching/oxidative quenching/triplet-triplet energy transfer (TT-EnT) pathway.	3
Figure 1.2 General pathways of heterogeneous photocatalysis. Photocatalyst (PC) first gets to excited state (PC*) by promoting electrons from VB to CB under visible light irradiation, and then participate in substrate activation via electron transfer (ET)/hole transfer (HT)/triplet-triplet energy transfer (TT-EnT) pathway.	11
Figure 1.3 Band structures of TiO ₂ (anatase and rutile). ²¹	13
Figure 1.4 Band structures of CdSe (TOPO) QDs ³³ and CdS ³⁴ . Note: The trapping of electrons and holes, in addition to columbic interaction, might cause difference between electrochemical band gap and optical band gap. ^{35,36} The redox potentials would be slightly altered if QDs are capped by different ligands. TOPO: trioctylphosphine oxide.	19
Figure 1.5 Band structures of representative carbon nitride variants (g-C ₃ N ₄ , ⁴⁶ K-PHI, ⁴⁷ g-CN-U ⁴⁸).....	24
Figure 1.6 Band structures of selected CMPs and COFs (<i>vide infra</i>).....	33
Figure 1.7 Structure of ABX ₃ MHP.....	40
Figure 1.8 Photoredox potentials of CsPbX ₃ (X = Cl, Br, I) perovskites (range highlighted in purple and green boxes) compared to other commonly used Ir- and Ru-based homogeneous photocatalysts.....	42
Figure 2.1 A) Stern-Volmer PL quenching study of CsPbBr ₃ NCs in the presence of various concentration of 1a . B) Radical trapping experiment by using TEMPO.....	62
Figure 2.2 A) Stern-Volmer PL quenching study of CsPbBr ₃ NCs in the presence of various concentration of 4a . B) Radical trapping experiment by using TEMPO.....	66
Figure 2.3 CV data of 2-bromoacetophenone (1a). $E_{red} = -1.11$ V vs. SCE.	88
Figure 2.4 CV data of (<i>E</i>)-1-benzylidene-2-phenylhydrazine (4a). $E_{ox} = +1.00$ V vs. SCE.	88
Figure 2.5 LC-MS evidence of int-i-TEMPO	90
Figure 2.6 LC-MS evidence of int-ii-TEMPO	90
Figure 2.7 LC-MS evidence of int-II-TEMPO	91
Figure 3.1 Proposed mechanism of the visible-light-induced CsPbBr ₃ NCs TET-mediated surface-templated intermolecular [2+2] cycloaddition.....	97
Figure 3.2 Stern-Volmer PL quenching studies of perovskite NCs with various olefins TEAs..	99
Figure 3.3 The carbonyl stretching frequency of 7c blueshifted after mixing with NCs. A) FTIR comparison indicating the surface binding of substrate via carboxylate group. B) Enlarged carbonyl stretching area.	100

Figure 3.4 Time-dependent NMR studies of cycloaddition of 7a in THF-d8 (signals of emerging 7aa are circled in red frames).	102
Figure 3.5 A) Pseudocolor image plot of the transient absorption (TA) experiments of NC, 7a' , 7b' and 7c' in THF; B) Normalized TA kinetics probed at the center of the NCs exciton bleach spectrum for NC, 7a' , 7b' and 7c' ; C) Normalized TA kinetics and fits for 7a' , 7b' and 7c' ...	107
Figure 3.6 A) Perovskite CsPbBr ₃ surface (frozen structure from crystal structure); B) Optimized binding structures of 7a and 7aa via <i>syn</i> - and <i>anti</i> -mode on NC; C) Binding enthalpy of the reaction path.....	110
Figure 3.7 CsPbBr ₃ NCs-photocatalyzed 7aa (<i>syn</i>) formation. No <i>anti</i> - 7aa was detected.	135
Figure 3.8 Ir(ppy) ₃ -photocatalyzed 7aa (<i>syn</i> and <i>anti</i>) formation.	135
Figure 3.9 PL quenching of CsPbBr ₃ NCs by (<i>E</i>)-4-phenylbut-3-en-2-one (6). $K_{SV} = 12.228 \text{ M}^{-1}$	136
Figure 3.10 PL quenching of CsPbBr ₃ NCs by (<i>E</i>)-4-(3-oxobut-1-en-1-yl)benzoic acid (7a). $K_{SV} = 746.73 \text{ M}^{-1}$	136
Figure 3.11 PL quenching of CsPbBr ₃ NCs by (<i>E</i>)-4-(3-oxo-3-phenylprop-1-en-1-yl)benzoic acid (7b). $K_{SV} = 754.68 \text{ M}^{-1}$	137
Figure 3.12 No PL quenching of CsPbBr ₃ NCs by 4-vinylbenzoic acid (7c) was observed.	137
Figure 3.13 PL quenching of CsPbBr ₃ NCs by (<i>E</i>)-4-(5-methyl-3-oxohex-1-en-1-yl)benzoic acid (7d). $K_{SV} = 157.41 \text{ M}^{-1}$	138
Figure 3.14 PL quenching of CsPbBr ₃ NCs by (<i>E</i>)-4-(3-(4-chlorophenyl)acryloyl)benzoic acid (7e). $K_{SV} = 836.36 \text{ M}^{-1}$	138
Figure 3.15 PL quenching of CsPbBr ₃ NCs by (<i>E</i>)-6-styryl-2-naphthoic acid (7f). $K_{SV} = 845.48 \text{ M}^{-1}$	139
Figure 3.16 PL quenching of CsPbBr ₃ NCs by methyl (<i>E</i>)-4-(3-oxobut-1-en-1-yl)benzoate (8).	139
Figure 3.17 PL quenching of CsPbBr ₃ NCs by (<i>E</i>)-4-(4-aminophenyl)but-3-en-2-one (9). $K_{SV} = 3049.1 \text{ M}^{-1}$	140
Figure 3.18 PL quenching of CsPbBr ₃ NCs by (<i>E</i>)-N-(4-(3-oxobut-1-en-1-yl)phenyl)acetamide (10). $K_{SV} = 557.15 \text{ M}^{-1}$	140
Figure 3.19 Time-dependent ¹ H NMR study was performed with 7a , CsPbBr ₃ NCs and THF-d8 in an NMR tube under blue LED irradiation. The timestamp of each measurement is marked on the left side of each stacked spectrum which is showing the graduate formation of the cyclobutane product 7aa . A polymeric byproduct was observed after 20h of reaction.	141
Figure 3.20 ¹ H NMR of the reaction mixture taken after blue LED irradiation for 30 min. Different symbols were used to identify each of the component presented in the reaction mixture (* for <i>trans</i> - 7a , + for <i>cis</i> - 7a , ^ for 7aa).	142
Figure 3.21 [7aa] vs. reaction time <i>t</i> (first 7h). The red curve represents the exponential fitting of [7aa] vs. reaction time <i>t</i>	144

Figure 3.22 The linear relationship between $d[7aa]/dt$ and $[7a]^2$ indicating the perovskite-photocatalyzed [2+2] cycloaddition follows law of second-order kinetics.	145
Figure 3.23 Comparison of the C=O stretching frequencies of Sample 1 (black), Sample 2 (red), Sample 3 (green) by IR. The $\sim 10\text{ cm}^{-1}$ shift of the C=O stretching frequency of Sample 3 towards higher wavenumber indicates the binding of 7c on CsPbBr ₃ NCs' surface via carboxylate group.....	146
Figure 3.24 ¹ H NMR of 7a (<i>x</i> mg) binding on CsPbBr ₃ NCs' (5.2 mg - <i>x</i> mg) surface.....	147
Figure 3.25 Powder XRD of as-prepared CsPbBr ₃ NCs (blue) and CsPbBr ₃ NCs after reaction and being left in THF for over 30 days (red) showing no sign of degradation.....	148
Figure 3.26 UV-Vis absorption spectra (left) and PL spectra (right) of the NCs solution in each catalytic cycle. The positions of characteristic peaks of perovskite NCs remained the same. ...	150
Figure 3.27 TEM measurements. Perovskite NCs samples were dispersed in THF solution and dropped on copper grids. TEM images of as-prepared CsPbBr ₃ NCs (A and B) and recycled CsPbBr ₃ NCs (C and D).	151
Figure 3.28 PL spectrum of CsPbBr ₃ NCs (black) and UV-Vis absorption spectrum of 7a (red). The non-overlapping rules out the possibility of NCs acting as a singlet sensitizer for the substrate 7a	152
Figure 3.29 PL spectrum of as-prepared CsPbBr ₃ NCs (black), CsPbBr ₃ NCs treated with 7c and OIAm (red). The PL of CsPbBr ₃ NCs clearly blue-shifted with the presence of both benzoic acid derivative and primary amine.	152
Figure 3.30 4x4 Cubic matrix of perovskite NCs: Cs ₁₆ Pb ₉ Br ₃₃ (+1 in overall charge) as shown from top view, tilt view and side view.....	154
Figure 3.31 Binding models of 7a on NC surface: 7a chelating to a single Cs atom, 7a bridging bind to two adjacent Cs atoms, and 7a bridging bind to two diagonal Cs atoms.	154
Figure 3.32 Binding of two 7a molecules on NC surface in <i>syn</i> - and <i>anti</i> -binding model.	154
Figure 3.33 Binding of 7aa molecules on NC surface in <i>syn</i> - and <i>anti</i> -binding model.	155
Figure 4.1 The as-synthesized CsPbBr ₃ perovskite nanocrystals under ambient light (left and middle) and under 365-nm UV excitation (right).....	178
Figure 4.2 Photocatalytic reaction setup with a 40-watt Kessil® PR160-456nm blue LED lamp.	188
Figure 4.3 ¹ H NMR analysis of the aliquots taken from the reaction mixture at different reaction time (24h/7 days/14 days) as indicated by the timestamp on top left of the stacked spectra showing the progressing benzyl bromide production.	212
Figure 4.4 The structural assignments of the crude reaction mixture (14 days) by ¹ H NMR spectroscopy showing high selectivity to benzyl bromide.	213
Figure 4.5 GC-MS analysis of the crude reaction mixture from 14h reveals groups of oligomer side products based on vinylcyclopropane, which is likely the result of ring-opening polymerization. ²⁵ A) GC chromatogram of the crude reaction mixture. B-D) Mass spectra of selected groups of compounds and their formation routes.	214

Figure 4.6 GC-MS analysis of the crude reaction mixture from **14I** reveals groups of oligomer side products based on vinylcyclopropane, which is likely the result of ring-opening polymerization.²⁵ **A)** GC chromatogram of the crude reaction mixture. **B-D)** Mass spectra of selected groups of compounds and their formation routes. 215

Figure 4.7 PL emission spectra of CsPbBr₃ NCs in DBM before and after blue LED (40 W, $\lambda_{\text{max}} = 456$ nm) irradiation (1h) showing slight increase in PL intensity, in line with previous reported bromide anion exchange of CsPbBr₃ perovskite NCs in DBM under visible light irradiation... 216

Figure 4.8 Cyclic voltammetry of CH₂Br₂..... 216

LIST OF SCHEMES

Scheme 1.1 Photocatalytic radical cation Diels-Alder reaction by Yoon and co-workers.	4
Scheme 1.2 Photoredox [2+2] cycloaddition by Yoon and co-workers.....	6
Scheme 1.3 Photocatalytic energy-transfer-mediated [2+2] cycloaddition by Yoon and co-workers.....	7
Scheme 1.4 Photocatalytic radical cascade cyclization by Stephenson and co-workers.	8
Scheme 1.5 Photocatalytic cyclopropylaniline ring-opening [3+2] cycloaddition by Zheng and co-workers.....	9
Scheme 1.6 TiO ₂ -photocatalyzed cyclizations by Scaiano and co-workers.....	14
Scheme 1.7 Photocatalytic oxidative [4+2] annulation of tertiary anilines with maleimides catalyzed by P25/NiO.	16
Scheme 1.8 Photocatalytic syntheses of aryltetralones catalyzed by TiO ₂	16
Scheme 1.9 Photocatalytic cyclobutylaniline ring-opening [4+2] cycloaddition catalyzed by Ti ³⁺ @TiO ₂	17
Scheme 1.10 Photocatalytic synthesis of 1,3,4-oxadiazoles from ketoacids with hydrazides catalyzed by GA-TiO ₂	17
Scheme 1.11 Photoredox [2+2] cyclodimerization of <i>N</i> -vinylcarbazole catalyzed by CdS.	19
Scheme 1.12 Photocatalytic CF ₂ -based radical cascade cyclization catalyzed by CdS QDs.....	20
Scheme 1.13 CdSe QDs-photocatalyzed energy-transfer-mediated [2+2] cycloaddition by Weiss and co-workers.....	21
Scheme 1.14 Cadmium chalcogenide QDs-photocatalyzed synthesis of tropane alkaloid skeletons.....	22
Scheme 1.15 mpg-C ₃ N ₄ -photocatalyzed cyclizations. A) Sequential oxidative coupling-cyclization for the synthesis of benzoxazoles, benzimidazoles and benzothiazoles. B) Intramolecular radical cyclization for the synthesis of cyclopentanes. C) Oxidative coupling of resveratrol derivatives for the synthesis of δ -viniferin and its analogues.....	25
Scheme 1.16 KPHI-photocatalyzed cyclizations by Savateev and co-workers.	26
Scheme 1.17 g-CN-U-photocatalyzed cyclizations by Wang and co-workers.	27
Scheme 1.18 g-C ₃ N ₄ -photocatalyzed cyclizations. A) Diels-Alder cycloaddition. B) Thiocyanated radical cyclization.	29
Scheme 1.18 (Continued) g-C ₃ N ₄ -photocatalyzed cyclizations. C) Intramolecular oxygen-centered radical cyclization of β,γ -unsaturated oximes. D) Intramolecular oxidative cyclization of thiobenzanilides. E) Dyhydrogenative [4+2] annulation of benzothioamides with alkynes.....	30
Scheme 1.19 Oxidative activation of <i>N</i> -aryl glycine for radical cascade cyclizations with imine derivatives photocatalyzed by carbon nitride.	31

Scheme 1.20 A) Proton coupled electron transfer (PCET) induced hydroamidation cyclization photocatalyzed by $^{NCN}CN_x$. B) Radical cascade hydrophosphorylated cyclization photocatalyzed by g- C_3N_4 -Ni.....	32
Scheme 1.21 CMP- and COF-photocatalyzed cyclizations by Zhang and co-workers.	34
Scheme 1.22 COF-photocatalyzed cyclizations. A) Tandem radical addition-cyclization of 2-aryl phenyl isocyanides. B) Oxidative coupling of thioamide for the synthesis 1,2,4-thiadiazole. C) Multi-component synthesis of pyridines from alkynes with nitriles or from aryl ketones with benzyl amines. D) Oxidative [3+2] cycloaddition of phenol with olefins.....	36
Scheme 1.23 CMP-photocatalyzed cyclizations. A) Oxidative intermolecular cyclization of 1,2-diaminobenzenes with aldehydes. B) Thiocyanation cyclization for the synthesis of thiocyano chromones.	38
Scheme 1.24 CsPbBr ₃ NCs-photocatalyzed α -alkylation of aldehyde.....	44
Scheme 1.25 Specific aim 1. LHP NCs-photocatalyzed N-heterocyclization for the syntheses of pyrrole and pyrazole derivatives.....	45
Scheme 1.26 Specific aim 2. LHP NCs-photocatalyzed surface-templated TT-EnT-mediated highly selective [2+2] cycloaddition. TT-EnT: triplet-triplet energy transfer. HH: head-to-head.	46
Scheme 1.27 Specific aim 3. LHP NCs-photocatalyzed bromine radical-mediated ring-opening [3+2] cycloaddition.....	47
Scheme 2.1 Small molecule drugs and ligands containing pyrrole and pyrazole scaffolds.....	58
Scheme 2.2 Photocatalytic design based on previous works. The key intermediates are highlighted in bracket for comparison. ET: electron transfer. HT: hole transfer.	59
Scheme 2.3 Proposed mechanism for the NCs-photocatalyzed synthesis of pyrrole derivatives. CB: conduction band. VB: valence band. int: intermediate. HT: hole transfer.	63
Scheme 2.4 Scope of NCs-photocatalyzed synthesis of pyrrole derivatives.....	64
Scheme 2.5 Proposed mechanism for the NCs-photocatalyzed synthesis of pyrazole derivatives. CB: conduction band. VB: valence band. int: intermediate.....	67
Scheme 2.6 Scope of NCs-photocatalyzed synthesis of pyrazole derivatives.	68
Scheme 2.7 The substrate scope for the NCs-photocatalyzed syntheses of pyrrole and pyrazole derivatives.....	71
Scheme 3.1 Schematic illustration of possible product outcomes from molecular photocatalyst vs. perovskite NCs photocatalyst. HH: head-to-head; HT: head-to-tail.	95
Scheme 3.2 Representative scope of bulk-like CsPbBr ₃ NCs-induced HH- <i>syn</i> -[2+2] cycloadditions. Reactions were performed under standard conditions. For heterocoupling, 7c (0.033 mmol, 3.0 equiv.) was used as coupling partner to react with other 4-vinylbenzoic acid derivatives (0.011 mmol, 1.0 equiv.). All yields are isolated yields.....	104
Scheme 3.3 Proposed reaction paths.	109
Scheme 3.4 Scope of Ir(ppy) ₃ -photocatalyzed [2+2] cycloaddition. Reactions ran using General Procedure C and D described above. All yields and diastereomeric ratios were determined by	

¹ H NMR using CH ₂ Br ₂ as an internal standard. Only the structures of the major diastereomers are shown.	133
Scheme 4.1 A-C) Previous focuses on LHP halide-exchange. D) Perovskite-induced Br radical in DBM for photocatalytic [3+2] cycloaddition.	162
Scheme 4.2 The trapping of bromine radicals.....	163
Scheme 4.3 Scope of vinylcyclopropanes and alkenes. Only the structures of the major diastereomers are shown. All yields are isolated yields. d.r. values were determined by ¹ H NMR integration.	167
Scheme 4.4 The plausible mechanism for NCs-photocatalyzed Br-mediated [3+2] cycloaddition.	170
Scheme 4.5 Merging with other organic transformations. General reaction conditions: substrate (0.15 mmol, 0.1 M), CsPbBr ₃ NCs (1.0 mg), DBM (1.5 mL). Reaction was performed under N ₂ and blue LED (40 W, λ _{max} = 456 nm) irradiation at room temperature. Isolated yields are shown.	174
Scheme 4.6 The substrate scope for [3+2].	179
Scheme 4.7 The mechanism for the hydrogen atom transfer of benzaldehyde acetal by bromine radical studied by Doyle group. ³⁷	210
Scheme 5.1 Proposed hole-transfer-initiated [2+2] cycloaddition of 4-vinylaniline derivatives photocatalyzed by LHP NCs. EDG: electron-donating group. HT: hole transfer. ET: electron transfer.	224
Scheme 5.2 Proposed pathway for construction of BCH via LHP NCs-photocatalyzed Br radical-mediated ring-opening [3+2] cycloaddition of vinylcyclopropane and BCB.....	225

LIST OF TABLES

Table 2.1 Condition investigation for the NCs-photocatalyzed synthesis of pyrrole derivatives.	61
Table 2.2 Condition exploration for the NCs-photocatalyzed synthesis of pyrazole derivatives.	65
Table 3.1 Control experiments of the NCs-photocatalyzed TET-mediated intermolecular [2+2] cycloaddition.	101
Table 3.2 TET fit parameters.	107
Table 3.3 Initial investigation of perovskite-photocatalyzed [2+2] cycloaddition of 6 . ^a	123
Table 3.4 Investigation of the types of perovskites for photocatalytic [2+2] cycloaddition of 7a .	124
Table 3.5 Investigation of the types of solvents for CsPbBr ₃ -photocatalyzed [2+2] cycloaddition of 7a .	125
Table 3.6 Investigation of other conditions for CsPbBr ₃ -photocatalyzed [2+2] cycloaddition of 7a .	126
Table 3.7 Concentration of each identified component as a function of reaction time.	143
Table 3.8 The yields of each catalytic cycle.	149
Table 3.9 Fitted time constant.	153
Table 4.1 Optimization studies and control experiments for perovskite photocatalytic Br-mediated [3+2] cycloaddition.	166
Table 4.2 Photocatalyst (PC) evaluation under standard conditions.	172
Table 4.3 Extended reaction conditions.	177
Table 4.4 NCs Catalyst Recycling experiments.	211
Table 4.5 Benzylic bromination of toluene.	213

LIST OF ABBREVIATIONS

A	ampere
Ac	acetyl
Ar	arene
calcd	calculated
cat	catalyst
cat*	excited-state catalyst
CB	conduction band
COSY	correlated spectroscopy
CV	cyclic voltammetry
d.r.	diastereomeric ratio
DBM	dibromomethane
DCM	dichloromethane
DFT	density functional theory
DMF	dimethylformamide
DMSO	dimethylsulfoxide
e ⁻	electron
$E_{1/2}$	half-wave potential
EDG	electron-donating group
EI	electron ionization
EnT	energy transfer
E_{ox}	oxidation potential
E_{red}	reduction potential

ESI	electrospray ionization
ET	electron transfer
Et	ethyl
E_T	excited-state triplet energy
eV	electron volt
EWG	electron-withdrawing group
GC-MS	gas chromatography-mass spectrometry
h^+	hole
HAT	hydrogen atom transfer
HOMO	highest occupied molecular orbital
HPLC	high-performance liquid chromatography
HT	hole transfer
$h\nu$	photon or energy of a photon
<i>i</i> -Pr	isopropyl
IR	infrared
K_{sv}	Stern-Volmer quenching constant
LC-MS	liquid chromatography-mass spectrometry
LED	light-emitting diode
LHP	lead-halide perovskite
LUMO	lowest unoccupied molecular orbital
M	molarity
m/z	mass per charge
Me	methyl

MHP	metal-halide perovskite
n.d.	no detection
NC	nanocrystal
<i>n</i> -Hex	normal hexyl
nm	nanometer
NMR	nuclear magnetic resonance
NOESY	nuclear overhauser effect spectroscopy
ns	nanosecond
OA	oleic acid
OlAm	oleylamine
PC	photocatalyst
PC*	excited-state photocatalyst
PET	photoinduced electron transfer
Ph	phenyl
PL	photoluminescence
PLQY	photoluminescence quantum yield
ps	picosecond
QD	quantum dot
R	substituent
SCE	saturated calomel electrode
SET	single-electron transfer
TA	transient absorption
<i>t</i> -Bu	<i>tert</i> -butyl

TEA	triplet energy acceptor
TEMPO	(2,2,6,6-Tetramethylpiperidin-1-yl)oxyl
TET	triplet energy transfer
THF	tetrahydrofuran
TLC	thin-layer chromatography
TON	turnover number
TT-EnT	triplet-triplet energy transfer
UV	ultraviolet
V	volt
VB	valence band
λ	wavelength
μs	microsecond
τ	lifetime

ACKNOWLEDGEMENTS

I would like to start by thanking my advisor, Dr. Yong Yan, for introducing me to the world of chemistry research, and for encouraging me not to give up on pursuing my research goals. Thank you for your support all these years and I appreciate the degree of freedom you had given me to explore projects that were often outside of Yan group's normal research interest.

I would like to thank the past Yan group members that I had the privilege to directly work with: Dr. Xiaolin Zhu, Yanhong Zhao, Yue Sun, Dian Zhu, Claudine Manabat, Dr. Jun Guo, Dr. Chuang Han, Dr. Xianghua Zeng, Tianshu Yang, Mariana Avvacumova, Dr. Yin Xu, Ruilin Zhao, Dr. Zhaoyuan Lyu. Thank you for sharing all the knowledge and being supportive whenever I needed a hand.

I want to thank the current Yan group members: Kanchan Mishra, Melad Shaikh, Jovan San Martin, Nhu Dang, Ramon Martinez. Thank you for creating an inspiring work environment and for interesting discussions. Good luck on your future endeavor.

I would like to thank my committee members: Prof. Haim Weizman, Prof. David Fenning and Prof. Jing Gu for your valuable suggestions and comments in the past. And I am grateful to Prof. Thomas Cole for accepting the role to serve on my committee. I would like to thank Prof. Douglas Grotjahn who had been incredibly kind and helpful to me during my PhD studies.

I would like to thank Prof. Guy Bertrand, Prof. Clifford Kubiak, Prof. Charles Perrin respectively for amazing lectures on Organometallic Chemistry, Inorganic Chemistry and NMR, Applied Spectroscopy during my studies at UCSD.

I would like to thank my colleagues and friends and faculty members in the chemistry department who provided help to me at some points: Dr. Pullman, Dr. Cooksy, Dr. Gustafson, Andrew, Sean, Mariel, Braden, Mark, David, Yuan, Nick, Sabrina, Hongxing, Ellen, Nobuyuki,

Harry, Laurie, for that I am always grateful. I hold the same level of gratitude for those whom I may not have the opportunity to include here.

I would like to thank my parents for believing in me and their unconditional support. And thank you my grandma, for the loving care and the wait.

Last but not least, thank you Yue Sun for standing by my side throughout the entire journey.

Chapter 2 contains unpublished materials and is reproduced in part as it appears in *Nature Communication* **2019**, 10, 2843. Zhu, X.; **Lin, Y.**; San Martin, J.; Sun, Y.; Zhu, D.; Yan, Y. The dissertation author was a co-author of this paper.

Chapter 3, in full, is a reprint of the material as it appears in *ACS Applied Materials & Interfaces* **2022**, 14 (22), 25357 – 25365. **Lin, Y.**; Avvacumova, M.; Zhao, R.; Chen, X.; Beard, M.; Yan, Y. The dissertation author was the primary investigator and author of this paper.

Chapter 4, in full, is a reprint of the material as it appears in *ChemSusChem* **2023**, e202301060. **Lin, Y.**; Yan, Y. The dissertation author was the primary investigator and author of this paper.

VITA

2017 Bachelor of Science in Chemistry, Wuhan University

2023 Doctor of Philosophy in Chemistry, University of California San Diego and San Diego State University

PUBLICATIONS

1. **Lin, Y.**; Yan, Y., CsPbBr₃ Perovskite Nanocrystals for Photocatalytic [3+2] Cycloaddition. *ChemSusChem* (Accepted manuscript online, **Aug 2023**) <https://doi.org/10.1002/cssc.202301060>
2. **Lin, Y.**; Avvacumova, M.; Zhao, R.; Chen, X.; Beard, M.; Yan, Y., Triplet Energy Transfer from Lead Halide Perovskite for Highly Selective Photocatalytic 2+2 Cycloaddition. *ACS Applied Materials & Interfaces* **2022**, 14 (22), 25357 – 25365.
3. Li, J.; Zan, W.; Kang, H.; Dong, Z.; Zhang, X.; **Lin, Y.**; Mu, Y.; Zhang, F.; Zhang, X.; Gu, J., Graphitic-N Highly Doped Graphene-Like Carbon: A Superior Metal-Free Catalyst for Efficient Reduction of CO₂. *Applied Catalysis B: Environmental* **2021**, 298, 120510.
4. San Martin, J.; Zeng, X.; Chen, X.; Miller, C.; Han, C.; **Lin, Y.**; Yamamoto, N.; Wang, X.; Yazdi, S.; Yan, Y.; Beard, M.; Yan, Y., A Nanocrystal Catalyst Incorporating a Surface Bound Transition Metal to Induce Photocatalytic Sequential Electron Transfer Events. *Journal of the American Chemical Society* **2021**, 143 (30), 11361 – 11369.
5. Liu, S.; DeFilippo, A.; Balasubramanian, M.; Liu, Z.; Wang, S.; Chen, Y.; Chariton, S.; Prakapenka, V.; Luo, X.; Zhao, L.; San Martin, J.; **Lin, Y.**; Yan, Y.; Ghose, S.; Tyson, T., High-Resolution In-Situ Synchrotron X-Ray Studies of Inorganic Perovskite CsPbBr₃: New Symmetry Assignments and Structural Phase Transitions. *Advanced Science* **2021**, 2003046.
6. **Lin, Y.**; Guo, J.; San Martin, J.; Han, C.; Martinez, R.; Yan, Y., Photoredox Organic Synthesis Employing Heterogeneous Photocatalysts with Emphasis on Halide Perovskite. *Chemistry – A European Journal* **2020**, 26 (58), 13118 – 13136.
7. Han, C.; Zhu, X.; San Martin, J.; **Lin, Y.**; Spears, S.; Yan, Y., Recent Progress in Engineering Metal Halide Perovskite for Efficient Visible Light-Driven Photocatalysis. *ChemSusChem* **2020**, 13 (16), 4005 – 4025.
8. Geng, Y.; Tao, C.; Duan, S.; San Martin, J.; **Lin, Y.**; Zhu, X.; Zhang, Q.; Kang, X.; He, S.; Zhao, Y.; Li, X.; Niu, L.; Qin, D.; Yan, Y., V-Rich Bi₂S₃ Nanowire with Efficient Charge Separation and Transport for High-Performance and Robust Photoelectrochemical Application under Visible Light. *Catalysis Today* **2020**, 350, 47 – 55.

9. Wang, K.; Lu, H.; Zhu, X.; **Lin, Y.**; Beard, M.; Yan, Y.; Chen, X., Ultrafast Reaction Mechanisms in Perovskite Based Photocatalytic C–C Coupling. *ACS Energy Letters* **2020**, 5 (2), 566 - 571.
10. Zhu, X.; **Lin, Y.**; San Martin, J.; Sun, Y.; Zhu, D.; Yan, Y., Lead Halide Perovskites for Photocatalytic Organic Synthesis. *Nature Communication* **2019**, 10, 2843.
11. Qin, D.-D.; Quan, J.-J.; Duan, S.-F.; San Martin, J.; **Lin, Y.**; Zhu, X.; Yao, X.-Q.; Su, J.-Z.; Rodríguez-Gutiérrez, I.; Tao, C.-L.; Yan, Y., High-Performance Photoelectrochemical Water Oxidation with Phosphorus-Doped and Metal Phosphide Cocatalyst-Modified g-C₃N₄ Formation Through Gas Treatment. *ChemSusChem* **2019**, 12 (4), 898 - 907.
12. Zhu, X.; **Lin, Y.**; Sun, Y.; Beard, M. C.; Yan, Y., Lead-Halide Perovskites for Photocatalytic α -Alkylation of Aldehydes. *Journal of the American Chemical Society* **2019**, 141 (2), 733-738.
13. Lei, Q.; Wang, S.; Hu, J.; **Lin, Y.**; Zhu, C.; Rong, L.; Zhang, X., Stimuli-Responsive “Cluster Bomb” for Programmed Tumor Therapy. *ACS Nano* **2017**, 11 (7), 7201-7214.

HONORS AND AWARDS

University Graduate Fellowship (2019/2020)

Provost’s Award for Research and Scholarship (2019)

Certificate of Appreciation for Outstanding Contribution as Graduate Mentor to NSF REU Summer Research Program (2018)

ABSTRACT OF THE DISSERTATION

Lead-Halide Perovskite for Visible-Light Photocatalytic Ring-Forming Reactions

by

Yixiong Lin

Doctor of Philosophy in Chemistry

University of California San Diego, 2023

San Diego State University, 2023

Professor Yong Yan, Chair

Cyclic compounds are ubiquitous in natural products and FDA approved drug molecules. A sustainable, efficient, and readily accessible method for direct access to cyclic compounds under mild reaction conditions is highly desired in modern synthetic chemistry. The emerging visible-light-driven photocatalysis, which shows complementary reactivity to the conventional method,

has been developed as a powerful tool for making valuable cyclic compounds. Among this catalytic category, heterogeneous photocatalysis showcases significant advantages, such as low cost, high photostability and facile regeneration of photocatalysts as well as unique photochemical selectivity and reactivity relative to those of homogeneous photocatalysis. Our group has shown that lead-halide perovskite nanocrystals (LHP NCs), a material with demonstrated excellent photophysical properties in photovoltaics, can be a promising heterogeneous visible-light photocatalyst for organic transformations. Because an efficient photocatalytic reaction can also essentially benefit from the LHP NCs' intensive visible light absorption, long charge carrier lifetime, long charge carrier diffusion length and high charge carrier mobility. These critical photophysical properties of LHP NCs along with the basic principles of visible-light-driven photocatalysis and an overview of other typical heterogeneous photocatalysts for ring-forming reactions have been discussed in **Chapter 1**. This dissertation further advances the application of the LHP NCs as visible-light photocatalysts towards some synthetically challenging, biorelevant cyclic compounds syntheses. Specifically, the photocatalytic synthesis of pharmaceutically important N-heterocycles (pyrroles and pyrazoles) is detailed in **Chapter 2**. The photocatalytic highly regio- and diastereoselective synthesis of cyclobutanes, a class of scaffolds that are widely present in natural compounds, is detailed in **Chapter 3**. Lastly, the photocatalytic synthesis of medicinally relevant vinylcyclopentanes is detailed in **Chapter 4**. The works described in this dissertation may lay the foundation for the design and development of highly valuable photocatalytic ring-forming reactions that directly benefit from the unique photophysical and photochemical properties of heterogeneous lead-halide perovskite nanocrystals photocatalysts.

Chapter 1 Introduction

1.1 Background Introduction

Ring- or cycle-containing compounds are ubiquitous in natural products and are privileged compounds in pharmaceutical industry. In fact, the majority of the top-selling small molecule drugs contains ring structures.^{1, 2} Therefore, readily accessible, highly efficient, and economic cyclization methodology for direct access to cyclic compounds is imperative in modern synthetic chemistry.

To date, tremendous number of successful examples to forge ring structures have been documented by employing traditional catalytic (transition metal catalysis, organocatalysis, Lewis acid catalysis) or non-catalytic approaches, which often require harsh reaction conditions. However, as sustainable chemistry has now become a critical topic in both industrial and academic society, chemical reactions that are driven by green energy source, highly selective and efficient for desired product formation (e.g., valuable cyclic compounds), but operable under mild conditions are still highly sought-after.

The recent renaissance of photocatalysis powered by visible light as a form of renewable energy, offers an appealing solution to address the sustainability issue while providing access to radical chemistry in a selective manner under benign reaction conditions which potentially invokes new chemical reactivity that is complimentary to conventional closed-shell, two-electron pathways.³ On top of that, photocatalysis combined with a secondary catalyst system have also shown feasible, allowing for a more diverse transformation.⁴ In contrast to tradition radical chemistry that often requires a highly reactive radical initiator and harsh reaction conditions, photocatalytic chemistry with a bench-stable photocatalyst can occur in an exceptionally mild conditions and provide access to new radical species such as radical ions and diradicals with unique

reactivity patterns that are otherwise hard to achieve using established traditional methods. Unlike high-energy ultraviolet light (UV) for non-selective, direct activation of the organic substrates that may cause undesirable side reactions, visible light-induced photocatalysis features a photocatalyst that is capable of absorbing visible light of appropriate wavelength, turning into its excited state then engaging in the subsequent substrate activation and transformation processes. Meanwhile, all other ingredients in the reaction mixture are generally chemically inert to visible light irradiation, as such, unproductive reactions can be circumvented from the event of photoexcitation of the substrate itself. The selectivity is governed by the redox potentials and charge transfer kinetics from the excited-state photocatalyst to the redox-active group present on the substrates, or regulated by the triplet energy levels of the involved species. Moreover, visible light can be harnessed from natural sunlight (44% visible light vs. 3% UV light) ⁵ or simple household light bulbs while UV light generation usually requires specialized apparatus which further limits its industrial applicability and scalability. Overall, visible light photocatalysis should be a promising strategy for cyclic compound synthesis.

1.2 General Mechanism of Visible-Light-Driven Homogeneous Photocatalysis

Homogeneous visible-light photocatalysts are the most studied photocatalysts applied for photocatalytic organic transformations in the past two decades, among which Iridium- and Ruthenium-based metal complexes are the most well-known. Towards the aim of obviating the use of noble metals and discovering new reactivity, metal-free organic dyes are also developed to be used as a type of photocatalyst. ⁶ These catalysts can become potent single-electron transfer (SET) or triplet-triplet energy transfer (TT-EnT) ⁷ agents once being excited by proper light irradiation.

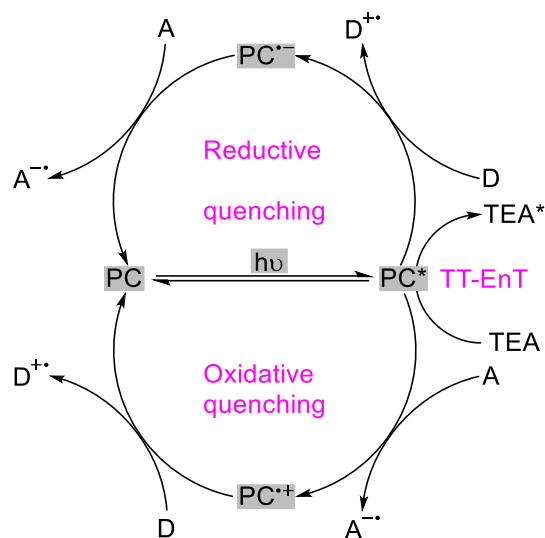


Figure 1.1 General pathways of homogeneous photocatalysis. Under visible light irradiation, photocatalyst (PC) first gets to its excited state (PC*) by promoting one electron from HOMO to LUMO. Then the resulting PC* participates in substrate activation via a reductive quenching/oxidative quenching/triplet-triplet energy transfer (TT-EnT) pathway. A: electron acceptor; D: electron donor; TEA: triplet energy acceptor; HOMO: highest occupied molecular orbital; LUMO: lowest unoccupied molecular orbital.

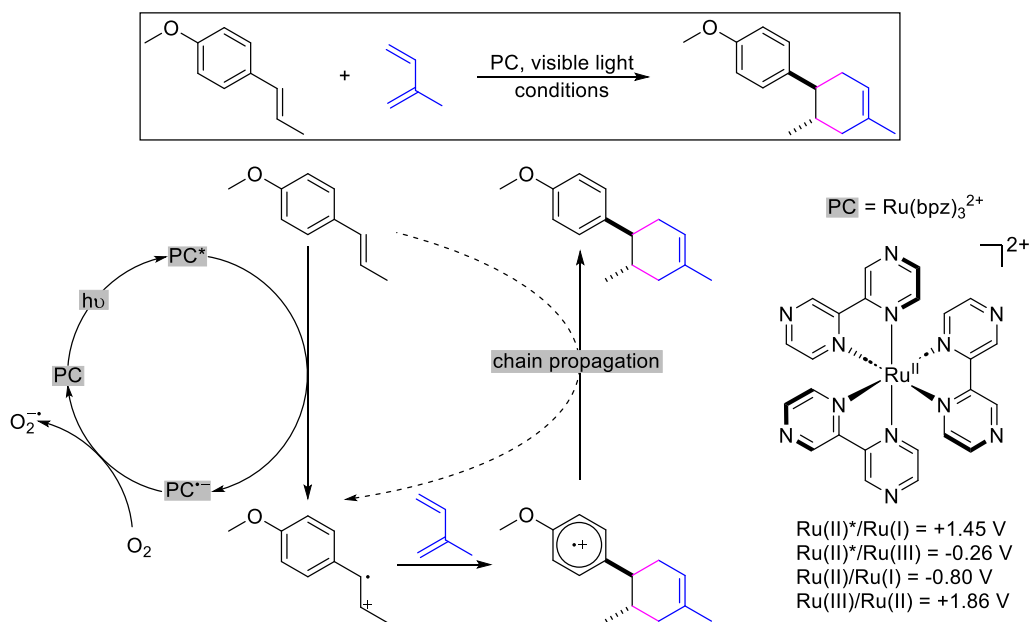
In a typical photocatalysis process, the photocatalyst (PC) absorbs visible light of appropriate wavelength to reach its excited state (PC*). Next, the PC* may initiate organic transformations via various pathways as shown in **Figure 1.1**. For the photoinduced electron transfer (PET)-based photoredox mechanism, an event of SET from or to the PC* may occur. The direction of electron flow is governed by the redox potentials, which measure the thermodynamic tendency of electron transfer from one specie to another. For instance, a PC* of a more positive potential than the oxidation potential of a substrate tends to oxidize the latter. As a result, the PC itself gains an electron from the substrate and gets reduced. Such process is commonly called reductive quenching, and *vice versa* for oxidative quenching. Therefore, to design a photoredox reaction, one must consider the redox potentials of each species involved in a photocatalytic cycle. Independent of the redox-active functional groups present on a substrate, interesting reactions may also be triggered via a triplet-triplet energy transfer (TT-EnT) mechanism. In this case, PC* acts

as a triplet sensitizer, transferring energy to the involved substrate or intermediate with lower triplet energy state. The photocatalytic TT-EnT mechanism is broadly explored towards triplet-energy-mediated cycloaddition, alkene isomerization, bond homolysis, and promotion of an organometallic catalysis cycle.⁸ In general, an efficient photocatalysis process necessitates a photocatalyst featuring intensive visible light absorption, long-lived excited state, facile electron transfer capability, matching photoredox potentials or triplet energy levels.

1.3 Representative Examples of Photocatalytic Ring-Forming Reactions

Ring-forming reaction is an imperative category in organic transformations (*vide supra*). To achieve sustainable and highly efficient ring-forming reactions while implement new reactivity, the emerging visible light photocatalysis has been explored as a powerful chemical tool towards this endeavor. Five typical photocatalytic mechanisms for the synthesis of ring compounds can be recognized.

1.3.1 Photocatalytic [4+2] Cycloaddition

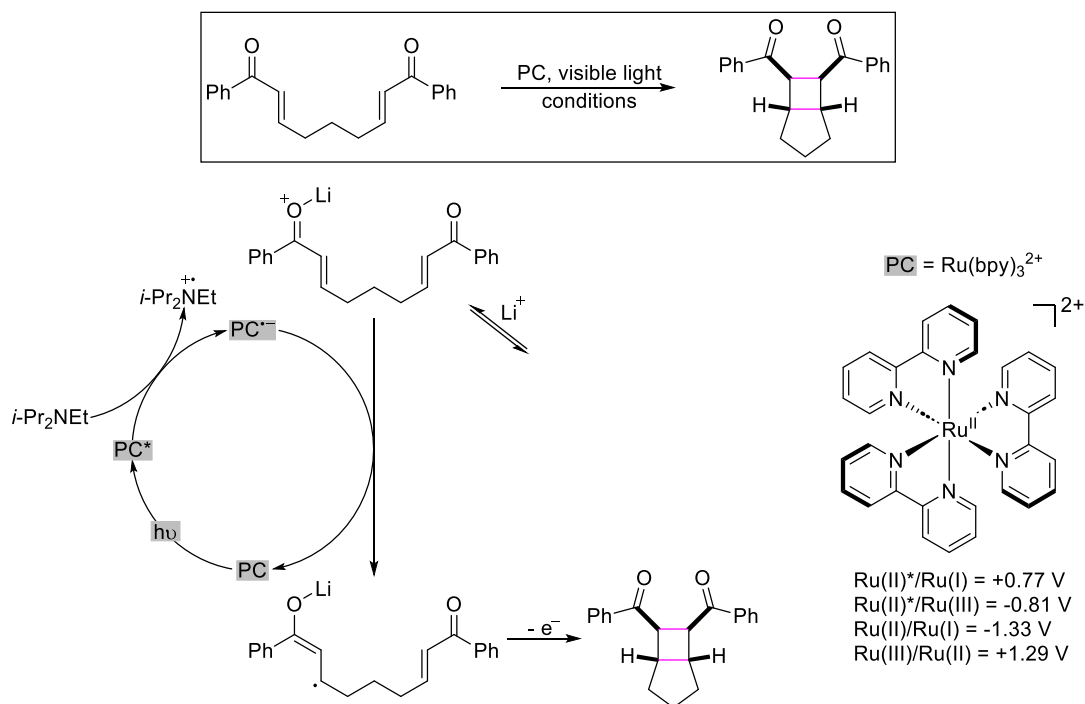


Lin *et al.*, *J. Am. Chem. Soc.* **2011**

Scheme 1.1 Photocatalytic radical cation Diels-Alder reaction by Yoon and co-workers.

Yoon group is among the pioneers for developing visible-light-induced photocatalytic cycloaddition reactions. For instance, in 2011, Lin *et al.* designed a photocatalytic protocol for radical cation Diels-Alder cycloaddition of electron-rich dienophiles promoted by ruthenium(II) polypyridyl complexes that would otherwise be unreactive in the classical thermal conditions because of electronical mismatch (**Scheme 1.1**).⁹ The electron-rich dienophile was proposed to undergo single-electron oxidation by the visible-light-induced excited-state PC* rendering an electron-poor radical cation, which now enables the electronically matching Diels-Alder cycloaddition reactivity with an electron-rich diene. The radical cation [4+2] cycloadduct can initiate a radical chain propagation via abstraction of an electron from another substrate, while the reduced-form PC is turned over by molecular oxygen to its photoactive ground state. This remarkable method provides an orthogonal reactivity to the classical thermal Diels-Alder cycloaddition.

1.3.2 Photocatalytic Redox-Based [2+2] Cycloaddition

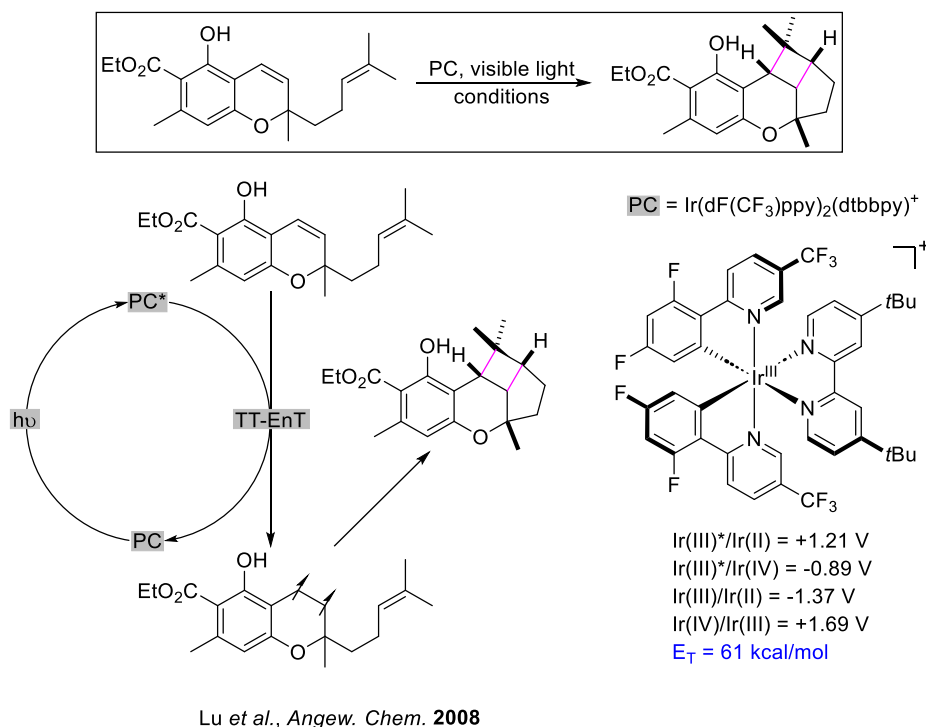


Ischay *et al.*, *J. Am. Chem. Soc.* **2008**

Scheme 1.2 Photoredox [2+2] cycloaddition by Yoon and co-workers.

[2+2] cycloaddition is an important ring-forming reaction pathway that leads to strained four-membered cycle formation. In 2008, Ischay *et al.* reported that a $\text{Ru}(\text{bpy})_3^{2+}$ photocatalyst can catalyze a formal [2+2] cycloaddition of tethered symmetrical bis(enone) via a critical radical anion intermediate (**Scheme 1.2**).¹⁰ The excited-state PC^* was proposed to undergo reductive quenching by Hünig's base to $\text{Ru}(\text{bpy})_3^+$, a potent reductant, which then reduces the lithium-activated enone via SET initiating the cycloaddition and regenerating the ground-state photocatalyst. The radical anion [2+2] cycloadduct can either be oxidized by the excited-state PC^* or by another equivalent of lithium-activated enone to furnish the final product. Notably, this strategy is also effective on unsymmetrical bis(enone) as well as untethered intermolecular dimerization.

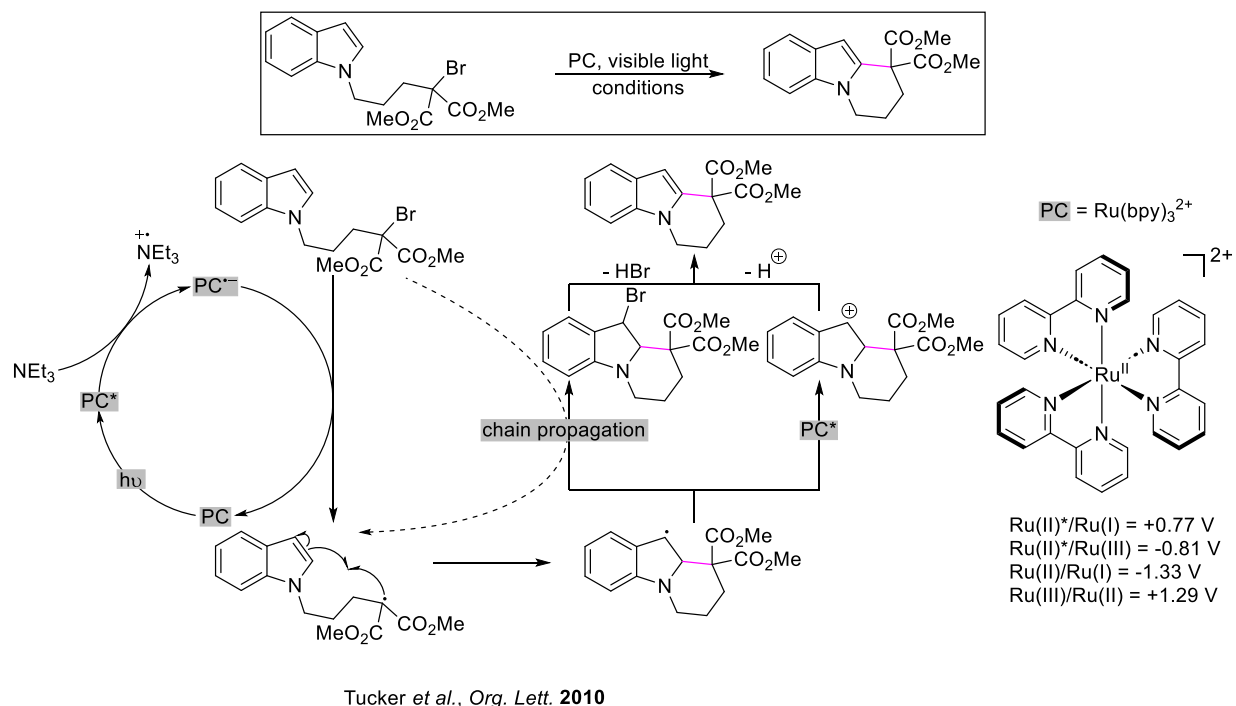
1.3.3 Photocatalytic Energy-Transfer-Based [2+2] Cycloaddition



Scheme 1.3 Photocatalytic energy-transfer-mediated [2+2] cycloaddition by Yoon and co-workers.

[2+2] cycloaddition can also be initiated by an energy-transfer (EnT) mechanism. Unlike a photoredox process that relies on the redox-active group present on the substrate, the alternative EnT method bypasses the electrochemical profile of the involved organic substrate. In 2012, Lu *et al.* reported an EnT-mediated intramolecular [2+2] cycloaddition of styrene derivatives whose oxidation potential is out of reach by the PC, however, excited-state triplet energy (E_T) is within reach (**Scheme 1.3**).¹¹ Experimental evidences such as the similar efficiencies are obtained in solvents of diverse polarity and PCs of lower triplet energies are incompetent catalysts further suggest this reaction is mediated by EnT instead of electron transfer. The involved styrene-based substrate conceivably goes through a diradical excited state after accepting EnT from the excited-state Ir-photocatalyst then undergoes intramolecular [2+2] cycloaddition with another double bond on the molecule to furnish the final cyclobutane product.

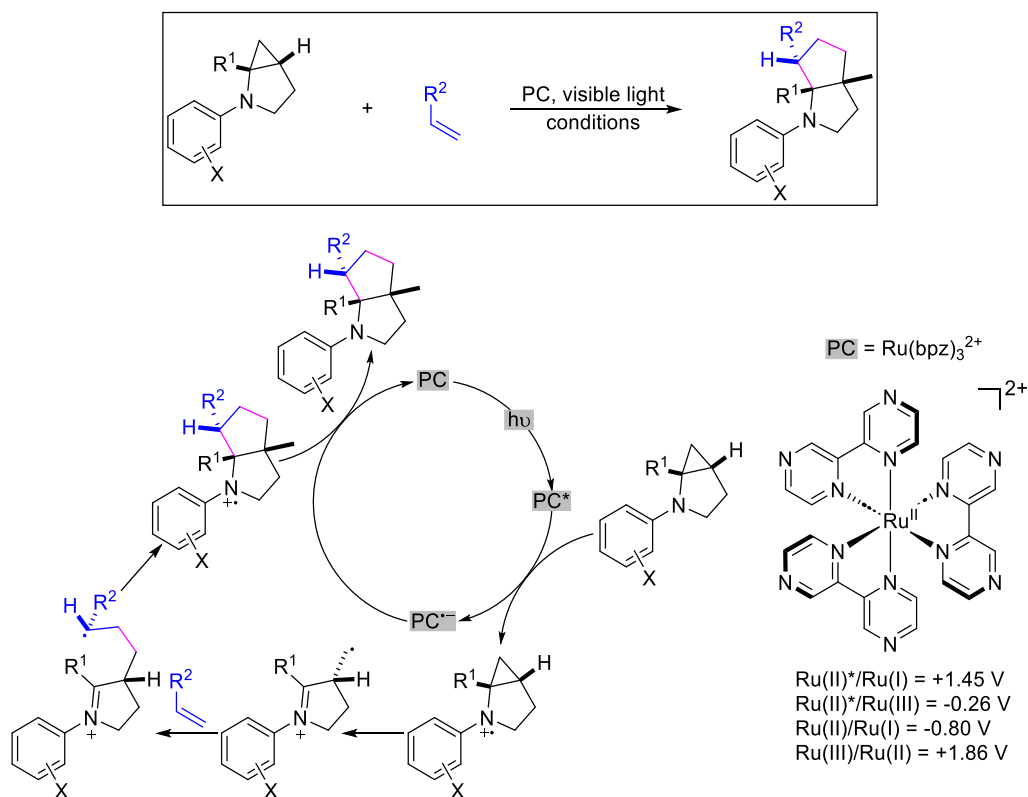
1.3.4 Photocatalytic Radical Cascade Cyclization



Scheme 1.4 Photocatalytic radical cascade cyclization by Stephenson and co-workers.

Radical addition to unsaturated bond is one of the most common ways to construct new C-C bond in photocatalytic chemistry. When such addition takes place intramolecularly, a cyclic architecture can be assembled, also known as radical cascade cyclization. As an early example shown in 2009, Tucker *et al.* reported a photocatalytic reductive radical cyclization approach for the C-H functionalization of indoles and pyrroles (**Scheme 1.4**).¹² Reductive quenching of the excited-state PC* by triethylamine results in Ru(bpy)₃³⁺ which then reduces the C(sp³)-Br bond of the bromomalonate functional group on the substrate via SET generating a carbon-centered radical while regenerating the ground-state PC. This electron-poor malonyl radical undergoes intramolecular cyclization with the electron-rich heterocycle, *i.e.*, indole, to a benzylic radical-based intermediate, which can either be oxidized by the PC* followed by elimination of a proton or abstract a Br atom from another equivalent of substrate followed by aromatization to furnish the final product.

1.3.5 Photocatalytic Ring-Opening Cyclization



Maity *et al.*, *Angew. Chem.* 2012

Scheme 1.5 Photocatalytic cyclopropylamine ring-opening [3+2] cycloaddition by Zheng and co-workers.

Ring-opening cycloaddition is yet another approach to construct a new ring and ring expansion can be achieved as a result. An example focused on amine radical cation-induced cyclopropane ring-opening was reported in 2011. Maity *et al.* designed a method that engages cyclopropylamines as three-carbon fragment for ring-opening [3+2] cycloaddition reactions with styrenes (**Scheme 1.5**).¹³ Single-electron oxidation of the cyclopropylamine substrate by the excited-state PC* results in a N-centered radical cation intermediate which then undergoes ring opening to an iminium ion tethered carbon-centered radical. Addition of this radical to a styrene results in a benzylic radical intermediate, which adds to the iminium C=N bond to afford the radical

cation [3+2] cycloadduct. The final product is furnished by obtaining an electron from the reduced-form PC, $\text{Ru}(\text{bpz})_3^+$, while regenerating the ground-state PC.

1.4 Visible-Light-Driven Heterogeneous Photocatalysis

In addition to homogeneous photocatalysts, heterogeneous catalysts are of high interest for chemical industrial applications and are outstanding candidates for developing catalyst-immobilized flow chemistry for large-scale product synthesis. Heterogeneous photocatalysts are particularly interesting because they are known for their recyclability from the reaction mixture as well as high photostability due to the restricted rotations. Heterogeneous photocatalysts are often excellent semiconductor materials that can absorb suitable light and realize charge separation, as such, they can be engineered and employed for visible light photocatalysis purposes. Furthermore, heterogeneous photocatalysis may offer novel reactivity and substrate activation mode that are distinct from or complementary to those of homogeneous photocatalysis due to their unique solid-state surface chemistry and photoelectronic properties. Heterogeneous photocatalysis has been explored towards renewable energy fuels generation (e.g., water splitting for hydrogen fuels,¹⁴ CO_2 reduction for carbon-based fuels¹⁵) using solar light as the energy input, pollutant degradation¹⁶ and biomass conversion¹⁷. Such heterogeneous photocatalysis shows promising results as well as great potential for applications in real life. Heterogeneous photocatalysis was also introduced to the realm of visible-light-driven photocatalytic organic transformations in recent years.

1.4.1 General Mechanism of Visible-Light-Driven Heterogeneous Photocatalysis

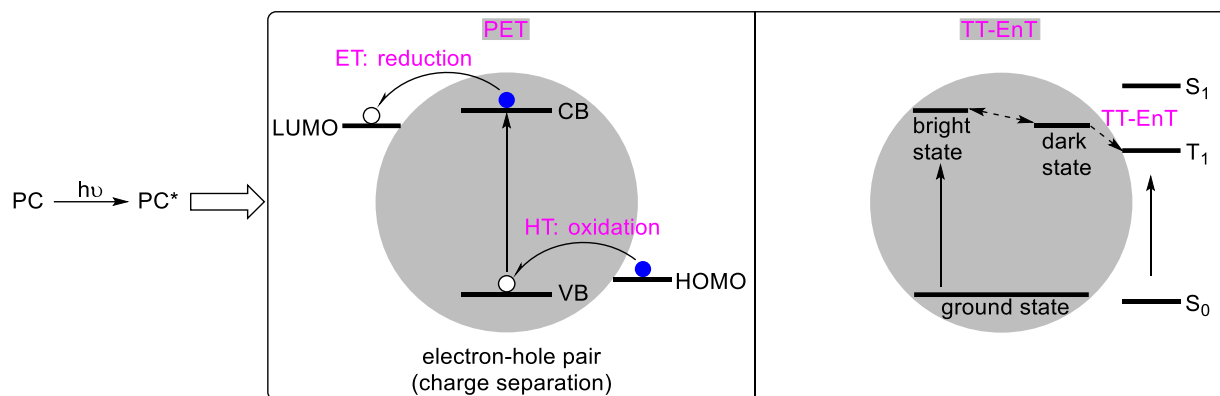


Figure 1.2 General pathways of heterogeneous photocatalysis. Photocatalyst (PC) first gets to excited state (PC^*) by promoting electrons from VB to CB under visible light irradiation, and then participate in substrate activation via electron transfer (ET)/hole transfer (HT)/triplet-triplet energy transfer (TT-EnT) pathway. PET: photoinduced electron transfer; VB: valence band; CB: conduction band.

Similar to homogeneous photocatalysis, two general mechanisms can be found for a visible-light-driven heterogeneous photocatalysis process (**Figure 1.2**). The heterogeneous PC first gets excited by the light of appropriate wavelength and reaches to its charge separation state, generating a hole in the valence band (VB), resembling the HOMO of a homogeneous PC, and an electron in the conduction band (CB), resembling the LUMO of a homogeneous PC. For a photoredox-based mechanism, interfacial single-electron transfer can either happen from CB to LUMO of a substrate (reduction), or from HOMO of a substrate to VB (oxidation). Such process shares the same mechanism with that of the traditional homogenous photocatalysis. However, in stark contrast to a homogeneous PC^* , where the same PC^* molecule exists either as an oxidizing or reducing specie at a disparate time, a heterogeneous PC^* can exist as a potent single-electron oxidant and reductant simultaneously on the same particle.

A TT-EnT mechanism is also operable in heterogeneous photocatalysis, the TT-EnT can happen from a triplet-like excited state (dark state) of a heterogeneous PC to promote a substrate to its reactive excited state. In stark contrast to a homogeneous molecular PC^* , the singlet-triplet

gap in a heterogeneous PC* is negligible or near-degeneracy.¹⁸ Therefore, the light input could be utilized more efficiently in the case of heterogeneous PC without losing a significant amount of energy when transitioning from singlet to triplet excited state.

1.4.2 Heterogeneous Photocatalysis for Ring-Forming Reactions

Heterogeneous photocatalysis has also been developed for the synthesis of ring-containing compounds. The recent advances of visible-light-driven semiconductor-like heterogeneous photocatalysis for ring-forming reactions have been summarized in this section with emphasis on typical materials, such as titanium oxide (TiO₂), cadmium chalcogenide (CdSe, CdS), covalent organic frameworks (COFs) and conjugated microporous polymers (CMPs) as the photocatalysts. The aim here is to summarize the applications of these heterogeneous photocatalysts in ring-forming reactions with highlight of their catalytic advantages. The comprehensive discussion of their individual reaction mechanisms, substrate scope tolerance, material design, synthesis, and engineering methods, and photoelectronic properties is out of the scope of this summary.

1.4.2a Titanium Oxide (TiO₂) for Photocatalytic Ring-Forming Reactions

TiO₂ is a low-cost, environmentally friendly, readily available material broadly applied in white pigment and cosmetic sunscreen, it is also a widely studied metal oxide-based heterogeneous semiconductor photocatalyst. TiO₂ can have two typical phases with different band gaps and reactivity, *i.e.*, rutile (3.0 eV) and anatase (3.2 eV).¹⁹ Degussa P25 is a commonly employed mixed-phase TiO₂ photocatalyst composed of polymorphs anatase and rutile in a ratio typically about 8:2. Pristine TiO₂ may not efficiently absorb visible light because of its large band gap, modification techniques such as dye sensitization, surface complexation, metal doping or nanoparticle decoration are often employed to enhance its absorptivity in visible spectrum as well as its photocatalytic efficiency.²⁰

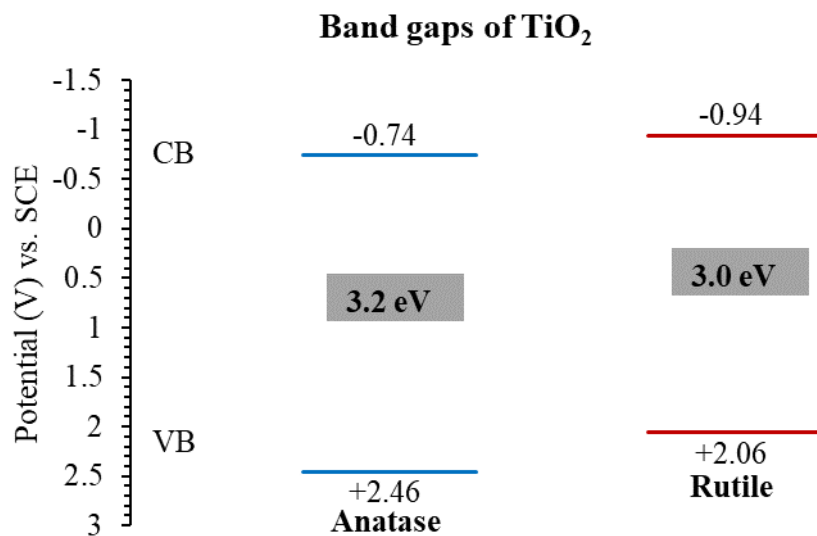
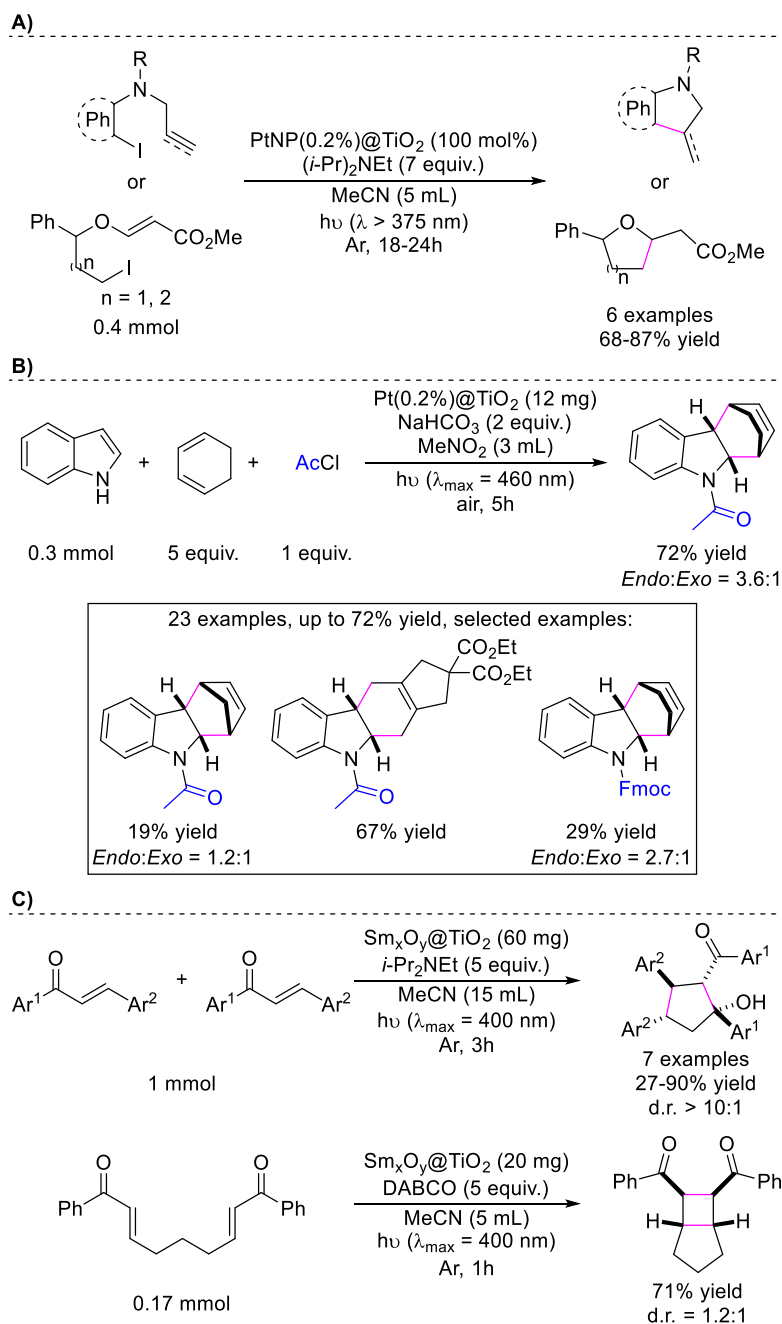


Figure 1.3 Band structures of TiO₂ (anatase and rutile). ²¹

In 2014, Scaiano group reported a platinum nanoparticle decorated TiO₂ photocatalyst (PtNP@TiO₂) that can induce a series of hydrodehalogenated intramolecular cyclization reactions of iodo compounds under ultraviolet A/visible light irradiation in the presence of diisopropylethylamine as a sacrificial electron donor. ²² A range of five- to six-membered heterocycles were obtained in good yields within 24h of reaction time. (**Scheme 1.6A**) The authors also showcased that their photocatalysts can induce intramolecular cycloaddition of bis(enone), however, with limited examples and selectivity (47–54%). It should be noted that the PtNP@TiO₂ demonstrates enhanced efficiency compared to undecorated TiO₂ owing to the NP's ability to enhance light absorption while inhibit the undesirable electron-hole pair recombination.

In 2017, Scaiano group collaborating with Yoon group discovered that TiO₂ together with indole can form a complex through substrate-surface interaction exhibiting a new absorption band that can extend to the visible light region. Such complex was verified by action spectrum, and was responsible for the Diels-Alder reactions observed between indole and 1,3-cyclohexadiene under

visible light irradiation.²³ Later on, they extended the scope of this reaction by employing platinum nanoparticles modified TiO₂ (Pt(0.2%)-TiO₂) as a photocatalyst.²⁴ (Scheme 1.6B)



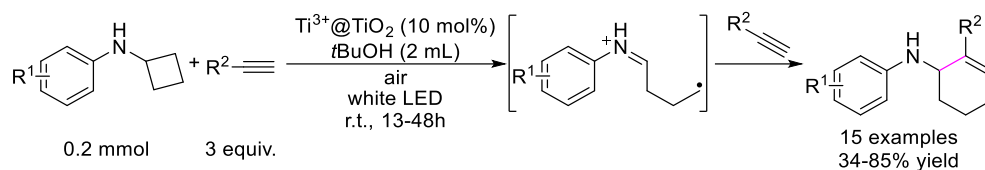
Scheme 1.6 TiO₂-photocatalyzed cyclizations by Scaiano and co-workers.

Scaiano and co-workers reported the first example of heterogeneous dual photoredox-Lewis acid catalysis in 2018, using a single bifunctional nanomaterial composed of samarium

oxide nanoparticles decorated TiO₂ (Sm_xO_y@TiO₂) for intermolecular net reductive and intramolecular redox neutral cyclization reactions (**Scheme 1.6C**).²⁵ This purely heterogeneous bifunctional nanocomposite allows the Lewis acid and the semiconductor support working synergistically and provides desired products comparable to the established yielding catalyzed by homogeneous photocatalysts in most cases. But this method provides extra opportunities for catalyst recycles, high turnovers and cost-effectiveness. Note that this system discussed here appears to have the same effect on the diastereoselectivity of the product as that with homogeneous photocatalysis.

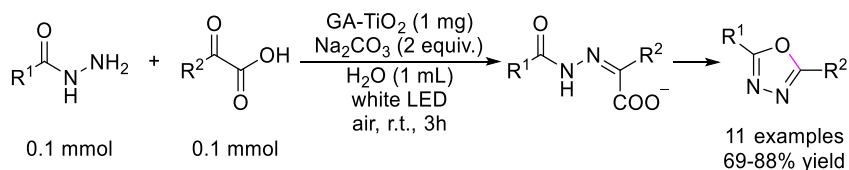
In 2015, Tang *et al.* reported a nickel oxide surface-modified TiO₂ photocatalyst (P25/NiO) that can induce oxidative cyclizations of tertiary anilines with maleimides affording tetrahydroquinolines in satisfactory to good yields under blue LED irradiation in the presence of oxygen from the air as an oxidant (**Scheme 1.7**).²⁶ The P25/NiO photocatalyst shows exceptionally higher catalytic efficiency compared to the pristine TiO₂ due to its extended visible light absorptivity and reduced electron-hole pair recombination tuned by nickel oxide clusters on the surface. Remarkably, their P25/NiO photocatalyst can be reused for at least 9 cycles of reactions without significant impact on the catalytic ability. In 2018, Sarvari group utilized the idea of organic dye Alizarin red S sensitized TiO₂ photocatalyst (ARS-TiO₂) to realize to same transformation.²⁷ In this strategy, the organic dye is covalently anchored on the TiO₂ surface, directly excited by the visible light while the semiconductor TiO₂ acts as an electron relay, thus alleviating the issue of generating undesirable strongly oxidizing species by the valence band of TiO₂. Later in 2020, their group was able to employ the same type of ARS-TiO₂ photocatalyst for synthesizing 2-aminobenzothiazoles from radical cyclization of anilines with thiocyanate radicals generated from photooxidation of ammonium thiocyanate.²⁸

cations followed by ring opening cyclization with alkynes. Such reaction mechanism was distinct from the rose Bengal photocatalyzed counterparts, which required an inert atmosphere.



Scheme 1.9 Photocatalytic cyclobutylaniline ring-opening [4+2] cycloaddition catalyzed by $\text{Ti}^{3+}@\text{TiO}_2$.

In 2022, Sciarretta *et al.* reported a graphene acid (GA) immobilized TiO_2 nanohybrid photocatalyst that can catalyze the synthesis of 1,3,4-oxadiazoles from ketoacids with hydrazides in reaction times as fast as 1h (**Scheme 1.10**).³¹ This GA- TiO_2 nanohybrid photocatalyst functioned cooperatively, where the GA is responsible for the imine formation and this hybrid material as an entity is mainly responsible for the subsequent photocatalyzed decarboxylative cyclization process. Such nanohybrid showed enhanced visible light absorptivity while maintaining conductivity.



Scheme 1.10 Photocatalytic synthesis of 1,3,4-oxadiazoles from ketoacids with hydrazides catalyzed by GA- TiO_2 .

Overall, TiO_2 was mostly employed for activation of substrates for ring-forming reactions via single-electron oxidation owing to its strong reduction potential (+2.46 V for anatase, +2.06 V for rutile, all vs. SCE). A few cases of reductive activation were also reported, however, for reactive substrates such as alkyl iodides and Lewis acid-activated enones. Proper modifications are often needed to reduce its charge-carrier recombination rate, prevent overoxidation, and induce

band gap red-shifting in order to enhance its photocatalytic efficiency under visible light irradiation.

1.4.2b Cadmium Chalcogenide (CdSe, CdS) for Photocatalytic Ring-Forming Reactions

Cadmium chalcogenide, namely, cadmium selenide (CdSe) and cadmium sulfide (CdS), in contrast to TiO₂ introduced above, are semiconductor materials of narrow band gaps capable of absorbing visible light. In fact, bulk CdSe has a band gap of 1.7 eV equivalent to absorb low energy photons down to 730 nm while bulk CdS has a band gap of 2.4 eV equivalent to 517 nm. Thanks to the advancement of colloidal nanocrystals synthesis methods, size-controlled, quantum-confined CdSe and CdS nanocrystals (quantum dots, QDs) of large surface-to-volume ratio can also be prepared. The CB and VB of such QDs are expected to shift towards more negative and more positive potentials respectively, result in increased band gaps, as the sizes of the QDs decrease smaller than their Bohr radii (5.3 nm and 2.8 nm for CdSe and CdS respectively ³²). **(Figure 1.4)** CdSe QDs are often needed to be synthesized for the purpose of visible-light-driven photocatalysis as its bulk band gap falls in the near-infrared region, whereas CdS with bulk-like properties are often employed.

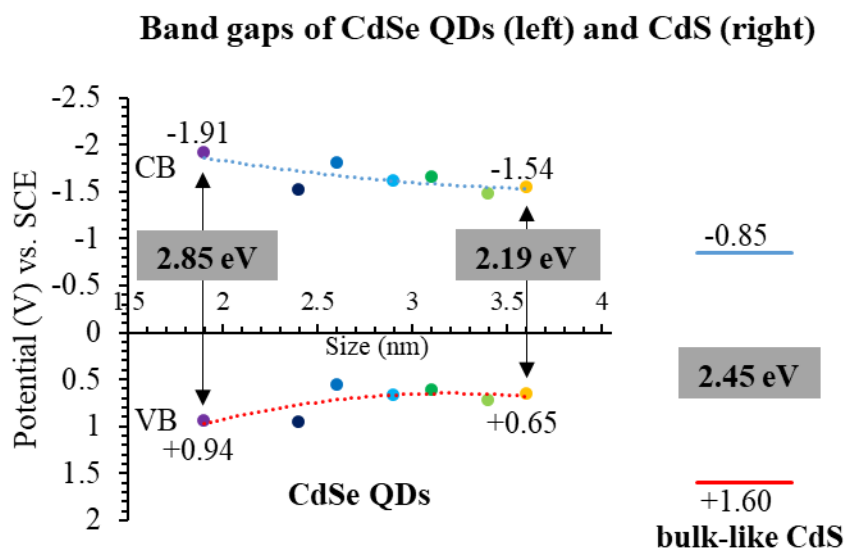
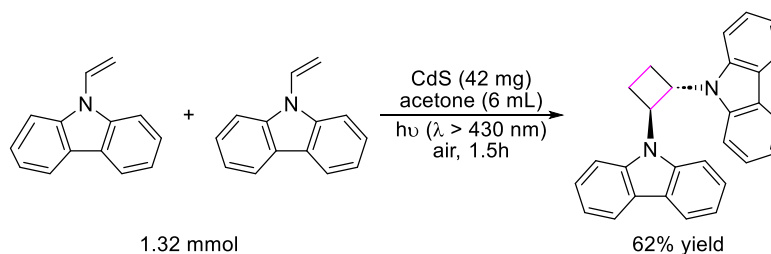


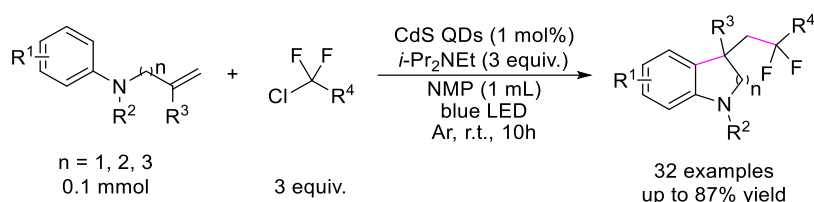
Figure 1.4 Band structures of CdSe (TOPO) QDs³³ and CdS³⁴. Note: The trapping of electrons and holes, in addition to coulombic interaction, might cause difference between electrochemical band gap and optical band gap.^{35, 36} The redox potentials would be slightly altered if QDs are capped by different ligands. TOPO: trioctylphosphine oxide.

An early example of CdS visible-light induced cycloaddition reaction can be traced back to 1986. De Mayo group reported that CdS can induce the dimerization of *N*-vinylcarbazole via [2+2] cycloaddition with the presence of oxygen and visible light irradiation.³⁷ (**Scheme 1.11**) Further investigation suggested that such reaction proceeded via a cation radical mechanism and appeared to follow the Langmuir-Hinshelwood and modified Eley-Rideal mechanism. They also obtained different activation energies from CdS catalysts purchased from two different commercial sources which may suggest different trapping efficiencies of the photoelectron by traps at different depths located below the conduction band of CdS.



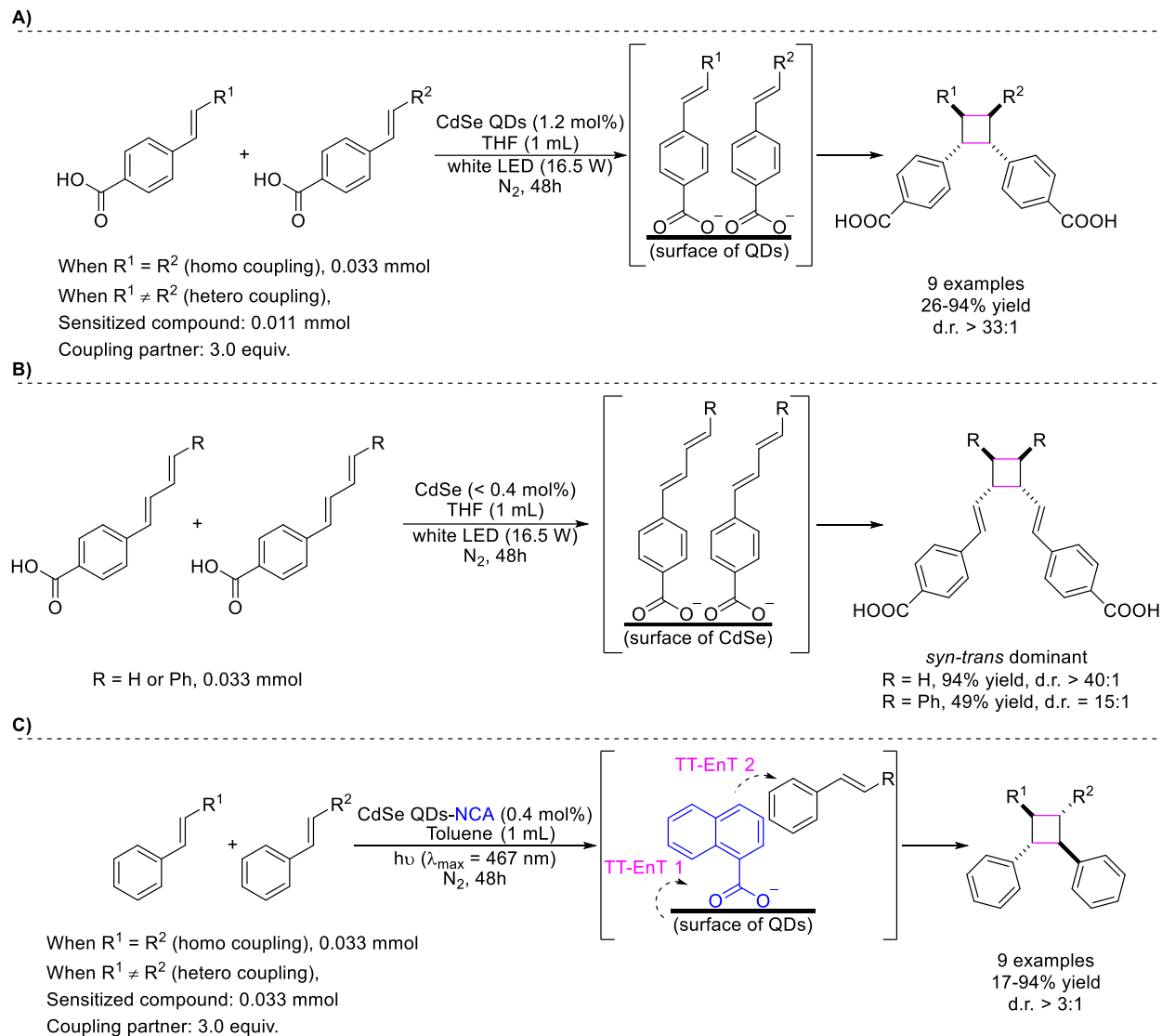
Scheme 1.11 Photoredox [2+2] cyclodimerization of *N*-vinylcarbazole catalyzed by CdS.

In 2018, Hu *et al.* reported that CdS QDs can efficiently photocatalyze the C(sp³)-Cl bond cleavage of functionalized difluoromethyl chlorides. The resulting CF₂-based radical can further involve in a radical cascade cyclization reaction with a phenyl-containing N-linked unactivated olefin to form an array of CF₂-containing five- or six-membered azaheterocycles such as indoline and tetrahydroquinoline.³⁸ (**Scheme 1.12**) Notably, the incorporation of a CF₂ group into such azaheterocycles may give them access to lead compounds with enhanced biological activities.



Scheme 1.12 Photocatalytic CF₂-based radical cascade cyclization catalyzed by CdS QDs.

A seminal report in 2019 from Weiss group found that a highly regio- and diastereoselective intermolecular [2+2] cycloaddition of 4-vinylbenzoic acid derivatives could be realized by CdSe QDs photocatalysis.³⁹ (**Scheme 1.13A**) They took advantages of the unique properties of the surface chemistry of the QDs, where the substrates needed to first anchor on the surface of the heterogeneous QDs via the -COOH group in order to be activated, thus allowing the access to exceptional head-to-head *syn* selectivity. Furthermore, such cycloaddition was found to proceed through a triplet energy transfer mechanism confirmed by transient absorption spectroscopic studies. Hence, the reactivity can be fine-tuned by size-controlled CdSe QDs photocatalysts possessing different triplet energy levels via the quantum confinement effect. The thermodynamics and mechanism of this reaction was further studied in details by groups of Weiss and Schatz collaboratively employing density functional theory (DFT) calculations.⁴⁰ They revealed that the reaction selectivity was resulted from the favorable *syn*-binding configuration of the substrate pairs on the QD surface which preserved during the dimerization via excitation.

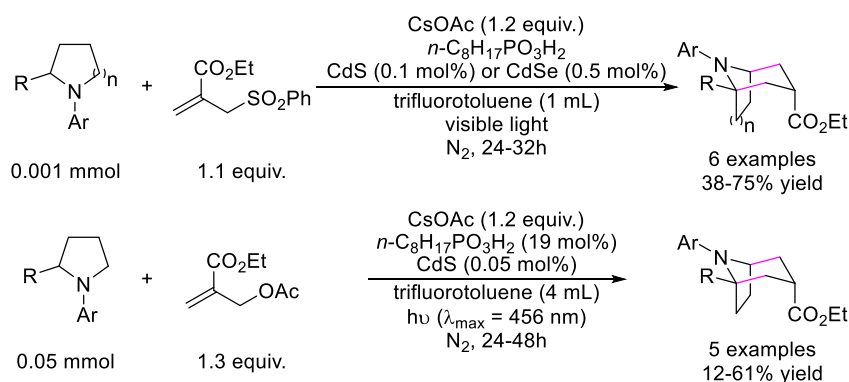


Scheme 1.13 CdSe QDs-photocatalyzed energy-transfer-mediated [2+2] cycloaddition by Weiss and co-workers.

Later in 2021, Weiss group reported a chemo- and stereoselective intermolecular [2+2] cycloaddition of conjugated dienes employing CdSe nanocrystals photocatalysis.¹⁸ (**Scheme 1.13B**) The high chemoselectivity was attributed to the negligible splitting of the singlet- and triplet-like excited state of the CdSe nanocrystals, which enables sufficient triplet energy transfer reactions while prevents undesirable redox-based side reactions. On the other hand, the high stereoselectivity was resulted from the reversible substrate-surface and product-surface tethering

which is closely related to the radius of curvature of the nanocrystal photocatalysts. In 2022, the same group further advanced their CdSe QDs-photocatalyzed intermolecular [2+2] cycloadditions to those freely diffused aromatic alkene substrates without a carboxyl anchoring group via an energy shuttle strategy.⁴¹ (**Scheme 1.13C**) Their results implied two sequential triplet-triplet energy transfer events where the first energy transfer happened from the QD to the polyaromatic energy shuttle followed by a second energy transfer from the shuttle to the transiently adsorbed substrate via van der Waals interactions.

In 2023, Dabbous *et al.* reported a cadmium chalcogenide QDs-photocatalyzed synthesis of tropane alkaloid skeletons from pyrrolidines (or piperidines) with allyl sulfones (or allyl acetates) radical traps via a radical cascade cyclization.⁴² (**Scheme 1.14**) This reaction was proposed to undergo two consecutive catalytic cycles where both cycles involved the oxidation of the amine substrate or intermediate to generate α -aminoalkyl radical. A phosphonate-based ligand was found beneficial to the second oxidation event, allowing the desired [3+3] cyclic product generated in a much higher yield.



Scheme 1.14 Cadmium chalcogenide QDs-photocatalyzed synthesis of tropane alkaloid skeletons.

Cadmium chalcogenide as a group of effective photocatalysts has been significantly benefited from the development of colloidal nanocrystals synthesis. These nanocrystals usually have large surface-to-volume ratio, hence exhibiting catalytic efficiencies similar to those of

homogenous molecular photocatalysts while remain highly recyclable. Cadmium chalcogenide nanocrystals have not only shown feasible for various photoredox-initiated radical cyclization reactions, their size-controlled QDs have also seen their unique application in a novel TT-EnT-mediated highly selective surface-templated synthesis of valuable cyclic compounds providing orthogonal methodologies to homogeneous photocatalysis.

1.4.2c Carbon Nitride (CN) for Photocatalytic Ring-Forming Reactions

Carbon nitride is a class of organic semiconductor material whose structure is composed of alternating carbon and nitrogen units with a typical ratio of 3:4. Among the carbon nitride family, two-dimensional graphitic carbon nitride (g-C₃N₄) is one of the most studied. These materials exhibit excellent thermostability and have suitable band gap which enables light absorption in visible spectrum (**Figure 1.5**). However, the photocatalytic ability of pristine g-C₃N₄ is usually low, because of small extinction coefficient in visible-light range, fast electron-hole recombination rate and small specific surface area. To enhance the photocatalytic performance, tunable parameters such as band structure, heterostructure, crystallinity, morphology can be accessed via using different functional-group precursors, copolymerization, metal doping, heteroatom doping, post treatment, etc.^{43, 44} As a result, an array of carbon nitride variants with different properties for specific applications can be produced, namely, mesoporous graphitic carbon nitride (mpg-C₃N₄), urea-derived graphitic carbon nitride (g-CN-U), etc. Their detailed synthesis and modification methods, photophysical and electrochemical properties, structure-performance relationship can be found in reviews authored by experts in this research field.⁴⁵ Here, we focus our discussion on the application of carbon nitride as photocatalysts for visible-light-driven ring-forming reactions.

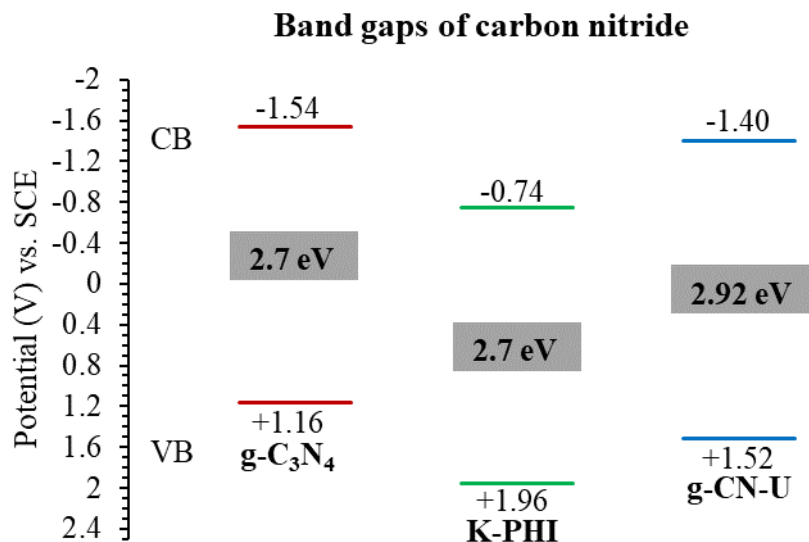
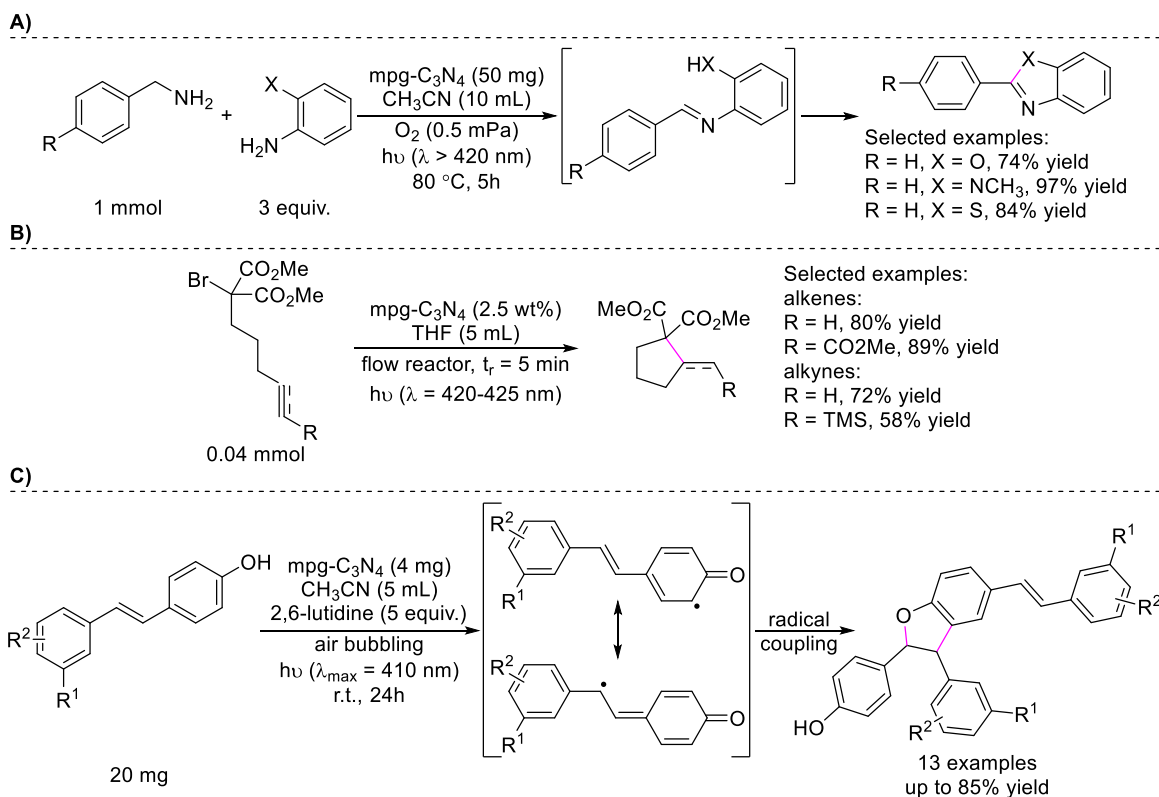


Figure 1.5 Band structures of representative carbon nitride variants (g-C₃N₄,⁴⁶ K-PHI,⁴⁷ g-CN-U⁴⁸).

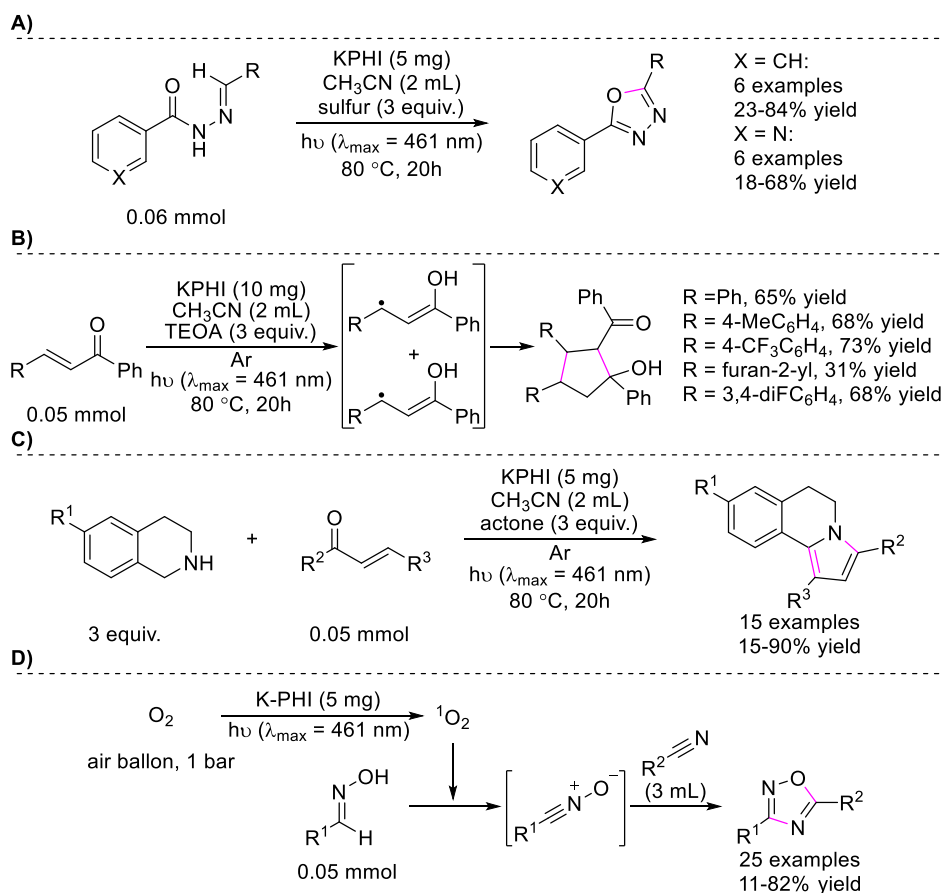
In 2010, Su *et al.* reported a protocol that employed mesoporous graphitic carbon nitride (mpg-C₃N₄) as a photocatalyst to oxidize amines into imines under aerobic condition and visible light irradiation. Then they further advanced this approach into one-pot synthesis of benzoxazoles, benzimidazoles and benzothiazoles through imine as an intermediate.⁴⁶ (**Scheme 1.15A**) Later in 2014, Blechert group developed a heterogeneous flow photochemistry method by using mpg-C₃N₄ photocatalyst for 5-*exo* radical cyclization of bromomalonates to produce substituted cyclopentanes.⁴⁹ (**Scheme 1.15B**) THF used here not only functioned as a solvent but also as an electron and hydron donor. Through fine tuning of the reaction conditions, the desired product was achieved in high yield and high selectivity. Oxidative coupling of resveratrol for biomimetic synthesis of bioactive δ -viniferin was achieved by Song *et al.* using mpg-C₃N₄ as a photocatalyst and molecular oxygen from the air as a mild oxidant.⁵⁰ (**Scheme 1.15C**) They found that the 4-hydroxy group was necessary in the stilbene starting material and the reactive oxygen species (ROS) was responsible for this transformation rather than singlet oxygen.



Scheme 1.15 mpg-C₃N₄-photocatalyzed cyclizations. **A)** Sequential oxidative coupling-cyclization for the synthesis of benzoxazoles, benzimidazoles and benzothiazoles. **B)** Intramolecular radical cyclization for the synthesis of cyclopentanes. **C)** Oxidative coupling of resveratrol derivatives for the synthesis of δ -viniferin and its analogues.

In 2018, Savateev group reported a method to employ potassium poly(heptazine imide) (KPHI), a type of well-crystallized carbon nitride, for photooxidative cyclization of *N*-acylhydrazones to synthesize 1,3,4-oxadiazoles.⁵¹ (**Scheme 1.16A**) It should be noted that sulfur, instead of oxygen, was used in this study as a highly selective electron scavenger. Such material was also reported to be active towards a photoreductive cyclodimerization of chalcones.⁴⁷ (**Scheme 1.16B**) Furthermore, the same group in 2019 reported a novel approach employing K-PHI for photocatalytic synthesis of *N*-fused pyrroles from tetrahydroisoquinoline (THIQ) and chalcones.⁵² (**Scheme 1.16C**) Such transformation was proposed to be initiated by a radical coupling of THIQ *N*-centered radical cation with chalcone radical anion, which is populated in the carbonyl group, and a series of intramolecular cyclization and aromatization steps.

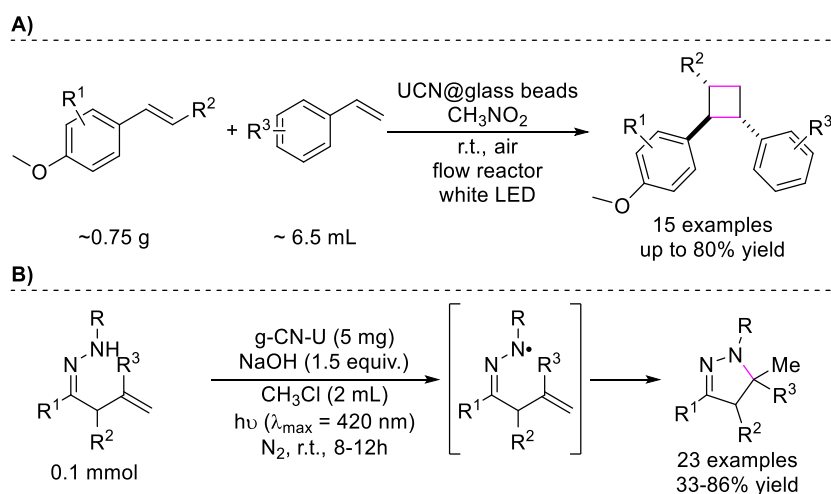
Collaboratively, Savateev group and Antonietti group refined the crystal structure of K-PHI by using powder XRD and TEM, then they used DFT method to calculate the density-of-states (DOS) and localize intra band states (IBS) of this material. The IBS was found to be responsible for the singlet-triplet intersystem crossing of the excited-state K-PHI. Photocatalysis application was demonstrated by the [3+2] cycloaddition of aldoximes with nitriles for the synthesis of 1,2,4-oxadiazoles initiated by triplet-excited K-PHI sensitized singlet oxygen.⁵³ (**Scheme 1.16D**)



Scheme 1.16 KPHI-photocatalyzed cyclizations by Savateev and co-workers.

In 2020, Wang group collaborated with Zhang group to develop a scalable and sustainable flow chemistry method for oxygen-mediated photocatalytic synthesis of cyclobutanes catalyzed by polymeric carbon nitride fabricated from urea (UCN). (**Scheme 1.17A**) This reaction was proposed to be initiated by hole transfer from photoexcited UCN to the anethole derivatives.⁵⁴

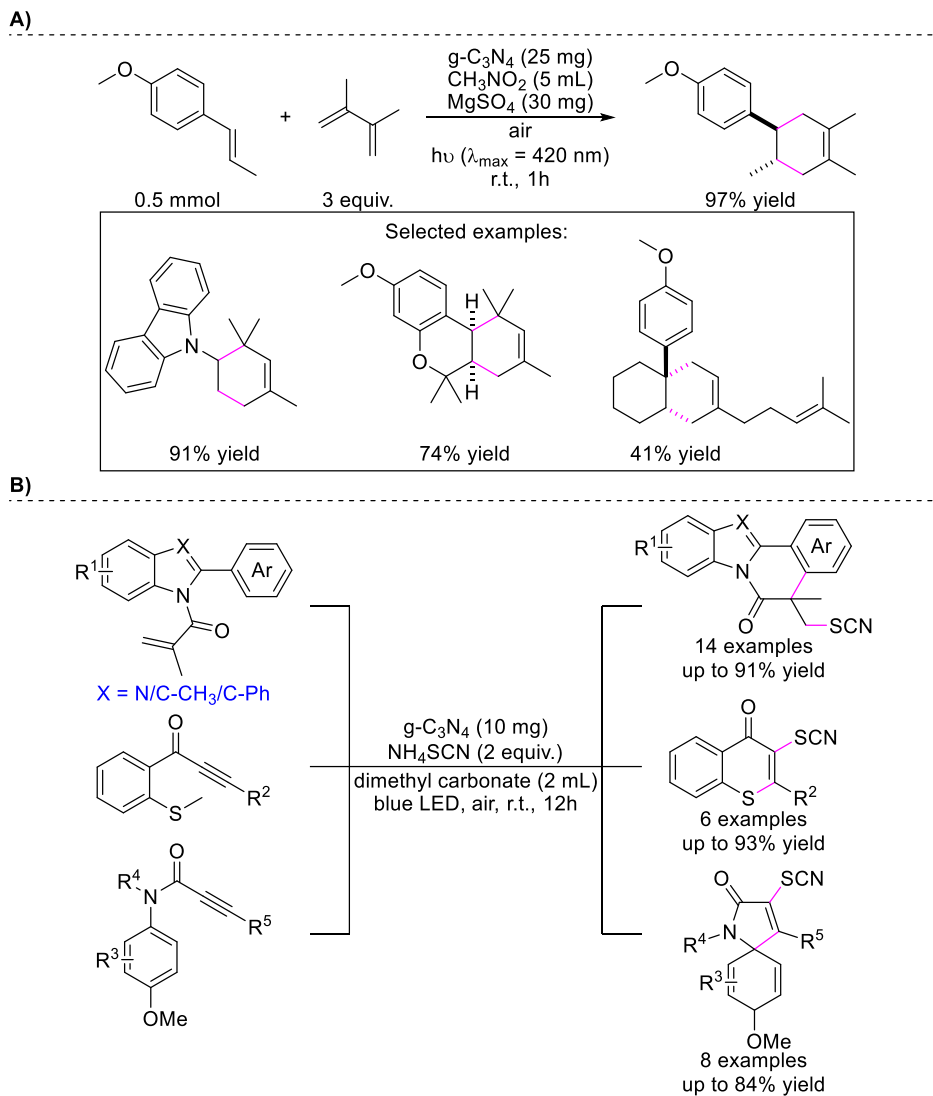
Here, the UCN photocatalyst was immobilized and coated on glass beads. Notably, this system is capable of gram-scale selectively producing magnosalin from α -asarone in a yield of 87%. Later in 2022, Wang group together with Cheng group found that the urea-derived polymeric carbon nitride (g-CN-U) offered enhanced substrate-surface complexation and electron abstraction kinetics particularly towards anionic intermediate. The synthetic utility of this system was demonstrated by the facile synthesis of dihydropyrazoles from cyclization of β,γ -unsaturated hydrazones via nitrogen-centered radical. ⁴⁸ (**Scheme 1.17B**) Additionally, cyclization of β,γ -unsaturated oximes via oxygen-centered radical were also amendable.



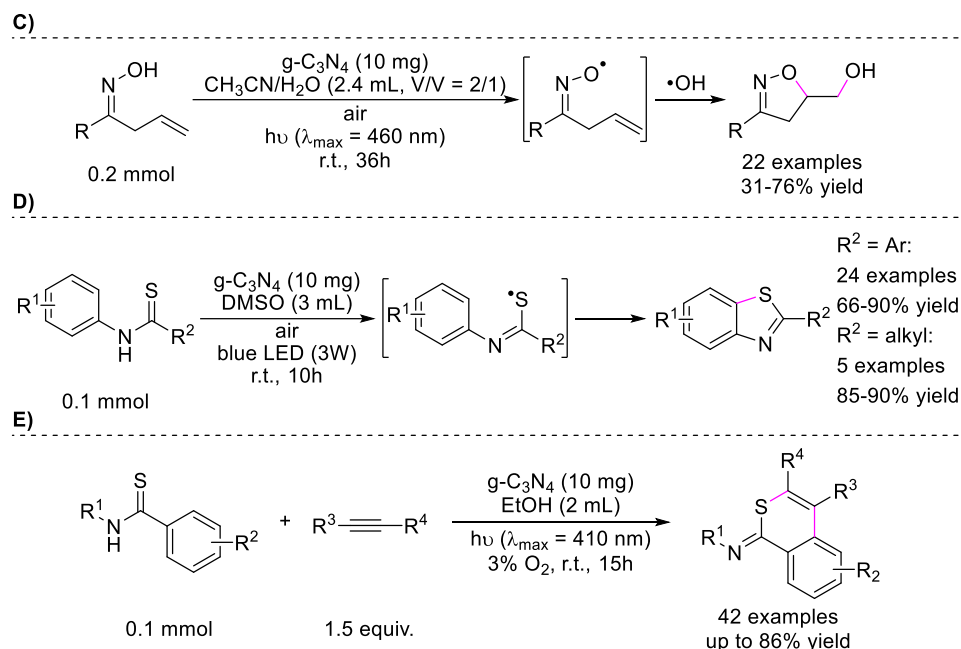
Scheme 1.17 g-CN-U-photocatalyzed cyclizations by Wang and co-workers.

Back in 2017, Zhao *et al.* reported a redox-neutral oxygen-mediated Diels-Alder reaction of electron rich dienophile photocatalyzed by graphitic carbon nitride (g-C₃N₄). ⁵⁵ (**Scheme 1.18A**) Such reaction underwent distinct mechanism from the Ru-based homogeneous photoredox system, where the cycloaddition process is a combination of direct [4+2] and [2+2] followed by photocatalytic rearrangement of a vinylcyclobutane intermediate. In 2021, collaborative work from groups of Yu and Chen employed g-C₃N₄ as a photocatalyst for generating SCN radical from ammonium thiocyanate via hole oxidation which then induced thiocyanated intramolecular radical

cyclization reactions to produce a series of thiocyanated indolo/benzimidazo[2,1-*a*]isoquinolin-6(*5H*)-one and thioflavone compounds.⁵⁶ (**Scheme 1.18B**) Later, they developed a visible-light-induced radical cyclization of β,γ -unsaturated oximes for the synthesis of isoxazolines catalyzed by g-C₃N₄, where oxygen-centered radical was generated by hole transfer, followed by intramolecular cyclization and terminated by hydroxyl radical generated by electron transfer from photoexcited g-C₃N₄ to molecular oxygen.⁵⁷ (**Scheme 1.18C**) In around the same period, groups of Zhou and Guo reported a visible light-driven oxidative cyclization of thiobenzanilides to afford benzothiazoles catalyzed by g-C₃N₄ under ambient air conditions with excellent recyclability.⁵⁸ (**Scheme 1.18D**) Recently, they reported a g-C₃N₄ photocatalyzed aerobic dyhydrogenative [4+2] annulation of benzothioamides with alkynes to afford benzo-fused six-membered S-heterocycles, *i.e.*, isothiochromenes.⁵⁹ (**Scheme 1.18E**) Mechanistic studies suggested that such reaction was initiated by hole oxidation of benzothioamide to form a sulfur-centered radical which then induced the subsequent radical cascade cyclization.



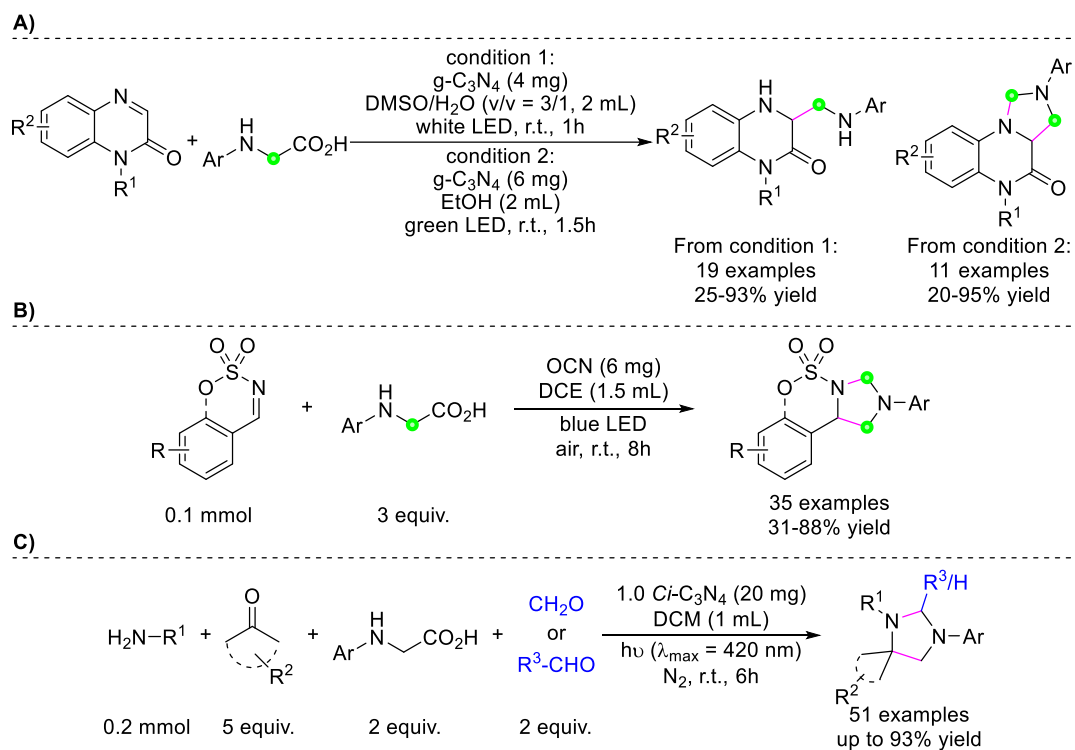
Scheme 1.18 g-C₃N₄-photocatalyzed cyclizations. **A)** Diels-Alder cycloaddition. **B)** Thiocyanated radical cyclization.



Scheme 1.18 (Continued) g-C₃N₄-photocatalyzed cyclizations. **C)** Intramolecular oxygen-centered radical cyclization of β,γ -unsaturated oximes. **D)** Intramolecular oxidative cyclization of thiobenzanilides. **E)** Dyhydrogenative [4+2] annulation of benzothioamides with alkynes.

Carbon nitride as a photocatalyst has been shown active towards single-electron oxidation of *N*-aryl glycine and the resulting α -amino methyl radical can effectively undergo imine addition. In 2020, groups of Yu and Chen together reported a g-C₃N₄ photocatalyzed divergent reaction of Quinoxalin-2(1*H*)-ones with *N*-aryl glycine to selectively afford the C-3 functionalized derivatives from radical addition and afford tetrahydroimidazo[1,5-*a*]quinoxalin-4(5*H*)-ones from radical cascade cyclization by changing the solvent.⁶⁰ (**Scheme 1.19A**) The key to a cyclic product was to use a solvent that has high solubility for oxygen, *i.e.*, EtOH, to facilitate the formation of an iminium intermediate from α -amino methyl radical as a bridge to create a ring structure. A similar annulation can be photocatalyzed by oxygen-doped graphitic carbon nitride (OCN) between *N*-sulfonyl ketimines and *N*-aryl glycines to synthesize imidazolidine-fused sulfamidates.⁶¹ (**Scheme 1.19B**) Interestingly, a redox-neutral one-pot four-component version of this type of

transformation was shown amendable by Tian *et al.* using a C₃N₄ photocatalyst modified by C2 insertion (1.0 Ci-C₃N₄) for the synthesis of spiro-imidazolidines.⁶² (Scheme 1.19C)



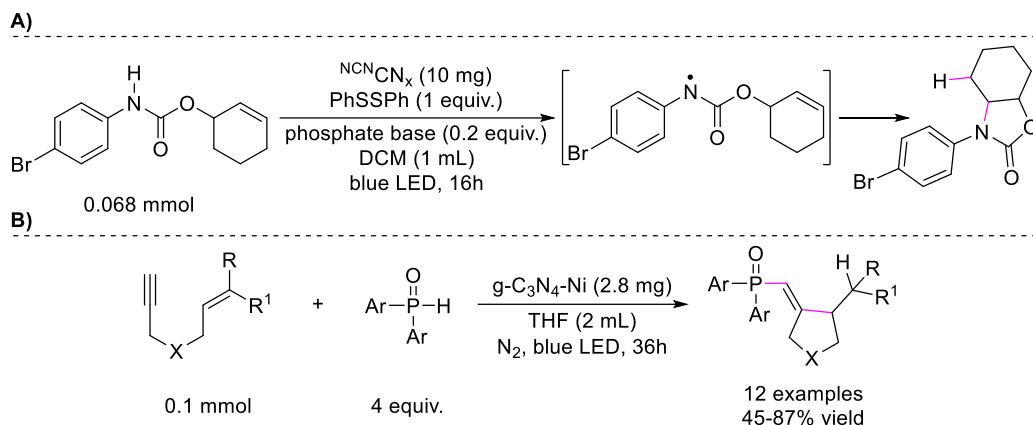
Scheme 1.19 Oxidative activation of *N*-aryl glycine for radical cascade cyclizations with imine derivatives photocatalyzed by carbon nitride.

Heterogeneous carbon nitride photocatalyst often suffers from asynchrony of photoredox rate and fast charge recombination thus significantly decreasing the photocatalytic efficiency. To circumvent these issues, Nocera group developed a sized-controlled, cyanamide modified carbon nitride (^NCN_x) material obtained by ball milling that took advantage of its well-defined long-lived triplet excited state.⁶³ The high photocatalytic efficiency of such material was demonstrated by a redox-neutral hydroamidation cyclization reaction (Scheme 1.20A), which required diffusive quenching and synchrony of redox events.

In 2022, Hou *et al.* reported a visible light-induced redox-neutral, radical cascade cyclization of nitrogen or carbon atom-tethered terminal alkyne containing 1,6-enynes to afford

hydrophosphorylated five-membered cycles catalyzed by nickel doped g-C₃N₄ (g-C₃N₄-Ni).⁶⁴

(Scheme 1.20B) This reaction was proposed to be initiated by a diphenylphosphine oxide radical generated from the hole oxidation by the excited-state g-C₃N₄-Ni photocatalyst.



Scheme 1.20 A) Proton coupled electron transfer (PCET) induced hydroamidation cyclization photocatalyzed by ^{NCN}CN_x. **B)** Radical cascade hydrophosphorylated cyclization photocatalyzed by g-C₃N₄-Ni.

1.4.2d Conjugated Microporous Polymers and Covalent Organic Frameworks for Photocatalytic Ring-Forming Reactions

In addition to carbon nitride, the other types of organic semiconductor photocatalysts for ring-forming reactions are also available. Conjugated microporous polymers (CMPs) and covalent organic frameworks (COFs) are among the most studied materials in this category. CMPs are a type of well-defined, amorphous, three-dimensional, highly porous polymers that have conjugated skeletons. In contrast to CMPs, COFs are a class of highly ordered, porous materials with two- or three-dimensional structures formed from covalently linked precursors. One of the drawbacks of both CMPs and COFs is their cumbersome synthetic procedures. Furthermore, the preparation of CMPs often involves transition-metal-catalyzed cross couplings while the preparation of COFs often involves harsh conditions such as high temperature and strong acid.^{65, 66} Given the widely available organic precursors, CMPs and COFs are accessible to various chemical structures with different properties for different purposes. Generally, these materials usually contain extended π -

conjugation or donor-acceptor moieties to ensure good photophysical properties for applications in photocatalysis, such as broad absorption range and slow electron-hole recombination rate.^{65, 66} To match the specific activation energies of individual photochemical reactions, their electrochemical profiles can be tailored via rational design of precursors and co-building block control.

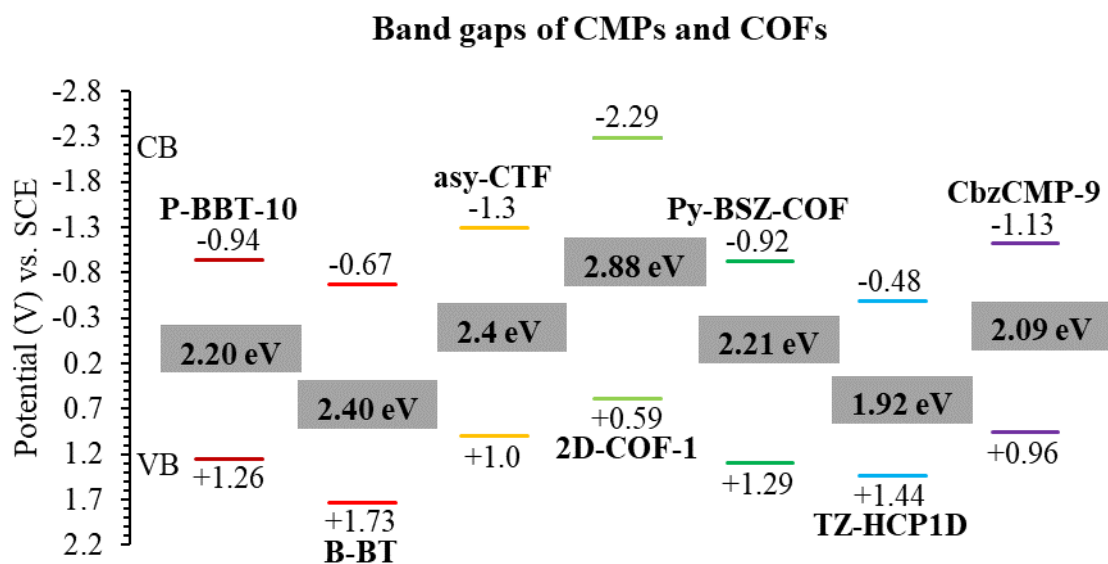
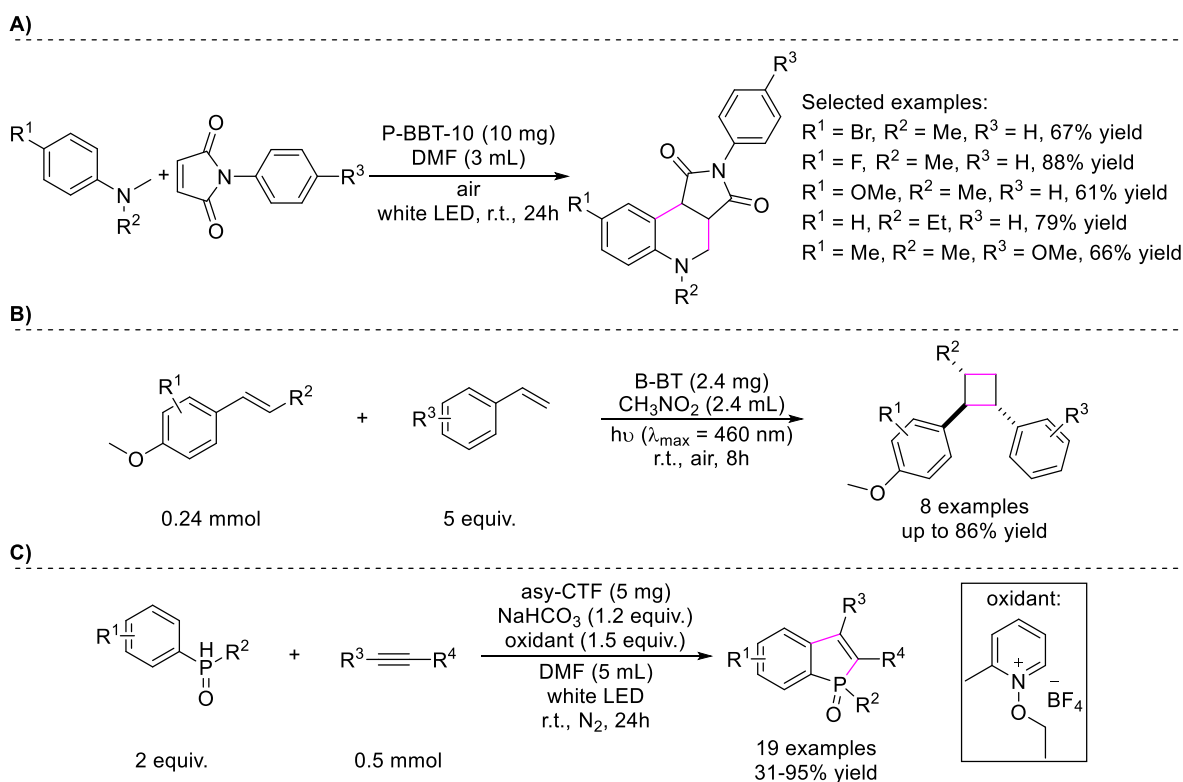


Figure 1.6 Band structures of selected CMPs and COFs (*vide infra*).

Zhang group is among the pioneers in the area of employing CMPs and COFs for photocatalytic cyclization reactions. In 2016, Zhang and co-workers reported that the band gap of a 1,3,5-cross-linked benzene-based conjugated nanoporous polymer (pore diameter of *ca.* 1.5 nm) can be engineered by copolymerization with electron-withdrawing comonomer, *i.e.*, benzobisthiadiazole (BBT).⁶⁷ By increasing the percentage of BBT versus benzene (B), a band gap narrowing of such polymer was observed thus the absorption of the photocatalyst was significantly extended to the visible light region. Through strategically aligning the conduction band (CB) and valence band (VB) positions of the polymer to bracket the redox potential of a targeted photoredox reaction, the P-BBT-10, where B/BBT = 90/10, was found to be an optimal

photocatalyst for the aerobic photooxidative cyclization of *N,N*-dimethylanilines with maleimides (**Scheme 1.21A**). In 2021, Almansaf *et al.* developed a new covalent organic framework based on imine bonds assembled from 2-(4-formylphenyl)-5-formylpyridine and 1,3,6,8-tetrakis(4-aminophenyl)pyrene and decorated with platinum (II), named COF-UARK-49-Pt, that can realize the same organic transformation.⁶⁸ Later in 2022, Jin *et al.* designed the first case of porphyrin-based 3D COFs with non-interpenetrated **scu** topology, such COF materials were demonstrated as excellent photocatalysts towards this oxidative [4+2] annulation thanks to the enriched porphyrin catalytic sites.⁶⁹

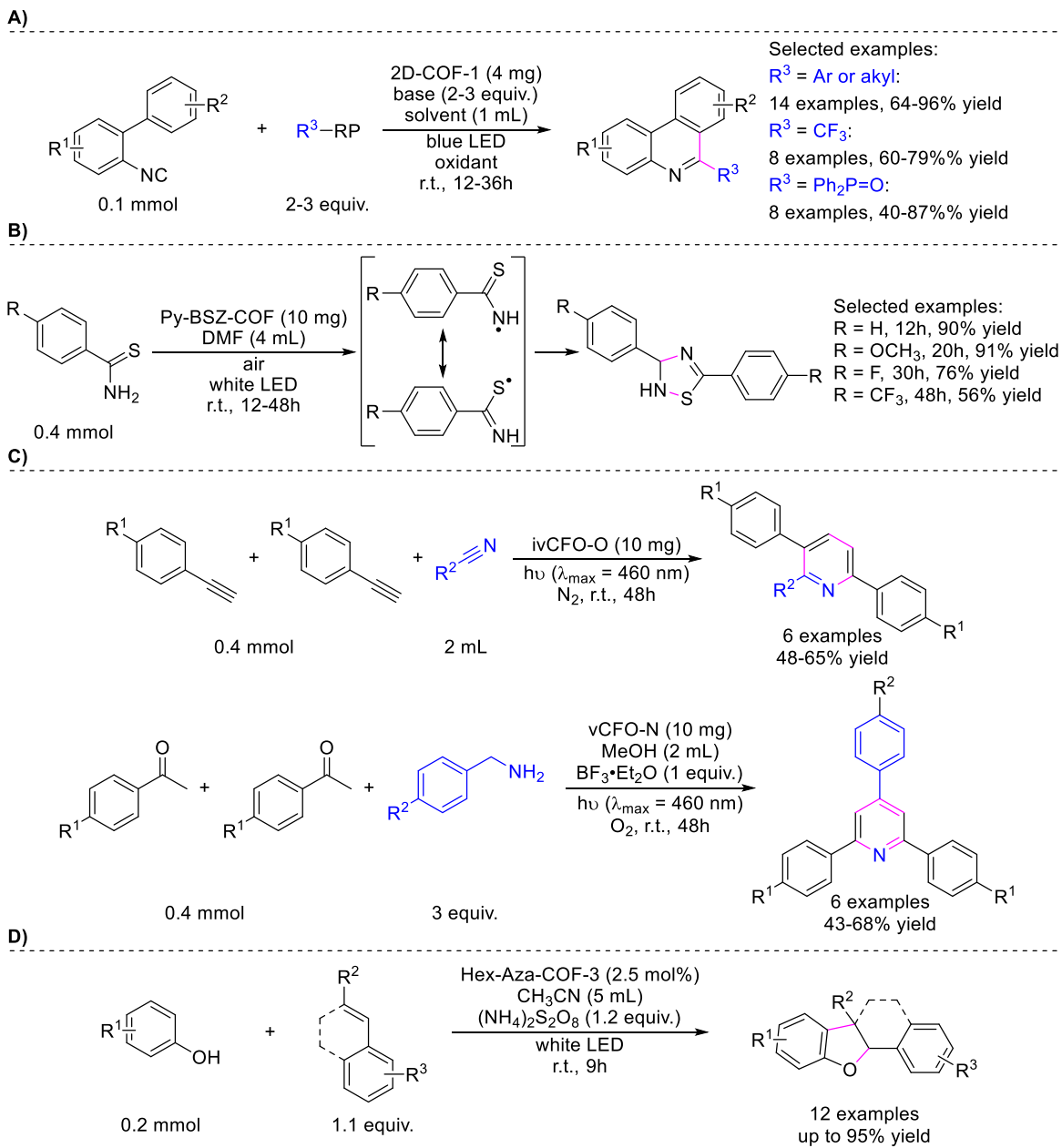


Scheme 1.21 CMP- and COF-photocatalyzed cyclizations by Zhang and co-workers.

In 2017, Zhang group reported the first example of photocatalytic [2+2] cycloaddition of anetholes with styrene derivatives using pure organic semiconductor (**Scheme 1.21B**).⁷⁰ A microporous cross-linked poly(benzothiadiazole) network (B-BT) was selected as their

photocatalyst, whose catalytic efficiency was proven comparable with that of the Ru- and Ir-based homogeneous photocatalysts. Later in 2018, they designed an asymmetric single-component covalent triazine framework (asy-CTF) fabricated by the trimerization of 5-(4-cyanophenyl)thiophene-2-carbonitrile, in which four different molecular donor-acceptor domains reside.⁷¹ The asy-CTF showed superior photocatalytic efficiency to that of its symmetric counterparts, owing to its enhanced charge-carrier separation via an intramolecular energy transfer cascade. Such enhancement was exemplified by the photocatalytic intermolecular cyclization of diphenylphosphine oxide with diphenylacetylene for the synthesis of benzophosphole oxide (**Scheme 1.21C**). In 2020, the same group developed a size-controllable CTF nanoparticles that is showing exceptionally high photocatalytic efficiency towards a [3+2] cycloaddition of *trans*-anethol and mequinol.⁷²

In 2019, collaborative work from groups of Yang, Xu and Yu reported a visible light-driven redox-neutral tandem radical addition-cyclization of 2-aryl phenyl isocyanide catalyzed by an imine-based two-dimensional covalent organic framework (2D-COF-1) that was fabricated by the condensation of 2,5-dimethoxyterephthalohydrazide with 1,3,5-triformylbenzene.⁷³ An array of diverse 6-substituted-phenanthridines were synthesized by this protocol using different radical precursors (**Scheme 1.22A**). Notably, such system was operable in a continuous flow reactor. In 2020, Li *et al.* designed a fully conjugated ethylene-linked donor-acceptor incorporating covalent organic framework that was constructed with a benzothiadiazole unit (Py-BSZ-COF). Such Py-BSZ-COF was found to be active towards photocatalytic generation of superoxide radical anion, which was further utilized to mediate a cyclization of thioamide to 1,2,4-thiadiazole (**Scheme 1.22B**).⁷⁴



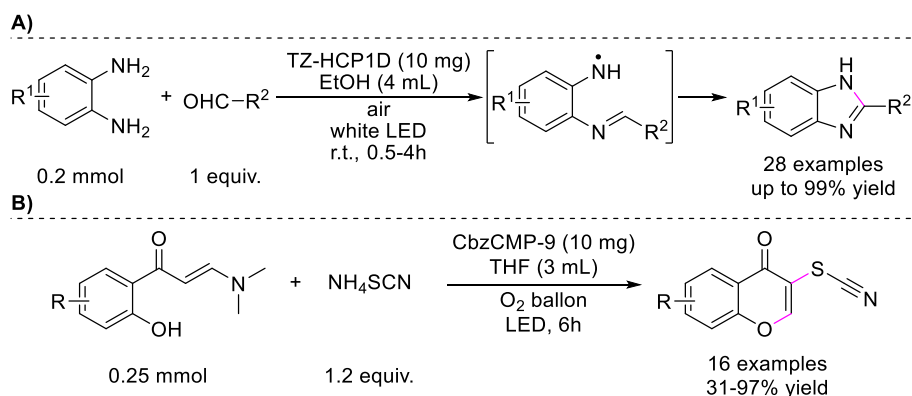
Scheme 1.22 COF-photocatalyzed cyclizations. **A)** Tandem radical addition-cyclization of 2-aryl phenyl isocyanides. **B)** Oxidative coupling of thioamide for the synthesis 1,2,4-thiadiazole. **C)** Multi-component synthesis of pyridines from alkynes with nitriles or from aryl ketones with benzyl amines. **D)** Oxidative [3+2] cycloaddition of phenol with olefins.

Two conceptually isoelectronic covalent organic frameworks were designed by Bi *et al.* in 2021, of which one features positively charged pyrylium core with vinylene linkages (ivCOF-O) while the other derived from the former under ammonia treatment features a neutral pyridine core

(vCOF-N).⁷⁵ This set of COFs has shown similar geometries but different states of charge, band gaps and energy levels. The ivCOF-O, with energy levels ranged from -5.7 eV (CB) to -7.3 eV (VB) (vs. vacuum), was found optimal for a photocatalytic multi-component synthesis of pyridines from alkynes with nitriles, while the vCOF-N, with energy levels ranged from -4.1 eV (CB) to -5.9 eV (VB) (vs. vacuum), was found optimal for a photocatalytic multi-component synthesis of pyridines from aryl ketones with benzyl amines (**Scheme 1.22C**). The former was proposed to be initiated by hole oxidation of alkynes and the latter to be initiated by hole oxidation of benzyl amines. This work demonstrates a well-controlled approach to design heteroatom-embedded COFs with tunable electronic properties. Lately, Parvatkar *et al.*, employed their previous developed Hex-Aza-COF-3, featuring phenazine and hexaazatriphenylene units that strengthen the covalent linkages, for photocatalytic synthesis of 2,3-dihydrobenzofurans via oxidative [3+2] cycloaddition of phenol with olefins (**Scheme 1.22D**).⁷⁶ The Hex-Aza-COF-3 showed high photocatalytic performance owing to an efficient photogenerated charge transfer process.

In 2021, An *et al.* reported two hyper-crosslinked polymer photocatalysts featuring s-tetrazine units (TZ-HCP) where the crosslinkers could be easily installed through Friedel-Crafts alkylation.⁷⁷ The TZ-HCP1D showed the highest photocatalytic ability among all samples towards an oxidative intermolecular cyclization of 1,2-diaminobenzenes with aldehydes for the synthesis of benzimidazoles (**Scheme 1.23A**). Remarkably, this photocatalyst can be recycled for 21 runs without noticeable loss of catalytic efficiency. Later, Wang *et al.* reported that tetrathienoanthracene-based conjugated microporous polymers (TTA-CMP) can also efficiently photocatalyze this type of cyclization.⁷⁸ Additionally, Luo *et al.* designed a benzotrithiophene and triphenylamine based covalent organic framework (BTT-TPA-COF) that can be applied as a photocatalyst for the same organic transformation.⁷⁹ In 2022, Deng *et al.* designed a series of

conjugated microporous polymers (CMPs) with tunable built-in electric field (BEF) by incorporating carbazole into various acceptor cores.⁸⁰ The CbzCMP-9 was identified as the one with the highest molecular dipole thus the strongest BEF, which provides it with fast charge-carrier separation and therefore good photocatalytic performances. Photocatalytic thiocyanation cyclization for the synthesis of thiocyano chromones was chosen as an example to demonstrate its synthetic utility (**Scheme 1.23B**).



Scheme 1.23 CMP-photocatalyzed cyclizations. **A)** Oxidative intermolecular cyclization of 1,2-diaminobenzenes with aldehydes. **B)** Thiocyanation cyclization for the synthesis of thiocyano chromones.

1.4.3 Conclusion

Significant advancement has been made to the field of heterogeneous photocatalytic ring-forming reactions as summarized above. Each type of commonly used heterogeneous photocatalysts showcased their specific advantages for photocatalytic ring-forming reactions. But the limitation of this category of photocatalysis also remains. Generally, they are still facing several challenges which may vary on a case-by-case basis: 1) Low visible-light absorptivity, e.g., TiO₂ and C₃N₄; 2) Limited active surface-to-volume ratio; 3) Poor chemical stability, e.g., C=C, C=N, and other unsaturated linkages in some COFs and CMPs are susceptible to radical addition and C=N linkage is vulnerable to hydrolysis conditions; 4) Low defect tolerance, e.g., cadmium chalcogenide; 5) Laborious or costly preparation, e.g., COFs and CMPs; 6) Fast electron-hole

recombination rate, e.g., TiO₂ and C₃N₄; 7) Poor dispersion in organic solvents. 8) Asynchronous photoredox rate which results in low catalytic efficiency and requires additional sacrificial donor; 9) Arduous or non-precise band gap tailoring. Our group is striving for a generic semiconductor photocatalytic system that may have the potential to address the above concerns in heterogeneous photocatalysis. We focus on developing lead-halide perovskite nanocrystals, that have been well-recognized to be a promising photovoltaic material in recent years, as photocatalysts for visible-light-driven organic transformations.

1.5 Lead-Halide Perovskite Nanocrystals as a Potential Candidate for Ring-Forming Reactions

1.5.1 Metal-Halide Perovskite as an Emerging Photovoltaic Material

Ever since Kojima *et al.* reported the seminal work on using lead-halide perovskite as a visible-light sensitizer in solar cells in 2009,⁸¹ there has been a dramatic growth of research interest in this area. The emerging single-junction perovskite-based solar cells have achieved significant advancement over the last decade. As demonstrated by the Best Research-Cell Efficiency Chart summarized by NREL,⁸² the state-of-the-art certified power conversion efficiency (PCE) of a single-junction perovskite cell has reached 26.1%, comparable to that of the traditional single-crystalline silicon-based solar cells. These perovskite materials have not only showcased its impressive potential in the solar cell research, but have been developed as promising candidates for applications in light-emitting-diodes (LEDs),⁸³ lasers,⁸⁴ photodetectors,⁸⁵ transistors,⁸⁶ piezoelectronics⁸⁷ and sensors⁸⁸.

1.5.2 APbX₃ Lead-Halide Perovskite Nanocrystals

Three-dimensional (3D) metal-halide perovskite (MHP) is a class of crystalline, ionic material with a general structural formula of ABX₃. The A-site monovalent cation can either be organic such as methylammonium (MA), formamidinium (FA), or inorganic such as cesium (Cs),

rubidium (Rb). The B-site divalent cation can be lead (Pb), tin (Sn), germanium (Ge), while the X-site anion is halide (Cl, Br, I). (**Figure 1.7**) An ideal crystal structure of an MHP is cubic, however, can be deviated by numerous factors including the Goldschmidt tolerance factor.⁸⁹ APbX₃ lead-halide perovskite (LHP) stands in the forefront of the MHP family, owing to their excellent optoelectronic properties such as intensive visible light absorption⁹⁰, long charge carrier lifetime⁹¹, long charge carrier diffusion length⁹² and high charge carrier mobility⁹¹. The development of colloidal nanocrystals (NCs) synthesis methods^{93, 94} has endowed the LHPs with greater advantages, since NCs have larger surface-to-volume ratio, and much less inherent defects compared to their bulk counterparts as demonstrated by their near-unity photoluminescence quantum yield (PLQY).

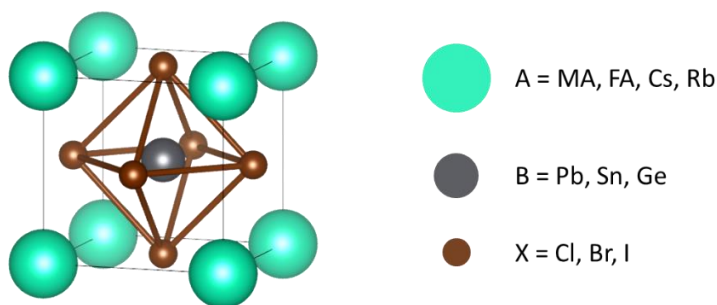


Figure 1.7 Structure of ABX₃ MHP.

1.5.3 LHP NCs as Potential Heterogeneous Photocatalysts

The rapid development of MHPs has sparked researcher's interest in employing them as heterogeneous photocatalysts, however, mainly in environmental applications. For instance, water splitting for H₂ evolution, CO₂ reduction, pollutant degradation, which are summarized comprehensively in the literature.^{95, 96} Our lab is among the pioneers for employing LHP NCs as heterogeneous photocatalysts for complex organic transformations that usually involve multi-step mechanisms and specifically tuned reaction conditions. As discussed above, LHPs have been proven to be promising materials for photovoltaic applications due to their intensive visible light

absorption, long charge carrier lifetime, long charge carrier diffusion length and high charge carrier mobility. Additionally, the band gaps of LHPs are tunable by synthesizing the quantum-confined LHP QDs of different sizes like the traditional quantum dots material, *i.e.*, CdSe QDs.⁹⁷ More importantly, the band-structure tailoring of LHPs can be precisely accessed by a unique and facile halide-tuning approach, changing the halide composition of the X-site in the ABX₃ perovskite structure. Our group hypothesized that these excellent optoelectronic properties of LHPs also make them excellent photocatalysts for visible-light-driven organic transformations, because an efficient photocatalyst essentially relies on the same set of parameters. In fact, via halide-based band gap tuning, the photoredox potentials of CsPbX₃ perovskites can cover mostly those of the commonly used Ir- and Ru- based homogeneous photocatalysts, (**Figure 1.8**)^{3, 98} rendering broad types of organic substrate activations thermodynamically feasible. Furthermore, the LHP NCs are readily available, they can be easily synthesized in large scale under ambient conditions from low-cost, bench-stable starting materials,⁹⁹ making them more attractive for potential industrial applications.

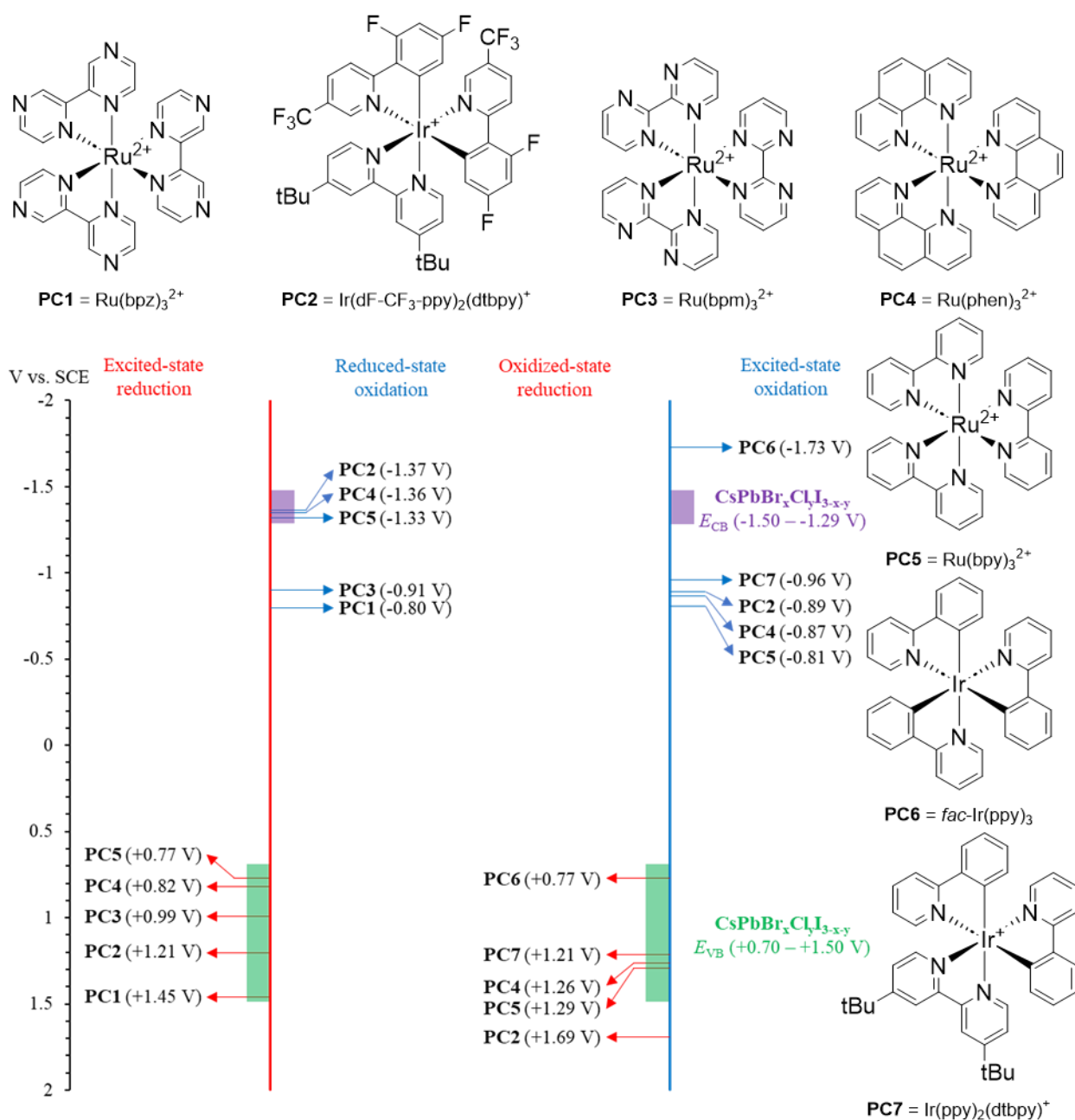
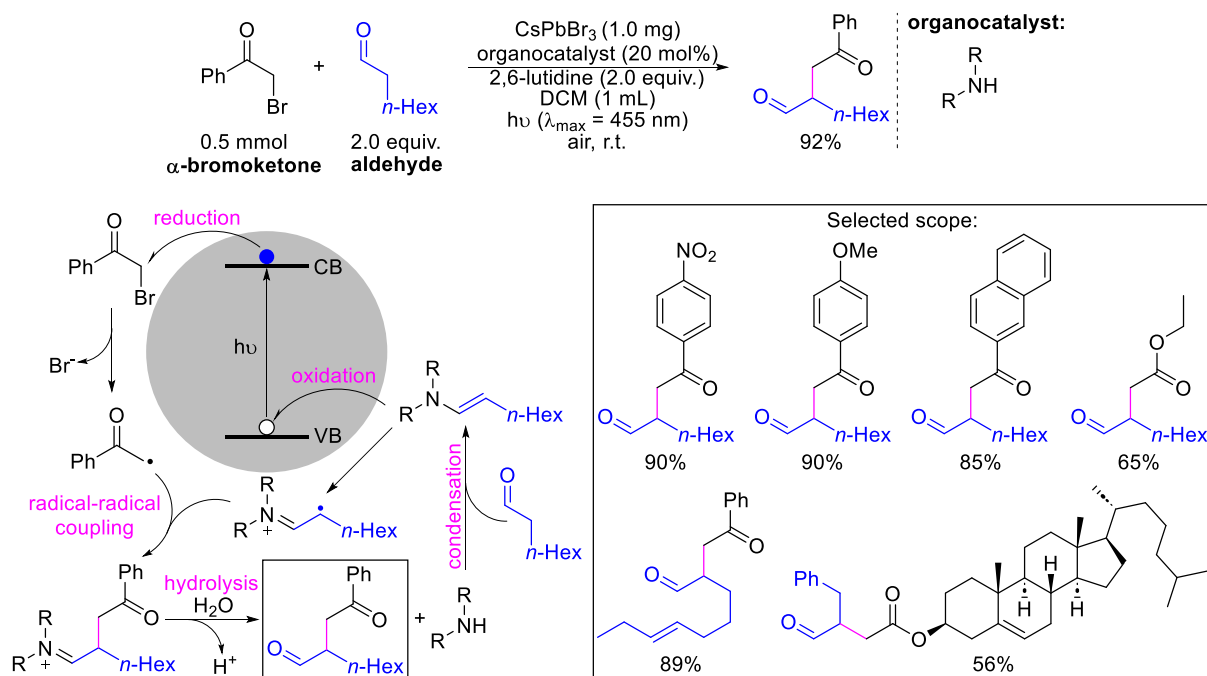


Figure 1.8 Photoredox potentials of CsPbX₃ (X = Cl, Br, I) perovskites (range highlighted in purple and green boxes) compared to other commonly used Ir- and Ru-based homogeneous photocatalysts.

1.5.4 Our Previous Work on Employing LHP NCs for Photocatalytic Organic Transformation

Our idea was to directly convert solar energy into chemical bond energy using already-proven-effective photovoltaic material LHP NCs as a photocatalyst. C-C bond formation is the

one of the most fundamental organic transformations, our initial assessment focused on photocatalytically forging a C-C bond between an aldehyde and an α -bromoketone, namely, α -alkylation of aldehyde. In 2019, our lab reported a merger of LHP NCs photoredox catalysis with enamine organocatalysis to realize this transformation and to validate the ability of LHP NCs as a photocatalyst.⁹⁹ In this study, we first performed gram-scale synthesis of the CsPbBr₃ NCs photocatalysts (*ca.* 2-100 nm) adopting a simple emulsion method.⁹⁴ Then we systematically examined their stability in organic solvents by measuring their photoluminescence (PL) lifetime and monitoring their PL intensity. The NCs show appreciable colloidal stability across a range of non- to mid-polar organic solvents including hexanes, dichloromethane (DCM), tetrahydrofuran (THF) and 1,4-dioxane which allows a potential photocatalytic reaction to be optimized in a wide selection of solvents. Notably, under optimized CsPbBr₃ NCs photocatalysis conditions, α -alkylation of aldehyde performed smoothly with a broad functional group tolerance and an exceptionally high turnover number (TON) over 52,000 based on Pb. (**Scheme 1.24**) Mechanistic studies including PL quenching study, and radical trapping experiments lead to a plausible biradical coupling mechanism. This reaction is proposed to be initiated by an electron transfer from CB of excited-state NCs (NCs*) to α -bromoketone generating an α -ketone radical and a hole transfer from VB of NCs* to enamine (in-situ formed from condensation of a secondary amine organocatalyst and an aldehyde) generating an enamine radical cation simultaneously. Radical-radical coupling between the α -ketone radical and the enamine radical cation followed by hydrolysis releases the final α -alkylated product and regenerates the organocatalyst.



Scheme 1.24 CsPbBr₃ NCs-photocatalyzed α -alkylation of aldehyde.

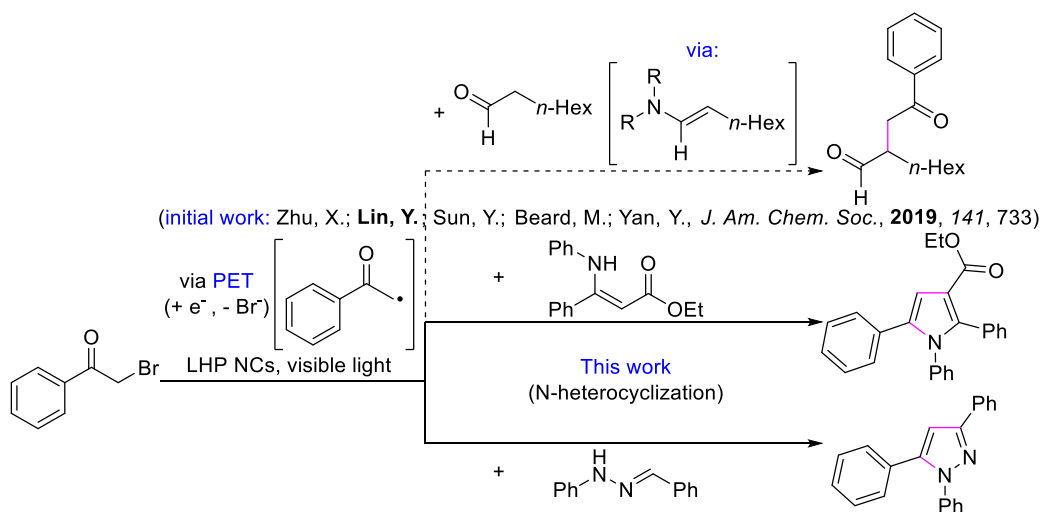
We further collaborated with Beard group to study this system by ultra-fast transient absorption spectroscopy and to demonstrate the kinetic feasibility of this proposed mechanism.¹⁰⁰ We observed an ultra-fast electron transfer from NCs* to α -bromoketone (~ 50 ps) and hole transfer from NCs* to enamine intermediate (~ 70 ps), resulting in charge separation states with microsecond-scale lifetime ($\sim 0.8 \mu\text{s}$ and $\sim 0.5 \mu\text{s}$ respectively) which allows the C-C bond formation undergo the proposed biradical pathway preferentially. (Scheme 1.24, bottom left) These LHP NCs not only provides tunable thermodynamic window for a wide range of substrate activations, but also provides new mechanism insights kinetically. The above results together validate our initial hypothesis: LHP NCs that has been proven to be an exceptional photovoltaic material can also be employed as an efficient and novel photocatalyst for organic transformations.

To date, the merits of LHP NCs to be employed as a photocatalyst such as: 1) Simple synthesis from readily available, low-cost starting materials; 2) Strong extinction coefficient in visible light region; 3) high PLQY results from high defect tolerance and low non-radiative loss;

3) Easy and rationalized band gap tunability for an ideal thermodynamic activation window; 4) Long-lived charge separation state and high charge carrier mobility; 5) Facile catalyst regeneration due to its heterogeneous nature, are recognized by researchers from whom the contributions to this field are thriving^{101, 102}. However, despite the growing interest in this research area, few efforts have been devoted to LHP NCs-photocatalyzed ring-forming reactions. We envision that LHP NCs can be employed for the synthesis of ring compounds, especially for those that of pharmaceutical relevance, via novel reaction mechanisms, thus provide complementary reactivity to currently existed methods.

1.6 Objectives of the Thesis

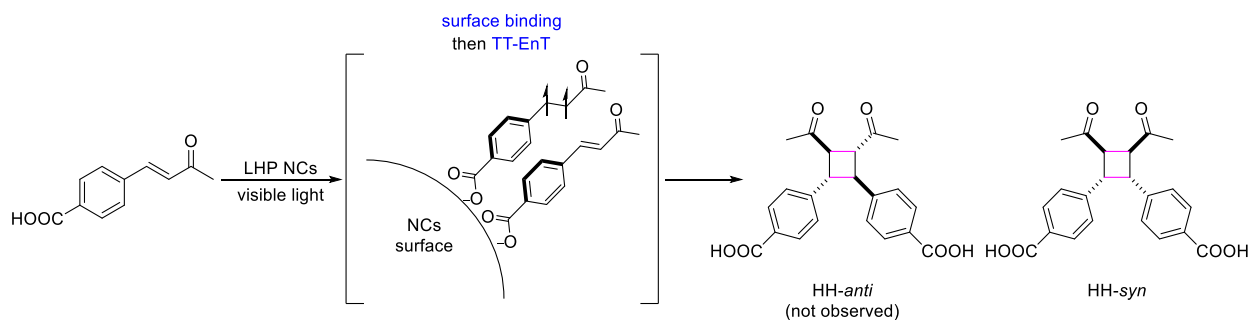
With demonstrated ability of LHP NCs to be used as a semiconductor-based heterogeneous photocatalyst for organic transformation according to our initial report,^{99, 100, 103} my doctoral research aims to expand the scope of LHP photocatalysis to photocatalytic ring-forming reactions, especially for the synthesis of biorelevant ring compounds.



Scheme 1.25 Specific aim 1. LHP NCs-photocatalyzed N-heterocyclization for the syntheses of pyrrole and pyrazole derivatives.

To achieve this objective, we set out to further examine our established protocol based on NCs-photocatalyzed α -alkylation of aldehyde.⁹⁹ We hypothesized that a stable enamine or

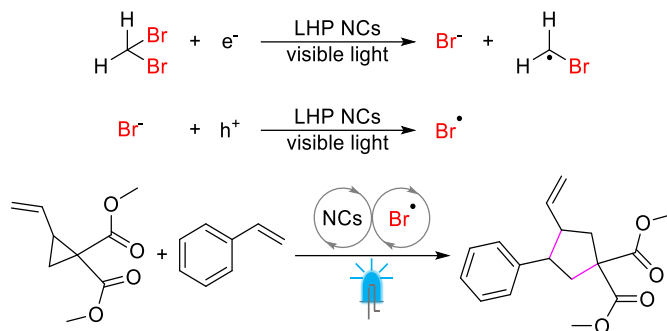
enamine derivative, in lieu of a transient-formed enamine intermediate, would engage in a radical cascade cyclization reaction with α -ketone radical inspired by the classical Hantzsch pyrrole synthesis. Two types of cyclic products could be expected from this photocatalytic pathway: pyrrole from stable enamine and pyrazole from stable hydrazone. (**Scheme 1.25**) Moreover, pyrrole and pyrazole are two pharmaceutically important scaffolds. Example such as Lipitor, one of the top-selling pharmaceutical products in the US, also contains pyrrole as its core structure. An efficient synthetic methodology for the syntheses of pyrrole and pyrazole derivatives under mild conditions is thus highly desired. I focused on exploring the substrate scope and investigating the reaction mechanism in this project.



Scheme 1.26 Specific aim 2. LHP NCs-photocatalyzed surface-templated TT-EnT-mediated highly selective [2+2] cycloaddition. TT-EnT: triplet-triplet energy transfer. HH: head-to-head.

We also questioned if LHP NCs could be employed to a triplet energy transfer-mediated [2+2] cycloaddition reaction, since it is a most common photocatalytic approach for cyclobutane synthesis. However, triplet energy is generally considered confined within the NCs. In fact, triplet energy transfer from LHP NCs has only been observed spectroscopically and never been employed for photocatalytic organic reactions. We first screened a set of styrene-based triplet energy acceptors (TEAs) with different functional groups, and found that carboxyl-containing TEAs are the most prominent. A diastereo- and regioselective [2+2] cycloaddition reaction was achieved when these carboxyl-containing TEAs were subjected to LHP NCs photocatalysis conditions.

(**Scheme 1.26**) Comprehensive mechanism investigations including NMR, IR spectroscopic studies, DFT calculations and transient absorption spectroscopic studies collaborated with Beard group at NREL were carried out to elaborate the proposed surface-templated TT-EnT mechanism.



Scheme 1.27 Specific aim 3. LHP NCs-photocatalyzed bromine radical-mediated ring-opening [3+2] cycloaddition.

One of the unique properties of LHP NCs is their facile band gap tuning via halide exchange. We found that bromine radical was generated as a key intermediate through a sequential electron transfer and hole transfer mechanism during the visible-light-induced bromide exchange between CsPbBr₃ NCs and Br-based solvent. We argued that such visible-light-induced Br radical intermediate may be of significance in the ring-forming organic synthesis. Here we aimed to harness such halogen radical intermediate for a Br radical-mediated ring-opening [3+2] cycloaddition reaction between vinylcyclopropanes and alkenes for the synthesis of vinylcyclopentanes. (**Scheme 1.27**) This strategy not only demonstrated broad substrate scope tolerance for syntheses of C(sp³)-enrich ring compounds, but also showcased promising results for engaging in other Br radical-related reactions, such as bromination and hydrogen atom transfer reactions. Moreover, the LHP NCs photocatalyst was maintaining high catalytic performance and highly recyclable during several consecutive reaction cycles.

Harnessing the merits of LHP NCs photocatalysts (intensive visible light absorption, long charge carrier lifetime, long charge carrier diffusion length and high charge carrier mobility, etc.),

the above specific aims were successfully achieved. The exploration and development of LHP NCs photocatalytic approaches for specific aim 1, 2 and 3 are described in **Chapter 2, 3 and 4** respectively in details. (*Vide infra*)

1.7 Reference

1. Taylor, R. D.; MacCoss, M.; Lawson, A. D. G., Rings in Drugs. *J. Med. Chem.* **2014**, *57* (14), 5845-5859.
2. Williams, R. E.; Njardarson, J. T. Top 200 Small Molecule Drugs by Retail Sales in 2022. <https://njardarson.lab.arizona.edu/sites/njardarson.lab.arizona.edu/files/NjardarsonGroup2022SmallMoleculeTopPosterV3.pdf> (accessed 08/07/2023).
3. Prier, C. K.; Rankic, D. A.; MacMillan, D. W. C., Visible Light Photoredox Catalysis with Transition Metal Complexes: Applications in Organic Synthesis. *Chem. Rev.* **2013**, *113* (7), 5322-5363.
4. Shaw, M. H.; Twilton, J.; MacMillan, D. W. C., Photoredox Catalysis in Organic Chemistry. *J. Org. Chem.* **2016**, *81* (16), 6898-6926.
5. Schultz, D. M.; Yoon, T. P., Solar Synthesis: Prospects in Visible Light Photocatalysis. *Science* **2014**, *343* (6174), 1239176.
6. Nicewicz, D. A.; Nguyen, T. M., Recent Applications of Organic Dyes as Photoredox Catalysts in Organic Synthesis. *ACS Catal.* **2014**, *4* (1), 355-360.
7. Strieth-Kalthoff, F.; James, M. J.; Teders, M.; Pitzer, L.; Glorius, F., Energy Transfer Catalysis Mediated by Visible Light: Principles, Applications, Directions. *Chem. Soc. Rev.* **2018**, *47* (19), 7190-7202.
8. Strieth-Kalthoff, F.; Glorius, F., Triplet Energy Transfer Photocatalysis: Unlocking the Next Level. *Chem* **2020**, *6* (8), 1888-1903.
9. Lin, S.; Ischay, M. A.; Fry, C. G.; Yoon, T. P., Radical Cation Diels–Alder Cycloadditions by Visible Light Photocatalysis. *J. Am. Chem. Soc.* **2011**, *133* (48), 19350-19353.
10. Ischay, M. A.; Anzovino, M. E.; Du, J.; Yoon, T. P., Efficient Visible Light Photocatalysis of [2+2] Enone Cycloadditions. *J. Am. Chem. Soc.* **2008**, *130* (39), 12886-12887.
11. Lu, Z.; Yoon, T. P., Visible Light Photocatalysis of [2+2] Styrene Cycloadditions by Energy Transfer. *Angew. Chem. Int. Ed.* **2012**, *51* (41), 10329-10332.
12. Tucker, J. W.; Narayanam, J. M. R.; Krabbe, S. W.; Stephenson, C. R. J., Electron Transfer Photoredox Catalysis: Intramolecular Radical Addition to Indoles and Pyrroles. *Org. Lett.* **2010**, *12* (2), 368-371.

13. Maity, S.; Zhu, M.; Shinabery, R. S.; Zheng, N., Intermolecular [3+2] Cycloaddition of Cyclopropylamines with Olefins by Visible-Light Photocatalysis. *Angew. Chem. Int. Ed.* **2012**, *51* (1), 222-226.
14. Kudo, A.; Miseki, Y., Heterogeneous Photocatalyst Materials for Water Splitting. *Chem. Soc. Rev.* **2009**, *38* (1), 253-278.
15. Li, K.; Peng, B.; Peng, T., Recent Advances in Heterogeneous Photocatalytic CO₂ Conversion to Solar Fuels. *ACS Catal.* **2016**, *6* (11), 7485-7527.
16. Herrmann, J.-M., Heterogeneous Photocatalysis: Fundamentals and Applications to the Removal of Various Types of Aqueous Pollutants. *Catal. Today* **1999**, *53* (1), 115-129.
17. Colmenares, J. C.; Luque, R., Heterogeneous Photocatalytic Nanomaterials: Prospects and Challenges in Selective Transformations of Biomass-Derived Compounds. *Chem. Soc. Rev.* **2014**, *43* (3), 765-778.
18. Jiang, Y.; Yang, M.; Wu, Y.; López-Arteaga, R.; Rogers, C. R.; Weiss, E. A., Chemo- and Stereoselective Intermolecular [2 + 2] Photocycloaddition of Conjugated Dienes Using Colloidal Nanocrystal Photocatalysts. *Chem Catal.* **2021**, *1* (1), 106-116.
19. Luttrell, T.; Halpegamage, S.; Tao, J.; Kramer, A.; Sutter, E.; Batzill, M., Why is Anatase a Better Photocatalyst than Rutile? - Model Studies on Epitaxial TiO₂ Films. *Sci. Rep.* **2014**, *4* (1), 4043.
20. Park, H.; Park, Y.; Kim, W.; Choi, W., Surface Modification of TiO₂ Photocatalyst for Environmental Applications. *J. Photochem. Photobiol. C* **2013**, *15*, 1-20.
21. Scanlon, D. O.; Dunnill, C. W.; Buckeridge, J.; Shevlin, S. A.; Logsdail, A. J.; Woodley, S. M.; Catlow, C. R. A.; Powell, M. J.; Palgrave, R. G.; Parkin, I. P.; Watson, G. W.; Keal, T. W.; Sherwood, P.; Walsh, A.; Sokol, A. A., Band Alignment of Rutile and Anatase TiO₂. *Nat. Mater.* **2013**, *12* (9), 798-801.
22. McTiernan, C. D.; Pitre, S. P.; Ismaili, H.; Scaiano, J. C., Heterogeneous Light-Mediated Reductive Dehalogenations and Cyclizations Utilizing Platinum Nanoparticles on Titania (PtNP@TiO₂). *Adv. Synth. Catal.* **2014**, *356* (13), 2819-2824.
23. Pitre, S. P.; Yoon, T. P.; Scaiano, J. C., Titanium Dioxide Visible Light Photocatalysis: Surface Association Enables Photocatalysis with Visible Light Irradiation. *Chem. Commun.* **2017**, *53* (31), 4335-4338.
24. Pitre, S. P.; Scaiano, J. C.; Yoon, T. P., Photocatalytic Indole Diels–Alder Cycloadditions Mediated by Heterogeneous Platinum-Modified Titanium Dioxide. *ACS Catal.* **2017**, *7* (10), 6440-6444.
25. Hodgson, G. K.; Scaiano, J. C., Heterogeneous Dual Photoredox-Lewis Acid Catalysis Using a Single Bifunctional Nanomaterial. *ACS Catal.* **2018**, *8* (4), 2914-2922.

26. Tang, J.; Grampp, G.; Liu, Y.; Wang, B.-X.; Tao, F.-F.; Wang, L.-J.; Liang, X.-Z.; Xiao, H.-Q.; Shen, Y.-M., Visible Light Mediated Cyclization of Tertiary Anilines with Maleimides Using Nickel(II) Oxide Surface-Modified Titanium Dioxide Catalyst. *J. Org. Chem.* **2015**, *80* (5), 2724-2732.
27. Hosseini-Sarvari, M.; Koohgard, M.; Firoozi, S.; Mohajeri, A.; Tavakolian, H., Alizarin Red S–TiO₂-Catalyzed Cascade C(sp³)–H to C(sp²)–H Bond Formation/Cyclization Reactions toward Tetrahydroquinoline Derivatives under Visible Light Irradiation. *New J. Chem.* **2018**, *42* (9), 6880-6888.
28. Koohgard, M.; Hosseinpour, Z.; Sarvestani, A. M.; Hosseini-Sarvari, M., ARS–TiO₂ Photocatalyzed Direct Functionalization of sp² C–H Bonds toward Thiocyanation and Cyclization Reactions under Visible Light. *Catal. Sci. Technol.* **2020**, *10* (5), 1401-1407.
29. Liu, Y.; Zhang, M.; Tung, C.-H.; Wang, Y., TiO₂ Photocatalytic Cyclization Reactions for the Syntheses of Aryltetralones. *ACS Catal.* **2016**, *6* (12), 8389-8394.
30. Wang, J.; Mao, C.; Feng, P.; Zheng, N., Visible-Light-Mediated [4+2] Annulation of N-Cyclobutylanilines with Alkynes Catalyzed by Self-Doped Ti³⁺@TiO₂. *Chem. Eur. J.* **2017**, *23* (61), 15396-15403.
31. Sciarretta, M.; Barawi, M.; Navío, C.; Shea, V. A. d. I. P. O.; Blanco, M.; Alemán, J., A Graphene Acid - TiO₂ Nanohybrid as Multifunctional Heterogeneous Photocatalyst for the Synthesis of 1,3,4-Oxadiazoles. *ACS Appl. Mater. Interfaces* **2022**, *14* (30), 34975-34984.
32. Mackenzie, J. D.; Bescher, E. P., Chemical Routes in the Synthesis of Nanomaterials Using the Sol–Gel Process. *Acc. Chem. Res.* **2007**, *40* (9), 810-818.
33. Inamdar, S. N.; Ingole, P. P.; Haram, S. K., Determination of Band Structure Parameters and the Quasi-Particle Gap of CdSe Quantum Dots by Cyclic Voltammetry. *ChemPhysChem* **2008**, *9* (17), 2574-2579.
34. Kohl, P. A.; Bard, A. J., Semiconductor Electrodes. 13. Characterization and Behavior of n-Type Zinc Oxide, Cadmium Sulfide, and Gallium Phosphide Electrodes in Acetonitrile Solutions. *J. Am. Chem. Soc.* **1977**, *99* (23), 7531-7539.
35. Haram, S. K.; Quinn, B. M.; Bard, A. J., Electrochemistry of CdS Nanoparticles: A Correlation between Optical and Electrochemical Band Gaps. *J. Am. Chem. Soc.* **2001**, *123* (36), 8860-8861.
36. Amelia, M.; Lincheneau, C.; Silvi, S.; Credi, A., Electrochemical Properties of CdSe and CdTe Quantum Dots. *Chem. Soc. Rev.* **2012**, *41* (17), 5728-5743.
37. Al-Ekabi, H.; De Mayo, P., Surface Photochemistry: The CdS Photoinduced Dimerization of N-Vinylcarbazole. *Tetrahedron* **1986**, *42* (22), 6277-6284.

38. Hu, J.; Pu, T.-J.; Xu, Z.-W.; Xu, W.-Y.; Feng, Y.-S., Cadmium Sulfide Quantum-Dot-Photocatalyzed Cascade Cyclization of Functionalized Difluoromethyl Chlorides with Unactivated Olefins. *Adv. Synth. Catal.* **2019**, *361* (4), 708-713.
39. Jiang, Y.; Wang, C.; Rogers, C. R.; Kodaimati, M. S.; Weiss, E. A., Regio- and Diastereoselective Intermolecular [2+2] Cycloadditions Photocatalysed by Quantum Dots. *Nat. Chem.* **2019**, *11* (11), 1034-1040.
40. Jones, L. O.; Mosquera, M. A.; Jiang, Y.; Weiss, E. A.; Schatz, G. C.; Ratner, M. A., Thermodynamics and Mechanism of a Photocatalyzed Stereoselective [2 + 2] Cycloaddition on a CdSe Quantum Dot. *J. Am. Chem. Soc.* **2020**, *142* (36), 15488-15495.
41. Jiang, Y.; López-Arteaga, R.; Weiss, E. A., Quantum Dots Photocatalyze Intermolecular [2 + 2] Cycloadditions of Aromatic Alkenes Adsorbed to their Surfaces via van der Waals Interactions. *J. Am. Chem. Soc.* **2022**, *144* (9), 3782-3786.
42. Dabbous, A.; Colson, E.; Chakravorty, D.; Mouesca, J.-M.; Lombard, C.; Caillat, S.; Ravanat, J.-L.; Dubois, F.; Dénès, F.; Renaud, P.; Maurel, V., Fine Tuning of Quantum Dots Photocatalysts for the Synthesis of Tropane Alkaloid Skeletons. *Chem. Eur. J.* **2023**, *29* (28), e202300303.
43. Yan, W.; Yan, L.; Jing, C., Impact of Doped Metals on Urea-Derived g-C₃N₄ for Photocatalytic Degradation of Antibiotics: Structure, Photoactivity and Degradation Mechanisms. *Appl. Catal. B* **2019**, *244*, 475-485.
44. Li, Y.; Li, X.; Zhang, H.; Fan, J.; Xiang, Q., Design and Application of Active Sites in g-C₃N₄-Based Photocatalysts. *J. Mater. Sci. Technol.* **2020**, *56*, 69-88.
45. Zheng, Y.; Lin, L.; Wang, B.; Wang, X., Graphitic Carbon Nitride Polymers toward Sustainable Photoredox Catalysis. *Angew. Chem. Int. Ed.* **2015**, *54* (44), 12868-12884.
46. Su, F.; Mathew, S. C.; Möhlmann, L.; Antonietti, M.; Wang, X.; Blechert, S., Aerobic Oxidative Coupling of Amines by Carbon Nitride Photocatalysis with Visible Light. *Angew. Chem. Int. Ed.* **2011**, *50* (3), 657-660.
47. Kurpil, B.; Markushyna, Y.; Savateev, A., Visible-Light-Driven Reductive (Cyclo)Dimerization of Chalcones over Heterogeneous Carbon Nitride Photocatalyst. *ACS Catal.* **2019**, *9* (2), 1531-1538.
48. Yang, M.; Lian, R.; Zhang, X.; Wang, C.; Cheng, J.; Wang, X., Photocatalytic Cyclization of Nitrogen-Centered Radicals with Carbon Nitride through Promoting Substrate/Catalyst Interaction. *Nat. Commun.* **2022**, *13* (1), 4900.
49. Woźnica, M.; Chaoui, N.; Taabache, S.; Blechert, S., THF: An Efficient Electron Donor in Continuous Flow Radical Cyclization Photocatalyzed by Graphitic Carbon Nitride. *Chem. Eur. J.* **2014**, *20* (45), 14624-14628.

50. Song, T.; Zhou, B.; Peng, G.-W.; Zhang, Q.-B.; Wu, L.-Z.; Liu, Q.; Wang, Y., Aerobic Oxidative Coupling of Resveratrol and its Analogues by Visible Light Using Mesoporous Graphitic Carbon Nitride (mpg-C₃N₄) as a Bioinspired Catalyst. *Chem. Eur. J.* **2014**, *20* (3), 678-682.
51. Kurpil, B.; Otte, K.; Antonietti, M.; Savateev, A., Photooxidation of N-Acylhydrazones to 1,3,4-Oxadiazoles Catalyzed by Heterogeneous Visible-Light-Active Carbon Nitride Semiconductor. *Appl. Catal. B* **2018**, *228*, 97-102.
52. Kurpil, B.; Otte, K.; Mishchenko, A.; Lamagni, P.; Lipiński, W.; Lock, N.; Antonietti, M.; Savateev, A., Carbon Nitride Photocatalyzes Regioselective Aminium Radical Addition to the Carbonyl Bond and Yields N-Fused Pyrroles. *Nat. Commun.* **2019**, *10* (1), 945.
53. Savateev, A.; Tarakina, N. V.; Strauss, V.; Hussain, T.; ten Brummelhuis, K.; Sánchez Vadillo, J. M.; Markushyna, Y.; Mazzanti, S.; Tyutyunnik, A. P.; Walczak, R.; Oschatz, M.; Guldi, D. M.; Karton, A.; Antonietti, M., Potassium Poly(Heptazine Imide): Transition Metal-Free Solid-State Triplet Sensitizer in Cascade Energy Transfer and [3+2]-cycloadditions. *Angew. Chem. Int. Ed.* **2020**, *59* (35), 15061-15068.
54. Yang, C.; Li, R.; Zhang, K. A. I.; Lin, W.; Landfester, K.; Wang, X., Heterogeneous Photoredox Flow Chemistry for the Scalable Organosynthesis of Fine Chemicals. *Nat. Commun.* **2020**, *11* (1), 1239.
55. Zhao, Y.; Antonietti, M., Visible-Light-Irradiated Graphitic Carbon Nitride Photocatalyzed Diels–Alder Reactions with Dioxygen as Sustainable Mediator for Photoinduced Electrons. *Angew. Chem. Int. Ed.* **2017**, *56* (32), 9336-9340.
56. Zeng, F.-L.; Zhu, H.-L.; Chen, X.-L.; Qu, L.-B.; Yu, B., Visible Light-Induced Recyclable g-C₃N₄ Catalyzed Thiocyanation of C(sp²)–H Bonds in Sustainable Solvents. *Green Chem.* **2021**, *23* (10), 3677-3682.
57. Fu, X.-Y.; Si, Y.-F.; Qiao, L.-P.; Zhao, Y.-F.; Chen, X.-L.; Yu, B., Visible Light-Promoted Recyclable Carbon Nitride-Catalyzed Dioxygenation of β,γ -Unsaturated Oximes. *Adv. Synth. Catal.* **2022**, *364* (3), 574-580.
58. Bai, J.; Yan, S.; Zhang, Z.; Guo, Z.; Zhou, C.-Y., Visible-Light Carbon Nitride-Catalyzed Aerobic Cyclization of Thiobenzanilides under Ambient Air Conditions. *Org. Lett.* **2021**, *23* (12), 4843-4848.
59. Guo, Y.; Chang, R.; Fu, Z.; Zhou, C.-Y.; Guo, Z., Heterogeneous Visible-Light Promoted Dehydrogenative [4 + 2] Annulation of Benzothioamides and Alkynes under Aerobic Conditions. *Green Chem.* **2023**, *25* (13), 5206-5212.
60. Si, Y.-F.; Chen, X.-L.; Fu, X.-Y.; Sun, K.; Song, X.; Qu, L.-B.; Yu, B., Divergent g-C₃N₄-catalyzed Reactions of Quinoxalin-2(1H)-ones with N-Aryl Glycines under Visible Light: Solvent-Controlled Hydroaminomethylation and Annulation. *ACS. Sustain. Chem. Eng.* **2020**, *8* (29), 10740-10746.

61. Shi, A.; Sun, K.; Wu, Y.; Xiang, P.; Krylov, I. B.; Terent'ev, A. O.; Chen, X.; Yu, B., Oxygen-Doped Carbon Nitride for Enhanced Photocatalytic Activity in Visible-Light-Induced Decarboxylative Annulation Reactions. *J. Catal.* **2022**, *415*, 28-36.
62. Tian, J.; Zhao, L.; Yang, C.; Yang, C.; Guo, L.; Xia, W., Four-Component Synthesis of Spiro-Imidazolidines Enabled by Carbon Nitride Photocatalysis. *ACS Catal.* **2023**, *13* (2), 866-876.
63. Rieth, A. J.; Qin, Y.; Martindale, B. C. M.; Nocera, D. G., Long-Lived Triplet Excited State in a Heterogeneous Modified Carbon Nitride Photocatalyst. *J. Am. Chem. Soc.* **2021**, *143* (12), 4646-4652.
64. Hou, H.; Wang, J.; Chen, X.; Han, Y.; Yu, H.; Yan, C.; Shi, Y.; Zhu, S., Graphitic Carbon Nitride as a Heterogeneous Photocatalyst for the Hydrophosphorylation and Hydrophosphorylative Cyclization Reactions of Terminal Alkyne and Its Derived Enynes. *ChemCatChem* **2022**, *14* (22), e202201073.
65. Xu, Y.; Jin, S.; Xu, H.; Nagai, A.; Jiang, D., Conjugated Microporous Polymers: Design, Synthesis and Application. *Chem. Soc. Rev.* **2013**, *42* (20), 8012-8031.
66. Geng, K.; He, T.; Liu, R.; Dalapati, S.; Tan, K. T.; Li, Z.; Tao, S.; Gong, Y.; Jiang, Q.; Jiang, D., Covalent Organic Frameworks: Design, Synthesis, and Functions. *Chem. Rev.* **2020**, *120* (16), 8814-8933.
67. Wang, Z. J.; Ghasimi, S.; Landfester, K.; Zhang, K. A. I., Bandgap Engineering of Conjugated Nanoporous Poly-benzobisthiadiazoles via Copolymerization for Enhanced Photocatalytic 1,2,3,4-Tetrahydroquinoline Synthesis under Visible Light. *Adv. Synth. Catal.* **2016**, *358* (16), 2576-2582.
68. Almansaf, Z.; Hu, J.; Zanca, F.; Shahsavari, H. R.; Kampmeyer, B.; Tsuji, M.; Maity, K.; Lomonte, V.; Ha, Y.; Mastroilli, P.; Todisco, S.; Benamara, M.; Oktavian, R.; Mirjafari, A.; Moghadam, P. Z.; Khosropour, A. R.; Beyzavi, H., Pt(II)-Decorated Covalent Organic Framework for Photocatalytic Difluoroalkylation and Oxidative Cyclization Reactions. *ACS Appl. Mater. Interfaces* **2021**, *13* (5), 6349-6358.
69. Jin, F.; Lin, E.; Wang, T.; Yan, D.; Yang, Y.; Chen, Y.; Cheng, P.; Zhang, Z., Rationally Fabricating 3D Porphyrinic Covalent Organic Frameworks with scu Topology as Highly Efficient Photocatalysts. *Chem* **2022**, *8* (11), 3064-3080.
70. Li, R.; Ma, B. C.; Huang, W.; Wang, L.; Wang, D.; Lu, H.; Landfester, K.; Zhang, K. A. I., Photocatalytic Regioselective and Stereoselective [2 + 2] Cycloaddition of Styrene Derivatives Using a Heterogeneous Organic Photocatalyst. *ACS Catal.* **2017**, *7* (5), 3097-3101.
71. Huang, W.; Byun, J.; Rörich, I.; Ramanan, C.; Blom, P. W. M.; Lu, H.; Wang, D.; Caire da Silva, L.; Li, R.; Wang, L.; Landfester, K.; Zhang, K. A. I., Asymmetric Covalent Triazine Framework for Enhanced Visible-Light Photoredox Catalysis via Energy Transfer Cascade. *Angew. Chem. Int. Ed.* **2018**, *57* (27), 8316-8320.

72. Huang, W.; Huber, N.; Jiang, S.; Landfester, K.; Zhang, K. A. I., Covalent Triazine Framework Nanoparticles via Size-Controllable Confinement Synthesis for Enhanced Visible-Light Photoredox Catalysis. *Angew. Chem. Int. Ed.* **2020**, *59* (42), 18368-18373.
73. Liu, S.; Pan, W.; Wu, S.; Bu, X.; Xin, S.; Yu, J.; Xu, H.; Yang, X., Visible-Light-Induced Tandem Radical Addition–Cyclization of 2-Aryl Phenyl Isocyanides Catalysed by Recyclable Covalent Organic Frameworks. *Green Chem.* **2019**, *21* (11), 2905-2910.
74. Li, S.; Li, L.; Li, Y.; Dai, L.; Liu, C.; Liu, Y.; Li, J.; Lv, J.; Li, P.; Wang, B., Fully Conjugated Donor–Acceptor Covalent Organic Frameworks for Photocatalytic Oxidative Amine Coupling and Thioamide Cyclization. *ACS Catal.* **2020**, *10* (15), 8717-8726.
75. Bi, S.; Zhang, Z.; Meng, F.; Wu, D.; Chen, J.-S.; Zhang, F., Heteroatom-Embedded Approach to Vinylene-Linked Covalent Organic Frameworks with Isoelectronic Structures for Photoredox Catalysis. *Angew. Chem. Int. Ed.* **2022**, *61* (6), e202111627.
76. Parvatkar, P. T.; Kandambeth, S.; Shaikh, A. C.; Nadinov, I.; Yin, J.; Kale, V. S.; Healing, G.; Emwas, A.-H.; Shekhah, O.; Alshareef, H. N.; Mohammed, O. F.; Eddaoudi, M., A Tailored COF for Visible-Light Photosynthesis of 2,3-Dihydrobenzofurans. *J. Am. Chem. Soc.* **2023**, *145* (9), 5074-5082.
77. An, W.-K.; Zheng, S.-J.; Zhang, H.-X.; Shang, T.-T.; Wang, H.-R.; Xu, X.-J.; Jin, Q.; Qin, Y.; Ren, Y.; Jiang, S.; Xu, C.-L.; Hou, M.-S.; Pan, Z., s-Tetrazine-Functionalized Hyper-Crosslinked Polymers for Efficient Photocatalytic Synthesis of Benzimidazoles. *Green Chem.* **2021**, *23* (3), 1292-1299.
78. Wang, C.-A.; Zhang, J.-P.; Nie, K.; Li, Y.-W.; Li, Q.; Jiao, G.-Z.; Chang, J.-G.; Han, Y.-F., Tetrathienoanthracene-Functionalized Conjugated Microporous Polymers as an Efficient, Metal-free Visible-Light Solid Organocatalyst for Heterogeneous Photocatalysis. *Catal. Sci. Technol.* **2021**, *11* (11), 3799-3809.
79. Luo, B.; Chen, Y.; Zhang, Y.; Huo, J., Benzotrithiophene and Triphenylamine Based Covalent Organic Frameworks as Heterogeneous Photocatalysts for Benzimidazole Synthesis. *J. Catal.* **2021**, *402*, 52-60.
80. Deng, Z.; Zhao, H.; Cao, X.; Xiong, S.; Li, G.; Deng, J.; Yang, H.; Zhang, W.; Liu, Q., Enhancing Built-in Electric Field via Molecular Dipole Control in Conjugated Microporous Polymers for Boosting Charge Separation. *ACS Appl. Mater. Interfaces* **2022**, *14* (31), 35745-35754.
81. Kojima, A.; Teshima, K.; Shirai, Y.; Miyasaka, T., Organometal Halide Perovskites as Visible-Light Sensitizers for Photovoltaic Cells. *J. Am. Chem. Soc.* **2009**, *131* (17), 6050-6051.
82. NREL Best Research-Cell Efficiency Chart. <https://www.nrel.gov/pv/assets/pdfs/best-research-cell-efficiencies.pdf> (accessed 08/23/2023).
83. Tan, Z.-K.; Moghaddam, R. S.; Lai, M. L.; Docampo, P.; Higler, R.; Deschler, F.; Price, M.; Sadhanala, A.; Pazos, L. M.; Credgington, D.; Hanusch, F.; Bein, T.; Snaith, H. J.; Friend,

R. H., Bright Light-Emitting Diodes Based on Organometal Halide Perovskite. *Nat. Nanotechnol.* **2014**, *9* (9), 687-692.

84. Zhu, H.; Fu, Y.; Meng, F.; Wu, X.; Gong, Z.; Ding, Q.; Gustafsson, M. V.; Trinh, M. T.; Jin, S.; Zhu, X. Y., Lead Halide Perovskite Nanowire Lasers with Low Lasing Thresholds and High Quality Factors. *Nat. Mater.* **2015**, *14* (6), 636-642.

85. Dou, L.; Yang, Y.; You, J.; Hong, Z.; Chang, W.-H.; Li, G.; Yang, Y., Solution-Processed Hybrid Perovskite Photodetectors with High Detectivity. *Nat. Commun.* **2014**, *5* (1), 5404.

86. Senanayak, S. P.; Abdi-Jalebi, M.; Kamboj, V. S.; Carey, R.; Shivanna, R.; Tian, T.; Schweicher, G.; Wang, J.; Giesbrecht, N.; Di Nuzzo, D.; Beere, H. E.; Docampo, P.; Ritchie, D. A.; Fairen-Jimenez, D.; Friend, R. H.; Sringhaus, H., A General Approach for Hysteresis-Free, Operationally Stable Metal Halide Perovskite Field-Effect Transistors. *Sci. Adv.* **6** (15), eaz4948.

87. You, Y.-M.; Liao, W.-Q.; Zhao, D.; Ye, H.-Y.; Zhang, Y.; Zhou, Q.; Niu, X.; Wang, J.; Li, P.-F.; Fu, D.-W.; Wang, Z.; Gao, S.; Yang, K.; Liu, J.-M.; Li, J.; Yan, Y.; Xiong, R.-G., An Organic-Inorganic Perovskite Ferroelectric with Large Piezoelectric Response. *Science* **2017**, *357* (6348), 306-309.

88. Deng, W.; Zhang, X.; Huang, L.; Xu, X.; Wang, L.; Wang, J.; Shang, Q.; Lee, S.-T.; Jie, J., Aligned Single-Crystalline Perovskite Microwire Arrays for High-Performance Flexible Image Sensors with Long-Term Stability. *Adv. Mater.* **2016**, *28* (11), 2201-2208.

89. Goldschmidt, V. M., Die Gesetze der Krystallochemie. *Naturwissenschaften* **1926**, *14* (21), 477-485.

90. Manser, J. S.; Christians, J. A.; Kamat, P. V., Intriguing Optoelectronic Properties of Metal Halide Perovskites. *Chem. Rev.* **2016**, *116* (21), 12956-13008.

91. Wehrenfennig, C.; Eperon, G. E.; Johnston, M. B.; Snaith, H. J.; Herz, L. M., High Charge Carrier Mobilities and Lifetimes in Organolead Trihalide Perovskites. *Adv. Mater.* **2014**, *26* (10), 1584-1589.

92. Xing, G.; Mathews, N.; Sun, S.; Lim, S. S.; Lam, Y. M.; Grätzel, M.; Mhaisalkar, S.; Sum, T. C., Long-Range Balanced Electron- and Hole-Transport Lengths in Organic-Inorganic $\text{CH}_3\text{NH}_3\text{PbI}_3$. *Science* **2013**, *342* (6156), 344-347.

93. Protesescu, L.; Yakunin, S.; Bodnarchuk, M. I.; Krieg, F.; Caputo, R.; Hendon, C. H.; Yang, R. X.; Walsh, A.; Kovalenko, M. V., Nanocrystals of Cesium Lead Halide Perovskites (CsPbX_3 , X = Cl, Br, and I): Novel Optoelectronic Materials Showing Bright Emission with Wide Color Gamut. *Nano Lett.* **2015**, *15* (6), 3692-3696.

94. Huang, H.; Zhao, F.; Liu, L.; Zhang, F.; Wu, X.-g.; Shi, L.; Zou, B.; Pei, Q.; Zhong, H., Emulsion Synthesis of Size-Tunable $\text{CH}_3\text{NH}_3\text{PbBr}_3$ Quantum Dots: An Alternative Route toward Efficient Light-Emitting Diodes. *ACS Appl. Mater. Interfaces* **2015**, *7* (51), 28128-28133.

95. Han, C.; Zhu, X.; Martin, J. S.; Lin, Y.; Spears, S.; Yan, Y., Recent Progress in Engineering Metal Halide Perovskites for Efficient Visible-Light-Driven Photocatalysis. *ChemSusChem* **2020**, *13* (16), 4005-4025.
96. Huang, H.; Pradhan, B.; Hofkens, J.; Roeffaers, M. B. J.; Steele, J. A., Solar-Driven Metal Halide Perovskite Photocatalysis: Design, Stability, and Performance. *ACS Energy Lett.* **2020**, *5* (4), 1107-1123.
97. Brennan, M. C.; Herr, J. E.; Nguyen-Beck, T. S.; Zinna, J.; Draguta, S.; Rouvimov, S.; Parkhill, J.; Kuno, M., Origin of the Size-Dependent Stokes Shift in CsPbBr₃ Perovskite Nanocrystals. *J. Am. Chem. Soc.* **2017**, *139* (35), 12201-12208.
98. Ravi, V. K.; Markad, G. B.; Nag, A., Band Edge Energies and Excitonic Transition Probabilities of Colloidal CsPbX₃ (X = Cl, Br, I) Perovskite Nanocrystals. *ACS Energy Lett.* **2016**, *1* (4), 665-671.
99. Zhu, X.; Lin, Y.; Sun, Y.; Beard, M. C.; Yan, Y., Lead-Halide Perovskites for Photocatalytic α -Alkylation of Aldehydes. *J. Am. Chem. Soc.* **2019**, *141* (2), 733-738.
100. Wang, K.; Lu, H.; Zhu, X.; Lin, Y.; Beard, M. C.; Yan, Y.; Chen, X., Ultrafast Reaction Mechanisms in Perovskite Based Photocatalytic C–C Coupling. *ACS Energy Lett.* **2020**, *5* (2), 566-571.
101. Lin, Y.; Guo, J.; San Martin, J.; Han, C.; Martinez, R.; Yan, Y., Photoredox Organic Synthesis Employing Heterogeneous Photocatalysts with Emphasis on Halide Perovskite. *Chem. Eur. J.* **2020**, *26* (58), 13118-13136.
102. Corti, M.; Bonomi, S.; Chiara, R.; Romani, L.; Quadrelli, P.; Malavasi, L., Application of Metal Halide Perovskites as Photocatalysts in Organic Reactions. *Inorganics* **2021**, *9* (7).
103. Lu, H.; Zhu, X.; Miller, C.; San Martin, J.; Chen, X.; Miller, E. M.; Yan, Y.; Beard, M. C., Enhanced Photoredox Activity of CsPbBr₃ Nanocrystals by Quantitative Colloidal Ligand Exchange. *J. Chem. Phys.* **2019**, *151* (20).

Chapter 2 Lead-Halide Perovskite Nanocrystals for Photocatalytic Redox-Neutral Syntheses of Pyrrole and Pyrazole Derivatives

2.1 Chapter Summary

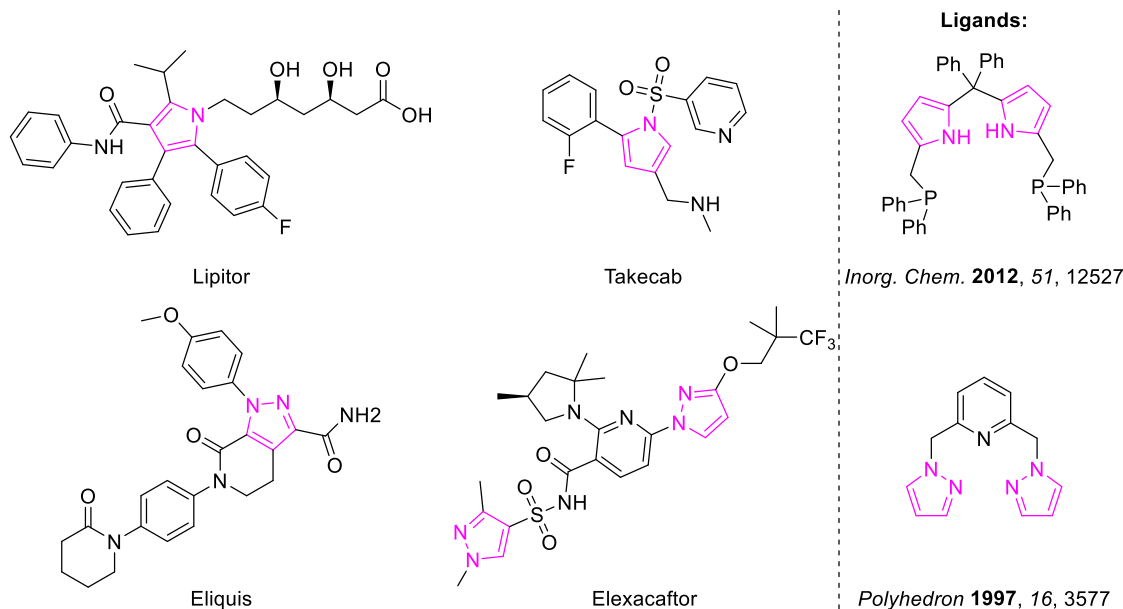
This chapter describes the application of lead-halide perovskite nanocrystals (LHP NCs) towards photocatalytic N-heterocyclization reactions for syntheses of 1,2,3,5-tetrasubstituted pyrroles and 1,3,5-trisubstituted pyrazoles. Mechanistic investigations including Stern-Volmer photoluminescence (PL) quenching studies, cyclic voltammetry measurements, and radical trapping experiments reveal that these two N-heterocyclization reactions may go through similar but slightly different reaction pathways: Both reactions involve a key α -ketone radical intermediate generated by electron transfer (ET) from the excited-state perovskite photocatalyst (NCs*) to the α -bromoketone starting material. For the synthesis of pyrroles, the α -ketone radical undergoes radical addition to enamine followed by hole transfer (HT)-enabled intramolecular cyclization and dehydration to afford the final product. But in the case of pyrazoles, while the radical addition pathway is also possible, the α -ketone radical may undergo radical-radical coupling with hydrazone radical (generated by hole transfer from NCs*) followed by intramolecular cyclization and dehydration to afford the final product. The broad functional group tolerance of these reactions has further demonstrated the synthetic utility of our perovskite photocatalysis strategy.

2.2 Introduction

Pyrrole and pyrazole are two pharmaceutically important five-membered N-heterocycles widely found in top 200 small molecule drugs (by retail sales) such as shown in **Scheme 2.1** (left).

¹ Additionally, many ligands studied in organometallic chemistry are also composed of pyrroles or pyrazoles as their core coordinating structures (**Scheme 2.1**, right), providing unique electronic and steric effects to the central metal atoms.^{2,3} As such, an efficient while simple and economic synthetic methodology for the preparation of these N-heterocycles that can operate in mild

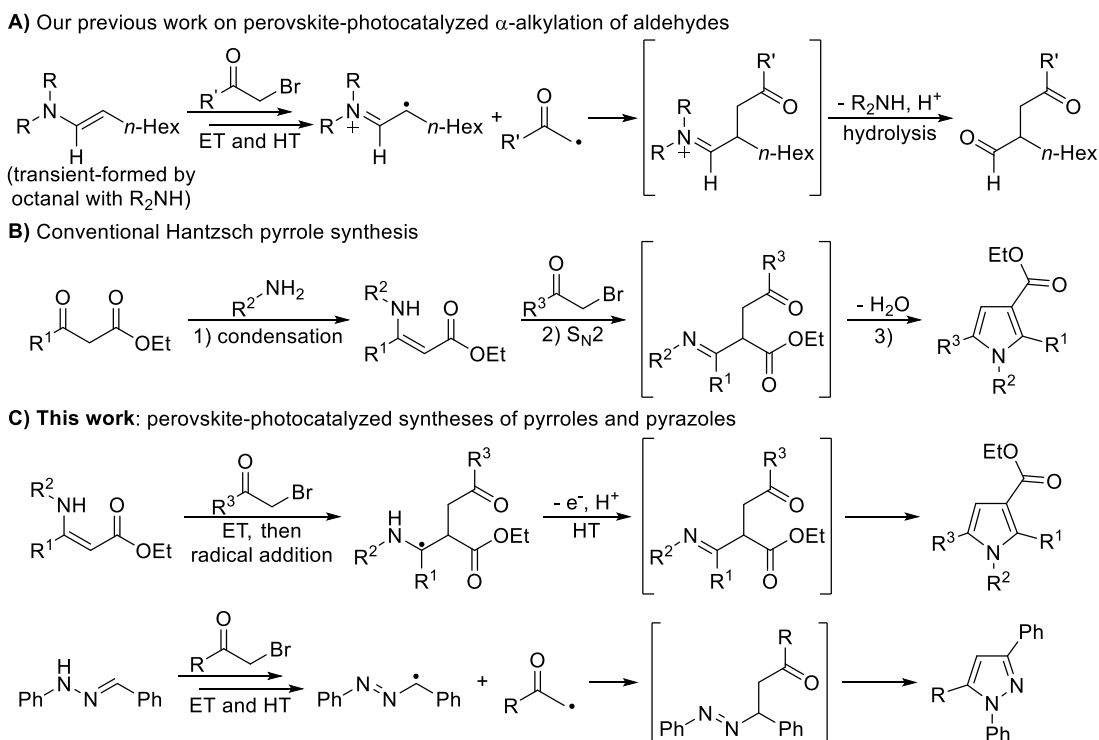
conditions and ambient atmosphere is highly desired. In fact, a series of seminal works have been reported for the syntheses of these motifs over the years, including Paal-Knorr synthesis,^{4, 5} Hantzsch pyrrole synthesis,⁶ Barton-Zard synthesis⁷ (for the synthesis of pyrroles) and Knorr pyrazole synthesis⁸ (for the synthesis of pyrazoles). However, these methods often require harsh reaction conditions, such as high temperature, and/or highly reactive reagents, such as strong base.



Scheme 2.1 Small molecule drugs and ligands containing pyrrole and pyrazole scaffolds.

LHP as an excellent photovoltaic material has recently been developed as a promising semiconductor-based heterogeneous photocatalyst.^{9, 10} Our group reported one of the first examples of employing LHP NCs for photocatalytic organic transformation, NCs-photocatalyzed α -alkylation of aldehydes.¹¹ As discussed in **Section 1.5.4**, such transformation involves an NCs photoredox cycle and an enamine organocatalysis cycle. The key C-C bond formation step is illustrated as a radical-radical coupling process between the α -ketone radical (formed from ET to α -bromoketone) and the enamine radical cation (formed from HT to the transient-formed enamine). (**Scheme 2.2A**) We recognized the similarity between this process and Hantzsch pyrrole synthesis⁶. The traditional Hantzsch pyrrole synthesis method can synthesize substituted pyrroles

from β -ketoesters, ammonia (or primary amines) and α -haloketones under reflux conditions, which involves three key steps: 1) enamine formation from amine and β -ketoester; 2) Nucleophilic substitution between enamine and α -haloketone; 3) Intramolecular cyclization by the nucleophilic addition of the enamine nitrogen to the 5-carbonyl carbon followed by dehydration. (**Scheme 2.2B**) We hypothesize that reaction between an α -bromoketone with a stable enamine in lieu of a transient-formed enamine under NCs photocatalysis conditions may synthesize pyrrole derivatives via a radical pathway. Specifically, α -ketone radical that is formed by ET from NCs* to α -bromoketone, reacts with a stable enamine, resulting in the key intermediate (**Scheme 2.2C**, top bracket) similar to that in step 2) in conventional Hantzsch pyrrole synthesis. Such intermediate may then undergo intramolecular cyclization and dehydration to arrive at the desired product. Furthermore, replacing the stable enamine with hydrazone may generate pyrazole (**Scheme 2.2C**, bottom).

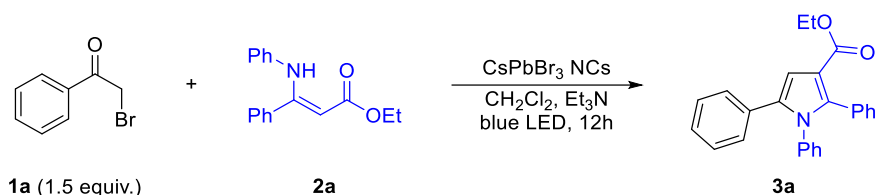


Scheme 2.2 Photocatalytic design based on previous works. The key intermediates are highlighted in bracket for comparison. ET: electron transfer. HT: hole transfer.

2.3 Results and Discussion

2.3.1 NCs-Photocatalyzed Synthesis of Pyrrole Derivatives

We set out to investigate the optimal reaction conditions for NCs-photocatalyzed synthesis of pyrrole derivatives using 2-bromoacetophenone (**1a**) and ethyl (*Z*)-3-phenyl-3-(phenylamino)acrylate (**2a**) as model substrates. To our delight, the desired pyrrole product **3a** could be observed in high yield under NCs photocatalysis as shown in **Table 2.1**. Running the reaction under air versus N₂ atmosphere gave similar yield, highlighting the good air tolerance of this system (entry 2). Changing the solvent from DCM to EtOAc or decreasing the photocatalyst loading mildly affected the yield (entry 3 and 4). A substoichiometric amount of Et₃N was found to promote the product yielding (entry 5), likely acting as an electron relay specie and a proton transfer agent. Omitting the CsPbBr₃ NCs or light irradiation shut down the reaction, suggesting the pivotal role of CsPbBr₃ NCs as a photocatalyst (entry 6 and 7).

Table 2.1 Condition investigation for the NCs-photocatalyzed synthesis of pyrrole derivatives.

entry	deviation from standard conditions ^a	yield, % ^b
1	None	93
2	Under N ₂	92
3	EtOAc as solvent	74
4	CsPbBr ₃ NCs (0.5 mg)	72
5	No Et ₃ N	68
6	No CsPbBr ₃ NCs	<1
7	No light	<1

^aStandard conditions: **1a** (0.15 mmol, 1.5 equiv.), **2a** (0.10 mmol, 0.05M), CsPbBr₃ NCs (2.0 mg), CH₂Cl₂ (DCM, 2.0 mL), Et₃N (35 mol%). Reaction was performed under household blue LED irradiation without N₂ sparging at room temperature for 12h.

^bYields were determined by ¹H NMR.

We commenced mechanistic studies to gain a better view of the reaction mechanism. Our electrochemical studies and previous report¹¹ both suggested that the excited-state CsPbBr₃ NCs ($E_{CB} = -1.3$ V, $E_{VB} = +1.1$ V, all vs. SCE) could single electronically reduce **1a** ($E_{red} = -1.11$ V vs. SCE, **Figure 2.3**). Stern-Volmer PL quenching study also verified the interaction between the excited-state NCs and starting material **1a**, with a quenching constant of 21.4 M⁻¹ (**Figure 2.1A**). Furthermore, addition of (2,2,6,6-Tetramethylpiperidin-1-yl)oxyl (TEMPO), a commonly used radical trapping agent, in the reaction solution decreased the product yielding dramatically, which indicates that this reaction is governed by radical pathways. LC-MS (liquid chromatography-mass spectrometry) analysis of such reaction mixture revealed that radical intermediate **int-i** and **int-ii** were likely involved in the reaction. (**Figure 2.1B** and **Scheme 2.3**)

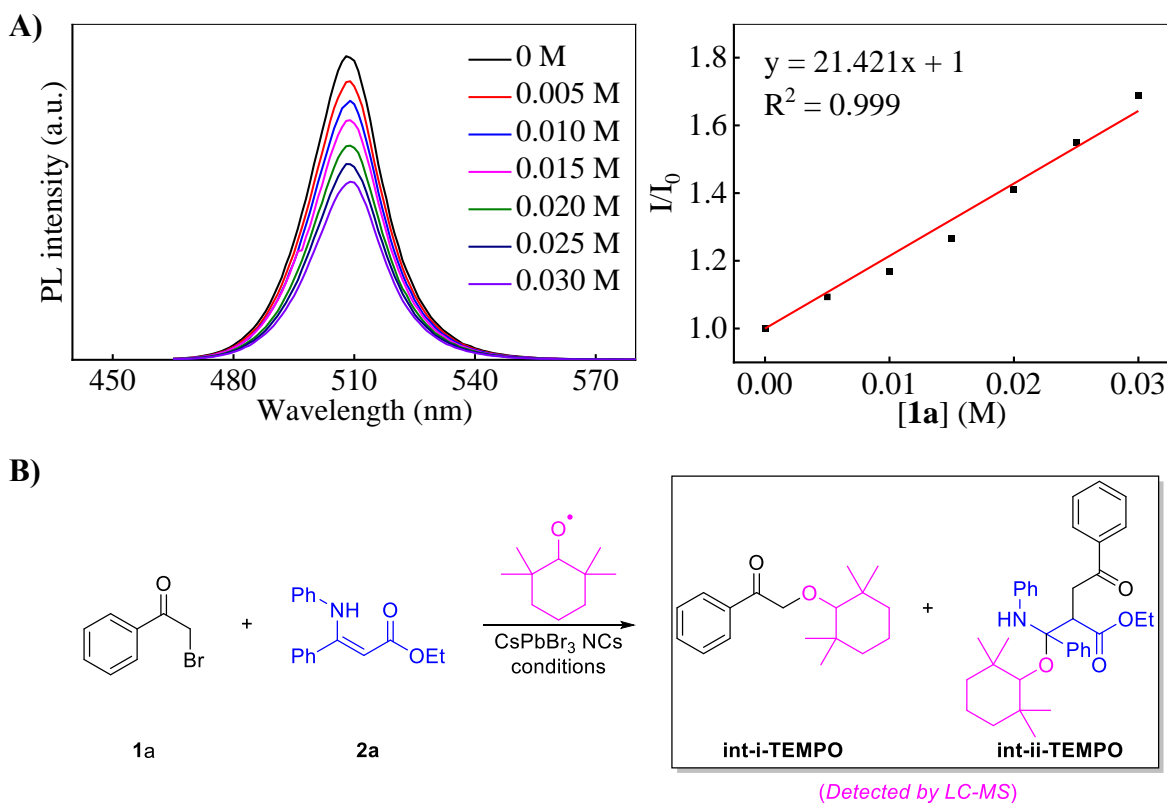
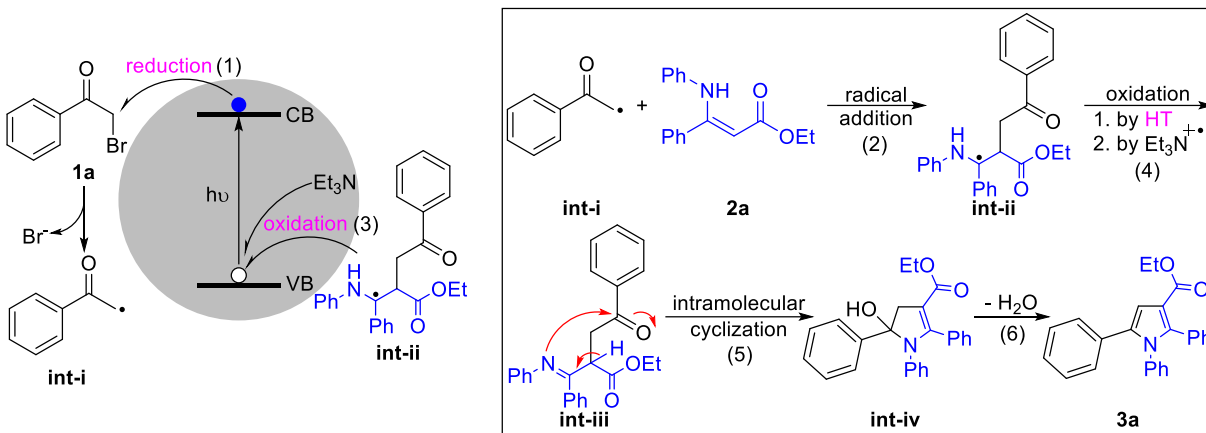


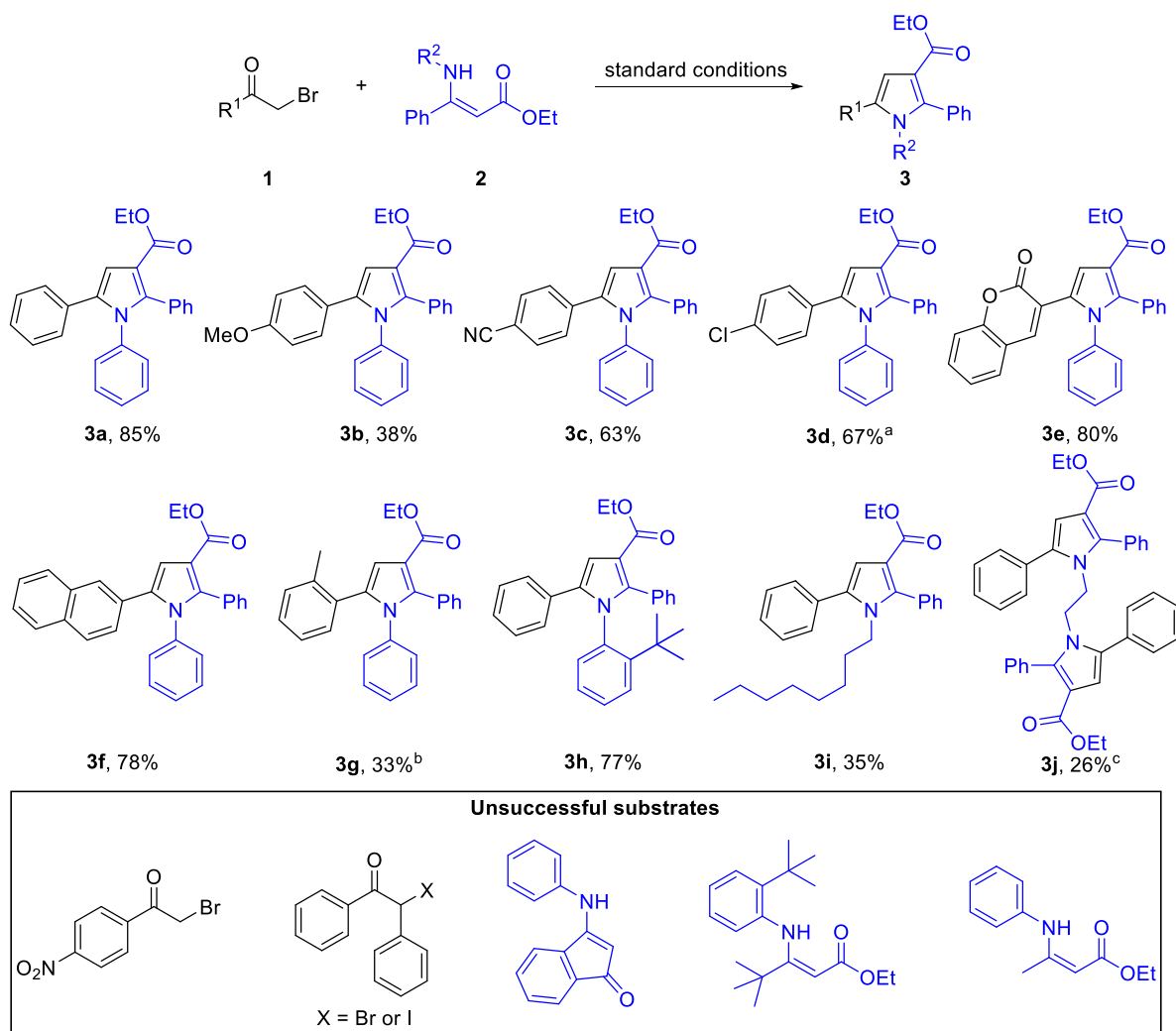
Figure 2.1 **A)** Stern-Volmer PL quenching study of CsPbBr₃ NCs in the presence of various concentration of **1a**. **B)** Radical trapping experiment by using TEMPO.

A reaction mechanism is proposed herein based on the above experimental results. (**Scheme 2.3**) Upon visible light excitation, (1) single electron transfer (SET) takes place from NCs* to reduce the starting material **1a** which then undergoes a rapid mesolytic cleavage to afford the radical intermediate **int-i**. (2) Subsequent radical addition of **int-i** to **2a** produces **int-ii**. (3) The CsPbBr₃ NCs photocatalyst can be regenerated via HT from the valence band (VB) of NCs to either **int-ii** or Et₃N, (4) producing the critical Hantzsch intermediate **int-iii** or Et₃N radical cation which may also oxidize **int-ii** to form **int-iii**. The substituted pyrrole product **3a** can be produced following the (5) intramolecular cyclization of **int-iii** and (6) subsequent dehydration.



Scheme 2.3 Proposed mechanism for the NCs-photocatalyzed synthesis of pyrrole derivatives. CB: conduction band. VB: valence band. int: intermediate. HT: hole transfer.

With the optimized reaction conditions and a plausible reaction mechanism in hand, we sought to explore the substrate scope of this reaction. (**Scheme 2.4**) With respect to the substrate **1**, we observed that 2-bromoacetophenone bearing a strong electron donating group (4'-OMe) only delivered product in moderate yield (**3b**). In contrast, electron-deficient 2-bromoacetophenone proceeded with good efficiency (**3c**). Not limited to the 2-bromoketones, 2,4'-dichloroacetophenone could also generate the desired product, leaving the para-chloro group unaffected thus providing a synthetic handle for further functionalization (**3d**). Remarkably, a natural compound derived 3-(bromoacetyl)coumarin was converted to the pyrrole product in very good yield (**3e**). 2-(Bromoacetyl)naphthalene featuring a fused aromatic ring was also a successful substrate (**3f**). Sterically hindered 2-bromo-2'-methylacetophenone affected the yield significantly (**3g**) while a much bulkier ortho *tert*-butyl group present on the *N*-phenyl substituent on the enamine substrate **2** only mildly affected the yield (**3h**). In addition to *N*-phenyl enamine, *N*-alkyl enamine was also shown feasible (**3i**). Finally, a bis-enamine with an *N*-ethylene linkage underwent two cyclization reactions on each molecule provided the desired bis-pyrrole product in acceptable yield (**3j**).



Scheme 2.4 Scope of NCs-photocatalyzed synthesis of pyrrole derivatives.

^a2,4'-Dichloroacetophenone was used as starting material **1**.

^bReaction run for 24h.

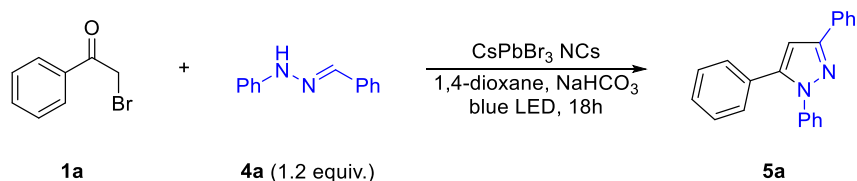
^c3.0 equivalent of starting material **1** was used.

2.3.2 NCs-Photocatalyzed Synthesis of Pyrazole Derivatives

To validate our hypothesis that the Hantzsch pyrrole synthesis via a radical pathway may be translated to pyrazole synthesis, (**Scheme 2.2C**) we replaced the enamine **2a** with a hydrazone **4a** to explore suitable reaction conditions. Gratifyingly, the expected pyrazole product **5a** could be produced in good yield as shown in **Table 2.2**. Notably, this reaction could also run without N_2 sparging with no significant impact on the product yielding (entry 1 and 2). Running the reaction without base was detrimental to the yield, probably because a stoichiometric amount of base helped

neutralizing the HBr side product which may cause unwanted degradation of starting material **4a** (e.g., hydrolysis). Both CsPbBr₃ NCs photocatalyst and light irradiation were found essential to a successful conversion (entry 6 and 7).

Table 2.2 Condition exploration for the NCs-photocatalyzed synthesis of pyrazole derivatives.



entry	deviation from standard conditions ^a	yield, % ^b
1	None	81
2	Under N ₂	83
3	Tetrahydrofuran as solvent	71
4	CsPbBr ₃ NCs (2.0 mg)	59
5	No NaHCO ₃	22
6	No CsPbBr ₃ NCs	<1
7	No light	<1

^aStandard conditions: **1a** (0.20 mmol, 0.1 M), **4a** (0.24 mmol, 1.2 equiv.), CsPbBr₃ NCs (5.0 mg), 1,4-dioxane (2.0 mL), NaHCO₃ (1.0 equiv.). Reaction was performed under household blue LED irradiation without N₂ sparging at room temperature for 18h.

^bYields were determined by ¹H NMR.

Mechanistic investigation was carried out after determining the reaction conditions. As discussed in the pyrrole section above, both electrochemical and spectroscopic studies suggested that NCs* could reduce **1a** (**Figure 2.1A** and **2.3**). On the other hand, we also observed a significant PL quenching of NCs by the starting material **4a**, with a quenching constant of 50.8 M⁻¹ (**Figure 2.2A**). Conducting cyclic voltammetry measurement on **4a** revealed that its oxidation potential ($E_{\text{ox}} = +1.00$ V vs. SCE, **Figure 2.4**) falls in the photoredox potentials of CsPbBr₃ NCs

($E_{CB} = -1.3$ V, $E_{VB} = +1.1$ V, all vs. SCE), suggesting the single-electron oxidation of **4a** by NCs* is thermodynamically feasible. Radical trapping experiment by adding TEMPO in the reaction mixture was again performed to study the involved radical species in this reaction. We successfully verified the TEMPO trapping product of **int-I** and identified the trapping product of **int-II** in LC-MS. (**Figure 2.2B** and **Scheme 2.5**)

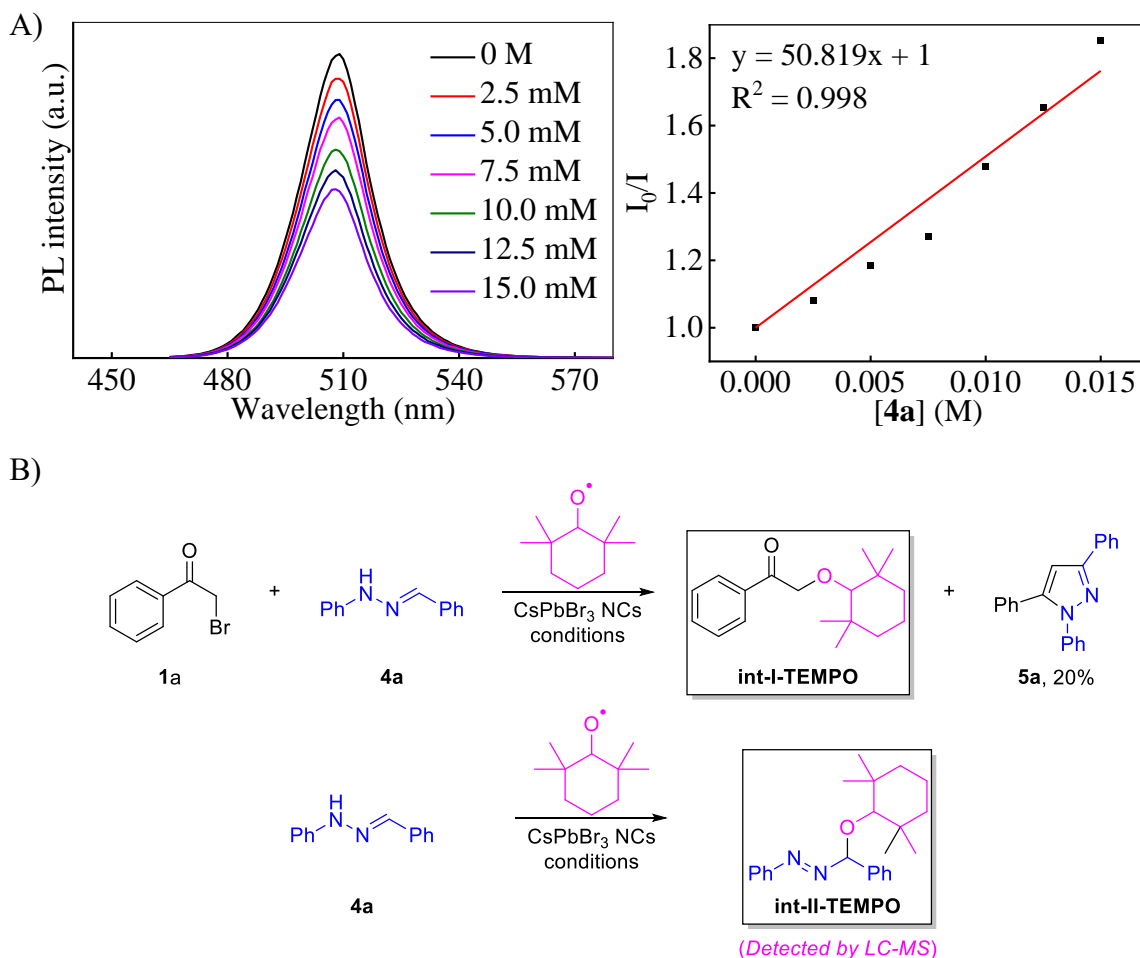
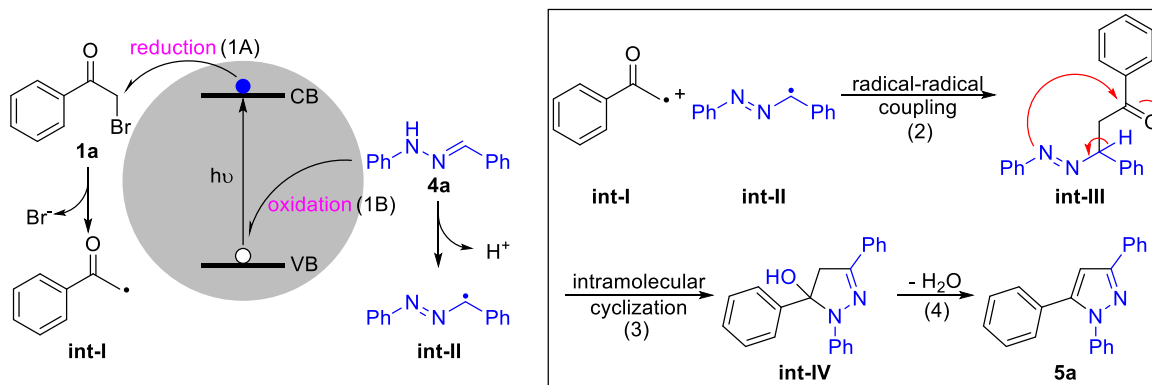


Figure 2.2 A) Stern-Volmer PL quenching study of CsPbBr₃ NCs in the presence of various concentration of **4a**. B) Radical trapping experiment by using TEMPO.

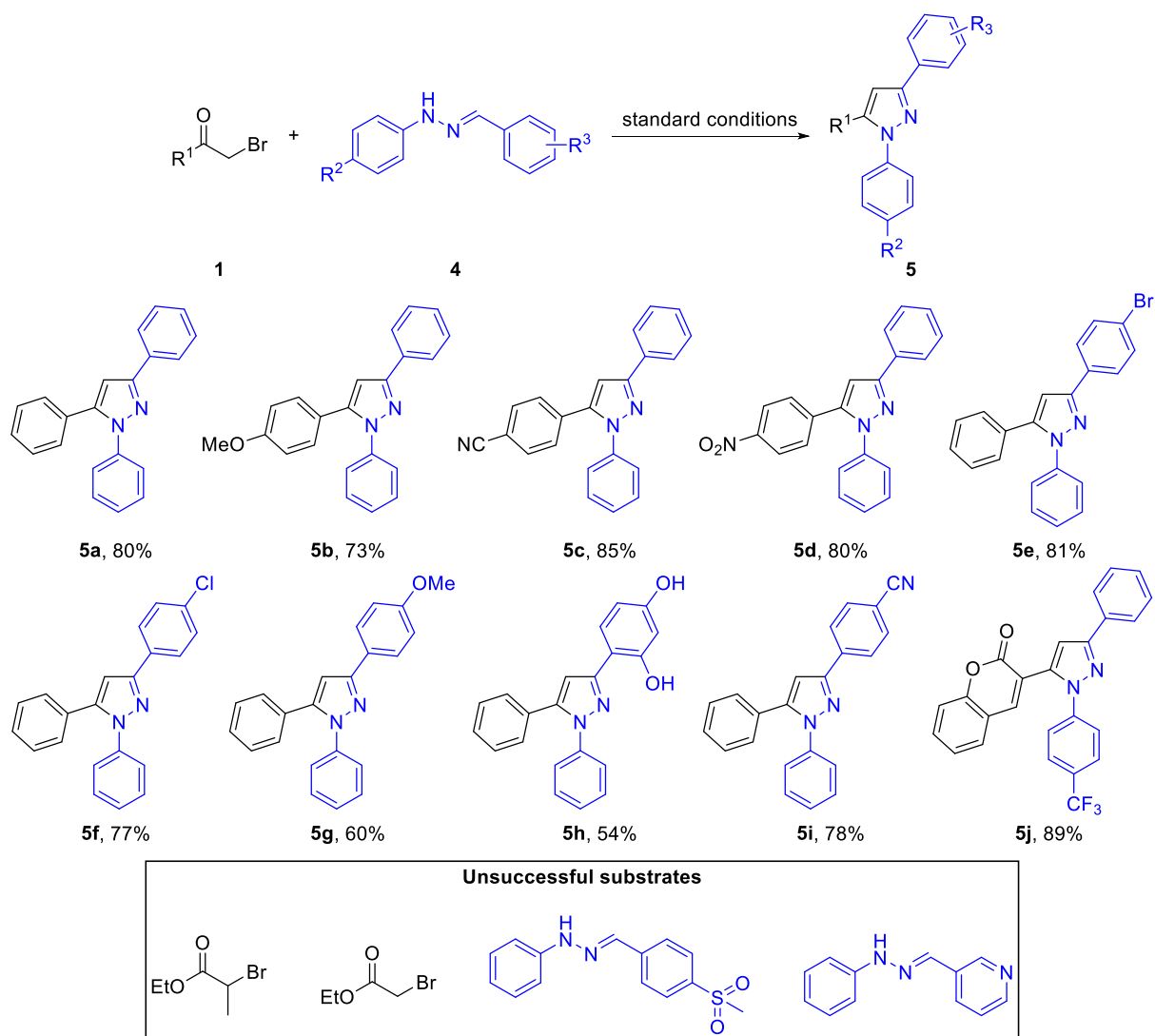
Collectively, this reaction is proposed to proceed first via (1A) single-electron reduction of **1a** and (1B) single electron oxidation of **4a** to give radical intermediate **int-I** and **int-II** respectively, meanwhile completing the photoredox cycle. (2) Subsequently, radical-radical

coupling between **int-I** and **int-II** leads to the critical Hantzsch-like intermediate **int-III**, which then undergoes sequential (3) intramolecular cyclization and (4) dehydration to produce the final substituted pyrazole product **5a**. (**Scheme 2.5**) Of note is that the mechanistic studies cannot rule out the pyrazole formation undergoes a radical addition mechanism like it is shown in the **Scheme 2.3**.



Scheme 2.5 Proposed mechanism for the NCs-photocatalyzed synthesis of pyrazole derivatives. CB: conduction band. VB: valence band. int: intermediate.

Similar to the study of pyrroles, we initiated the substrate scope survey for the photocatalytic synthesis of pyrazoles. (**Scheme 2.6**) Gratifyingly, various electronically biased 2-bromoacetophenone were well-tolerated (**5a-d**). Variations on the hydrazones **4** were also found viable. 4-halobenzaldehyde derived hydrazones were highly successful substrates (**5e and 5f**). Both electron-rich and electron-deficient hydrazones were converted to respective pyrazole derivatives with good to excellent efficiencies (**5g-i**). Notably, **5h** with a highly polar 1,3-dihydroxyphenyl group was produced in good yield, highlighting an opportunity to introduce hydrophilic functional group to these pyrazole scaffolds to optimize their aqueous solubility, which is an important physicochemical property of compounds in drug discovery. Lastly, an analog to an anti-inflammatory agent was synthesized in excellent yield using this method (**5j**).



Scheme 2.6 Scope of NCs-photocatalyzed synthesis of pyrazole derivatives.

2.4 Chapter Conclusion

In conclusion, we have developed a benign, efficient, and experimentally simple CsPbBr₃ NCs-photocatalyzed approach to synthesize a diverse array of substituted pyrrole and pyrazole derivatives. Both types of reactions were proposed to proceed through a key α -ketone radical generated by the conduction band-based single electron transfer from excited-state NCs to the α -bromoketone starting material. Such α -ketone radical readily engages in cascade reactions with stable enamine or hydrazone radical to produce the targeted pyrrole or pyrazole products. This

method reported herein demonstrates the versatility of lead-halide perovskite photocatalysis and expands its application in the realm of N-heterocycle synthesis.

2.5 Experimental Section

2.5.1 General Information

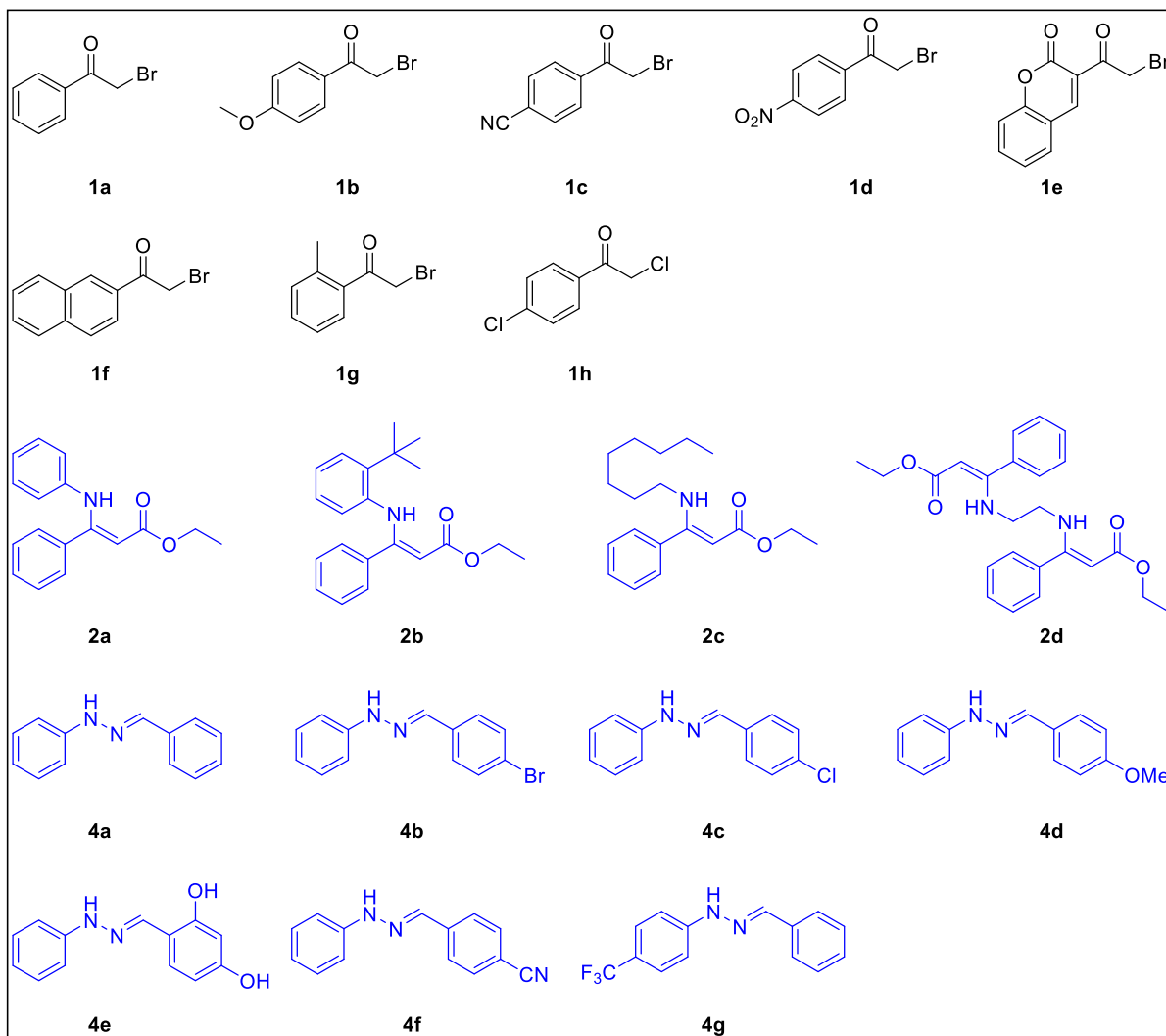
Commercially available reagents and solvents were purchased from TCI Chemicals, Fisher Scientific and Sigma-Aldrich and were used as received if not stated otherwise. Two household blue LED lamps (12 W) were used for all photochemical reactions. Silica gels (P60, 40-63 μm , 60 Å) used for column chromatography were purchased from SILICYCLE. Thin layer chromatography (TLC) analysis was carried out on aluminum backed silica gel coated plates (200 μm , SILICYCLE). Visualization was completed by a Analytikjena hand-held UV lamp (254 nm).

^1H , ^{13}C , ^{19}F NMR spectra were acquired on a Varian VNMRS 400 spectrometer/Varian Inova 500 spectrometer/Bruker AVANCE Neo 500 spectrometer/Bruker Avance AV1 400 spectrometer. All chemical shifts are reported in parts per million (ppm) referenced to residual chloroform (7.26 ppm and 77.16 ppm, respectively for ^1H and ^{13}C NMR), unless otherwise noted. All coupling constants (J) are reported in hertz (Hz). Abbreviations for multiplicity are: s, singlet; br s, broad singlet; d, doublet; t, triplet; q, quartet; p, pentet; hept, heptet; m, multiplet. All the NMR spectra were processed using Mestrenova software applying standard baseline corrections. ^1H NMR data were recorded for all compounds for characterization purposes. Mass spectra were recorded on an Agilent 7890A GC system coupled with a 5975 MSD (Gas Chromatography-Mass Spectrometry, GC-MS) with an electron ionization (EI) method or Agilent 1100 series LC system coupled with a FINNIGAN LTQ MSD (Liquid Chromatography-Mass Spectrometry, LC-MS) with an electrospray ionization (ESI) method. Steady-state emission spectra were acquired using a HORIBA Fluoromax-4 spectrofluorometer. Cyclic voltammetry data were recorded on a CH Instruments CHI660E Electrochemical Analyzer.

2.5.2 Preparation of CsPbBr₃ NCs Photocatalyst

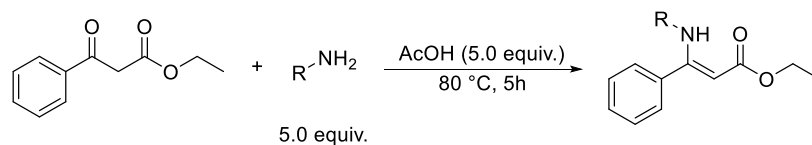
The synthesis of CsPbBr₃ perovskite nanocrystals was adapted from literature with minor modifications.^{11, 12} PbBr₂ solution (3.0 mL, 0.67 M in DMF) and CsBr solution (2.0 mL, 1.0 M in H₂O) were prepared in advance as precursor solutions. To a vigorously stirring solution containing hexanes (500 mL), oleic acid (8.0 mL) and *n*-octylamine (1.5 mL), the PbBr₂ and CsBr precursor solutions were added dropwise. Along with mixing, an emulsion formed and the color of the resulting mixture turned from clear to slightly pale yellow. After that, acetone (400 mL) was added for the demulsion process. The CsPbBr₃ nanocrystals were isolated by centrifugation at 7000 rpm for 10 min then dried under open air.

2.5.3 Preparation of Starting Materials



Scheme 2.7 The substrate scope for the NCs-photocatalyzed syntheses of pyrrole and pyrazole derivatives.

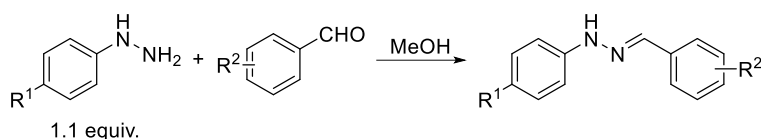
General Procedure A for the Synthesis of Stable Enamines¹³:



To a scintillation vial with a magnetic stirring bar was added primary amine (5.0 equiv.), acetic acid (5.0 equiv.) and ethyl benzoylacetate (1.0 equiv.). The resulting mixture was allowed to react at 80 °C for 5h. Upon completion, the reaction mixture was diluted with water and

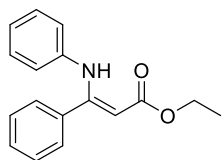
extracted with CH₂Cl₂ for three times. The combined organic phase was washed with brine, dried over Na₂SO₄, and concentrated using a rotary evaporator. Then the product was purified by flash column chromatography on silica gel using a combination of hexanes and EtOAc as eluent.

General Procedure B for the Synthesis of Hydrazones:



To a stirring phenylhydrazine solution (1.1 equiv., 3 M in MeOH) in a scintillation vial, benzaldehyde solution (1.0 equiv., 1 M in MeOH) was added dropwise at room temperature. The product would generally precipitate out from the solution during the course of addition. The resulting mixture was allowed to stir at room temperature or reflux temperature for a prolonged period of time until the conversion of benzaldehydes was complete (monitored by TLC). Finally, the product was collected via vacuum filtration and purified by washing with cold MeOH solvent.

Synthesis of Stable Enamines (2a-d)

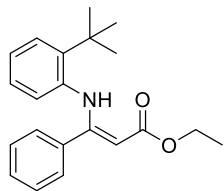


ethyl (Z)-3-phenyl-3-(phenylamino)acrylate (2a)

The titled compound was synthesized following **General Procedure A**:

Aniline (2282.6 μ L, 25.0 mmol, 5.0 equiv.), acetic acid (1429.8 μ L, 25.0 mmol, 5.0 equiv.) and ethyl benzoylacetate (865.8 μ L, 5.0 mmol, 1.0 equiv.) were used. The product was purified by flash column chromatography on silica gel (Hexanes/EtOAc = 20/1) as light-yellow solid (83% **yield**, 1109 mg). The ¹H NMR spectra matched those reported in the literature.¹³

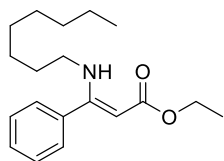
¹H NMR (500 MHz, CDCl₃) δ 7.76 – 7.71 (m, 1H), 7.66 – 7.57 (m, 3H), 7.44 – 7.39 (m, 2H), 7.23 – 7.20 (m, 5H), 7.18 – 7.12 (m, 4H), 7.07 (s, 1H), 6.97 (d, *J* = 7.5 Hz, 2H), 4.19 (q, *J* = 7.0 Hz, 2H), 1.19 (t, *J* = 7.0 Hz, 3H).



ethyl (Z)-3-((2-(tert-butyl)phenyl)amino)-3-phenylacrylate (2b)

The titled compound was synthesized following **General Procedure A** with minor modification: 2-*tert*-Butylaniline (1247.5 μ L, 8.0 mmol, **4.0 equiv.**), acetic acid (457.5 μ L, 8.0 mmol, **4.0 equiv.**) and ethyl benzoylacetate (346.3 μ L, 2.0 mmol, 1.0 equiv.) were used and the reaction was run **overnight**. The product was purified by flash column chromatography on silica gel (Hexanes/EtOAc = 20/1) as viscous red oil (90% **yield**, 582 mg).

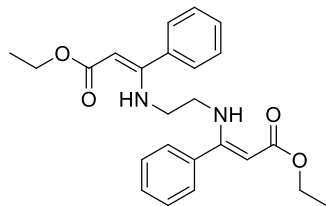
$^1\text{H NMR}$ (400 MHz, CDCl_3) δ 10.41 (s, 1H), 7.36 (dd, $J = 8.0, 1.6$ Hz, 1H), 7.31 – 7.19 (m, 5H), 6.96 – 6.88 (m, 1H), 6.76 (td, $J = 7.6, 1.6$ Hz, 1H), 6.37 – 6.32 (m, 1H), 5.06 (s, 1H), 4.22 (q, $J = 7.2$ Hz, 2H), 1.60 (s, 9H), 1.32 (t, $J = 7.2$ Hz, 3H).



ethyl (Z)-3-(octylamino)-3-phenylacrylate (2c)

The titled compound was synthesized following **General Procedure A**: *n*-Octylamine (1652.7 μ L, 10.0 mmol, 5.0 equiv.), acetic acid (571.9 μ L, 10.0 mmol, 5.0 equiv.) and ethyl benzoylacetate (346.3 μ L, 2.0 mmol, 1.0 equiv.) were used. The product was purified by flash column chromatography on silica gel (Hexanes/EtOAc = 20/1) as colorless oil (85% **yield**, 516 mg).

$^1\text{H NMR}$ (400 MHz, CDCl_3) δ 8.54 (s, 1H), 7.44 – 7.32 (m, 5H), 4.56 (s, 1H), 4.15 (q, $J = 7.2$ Hz, 2H), 3.08 – 2.99 (m, 2H), 1.46 (p, $J = 7.2$ Hz, 2H), 1.31 – 1.16 (m, 13H), 0.86 (t, $J = 7.2$ Hz, 3H).



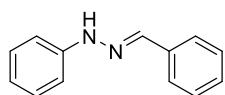
diethyl 3,3'-(ethane-1,2-diylbis(azanediyl))(2Z,2'Z)-bis(3-phenylacrylate) (2d)

The titled compound was synthesized according to the following procedure: To a 50-mL round bottom flask with a magnetic stirring bar, toluene (2 mL), ethyl benzoylacetate (346.3 μ L, 2.0 mmol, 2.0 equiv.), ethylenediamine (66.9 μ L, 1.0 mmol, 1.0 equiv.) and MgSO_4 (1204 mg, 10 mmol, 10 equiv.) were added. Then the resulting mixture was allowed

to react at reflux temperature for 8h. Upon completion, the reaction mixture was first filtered, then concentrated using a rotary evaporator. The product was purified by flash column chromatography on silica gel (Hexanes/EtOAc = 10/1) as white solid (73% **yield**, 297 mg).

¹H NMR (400 MHz, CDCl₃) δ 8.47 (br s, 2H), 7.43 – 7.29 (m, 6H), 7.24 – 7.16 (m, 4H), 4.58 (s, 2H), 4.14 (q, *J* = 7.2 Hz, 4H), 3.15 – 3.04 (m, 4H), 1.28 (t, *J* = 7.2 Hz, 6H).

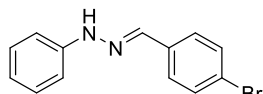
Synthesis of Hydrazones (4a-g)



(E)-1-benzylidene-2-phenylhydrazine (4a)

The titled compound was synthesized following **General Procedure B**: Phenylhydrazine (540.7 μL, 5.5 mmol, 1.1 equiv.), benzaldehyde (510.2 μL, 5.0 mmol, 1.0 equiv.) and MeOH (7 mL) were used. The product was obtained as a light-yellow solid (93% **yield**, 913 mg). The ¹H NMR spectra matched those reported in the literature.¹⁴

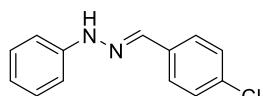
¹H NMR (400 MHz, CDCl₃) δ 7.75 – 7.62 (m, 3H), 7.41 – 7.27 (m, 5H), 7.18 – 7.05 (m, 2H), 6.92 – 6.83 (m, 1H).



(E)-1-(4-bromobenzylidene)-2-phenylhydrazine (4b)

The titled compound was synthesized following **General Procedure B**: Phenylhydrazine (324.4 μL, 3.3 mmol, 1.1 equiv.), 4-bromobenzaldehyde (555.1 mg, 3.0 mmol, 1.0 equiv.) and MeOH (4 mL) were used. The product was obtained as a light-yellow solid (86% **yield**, 710 mg). The ¹H NMR spectra matched those reported in the literature.¹⁴

¹H NMR (400 MHz, CDCl₃) δ 7.66 (s, 1H), 7.62 (s, 1H), 7.55 – 7.46 (m, 4H), 7.32 – 7.26 (m, 2H), 7.14 – 7.08 (m, 2H), 6.93 – 6.85 (m, 1H).

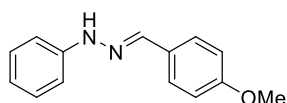


(E)-1-(4-chlorobenzylidene)-2-phenylhydrazine (4c)

The titled compound was synthesized following **General Procedure B**: Phenylhydrazine (324.4 μL, 3.3 mmol, 1.1 equiv.), 4-chlorobenzaldehyde (421.7 mg, 3.0 mmol,

1.0 equiv.) and MeOH (4 mL) were used. The product was obtained as a light-yellow solid (55% **yield**, 381 mg). The ^1H NMR spectra matched those reported in the literature.¹⁴

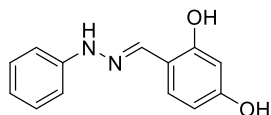
^1H NMR (400 MHz, CDCl_3) δ 7.70 – 7.61 (m, 2H), 7.59 (d, $J = 8.8$ Hz, 2H), 7.34 (d, $J = 8.8$ Hz, 2H), 7.31 – 7.26 (m, 2H), 7.15 – 7.06 (m, 2H), 6.93 – 6.85 (m, 1H).



(E)-1-(4-methoxybenzylidene)-2-phenylhydrazine (4d)

The titled compound was synthesized following **General Procedure B**: Phenylhydrazine (324.4 μL , 3.3 mmol, 1.1 equiv.), 4-anisaldehyde (364.7 μL , 3.0 mmol, 1.0 equiv.) and MeOH (4 mL) were used. The product was obtained as a light-yellow solid (77% **yield**, 523 mg). The ^1H NMR spectra matched those reported in the literature.¹⁵

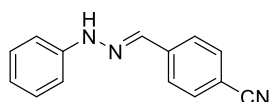
^1H NMR (400 MHz, CDCl_3) δ 7.66 (s, 1H), 7.60 (d, $J = 8.8$ Hz, 2H), 7.49 (br s, 1H), 7.30 – 7.24 (m, 2H), 7.14 – 7.06 (m, 2H), 6.91 (d, $J = 8.8$ Hz, 2H), 6.88 – 6.83 (m, 1H), 3.84 (s, 3H).



(E)-4-((2-phenylhydrazineylidene)methyl)benzene-1,3-diol (4e)

The titled compound was synthesized following **General Procedure B** with minor modification: Phenylhydrazine (324.4 μL , 3.3 mmol, 1.1 equiv.), 2,4-dihydroxybenzaldehyde (414.4 mg, 3.0 mmol, 1.0 equiv.) and MeOH (4 mL) were used. No precipitation was observed during the reaction. Upon completion, the reaction mixture was first concentrated using a rotary evaporator, then transferred to an **antisolvent** Et_2O . The product was collected via vacuum filtration and purified by washing with cold Et_2O solvent as a light-brown solid (47% **yield**, 322 mg).

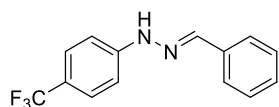
^1H NMR (400 MHz, CDCl_3) δ 11.10 (s, 1H), 7.83 (s, 1H), 7.35 – 7.27 (m, 3H), 7.03 (d, $J = 8.4$ Hz, 1H), 6.99 – 6.94 (m, 2H), 6.93 – 6.88 (m, 1H), 6.47 (d, $J = 2.4$ Hz, 1H), 6.40 (dd, $J = 8.4, 2.4$ Hz, 1H), 4.94 (br s, 1H).



(E)-4-((2-phenylhydrazineylidene)methyl)benzonitrile (4f)

The titled compound was synthesized following **General Procedure B**: Phenylhydrazine (324.4 μL , 3.3 mmol, 1.1 equiv.), 4-formylbenzotrile (393.4 mg, 3.0 mmol, 1.0 equiv.) and MeOH (4 mL) were used. Reflux temperature was applied. The product was obtained as a bright -yellow solid (91% **yield**, 604 mg). The ^1H NMR spectra matched those reported in the literature. ¹⁴

^1H NMR (400 MHz, CDCl_3) δ 7.90 (s, 1H), 7.73 (d, $J = 8.4$ Hz, 2H), 7.67 – 7.61 (m, 3H), 7.34 – 7.27 (m, 2H), 7.16 – 7.10 (m, 2H), 6.97 – 6.91 (m, 1H).



(E)-1-benzylidene-2-(4-(trifluoromethyl)phenyl)hydrazine (4g)

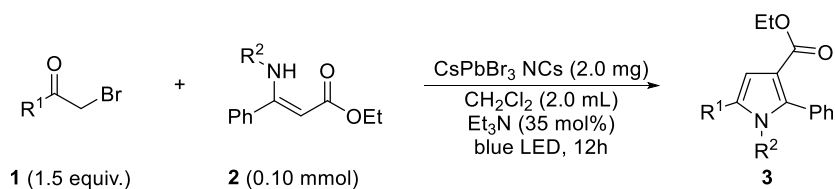
The titled compound was synthesized following **General Procedure B** with minor modification: 4-(trifluoromethyl)phenylhydrazine solution (3.3 mL, **1 M in MeOH**) and benzaldehyde solution (1.0 mL, **3 M in MeOH**) were used. Reflux temperature was applied. No precipitation was observed during the reaction. Upon completion, the reaction mixture was first concentrated using a rotary evaporator, then transferred to a mixed **antisolvent** Hexanes/ Et_2O . The product was collected via vacuum filtration and purified by washing with cold Hexanes/ Et_2O solvent as a light-yellow solid (42% **yield**, 333 mg). The ^1H NMR spectra matched those reported in the literature. ¹⁶

^1H NMR (400 MHz, CDCl_3) δ 7.78 (br s, 1H), 7.74 (s, 1H), 7.72 – 7.63 (m, 2H), 7.51 (d, $J = 8.4$ Hz, 2H), 7.44 – 7.30 (m, 3H), 7.16 (d, $J = 8.4$ Hz, 2H).

^{19}F NMR (376 MHz, CDCl_3) δ -61.33.

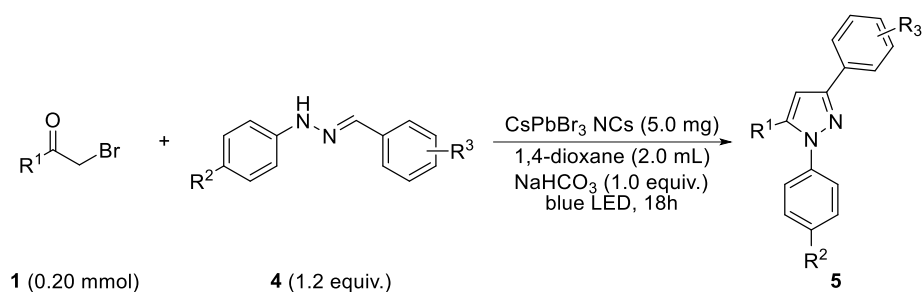
2.5.4 Photocatalytic Synthesis of Products

General Procedure C for the NCs-Photocatalyzed Synthesis of Pyrrole Derivatives:



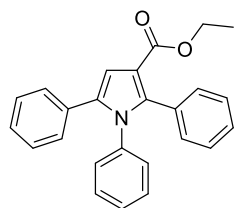
To a 1-dram vial with a magnetic stirring bar was added 2-bromoketone **1** (0.15 mmol, 1.5 equiv.), enamine **2** (0.10 mmol, 1.0 equiv.), CsPbBr₃ perovskite photocatalyst (2.0 mg), CH₂Cl₂ (2.0 mL) and Et₃N (0.035 mmol, 35 mol%). The resulting mixture was allowed to react at room temperature under blue LED (12 W *2) irradiation for 12h. Upon completion, the solvent was removed using a rotary evaporator. Then the product **3** was purified by flash column chromatography on silica gel using a combination of hexanes and EtOAc as eluent.

General Procedure D for the NCs-Photocatalyzed Synthesis of Pyrazole Derivatives:



To a 1-dram vial with a magnetic stirring bar was added 2-bromoketone **1** (0.20 mmol, 1.0 equiv.), hydrazone **4** (0.24 mmol, 1.2 equiv.), NaHCO₃ (0.2 mmol, 1.0 equiv.), CsPbBr₃ perovskite photocatalyst (5.0 mg) and 1,4-dioxane (2.0 mL). The resulting mixture was allowed to react at room temperature under blue LED (12 W *2) irradiation for 18h. Upon completion, the reaction mixture was first diluted with CH₂Cl₂ and transferred to a separatory funnel. Next, it was washed with water and extracted with CH₂Cl₂. The combined organic phase was washed with brine and dried over Na₂SO₄ before the solvent was removed using a rotary evaporator. Then the product **5** was purified by flash column chromatography on silica gel using a combination of hexanes and EtOAc as eluent.

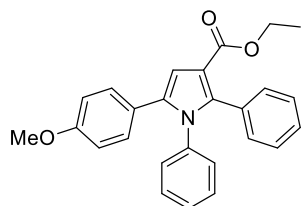
Photocatalytic Synthesis of Pyrrole Derivatives (3a-j)



ethyl 1,2,5-triphenyl-1H-pyrrole-3-carboxylate (3a)

The titled compound was synthesized following **General Procedure C**: 2-Bromoacetophenone (**1a**, 29.9 mg, 0.15 mmol, 1.5 equiv.), ethyl (*Z*)-3-phenyl-3-(phenylamino)acrylate (**2a**, 26.7 mg, 0.10 mmol, 1.0 equiv.), CsPbBr₃ perovskite photocatalyst (2.0 mg), CH₂Cl₂ (2.0 mL) and Et₃N (4.88 μL, 0.035 mmol, 35 mol%) were used. The product was purified by flash column chromatography on silica gel (Hexanes/EtOAc = 33/1 – 25/1) as white solid (80% **yield**, 31.2 mg). The ¹H NMR spectra matched those reported in the literature.¹⁷

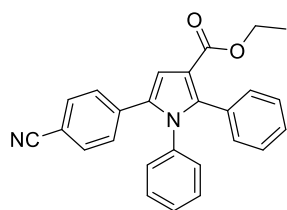
¹H NMR (400 MHz, CDCl₃) δ 7.23 – 7.12 (m, 11H), 7.11 – 7.06 (m, 2H), 6.95 (s, 1H), 6.94 – 6.90 (m, 2H), 4.18 (q, *J* = 7.2 Hz, 2H), 1.19 (t, *J* = 7.2 Hz, 3H).



ethyl 5-(4-methoxyphenyl)-1,2-diphenyl-1H-pyrrole-3-carboxylate (3b)

The titled compound was synthesized following **General Procedure C**: 2-Bromo-4'-methoxyacetophenone (**1b**, 34.4 mg, 0.15 mmol, 1.5 equiv.), ethyl (*Z*)-3-phenyl-3-(phenylamino)acrylate (**2a**, 26.7 mg, 0.10 mmol, 1.0 equiv.), CsPbBr₃ perovskite photocatalyst (2.0 mg), CH₂Cl₂ (2.0 mL) and Et₃N (4.88 μL, 0.035 mmol, 35 mol%) were used. The product was purified by flash column chromatography on silica gel (Hexanes/EtOAc = 30/1 – 20/1) as white solid (38% **yield**, 15.1 mg).

¹H NMR (500 MHz, CDCl₃) δ 7.22 – 7.12 (m, 8H), 7.00 (d, *J* = 9.0 Hz, 2H), 6.91 (dd, *J* = 8.0, 1.5 Hz, 2H), 6.86 (s, 1H), 6.72 (d, *J* = 9.0 Hz, 2H), 4.17 (q, *J* = 7.0 Hz, 2H), 3.75 (s, 3H), 1.17 (t, *J* = 7.0 Hz, 3H).

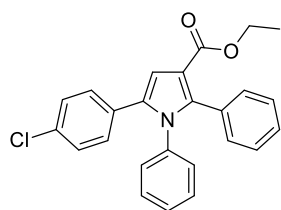


ethyl 5-(4-cyanophenyl)-1,2-diphenyl-1H-pyrrole-3-carboxylate (3c)

The titled compound was synthesized following **General Procedure C**:

2-Bromo-4'-cyanoacetophenone (**1c**, 33.6 mg, 0.15 mmol, 1.5 equiv.), ethyl (*Z*)-3-phenyl-3-(phenylamino)acrylate (**2a**, 26.7 mg, 0.10 mmol, 1.0 equiv.), CsPbBr₃ perovskite photocatalyst (2.0 mg), CH₂Cl₂ (2.0 mL) and Et₃N (4.88 μL, 0.035 mmol, 35 mol%) were used. The product was purified by flash column chromatography on silica gel (Hexanes/EtOAc = 20/1 – 10/1) as white solid (63% **yield**, 24.7 mg).

¹H NMR (500 MHz, CDCl₃) δ 7.45 (d, *J* = 8.0 Hz, 2H), 7.25 – 7.13 (m, 10H), 7.07 (s, 1H), 6.92 (d, *J* = 8.0 Hz, 2H), 4.17 (q, *J* = 7.0 Hz, 2H), 1.17 (t, *J* = 7.0 Hz, 3H).

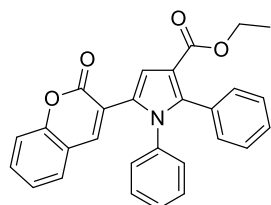


ethyl 5-(4-chlorophenyl)-1,2-diphenyl-1H-pyrrole-3-carboxylate (3d)

The titled compound was synthesized following **General Procedure C** with minor modification: **2,4'-Dichloroacetophenone (1h**, 28.4 mg,

0.15 mmol, 1.5 equiv.), ethyl (*Z*)-3-phenyl-3-(phenylamino)acrylate (**2a**, 26.7 mg, 0.10 mmol, 1.0 equiv.), CsPbBr₃ perovskite photocatalyst (2.0 mg), CH₂Cl₂ (2.0 mL) and Et₃N (4.88 μL, 0.035 mmol, 35 mol%) were used. The product was purified by flash column chromatography on silica gel (Hexanes/EtOAc = 20/1 – 10/1) as white solid (67% **yield**, 26.9 mg).

¹H NMR (400 MHz, CDCl₃) δ 7.22 – 7.12 (m, 10H), 7.02 – 6.98 (m, 2H), 6.94 (s, 1H), 6.92 – 6.88 (m, 2H), 4.17 (q, *J* = 7.2 Hz, 2H), 1.17 (t, *J* = 7.2 Hz, 3H).



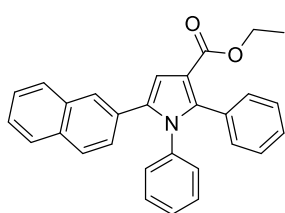
ethyl 5-(2-oxo-2H-chromen-3-yl)-1,2-diphenyl-1H-pyrrole-3-carboxylate (3e)

The titled compound was synthesized following **General Procedure C**: 3-(Bromoacetyl)coumarin (**1e**, 40.1 mg, 0.15 mmol, 1.5 equiv.), ethyl (*Z*)-3-phenyl-3-

(phenylamino)acrylate (**2a**, 26.7 mg, 0.10 mmol, 1.0 equiv.), CsPbBr₃ perovskite photocatalyst (2.0 mg), CH₂Cl₂ (2.0 mL) and Et₃N (4.88 μL, 0.035 mmol, 35 mol%) were used. The product was purified by flash column chromatography on silica gel (Hexanes/EtOAc = 10/1 – 4/1) as light-yellow solid (80% **yield**, 34.8 mg).

¹H NMR (400 MHz, CDCl₃) δ 7.46 (ddd, *J* = 8.8, 6.8, 2.0 Hz, 1H), 7.32 (s, 1H), 7.28 – 7.17 (m, 12H), 7.07 – 7.02 (m, 2H), 4.18 (q, *J* = 7.2 Hz, 2H), 1.19 (t, *J* = 7.2 Hz, 3H).

GC-MS (EI) *m/z* calcd for C₂₈H₂₁NO₄⁺ [*M*]⁺ 435.1, found: 435.1.

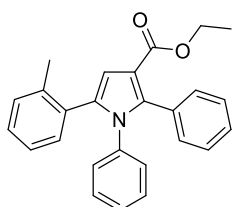


ethyl 5-(naphthalen-2-yl)-1,2-diphenyl-1*H*-pyrrole-3-carboxylate (3f**)**

The titled compound was synthesized following **General Procedure C**:

2-Bromo-2'-acetone (1f, 37.4 mg, 0.15 mmol, 1.5 equiv.), ethyl (*Z*)-3-phenyl-3-(phenylamino)acrylate (**2a**, 26.7 mg, 0.10 mmol, 1.0 equiv.), CsPbBr₃ perovskite photocatalyst (2.0 mg), CH₂Cl₂ (2.0 mL) and Et₃N (4.88 μL, 0.035 mmol, 35 mol%) were used. The product was purified by flash column chromatography on silica gel (Hexanes/EtOAc = 33/1 – 25/1) as white solid (78% **yield**, 32.6 mg). The ¹H NMR spectra matched those reported in the literature.¹⁷

¹H NMR (500 MHz, CDCl₃) δ 7.76 – 7.71 (m, 1H), 7.66 – 7.57 (m, 3H), 7.44 – 7.39 (m, 2H), 7.23 – 7.20 (m, 5H), 7.18 – 7.12 (m, 4H), 7.07 (s, 1H), 6.97 (d, *J* = 7.5 Hz, 2H), 4.19 (q, *J* = 7.0 Hz, 2H), 1.19 (t, *J* = 7.0 Hz, 3H).

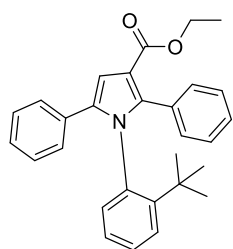


ethyl 1,2-diphenyl-5-(*o*-tolyl)-1*H*-pyrrole-3-carboxylate (3g**)**

The titled compound was synthesized following **General Procedure C**: 2-Bromo-2'-methylacetone (**1g**, 32.0 mg, 0.15 mmol, 1.5 equiv.), ethyl (*Z*)-3-phenyl-3-(phenylamino)acrylate (**2a**, 26.7 mg, 0.10 mmol, 1.0 equiv.), CsPbBr₃ perovskite photocatalyst (2.0 mg), CH₂Cl₂ (2.0 mL) and Et₃N (4.88 μL, 0.035 mmol, 35 mol%) were used to

react for 24h. The product was purified by flash column chromatography on silica gel (Hexanes/EtOAc = 33/1 – 25/1) as light-yellow solid (33% **yield**, 12.6 mg).

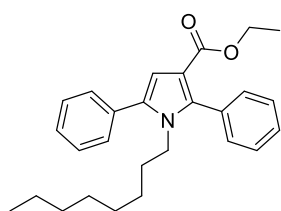
¹H NMR (400 MHz, CDCl₃) δ 7.22 – 7.19 (m, 5H), 7.16 – 6.99 (m, 7H), 6.82 – 6.77 (m, 3H), 4.18 (q, *J* = 7.2 Hz, 2H), 2.12 (s, 3H), 1.18 (t, *J* = 7.2 Hz, 3H).



ethyl 1-(2-(*tert*-butyl)phenyl)-2,5-diphenyl-1H-pyrrole-3-carboxylate (3h)

The titled compound was synthesized following **General Procedure C**: 2-Bromoacetophenone (**1a**, 29.9 mg, 0.15 mmol, 1.5 equiv.), ethyl (*Z*)-3-((2-(*tert*-butyl)phenyl)amino)-3-phenylacrylate (**2b**, 32.3 mg, 0.10 mmol, 1.0 equiv.), CsPbBr₃ perovskite photocatalyst (2.0 mg), CH₂Cl₂ (2.0 mL) and Et₃N (4.88 μL, 0.035 mmol, 35 mol%) were used. The product was purified by flash column chromatography on silica gel (Hexanes/EtOAc = 20/1 – 10/1) as white solid (77% **yield**, 32.6 mg).

¹H NMR (500 MHz, CDCl₃) δ 7.33 (d, *J* = 8.0 Hz, 1H), 7.26 – 7.07 (m, 13H), 7.01 (s, 1H), 4.24 – 4.12 (m, 2H), 1.19 (t, *J* = 7.0 Hz, 3H), 0.89 (s, 9H).

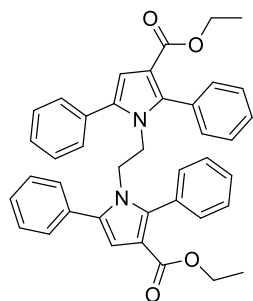


ethyl 1-octyl-2,5-diphenyl-1H-pyrrole-3-carboxylate (3i)

The titled compound was synthesized following **General Procedure C**: 2-Bromoacetophenone (**1a**, 29.9 mg, 0.15 mmol, 1.5 equiv.), ethyl (*Z*)-3-(octylamino)-3-phenylacrylate (**2c**, 30.3 mg, 0.10 mmol, 1.0 equiv.), CsPbBr₃ perovskite photocatalyst (2.0 mg), CH₂Cl₂ (2.0 mL) and Et₃N (4.88 μL, 0.035 mmol, 35 mol%) were used. The product was purified by flash column chromatography on silica gel (Hexanes/EtOAc = 20/1 – 10/1) as colorless oil (35% **yield**, 14.1 mg).

¹H NMR (500 MHz, CDCl₃) δ 7.47 – 7.34 (m, 10H), 6.70 (s, 1H), 4.11 (q, *J* = 7.0 Hz, 2H), 3.84 – 3.79 (m, 2H), 1.25 – 0.94 (m, 15H), 0.82 (t, *J* = 7.5 Hz, 3H).

GC-MS (EI) m/z calcd for $C_{27}H_{33}NO_2^+$ $[M]^+$ 403.3, found: 403.3.



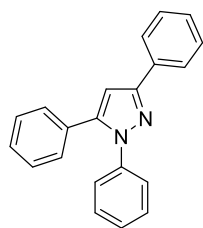
diethyl 1,1'-(ethane-1,2-diyl)bis(2,5-diphenyl-1H-pyrrole-3-carboxylate) (3j)

The titled compound was synthesized following **General Procedure C** with minor modification: 2-Bromoacetophenone (**1a**, 59.7 mg, 0.30 mmol, **3.0 equiv.**), diethyl 3,3'-(ethane-1,2-diylbis(azanediyl))(2Z,2'Z)-bis(3-phenylacrylate) (**2d**, 40.9 mg, 0.10 mmol, 1.0 equiv.), CsPbBr₃ perovskite photocatalyst (2.0 mg), CH₂Cl₂ (2.0 mL) and Et₃N (4.88 μ L, 0.035 mmol, 35 mol%) were used. The product was purified by flash column chromatography on silica gel (Hexanes/EtOAc = 10/1) as white solid (26% **yield**, 15.8 mg).

¹H NMR (400 MHz, CDCl₃) δ 7.36 – 7.27 (m, 12H), 6.92 – 6.86 (m, 4H), 6.76 – 6.72 (m, 4H), 6.47 (s, 2H), 4.08 (q, $J = 7.2$ Hz, 4H), 3.72 (s, 4H), 1.10 (t, $J = 7.2$ Hz, 6H).

LC-MS (ESI⁺) m/z calcd for $C_{40}H_{37}N_2O_4^+$ $[M+H]^+$ 609.3, found: 609.3.

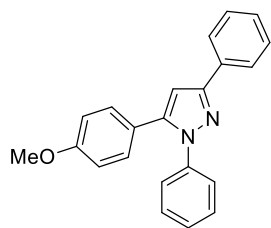
Photocatalytic Synthesis of Pyrazole Derivatives (5a-j)



1,3,5-triphenyl-1H-pyrazole (5a)

The titled compound was synthesized following **General Procedure D**: 2-Bromoacetophenone (**1a**, 39.8 mg, 0.20 mmol, 1.0 equiv.), (*E*)-1-benzylidene-2-phenylhydrazine (**4a**, 47.1 mg, 0.24 mmol, 1.2 equiv.), NaHCO₃ (16.8 mg, 0.2 mmol, 1.0 equiv.), CsPbBr₃ perovskite photocatalyst (5.0 mg) and 1,4-dioxane (2.0 mL) were used. The product was purified by flash column chromatography on silica gel (Hexanes/EtOAc = 33/1) as white solid (80% **yield**, 47.4 mg). The ¹H NMR spectra matched those reported in the literature.

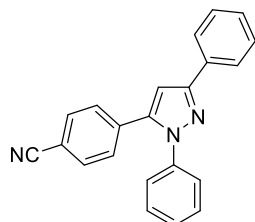
¹H NMR (400 MHz, CDCl₃) δ 7.96 – 7.91 (m, 2H), 7.47 – 7.41 (m, 2H), 7.40 – 7.27 (m, 11H), 6.84 (s, 1H).



5-(4-methoxyphenyl)-1,3-diphenyl-1H-pyrazole (5b)

The titled compound was synthesized following **General Procedure D**: 2-Bromo-4'-methoxyacetophenone (**1b**, 45.8 mg, 0.20 mmol, 1.0 equiv.), (*E*)-1-benzylidene-2-phenylhydrazine (**4a**, 47.1 mg, 0.24 mmol, 1.2 equiv.), NaHCO₃ (16.8 mg, 0.2 mmol, 1.0 equiv.), CsPbBr₃ perovskite photocatalyst (5.0 mg) and 1,4-dioxane (2.0 mL) were used. The product was purified by flash column chromatography on silica gel (Hexanes/EtOAc = 10/1) as white solid (73% **yield**, 47.7 mg). The ¹H NMR spectra matched those reported in the literature.¹⁸

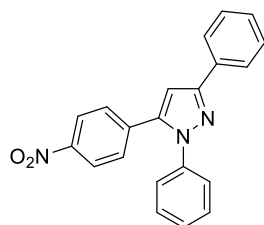
¹H NMR (500 MHz, CDCl₃) δ 7.93 (d, *J* = 8.0 Hz, 2H), 7.46 – 7.28 (m, 8H), 7.21 (d, *J* = 8.0 Hz, 2H), 6.85 (d, *J* = 8.0 Hz, 2H), 6.77 (s, 1H), 3.82 (s, 3H).



4-(1,3-diphenyl-1H-pyrazol-5-yl)benzonitrile (5c)

The titled compound was synthesized following **General Procedure D**: 2-Bromo-4'-cyanoacetophenone (**1c**, 44.8 mg, 0.20 mmol, 1.0 equiv.), (*E*)-1-benzylidene-2-phenylhydrazine (**4a**, 47.1 mg, 0.24 mmol, 1.2 equiv.), NaHCO₃ (16.8 mg, 0.2 mmol, 1.0 equiv.), CsPbBr₃ perovskite photocatalyst (5.0 mg) and 1,4-dioxane (2.0 mL) were used. The product was purified by flash column chromatography on silica gel (Hexanes/EtOAc = 20/1 – 15/1) as light-yellow solid (85% **yield**, 54.6 mg).

¹H NMR (500 MHz, CDCl₃) δ 7.92 (d, *J* = 7.5 Hz, 2H), 7.60 (d, *J* = 8.0 Hz, 2H), 7.47 – 7.32 (m, 10H), 6.90 (s, 1H).

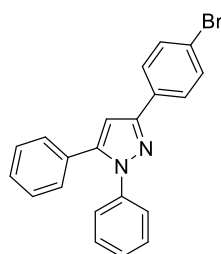


5-(4-nitrophenyl)-1,3-diphenyl-1H-pyrazole (**5d**)

The titled compound was synthesized following **General Procedure D**: 2-Bromo-4'-nitroacetophenone (**1d**, 48.8 mg, 0.20 mmol, 1.0 equiv.), (*E*)-1-benzylidene-2-phenylhydrazine (**4a**, 47.1 mg, 0.24 mmol, 1.2 equiv.), NaHCO₃ (16.8 mg, 0.2 mmol, 1.0 equiv.), CsPbBr₃ perovskite photocatalyst (5.0 mg) and 1,4-dioxane (2.0 mL) were used. The product was purified by flash column chromatography on silica gel (Hexanes/EtOAc = 8/1) as white solid (80% **yield**, 54.6 mg). The ¹H NMR spectra matched those reported in the literature.

18

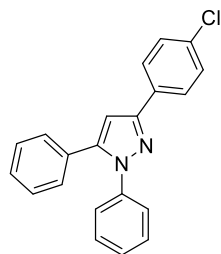
¹H NMR (500 MHz, CDCl₃) δ 8.18 (d, *J* = 8.5 Hz, 2H), 7.92 (d, *J* = 8.0 Hz, 2H), 7.48 – 7.33 (m, 10H), 6.95 (s, 1H).



3-(4-bromophenyl)-1,5-diphenyl-1H-pyrazole (**5e**)

The titled compound was synthesized following **General Procedure D**: 2-Bromoacetophenone (**1a**, 39.8 mg, 0.20 mmol, 1.0 equiv.), (*E*)-1-(4-bromobenzylidene)-2-phenylhydrazine (**4b**, 66.0 mg, 0.24 mmol, 1.2 equiv.), NaHCO₃ (16.8 mg, 0.2 mmol, 1.0 equiv.), CsPbBr₃ perovskite photocatalyst (5.0 mg) and 1,4-dioxane (2.0 mL) were used. The product was purified by flash column chromatography on silica gel (Hexanes/EtOAc = 33/1) as white solid (81% **yield**, 60.8 mg). The ¹H NMR spectra matched those reported in the literature.¹⁸

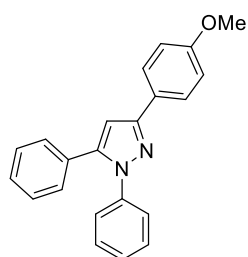
¹H NMR (400 MHz, CDCl₃) δ 7.81 (d, *J* = 8.4 Hz, 2H), 7.56 (d, *J* = 8.4 Hz, 2H), 7.40 – 7.26 (m, 10H), 6.80 (s, 1H).



3-(4-chlorophenyl)-1,5-diphenyl-1H-pyrazole (5f)

The titled compound was synthesized following **General Procedure D**: 2-Bromoacetophenone (**1a**, 39.8 mg, 0.20 mmol, 1.0 equiv.), (*E*)-1-(4-chlorobenzylidene)-2-phenylhydrazine (**4c**, 55.4 mg, 0.24 mmol, 1.2 equiv.), NaHCO₃ (16.8 mg, 0.2 mmol, 1.0 equiv.), CsPbBr₃ perovskite photocatalyst (5.0 mg) and 1,4-dioxane (2.0 mL) were used. The product was purified by flash column chromatography on silica gel (Hexanes/EtOAc = 33/1) as white solid (77% **yield**, 50.9 mg). The ¹H NMR spectra matched those reported in the literature.¹⁸

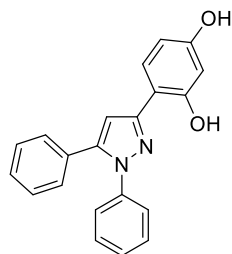
¹H NMR (400 MHz, CDCl₃) δ 7.89 (d, *J* = 8.4 Hz, 2H), 7.39 – 7.26 (m, 12H), 6.81 (s, 1H).



3-(4-methoxyphenyl)-1,5-diphenyl-1H-pyrazole (5g)

The titled compound was synthesized following **General Procedure D**: 2-Bromoacetophenone (**1a**, 39.8 mg, 0.20 mmol, 1.0 equiv.), (*E*)-1-(4-methoxybenzylidene)-2-phenylhydrazine (**4d**, 54.3 mg, 0.24 mmol, 1.2 equiv.), NaHCO₃ (16.8 mg, 0.2 mmol, 1.0 equiv.), CsPbBr₃ perovskite photocatalyst (5.0 mg) and 1,4-dioxane (2.0 mL) were used. The product was purified by flash column chromatography on silica gel (Hexanes/EtOAc = 8/1) as white solid (60% **yield**, 39.2 mg). The ¹H NMR spectra matched those reported in the literature.¹⁸

¹H NMR (500 MHz, CDCl₃) δ 7.85 (d, *J* = 9.0 Hz, 2H), 7.38 – 7.27 (m, 10H), 6.97 (d, *J* = 9.0 Hz, 2H), 6.76 (s, 1H), 3.86 (s, 3H).



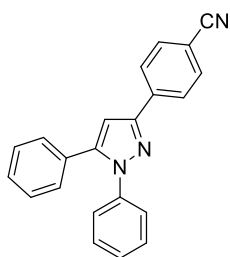
4-(1,5-diphenyl-1H-pyrazol-3-yl)benzene-1,3-diol (5h)

The titled compound was synthesized following **General Procedure D**: 2-Bromoacetophenone (**1a**, 39.8 mg, 0.20 mmol, 1.0 equiv.), (*E*)-4-((2-

phenylhydrazineylidene)methyl)benzene-1,3-diol (**4e**, 54.8 mg, 0.24 mmol, 1.2 equiv.), NaHCO₃ (16.8 mg, 0.2 mmol, 1.0 equiv.), CsPbBr₃ perovskite photocatalyst (5.0 mg) and 1,4-dioxane (2.0 mL) were used. The product was purified by flash column chromatography on silica gel (Hexanes/EtOAc = 5/1 – 2/1) as light-yellow solid (54% **yield**, 35.5 mg).

¹H NMR (500 MHz, CDCl₃) δ 10.98 (s, 1H), 7.50 (d, *J* = 8.5 Hz, 1H), 7.38 – 7.27 (m, 10H), 6.78 (s, 1H), 6.52 (d, *J* = 2.5 Hz, 1H), 6.46 (dd, *J* = 8.5, 2.5 Hz, 1H).

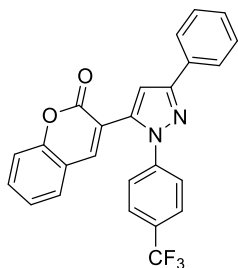
LC-MS (ESI⁺) *m/z* calcd for C₂₁H₁₇N₂O₂⁺ [M+H]⁺ 329.1, found: 329.1.



4-(1,5-diphenyl-1H-pyrazol-3-yl)benzonitrile (5i)

The titled compound was synthesized following **General Procedure D**: 2-Bromoacetophenone (**1a**, 39.8 mg, 0.20 mmol, 1.0 equiv.), (*E*)-4-((2-phenylhydrazineylidene)methyl)benzonitrile (**4f**, 53.1 mg, 0.24 mmol, 1.2 equiv.), NaHCO₃ (16.8 mg, 0.2 mmol, 1.0 equiv.), CsPbBr₃ perovskite photocatalyst (5.0 mg) and 1,4-dioxane (2.0 mL) were used. The product was purified by flash column chromatography on silica gel (Hexanes/EtOAc = 20/1) as light-yellow solid (78% **yield**, 50.1 mg). The ¹H NMR spectra matched those reported in the literature.¹⁸

¹H NMR (500 MHz, CDCl₃) δ 8.03 (d, *J* = 8.0 Hz, 2H), 7.72 (d, *J* = 8.0 Hz, 2H), 7.41 – 7.26 (m, 10H), 6.87 (s, 1H).



3-(3-phenyl-1-(4-(trifluoromethyl)phenyl)-1H-pyrazol-5-yl)-2H-chromen-2-one (5j)

The titled compound was synthesized following **General Procedure D**: 3-(Bromoacetyl)coumarin (**1e**, 53.4 mg, 0.20 mmol, 1.0 equiv.), (*E*)-1-benzylidene-2-(4-(trifluoromethyl)phenyl)hydrazine (**4g**, 63.4 mg, 0.24 mmol, 1.2 equiv.), NaHCO₃ (16.8 mg, 0.2 mmol, 1.0 equiv.), CsPbBr₃ perovskite photocatalyst (5.0 mg) and 1,4-

dioxane (2.0 mL) were used. The product was purified by flash column chromatography on silica gel (Hexanes/EtOAc = 10/1 – 8/1) as light-yellow solid (89% **yield**, 77.0 mg).

¹H NMR (400 MHz, CDCl₃) δ 7.93 – 7.89 (m, 2H), 7.75 (s, 1H), 7.70 – 7.63 (m, 4H), 7.60 (ddd, *J* = 8.4, 7.6, 1.6 Hz, 1H), 7.49 – 7.42 (m, 3H), 7.40 – 7.35 (m, 2H), 7.33 (td, *J* = 7.6, 0.8 Hz, 1H), 7.05 (s, 1H).

¹⁹F NMR (376 MHz, CDCl₃) δ -62.44.

¹³C NMR (126 MHz, CDCl₃) δ 158.7, 154.0, 152.9, 143.3, 143.1, 137.7, 132.9, 132.4, 129.7 (q, *J* = 32.8 Hz), 128.9, 128.6, 128.5, 126.6 (q, *J* = 3.8 Hz), 126.0, 125.1, 124.2, 123.9 (q, *J* = 273.4 Hz), 118.9, 118.6, 117.0, 108.6.

GC-MS (EI) *m/z* calcd for C₂₅H₁₅F₃N₂O₂⁺ [M]⁺ 432.1, found: 432.2.

2.5.5 Cyclic Voltammetry (CV) Data

The electrochemical experiments were performed using a CH Instruments CHI660E Electrochemical Analyzer, a Pt disc carbon working electrode, a Pt wire counter electrode, and a Ag/AgCl reference electrode (Ag in 0.1 M AgNO₃ solution). The samples were prepared with 0.1 M tetrabutylammonium hexafluorophosphate (0.1 M) as supporting electrolyte in CH₃CN and sparged with N₂ for 20 minutes. The potential values obtained in reference to Ag/AgCl were converted to the saturated calomel electrode (SCE) in order to directly compare with literature.

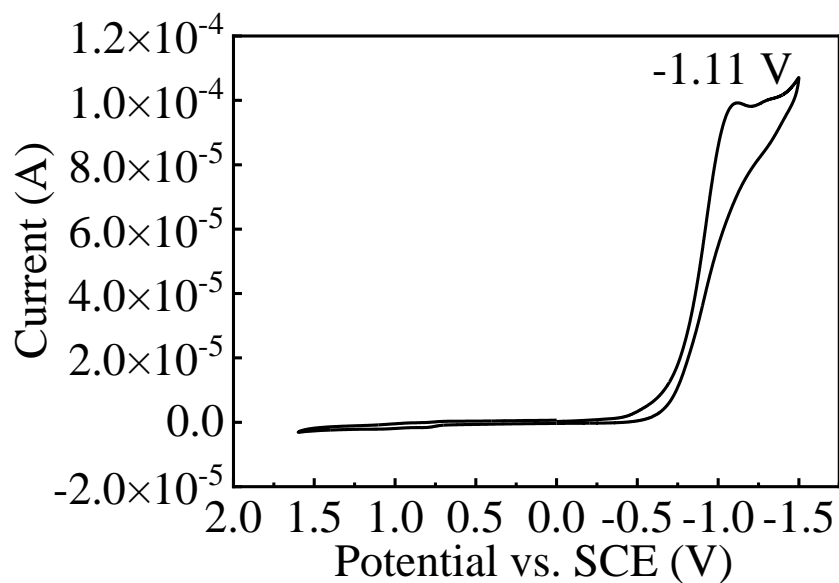


Figure 2.3 CV data of 2-bromoacetophenone (**1a**). $E_{\text{red}} = -1.11$ V vs. SCE.

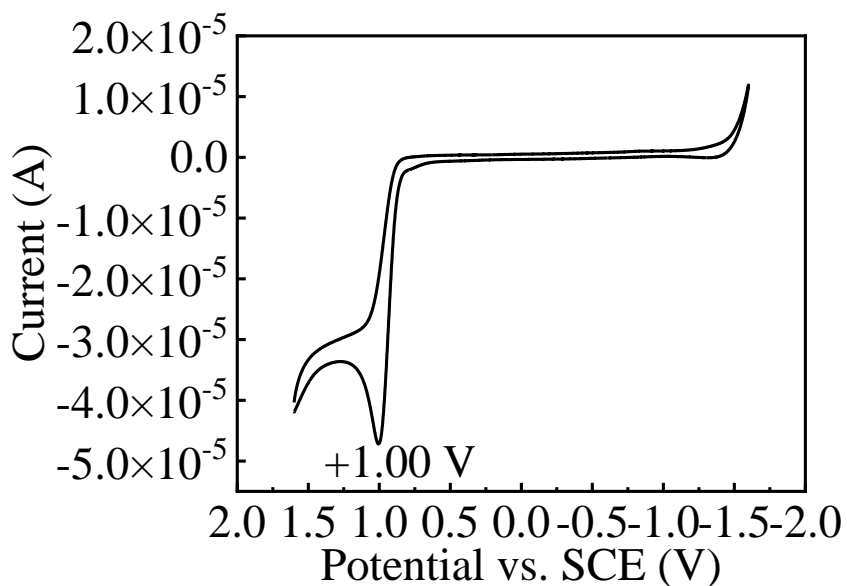


Figure 2.4 CV data of (*E*)-1-benzylidene-2-phenylhydrazine (**4a**). $E_{\text{ox}} = +1.00$ V vs. SCE.

2.5.6 Photoluminescence (PL) Quenching Study

Stern-Volmer PL quenching studies of CsPbBr₃ NCs were conducted using 2-bromoacetophenone (**1a**) and (*E*)-1-benzylidene-2-phenylhydrazine (**4a**) respectively as quenchers. The quenching constants (K_{sv}) were determined using Stern-Volmer kinetics following equation:

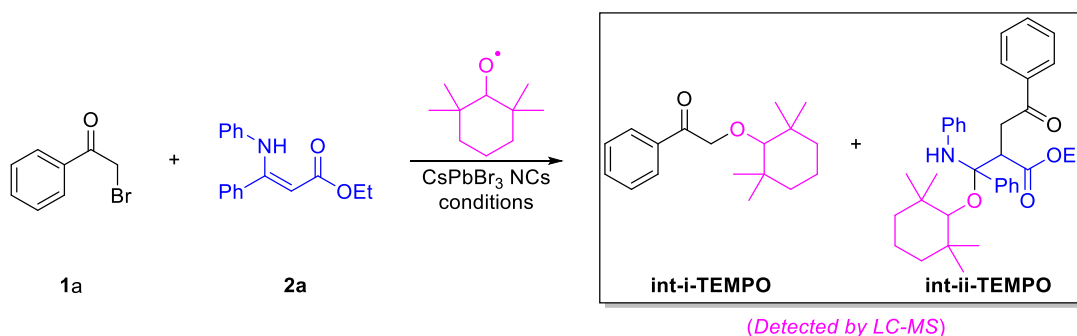
$$\frac{I_0}{I} = K_{SV}[\text{quencher}]$$

where I_0 is the original PL intensity of NCs without the presence of a quencher, I is the PL intensity of NCs after the addition of a quencher.

A standard fluorometer setup was used to perform the quenching studies with an excitation wavelength of 455 nm. Samples were prepared by a gently stirring mixture of CsPbBr₃ NCs (1.0 mg), solvent (2.0 mL) and increasing amount of quencher. Emission intensities at 510 nm were used for plotting the Stern-Volmer relationship. Stern-Volmer kinetics equation was derived by linear fitting using OriginPro© software.

2.5.7 Radical Trapping Experiments

The Radical Trapping Experiment for **int-i** and **int-ii** in the Photocatalytic Synthesis of Pyrroles



To a 1-dram vial with a magnetic stirring bar was added 2-bromoacetophenone (**1a**, 0.15 mmol), ethyl (Z)-3-phenyl-3-(phenylamino)acrylate (**2a**, 0.10 mmol), TEMPO (0.3 mmol), CsPbBr₃ perovskite photocatalyst (2.0 mg), CH₂Cl₂ (1.0 mL) and Et₃N (5 μL). The resulting mixture was allowed to react at room temperature under blue LED (12 W *2) irradiation for 24h. LC-MS analysis of such reaction mixture found **int-i-TEMPO** and **int-ii-TEMPO**.

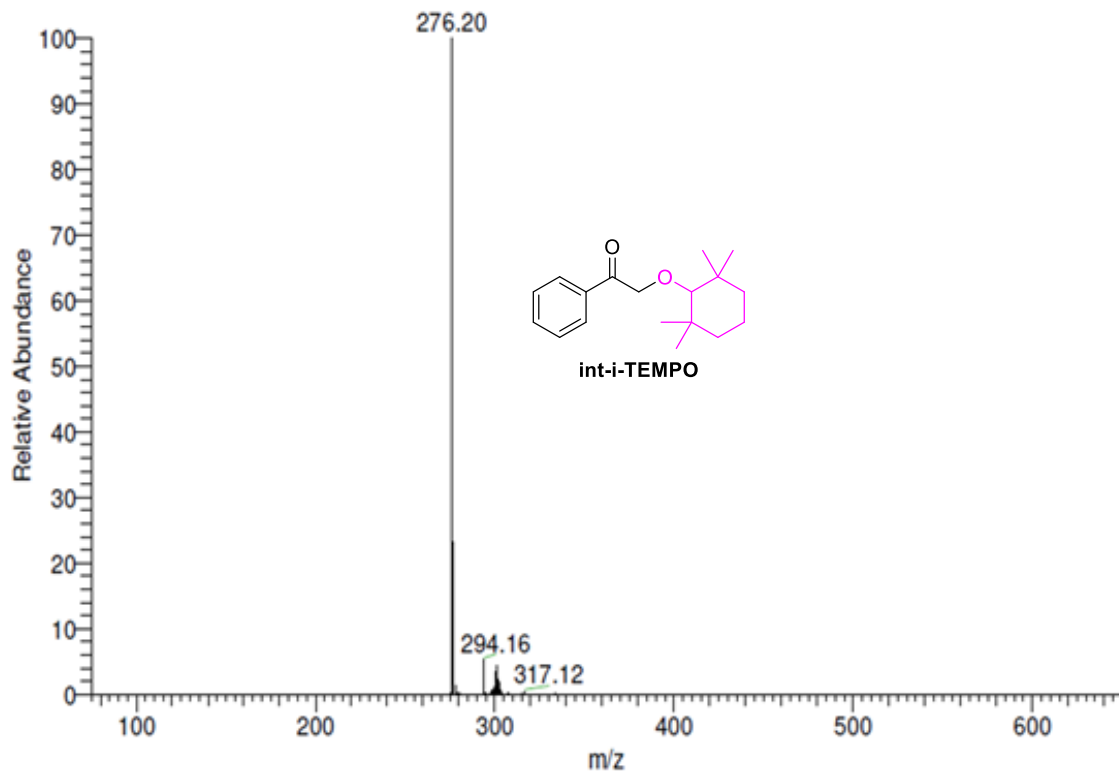


Figure 2.5 LC-MS evidence of **int-i-TEMPO**.

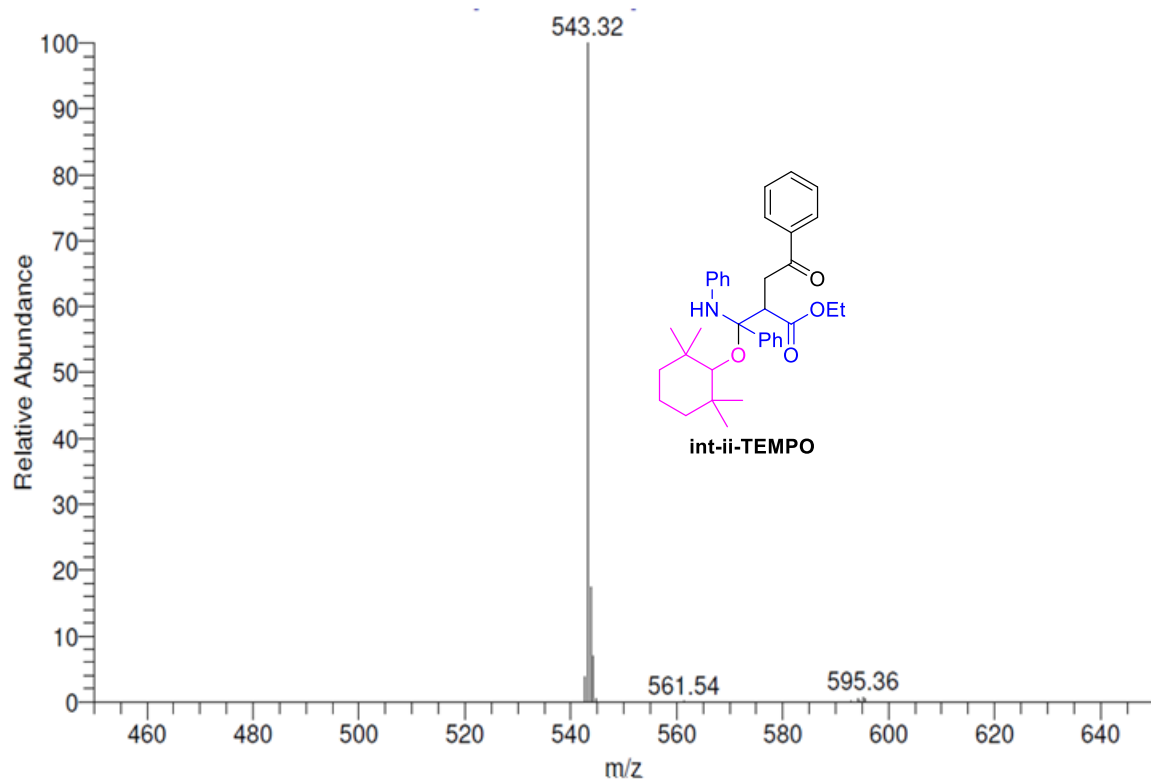
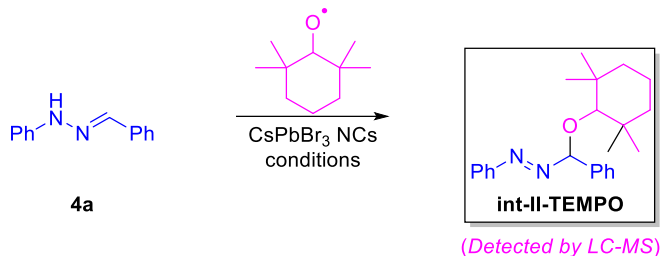


Figure 2.6 LC-MS evidence of **int-ii-TEMPO**.

The Radical Trapping Experiment for int-II in the Photocatalytic Synthesis of Pyrazoles



To a 1-dram vial with a magnetic stirring bar was added (*E*)-1-benzylidene-2-phenylhydrazine (**4a**, 0.1 mmol), TEMPO (0.2 mmol), CsPbBr₃ perovskite photocatalyst (2.0 mg) and CH₂Cl₂ (1.0 mL). The resulting mixture was allowed to react at room temperature under blue LED (12 W *2) irradiation for 24h. LC-MS analysis of such reaction mixture found **int-II-TEMPO**.

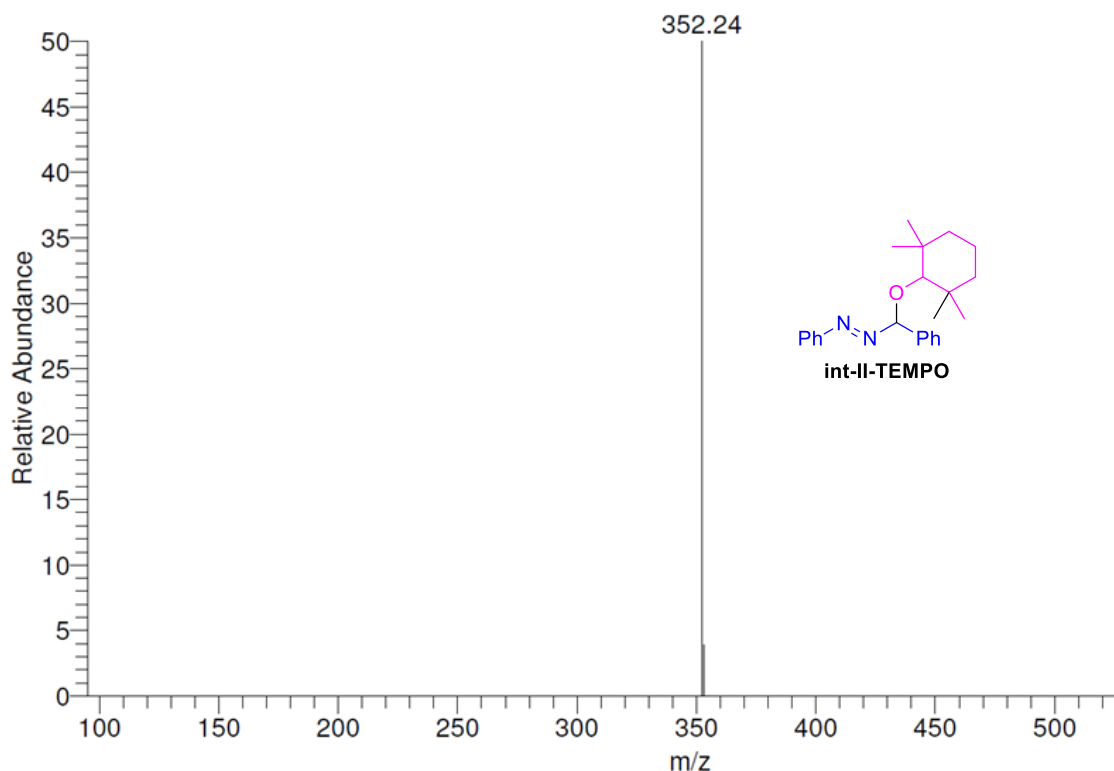


Figure 2.7 LC-MS evidence of **int-II-TEMPO**.

2.6 Acknowledgements

Chapter 2 contains unpublished materials and is reproduced in part as it appears in *Nature Communication* **2019**, 10, 2843. Zhu, X.; **Lin, Y.**; San Martin, J.; Sun, Y.; Zhu, D.; Yan, Y. The dissertation author was a co-author of this paper.

The data for reaction condition exploration and mechanistic studies was adapted from the above-mentioned publication. I provided work for reaction condition exploration and mechanistic studies led by Dr. Xiaolin Zhu. I was the primary researcher for the pyrroles and pyrazoles scopes evaluation, compound synthesis/purification/characterization. I organized and wrote the dissertation presented in this chapter.

2.7 Reference

1. Williams, R. E.; Njardarson, J. T. Top 200 Small Molecule Drugs by Retail Sales in 2022. <https://njardarson.lab.arizona.edu/sites/njardarson.lab.arizona.edu/files/NjardarsonGroup2022SmallMoleculeTopPosterV3.pdf> (accessed 08/07/2023).
2. Kumar Lal, T.; Mukherjee, R., New Cobalt(II) and Nickel(II) Complexes with 2-(Pyrazol-1-ylmethyl)pyridine. Stereochemical Variations in Cobalt(II) Complexes and X-Ray Crystal Structure of Bis[2-(pyrazol-1-ylmethyl) pyridine]Dichlorocobalt(II) Tetrahydrate. *Polyhedron* **1997**, 16 (20), 3577-3583.
3. Kumar, S.; Mani, G.; Mondal, S.; Chattaraj, P. K., Pyrrole-Based New Diphosphines: Pd and Ni Complexes Bearing the PNP Pincer Ligand. *Inorg. Chem.* **2012**, 51 (22), 12527-12539.
4. Paal, C., Ueber die Derivate des Acetophenonacetessigesters und des Acetonylacetessigesters. *Ber. Dtsch. Chem. Ges.* **1884**, 17 (2), 2756-2767.
5. Knorr, L., Synthese von Furfuranderivaten aus dem Diacetbernsteinsäureester. *Ber. Dtsch. Chem. Ges.* **1884**, 17 (2), 2863-2870.
6. Hantzsch, A., Neue Bildungsweise von Pyrrolderivaten. *Ber. Dtsch. Chem. Ges.* **1890**, 23 (1), 1474-1476.
7. Barton, D. H. R.; Zard, S. Z., A New Synthesis of Pyrroles from Nitroalkenes. *J. Chem. Soc., Chem. Commun.* **1985**, (16), 1098-1100.
8. Knorr, L., Einwirkung von Acetessigester auf Phenylhydrazin. *Ber. Dtsch. Chem. Ges.* **1883**, 16 (2), 2597-2599.

9. Han, C.; Zhu, X.; Martin, J. S.; Lin, Y.; Spears, S.; Yan, Y., Recent Progress in Engineering Metal Halide Perovskites for Efficient Visible-Light-Driven Photocatalysis. *ChemSusChem* **2020**, *13* (16), 4005-4025.
10. Lin, Y.; Guo, J.; San Martin, J.; Han, C.; Martinez, R.; Yan, Y., Photoredox Organic Synthesis Employing Heterogeneous Photocatalysts with Emphasis on Halide Perovskite. *Chem. Eur. J.* **2020**, *26* (58), 13118-13136.
11. Zhu, X.; Lin, Y.; Sun, Y.; Beard, M. C.; Yan, Y., Lead-Halide Perovskites for Photocatalytic α -Alkylation of Aldehydes. *J. Am. Chem. Soc.* **2019**, *141* (2), 733-738.
12. Huang, H.; Zhao, F.; Liu, L.; Zhang, F.; Wu, X.-g.; Shi, L.; Zou, B.; Pei, Q.; Zhong, H., Emulsion Synthesis of Size-Tunable $\text{CH}_3\text{NH}_3\text{PbBr}_3$ Quantum Dots: An Alternative Route toward Efficient Light-Emitting Diodes. *ACS Appl. Mater. Interfaces* **2015**, *7* (51), 28128-28133.
13. Würtz, S.; Rakshit, S.; Neumann, J. J.; Dröge, T.; Glorius, F., Palladium-Catalyzed Oxidative Cyclization of N-Aryl Enamines: From Anilines to Indoles. *Angew. Chem. Int. Ed.* **2008**, *47* (38), 7230-7233.
14. Török, B.; Sood, A.; Bag, S.; Tulsan, R.; Ghosh, S.; Borkin, D.; Kennedy, A. R.; Melanson, M.; Madden, R.; Zhou, W.; LeVine, H., III; Török, M., Diaryl Hydrazones as Multifunctional Inhibitors of Amyloid Self-Assembly. *Biochemistry* **2013**, *52* (7), 1137-1148.
15. Li, P.; Wu, C.; Zhao, J.; Rogness, D. C.; Shi, F., Synthesis of Substituted 1*H*-Indazoles from Arynes and Hydrazones. *J. Org. Chem.* **2012**, *77* (7), 3149-3158.
16. Lundgren, R. J.; Stradiotto, M., Palladium-Catalyzed Cross-Coupling of Aryl Chlorides and Tosylates with Hydrazine. *Angew. Chem. Int. Ed.* **2010**, *49* (46), 8686-8690.
17. Lei, T.; Liu, W.-Q.; Li, J.; Huang, M.-Y.; Yang, B.; Meng, Q.-Y.; Chen, B.; Tung, C.-H.; Wu, L.-Z., Visible Light Initiated Hantzsch Synthesis of 2,5-Diaryl-Substituted Pyrroles at Ambient Conditions. *Org. Lett.* **2016**, *18* (10), 2479-2482.
18. Fan, X.-W.; Lei, T.; Zhou, C.; Meng, Q.-Y.; Chen, B.; Tung, C.-H.; Wu, L.-Z., Radical Addition of Hydrazones by α -Bromo Ketones To Prepare 1,3,5-Trisubstituted Pyrroles via Visible Light Catalysis. *J. Org. Chem.* **2016**, *81* (16), 7127-7133.

Chapter 3 Triplet Energy Transfer from Lead Halide Perovskite for Highly Selective Photocatalytic [2+2] Cycloaddition

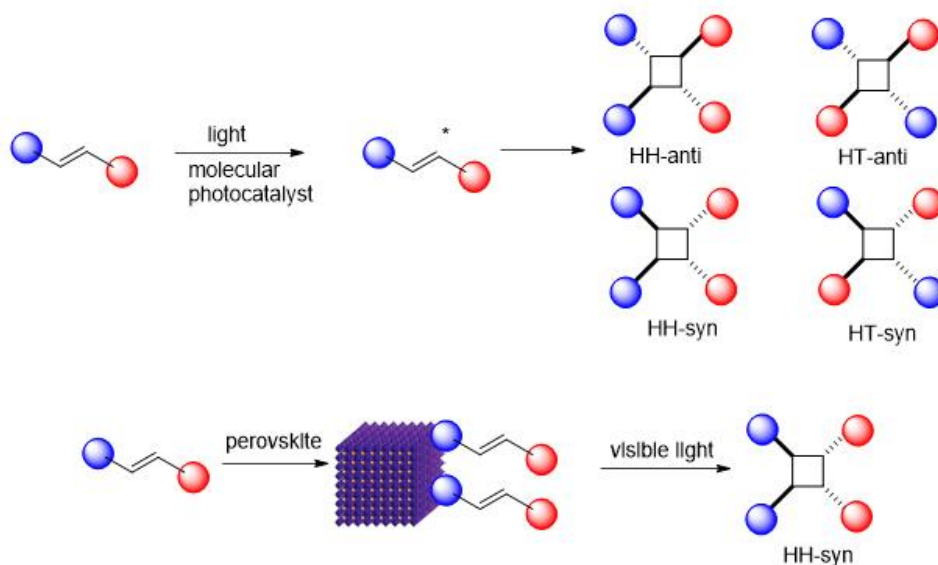
3.1 Chapter Summary

This chapter describes the application of lead-halide perovskite nanocrystals (LHP NCs) towards photocatalytic triplet energy transfer (TET)-mediated [2+2] cycloaddition reactions for the synthesis of head-to-head (HH) *syn*-cyclobutanes. Triplet excitons are generally confined within the semiconductor, hence solar energy utilization via direct TET from semiconductors is challenging. TET from LHP semiconductors to nearby organic molecules has been illustrated with ultra-fast spectroscopy. Direct utilization of solar energy, *i.e.*, visible light, for photocatalysis via TET is an important route, has yet been demonstrated with lead-halide perovskite semiconductors. Here we show that a photocatalytic [2+2] cycloaddition reaction can be successfully demonstrated via TET from LHP NCs. The triplet excitons are shown to induce a highly HH- and *syn*-selective [2+2] cycloaddition starting from olefins. Such photocatalytic reactions probe the TET process previously only observed spectroscopically. Moreover, our observation demonstrates that bulk-like LHP NCs (Size > 10 nm, emission $\lambda_{\text{max}} = 530$ nm), in addition to quantum-confined smaller NCs, are also effective for TET. Our findings may render a new energy conversion pathway to employ LHP NCs via direct TET for photocatalytic highly selective organic synthesis.

3.2 Introduction

Direct utilization of long-lived triplets state using molecular chromophores for organic activation has been extensively explored.¹⁻⁶ However, employment of triplet excitons from inorganic semiconductors is usually challenging, because such excitons are generally tightly confined within the semiconductor. Noticeable exceptions have been recently reported, *e.g.* pioneering work of the direct observation of TET from CdSe quantum dots (QDs) to organic molecules,⁷ triplet exciton transfer from CdSe QDs for organic substrate activation and subsequent

regio- and diastereoselective or chemo- and stereoselective cycloadditions that could not otherwise be achieved by molecular photocatalysts under the same conditions.^{8, 9} Lately, TET from perovskite NCs to the triplet state of suitable organic molecules (*e.g.* polycyclic aromatic hydrocarbons, PAH^{10, 11}, rhodamine B¹²) has been explored via ultrafast spectroscopy. Overall, such energy transfer processes were mainly observed via the organic triplet energy acceptor (TEA) that further induced a triplet-triplet annihilation upconversion (TTA-UC). Notably, the early report of triplet sensitization of perovskite NCs for such TTA-UC application can be traced back to 2017, where Mase *et al.* employed LHP NCs to triplet excite the surface-bound organic dye and achieved the efficient upconversion via a tandem TET to the 9,10-Diphenylanthracene (DPA).¹³ Direct application of such energy transfer process in organic substrate activation via LHP NCs for photocatalysis^{12, 14} had been predicted, however, has not yet been experimentally achieved.



Scheme 3.1 Schematic illustration of possible product outcomes from molecular photocatalyst vs. perovskite NCs photocatalyst. HH: head-to-head; HT: head-to-tail.

Here we report the first LHP-based TET process employed in a photocatalytic organic synthesis and that bulk-like CsPbBr₃ NCs (Size > 10 nm, larger than Bohr radius; $E_{CB} = -1.3$ V,

$E_{\text{VB}} = +1.1$ V, all vs. SCE; ¹⁵ Excited-state triplet energy, $E_{\text{T}} = 2.4$ eV) can induce highly selective [2+2] olefin cycloadditions. Lately, visible-light-induced TET-mediated intermolecular [2+2] cycloaddition has been studied by Yoon,^{2, 16} Bach,¹⁷ Wu¹ and others^{18, 19} where an organic chromophore or Ir, Ru-based transition metal complex photocatalysts were utilized. Therefore, the visible-light-induced intermolecular [2+2] cycloaddition was chosen here as a model reaction to probe the TET ability of the LHP NCs. TET from the long-lived triplet states of molecular photocatalyst usually leads to a free (unbounded) triplet-excited substrate which may result in non-selective [2+2] couplings, as shown in **Scheme 3.1**. Our approach here utilizes the LHP NCs' surface as a template for a dynamic anchoring of the organic substrates. Such anchoring encourages efficient TET from the NCs to the surface-bound substrates, followed by the [2+2] cycloaddition on the NCs' surface, hence leading to a regio- and diastereoselective HH-*syn*-cyclobutane product (**Figure 3.1**). Note that a charge-transfer induced stereoselective C-C coupling reaction via perovskite QDs was reported lately,²⁰ but the selectivity remained governed by a thermodynamic driving force similar to previous work.²¹ Here our TET approach induces a unique thermodynamically unfavored *syn*-selective [2+2] cycloaddition which is distinct from those catalyzed by commonly studied molecular photocatalysts.

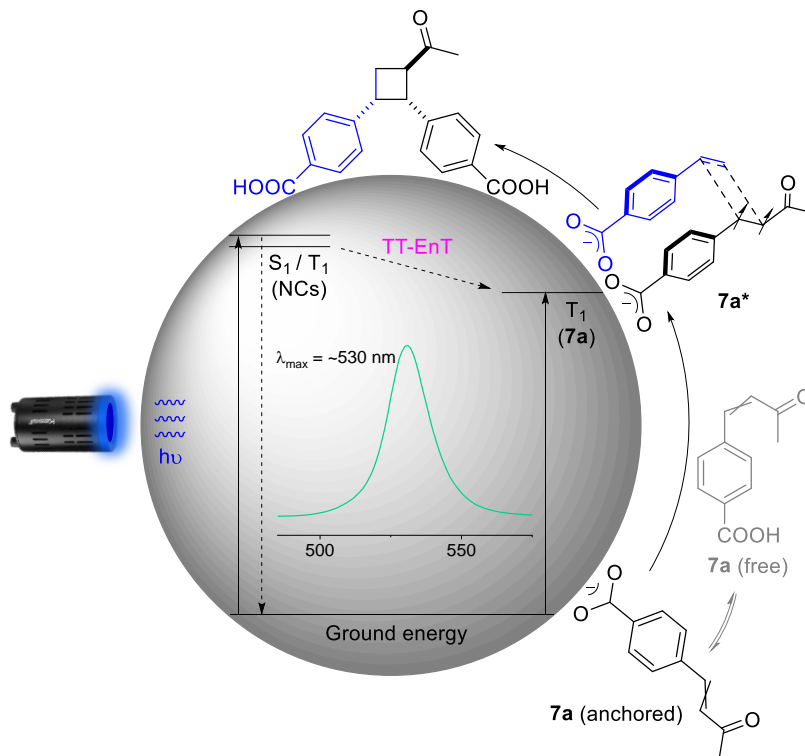


Figure 3.1 Proposed mechanism of the visible-light-induced CsPbBr₃ NCs TET-mediated surface-templated intermolecular [2+2] cycloaddition.

3.3 Results and Discussion

3.3.1 Screening of Triplet Energy Acceptor

Triplet energy acceptor (TEA) plays a vital role for the NCs-based TET process. Spectroscopically, Wu group reported that strong quantum confinement is imperative for an efficient TET from the perovskite NCs to carboxyl-linked PAH acceptors.^{10, 12} Castellano group used polyaromatic carboxylic acid as a TEA to directly observe the TET from CdSe semiconductor NCs via transient absorption spectroscopy⁷ and to study the delayed molecular triplet generation from PbS QDs.²² Tang group used a series of anthracene carboxylic acid derivatives with variable bridging length to study the distance-dependent TET of CdSe NCs²³ and the carboxyl-bearing transmitters were also discussed.²⁴ Weiss group demonstrated TET to vinyl benzoic acid derivatives from CdSe QDs.^{8, 9}

Here we screened the olefin substrates to probe the TET process from CsPbBr₃ NCs. We first explored the TET to olefin substrates via Stern-Volmer photoluminescence (PL) quenching studies as shown in **Figure 3.2**. Meaningful PL quenching as indicated by the quenching constant, K_{SV} , was observed on the TEAs with amino or carboxyl anchoring groups, such as **7a**, **7e**, and **9** respectively. Neglectable quenching was shown when such anchoring group was missing in **6** or diminishing upon esterification of the carboxylic acid in **8**. Compound **7c** also illustrated no TET, probably because its triplet energy (2.51 eV)⁸ is higher than that of the bulk-like CsPbBr₃ NCs (2.4 eV). Overall, suitable olefin candidates for CsPbBr₃ NCs are generally substrates with lower E_T and with amino or carboxyl anchoring group. It is important to note here that we cannot distinguish the quenching process by amino-containing **9** is via TET or charge transfer^{12,25}, although a highest quenching constant was observed. Additionally, **10** also demonstrated a significant quenching to the PL of NCs even after acetylation of the amino group that may decrease its binding ability to the NCs' surface. However, NCs-photocatalyzed cycloaddition of **9** and **10** were not successful (*vide infra*), likely because the VB-based amine oxidation (charge transfer process)^{12,25} rather than TET was dominant.

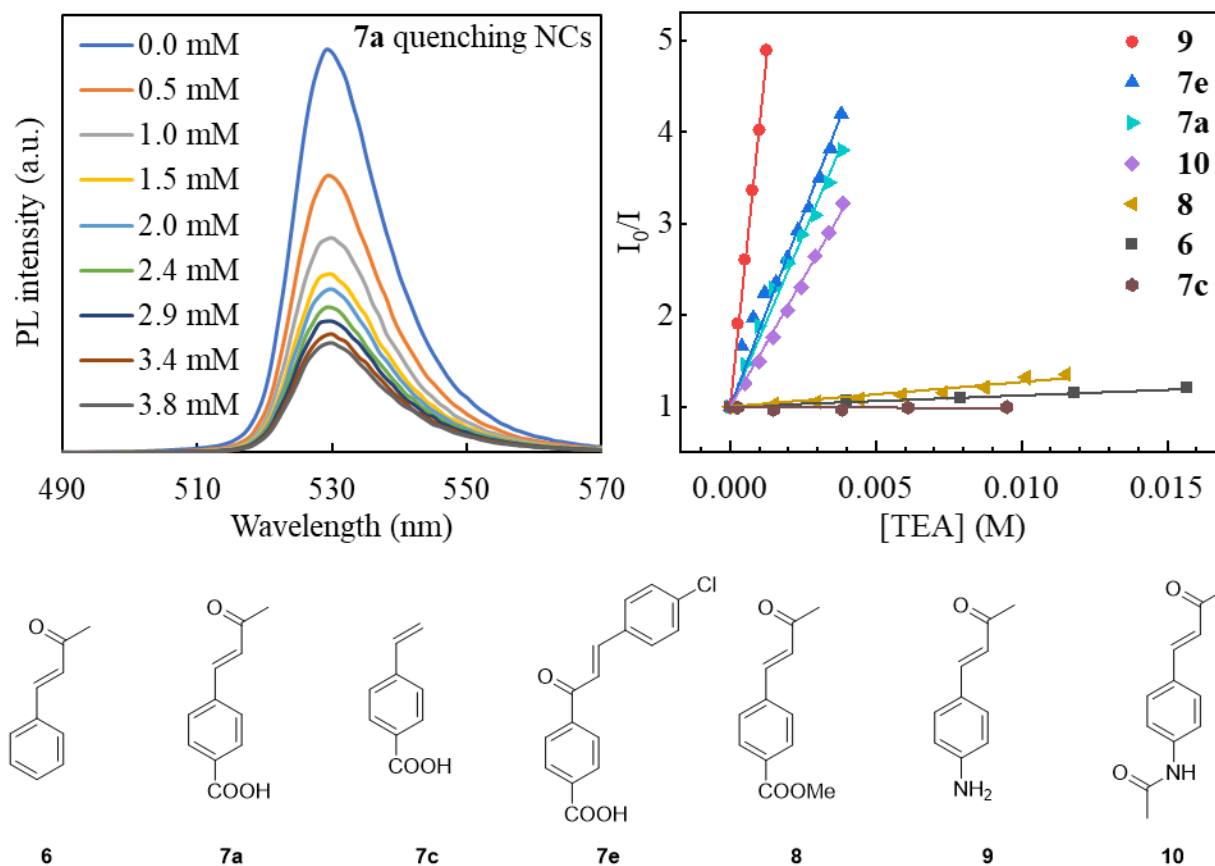


Figure 3.2 Stern-Volmer PL quenching studies of perovskite NCs with various olefins TEAs.

3.3.2 Studies of the Surface Binding

Surface binding is imperative for surface-templated photocatalytic reactions. TEA's dynamic binding to the CsPbBr₃ NCs' surfaces was explored using ¹H NMR. The binding of substrate, *i.e.*, **7a**, was first validated via quantitative NMR measurements in which **7a**-saturated NCs were centrifuged, isolated, and re-dissolved in DMSO-d₆ to break the perovskite NCs into free soluble molecules. An internal reference was added to calculate the binding amount of **7a**, demonstrating ~1 wt% of **7a** binding to the NCs (**Figure 3.24**). Such binding experiments implied roughly 130 substrate molecules per NC (estimated from 10 nm NC). Surface TEA binding was also elucidated with IR spectroscopy (**Figure 3.3**). To understand the interaction between the substrate and CsPbBr₃ NCs, **7c** was employed for the IR comparisons. After stirring with CsPbBr₃

NCs in solution under dark, the carbonyl stretches of **7c** shifted towards higher wavenumbers (~10 cm^{-1}). Such blue-shifted stretching mode likely resulted from the positively charged perovskite NCs surface, suggesting a binding interaction between the TEA and NCs surface.

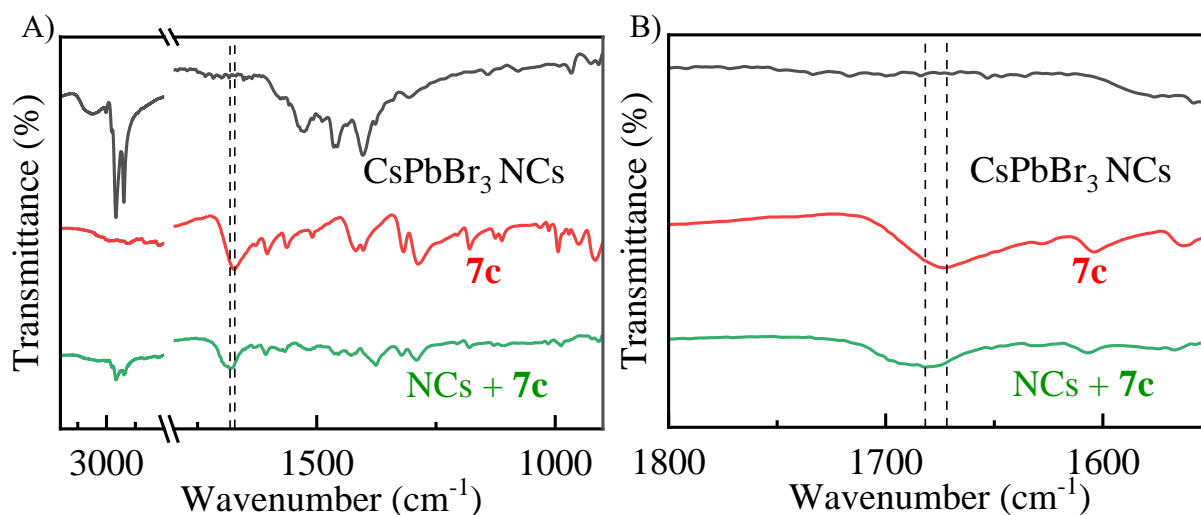


Figure 3.3 The carbonyl stretching frequency of **7c** blueshifted after mixing with NCs. **A)** FTIR comparison indicating the surface binding of substrate via carboxylate group. **B)** Enlarged carbonyl stretching area.

3.3.3 TET-Induced [2+2] Cycloaddition Reactions

To corroborate the quenching studies, photocatalytic [2+2] cycloaddition reactions were set up with TEAs as the reaction starting materials and bulk-like CsPbBr_3 NCs as the photocatalyst in THF solvent under blue LED irradiation (**Table 3.1**). Control experiment revealed that light and CsPbBr_3 NCs were all essential for this reaction. Such neat reaction setup provided a viable model to directly monitor the reaction progress with ^1H NMR. As shown in **Figure 3.4**, upon irradiation with blue LED for 30 min, a readily E/Z olefin isomerization of **7a** was observed and more importantly, an HH-*syn*-[2+2] product **7aa** emerged with characteristic cyclobutane peaks at 4.05 and 4.25 ppm. The rate of formation suggested that **7aa** was dependent on the concentration of **7a** in a pseudo second-order relationship (**Figure 3.22**). Further irradiation led to the accumulation of **7aa**, and the consumption of substrate **7a** and overall resulted in a 42% isolated yield.

Table 3.1 Control experiments of the NCs-photocatalyzed TET-mediated intermolecular [2+2] cycloaddition.

entry	deviation from standard conditions ^a	yield, % ^b	d.r. ^b
1	None	44	>30:1
2	Without light	0	N/A
3	Without CsPbBr ₃ NCs	0	N/A
4	With green LED (525 nm) instead of blue LED	17	>30:1
5	Without N ₂ sparging	31	>30:1

^aStandard conditions: **7a** (0.033 mmol), CsPbBr₃ NCs (2.0 mg), THF (1.2 mL). Reaction was performed under N₂ and blue LED irradiation at room temperature for 20h.

^bYields and diastereomeric ratios were determined by ¹H NMR of crude reaction mixture using CH₂Br₂ as an internal standard.

It is important to point out that neither HT- nor *anti*-[2+2] product, as shown in **Scheme 3.1** was observed on NMR or HPLC scale (**Figure 3.7**), rendering a highly regio- and diastereoselective perovskite NCs photocatalysis. Whereas molecular photocatalyst, *i.e.*, Ir(ppy)₃, led to a mixture of the [2+2] products as HH-*anti* (major) and HH-*syn* (minor). (**Scheme 3.4**) Correspondingly, NMR studies on TEAs with little or no *K_{sv}* discussed above failed to deliver [2+2] product. Substrate **9** and **10**, although showed significant *K_{sv}*, rendered no [2+2] product, likely due to a charge-transfer quenching process and not TET. The cycloaddition of **7a** under otherwise identical conditions but with irradiation under a green LED (525 nm) also led to the formation of **7aa** (**Table 3.1**, entry 4). This result implied that bulk-like perovskite NCs were effective for the TET process observed here, while quantum-confined NCs which were not excited

by the green LED, were not necessary for the TET process in this reaction. Together these results demonstrates that: 1) TEAs for perovskite NCs necessitate a suitable anchoring group; 2) If the excited-state TEA under unbounded form for [2+2] cycloaddition, an *anti*-[2+2] product would be preferred; 3) Bulk-like CsPbBr₃ NCs are also effective towards TET-mediated [2+2] cycloadditions.

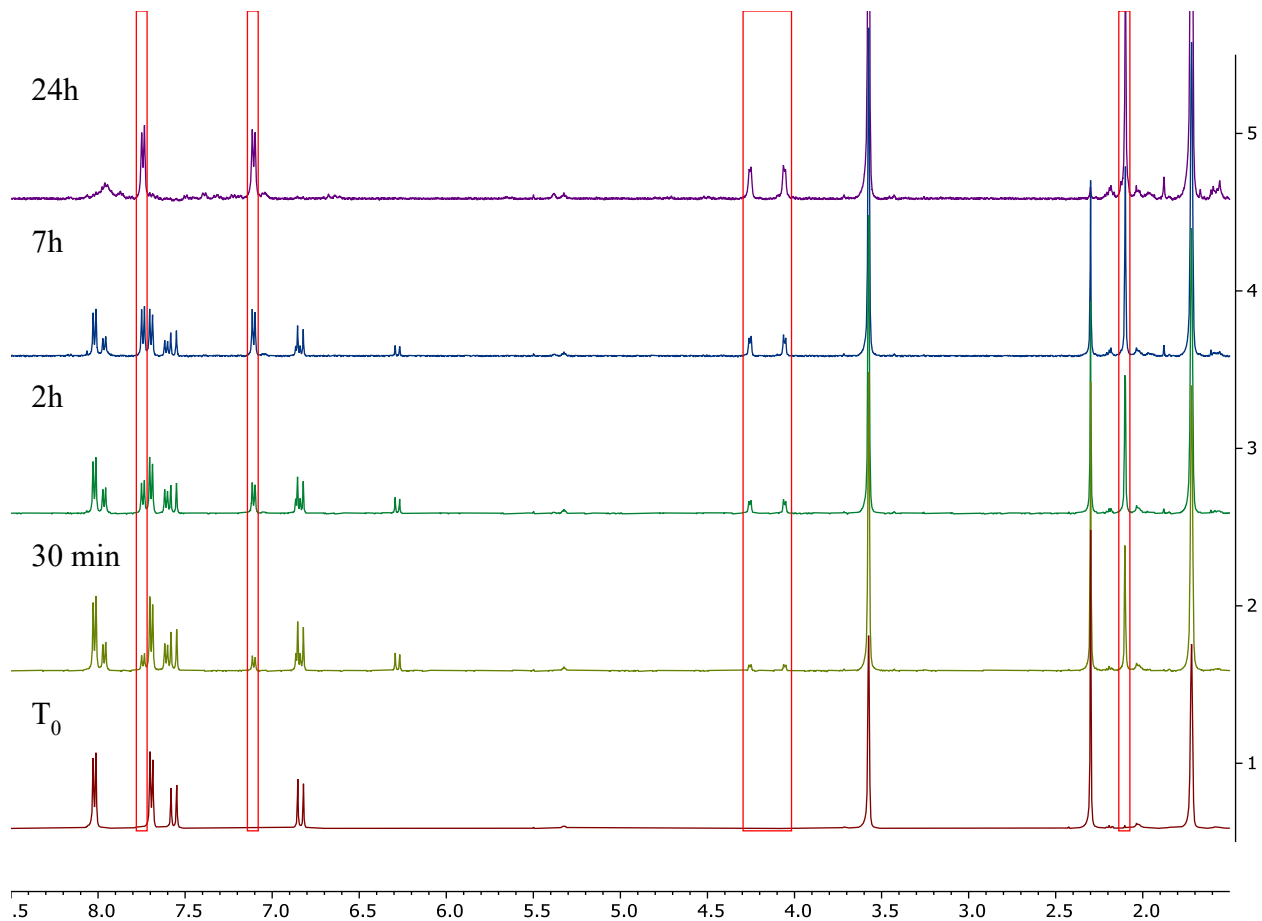
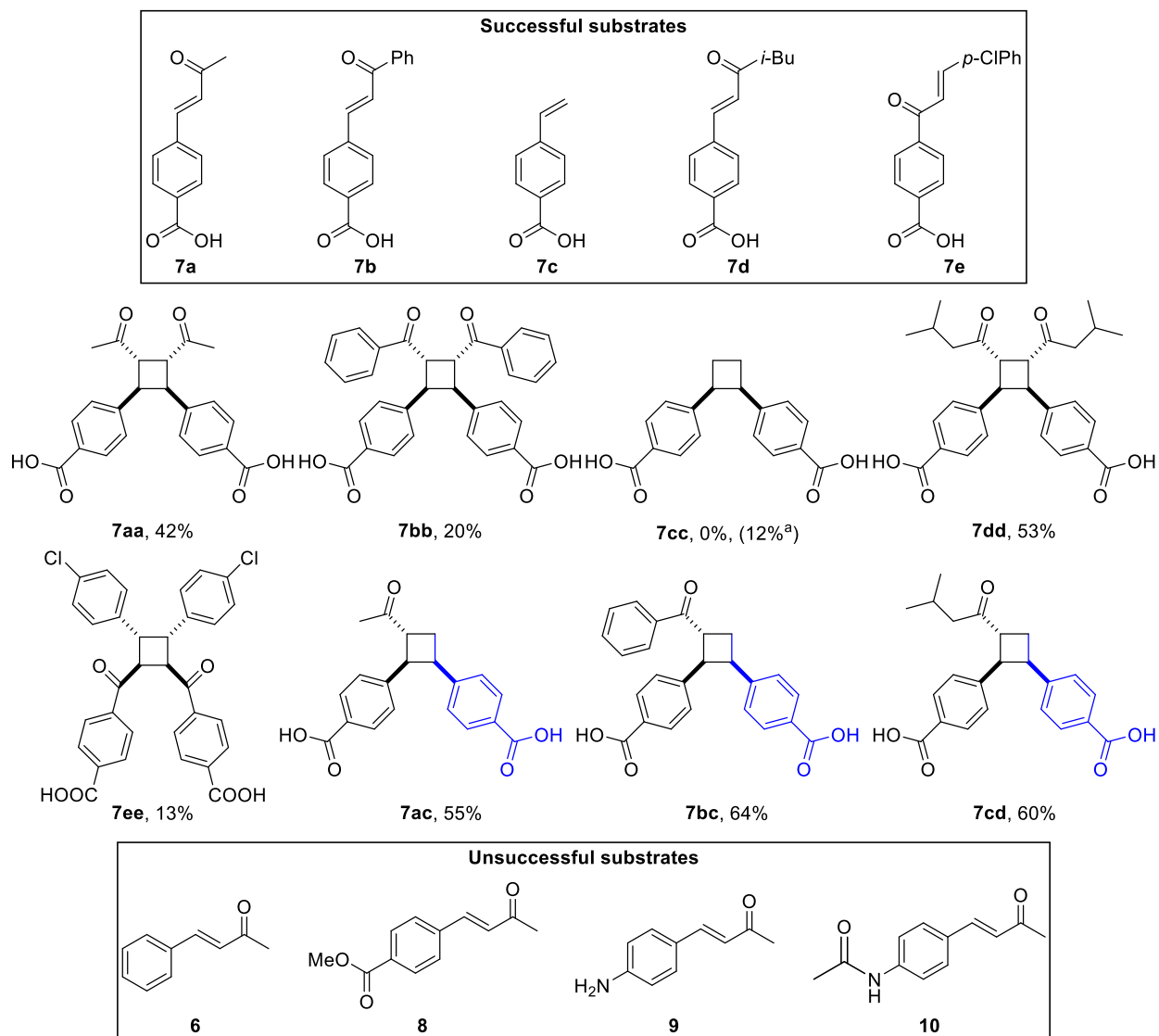


Figure 3.4 Time-dependent NMR studies of cycloaddition of **7a** in THF-d₈ (signals of emerging **7aa** are circled in red frames).

We next extended the scope of the photocatalytic [2+2] cycloadditions and synthesized an array of *homo* and *hetero* HH-*syn*-[2+2] products as shown in **Scheme 3.2** with bulk-like CsPbBr₃ NCs. In general, the heterocouplings (*e.g.*, **7ac**, **7bc**, **7cd**) were observed with higher yields than the homocouplings. The *homo* [2+2] cycloaddition generated a polymeric byproduct as evidenced

by ^1H NMR (**Figure 3.19**), perhaps resulting from NCs surface-templated polymerization of the excited-state olefin TEAs. **7c** ($E_{\text{T}} = 2.51$ eV) cannot be triplet excited by bulk-like CsPbBr₃ NCs ($E_{\text{T}} = 2.4$ eV) under the standard reaction conditions, but when added in excess, can function as a coupling partner to capture the other excited-state TEAs for *hetero* [2+2] cycloaddition, thus inhibiting the polymeric byproduct formation route. The *homo* [2+2] cycloaddition of **7c** under standard conditions was unsuccessful, however, could be achieved by adding a catalytic amount of oleylamine to the reaction mixture. This may result from a previously observed etching effect²⁶ of the perovskite NCs with the presence of both aromatic acids and primary amines. Such effect induced a blue-shift of the PL of CsPbBr₃ NCs (**Figure 3.29**) indicating an increased E_{T} , hence enabled the activation of substrate **7c**.



Scheme 3.2 Representative scope of bulk-like CsPbBr₃ NCs-induced HH-*syn*-[2+2] cycloadditions. Reactions were performed under standard conditions. For heterocoupling, **7c** (0.033 mmol, 3.0 equiv.) was used as coupling partner to react with other 4-vinylbenzoic acid derivatives (0.011 mmol, 1.0 equiv.). All yields are isolated yields.

^aReaction ran for 40 hours and oleylamine (5 μ L) was used as an additive.

3.3.4 TET Dynamics

Ultrafast spectroscopy is critical to understand the dynamics of a photocatalytic reaction. Here we relied on it to illustrate the TET process within this visible-light-induced cycloaddition pathway. Previous ultrafast studies demonstrated that TET to TEAs, *i.e.*, PAHs, was not observed for bulk-like CsPbBr₃ perovskite NCs while the TET efficiency gradually increased when quantum

confined perovskite NCs were employed.¹⁰ A highly size-dependent TET rate was obtained as a function of carrier probability density at the NC surface ($|\Psi_s|^2$) for varying NC sizes. A highest TET efficiency was observed for a blue NC (size = 3.5 nm) with the strongest quantum confinement.

The TET dynamics is drastically different in the current [2+2] cycloaddition system. TET dynamics was compared among three representative TEAs. (**Figure 3.5**) Typical pseudocolor images corresponding to NC, NC+**7a** (labelled **7a'**), NC+**7b** (labelled **7b'**) and NC+**7c** (labelled **7c'**) in THF were generated. The color indicates the intensity of the photo-induced absorption (PIA) or photo-induced ground state bleach (GSB). The GSB dynamics can be followed to monitor the reaction progress.^{25, 27, 28} In the pseudocolor image, the bright red color corresponds to the photo-induced GSB of the perovskite NCs. The dynamics for **7b'** exhibited a faster overall decay than that observed for the isolated NCs, indicating a fast TET. The dynamics for **7a'**, on the other hand, showed an initial faster decay around 107 ps followed by a much slower decay. This indicates the energy of the triplet of **7a** ($E_T = 2.36$ eV⁸) can transfer back to the NCs since they have similar energies.¹¹ In the case of **7c'**, the dynamics was almost identical to the isolated NCs, suggesting no TET or charge transfer to **7c** ($E_T = 2.51$ eV). This also corroborates well with the experimental observation that *homo*-cycloaddition of **7c** to **7cc** was not occurring under our standard reaction conditions. To further elucidate the TET, we extended the kinetic studies of **7a'**, **7b'** and **7c'** to 10 μ s. We first analyzed the kinetics for **7c'**. Since there is no TET for **7c'**, we can use a previously established fitting procedure to model its kinetics.²⁵ We described the TA kinetics with three parallel processes in **Eq. 3.1** (**Table 3.9**):

$$[N(t)] = -A_1 \cdot e^{-\frac{t}{\tau_1}} - A_2 \cdot e^{-\frac{t}{\tau_2}} - A_3 \cdot e^{-\frac{t}{\tau_3}} \quad (\text{Eq. 3.1})$$

where $N(t)$ is the exciton population at a pump-probe delay of t , τ_1 , τ_2 and τ_3 are the three processes that describe charge recombination of the NCs²⁹. For **7c'**, the best-fit time constants are 922 ± 47 ps, 16.6 ± 1.0 ns and 840 ± 49 ns which corresponds to surface trapping (922 ps) and radiative recombination (16.6 and 840 ns, possibly due to electrons and holes, **Table 3.9**) respectively.³⁰ When TET occurs, we introduced a term to describe the fraction of nanocrystals (f_2) that undergo TET and subsequent recombination. Due to the heterogeneous nature of the reaction, a portion of NCs might not have a TEA nearby and therefore this fraction (f_1) remains unchanged.²⁵ Thus, **Eq. 3.1** can be rewritten as following:

$$[N(t)] = f_1 \left(-A_1 \cdot e^{-\frac{t}{\tau_1}} - A_2 \cdot e^{-\frac{t}{\tau_2}} - A_3 \cdot e^{-\frac{t}{\tau_3}} \right) + f_2 \left(-B_1 \cdot e^{-\frac{t}{\tau_4}} - B_2 \cdot e^{-\frac{t}{\tau_5}} \right) \quad (\text{Eq. 3.2})$$

Here τ_4 is energy transfer time and τ_5 is recombination lifetime. Note here when TET occurs to induce [2+2] cycloaddition reactions, there will be no recombination afterward and the whole process is dominated by τ_4 . In colloidal systems, characteristic charge/energy transfer times from nanocrystals to molecules can span from a few ps to a few ns.³¹⁻³³ Here the fitting results are shown in **Figure 3.5C** and the best-fit parameters are listed in **Table 3.2**, rendering a ~110 ps fast TET from bulk-like perovskite NCs to TEAs under the current reaction pathway, and a moderate fraction of *ca.* 13-20% bulk-like perovskite NCs undergoing the TET process to the TEAs.

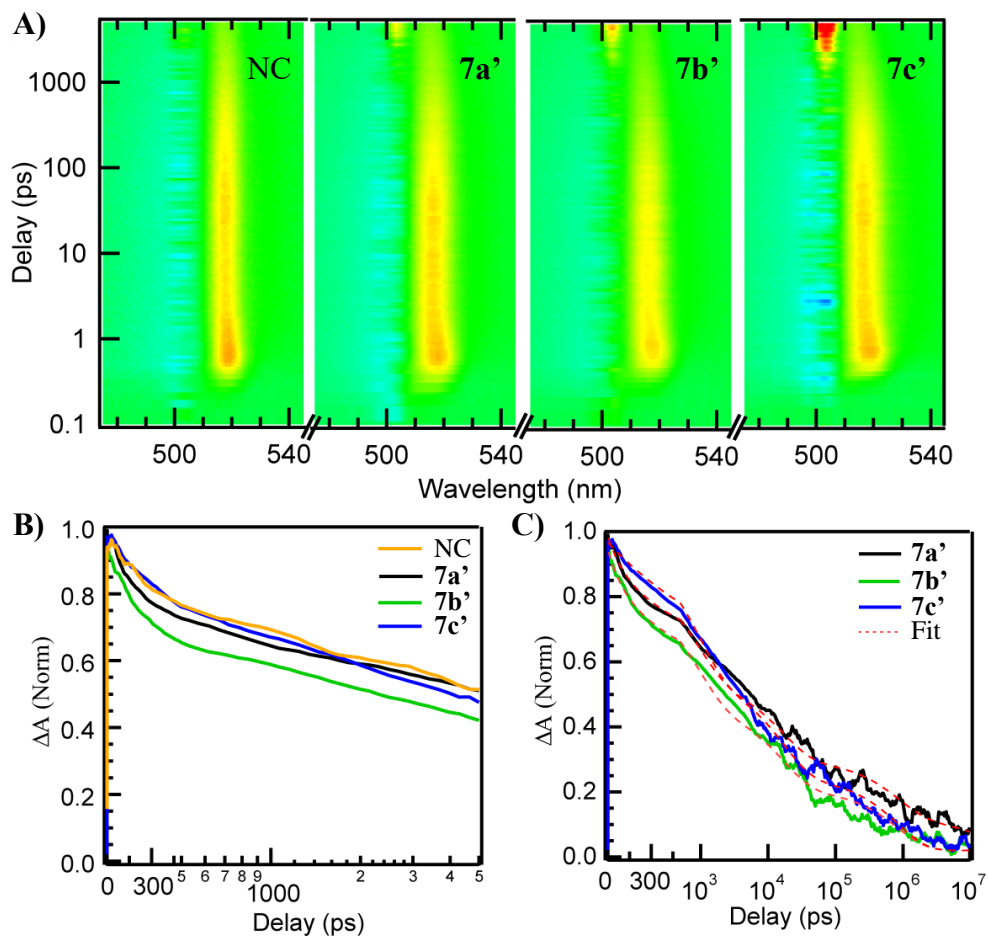


Figure 3.5 A) Pseudocolor image plot of the transient absorption (TA) experiments of NC, **7a'**, **7b'** and **7c'** in THF. The y-axis indicates pump-probe delay time and the x-axis indicates the probe wavelength. The bright red color corresponds to a photoinduced NCs exciton ground state bleach while blue is a photoinduced absorption; B) Normalized TA kinetics probed at the center of the NCs exciton bleach spectrum for NC, **7a'**, **7b'** and **7c'**; C) Normalized TA kinetics and fits for **7a'**, **7b'** and **7c'**.

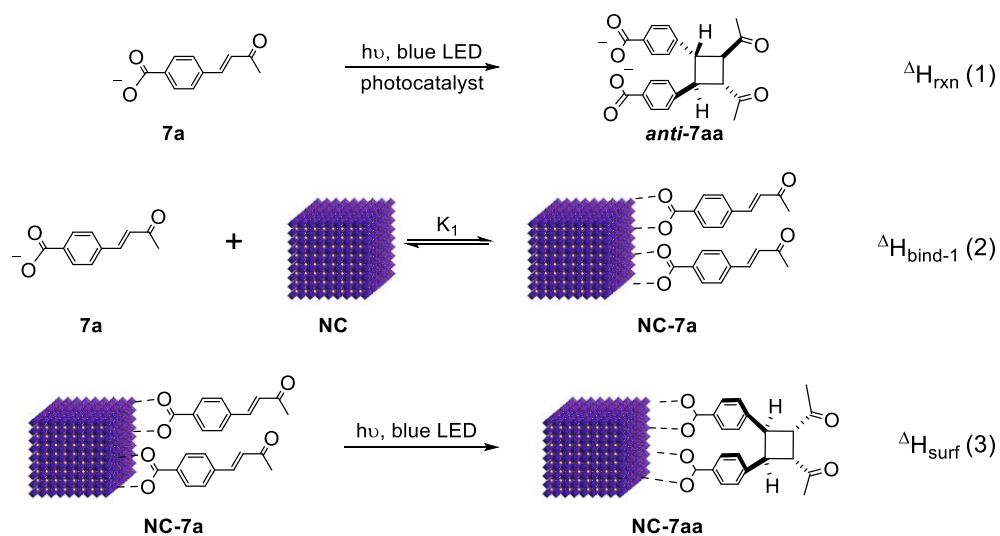
Table 3.2 TET fit parameters.

Reactants	τ_4 (ps)	f_2
7a	107 ± 19	$13 \pm 3\%$
7b	109 ± 18	$20 \pm 5\%$
7c	no TET	N/A

Previous ultrafast study demonstrated that efficiencies of TET to TEAs gradually increased when quantum confined perovskite NCs were employed.¹⁰ For bulk-like CsPbBr₃ NCs, the TET efficiency was very low (0.006) which is quite different from our [2+2] cycloaddition system studied here. A fast TET rate on the order of ~110 ps, was illustrated by transient absorption spectroscopy in our system. Such a trend might be related to a surface state mediated energy transfer process which was observed for PbS quantum dots^{34, 35} and bulk metal-halide perovskite systems³⁶. With a surface state mediation, triplet energies could efficiently transfer to the TEAs and result in a [2+2] cycloaddition reaction.

3.3.5 DFT Studies

We employed DFT calculations to illustrate the surface binding thermodynamics that are responsible for the highly *syn*-selective [2+2] product. DFT calculations were applied to estimate the binding energy in **Scheme 3.3**, employing the same methodology as reported lately on a CdSe quantum dot system.³⁷ A 4x4 cubic matrix from perovskite crystal structure (Pb-Br 2.97 Å, Cs-Cs 5.94 Å)³⁸ with Cs-rich surface was used without optimization as shown in **Figure 3.6A**. The binding energies were computed with DFT using a B3LYP functional and the Ahlrich's double- ζ basis with a polarization function, Def2-SVP, with the dispersion terms including D3BJ (Grimme's third-generation dispersion and Becke-Johnson damping). (More details are shown in **Section 3.5.13**)



Scheme 3.3 Proposed reaction paths.

We employed **7a** as an example to illustrate the highly diastereomeric selectivity in this reaction pathway as proposed in **Scheme 3.3**. We found that reaction (1) is exothermic, $\Delta H_{\text{rxn}} \sim -6$ kcal/mol in *syn*-mode while ~ -11 kcal/mol in *anti*-addition in THF. Without surface binding, *i.e.*, under unbound TET from molecular photocatalyst, an *anti*-addition [2+2] product will be preferred. This is corroborating with previous reports that reaction (1) with homogenous Ir- or Ru-based molecular sensitizer, *anti*-[2+2] cyclobutanes were dominant.¹⁻⁶

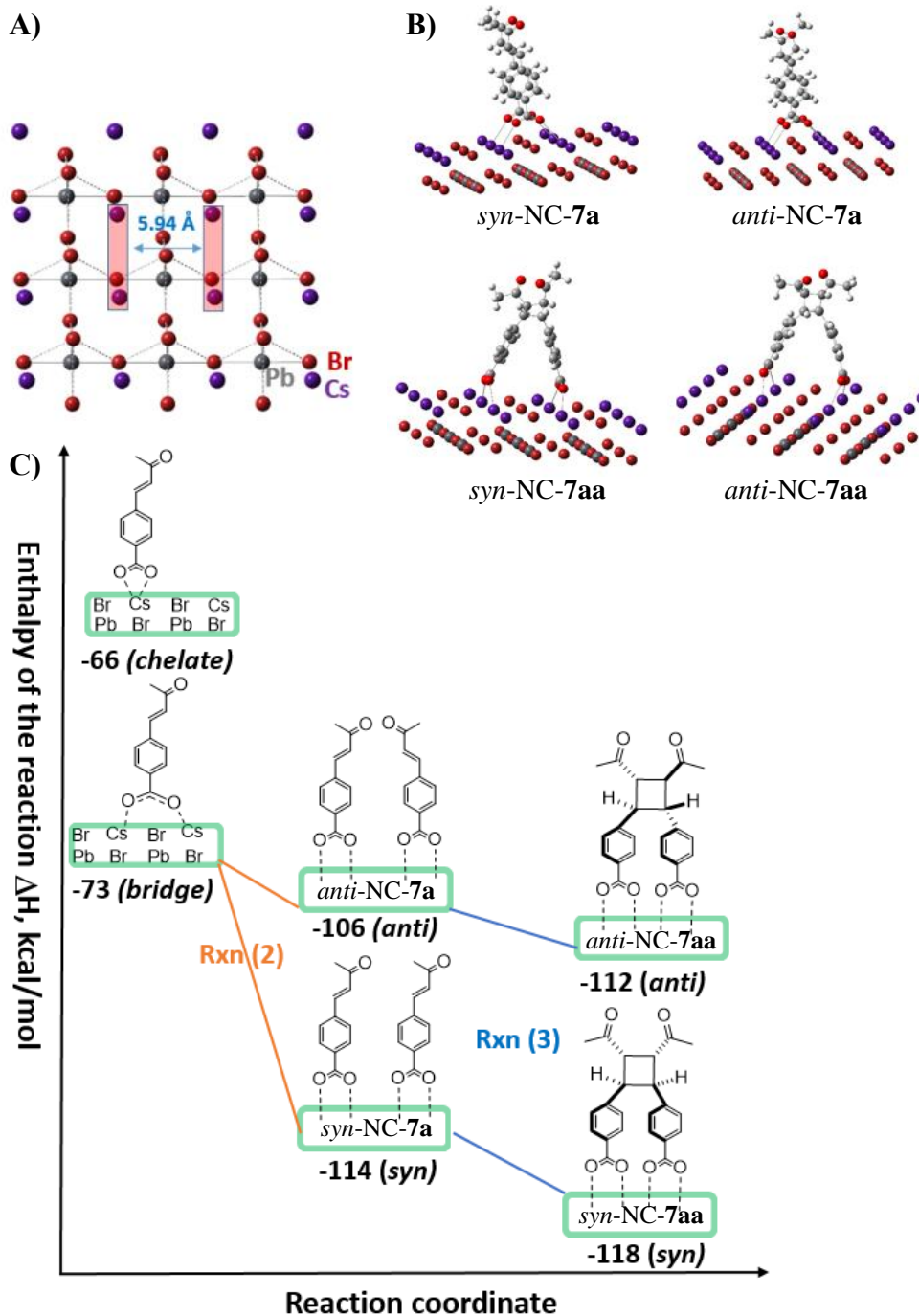


Figure 3.6 A) Perovskite CsPbBr₃ surface (frozen structure from crystal structure); B) Optimized binding structures of **7a** and **7aa** via *syn*- and *anti*-mode on NC; C) Binding enthalpy of the reaction path.

With NCs surface binding, a clear discrepancy of reaction paths was shown in **Scheme 3.3**.

Previous experimental evidence³⁹ and theoretical explorations⁴⁰ both suggested that CsPbBr₃ NCs

present an excess Cs^+ with positively charged surface. We adopted positively charged Cs-rich NCs surface which prefers the binding to the carboxyl substrates as shown in **Figure 3.6A** and **3.6B** accordingly.⁴⁰ Three carboxylate-binding modes, **7a**-chelating to one Cs-ion, **7a**-bridging to two-adjacent Cs-ions, and **7a**-bridging to two-diagonal Cs-ions were compared. (**Figure 3.31**) The binding energy comparison indicated that **7a**-bridging (shown in **Figure 3.6C**) demonstrated the most stable binding enthalpy and therefore was selected for further binding modes exploration. Respective binding-intermediates in reaction (2) and (3), **Scheme 3.3**, were optimized as shown in **Figure 3.6B** and their energy comparison were illustrated in **Figure 3.6C**. The key intermediate NC-**7a** demonstrated stark discrepancy with reaction (1) in which the *syn*-NC-**7a** demonstrate \sim -8 kcal/mol enthalpy more stable than the *anti*-NC-**7a**. The NC-**7aa** intermediate also demonstrated about the similar energy discrepancy, -6 kcal/mol with preference to the *syn*-NC-**2aa**. This DFT results demonstrated similar energy discrepancy on a CdSe quantum dots surface where ca. -17 kcal/mol energy stabilization was noted of *syn*- over *anti*-intermediate. In general, these DFT results corroborate well with our experimental observation where *syn*-product is dominant in this TET-based perovskite NCs photocatalysis.

The two **7a** substrates, *syn*- or *anti*-binding on the NC surface, after TET-induced [2+2] cycloaddition, determined the final *syn*- or *anti*-**7aa** product respectively. ΔH_{rxn} of overall reaction (1) does not necessarily govern the final diastereomeric selectivity under the templated reaction path. Rather, both binding intermediates show lower energy path in *syn*-mode than respective *anti*-mode. We may rationale that the π -orbital overlap between **7a** substrates in *syn*-mode delocalized extensively from the phenyl group to conjugate motifs, *i.e.*, C=C and C=O bonds, however, such overlap is significantly diminished in *anti*-mode, with only phenyl-based π -overlap but excluding effective π -interaction in the C=C-C=O area. Such π -orbital overlap extension here might play a

more significant role on a flat cubic surface of the perovskite NCs. Therefore, *syn*-binding **NC-7a** is preferred with ca. -8 kcal/mol energy stabilization. Such energy term might be the key energy component for our observation here in this highly diastereomeric *syn*-selective cycloaddition.

3.4 Chapter Conclusions

In conclusion, triplet excitons that are generally confined within semiconductors have been successfully transferred from perovskite NCs to organic olefins substrates and induced a highly selective photocatalytic [2+2] cycloaddition reaction. We found that under our designed reaction pathway, the quantum confinement is not necessary to entail the TET event, perhaps indicating a discrepant TET mechanism from perovskite to PAHs. Bulk-like CsPbBr₃ NCs with uncontrolled size (>10 nm) are significantly more accessible for catalyst production and hence a reliable and economical photocatalyst for this type of *syn*-selective reaction. The TET-induced reaction dynamics has been illustrated with ultrafast spectroscopy. Fast dynamics (~110 ps) and moderate fraction (~20%) of TET were observed from NCs to the respective TEAs. DFT theoretical method that was previously employed on a CdSe QD system, was successfully explored here to elucidate the high selectivity in this CsPbBr₃ perovskite NCs surface-templated [2+2] reaction path. A non-trivial amount of binding enthalpy, up to -8 kcal/mol, likely accounting from the extended π -orbital overlap under *syn*-mode, was found to stabilize the key *syn*-addition intermediate. Our exploration here may reveal a new triplet energy conversion pathway to employ bulk-like semiconductors for photocatalytic organic synthesis.

3.5 Experimental Section

3.5.1 General Information

Commercially available reagents were purchased from Sigma-Aldrich or TCI Chemicals (US). Anhydrous, unstable tetrahydrofuran (THF) was purchased from Alfa Aesar and was used directly under N₂ protection for photochemical reaction setup. All other solvents were purchased

from Alfa Aesar or Fisher Scientific and were used as received. Household blue LED light bulbs (14 W) were purchased from Amazon and were used for all photochemical reactions unless otherwise noted. Silica gels (P60, 40-63 μm , 60 \AA) used for column chromatography were purchased from SILICYCLE (Canada). Thin layer chromatography (TLC) analysis was carried out on aluminum or glass backed silica gel coated plates (200 μm , SILICYCLE). Visualization was completed by a Analytikjena hand-held UV lamp (254 nm).

^1H NMR and ^{13}C NMR spectra were acquired on a Varian VNMRS 400 spectrometer or Varian Inova 500 spectrometer. All chemical shifts are reported in parts per million (ppm) referenced to residual dimethyl sulfoxide- d_6 (2.50 ppm and 39.52 ppm, respectively for ^1H and ^{13}C NMR), unless otherwise noted. All coupling constants (J) are reported in hertz (Hz). Abbreviations are: s, singlet; br s, broad singlet; d, doublet; t, triplet; q, quartet; m, multiplet. ^1H NMR data were acquired for all compounds for characterization purposes. ^{13}C NMR and high-resolution mass spectra (HRMS) were acquired for all new compounds. CH_2Br_2 was used as an internal standard for calculating the NMR yields. Diastereomeric ratio was calculated from ^1H NMR integration.

HRMS were recorded on an Agilent 6530 Accurate Mass Q-TOF with an electrospray ionization (ESI) method. High-performance liquid chromatography (HPLC) data was acquired on an Agilent 1100 series HPLC equipped with a C18 column (4.6 x 100 mm, 3.5 micron). Steady-state emission spectra were acquired using a HORIBA Fluoromax-4 spectrofluorometer. Powder XRD analysis was taken on an X-ray Powder Diffraction Philips Empyrean using a piece of glass slide as the sample holder. UV-Vis absorption spectra were acquired using a Thermo Scientific GENESYS 30 Visible Spectrophotometer. IR spectra were recorded on a Thermo Fisher Scientific

Nicolet iS50 FTIR Spectrometer. Transmission Electron Microscope (TEM) images were collected on an FEC Tecnai 12 Transmission Electron Microscope.

3.5.2 Preparation of Perovskite Photocatalysts

Room-temperature synthesis of CsPbBr₃ perovskite NCs: Large-sized CsPbBr₃ NCs were synthesized by minor modification of the literature method.⁴¹ CsBr solution (2.0 mL, 1.0 M in H₂O) and PbBr₂ solution (2.0 mL, 1.0 M in dimethylformamide, DMF) were prepared as two respective precursor stock solutions. To a vigorously stirring mixture of hexanes (10.0 mL), oleic acid (OA, 2.0 mL) and *n*-octylamine (0.25 mL) was added the above-mentioned PbBr₂ solution (300 μL) and CsBr solution (300 μL) dropwise. A white-yellowish emulsion formed along with mixing. Subsequently, acetone (8.0 mL) was added in one time for demulsification purpose. After that, the resulting mixture was subjected to centrifugation at 4k rpm for 5 min to afford the CsPbBr₃ NCs which was then further washed by hexanes (3 mL) for 2 times. The residual solvent was removed by house vacuum for 2h.

Hot-injection synthesis of CsPbBr₃ perovskite NCs: CsPbBr₃ NCs were synthesized by minor modification of the literature method.⁴² A Cs-oleate precursor solution was prepared by loading Cs₂CO₃ (0.204 g), OA (625 μL) and 1-octadecene (1-ODE, 10.0 mL) in a 50-mL 2-neck round-bottom flask equipped with a suitable magnetic stirring bar. The resulting dispersion was subjected to vacuum dry at 120 °C for 1h and then charged with N₂ before heating to 150 °C until all the Cs₂CO₃ reacted with OA. The Cs-oleate precursor solution was kept at 120 °C for use in next step. Meanwhile, 1-ODE (5.0 mL) and PbBr₂ (0.069 g, 0.188 mmol) were loaded into a 25-mL Schlenk tube equipped with a suitable magnetic stirring bar and dried under vacuum at 120 °C for 1h. It was then charged with N₂ followed by the addition of dried oleylamine (OlAm, 0.5 mL) and dried OA (0.5 mL). After complete solubilization of PbBr₂, the temperature of the resulting solution was raised to and kept at 170 °C. The prepared Cs-oleate solution (0.40 mL, 0.125 M in

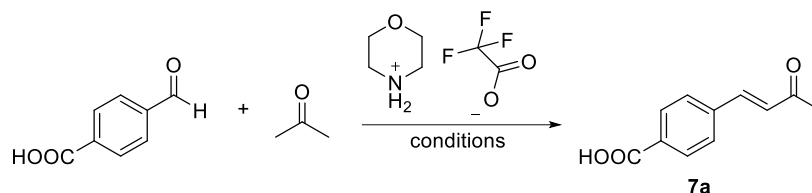
1-ODE) was quickly injected by using a 1-mL syringe and 5s later, the reaction mixture was taken out from the hot plate and cooled by immersion in an ice-water bath for 1 min. The resulting yellow-greenish mixture was added the same volume of methyl acetate (MeOAc, ~ 6.5 mL), CsPbBr₃ NCs were then collected by centrifugation at 4k rpm for 30 min and further washed by MeOAc (3 mL). The residual solvent was removed by house vacuum for 2h.

Synthesis of amine-free CsPbBr₃: The amine-free CsPbBr₃ NCs were synthesized by modification of the literature method.⁴³ A 50-mL Schlenk tube equipped with a suitable-sized magnetic stirring bar was loaded with CsOAc (48.0 mg, 0.25 mmol), Pb(OAc)₂ (163.0 mg, 0.5 mmol), OA (2.0 mL) and 1-ODE (5.0 mL). The resulting mixture was then heated at 120 °C under vacuum for 30 min to remove moisture before being refilled with N₂. The reaction mixture was allowed to react for another 30 min at 100 °C before lowering the temperature to 80 °C. A preheated (80 °C) tetraoctylammonium bromide (TOABr) solution (5.0 mL, 0.1 M in toluene) was swiftly injected to the Schlenk tube, a yellowish solution was observed and the resulting mixture was removed from the heating source and cooled down to room temperature. A hexanes/acetone solution (1:2, 45 mL) was added as an anti-solvent and the CsPbBr₃ NCs were collected by centrifugation at 4k rpm for 10 min. The CsPbBr₃ NCs were washed again by a hexanes/acetone solution (1:2, 10 mL) and dried under house vacuum for 2h to remove residual solvents.

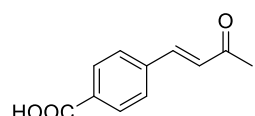
Synthesis of zero-dimension Cs₄PbBr₆: Cs₄PbBr₆ was synthesized according to the reported method.⁴⁴ A 50-mL round-bottom flask was charged with PbBr₂ (1.835 g, 5.0 mmol), CsBr (1.064 g, 5.0 mmol) and dimethyl sulfoxide (DMSO, 5.0 mL). The resulting mixture was allowed to stir at room temperature for 1h before the solution was filtered and heated at 120 °C for 3h. The resulting precipitate was collected by vacuum filtration and washed by DMSO. Then the collected solid was subjected to vacuum oven drying at 100 °C for overnight.

3.5.3 Preparation of Substrates

(*E*)-4-(3-oxobut-1-en-1-yl)benzoic acid (**7a**)

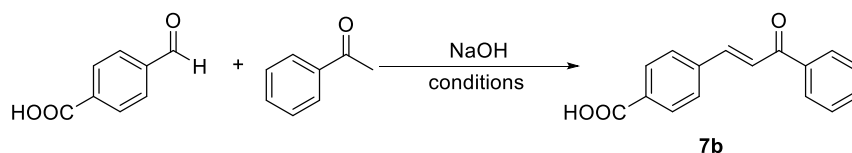


The titled compound (**7a**) was prepared by literature reported method.⁴⁵ Firstly, the morpholinium trifluoroacetate was prepared by slow addition of trifluoroacetic acid (842 μL , 11 mmol) in morpholine solution (20 mL, 0.5 M in diethyl ether) at 0 $^{\circ}\text{C}$. The reaction solution was stirring for 1h before warming up to room temperature followed by collecting the catalyst as white solid with Büchner funnel and being washed with diethyl ether. The aldol condensation reaction was performed in a 50-mL sealed vial, to which terephthalaldehydic acid (900 mg, 6.0 mmol, 1.0 equiv.), acetone (15 mL), morpholinium trifluoroacetate (240 mg, 1.2 mmol, 20 mol%) was added accordingly. The reaction mixture was allowed to stir at 75 $^{\circ}\text{C}$ for 48h before being cooled down to room temperature. The over-excess acetone was removed by rotary evaporation and the resulting solid was washed by water for two times and recrystallized from ethanol to afford the titled compound as white solid in a yield of 80% (913 mg). The ^1H NMR spectra matched those reported in the literature.⁴⁵

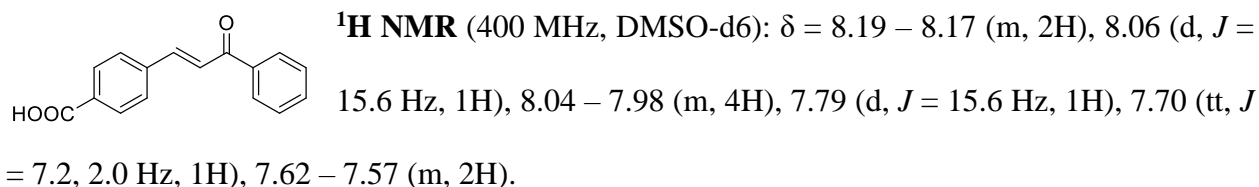


^1H NMR (500 MHz, DMSO- d_6): δ = 7.97 (d, J = 8.0 Hz, 2H), 7.82 (d, J = 8.0 Hz, 2H), 7.67 (d, J = 16.5 Hz, 1H), 6.90 (d, J = 16.5 Hz, 1H), 2.36 (s, 3H).

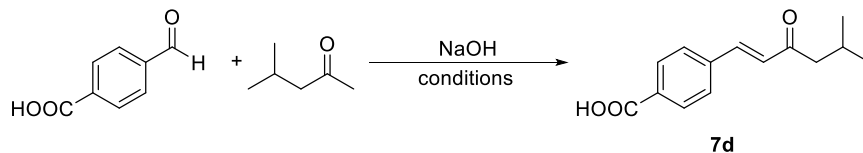
(*E*)-4-(3-oxo-3-phenylprop-1-en-1-yl)benzoic acid (**7b**)



The titled compound (**7b**) was prepared by the following procedure: A 50-mL round-bottom flask was charged with terephthalaldehydic acid (450 mg, 3.0 mmol, 1.0 equiv.), acetophenone (386 μ L, 3.3 mmol, 1.1 equiv.), and methanol (20 mL). Under stirring, NaOH solution (3 mL, 3.0 M in H₂O) was added in the reaction mixture dropwise, then it was allowed to react at room temperature for overnight before the pH value of the reaction mixture was adjusted to ~2 using HCl solution (2.0 M in H₂O). The resulting solid was collected by vacuum filtration and washed with water and ethanol for two times respectively to afford the titled compound as white solid in a yield of 51% (386 mg). The ¹H NMR spectra matched those reported in the literature.⁸

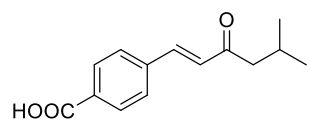


(E)-4-(5-methyl-3-oxohex-1-en-1-yl)benzoic acid (7d)



The titled compound (**7d**) was prepared by the following procedure: A 50-mL round-bottom flask was charged with terephthalaldehydic acid (450 mg, 3.0 mmol, 1.0 equiv.), methyl isobutyl ketone (1.135 mL, 9.0 mmol, 3.0 equiv.), and ethanol (10 mL). Under stirring, NaOH solution (3 mL, 3.0 M in H₂O) was added in the reaction mixture dropwise, then it was allowed to react at room temperature for 48h before the pH value of the reaction mixture was adjusted to ~2 using HCl solution (2.0 M in H₂O). The ethanol was then removed by rotary evaporation and the

resulting solid was collected by vacuum filtration and washed with water. After recrystallization from ethanol, the titled compound was afforded as white solid in a yield of 54 % (375 mg).

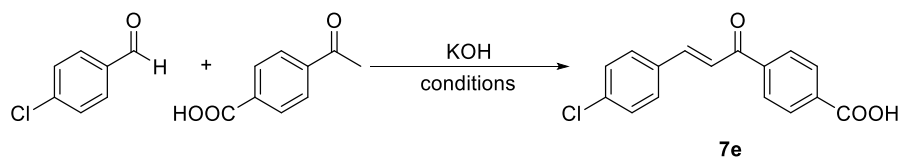


¹H NMR (400 MHz, DMSO-d₆): δ = 7.96 (d, *J* = 8.4 Hz, 2H), 7.83 (d, *J* = 8.4 Hz, 2H), 7.64 (d, *J* = 16.4 Hz, 4H), 6.98 (d, *J* = 16.4 Hz, 1H), 2.59 (d, *J* = 6.8 Hz, 2H), 2.17 – 2.07 (m, 1H), 0.91 (d, *J* = 6.8 Hz, 6H).

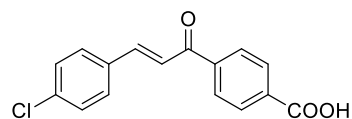
¹³C NMR (126 MHz, acetone-d₆): δ = 199.8, 167.1, 141.1, 140.2, 131.0, 129.7, 129.6, 129.1, 50.3, 25.6, 22.9.

HRMS (ESI⁺) (*m/z*): [M-H]⁺ calculated for C₁₄H₁₅O₃, 231.1021; found 231.1033.

(E)-4-(3-(4-chlorophenyl)acryloyl)benzoic acid (7e)

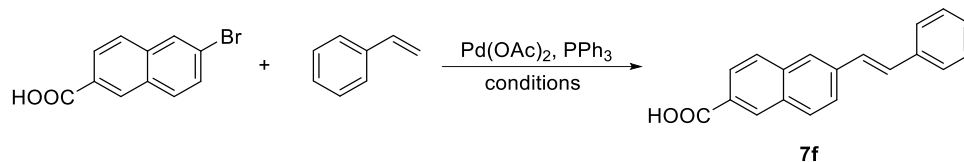


The titled compound (**7e**) was prepared by the following procedure: A 50-mL round-bottom flask was charged with 4-chlorobenzaldehyde (428 mg, 3.05 mmol, 1.0 equiv.), 4-acetylbenzoic acid (500 mg, 3.05 mmol, 1.0 equiv.), and ethanol (20 mL). Under stirring, KOH solution (3.05 mL, 3.0 M in H₂O) was added in the reaction mixture dropwise, then it was allowed to react at room temperature for overnight before the pH value of the reaction mixture was adjusted to ~2 using HCl solution (2.0 M in H₂O). The solid was collected by vacuum filtration and washed with water and ethanol for two times respectively to afford the titled compound as white solid in a yield of 56 % (490 mg). The ¹H NMR spectra matched those reported in the literature.⁴⁶

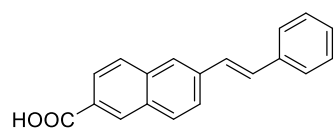


¹H NMR (500 MHz, DMSO-d₆): δ = 8.23 (d, *J* = 8.0 Hz, 2H), 8.10 (d, *J* = 8.0 Hz, 2H), 7.98 – 7.94 (m, 3H), 7.76 (d, *J* = 15.5 Hz, 1H), 7.54 (d, *J* = 8.5 Hz, 2H).

(E)-6-styryl-2-naphthoic acid (7f)

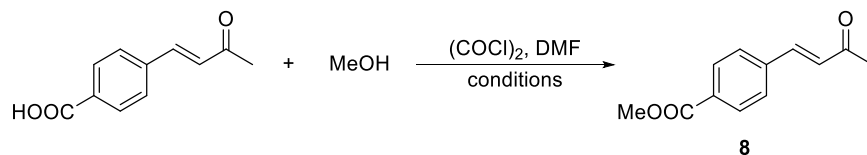


The titled compound (**7f**) was prepared by modified literature reported method.⁸ A 100-mL Schlenk tube equipped with a suitable magnetic stirring bar was charged with 6-bromo-2-naphthoic acid (627.7 mg, 2.5 mmol, 1.0 equiv.), triphenylphosphine (52.0 mg, 0.2 mmol, 8 mol%), K₂CO₃ (346 mg, 2.5 mmol, 1.0 equiv.), DMF (16 mL), styrene (372 μ L, 3.25 mmol, 1.3 equiv.), Pd(OAc)₂ (22.5 mg, 0.1 mmol, 4 mol%) under a continuous flow of N₂. And then Et₃N (4 mL) was quickly added. Three vacuum/N₂ cycles were carried out immediately to get rid of residual oxygen from the reaction system. Then the Schlenk tube was sealed but connected with a N₂ balloon and it was allowed to react at 110 °C for 16h. The reaction mixture was then cooled to room temperature and diluted with water (~100 mL). The resulting aqueous suspension was first washed twice with EtOAc then the pH value of the aqueous phase was the adjusted to ~3 with HCl (1.0 M in H₂O) and extracted twice with EtOAc. The combined organic phase was dried over Na₂SO₄ and the solvent was removed under rotary evaporation. The resulting solid was triturated with hot CHCl₃ to afford the titled compound as pale brown solid in a yield of 35% (235 mg). The ¹H NMR spectra matched those reported in the literature.⁸

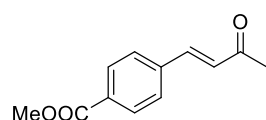


¹H NMR (400 MHz, DMSO-d₆): δ 8.57 (s, 1H), 8.11 (d, J = 9.2 Hz, 2H), 7.98 - 7.95 (m, 3H), 7.68 (d, J = 7.6 Hz, 2H), 7.53 - 7.44 (m, 2H), 7.42 (t, J = 7.6 Hz, 2H), 7.31 (t, J = 7.6 Hz, 1H).

methyl (*E*)-4-(3-oxobut-1-en-1-yl)benzoate (8**)**

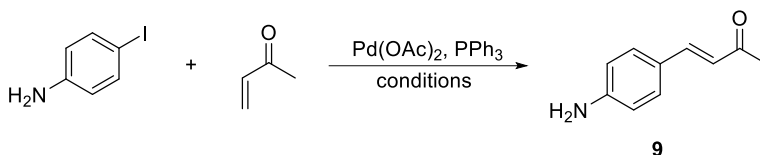


The titled compound (**8**) was prepared by modified literature reported method.⁴⁷ A 20-mL vial equipped with a suitable magnetic stirring bar was charged with (*E*)-4-(3-oxobut-1-en-1-yl)benzoic acid (**7a**, 190.2 mg, 1.0 mmol, 1.0 equiv.), dichloromethane (DCM, 3.2 mL), DMF (130 μ L) and oxalyl chloride (93.5 μ L, 1.1 mmol, 1.1 equiv.). The reaction mixture was allowed to stir at room temperature for 50 min. Then MeOH (500 μ L) was added in the reaction mixture dropwise at 0 $^{\circ}$ C. The reaction was then allowed to react at room temperature for another 2h before it was neutralized with saturated NaHCO₃ solution and extracted by DCM. The combined organic phase was washed twice with water and once with brine. The organic phase was then collected, dried over Na₂SO₄ and the solvent was removed under rotary evaporation. Column chromatography was performed using Hexanes/EtOAc (5/1) as eluent to afford the titled compound as white solid in a yield of 30% (61 mg). The ¹H NMR spectra matched those reported in the literature.⁴⁵



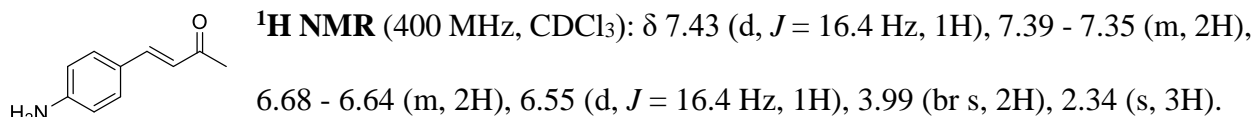
¹H NMR (400 MHz, CDCl₃): δ 8.06 (d, J = 8.4 Hz, 2H), 7.60 (d, J = 8.4 Hz, 2H), 7.52 (d, J = 16.4 Hz, 1H), 6.78 (d, J = 16.4 Hz, 1H), 3.93 (s, 3H), 2.40 (s, 3H).

(*E*)-4-(4-aminophenyl)but-3-en-2-one (9**)**

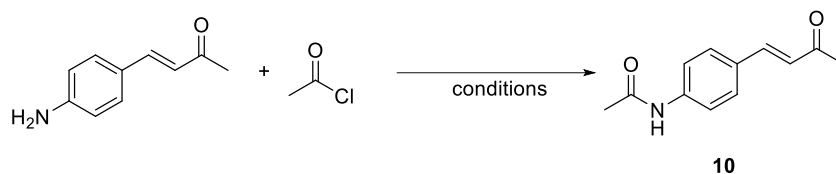


The titled compound (**9**) was prepared by the following procedure: A 100-mL Schlenk tube equipped with a suitable magnetic stirring bar was charged with 4-Iodoaniline (876.1 mg, 4.0

mmol, 1.0 equiv.), triphenylphosphine (104.9 mg, 0.4 mmol, 10 mol%), CH₃CN (20 mL), 3-Buten-2-one (466.7 μ L, 5.6 mmol, 1.4 equiv.) and Pd(OAc)₂ (44.9 mg, 0.2 mmol, 5 mol%) under a continuous flow of N₂. And then Et₃N (669 μ L, 4.8 mmol, 1.2 equiv.) was quickly added. Three vacuum/N₂ cycles were carried out immediately to get rid of residual oxygen from the reaction system. Then the Schlenk tube was sealed but connected with a N₂ balloon and it was allowed to react at 82 °C for 36h. The reaction mixture was then cooled to room temperature and the solvent, Et₃N, 3-Buten-2-one was removed under rotary evaporation. Column chromatography was performed using Hexanes/EtOAc (from 4/1 to 1/1) as eluent to afford the titled compound as pale brown solid in a yield of 21% (135 mg). The ¹H NMR spectra matched those reported in the literature.⁴⁸

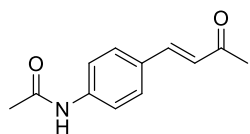


(E)-N-(4-(3-oxobut-1-en-1-yl)phenyl)acetamide (10)



The titled compound (**10**) was prepared by literature reported method.⁴⁹ A 20-mL vial equipped with a suitable magnetic stirring bar was charged with (*E*)-4-(4-aminophenyl)but-3-en-2-one (48.4 mg, 0.3 mmol, 1.0 equiv.), DCM (4 mL) and Et₃N (52.3 μ L, 0.375 mmol, 1.25 equiv.). While stirring at 0 °C, acetyl chloride (26.8 μ L, 0.375 mmol, 1.25 equiv.) was added dropwise to the reaction mixture. The reaction was then allowed to warm up to room temperature and continue to react until the complete conversion of the aniline (monitored by TLC). The reaction was quenched with saturated NaHCO₃ solution. The organic phase was washed with HCl solution (2.0 M in H₂O) and water, dried over Na₂SO₄ and concentrated under rotary evaporation. Further

purification of the product was needed via column chromatography using Hexanes/EtOAc (1/1, 1% DCM as additive) as eluent to afford the titled compound as pale yellow solid in a yield of 62% (38 mg). The ^1H and ^{13}C NMR spectra matched those reported in the literature.⁴⁵

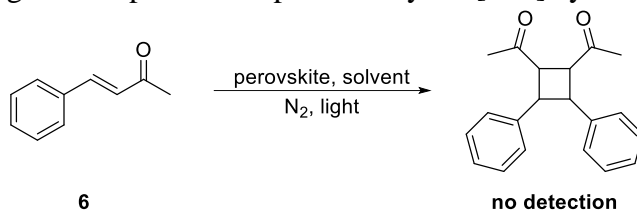


$^1\text{H NMR}$ (400 MHz, THF- d_8): δ = 9.26 (br s, 1H), 7.64 (d, J = 8.8 Hz, 2H), 7.51 (d, J = 8.8 Hz, 2H), 7.46 (d, J = 16.0 Hz, 1H), 6.63 (d, J = 16.0 Hz, 1H), 2.25 (s, 3H), 2.03 (s, 3H).

$^{13}\text{C NMR}$ (126 MHz, THF- d_8): δ = 196.7, 168.5, 143.0, 142.7, 130.4, 129.7, 126.4, 119.7, 27.2, 24.1.

3.5.4 Condition Exploration for Perovskite-Photocatalyzed [2+2] Cycloaddition

Table 3.3 Initial investigation of perovskite-photocatalyzed [2+2] cycloaddition of **6**.^a



Entry	Type of perovskite	Solvent	Light
1	room-temp. CsPbBr ₃	DCM	blue LED
2	room-temp. CsPbBr ₃	Toluene	blue LED
3	room-temp. CsPbBr ₃	THF	blue LED
4	room-temp. CsPbBr ₃	DCM	CFL
5	hot-injection CsPbBr ₃	DCM	blue LED
6	hot-injection CsPbBr ₃	Toluene	blue LED
7	hot-injection CsPbBr ₃	THF	blue LED
8	hot-injection CsPbBr ₃	DCM	CFL
9 ^b	hot-injection CsPbBr ₃	Toluene	blue LED
10 ^c	hot-injection CsPbBr ₃	Toluene	blue LED
11 ^d	hot-injection CsPbBr ₃	THF	blue LED

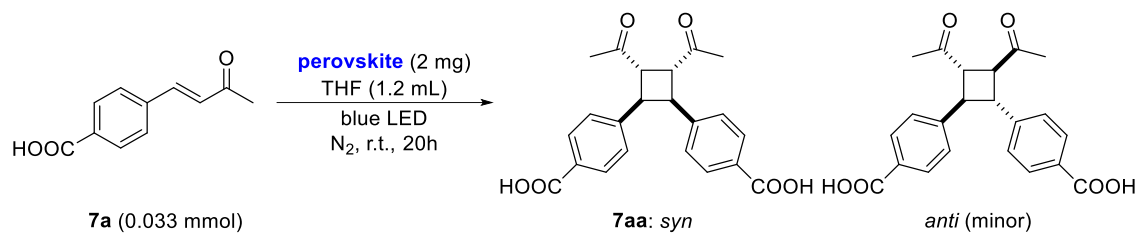
^aReaction ran with **6** (0.2 mmol), perovskite (2 mg) and solvent (2 mL) under visible light irradiation at room temperature for overnight.

^b**6** (2 mmol).

^cTrimethylsilyl chloride (1 μL) as additive.

^dEu(OTf)₃ (10 mol%) as additive.

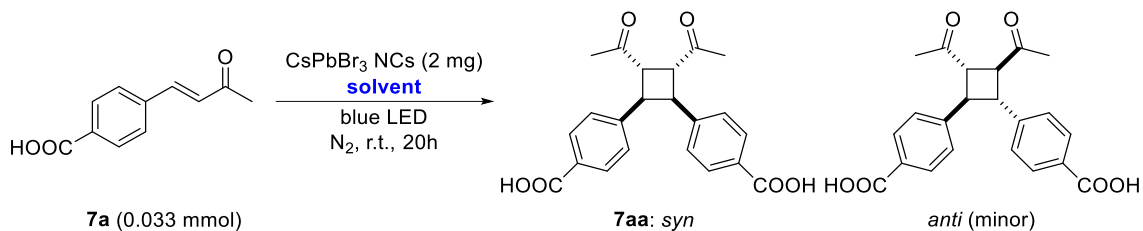
All the above conditions resulted in no product formation confirmed by TLC, GC-MS and ¹H NMR. CFL: compact fluorescence lamp.

Table 3.4 Investigation of the types of perovskites for photocatalytic [2+2] cycloaddition of **7a**.

Entry	Type of perovskite	7aa , % ^a	d.r. ^a
1	hot-injection CsPbBr ₃	44	>30:1
2	amine-free CsPbBr ₃	28	>30:1
3	room-temp. CsPbBr ₃	9	>30:1
4	Cs ₄ PbBr ₆	0	N/A
5	Without perovskite	0	N/A

^aYields and diastereomeric ratios were determined by crude ¹H NMR using CH₂Br₂ as an internal standard.

Table 3.5 Investigation of the types of solvents for CsPbBr₃-photocatalyzed [2+2] cycloaddition of **7a**.

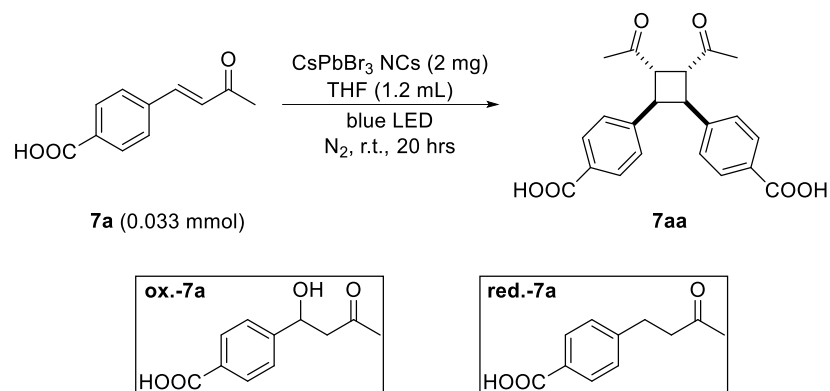


Entry	Type of solvent	7aa , % ^a	d.r. ^a
1	THF (1.2 mL)	44	>30:1
2	Toluene (1.2 mL)	5	n.d. ^b
3	THF/Tol (1/2, 1.2 mL)	22	>30:1
4	THF (10 mL)	17	>30:1

^aYields and diastereomeric ratios were determined by crude ¹H NMR using CH₂Br₂ as an internal standard.

^bNo detection due to detection limit.

CsPbBr₃ NCs: perovskite synthesized by hot-injection method.

Table 3.6 Investigation of other conditions for CsPbBr₃-photocatalyzed [2+2] cycloaddition of **7a**.

Entry	Deviation from standard conditions	7aa , % ^a
1	None	44
2	React for 12h instead of 20h	37
3	React for 48h instead of 20h	46
4	Green LED instead of blue LED	17
5	Red LED instead of blue LED	0
6	Without light	0
7	With CsPbBr ₃ NCs (12 mg)	29
8	Without N ₂ sparging	31 ^b
9	Benzoic acid (3 equiv.) as additive	40 ^c

^aYields were determined by crude ¹H NMR using CH₂Br₂ as an internal standard.

^bObserved with byproduct formation of **ox.-7a**.

^cObserved with byproduct formation of **red.-7a**.

CsPbBr₃ NCs: perovskite synthesized by hot-injection method.

3.5.5 Photocatalytic Synthesis of Products

General Procedure A for the NCs-Photocatalyzed [2+2] *Homo*-Cycloaddition:

A 4-mL vial was charged with 4-vinylbenzoic acid derivative (0.033 mmol), CsPbBr₃ NCs (2 mg) and a suitable-sized magnetic stirring bar. N₂-protected preservative-free THF (1.2 mL) was used as solvent. While stirring slowly, the reaction solution was purged with 99.998% N₂ for

20 min through a cap with Teflon septa and sealed with parafilm. The reaction vial was then placed in the middle of two face-to-face (~10 cm away) household blue LED bulbs (14 W) and stirred at 1200 rpm without heating for 20h.

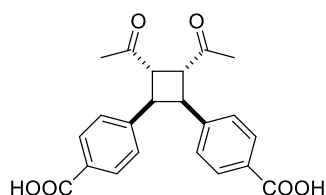
General Procedure B for the NCs-Photocatalyzed [2+2] *Hetero*-Cycloaddition:

A 4-mL vial was charged with 4-vinylbenzoic acid derivative (0.011 mmol, 1.0 equiv.), 4-vinylbenzoic acid (**7c**, 0.033 mmol, 3.0 equiv.), CsPbBr₃ NCs (2 mg) and a suitable-sized magnetic stirring bar. N₂-protected preservative-free THF (1.2 mL) was used as solvent. While stirring slowly, the reaction solution was purged with 99.998% N₂ for 20 min through a cap with Teflon septa and sealed with parafilm. The reaction vial was then placed in the middle of two face-to-face (~10 cm away) household blue LED bulbs (14 W) and stirred at 1200 rpm without heating for 20h.

Post-Reaction Work-Up for General Procedure A and B:

Once the reaction was finished, the reaction mixture was transferred to a 25-mL recovery flask to remove the THF solvent under rotary evaporation and the product was purified by silica gel column chromatography using AcOH/DCM (1% - 2%) as eluent (or a crude ¹H NMR using CH₂Br₂ as an internal standard was taken to determine the NMR yield before the purification).

Photocatalytic Synthesis of HH-Syn-Cyclobutanes

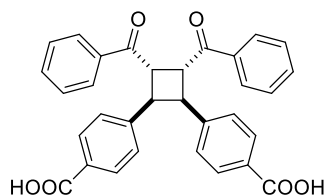


***syn*-4,4'-(3,4-diacetylcyclobutane-1,2-diyl)dibenzoic acid (**7aa**)**

The titled compound was synthesized according to **General**

Procedure A: (*E*)-4-(3-oxobut-1-en-1-yl)benzoic acid (**7a**, 6.3 mg, 0.033 mmol), CsPbBr₃ NCs (2 mg) and THF (1.2 mL) were used. The product was purified by flash column chromatography (AcOH/DCM = 1% - 2%) as white solid (42% **yield**, 2.6 mg). The ¹H NMR spectra matched those reported in the literature.⁸

¹H NMR (400 MHz, DMSO-d₆): δ = 7.65 (d, *J* = 7.6 Hz, 4H), 7.15 (d, *J* = 7.6 Hz, 4H), 4.16 (m, 4H), 2.12 (s, 6H).

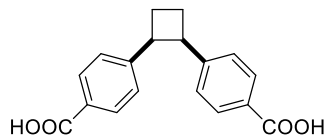


***syn*-4,4'-(3,4-dibenzoylcyclobutane-1,2-diyl)dibenzoic acid (7bb)**

The titled compound was synthesized according to **General**

Procedure A: (*E*)-4-(3-oxo-3-phenylprop-1-en-1-yl)benzoic acid (**7b**, 8.3 mg, 0.033 mmol), CsPbBr₃ NCs (2 mg) and THF (1.2 mL) were used. The product was purified by flash column chromatography (AcOH/DCM = 2%) as white solid (20% **yield**, 1.7 mg). The ¹H NMR spectra matched those reported in the literature.⁸

¹H NMR (400 MHz, DMSO-d₆): δ = 7.84 (d, *J* = 7.2 Hz, 4H), 7.69 (d, *J* = 8.0 Hz, 4H), 7.55 (t, *J* = 7.2 Hz, 2H), 7.42 (t, *J* = 8.0 Hz, 4H), 7.31 (d, *J* = 7.2 Hz, 4H), 5.20 – 5.19 (m, 2H), 4.38 – 4.37 (m, 2H).

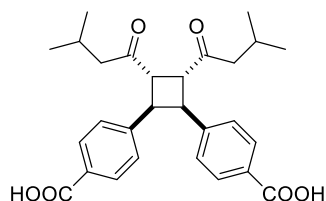


***syn*-4,4'-(cyclobutane-1,2-diyl)dibenzoic acid (7cc)**

The titled compound was synthesized according to **General**

Procedure A with minor modification: 4-vinylbenzoic acid (**7c**, 4.9 mg, 0.033 mmol), CsPbBr₃ NCs (2 mg), **OIAm** (5 μL) and THF (1.2 mL) were used. After blue LED irradiation for **40h**, two parallel reaction mixtures were combined and the product was purified by flash column chromatography (AcOH/DCM = 1%) as white solid (12% **yield**, 1.2 mg). The ¹H NMR spectra matched those reported in the literature.⁸

¹H NMR (400 MHz, DMSO-d₆): δ = 7.64 (d, *J* = 7.6 Hz, 4H), 7.10 (d, *J* = 7.6 Hz, 4H), 4.14 – 4.12 (m, 2H), 2.47 – 2.45 (m, 4H).



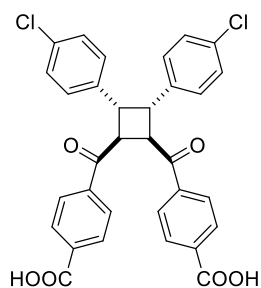
***syn*-4,4'-(3,4-bis(3-methylbutanoyl)cyclobutane-1,2-diyl)dibenzoic acid (7dd)**

The titled compound was synthesized according to **General Procedure A**: (*E*)-4-(5-methyl-3-oxohex-1-en-1-yl)benzoic acid (**7d**, 7.7 mg, 0.033 mmol), CsPbBr₃ NCs (2 mg) and THF (1.2 mL) were used. The product was purified by flash column chromatography (AcOH/DCM = 2%) as white solid (53% **yield**, 4.1 mg).

¹H NMR (400 MHz, DMSO-d₆): δ = 7.65 (d, *J* = 7.6 Hz, 4H), 7.16 (d, *J* = 7.6 Hz, 4H), 4.13 – 4.11 (m, 4H), 2.38 (dd, *J* = 16.4, 6.8 Hz, 2H), 2.26 (dd, *J* = 16.4, 6.8 Hz, 2H), 2.07 – 1.97 (m, 2H), 0.87 (d, *J* = 6.8 Hz, 6H), 0.85 (d, *J* = 6.8 Hz, 6H).

¹³C NMR (126 MHz, DMSO-d₆): δ = 208.7, 167.1, 144.1, 128.9, 128.8, 128.1, 49.3, 49.2, 43.6, 23.7, 22.5, 22.4.

HRMS (ESI⁻) (*m/z*): [M-H]⁻ calculated for C₂₈H₃₁O₆, 463.2121; found 463.2127.



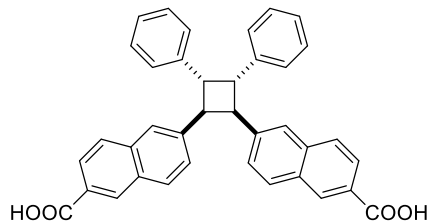
***syn*-4,4'-(3,4-bis(4-chlorophenyl)cyclobutane-1,2-dicarbonyl)dibenzoic acid (**7ee**)**

The titled compound was synthesized according to **General Procedure A** with minor modification: (*E*)-4-(3-(4-chlorophenyl)acryloyl)benzoic acid (**7e**, 9.5 mg, 0.033 mmol), CsPbBr₃ NCs (2 mg) and THF (**1.4 mL**) were used. Two parallel reaction mixtures were combined and the product was purified by flash column chromatography (AcOH/DCM = 2%) as white solid (13% **yield**, 2.5 mg).

¹H NMR (400 MHz, DMSO-d₆): δ = 7.92 (m, 8H), 7.22 (m, 8H), 5.18 – 5.17 (m, 2H), 4.28 – 4.27 (m, 2H).

¹³C NMR (126 MHz, DMSO-d₆): δ = 197.89, 166.48, 138.19, 137.77, 130.86, 129.99, 129.50, 128.03, 127.79, 47.42, 43.56.

HRMS (ESI⁻) (*m/z*): [M-H]⁻ calculated for C₃₂H₂₁Cl₂O₆, 571.0715; found 571.0724.

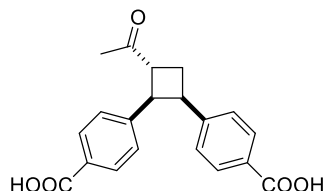


***syn*-6,6'-(3,4-diphenylcyclobutane-1,2-diyl)bis(2-naphthoic acid) (7ff)**

The titled compound was synthesized according to **General Procedure A** with minor modification: (*E*)-6-styryl-2-

naphthoic acid (**7f**, 9.1 mg, 0.033 mmol), CsPbBr₃ NCs (2 mg), **OlAm** (5 μL) and THF (1.4 mL) were used. After blue LED irradiation for **40h**, two parallel reaction mixtures were combined and the product was purified by flash column chromatography (AcOH/DCM = 1%) as white solid (15% yield, 2.7 mg). The ¹H NMR spectra matched those reported in the literature.⁸

¹H NMR (500 MHz, DMSO-d₆): δ = 8.35 (s, 2H), 7.90 (s, 2H), 7.83 (m, 4H), 7.75 (d, *J* = 8.5 Hz, 2H), 7.45 (d, *J* = 8.5 Hz, 2H), 7.27 (d, *J* = 7.5 Hz, 4H), 7.16 (t, *J* = 7.5 Hz, 4H), 7.05 (t, *J* = 7.5 Hz, 2H), 4.81 – 4.77 (m, 4H).



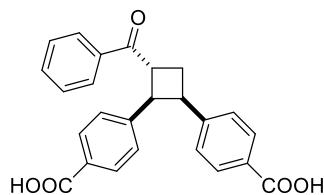
***syn*-4,4'-(3-acetylcyclobutane-1,2-diyl)dibenzoic acid (7ac)**

The titled compound was synthesized according to **General**

Procedure B: (*E*)-4-(3-oxobut-1-en-1-yl)benzoic acid (**7a**, 2.1 mg, 0.011 mmol), 4-vinylbenzoic acid (**7c**, 4.9 mg, 0.033 mmol), CsPbBr₃ NCs (2 mg) and THF (1.2 mL) were used. The product was purified by flash column chromatography (AcOH/DCM = 1%) as white solid (54% **yield**, 2.0 mg). The ¹H NMR spectra matched those reported in the literature.⁸

8

¹H NMR (400 MHz, DMSO-d₆): δ = 7.67 – 7.63 (m, 4H), 7.17 (d, *J* = 7.2 Hz, 2H), 7.10 (d, *J* = 7.2 Hz, 2H), 4.25 (t, *J* = 9.2 Hz, 1H), 4.01 (q, *J* = 9.2 Hz, 1H), 3.92 (td, *J* = 9.6, 4.4 Hz, 1H), 2.67 – 2.60 (m, 1H), 2.56 – 2.51 (m, 1H), 2.10 (s, 3H).

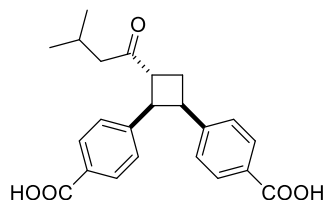


***syn*-4,4'-(3-benzoylcyclobutane-1,2-diyl)dibenzoic acid (7bc)**

The titled compound was synthesized according to **General**

Procedure B: (*E*)-4-(3-oxo-3-phenylprop-1-en-1-yl)benzoic acid (**7b**, 2.8 mg, 0.011 mmol), 4-vinylbenzoic acid (**7c**, 4.9 mg, 0.033 mmol), CsPbBr₃ NCs (2 mg) and THF (1.2 mL) were used. The product was purified by flash column chromatography (AcOH/DCM = 1%) as white solid (64% **yield**, 2.8 mg). The ¹H NMR spectra matched those reported in the literature.⁸

¹H NMR (400 MHz, DMSO-d₆): δ = 8.21 (d, *J* = 7.2 Hz, 2H), 7.70 – 7.63 (m, 5H), 7.54 (t, *J* = 7.6 Hz, 2H), 7.29 (d, *J* = 7.6 Hz, 2H), 7.15 (d, *J* = 7.6 Hz, 2H), 4.81 – 4.74 (m, 1H), 4.47 (t, *J* = 9.2 Hz, 1H), 4.08 – 4.02 (m, 1H), 2.84 (td, *J* = 11.6, 4.8 Hz, 1H), 2.68 (dt, *J* = 11.6, 4.8 Hz, 1H).



***syn*-4,4'-(3-(3-methylbutanoyl)cyclobutane-1,2-diyl)dibenzoic acid**

(7cd)

The titled compound was synthesized according to **General**

Procedure B: (*E*)-4-(5-methyl-3-oxohex-1-en-1-yl)benzoic acid (**7d**, 2.6 mg, 0.011 mmol), 4-vinylbenzoic acid (**7c**, 4.9 mg, 0.033 mmol), CsPbBr₃ NCs (2 mg) and THF (1.2 mL) were used. The product was purified by flash column chromatography (AcOH/DCM = 1%) as white solid (59% **yield**, 2.5 mg).

¹H NMR (400 MHz, DMSO-d₆): δ = 7.67 – 7.63 (m, 4H), 7.18 (d, *J* = 8.0 Hz, 2H), 7.09 (d, *J* = 8.0 Hz, 2H), 4.24 (t, *J* = 9.2 Hz, 1H), 4.02 – 3.90 (m, 2H), 2.65 – 2.52 (m, 2H), 2.38 – 2.27 (m, 2H), 2.11 – 2.00 (m, 1H), 0.84 (d, *J* = 6.8 Hz, 6H).

¹³C NMR (126 MHz, DMSO-d₆): δ = 209.9, 167.1, 167.0, 145.8, 144.6, 128.8, 128.5, 128.2, 127.9, 48.8, 46.4, 45.6, 41.0, 25.5, 23.6, 22.4, 22.4.

HRMS (ESI⁺) (*m/z*): [M-H]⁺ calculated for C₂₃H₂₃O₅, 379.1545; found 379.1549.

General Procedure C for the Ir(ppy)₃-Photocatalyzed [2+2] *Homo*-Cycloaddition:

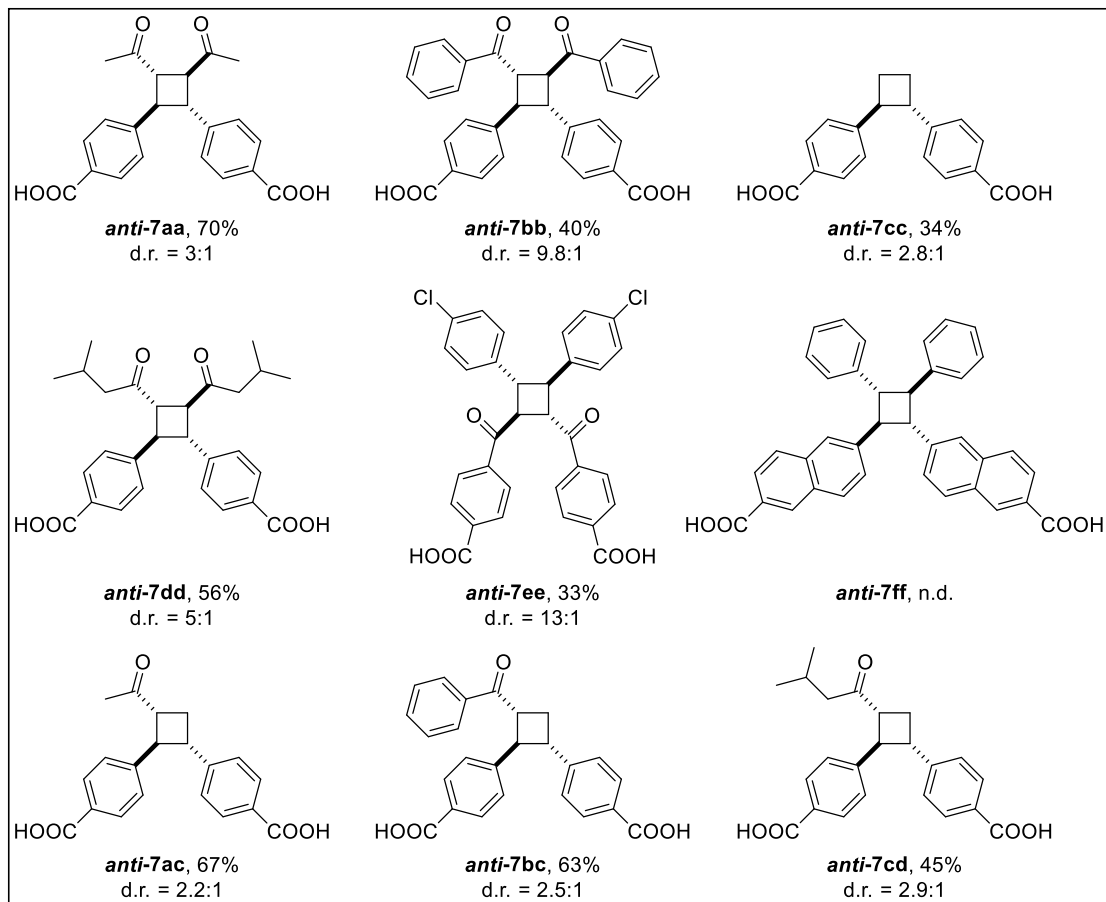
An Ir(ppy)₃ solution (0.013 mg/mL in THF) was prepared as a catalyst stock solution. First, A 4-mL vial was charged with 4-vinylbenzoic acid derivative (0.033 mmol), a suitable-sized magnetic stirring bar and Ir(ppy)₃ stock solution (1.2 mL, for substrates **7e** and **7f** with poor solubility, additional 0.2 mL fresh THF was added). While stirring slowly, the reaction solution was purged with 99.998% N₂ for 20 min through a cap with Teflon septa and sealed with parafilm. The reaction vial was then placed in the middle of two face-to-face (~10 cm away) household blue LED bulbs (14 W) and stirred at 1200 rpm without heating for 40h.

General Procedure D for the Ir(ppy)₃-Photocatalyzed [2+2] *Hetero*-Cycloaddition:

An Ir(ppy)₃ solution (0.013 mg/mL in THF) was prepared as a catalyst stock solution. First, A 4-mL vial was charged with 4-vinylbenzoic acid derivative (0.011 mmol, 1.0 equiv.), 4-vinylbenzoic acid (**7c**, 0.033 mmol, 3.0 equiv.), a suitable-sized magnetic stirring bar and Ir(ppy)₃ stock solution (1.2 mL, for substrates **7e** and **7f** with poor solubility, additional 0.2 mL fresh THF was added). While stirring slowly, the reaction solution was purged with 99.998% N₂ for 20 min through a cap with Teflon septa and sealed with parafilm. The reaction vial was then placed in the middle of two face-to-face (~10 cm away) household blue LED bulbs (14 W) and stirred at 1200 rpm without heating for 40h.

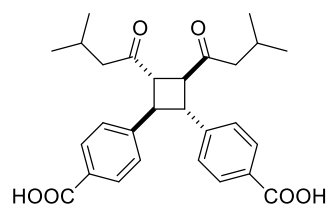
Post-Reaction Work-Up for General Procedure C and D:

Once the reaction was finished, the reaction mixture was transferred to a 25-mL recovery flask to remove the THF solvent under rotary evaporation and the crude ¹H NMR using CH₂Br₂ as an internal standard was taken to determine the NMR yield and diastereomeric ratio.



Scheme 3.4 Scope of Ir(ppy)₃-photocatalyzed [2+2] cycloaddition. Reactions ran using **General Procedure C and D** described above. All yields and diastereomeric ratios were determined by ¹H NMR using CH₂Br₂ as an internal standard. Only the structures of the major diastereomers are shown.

Characterizations of New [2+2] Compounds Formed by Ir(ppy)₃ Photocatalysis

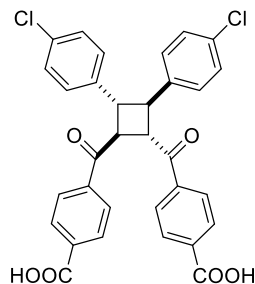


anti-4,4'-(3,4-bis(3-methylbutanoyl)cyclobutane-1,2-diyl)dibenzoic acid (*anti-7dd*)

¹H NMR (400 MHz, DMSO-d₆): δ = 7.90 (d, *J* = 8.0 Hz, 4H), 7.43 (d, *J* = 8.0 Hz, 4H), 3.63 – 3.57 (m, 4H), 2.29 – 2.17 (m, 4H), 2.04 – 1.94 (m, 2H), 0.81 (d, *J* = 6.8 Hz, 6H), 0.79 (d, *J* = 6.8 Hz, 6H).

¹³C NMR (126 MHz, DMSO-d₆): δ = 208.1, 167.1, 145.8, 129.7, 127.4, 127.4, 50.1, 49.3, 46.2, 23.5, 22.3.

HRMS (ESI⁻) (m/z): [M-H]⁻ calculated for C₂₈H₃₁O₆, 463.2121; found 463.2132.

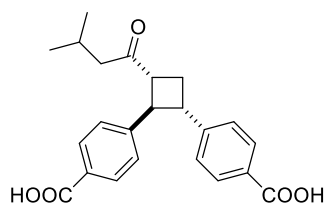


anti-4,4'-(3,4-bis(4-chlorophenyl)cyclobutane-1,2-dicarbonyl)dibenzoic acid (*anti*-7ee)

¹H NMR (400 MHz, DMSO-d₆): δ = 7.88 – 7.83 (m, 8H), 7.39 – 7.34 (m, 8H), 4.66 – 4.64 (m, 2H), 3.89 – 3.87 (m, 2H).

¹³C NMR (126 MHz, DMSO-d₆): δ = 198.0, 166.5, 139.6, 138.3, 131.8, 129.3, 129.2, 129.1, 128.6, 47.3, 46.3.

HRMS (ESI⁻) (m/z): [M-H]⁻ calculated for C₃₂H₂₁Cl₂O₆, 571.0715; found 571.0719.



anti-4,4'-(3-(3-methylbutanoyl)cyclobutane-1,2-diyl)dibenzoic acid (*anti*-7cd)

¹H NMR (400 MHz, DMSO-d₆): δ = 7.88 (d, *J* = 8.4 Hz, 2H), 7.85 (d, *J* = 8.4 Hz, 2H), 7.43 (d, *J* = 8.4 Hz, 2H), 7.31 (d, *J* = 8.4 Hz, 2H), 3.68 – 3.58 (m, 2H), 3.49 – 3.42 (m, 1H), 2.60 – 2.53 (m, 1H), 2.28 – 2.18 (m, 2H), 2.17 – 2.10 (m, 1H), 2.03 – 1.93 (m, 1H), 0.81 – 0.77 (m, 6H).

¹³C NMR (126 MHz, DMSO-d₆): δ = 209.5, 167.1, 167.1, 148.0, 146.9, 129.6, 129.6, 129.3, 129.0, 127.3, 126.8, 49.4, 49.1, 48.2, 42.2, 28.3, 23.6, 22.4, 22.4.

HRMS (ESI⁻) (m/z): [M-H]⁻ calculated for C₂₃H₂₃O₅, 379.1545; found 379.1555.

3.5.6 HPLC Analysis on the Reaction Mixture of Cycloaddition of 7a

HPLC data was collected on an Agilent 1100 series HPLC equipped with a C18 column (4.6 x 100 mm, 3.5 micron). Run parameters were: 1 mL/min, gradient 30% - 70% (MeCN/water with 0.1% formic acid) for the total of 10 min, DAD detector set at 270 nm.

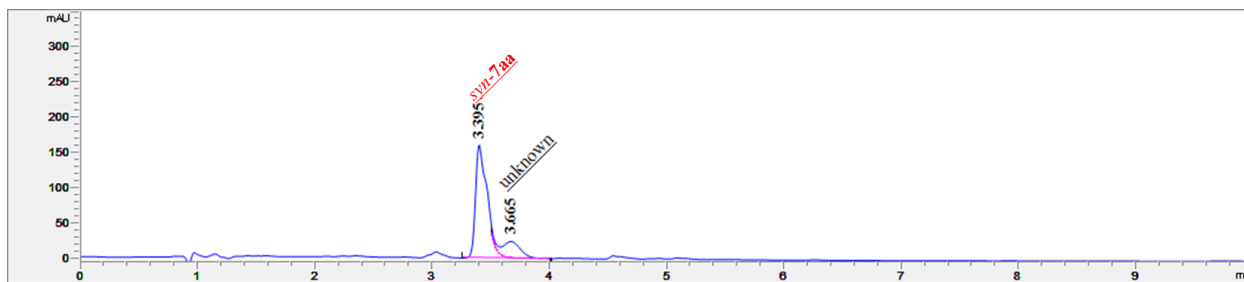


Figure 3.7 CsPbBr₃ NCs-photocatalyzed **7aa** (*syn*) formation. No *anti-7aa* was detected.

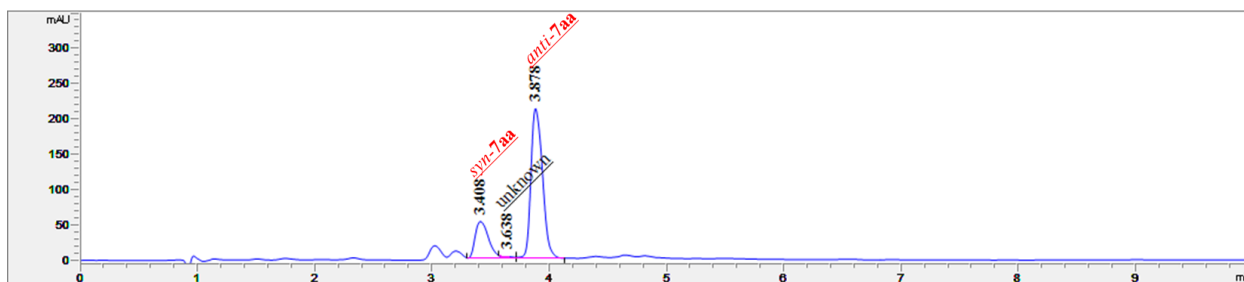


Figure 3.8 Ir(ppy)₃-photocatalyzed **7aa** (*syn* and *anti*) formation.

3.5.7 Photoluminescence (PL) Quenching Study

Photoluminescence quenching studies of CsPbBr₃ NCs solution (2 mL, 1 mg/mL in THF) by titration of various substrates were measured in a 1-cm quartz cuvette. The excitation wavelength was set at 365 nm and the emission intensities at 530 nm were used for Stern-Volmer plot. The quenching constants (K_{SV}) were determined by the Stern-Volmer kinetics following equation:

$$\frac{I_0}{I} = K_{SV}[\text{quencher}]$$

where I_0 is the original PL intensity of NCs without the presence of a quencher, I is the PL intensity of NCs after the addition of a quencher.

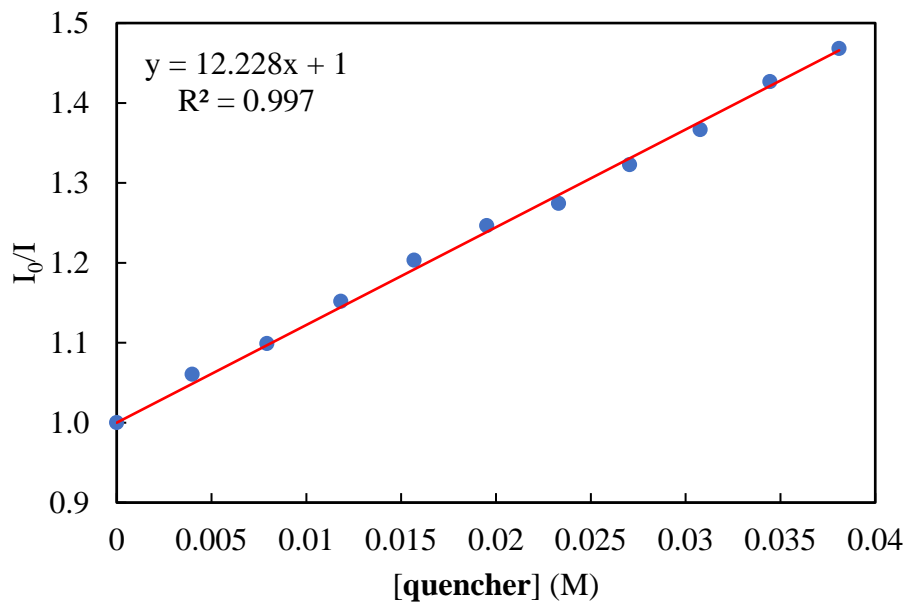


Figure 3.9 PL quenching of CsPbBr₃ NCs by (*E*)-4-phenylbut-3-en-2-one (**6**). $K_{sv} = 12.228 \text{ M}^{-1}$.

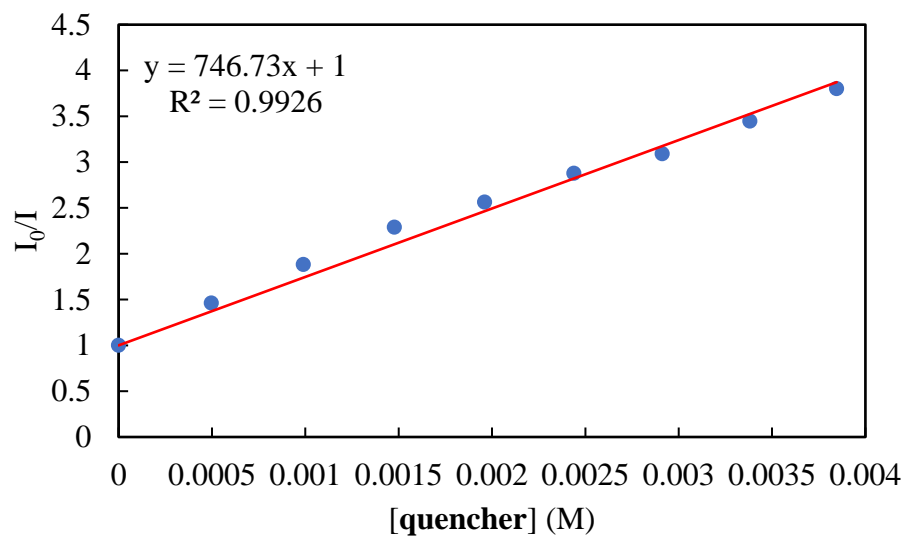


Figure 3.10 PL quenching of CsPbBr₃ NCs by (*E*)-4-(3-oxobut-1-en-1-yl)benzoic acid (**7a**). $K_{sv} = 746.73 \text{ M}^{-1}$.

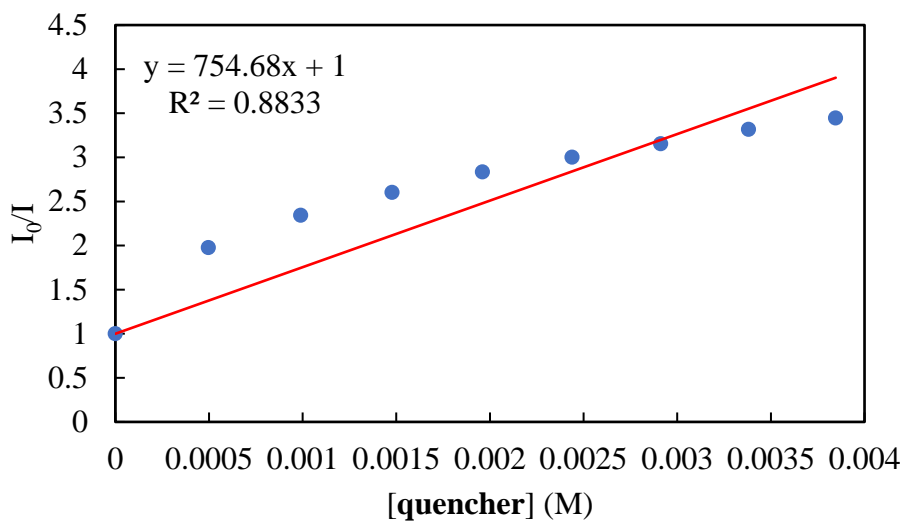


Figure 3.11 PL quenching of CsPbBr₃ NCs by (E)-4-(3-oxo-3-phenylprop-1-en-1-yl)benzoic acid (7b). $K_{SV} = 754.68 \text{ M}^{-1}$.

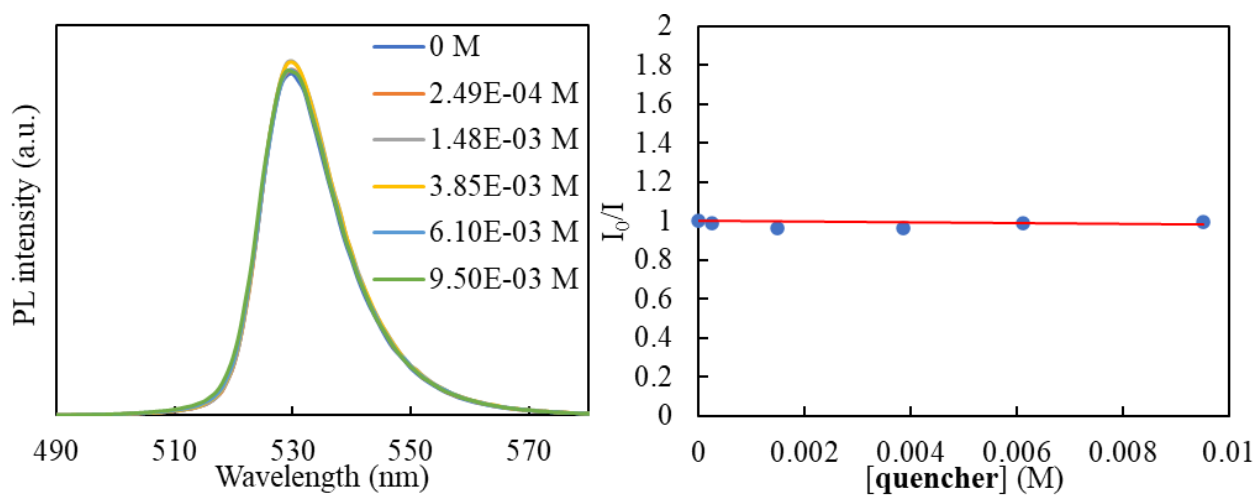


Figure 3.12 No PL quenching of CsPbBr₃ NCs by 4-vinylbenzoic acid (7c) was observed.

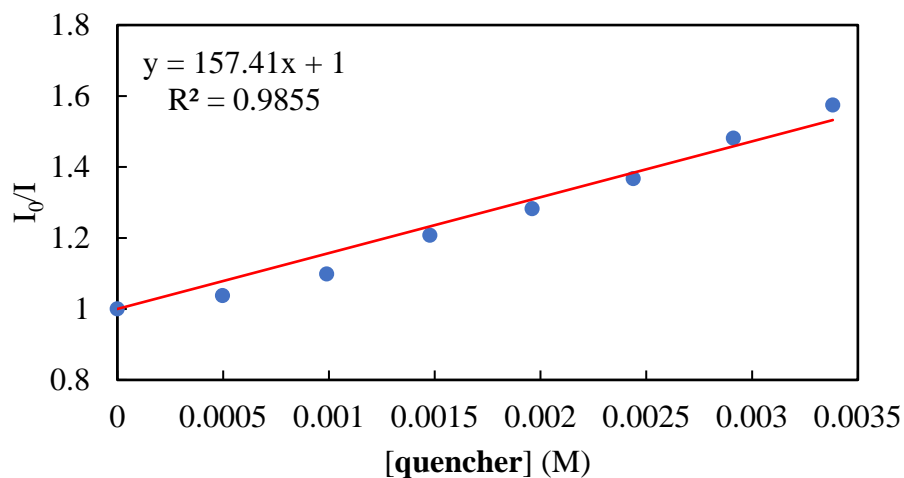


Figure 3.13 PL quenching of CsPbBr₃ NCs by (*E*)-4-(5-methyl-3-oxohex-1-en-1-yl)benzoic acid (**7d**). $K_{SV} = 157.41 \text{ M}^{-1}$.

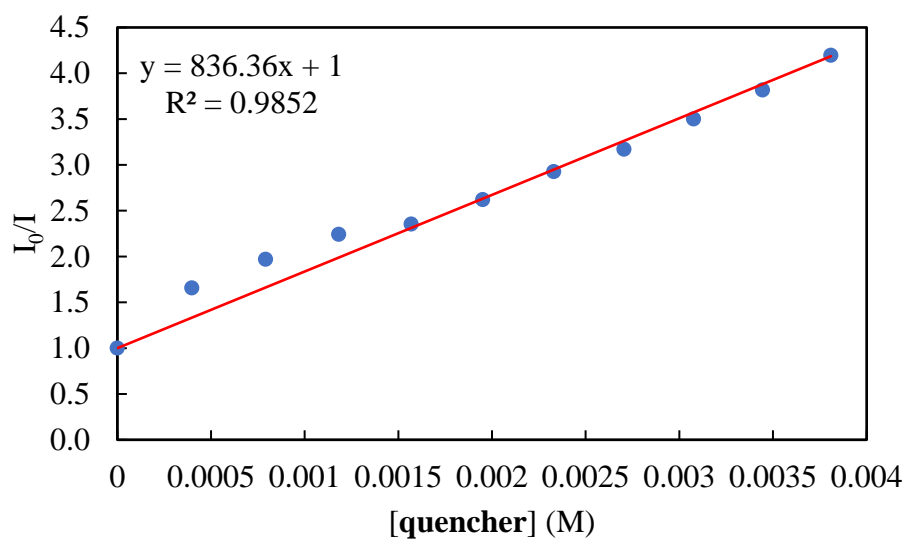


Figure 3.14 PL quenching of CsPbBr₃ NCs by (*E*)-4-(3-(4-chlorophenyl)acryloyl)benzoic acid (**7e**). $K_{SV} = 836.36 \text{ M}^{-1}$.

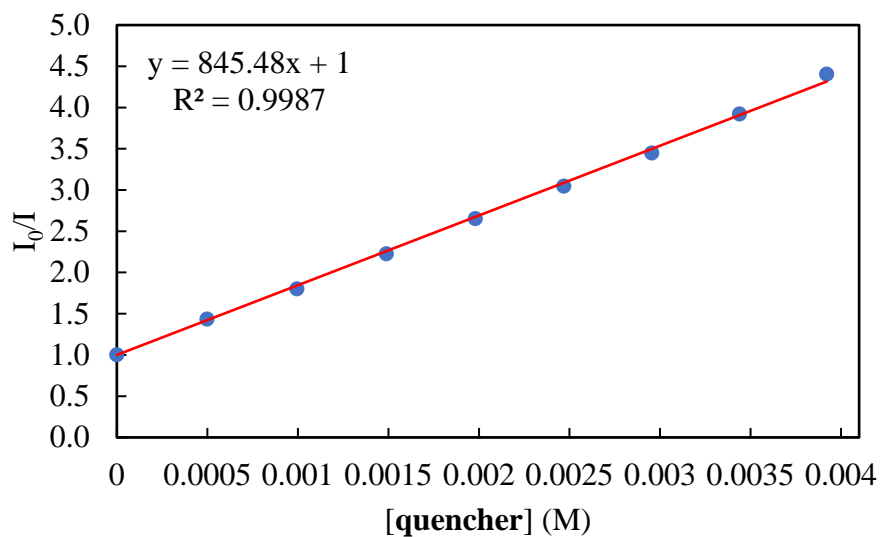


Figure 3.15 PL quenching of CsPbBr₃ NCs by (*E*)-6-styryl-2-naphthoic acid (**7f**). $K_{SV} = 845.48 \text{ M}^{-1}$.

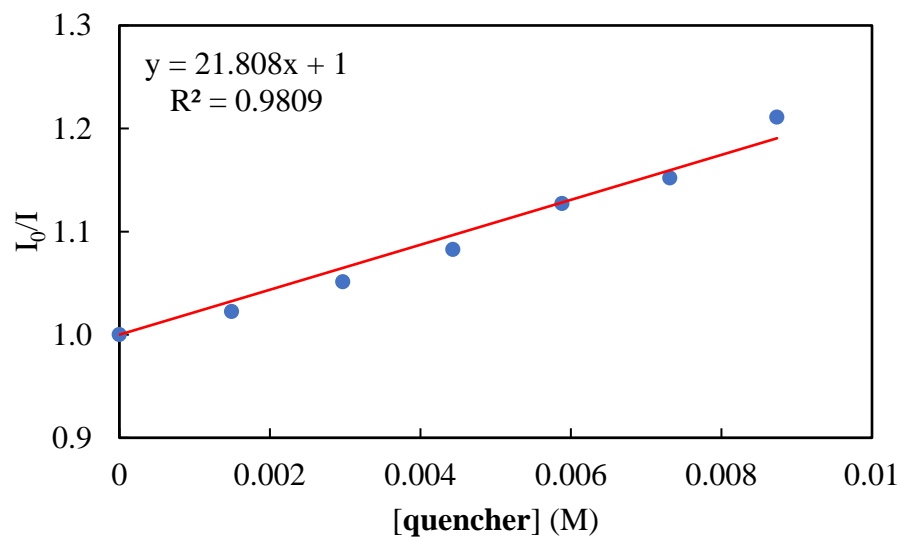


Figure 3.16 PL quenching of CsPbBr₃ NCs by methyl (*E*)-4-(3-oxobut-1-en-1-yl)benzoate (**8**). $K_{SV} = 21.808 \text{ M}^{-1}$.

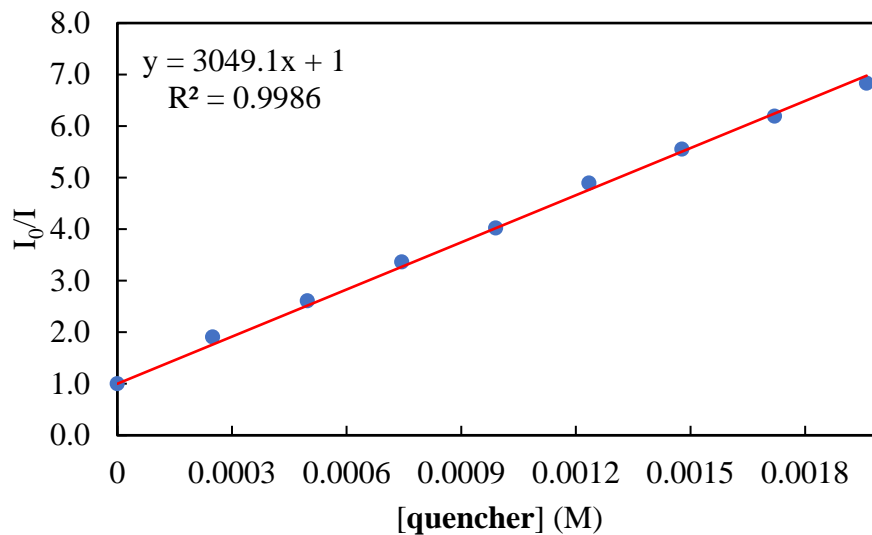


Figure 3.17 PL quenching of CsPbBr₃ NCs by (*E*)-4-(4-aminophenyl)but-3-en-2-one (**9**). $K_{SV} = 3049.1 \text{ M}^{-1}$.

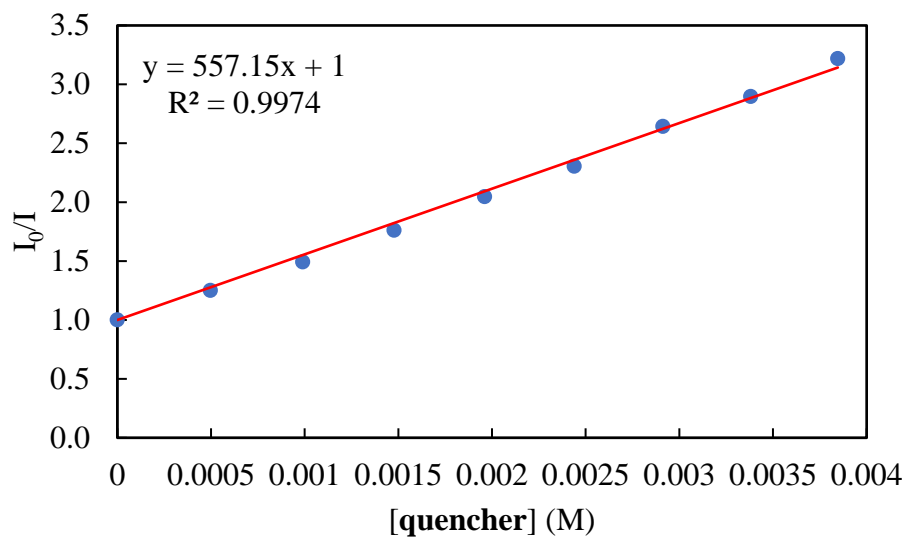


Figure 3.18 PL quenching of CsPbBr₃ NCs by (*E*)-*N*-(4-(3-oxobut-1-en-1-yl)phenyl)acetamide (**10**). $K_{SV} = 557.15 \text{ M}^{-1}$.

3.5.8 Time-Dependent NMR Study

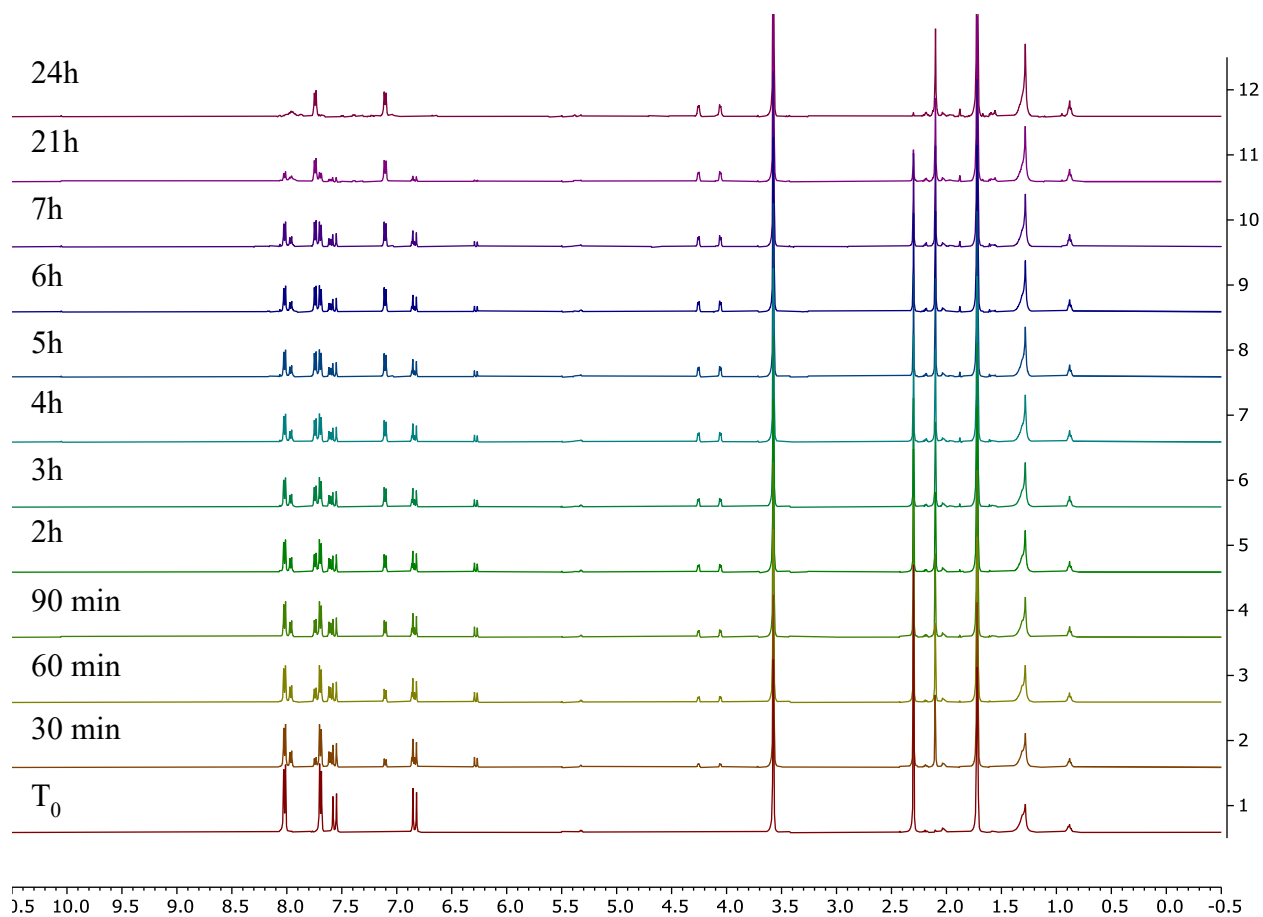


Figure 3.19 Time-dependent ¹H NMR study was performed with **7a**, CsPbBr₃ NCs and THF-d₈ in an NMR tube under blue LED irradiation. The timestamp of each measurement is marked on the left side of each stacked spectrum which is showing the gradual formation of the cyclobutane product **7aa**. A polymeric byproduct was observed after 20h of reaction.

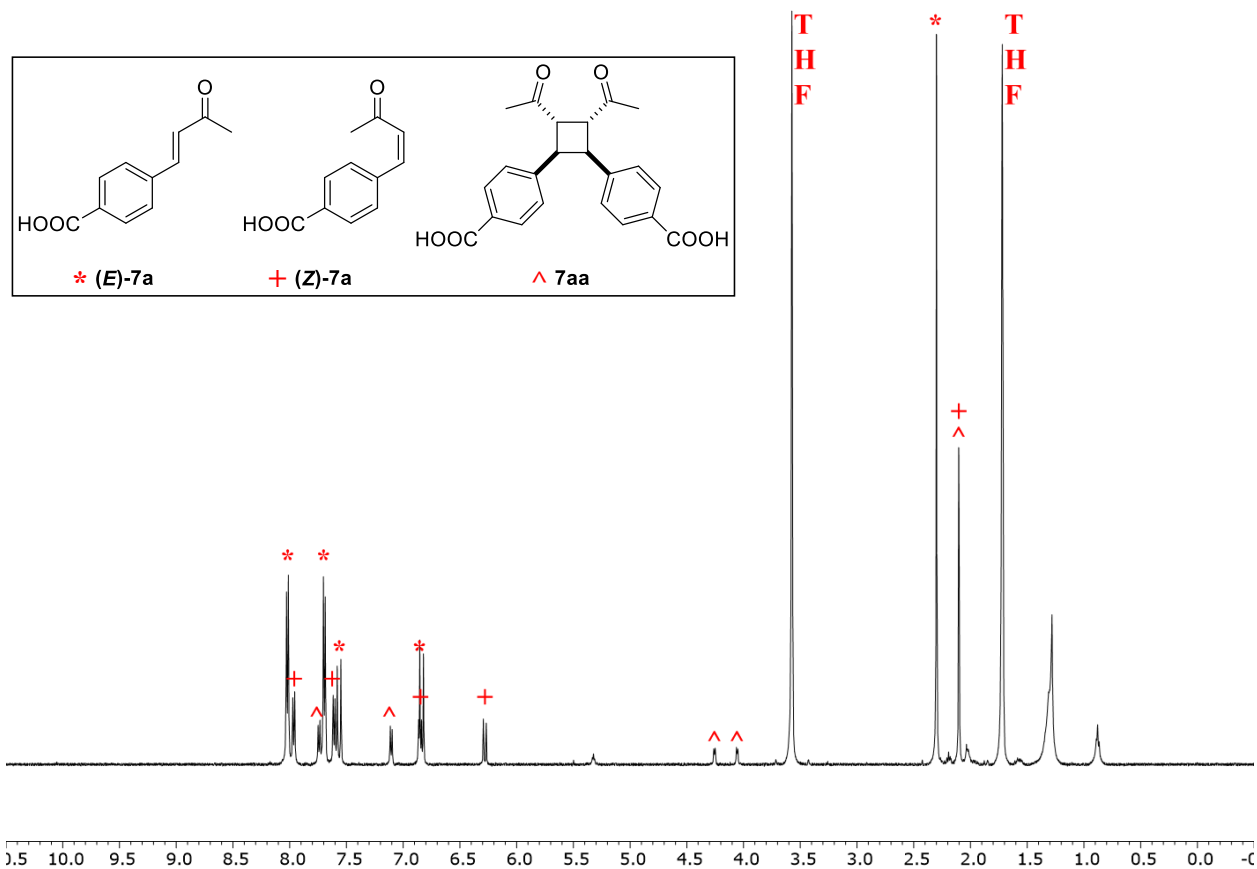


Figure 3.20 ^1H NMR of the reaction mixture taken after blue LED irradiation for 30 min. Different symbols were used to identify each of the component presented in the reaction mixture (* for *trans*-7a, + for *cis*-7a, ^ for 7aa).

Table 3.7 Concentration of each identified component as a function of reaction time.

t (h)	[7aa] (M)	Total [7a] (M)	[(E)-7a] (M)	[(Z)-7a] (M)
0	0	0.07	0.07	0
0.5	0.004084	0.057014	0.041658	0.008168
1	0.006592	0.051416	0.03586	0.013184
1.5	0.007896	0.047373	0.033161	0.015791
2	0.009022	0.045109	0.031757	0.018044
3	0.01022	0.040471	0.029025	0.02044
4	0.011032	0.036626	0.026477	0.022064
5	0.011763	0.034349	0.025409	0.023527
6	0.011939	0.031997	0.023879	0.023879
7	0.012098	0.030486	0.022743	0.024195
21	0.013419	0.013419	0.010199	0.026838
24	0.013419	0.011809	0.009125	0.026838

The fitting of rate law: The reaction could not directly fit in the integrated rate law because of other possible side reactions from starting material **7a** to unknown species. Instead, we firstly figured out the rate of change of product concentration [7aa] by plotting and fitting [7aa] vs. reaction time *t*.

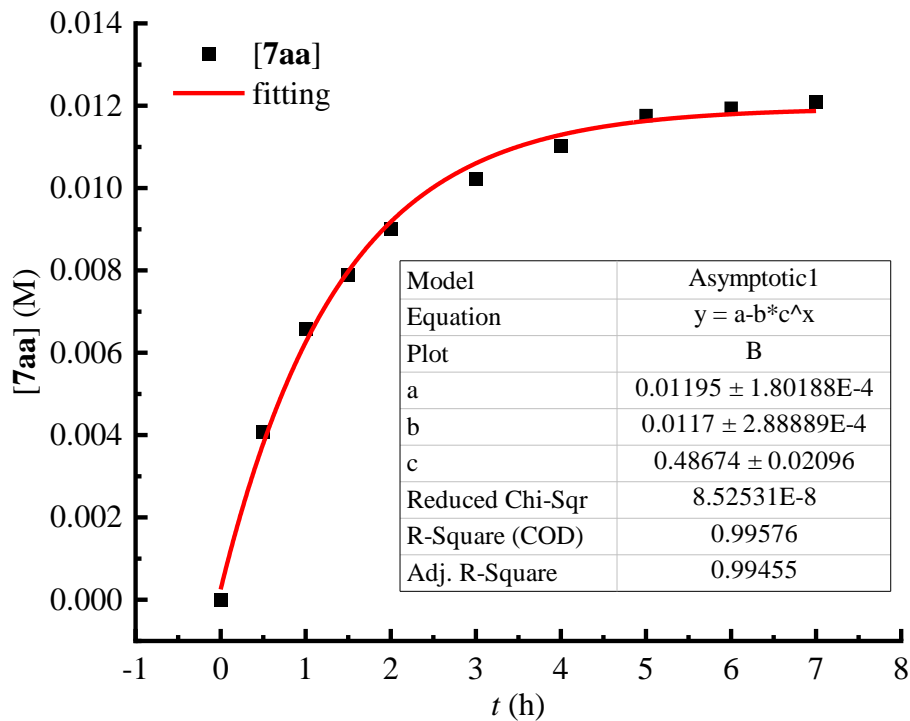


Figure 3.21 [7aa] vs. reaction time t (first 7h). The red curve represents the exponential fitting of [7aa] vs. reaction time t .

Taking the first derivative of the fitting equation (**Figure 3.21**, inset), the rate of change of [7aa] can be described by:

$$d[7aa]/dt = 0.00842 * 0.487^t \quad (\text{Eq. 3.3})$$

Substitute the reaction time t in **Eq. 3.3**, the rate of change of [7aa] at each time point can be obtained. We found good linear relationship between $d[7aa]/dt$ and $[7a]^2$:

$$d[7aa]/dt = k[7a]^2 \quad (\text{Eq. 3.4})$$

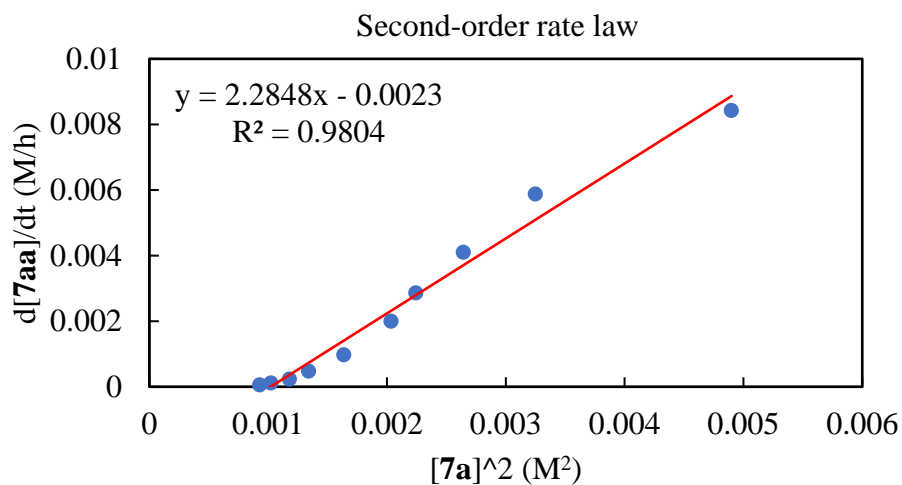


Figure 3.22 The linear relationship between $d[7aa]/dt$ and $[7a]^2$ indicating the perovskite-photocatalyzed [2+2] cycloaddition follows law of second-order kinetics.

3.5.9 Investigation of Surface Binding

Qualitative analysis: IR spectra were measured on a Thermo Fisher Scientific Nicolet iS50 FTIR

Spectrometer. Samples were prepared as followed:

Sample 1: CsPbBr₃ NCs alone;

Sample 2: Substrate **7c** alone;

Sample 3: Collected by centrifugation after CsPbBr₃ NCs (2 mg) stirring with **7c** in THF (1.2 mL) for 1h under dark.

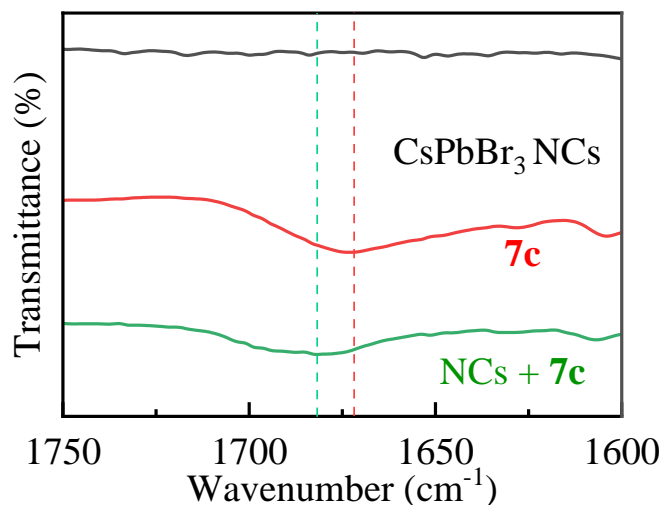


Figure 3.23 Comparison of the C=O stretching frequencies of **Sample 1** (black), **Sample 2** (red), **Sample 3** (green) by IR. The $\sim 10\text{ cm}^{-1}$ shift of the C=O stretching frequency of **Sample 3** towards higher wavenumber indicates the binding of **7c** on CsPbBr₃ NCs' surface via carboxylate group.

Quantitative analysis: ¹H NMR experiment was carried out to determine the amount of substrate binding on cubic perovskite nanocrystal surface.

CsPbBr₃ NCs (10 mg) was stirred under dark with **7a** (31.5 mg, 0.165 mmol) in degassed THF (6 mL) for 30 min. Then, the mixture was transferred to a 15-mL centrifuge tube and subjected to centrifugation at 10k rpm for 1h. The supernatant was decanted and the resulting precipitate was dried under *vacuo* for 3h. Part of the dried solid was carefully obtained using a small spatula and weighted 5.2 mg. The above solid was then dissolved in DMSO-d₆ (600 μ L) with CH₂Br₂ (3.48 μ L, 0.05 mmol) added as an internal standard. Finally, the ¹H NMR data was acquired on a Varian VNMRs 400 spectrometer.

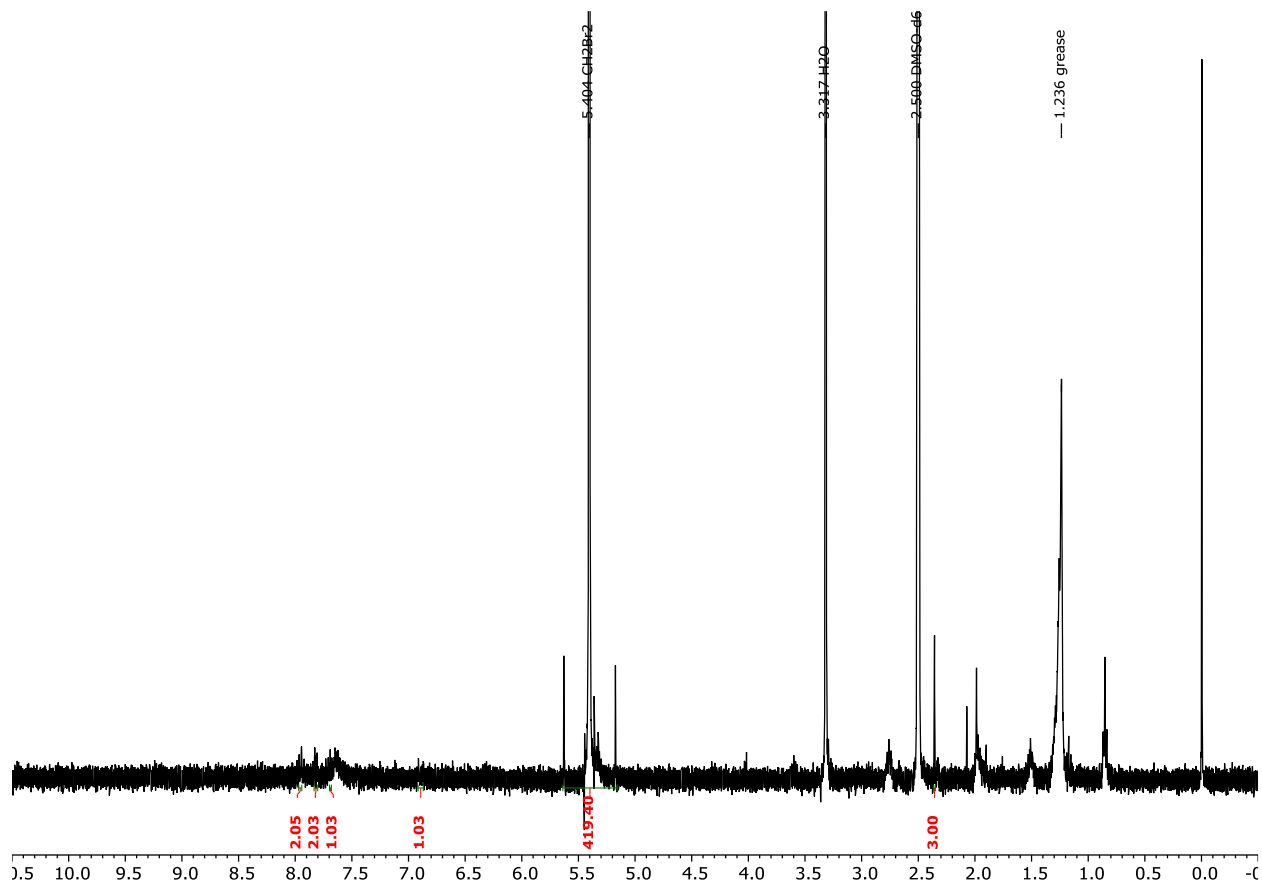


Figure 3.24 ^1H NMR of **7a** (x mg) binding on CsPbBr_3 NCs' (5.2 mg - x mg) surface.

The total number of **7a** present on CsPbBr_3 NCs' surface (from ^1H NMR integration):

$$N(\mathbf{7a}) = 0.1 \text{ mmol} / 419.40 * 1 * N_A = 1.44 * 10^{17} \quad (\text{Eq. 3.5})$$

where 419.40 is the integral of the total protons (0.1 mmol) on CH_2Br_2 , 1 is the integral of **7a**, N_A is the Avogadro constant.

Similarly, the total mass of **7a** present on CsPbBr_3 NCs' surface can be described as:

$$m(\mathbf{7a}) = 0.1 \text{ mmol} / 419.40 * 1 * 190.2 \text{ mg/mmol} = 0.045 \text{ mg} \quad (\text{Eq. 3.6})$$

where 190.2 is the molecular weight of compound **7a**.

The volume of a single 10-nm CsPbBr_3 perovskite cubic nanocrystal is:

$$V(\text{NC}) = (10 \text{ nm})^3 = 1.0 * 10^{-21} \text{ L} \quad (\text{Eq. 3.7})$$

The mass of a single 10-nm CsPbBr_3 perovskite cubic nanocrystal is:

$$m(\text{NC}) = V * d = 4.75 * 10^{-21} \text{kg} \quad (\text{Eq. 3.8})$$

where d is the density of CsPbBr₃ perovskite (4.75 kg/L) adopted from the literature.⁵⁰

The total number of CsPbBr₃ NCs present in a (5.2 mg – 0.045 mg) sample:

$$N(\text{NCs}) = 5.16 \text{ mg}/m(\text{NC}) = 1.09 * 10^{15} \quad (\text{Eq. 3.9})$$

The average number of **7a** binding on a single 10-nm CsPbBr₃ perovskite cubic nanocrystal is:

$$N(\text{binding number}) = N(\mathbf{7a})/N(\text{NCs}) = 132 \quad (\text{Eq. 3.10})$$

3.5.10 Catalyst Stability and Recyclability

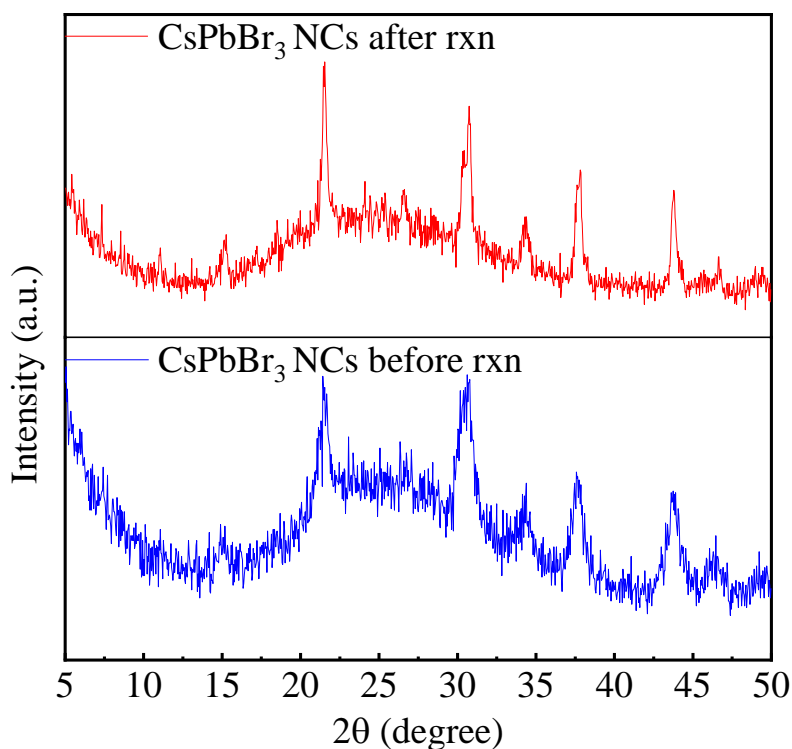
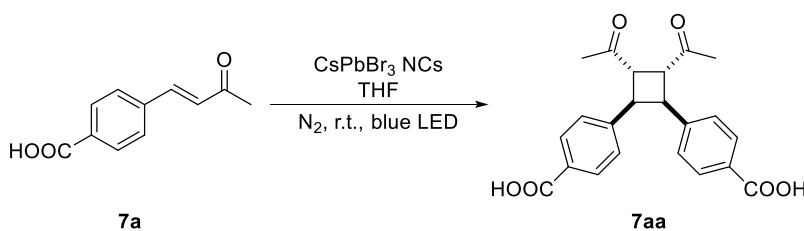


Figure 3.25 Powder XRD of as-prepared CsPbBr₃ NCs (blue) and CsPbBr₃ NCs after reaction and being left in THF for over 30 days (red) showing no sign of degradation.

Catalyst recycling experiment: A 4-mL vial was charged with (*E*)-4-(3-oxobut-1-en-1-yl)benzoic acid (**7a**, 6.3 mg, 0.033 mmol), CsPbBr₃ NCs (2 mg) and a suitable-sized magnetic stirring bar. N₂-protected preservative-free THF (1.2 mL) was used as solvent. While stirring slowly, the reaction solution was purged with 99.998% N₂ for 20 min through a cap with Teflon

septa and sealed with parafilm. The reaction vial was then placed in the middle of two face-to-face (~10 cm away) household blue LED bulbs (14 W) and stirred at 1200 rpm without heating for 20h. Once the reaction was finished, the reaction solution was transferred to a micro centrifuge tube and subjected to centrifugation at 10k rpm for 30 min. The liquid was transferred to a 25-mL recovery flask to remove the THF solvent under rotary evaporation, a crude ¹H NMR using DMSO-d₆ as solvent and CH₂Br₂ as an internal standard was taken to determine the NMR yield. The perovskite NCs (precipitate) was collected and reused for the next reaction cycle.

Table 3.8 The yields of each catalytic cycle.



Cycle	7aa , %
1	43
2	8
3	3

An aliquot of the reaction mixture was taken before each catalytic cycle (visible light irradiation) and diluted in THF and was used to measure the UV-Vis spectra. The entire reaction mixture before each catalytic cycle (visible light irradiation) was used to measure the PL spectra.

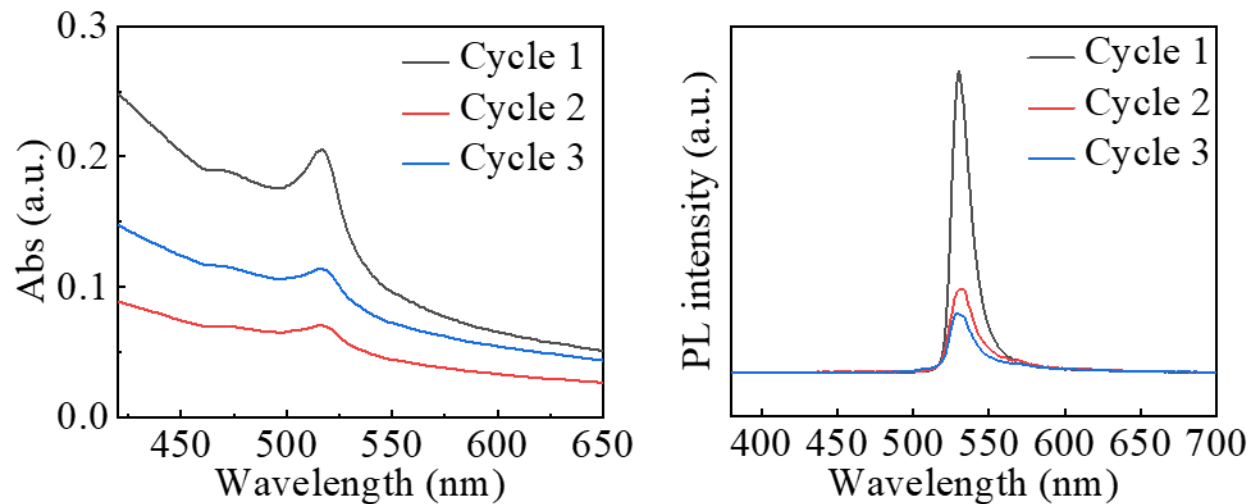


Figure 3.26 UV-Vis absorption spectra (left) and PL spectra (right) of the NCs solution in each catalytic cycle. The positions of characteristic peaks of perovskite NCs remained the same.

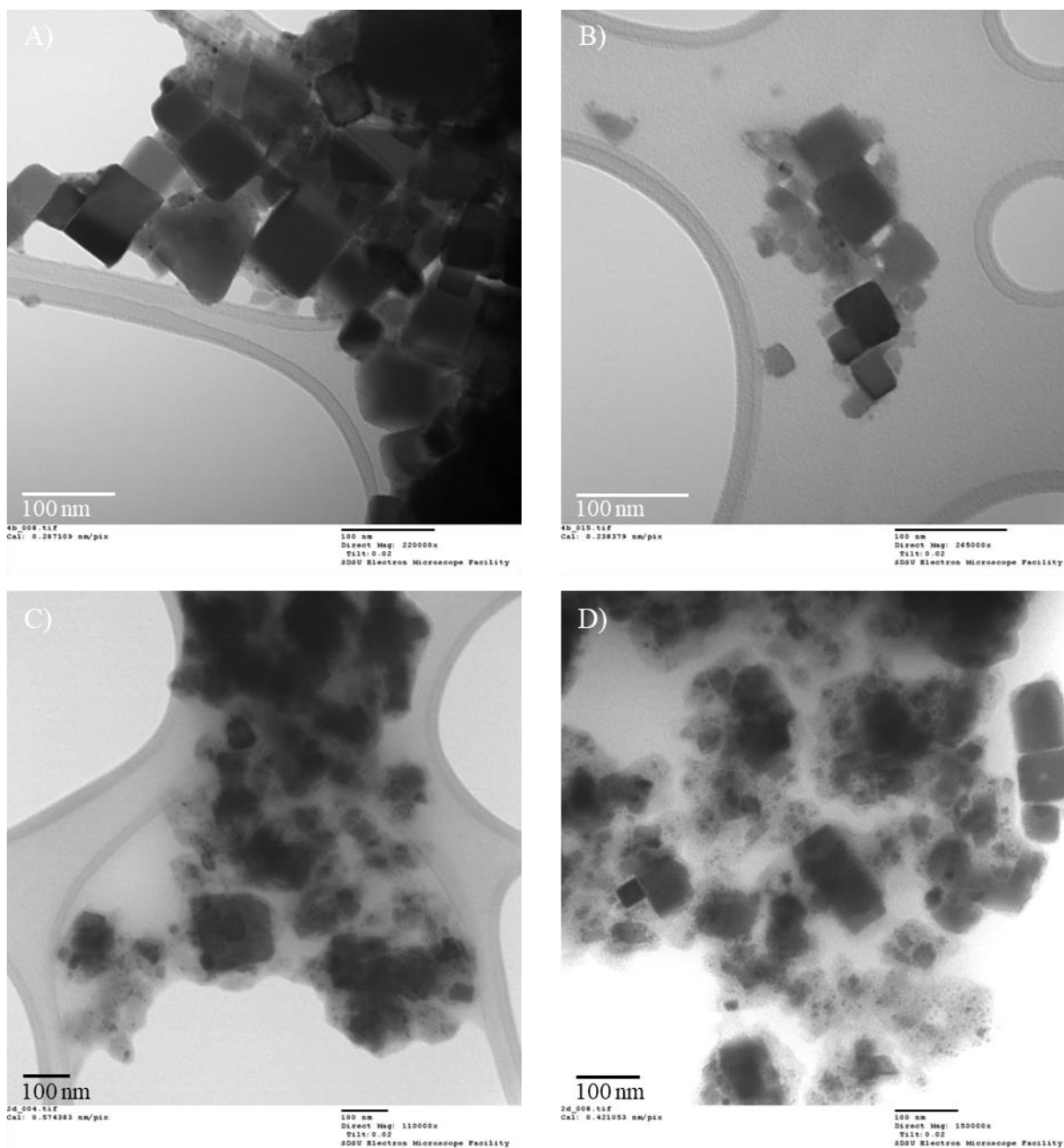


Figure 3.27 TEM measurements. Perovskite NCs samples were dispersed in THF solution and dropped on copper grids. TEM images of as-prepared CsPbBr₃ NCs (**A** and **B**) and recycled CsPbBr₃ NCs (**C** and **D**).

In summary, we conclude that the perovskite structure remained intact after reactions but the NCs were susceptible to aggregation probably via being wrapped by the polymers generated from the side reactions, thus diminishing the efficiency of this surface binding-dependent reaction.

3.5.11 UV-Vis Spectra of Substrate and PL Spectra of CsPbBr₃ NCs

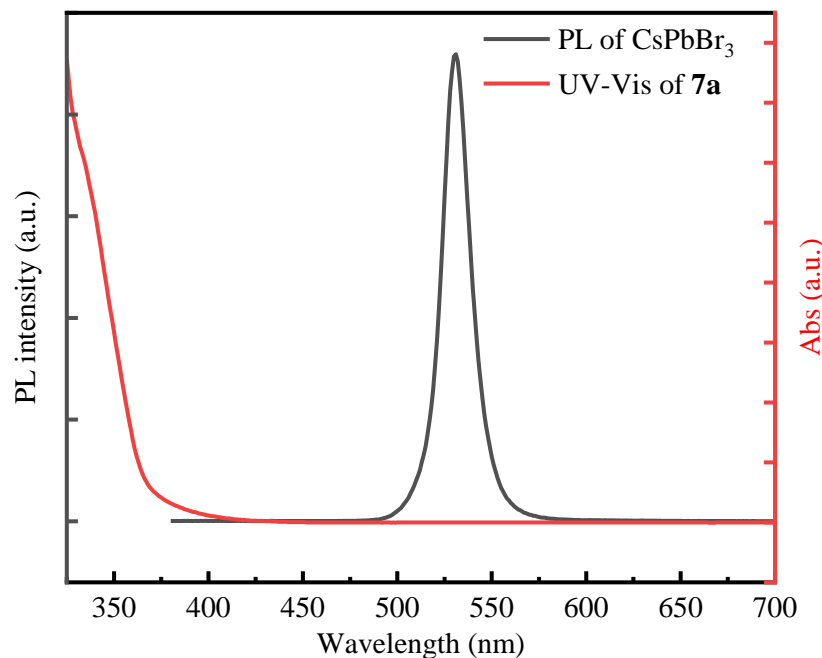


Figure 3.28 PL spectrum of CsPbBr₃ NCs (black) and UV-Vis absorption spectrum of **7a** (red). The non-overlapping rules out the possibility of NCs acting as a singlet sensitizer for the substrate **7a**.

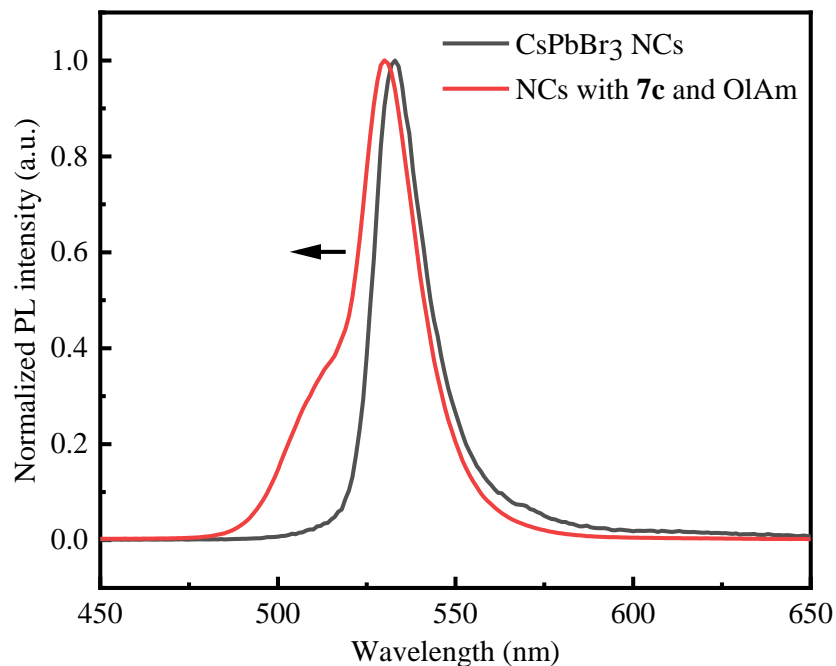


Figure 3.29 PL spectrum of as-prepared CsPbBr₃ NCs (black), CsPbBr₃ NCs treated with **7c** and OlAm (red). The PL of CsPbBr₃ NCs clearly blue-shifted with the presence of both benzoic acid derivative and primary amine.

3.5.12 Transient Absorption (TA) Spectroscopy Experiment Setup

Transient absorption measurement is based on the Ti:sapphire laser amplifier (Coherent Libra, 800 nm, pulse duration ~200 fs, ~4 mJ/pulse and 1 kHz repetition rate) and the pump-probe transient absorption spectrometer (Helios, Ultrafast System). The fundamental beam (800 nm) is split in two beams. One beam is sent to an optical parametric amplifier to generate the pump pulse at 500 nm (2.48 eV), and its intensity is attenuated by two neutral density filter wheels. The other 800 nm beam was focused into a sapphire to generate white light probe (450-780 nm). Probe delay can be up to ~5 ns, is tuned by a delay line. For time delay longer than 5 ns, a fiber laser is used to generate the white light probe pulse and the delay is controlled electronically (EOS, Ultrafast systems). The pump and probe are focused and overlapped onto the sample. The probe size is ~200 μm , and pump beam size is ~500 μm . The beam size is defined as the radius of an aperture that contains $(1/e^2)$ of the total power. The samples are constantly stirred to give reactants enough time to diffuse.

Table 3.9 Fitted time constant.

Reactants	A ₁	τ_1 (ps)	A ₂	τ_2 (ns)	A ₃	τ_3 (μs)	B ₁	τ_4 (ps)	B ₂	τ_5 (μs)	f_1 (%)	f_2 (%)
7a	0.42	922	0.31	16.6	0.22	0.84	1	107 \pm 19	-	-	87 \pm 3	13 \pm 3
7b	0.42	922	0.31	16.6	0.22	0.84	0.45	109 \pm 18	0.55	17.7 \pm 3.0	80 \pm 5	20 \pm 5
NC	0.42	922	0.31	16.6	0.22	0.84	-	-	-	-	1	0

3.5.13 DFT Calculations

All DFT calculations were carried out with Gaussian 16. The geometries were visualized with GaussView 6. The DFT methodology was employed following a previous report on a CdSe quantum dots system.³⁷ A 4x4 cubic matrix from perovskite crystal structure (Pb-Br 2.97 Å, Cs-

Cs 5.94 Å)³⁸ with Cs-rich surface is used without optimization as shown in details below in Figure below. The binding energies were computed with DFT using B3LYP functional and the Ahlrich's double- ζ basis with a polarization function Def2-SVP with the dispersion terms including D3BJ (Grimme's third-generation dispersion and Becke-Johnson damping).

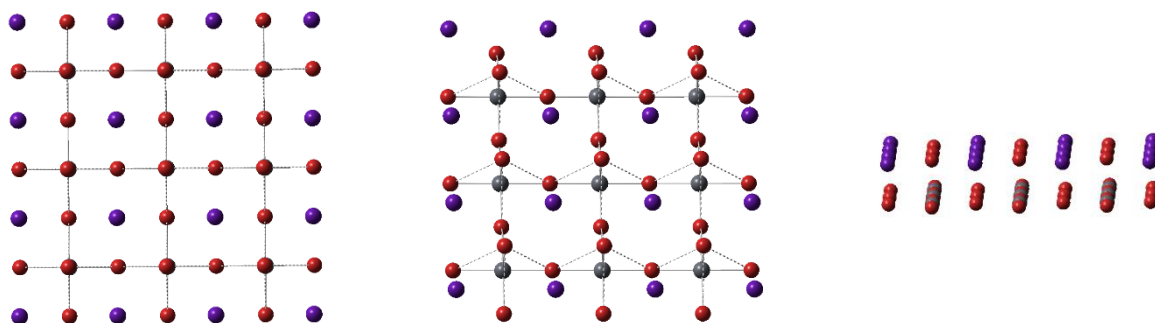


Figure 3.30 4x4 Cubic matrix of perovskite NCs: Cs₁₆Pb₉Br₃₃ (+1 in overall charge) as shown from top view, tilt view and side view.

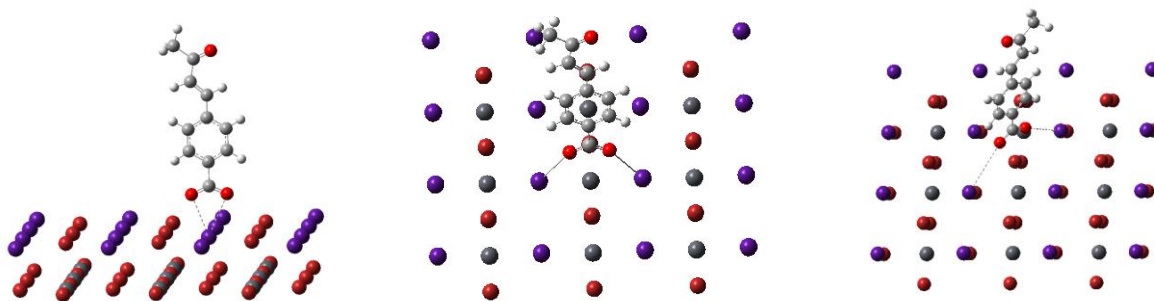


Figure 3.31 Binding models of **7a** on NC surface: **7a** chelating to a single Cs atom, **7a** bridging bind to two adjacent Cs atoms, and **7a** bridging bind to two diagonal Cs atoms.

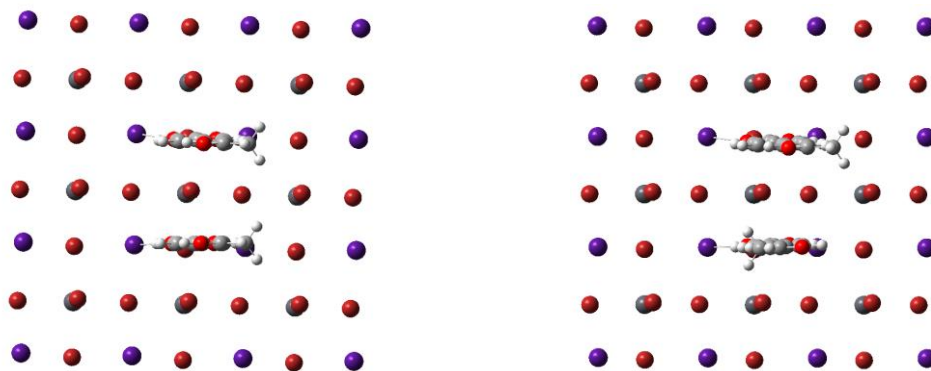


Figure 3.32 Binding of two **7a** molecules on NC surface in *syn*- and *anti*-binding model.

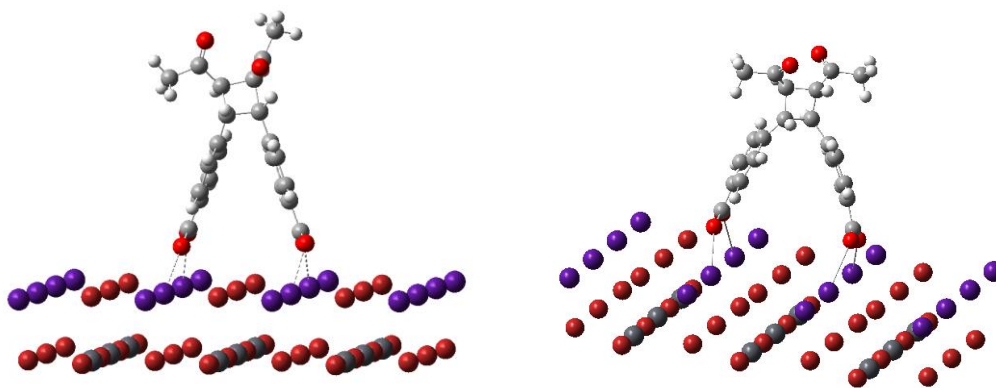


Figure 3.33 Binding of **7aa** molecules on NC surface in *syn*- and *anti*-binding model.

3.6 Acknowledgements

Chapter 3, in full, is a reprint of the material as it appears in *ACS Applied Materials & Interfaces* **2022**, 14 (22), 25357 – 25365. **Lin, Y.**; Avvacumova, M.; Zhao, R.; Chen, X.; Beard, M.; Yan, Y. The dissertation author was the primary investigator and author of this paper.

I led the initial reaction investigation, steady-state spectroscopic studies, surface ligand binding studies, reaction condition exploration, time-dependent NMR studies, substrate scope evaluation, catalyst synthesis, compound synthesis/purification/characterization. I wrote the first draft of the manuscript.

3.7 Reference

1. Lei, T.; Zhou, C.; Huang, M.-Y.; Zhao, L.-M.; Yang, B.; Ye, C.; Xiao, H.; Meng, Q.-Y.; Ramamurthy, V.; Tung, C.-H.; Wu, L.-Z., General and Efficient Intermolecular [2+2] Photodimerization of Chalcones and Cinnamic Acid Derivatives in Solution through Visible-Light Catalysis. *Angew. Chem. Int. Ed.* **2017**, 56 (48), 15407-15410.
2. Blum, T. R.; Miller, Z. D.; Bates, D. M.; Guzei, I. A.; Yoon, T. P., Enantioselective Photochemistry through Lewis Acid-Catalyzed Triplet Energy Transfer. *Science* **2016**, 354 (6318), 1391-1395.
3. Daub, M. E.; Jung, H.; Lee, B. J.; Won, J.; Baik, M.-H.; Yoon, T. P., Enantioselective [2+2] Cycloadditions of Cinnamate Esters: Generalizing Lewis Acid Catalysis of Triplet Energy Transfer. *J. Am. Chem. Soc.* **2019**, 141 (24), 9543-9547.

4. Zheng, J.; Swords, W. B.; Jung, H.; Skubi, K. L.; Kidd, J. B.; Meyer, G. J.; Baik, M.-H.; Yoon, T. P., Enantioselective Intermolecular Excited-State Photoreactions Using a Chiral Ir Triplet Sensitizer: Separating Association from Energy Transfer in Asymmetric Photocatalysis. *J. Am. Chem. Soc.* **2019**, *141* (34), 13625-13634.
5. Strieth-Kalthoff, F.; James, M. J.; Teders, M.; Pitzer, L.; Glorius, F., Energy Transfer Catalysis Mediated by Visible Light: Principles, Applications, Directions. *Chem. Soc. Rev.* **2018**, *47* (19), 7190-7202.
6. Strieth-Kalthoff, F.; Glorius, F., Triplet Energy Transfer Photocatalysis: Unlocking the Next Level. *Chem* **2020**, *6* (8), 1888-1903.
7. Mongin, C.; Garakyaraghi, S.; Razgoniaeva, N.; Zamkov, M.; Castellano, F. N., Direct Observation of Triplet Energy Transfer from Semiconductor Nanocrystals. *Science* **2016**, *351* (6271), 369-372.
8. Jiang, Y.; Wang, C.; Rogers, C. R.; Kodaimati, M. S.; Weiss, E. A., Regio- and Diastereoselective Intermolecular [2+2] Cycloadditions Photocatalysed by Quantum Dots. *Nat. Chem.* **2019**, *11* (11), 1034-1040.
9. Jiang, Y.; Yang, M.; Wu, Y.; López-Arteaga, R.; Rogers, C. R.; Weiss, E. A., Chemo- and Stereoselective Intermolecular [2 + 2] Photocycloaddition of Conjugated Dienes Using Colloidal Nanocrystal Photocatalysts. *Chem Catal.* **2021**, *1* (1), 106-116.
10. Luo, X.; Lai, R.; Li, Y.; Han, Y.; Liang, G.; Liu, X.; Ding, T.; Wang, J.; Wu, K., Triplet Energy Transfer from CsPbBr₃ Nanocrystals Enabled by Quantum Confinement. *J. Am. Chem. Soc.* **2019**, *141* (10), 4186-4190.
11. Luo, X.; Han, Y.; Chen, Z.; Li, Y.; Liang, G.; Liu, X.; Ding, T.; Nie, C.; Wang, M.; Castellano, F. N.; Wu, K., Mechanisms of Triplet Energy Transfer Across the Inorganic Nanocrystal/Organic Molecule Interface. *Nat. Commun.* **2020**, *11* (1), 28.
12. Luo, X.; Liang, G.; Han, Y.; Li, Y.; Ding, T.; He, S.; Liu, X.; Wu, K., Triplet Energy Transfer from Perovskite Nanocrystals Mediated by Electron Transfer. *J. Am. Chem. Soc.* **2020**, *142* (25), 11270-11278.
13. Mase, K.; Okumura, K.; Yanai, N.; Kimizuka, N., Triplet sensitization by perovskite nanocrystals for photon upconversion. *Chem. Commun.* **2017**, *53* (59), 8261-8264.
14. Jiang, Y.; Weiss, E. A., Colloidal Quantum Dots as Photocatalysts for Triplet Excited State Reactions of Organic Molecules. *J. Am. Chem. Soc.* **2020**, *142* (36), 15219-15229.
15. Ravi, V. K.; Markad, G. B.; Nag, A., Band Edge Energies and Excitonic Transition Probabilities of Colloidal CsPbX₃ (X = Cl, Br, I) Perovskite Nanocrystals. *ACS Energy Lett.* **2016**, *1* (4), 665-671.
16. Lu, Z.; Yoon, T. P., Visible Light Photocatalysis of [2+2] Styrene Cycloadditions by Energy Transfer. *Angew. Chem. Int. Ed.* **2012**, *51* (41), 10329-10332.

17. Alonso, R.; Bach, T., A Chiral Thioxanthone as an Organocatalyst for Enantioselective [2+2] Photocycloaddition Reactions Induced by Visible Light. *Angew. Chem. Int. Ed.* **2014**, *53* (17), 4368-4371.
18. Zhao, J.; Brosmer, J. L.; Tang, Q.; Yang, Z.; Houk, K. N.; Diaconescu, P. L.; Kwon, O., Intramolecular Crossed [2+2] Photocycloaddition through Visible Light-Induced Energy Transfer. *J. Am. Chem. Soc.* **2017**, *139* (29), 9807-9810.
19. Münster, N.; Parker, N. A.; van Dijk, L.; Paton, R. S.; Smith, M. D., Visible Light Photocatalysis of 6π Heterocyclization. *Angew. Chem. Int. Ed.* **2017**, *56* (32), 9468-9472.
20. Yuan, Y.; Zhu, H.; Hills-Kimball, K.; Cai, T.; Shi, W.; Wei, Z.; Yang, H.; Candler, Y.; Wang, P.; He, J.; Chen, O., Stereoselective C–C Oxidative Coupling Reactions Photocatalyzed by Zwitterionic Ligand Capped CsPbBr₃ Perovskite Quantum Dots. *Angew. Chem. Int. Ed.* **2020**, *59* (50), 22563-22569.
21. Du, Y.; Zhang, Y.; Wang, S.; Zhao, K., Highly Stereoselective Dimerization of 3-Alkoxyimino-2-aryl-alkylnitriles via Oxidative Carbon-Carbon. *Synlett* **2009**, (11), 1835-1841.
22. Garakyaraghi, S.; Mongin, C.; Granger, D. B.; Anthony, J. E.; Castellano, F. N., Delayed Molecular Triplet Generation from Energized Lead Sulfide Quantum Dots. *J. Phys. Chem. Lett.* **2017**, *8* (7), 1458-1463.
23. Li, X.; Huang, Z.; Zavala, R.; Tang, M. L., Distance-Dependent Triplet Energy Transfer between CdSe Nanocrystals and Surface Bound Anthracene. *J. Phys. Chem. Lett.* **2016**, *7* (11), 1955-1959.
24. Huang, Z.; Tang, M. L., Designing Transmitter Ligands That Mediate Energy Transfer between Semiconductor Nanocrystals and Molecules. *J. Am. Chem. Soc.* **2017**, *139* (28), 9412-9418.
25. Wang, K.; Lu, H.; Zhu, X.; Lin, Y.; Beard, M. C.; Yan, Y.; Chen, X., Ultrafast Reaction Mechanisms in Perovskite Based Photocatalytic C-C Coupling. *ACS Energy Lett.* **2020**, *5* (2), 566-571.
26. Koscher, B. A.; Nett, Z.; Alivisatos, A. P., The Underlying Chemical Mechanism of Selective Chemical Etching in CsPbBr₃ Nanocrystals for Reliably Accessing Near-Unity Emitters. *ACS Nano* **2019**, *13* (10), 11825-11833.
27. Chen, X.; Lu, H.; Li, Z.; Zhai, Y.; Ndione, P. F.; Berry, J. J.; Zhu, K.; Yang, Y.; Beard, M. C., Impact of Layer Thickness on the Charge Carrier and Spin Coherence Lifetime in Two-Dimensional Layered Perovskite Single Crystals. *ACS Energy Lett.* **2018**, *3* (9), 2273-2279.
28. Chen, X.; Lu, H.; Yang, Y.; Beard, M. C., Excitonic Effects in Methylammonium Lead Halide Perovskites. *J. Phys. Chem. Lett.* **2018**, *9* (10), 2595-2603.

29. Koscher, B. A.; Swabeck, J. K.; Bronstein, N. D.; Alivisatos, A. P., Essentially Trap-Free CsPbBr₃ Colloidal Nanocrystals by Postsynthetic Thiocyanate Surface Treatment. *J. Am. Chem. Soc.* **2017**, *139* (19), 6566-6569.
30. Li, B.; Huang, H.; Zhang, G.; Yang, C.; Guo, W.; Chen, R.; Qin, C.; Gao, Y.; Biju, V. P.; Rogach, A. L.; Xiao, L.; Jia, S., Excitons and Biexciton Dynamics in Single CsPbBr₃ Perovskite Quantum Dots. *J. Phys. Chem. Lett.* **2018**, *9* (24), 6934-6940.
31. Wu, K.; Liang, G.; Shang, Q.; Ren, Y.; Kong, D.; Lian, T., Ultrafast Interfacial Electron and Hole Transfer from CsPbBr₃ Perovskite Quantum Dots. *J. Am. Chem. Soc.* **2015**, *137* (40), 12792-12795.
32. Mandal, S.; George, L.; Tkachenko, N. V., Charge Transfer Dynamics in CsPbBr₃ Perovskite Quantum Dots–Anthraquinone/Fullerene (C60) Hybrids. *Nanoscale* **2019**, *11* (3), 862-869.
33. Kobosko, S. M.; DuBose, J. T.; Kamat, P. V., Perovskite Photocatalysis. Methyl Viologen Induces Unusually Long-Lived Charge Carrier Separation in CsPbBr₃ Nanocrystals. *ACS Energy Lett.* **2020**, *5* (1), 221-223.
34. Bender, J. A.; Raulerson, E. K.; Li, X.; Goldzak, T.; Xia, P.; Van Voorhis, T.; Tang, M. L.; Roberts, S. T., Surface States Mediate Triplet Energy Transfer in Nanocrystal–Acene Composite Systems. *J. Am. Chem. Soc.* **2018**, *140* (24), 7543-7553.
35. Mahboub, M.; Xia, P.; Van Baren, J.; Li, X.; Lui, C. H.; Tang, M. L., Midgap States in PbS Quantum Dots Induced by Cd and Zn Enhance Photon Upconversion. *ACS Energy Lett.* **2018**, *3* (4), 767-772.
36. Wang, L.; Yoo, J. J.; Lin, T.-A.; Perkinson, C. F.; Lu, Y.; Baldo, M. A.; Bawendi, M. G., Interfacial Trap-Assisted Triplet Generation in Lead Halide Perovskite Sensitized Solid-State Upconversion. *Adv. Mater.* **2021**, *33* (27), 2100854.
37. Jones, L. O.; Mosquera, M. A.; Jiang, Y.; Weiss, E. A.; Schatz, G. C.; Ratner, M. A., Thermodynamics and Mechanism of a Photocatalyzed Stereoselective [2 + 2] Cycloaddition on a CdSe Quantum Dot. *J. Am. Chem. Soc.* **2020**, *142* (36), 15488-15495.
38. Goesten, M. G.; Hoffmann, R., Mirrors of Bonding in Metal Halide Perovskites. *J. Am. Chem. Soc.* **2018**, *140* (40), 12996-13010.
39. Wei, S.; Yang, Y.; Kang, X.; Wang, L.; Huang, L.; Pan, D., Room-Temperature and Gram-Scale Synthesis of CsPbX₃ (X = Cl, Br, I) Perovskite Nanocrystals with 50–85% Photoluminescence Quantum Yields. *Chem. Commun.* **2016**, *52* (45), 7265-7268.
40. ten Brinck, S.; Infante, I., Surface Termination, Morphology, and Bright Photoluminescence of Cesium Lead Halide Perovskite Nanocrystals. *ACS Energy Lett.* **2016**, *1* (6), 1266-1272.

41. Huang, H.; Zhao, F.; Liu, L.; Zhang, F.; Wu, X.-g.; Shi, L.; Zou, B.; Pei, Q.; Zhong, H., Emulsion Synthesis of Size-Tunable $\text{CH}_3\text{NH}_3\text{PbBr}_3$ Quantum Dots: An Alternative Route toward Efficient Light-Emitting Diodes. *ACS Appl. Mater. Interfaces* **2015**, *7* (51), 28128-28133.
42. Protesescu, L.; Yakunin, S.; Bodnarchuk, M. I.; Krieg, F.; Caputo, R.; Hendon, C. H.; Yang, R. X.; Walsh, A.; Kovalenko, M. V., Nanocrystals of Cesium Lead Halide Perovskites (CsPbX_3 , X = Cl, Br, and I): Novel Optoelectronic Materials Showing Bright Emission with Wide Color Gamut. *Nano Lett.* **2015**, *15* (6), 3692-3696.
43. Yassitepe, E.; Yang, Z.; Voznyy, O.; Kim, Y.; Walters, G.; Castañeda, J. A.; Kanjanaboos, P.; Yuan, M.; Gong, X.; Fan, F.; Pan, J.; Hoogland, S.; Comin, R.; Bakr, O. M.; Padilha, L. A.; Nogueira, A. F.; Sargent, E. H., Amine-Free Synthesis of Cesium Lead Halide Perovskite Quantum Dots for Efficient Light-Emitting Diodes. *Adv. Funct. Mater.* **2016**, *26* (47), 8757-8763.
44. Saidaminov, M. I.; Almutlaq, J.; Sarmah, S.; Dursun, I.; Zhumeckenov, A. A.; Begum, R.; Pan, J.; Cho, N.; Mohammed, O. F.; Bakr, O. M., Pure Cs_4PbBr_6 : Highly Luminescent Zero-Dimensional Perovskite Solids. *ACS Energy Lett.* **2016**, *1* (4), 840-845.
45. Zumbansen, K.; Döhring, A.; List, B., Morpholinium Trifluoroacetate-Catalyzed Aldol Condensation of Acetone with both Aromatic and Aliphatic Aldehydes. *Adv. Synth. Catal.* **2010**, *352* (7), 1135-1138.
46. Nielsen, S. F.; Boesen, T.; Larsen, M.; Schønning, K.; Kromann, H., Antibacterial Chalcones—Bioisosteric Replacement of the 4' -Hydroxy Group. *Bioorg. Med. Chem.* **2004**, *12* (11), 3047-3054.
47. Pollock, J. A.; Sharma, N.; Ippagunta, S. K.; Redecke, V.; Häcker, H.; Katzenellenbogen, J. A., Triaryl Pyrazole Toll-Like Receptor Signaling Inhibitors: Structure–Activity Relationships Governing Pan- and Selective Signaling Inhibitors. *ChemMedChem* **2018**, *13* (20), 2208-2216.
48. Cui, M.; Ono, M.; Kimura, H.; Liu, B.; Saji, H., Synthesis and Structure–Affinity Relationships of Novel Dibenzylideneacetone Derivatives as Probes for β -Amyloid Plaques. *J. Med. Chem.* **2011**, *54* (7), 2225-2240.
49. Nocentini, A.; Lucidi, A.; Perut, F.; Massa, A.; Tomaselli, D.; Gratteri, P.; Baldini, N.; Rotili, D.; Mai, A.; Supuran, C. T., α,γ -Diketocarboxylic Acids and Their Esters Act as Carbonic Anhydrase IX and XII Selective Inhibitors. *ACS Med. Chem. Lett.* **2019**, *10* (4), 661-665.
50. *CsPbBr₃ Crystal Structure: Datasheet from "PAULING FILE Multinaries Edition – 2012" in SpringerMaterials* (https://materials.springer.com/isp/crystallographic/docs/sd_0545372), Springer-Verlag Berlin Heidelberg & Material Phases Data System (MPDS), Switzerland & National Institute for Materials Science (NIMS), Japan.

Chapter 4 CsPbBr₃ Perovskite Nanocrystals for Photocatalytic [3+2] Cycloaddition

4.1 Chapter Summary

This chapter describes the application of CsPbBr₃ perovskite nanocrystals (NCs) for the photocatalytic generation of bromine radicals (Br•) in Br-based organic solvents and towards a Br radical-mediated ring-opening [3+2] cycloaddition reaction for vinylcyclopentane synthesis. Visible-light-induced halide-exchange between halide perovskite and organohalide solvents has been studied in which photoinduced electron transfer from CsPbBr₃ NCs to dihalomethane solvent molecules produces halide anions via reductive dissociation, followed by a spontaneous anion-exchange. Photogenerated holes in this process are less focused. Here, for CsPbBr₃ in dibromomethane (DBM), we discover that Br• is a key intermediate resulting from the hole oxidation. We successfully trapped Br• with reported methods and found that Br• is in continuous generation in DBM under visible light irradiation, hence imperative for catalytic reaction design. Continuous Br• within this halide-exchange process is active for photocatalytic [3+2] cycloaddition for the synthesis of vinylcyclopentane, a privileged scaffold in medicinal chemistry, with good yield and rationalized diastereoselectivity. The NCs photocatalyst is highly recyclable due to Br-based self-healing, leading to a particularly economic and neat heterogeneous reaction where the solvent DBM also behaves as a co-catalyst for perovskite photocatalysis. Halide perovskites, notable for efficient solar energy conversion, herein are demonstrated as exceptional photocatalysts for Br radical-mediated [3+2] cycloaddition. We envisage such perovskite-induced Br radical strategy may serve as a powerful chemical tool to develop valuable halogen radical-involved reactions.

4.2 Introduction

One of the unique properties of lead-halide perovskites (LHP) is their easily accessible band tunings in which simple halide-exchange may tune the bandgaps of perovskites that essentially span the entire visible light spectrum.¹⁻³ As shown in **Scheme 4.1A**, LHP demonstrated spontaneous halide-exchange with free halogen ions in solution, *i.e.*, CsPbBr₃ readily exchanged with I⁻ ions, forming CsPbBr_{3-x}I_x, or with Cl⁻ ions forming CsPbBr_{3-x}Cl_x.¹⁻³ Visible-light-induced halide-exchange of perovskite NCs was discovered by Parobek *et al.* directly between an organohalide solvent and LHP, *i.e.*, CsPbBr₃ with dichloromethane forming CsPbBr_{3-x}Cl_x (**Scheme 4.1B**),⁴ implying a potential application in halogen activations. We also reported a perovskite-induced photocatalytic organic reaction for the synthesis of N-heterocycles, forming a critical pharmaceutical-related *N*-aryl pyrrole scaffold, that involved *in-situ* light-induced halide-exchange between α -haloketone and CsPbBr₃, leading to a wider photoredox potential of the perovskite photocatalyst thus enabling a broader range of substrate activation (**Scheme 4.1C**).⁵

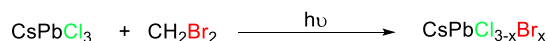
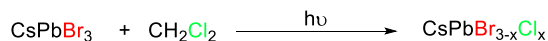
Halide-exchange has been focused on tuning the bandgap of halide perovskite, therefore tuning its respective optoelectronic properties. The proposed mechanism for light-induced halide-exchange with organohalides involves a key electron transfer step from excited-state NCs (conduction band) to reduce haloalkane, forming respective halide anion and alkyl radical.^{4,6} Fewer attentions have been paid to the halide itself, particularly organohalides, one of the most common organic compounds. Noticeable exception was reported for halogenation of electron-rich arenes where halogen sourced from dihalomethane solvent.⁷ Wong *et al.* illustrated the exchange kinetics using primary, secondary, and tertiary haloalkanes and demonstrated that the exchange rate is determined by the activation barrier of C-X bond breakage, and closely corresponds to the C-X bond energy and respective carbon radical stability.⁶ However, the hole transfer counterpart

(valance band-based oxidation), which is an imperative half-cell reaction of the full cycle, of such light-induced halide-exchange process has been less discussed.

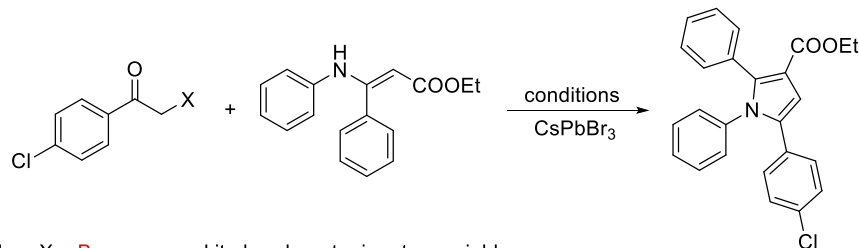
A) Spontaneous perovskite halide-exchange (X = Cl, Br, I):



B) Parobek *et al.*: light-induced halide-exchange between perovskite and halogen solvents



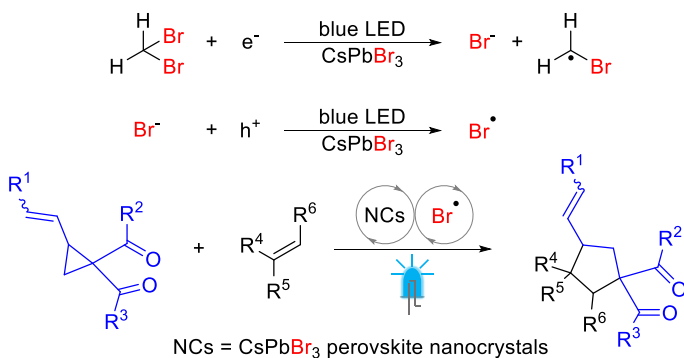
C) Our previous report: halide-exchange for perovskite photocatalyst activation



When X = Br, no perovskite bandgap tuning, trace yield.

When X = Cl, bandgap blue-tuning, forming $\text{CsPbBr}_{3-x}\text{Cl}_x$, wider photoredox potential, high yield.

D) This work: halide-exchange for continuous Br radical for photocatalytic [3+2] cycloaddition



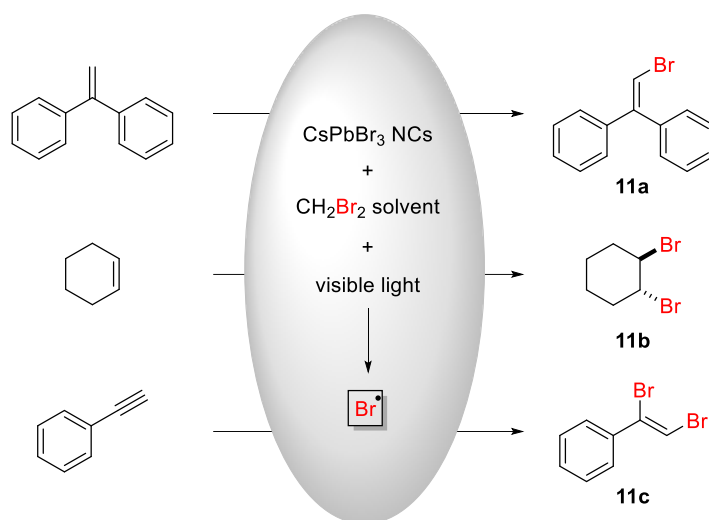
Scheme 4.1 A-C) Previous focuses on LHP halide-exchange. **D)** Perovskite-induced Br radical in DBM for photocatalytic [3+2] cycloaddition.

4.3 Results and Discussion

4.3.1 Bromine Radicals

Our initial exploration of this oxidative half-cell reaction revealed that the photogenerated holes may directly transfer to the halide anions, *i.e.*, Br^- , that has been generated from the reductive half-cell reaction (electron transfer process), forming Br^\bullet in DBM solvent as shown in **Scheme**

4.1D. We employed reported method to verify such $\text{Br}\cdot$ intermediate.⁸ For instance, when 1,1-diphenylethylene, a commonly known radical acceptor, was added to a DBM solution containing catalytic amount of CsPbBr_3 NCs, a substantial portion of 2-bromo-1,1-diphenylethylene (**11a**) was found as product after irradiation under blue LED in anaerobic condition (**Scheme 4.2**, also see **Section 4.5.6**). Furthermore, when cyclohexene and phenylacetylene were subjected to the same experimental conditions respectively, their bromo-addition products (**11b** and **11c**) were also isolated. The production of the bromo-trapping products (**11a-c**) under CsPbBr_3 NCs photocatalysis conditions in DBM underpins the $\text{Br}\cdot$ formation from the hole oxidation of the Br^- that are generated from the first electron transfer step.



Scheme 4.2 The trapping of bromine radicals.

Interestingly, we also found that such perovskite-induced $\text{Br}\cdot$ generation in DBM is a continuous process under the visible light irradiation. $\text{Br}\cdot$ is known to brominate the reactive C-H bonds, *i.e.*, benzylic C-H, via free-radical substitution. Our experiment of gram-scale benzylic bromination of toluene showed that the yield of benzyl bromide steadily increased over 14 days. (**Table 4.5**) This remarkable result further demonstrates two important points: 1) the steady-state concentration of $\text{Br}\cdot$ during the light-induced perovskite bromide-exchange process is low,

otherwise multi-bromination byproduct could be seen; 2) Br• can be continuously generated without undesirable quenching during the photocatalysis process. The presence of small amount but continuous generation of Br• in such a neat reaction setup might be of significance for further development of valuable photocatalytic reactions, given that Br• has been widely explored as an agent for bromination, hydrogen atom transfer (HAT) ⁸⁻¹¹ and other elegant organic transformations. ^{12, 13}

4.3.2 Photocatalytic Design

We focused on exploiting the perovskite-induced continuous Br• for photocatalytic organic reaction purposes. Here we explored the synthetic application of this system by designing a protocol for Br radical-mediated [3+2] cycloaddition for vinylcyclopentane synthesis. Five-membered cyclic scaffolds are privileged in medicinal chemistry and being found in over 10 of the top 30 Bemis–Murcko frameworks. ¹⁴ Several seminal works were reported to achieve [3+2] cycloaddition between vinylcyclopropanes and alkenes. Examples by thiyl radical were found in early cases under thermal condition or with a radical initiator under intense UV excitation. ¹⁵⁻¹⁷ Organotin hydride, a classical radical precursor, was reported to be active towards this endeavor with the presence of a suitable radical initiator. ¹⁸ As the rapid development of visible-light photocatalysis, Miyake group reported that a cinnamyl bromide co-catalyst could accept triplet energy from an excited-state iridium photocatalyst to mediate such valuable organic transformation. ¹⁹ Most recently, isothiouronyl radical cation coupled with an Ir-based photocatalyst was utilized to catalyze this [3+2] cycloaddition. ²⁰ Overall, the harsh reaction conditions, radical initiator, delicately designed co-catalyst or noble metal complex-based photocatalyst were required for the success of the aforementioned reactions.

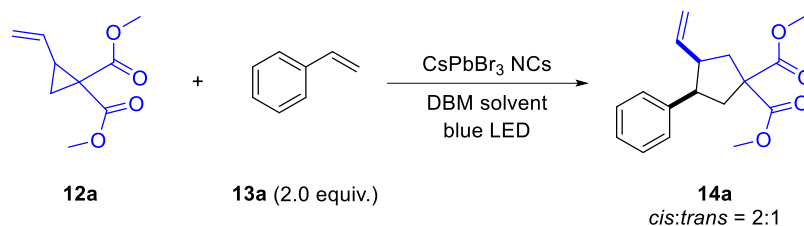
Such radical-mediated [3+2] cycloaddition mechanism necessitates a highly reversible addition of the catalytic radical (*i.e.*, Br•) to the C(sp²)-C(sp²) bond of vinylcyclopropane substrate

achieving ring opening and then to release the added radical after a cyclization step.²¹ However, the continuous radical generation may be beneficial to the [3+2] product formation because the undesirable but inevitable off-cycle quenching of such radicals will terminate the reaction and result in a diminished yield.²² Our approach here featuring a benign reaction condition with recyclable CsPbBr₃ NCs as the photocatalyst, DBM as the co-catalyst and solvent, demonstrates a high turnover pathway to exploit the photogenerated holes during the perovskite halide-exchange process. The CsPbBr₃ perovskite-induced continuous Br• generation under visible light irradiation in our simple reaction setup may offer an appealing strategy for photocatalytic Br radical-mediated organic transformations.

4.3.3 Reaction Development

To our delight, visible-light-induced continuous Br• generated from CsPbBr₃ NCs in DBM resulted in the [3+2] cycloaddition of vinylcyclopropane **12a** with alkene **13a** in a high yield as shown in **Table 4.1**. The desired product vinylcyclopentane **14a** was observed with a diastereomeric ratio (d.r.) of 2:1 (*cis:trans*) in 94% yield after blue LED irradiation for 4h (**Table 4.1**, entry 1). Omitting the light or NCs resulted in complete recovery of the starting materials (entry 2, 3 and 4), demonstrating the pivotal role of CsPbBr₃ NCs as a photocatalyst. Furthermore, non-Br solvent resulted in no reaction (entry 5 and 6) or trace yield (entry 7). Altering the Br-based solvent, ratio between the starting materials **12a** and **13a** resulted in compromised yields (entry 8, 9 and 10). Note that a stoichiometric instead of solvent amount of DBM could also achieve a similar yield to the optimized conditions, but a longer reaction time was required. (See **Table 4.3** for full condition exploration)

Table 4.1 Optimization studies and control experiments for perovskite photocatalytic Br-mediated [3+2] cycloaddition.



Entry	Deviation from standard conditions ^a	Yield, % ^b
1	None	94 (87)
2	No light	0
3	No CsPbBr ₃ NCs	0
4	PbBr ₂ instead of CsPbBr ₃ NCs	0
5	Toluene as solvent	0
6	Tetrahydrofuran as solvent	0
7	Dichloromethane as solvent	Trace
8	1-Bromobutane as solvent	91
9	13a (1.0 equiv.)	68
10	13a (3.0 equiv.)	92

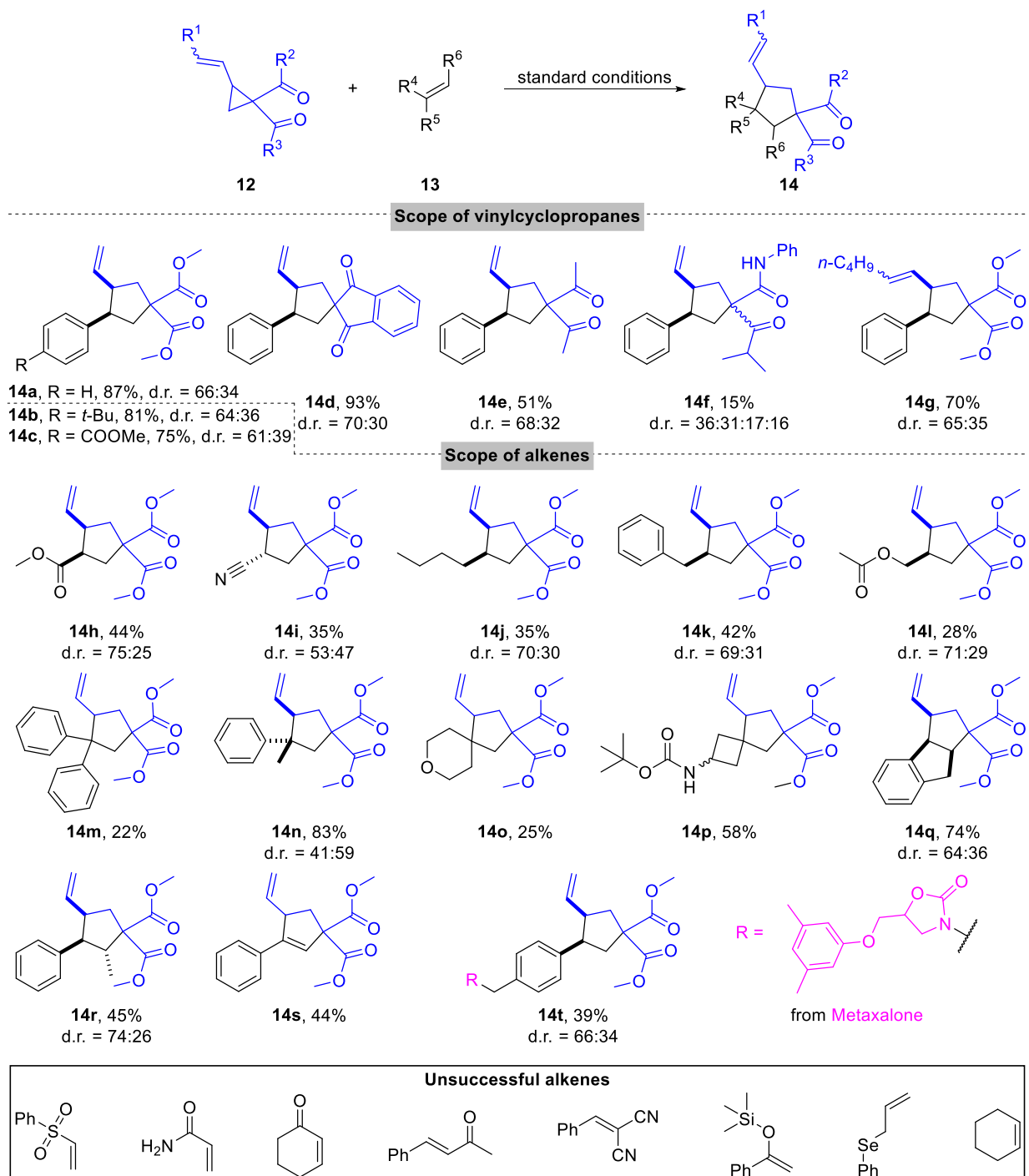
^aStandard conditions: **12a** (0.15 mmol, 0.1 M), **13a** (0.30 mmol, 2.0 equiv.), CsPbBr₃ NCs (1.0 mg), DBM (1.5 mL). Reaction was performed under N₂ and blue LED (40 W, $\lambda_{\text{max}} = 456 \text{ nm}$) irradiation at room temperature for 4h.

^bYields were determined by ¹H NMR using 3,4,5-trichloropyridine as an internal standard. Isolated yield is shown in parentheses.

4.3.4 Reaction Scope

The reaction scope with regard to both vinylcyclopropanes **12** and alkenes **13** were investigated (**Scheme 4.3**). **12** with different substituents cyclized with styrenes in yields up to 93%. Compound **14f** was obtained in a noticeable lower yield (15%), probably due to the steric hindrance from the isopropyl group and that the *N*-phenylacetamido group may function as a

competitive hole scavenger, having a detrimental effect on the product yielding.²³ Notably, the double bond on **12** does not need to be terminal (**14g**, 70% yield).



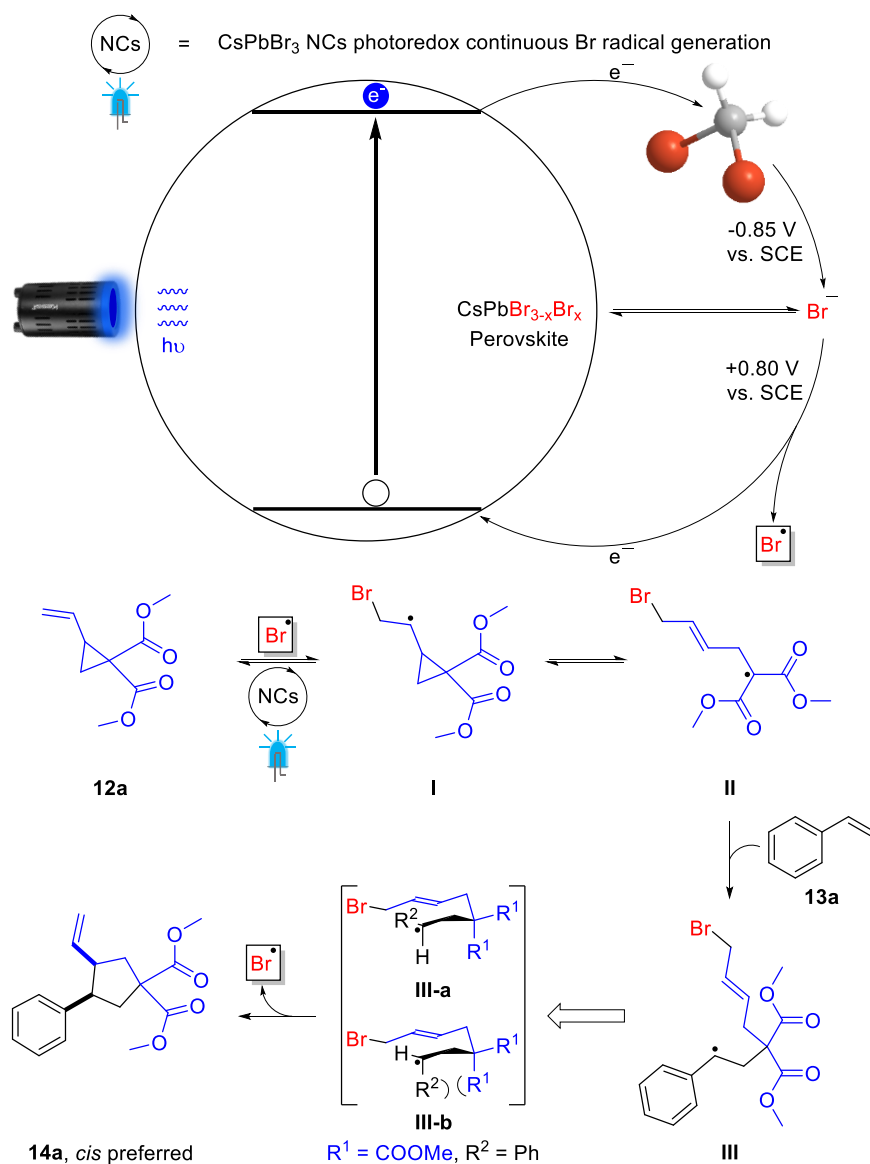
Scheme 4.3 Scope of vinylcyclopropanes and alkenes. Only the structures of the major diastereomers are shown. All yields are isolated yields. d.r. values were determined by ¹H NMR integration.

We next examined the scope of alkenes. In general, styrenes could tolerate both electron-donating and electron-withdrawing para-substituents, making them highly successful reaction partners (**14a-c**, 75-87% yield). Michael acceptors only delivered products in moderate yields (**14h, i**, 35-44% yield), likely because the undesired polymerization reaction competed with the desired reaction pathway.²⁴ Another reason perhaps could be attributed to less-than-optimal matching of orbitals energies, considering an electron-poor malonyl radical (**Scheme 4.4**, intermediate **II**) attacking an electron-deficient alkene. Non-activated primary alkenes are also successful substrates albeit with lower yield (**14j-l**, 28-42% yield), we attribute such observation to a less stable radical intermediate (**Scheme 4.4**, variant of **III**). (*Vide infra*) Overall, both Michael acceptors and non-activated primary alkenes delivered products in modest yields. However, the conversions based on starting material **12a** were all nearly quantitative in these cases. Further analysis on the side products revealed a ring-opening polymerization pathway, consistent to a mechanism disclosed by Chen *et al.*,²⁵ which consumed the vinylcyclopropane starting material in an unproductive way (**Figure 4.5** and **4.6**). These observations indicate that both the transition from intermediate **II** to **III** and the stability of **III** are imperative for an efficient transformation. Saturated (hetero)cycle compounds with an *exo*-methylene group generated useful three-dimensional-enrich spiro-products (**14o, p**, 25-58% yield). Indene, a cyclic alkene, could be employed to generate a fused-ring product (**14q**, 74% yield) that is an important category in drug discovery. Alpha-methyl substituted styrene did not appear to affect the cycloaddition for **14n**, creating a quaternary carbon stereocenter, with a yield of 83% that is comparable to non-substituted styrenes. However, beta-methyl substituted styrene delivered product in a lower yield (**14r**, 45% yield). As expected, 1,1-diphenylethylene only resulted in 22% yield of desired product (**14m**) with high yielding of **11a** as a byproduct, because 1,1-diphenylethylene itself is a good

bromine radical acceptor, consuming Br• during the photocatalytic process as shown in **Scheme 4.2**. Interestingly, this [3+2] cycloaddition is not limited to alkenes. Phenylacetylene bearing a triple bond is also a successful substrate to form [3+2] cycloaddition product, **14s**. Further studies focusing on the alkyne substrates are currently under investigation in our laboratory. Finally, an alkene derived from the commercially available drug molecule, Metaxalone, provided the expected product (**14t**) in 39% yield, indicating a potential application in late-stage pharmaceutical functionalization, an extremely important methodology for drug development.

4.3.5 Mechanistic Investigation

The plausible mechanism (**Scheme 4.4**) is premised on our experimental results and previous reported studies. Under visible light irradiation, CsPbBr₃ NCs undergo photoinduced electron transfer from conduction band to DBM ($E_{1/2}^{\text{red}} = -0.85$ V vs. SCE, ⁷ also see **Figure 4.8**), generating Br⁻ (**Scheme 4.1D** and **Scheme 4.4**), while the photogenerated holes from valence band further oxidize the Br⁻ into Br• ($E_{1/2}^{\text{ox}} = +0.80$ V vs. SCE) ²⁶. Here, the bromide-exchange between the DBM solvent and CsPbBr₃ NCs is a dynamic process under light irradiation, meaning that Br• generation is continuous in the photoredox cycle. Note that direct single-electron oxidation of DBM is not viable because the oxidation potential of DBM ($E_{1/2}^{\text{ox}} = +1.62$ V vs. SCE) ⁸ is out of reach for the photoredox potential of CsPbBr₃ NCs. The reversible addition of Br• to vinylcyclopropane **12a** leads to intermediate **I**, followed by ring opening to form **II**, which is then trapped by alkene **13a** to produce **III**. The optimal reaction condition requires an excessive amount of **13a** (**Table 4.1**, entry 9), probably because of the reversible nature of intermediate **II** which resonates with **I**. But over-excess amount of **13a** slightly reduces the yield (**Table 1**, entry 10), because **13a** may compete with **12a** for the Br• addition (such as shown in **Scheme 4.2**), therefore consuming Br• in an undesirable way.



Scheme 4.4 The plausible mechanism for NCs-photocatalyzed Br-mediated [3+2] cycloaddition.

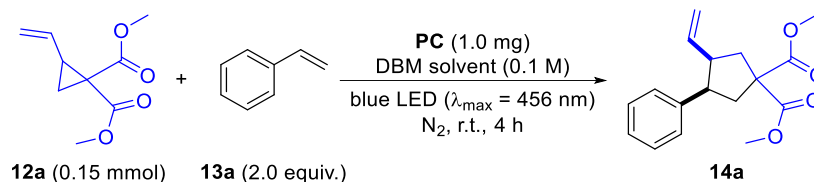
The diastereoselectivity is governed by the intermediate **III**, whose chair-like transition states have been proposed in **Scheme 4.4**, bracket.¹⁶ Two likely configurations **III-a** and **III-b** are illustrated as the key transition states for the de-brominated (Br^\bullet regeneration) cyclization step and determine the diastereoselectivity. For instance, **III-a** will lead to the formation of *cis*-**14a** while **III-b** results in the *trans*-**14a** product. Here, the steric hindrance from the 1,3-diaxial interaction of **III-b** (*i.e.*, R^1 and R^2) disfavors the **III-b** configuration compared to the **III-a** that dictates the

preference for *cis*-product formation, corroborating with the general diastereomeric ratios shown in **Scheme 4.3**.²⁷ The diastereomeric conformation of the product is confirmed by Nuclear Overhauser Effect Spectroscopy (NOESY, see **Appendix B**). It is worth noting that our illustration of the diastereoselectivity of this transformation is distinct from the lately reported photocatalytic approach.^{19,20}

Photocatalyst evaluation studies were carried out employing a few commonly used homogeneous molecular photocatalysts (**Table 4.2**). Note that the key to a successful transformation is to efficiently produce continuous Br• without perturbing the subsequent catalytic cycle. Under otherwise the same standard conditions, Ru(bpy)₃²⁺ yielded no product because the redox potential of it cannot reach that of DBM (**Table 4.2**, entry 2). Although *fac*-Ir(ppy)₃ can photoreduce DBM to Br⁻ (Ir^{IV}/Ir^{III*} = -1.73 V vs. SCE), it barely reaches the oxidation potential of Br⁻ to Br• (Ir^{IV}/Ir^{III} = +0.77 V vs. SCE). The key oxidation step to generate Br• might be impeded, hence only trace amount of product was observed. [Acr-Mes]⁺(ClO₄)⁻ photocatalyst yielded trace amount of desired product owing to its highly oxidizing excited state (cat^{*}/cat• = +2.06 V vs. SCE), which allows it to directly oxidize the DBM to generate Br•. However, the Br• generation is not continuous hence not sustainable because now the other half-cell reaction (reduction) is problematic due to the absence of a proper reagent to regenerate the ground-state acridinium photocatalyst, causing the following Br radical-mediated catalytic cycle susceptible to termination once the limited amount of Br• being produced is intercepted by an off-cycle pathway. 4-CzIPN photocatalyst furnished a good amount of product, likely going through a reduction (DBM/Br⁻) then oxidation (Br⁻/Br•) mechanism. Since the photoredox potentials of 4-CzIPN (cat⁺/cat* = -1.04 V, cat⁺/cat = +1.52 V vs. SCE) are amendable to cover both the reduction potential of DBM and the oxidation potential of Br⁻. Finally, a Br-containing fluorescein-based

PC, eosin Y, with suitable excited-state photoredox potentials was subjected to this study. However, the product was only observed in a modest yield even with the presence of CsBr salt as an additive (**Table 4.2**, entry 6). The above results further support our photoredox-based continuous Br• generation mechanism.

Table 4.2 Photocatalyst (PC) evaluation under standard conditions.



Entry	PC	M ⁺ /M* (V) ^a	M*/M ⁻ (V) ^a	M ⁺ /M (V) ^a	M/M ⁻ (V) ^a	Yield, % ^b
1	CsPbBr ₃ NCs	-1.3	+1.1			94
2	Ru(bpy) ₃ ²⁺	-0.81	+0.77	+1.29	-1.33	n.d.
3	<i>fac</i> -Ir(ppy) ₃	-1.73	+0.31	+0.77	-2.19	trace
4	[Acr-Mes] ⁺ (ClO ₄) ⁻		+2.06		-0.57	trace
5	4-CzIPN	-1.04	+1.35	+1.52	-1.21	68
6	Eosin Y	-1.11	+0.83	+0.78	-1.06	21 (24)

^aAll potentials vs. saturated calomel electrode (SCE). Photoredox potentials of PC are referenced from literature.²⁸⁻³²

^bYields were determined by ¹H NMR using 3,4,5-trichloropyridine as an internal standard. Yield with CsBr (1.0 mg) as an additive is shown in parentheses.

4.3.6 Catalyst Recycling

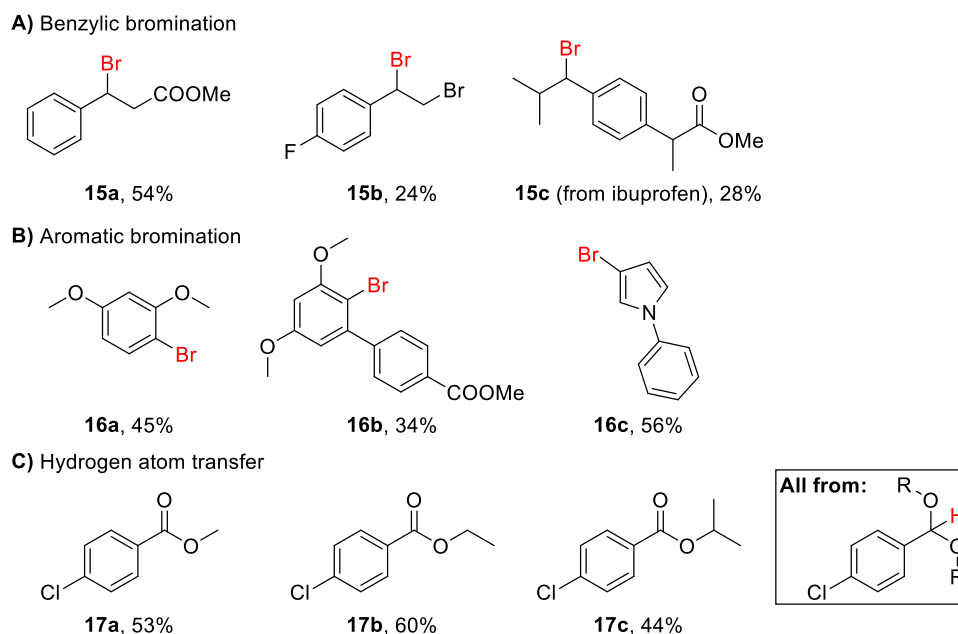
Our heterogenous approach may be advantageous over homogenous photocatalysts for such [3+2] cycloaddition in the following aspects: 1) The localized concentration of Br⁻ is higher in the case of CsPbBr₃ NCs owing to its positively-charged surface^{33, 34} hence more capable of adsorbing Br⁻ as the potential hole acceptor. 2) The Br⁻ may also come from CsPbBr₃'s own

surface, which is supported by our observation (**Table 4.1**, entry 7) ³⁵, meaning NCs are intrinsically superior in the context of bromide oxidation. Note that this pathway is not necessarily detrimental to the perovskite structure since Br⁻ diffusing from the bulk solution would compensate for the loss from the NCs' surface. Conversely, the density of surface vacancy defects of CsPbBr₃ NCs could be reduced via such “self-bromide exchange” process. ⁴ 3) The enhancement of the PL intensity of CsPbBr₃ NCs after irradiation in DBM was observed in our study (**Figure 4.7**), in line with previous report, ⁴ indicating the defects healing during the “self-bromide exchange” process. Catalyst deactivation remains a long-term issue. ³⁶ However, our recycling experiments showed that the perovskite NCs demonstrated no sign of decrease in catalytic performance during three consecutive cycles of reactions (**Table 4.4**), probably attributed to this self-healing process. These aspects together undoubtedly render a high-turnover photocatalytic strategy.

4.3.7 More Applications

We moved on to examine the robustness of our system by merging it with other bromination or Br-mediated reactions. The preliminary results without optimization are very promising. Various alkylbenzene compounds were successfully brominated at the benzylic position in moderate yields (**Scheme 4.5A**). Notably, ibuprofen, a commonly used anti-inflammatory drug molecule, derived methyl ester could undergo bromination to generate **15c** (28% yield). Gram-scale selective synthesis of an important building block, benzyl bromide, from widely available toluene was performed to demonstrate the scale-up capability of this system. (**Table 4.5**) We also discovered that mono-bromomethane was a key side product generated from DBM in this benzylic bromination. A series of electron-rich (hetero)arenes could be brominated at the predictable position (**Scheme 4.5B, 16a-c**, 34-56% yield). Gratifyingly, our system could also be applied to an HAT reaction, where the tertiary C(sp³)-H of benzaldehyde acetals could be

abstracted by Br• then undergo β -fragmentation to produce respective esters (**Scheme 4.5C**). This type of mechanism was well-documented by Doyle Group^{11, 37} (also see **Scheme 4.7**). More synthetic applications utilizing this strategy are currently under development in our group.



Scheme 4.5 Merging with other organic transformations. General reaction conditions: **substrate** (0.15 mmol, 0.1 M), CsPbBr₃ NCs (1.0 mg), DBM (1.5 mL). Reaction was performed under N₂ and blue LED (40 W, $\lambda_{\text{max}} = 456 \text{ nm}$) irradiation at room temperature. Isolated yields are shown.

4.4 Conclusion

Mechanistic investigation of visible-light-induced halide-exchange between LHP NCs and organohalide solvents leads to the discovery of an important Br• intermediate. Such Br• is concluded to be generated in a continuous manner in DBM solvent under visible light irradiation. We also prove that such continuous generation of Br• plays an important role in further design of photocatalytic organic reactions. Most prominently, such mechanism allows us to utilize DBM as a co-catalyst and solvent to mediate the perovskite-photoinduced [3+2] cycloadditions with broad substrate scope tolerance, for the synthesis of a critical category in medicinal chemistry. The respective diastereoselectivity for the preference of *cis*-product formation has been revealed due to the 1,3-diaxial interaction of the chair-like transition states (**III-a** vs. **III-b**). Additionally, this

strategy can be extended to other Br radical-related reactions, *i.e.*, benzylic bromination, aromatic bromination, and Br radical-mediated HAT, demonstrating a great potential for LHP to be applied in halogen radical-involved organic reactions.

Among the photocatalysts for photoredox organic synthesis, LHP is not only economic but also highly efficient, paving the path to render the ease of product separation, simple catalyst regeneration, and usually high stability of solid catalysts facilitating continuous flow production processes. The design and development of heterogeneous catalysts for vast and large-scale production of value-added organic molecules, particularly those of pharmaceutical significance, *i.e.*, [3+2] cycles here, should be an essential ingredient in the chemical synthetic toolbox.

4.5 Experimental Section

4.5.1 General Information

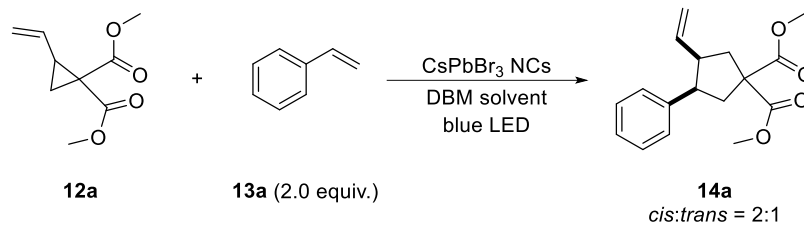
Commercially available reagents and solvents were purchased from TCI Chemicals, Fisher Scientific and Sigma-Aldrich and were used as received if not stated otherwise. A 40-watt Kessil® PR160-456nm blue LED lamp was used for all photochemical reactions. Silica gels (P60, 40-63 μm , 60 \AA) used for column chromatography were purchased from SILICYCLE. Thin layer chromatography (TLC) analysis was carried out on aluminum backed silica gel coated plates (200 μm , SILICYCLE). Visualization was completed by a Analytikjena hand-held UV lamp (254 nm) and basic KMnO_4 solution.

^1H , ^{13}C , ^{19}F NMR spectra were acquired on a Varian VNMRS 400 spectrometer or Varian Inova 500 spectrometer. Nuclear Overhauser Effect Spectroscopy (NOESY) were acquired on a Varian Inova 500 spectrometer. Homonuclear Correlation Spectroscopy (COSY) were acquired on a Varian VNMRS 400 spectrometer. All chemical shifts are reported in parts per million (ppm) referenced to residual chloroform (7.26 ppm and 77.16 ppm, respectively for ^1H and ^{13}C NMR), unless otherwise noted. All coupling constants (J) are reported in hertz (Hz). Abbreviations for

multiplicity are: s, singlet; br s, broad singlet; d, doublet; t, triplet; q, quartet; hept, heptet; m, multiplet. All the NMR spectra were processed using Mestrenova software applying standard baseline corrections. ^1H NMR data were recorded for all compounds for characterization purposes. Crude yields were determined by ^1H NMR using 3,4,5-Trichloropyridine as an internal standard. Diastereomeric ratios were calculated from ^1H NMR integration. Mass spectra were recorded on an Agilent 7890A GC system coupled with a 5975 MSD (Gas Chromatography-Mass Spectrometry, GC-MS) with an electron ionization (EI) method. High-resolution mass spectra (HRMS) were recorded on an Agilent 6530 Accurate Mass Q-TOF with an electrospray ionization (ESI) method. Steady-state emission spectra were acquired using a HORIBA Fluoromax-3 spectrofluorometer.

4.5.2 Condition Exploration

Table 4.3 Extended reaction conditions.

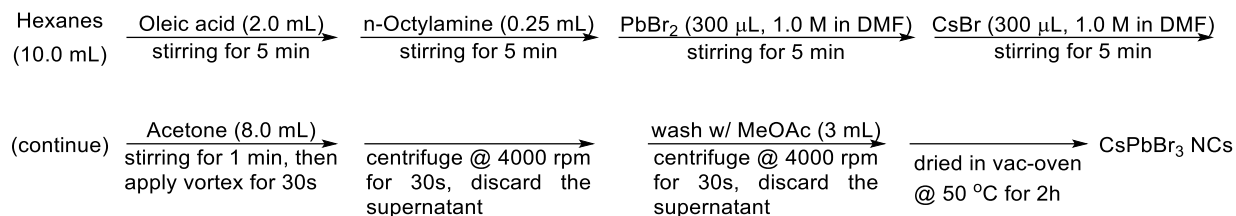


Entry	Deviation from standard conditions ^a	yield, % ^b
1	none	94
2	no light	0
3	no CsPbBr ₃ NCs	0
4	PbBr ₂ instead of CsPbBr ₃ NCs	0
5	toluene as solvent	0
6	tetrahydrofuran (THF) as solvent	0
7	dichloromethane (DCM) as solvent	trace
8	1-bromobutane as solvent	91
9	13a (1.0 equiv.)	68
10	13a (3.0 equiv.)	92
11	THF as solvent with DBM (1.0 equiv.)	18
12	MeOAc as solvent with DBM (1.0 equiv.) react for 32h	52
13	MeOAc (1.4 mL) and DBM (10.0 equiv., 0.1 mL) as solvent	42
14	MeOAc (1.4 mL) and DBM (10.0 equiv., 0.1 mL) as solvent react for 16h	87
15	MeOAc (1.4 mL) and DBM (10.0 equiv., 0.1 mL) as solvent react for 20h	95

^aStandard conditions: **12a** (0.15 mmol, 0.1 M), **13a** (0.30 mmol, 2.0 equiv.), CsPbBr₃ NCs (1.0 mg), DBM (1.5 mL). Reaction was performed under N₂ and blue LED (40 W, λ_{max} = 456 nm) irradiation at room temperature for 4h.

^bYields were determined by ¹H NMR using 3,4,5-trichloropyridine as an internal standard.

4.5.3 Preparation of CsPbBr₃ NCs Photocatalyst



The synthesis of CsPbBr₃ perovskite nanocrystals was adapted from literature.³⁸ CsBr solution (3.0 mL, 1.0 M in H₂O) and PbBr₂ solution (7.0 mL, 1.0 M in dimethylformamide, DMF) were prepared as two respective precursor stock solutions. To a 20-mL vial with a magnetic stirring bar, hexanes (10.0 mL) and oleic acid (2.0 mL) were added and the resulting mixture was allowed to vigorously stir at room temperature for 5 min. Then, *n*-octylamine (0.25 mL) was added and continued stirring for another 5 min. Next, the PbBr₂ stock solution (300 μ L, 1.0 M in DMF) was added dropwise. After 5 min stirring, the CsBr stock solution (300 μ L, 1.0 M in H₂O) was added dropwise. The resulting mixture was allowed to stir for another 5 min followed by adding acetone (8.0 mL) in one batch. A large amount of precipitate was formed and the mixture stayed stirring for 1 min and was subjected to vortex for 30s. Finally, the solid was collected via centrifugation and washed with MeOAc (3 mL). The residual solvent was removed by vacuum oven at 50 °C for 2h.

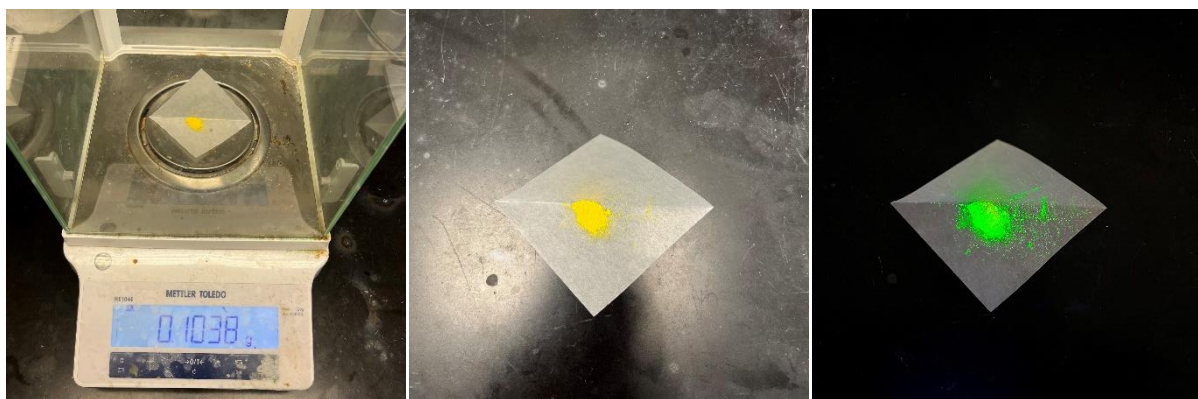
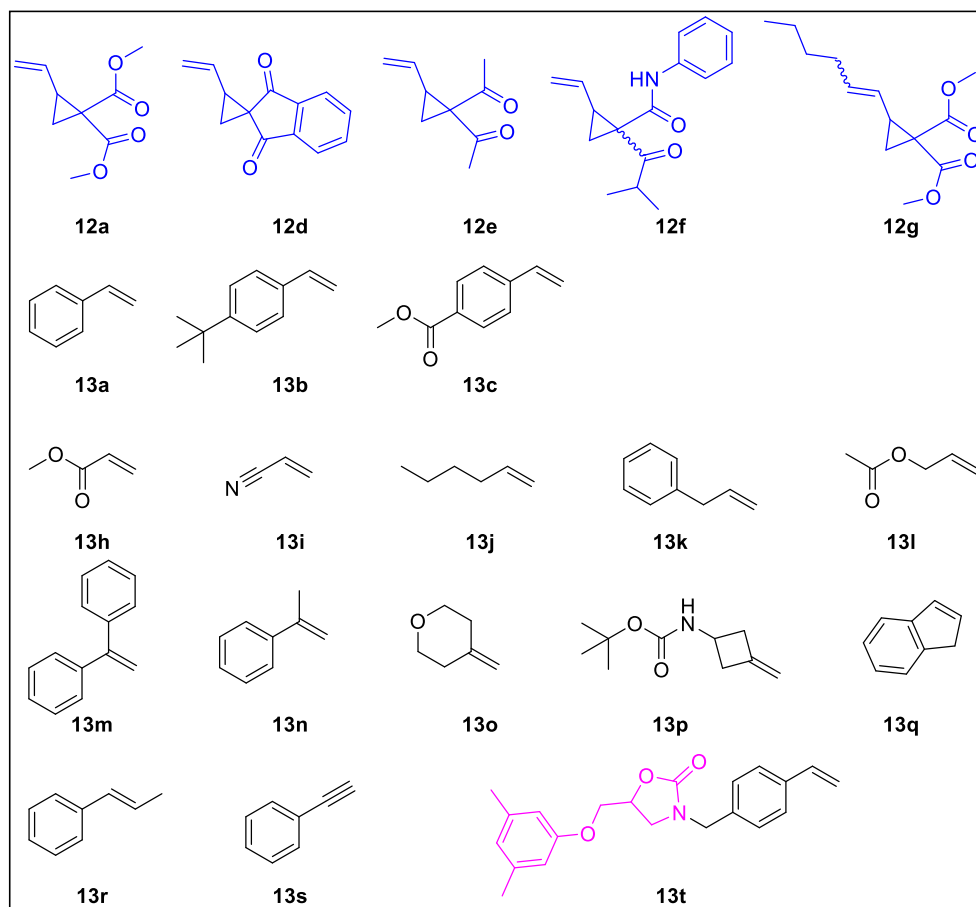


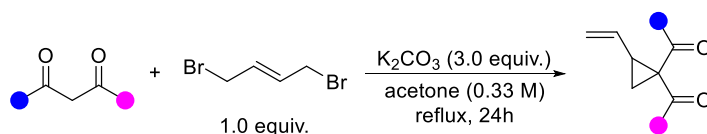
Figure 4.1 The as-synthesized CsPbBr₃ perovskite nanocrystals under ambient light (left and middle) and under 365-nm UV excitation (right).

4.5.4 Preparation of Starting Materials



Scheme 4.6 The substrate scope for [3+2].

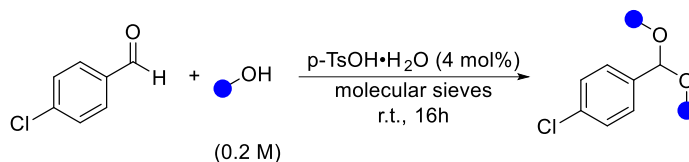
General Procedure A for the Synthesis of Vinylcyclopropanes³⁹:



To a round-bottom flask with a magnetic stirring bar was added *trans*-1,4-dibromo-2-butene (1.0 equiv.), K_2CO_3 (3.0 equiv.), acetone (0.33 M) and 1,3-dione (1.0 equiv.). The resulting mixture was allowed to react at reflux temperature around 60 °C for 24h. Upon completion, the reaction mixture was filtered and the solvent was removed by rotary evaporator. Then the product was purified by flash column chromatography on silica gel using a combination of hexanes and

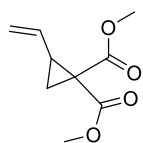
EtOAc as eluent. TLC was employed to detect the product and the basic KMnO₄ solution was necessary in most of the cases for visualization in addition to UV lamp (254 nm).

General Procedure B for the Synthesis of Benzaldehyde Acetals¹¹:



To a round-bottom flask with a magnetic stirring bar was added 4-chlorobenzaldehyde (1.0 equiv.), alcohol as solvent (0.2 M) and *p*-toluenesulfonic acid monohydrate (4 mol%). A suitable amount of activated 4Å molecular sieves (vac-oven dried at 120 °C for 24h) were also added to remove the water side-product. The resulting mixture was allowed to react at room temperature for 16h. Upon completion, the reaction mixture was filtered and the solvent was removed by rotary evaporator. Then the product was purified by flash column chromatography on silica gel using a combination of hexanes and EtOAc as eluent. TLC was employed to detect the product. Although acetals were reported unstable in the silica gel column chromatography condition, we managed to obtain reasonable yields in all our cases.

Synthesis of Vinylcyclopropanes

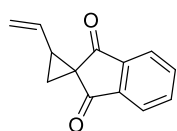


dimethyl 2-vinylcyclopropane-1,1-dicarboxylate (12a)

The titled compound was synthesized following **General Procedure A**: *trans*-1,4-Dibromo-2-butene (2139 mg, 10.0 mmol, 1.0 equiv.), K₂CO₃ (4146 mg, 30.0 mmol, 3.0 equiv.), acetone (30 mL, 0.33 M) and dimethyl malonate (1149 μL, 10.0 mmol, 1.0 equiv.) were used. The product was purified by flash column chromatography on silica gel (Hexanes/EtOAc = 20/1 - 15/1) as colorless oil (79% **yield**, 1455 mg). The analytical data is in good agreement with the reported data.¹⁹

¹H NMR (400 MHz, CDCl₃) δ 5.43 (ddd, *J* = 16.8, 10.0, 8.0 Hz, 1H), 5.30 (dd, *J* = 16.8, 1.6 Hz, 1H), 5.14 (dd, *J* = 10.0, 1.6 Hz, 1H), 3.74 (s, 6H), 2.59 (q, *J* = 8.4 Hz, 1H), 1.72 (dd, *J* = 7.6, 4.8 Hz, 1H), 1.59 (dd, *J* = 8.8, 4.8 Hz, 1H).

¹³C NMR (101 MHz, CDCl₃) δ 170.2, 167.9, 133.1, 118.9, 52.8, 35.9, 31.7, 20.8.

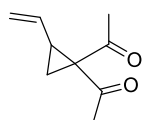


2-vinylspiro[cyclopropane-1,2'-indene]-1',3'-dione (12d)

The titled compound was synthesized following **General Procedure A** with minor modification: *trans*-1,4-Dibromo-2-butene (427.8 mg, 2.0 mmol, 1.0 equiv.), K₂CO₃ (691 mg, 5.0 mmol, **2.5 equiv.**), **dimethylformamide (DMF, 10 mL, 0.2 M)** and 1,3-indandione (292.4 mg, 2.0 mmol, 1.0 equiv.) were used. The product was purified by flash column chromatography on silica gel (Hexanes/EtOAc = 13/1) as light-yellow solid (52% **yield**, 205 mg). The analytical data is in good agreement with the reported data.⁴⁰

¹H NMR (400 MHz, CDCl₃) δ 7.98 – 7.90 (m, 2H), 7.83 – 7.76 (m, 2H), 6.03 (dt, *J* = 17.2, 10.0 Hz, 1H), 5.29 (dd, *J* = 17.2, 1.2 Hz, 1H), 5.15 (dd, *J* = 10.0, 1.2 Hz, 1H), 2.82 (q, *J* = 8.8 Hz, 1H), 2.14 (dd, *J* = 8.8, 4.0 Hz, 1H), 1.99 (dd, *J* = 8.0, 4.0 Hz, 1H).

¹³C NMR (101 MHz, CDCl₃) δ 198.1, 197.3, 142.7, 141.9, 135.0, 134.9, 133.1, 122.6, 122.6, 118.7, 42.3, 40.3, 24.7.

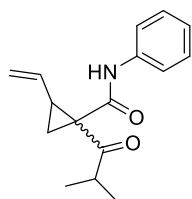


1,1'-(2-vinylcyclopropane-1,1-diyl)bis(ethan-1-one) (12e)

The titled compound was synthesized following **General Procedure A**: *trans*-1,4-Dibromo-2-butene (2139 mg, 10.0 mmol, 1.0 equiv.), K₂CO₃ (4146 mg, 30.0 mmol, 3.0 equiv.), acetone (30 mL, 0.33 M) and acetylacetone (1022 μL, 10.0 mmol, 1.0 equiv.) were used. The product was purified by flash column chromatography on silica gel (Hexanes/EtOAc = 50/1 - 20/1) as colorless oil (48% **yield**, 730 mg). The analytical data is in good agreement with the reported data.³⁹

¹H NMR (400 MHz, CDCl₃) δ 5.33 – 5.27 (m, 2H), 5.17 – 5.12 (m, 1H), 2.66 – 2.58 (m, 1H), 2.27 (s, 3H), 2.17 (s, 3H), 1.84 (dd, *J* = 7.6, 4.8 Hz, 1H), 1.49 (dd, *J* = 8.8, 4.8 Hz, 1H).

¹³C NMR (101 MHz, CDCl₃) δ 202.9, 202.6, 133.0, 119.1, 51.5, 32.6, 31.0, 27.1, 20.5.



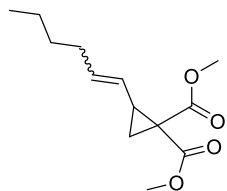
1-isobutyryl-*N*-phenyl-2-vinylcyclopropane-1-carboxamide (12f) (*cis:trans* = 1:1)

The titled compound was synthesized following **General Procedure A**: *trans*-1,4-Dibromo-2-butene (427.8 mg, 2.0 mmol, 1.0 equiv.), K₂CO₃ (829.2 mg, 6.0 mmol, 3.0 equiv.), acetone (6 mL, 0.33 M) and *N*-phenyl-isobutyrylacetamide (410.6 mg, 2.0 mmol, 1.0 equiv.) were used. The product was purified by flash column chromatography on silica gel (Hexanes/EtOAc = 15/1 - 10/1) as white solid (inseparable diastereomers, 68% **yield**, 350 mg).

¹H NMR (400 MHz, CDCl₃) δ 9.88 (s, 0.5H), 9.77 (s, 0.5H), 7.61 – 7.51 (m, 2H), 7.37 – 7.28 (m, 2H), 7.14 – 7.06 (m, 1H), 5.71 (ddd, *J* = 16.8, 10.0, 8.8 Hz, 0.5H), 5.56 (ddd, *J* = 17.2, 10.0, 7.6 Hz, 0.5H), 5.41 – 5.29 (m, 1H), 5.26 – 5.13 (m, 1H), 2.83 – 2.65 (m, 1H), 2.55 (q, *J* = 8.0 Hz, 0.5H), 2.41 (q, *J* = 8.4 Hz, 0.5H), 2.33 – 2.23 (m, 1H), 1.88 (dd, *J* = 7.6, 5.2 Hz, 0.5H), 1.82 (dd, *J* = 9.2, 5.2 Hz, 0.5H), 1.19 – 1.09 (m, 4.5H), 1.04 (d, *J* = 6.4 Hz, 1.5H).

¹³C NMR (101 MHz, CDCl₃) δ 212.7, 166.4, 138.1, 132.6, 132.6, 129.1, 129.1, 129.0, 124.4, 124.3, 120.2, 112.0, 41.6, 39.2, 39.1, 36.1, 35.9, 19.4, 19.2, 19.1, 16.6, 16.4.

Inseparable: **GC-MS** (EI, 70 eV) *m/z* (%) 257 (M⁺, 51), 214 (100), 196 (9), 186 (30), 165 (94), 132 (20), 121 (41), 93 (87), 77 (63), 71 (30), 65 (79).



dimethyl 2-(hex-1-en-1-yl)cyclopropane-1,1-dicarboxylate (12g) (*cis:trans* = 1:5)

The titled compound was synthesized via Grubbs olefin metathesis. To an 8-mL vial with a magnetic stirring bar, dimethyl 2-vinylcyclopropane-1,1-dicarboxylate (**12a**, 73.7

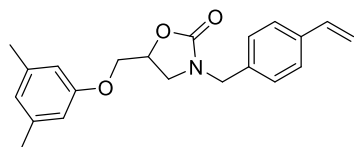
mg, 0.4 mmol, 1.0 equiv.), DCM (2.5 mL, 0.16 M), 1-hexene (500 μ L, 4 mmol, 10 equiv.) and Grubbs catalyst 2nd gen (8.5 mg, 0.01 mmol, 2.5 mol%) were added. Then the resulting mixture was degassed with N₂ and sealed with electric tape. It was allowed to react at reflux temperature for 20h. Upon completion, the solvent was removed by rotary evaporator. The product was purified by flash column chromatography on silica gel (Hexanes/EtOAc = 33/1 – 20/1) as colorless oil (inseparable stereoisomers, 50% **yield**, 49.8 mg).

¹H NMR (400 MHz, CDCl₃) δ 5.69 (dt, J = 15.2, 6.8 Hz, 0.83H), 5.55 (dt, J = 10.8, 7.6 Hz, 0.17H), 5.03 (dd, J = 15.2, 8.0 Hz, 0.83H), 4.85 (dd, J = 10.8, 9.2 Hz, 0.17H), 3.75 – 3.66 (m, 6H), 2.71 (dt, J = 9.6, 8.0 Hz, 0.17H), 2.52 (q, J = 8.4 Hz, 0.83H), 2.20 – 2.09 (m, 0.34H), 2.02 – 1.91 (m, 1.67H), 1.71 – 1.50 (m, 2H), 1.38 – 1.20 (m, 4H), 0.91 – 0.81 (m, 3H).

¹³C NMR (101 MHz, CDCl₃) δ 170.4, 170.4, 168.2, 168.1, 135.7, 135.6, 124.4, 124.3, 52.8, 52.7, 52.6, 52.5, 35.7, 35.7, 32.2, 31.6, 31.4, 31.3, 27.6, 27.0, 22.3, 22.1, 22.0, 20.9, 14.0, 14.0.

Minor: **GC-MS** (EI, 70 eV) m/z (%) 240 (M⁺, 6), 208 (11), 180 (23), 176 (20), 165 (20), 152 (59), 148 (20), 138 (31), 133 (41), 127 (19), 120 (94), 113 (26), 105 (53), 97 (26), 91 (65), 79 (100), 71 (26), 65 (44), 59 (96). Major: **GC-MS** (EI, 70 eV) m/z (%) 240 (M⁺, 9), 208 (16), 180 (20), 176 (26), 165 (21), 152 (62), 147 (22), 138 (34), 133 (43), 127 (24), 120 (100), 113 (19), 105 (45), 97 (19), 91 (46), 79 (68), 71 (25), 65 (28), 59 (59).

Synthesis of Other Starting Materials



5-((3,5-dimethylphenoxy)methyl)-3-(4-vinylbenzyl)oxazolidin-2-one (13t)

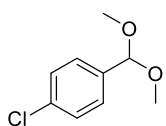
The titled compound was synthesized according to the following procedure: To a 20-mL vial with a magnetic stirring bar, Metaxalone (331.9 mg, 1.5 mmol, 1.0 equiv.), K₂CO₃ (414.6 mg, 3.0 mmol, 2.0 equiv.), DMF (5 mL, 0.3 M) and 4-

(Chloromethyl)styrene (318 μ L, 2.25 mmol, 1.5 equiv.) were added. Then the resulting mixture was allowed to react at room temperature for 20h. Upon completion, the reaction mixture was first filtered. Then, in a separatory funnel, washed w/ water and extract w/ EtOAc for three times. The combined organic layer was washed w/ brine then transferred to a rotary evaporator to remove solvent. The product was purified by flash column chromatography on silica gel (Hexanes/EtOAc = 3/1 – 2/1) as white solid (72% **yield**, 362.5 mg).

$^1\text{H NMR}$ (400 MHz, CDCl_3) δ 7.40 (d, $J = 8.0$ Hz, 2H), 7.27 (d, $J = 8.0$ Hz, 2H), 6.71 (dd, $J = 17.6, 10.8$ Hz, 1H), 6.62 (s, 1H), 6.47 (s, 2H), 5.75 (d, $J = 17.6$ Hz, 1H), 5.27 (d, $J = 10.8$ Hz, 1H), 4.84 – 4.74 (m, 1H), 4.49 (d, $J = 15.2$ Hz, 1H), 4.41 (d, $J = 15.2$ Hz, 1H), 4.10 – 4.02 (m, 2H), 3.56 (t, $J = 8.8$ Hz, 1H), 3.42 (dd, $J = 8.8, 5.6$ Hz, 1H), 2.27 (s, 6H).

$^{13}\text{C NMR}$ (101 MHz, CDCl_3) δ 158.3, 157.8, 139.5, 137.5, 136.4, 135.3, 128.5, 126.8, 123.5, 114.4, 112.5, 71.0, 68.1, 48.2, 46.2, 21.5.

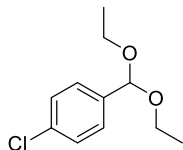
GC-MS (EI, 70 eV) m/z (%) 337 (M^+ , 32), 172 (27), 147 (19), 130 (18), 122 (20), 117 (100), 105 (21), 91 (56), 77 (40), 65 (12).



1-chloro-4-(dimethoxymethyl)benzene

The titled compound was synthesized following **General Procedure B**: 4-chlorobenzaldehyde (703 mg, 5.0 mmol, 1.0 equiv.), *p*-Toluenesulfonic acid monohydrate (35 mg, 0.2 mmol, 4 mol%) and MeOH (25 mL, 0.2 M) were used. The product was purified by flash column chromatography on silica gel (Hexanes/EtOAc = 30/1 - 25/1) as colorless oil (43% **yield**, 400 mg). The analytical data is in good agreement with the reported data.⁴¹

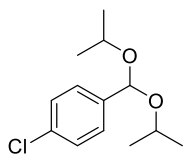
$^1\text{H NMR}$ (400 MHz, CDCl_3) δ 7.39 (d, $J = 8.0$ Hz, 2H), 7.34 (d, $J = 8.0$ Hz, 2H), 5.37 (s, 1H), 3.31 (s, 6H).



1-chloro-4-(diethoxymethyl)benzene

The titled compound was synthesized following **General Procedure B**: 4-chlorobenzaldehyde (703 mg, 5.0 mmol, 1.0 equiv.), *p*-Toluenesulfonic acid monohydrate (35 mg, 0.2 mmol, 4 mol%) and EtOH (25 mL, 0.2 M) were used. The product was purified by flash column chromatography on silica gel (Hexanes/EtOAc = 50/1 - 30/1) as colorless oil (27% **yield**, 285.1 mg). The analytical data is in good agreement with the reported data. ⁴¹

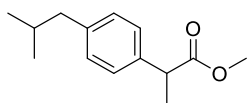
¹H NMR (400 MHz, CDCl₃) δ 7.41 (d, *J* = 8.0 Hz, 2H), 7.33 (d, *J* = 8.0 Hz, 2H), 5.48 (s, 1H), 3.64 – 3.47 (m, 4H), 1.26 – 1.20 (m, 6H).



1-chloro-4-(diisopropoxymethyl)benzene

The titled compound was synthesized following **General Procedure B**: 4-chlorobenzaldehyde (703 mg, 5.0 mmol, 1.0 equiv.), *p*-Toluenesulfonic acid monohydrate (35 mg, 0.2 mmol, 4 mol%) and *i*-PrOH (25 mL, 0.2 M) were used. The product was purified by flash column chromatography on silica gel (Hexanes/EtOAc = 50/1 - 30/1) as colorless oil (43% **yield**, 526.5 mg). The analytical data is in good agreement with the reported data. ⁴²

¹H NMR (400 MHz, CDCl₃) δ 7.41 (d, *J* = 8.4 Hz, 2H), 7.32 (d, *J* = 8.4 Hz, 2H), 5.52 (s, 1H), 3.89 (hept, *J* = 6.0 Hz, 2H), 1.19 (d, *J* = 6.0 Hz, 6H), 1.16 (d, *J* = 6.0 Hz, 6H).

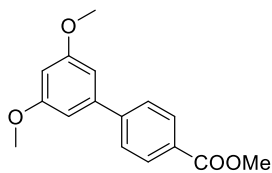


methyl 2-(4-isobutylphenyl)propanoate

The titled compound was synthesized according to the following procedure: To a 200-mL round bottom flask with a magnetic stirring bar, ibuprofen (2063 mg, 10 mmol), conc. H₂SO₄ (1.5 mL) and MeOH (50 mL, 0.2 M) were added. Then the resulting mixture was allowed to react at reflux temperature for 18h. Upon completion, the solvent was removed by rotary evaporator. Then, the reaction mixture was transferred to a separatory funnel, washed w/ water and extract w/ DCM for three times. The combined organic layer was transferred to a rotary

evaporator to concentrate. The product was purified by flash column chromatography on silica gel (Hexanes/EtOAc = 20/1) as colorless oil (94% **yield**, 2088 mg). The analytical data is in good agreement with the reported data.⁴³

¹H NMR (400 MHz, CDCl₃) δ 7.20 (d, *J* = 8.0 Hz, 2H), 7.09 (d, *J* = 8.0 Hz, 2H), 3.70 (q, *J* = 7.2 Hz, 1H), 3.66 (s, 3H), 2.45 (d, *J* = 7.2 Hz, 2H), 1.92 – 1.77 (m, 1H), 1.49 (d, *J* = 7.2 Hz, 3H), 0.90 (d, *J* = 6.8 Hz, 6H).



methyl 3',5'-dimethoxy-[1,1'-biphenyl]-4-carboxylate

The titled compound was synthesized via Suzuki-Miyaura cross coupling.

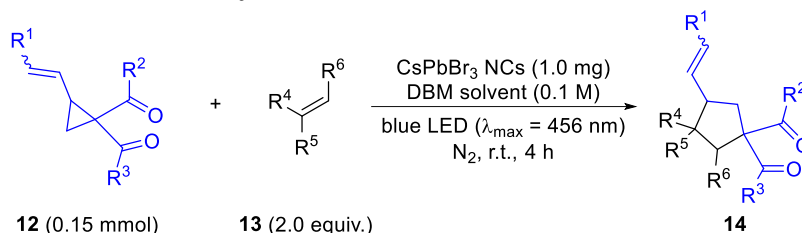
To an 8-mL vial with a magnetic stirring bar, 1-bromo-3,5-dimethoxybenzene (434.1 mg, 2.0 mmol, 1.0 equiv.), 4-methoxycarbonylphenylboronic acid (431.9 mg, 2.4 mmol, 1.2 equiv.), K₃PO₄ (1061.4 mg, 5.0 mmol, 2.5 equiv.) and dioxane/H₂O (3.2/0.8 mL, 0.5 M) were first added. Next, Pd(PPh₃)₄ (57.8 mg, 0.05 mmol, 2.5 mol%) was added under N₂. Then the resulting mixture was degassed with N₂ and sealed with electric tape. It was allowed to react at 100 °C for 28h. Upon completion, the reaction mixture was first filtered. Then, in a separatory funnel, washed w/ water and extract w/ DCM for three times. The combined organic layer was washed w/ brine then transferred to a rotary evaporator to remove solvent. The product was purified by flash column chromatography on silica gel (Hexanes/EtOAc = 20/1 – 10/1) as white solid (60% **yield**, 324.2 mg). The analytical data is in good agreement with the reported data.

44

¹H NMR (400 MHz, CDCl₃) δ 8.09 (d, *J* = 8.4 Hz, 2H), 7.64 (d, *J* = 8.4 Hz, 2H), 6.75 (d, *J* = 2.4 Hz, 2H), 6.51 (t, *J* = 2.4 Hz, 1H), 3.94 (s, 3H), 3.86 (s, 6H).

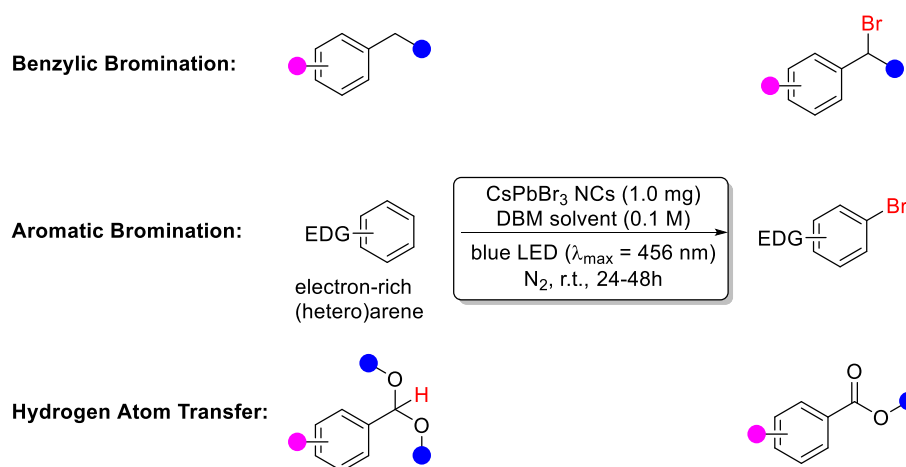
4.5.5 Photocatalytic Synthesis of Products

General Procedure C for [3+2] Cycloaddition:



To a 1-dram vial with a magnetic stirring bar was added vinylcyclopropane **12** (0.15 mmol, 1.0 equiv.), DBM (1.5 mL, 0.1 M), CsPbBr₃ perovskite photocatalyst (1.0 mg) and alkene **13** (0.30 mmol, 2.0 equiv.). The resulting mixture was degassed with N₂ for 20 min and sealed with parafilm. It was allowed to react at room temperature under blue LED (Kessil®, 40 W, λ_{max} = 456 nm) irradiation for 4h. Upon completion, the solvent was removed by rotary evaporator. Then the product **14** was purified by flash column chromatography on silica gel using a combination of hexanes and EtOAc as eluent. TLC was employed to detect the product and the basic KMnO₄ solution was necessary in most of the cases for visualization in addition to UV lamp (254 nm).

General Procedure D for Other Synthetic Applications (Benzylic Bromination, Aromatic Bromination, Hydrogen Atom Transfer):



To a 1-dram vial with a magnetic stirring bar was added alkylbenzene (for benzylic bromination), or electron-rich arene (for aromatic bromination), or benzaldehyde acetal (for

hydrogen atom transfer) (0.15 mmol, 1.0 equiv.), DBM (1.5 mL, 0.1 M) and CsPbBr₃ perovskite photocatalyst (1.0 mg). The resulting mixture was degassed with N₂ for 20 min and sealed with parafilm. It was allowed to react at room temperature under blue LED (Kessil®, 40 W, $\lambda_{\text{max}} = 456$ nm) irradiation for 24-48h. Upon completion, the solvent was removed by rotary evaporator. Then the product was purified by flash column chromatography on silica gel using a combination of hexanes and EtOAc as eluent. TLC was employed to detect the product.

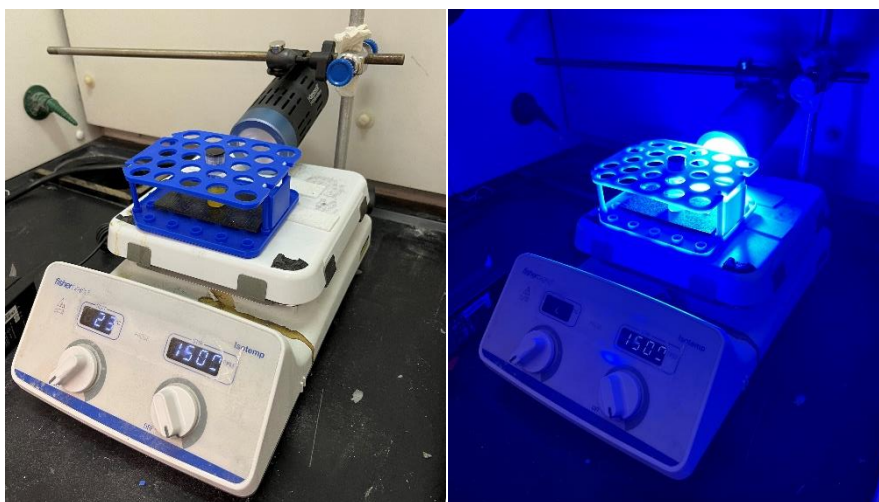
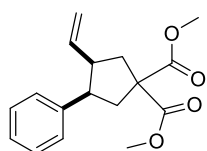


Figure 4.2 Photocatalytic reaction setup with a 40-watt Kessil® PR160-456nm blue LED lamp.

Photocatalytic Synthesis of Vinylcyclopentanes



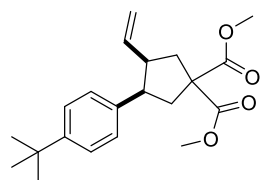
dimethyl 3-phenyl-4-vinylcyclopentane-1,1-dicarboxylate (14a) (*cis:trans* = 66:34)

The titled compound was synthesized following **General Procedure C**: dimethyl 2-vinylcyclopropane-1,1-dicarboxylate (**12a**, 27.6 mg, 0.15 mmol, 1.0 equiv.), DBM (1.5 mL), CsPbBr₃ perovskite photocatalyst (1.0 mg) and styrene (**13a**, 34.4 μ L, 0.30 mmol, 2.0 equiv.) were used. The product was purified by flash column chromatography on silica gel (Hexanes/EtOAc = 20/1) as colorless oil (inseparable diastereomers, 87% **yield**, 37.6 mg).

¹H NMR (400 MHz, CDCl₃) δ 7.31 – 7.14 (m, 5H), 5.65 (ddd, *J* = 17.2, 10.8, 6.8 Hz, 0.34H), 5.37 (ddd, *J* = 17.6, 10.4, 8.0 Hz, 0.66H), 4.91 – 4.80 (m, 2H), 3.78 – 3.77 (m, 6H), 3.48 – 3.42 (m, 0.67H), 3.06 – 2.99 (m, 0.67H), 2.91 – 2.55 (m, 3.44H), 2.42 – 2.32 (m, 1H), 2.17 (dd, *J* = 12.8, 10.0 Hz, 0.34H).

¹³C NMR (101 MHz, CDCl₃) δ 173.3, 173.1, 173.1, 172.8, 141.6, 140.9, 138.8, 138.3, 128.5, 128.5, 128.2, 127.7, 126.7, 126.4, 115.7, 115.5, 59.1, 58.2, 53.1, 53.0, 51.6, 51.0, 48.1, 47.5, 42.6, 40.4, 39.1, 38.2.

Minor: **GC-MS** (EI, 70 eV) *m/z* (%) 288 (M⁺, 2), 228 (13), 202 (14), 170 (36), 152 (14), 145 (100), 141 (16), 128 (21), 121 (20), 115 (40), 104 (11), 91 (28), 77 (11), 59 (17). Major: **GC-MS** (EI, 70 eV) *m/z* (%) 288 (M⁺, 2), 228 (14), 202 (12), 170 (33), 152 (12), 145 (100), 141 (15), 129 (18), 121 (19), 115 (35), 104 (11), 91 (25), 77 (10), 59 (13).



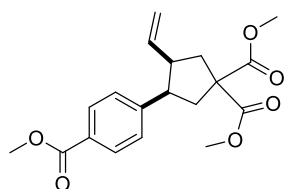
dimethyl 3-(4-(*tert*-butyl)phenyl)-4-vinylcyclopentane-1,1-dicarboxylate (14b) (*cis:trans* = 64:36)

The titled compound was synthesized following **General Procedure C**: dimethyl 2-vinylcyclopropane-1,1-dicarboxylate (**12a**, 27.6 mg, 0.15 mmol, 1.0 equiv.), DBM (1.5 mL), CsPbBr₃ perovskite photocatalyst (1.0 mg) and 4-*tert*-butylstyrene (**13b**, 54.9 μL, 0.30 mmol, 2.0 equiv.) were used. The product was purified by flash column chromatography on silica gel (Hexanes/EtOAc = 33/1 – 20/1) as colorless oil (inseparable diastereomers, 81% **yield**, 41.7 mg).

¹H NMR (400 MHz, CDCl₃) δ 7.32 – 7.29 (m, 2H), 7.15 (d, *J* = 8.0 Hz, 0.75H), 7.08 (d, *J* = 8.0 Hz, 1.30H), 5.67 (ddd, *J* = 17.2, 10.4, 6.8 Hz, 0.36H), 5.39 (ddd, *J* = 17.6, 10.0, 8.4 Hz, 0.64H), 4.95 – 4.83 (m, 2H), 3.78 – 3.76 (m, 6H), 3.41 (dt, *J* = 10.4, 7.6 Hz, 0.64H), 3.01 (p, *J* = 7.2 Hz, 0.66H), 2.90 – 2.54 (m, 3.54H), 2.41 (dd, *J* = 14.0, 6.4 Hz, 0.66H), 2.35 – 2.29 (m, 0.38H), 2.16 (dd, *J* = 12.8, 9.6 Hz, 0.38H).

^{13}C NMR (101 MHz, CDCl_3) δ 173.3, 173.2, 173.1, 172.9, 149.4, 149.1, 139.1, 138.5, 138.5, 137.8, 128.1, 127.3, 125.4, 125.1, 115.6, 115.4, 59.1, 58.2, 53.0, 52.9, 51.0, 50.6, 47.7, 47.3, 42.7, 40.4, 39.0, 38.4, 34.5, 34.5, 31.5.

Minor: **GC-MS** (EI, 70 eV) m/z (%) 344 (M^+ , 9), 329 (31), 312 (27), 297 (10), 284 (27), 269 (13), 257 (13), 225 (21), 211 (10), 195 (12), 177 (19), 170 (46), 167 (26), 152 (27), 145 (100), 141 (18), 128 (22), 113 (23), 105 (11), 91 (29), 57 (35). Major: **GC-MS** (EI, 70 eV) m/z (%) 344 (M^+ , 11), 329 (33), 312 (32), 297 (12), 284 (33), 269 (16), 257 (12), 225 (26), 211 (12), 195 (15), 184 (11), 177 (24), 170 (56), 167 (32), 152 (32), 145 (100), 141 (20), 128 (24), 113 (26), 105 (14), 91 (34), 57 (49).



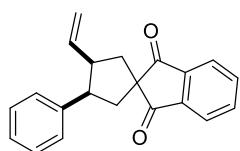
dimethyl 3-(4-(methoxycarbonyl)phenyl)-4-vinylcyclopentane-1,1-dicarboxylate (14c) (*cis:trans* = 61:39)

The titled compound was synthesized following **General Procedure C**: dimethyl 2-vinylcyclopropane-1,1-dicarboxylate (**12a**, 27.6 mg, 0.15 mmol, 1.0 equiv.), DBM (1.5 mL), CsPbBr_3 perovskite photocatalyst (1.0 mg) and methyl 4-vinylbenzoate (**13c**, 48.7 mg, 0.30 mmol, 2.0 equiv.) were used. The product was purified by flash column chromatography on silica gel (Hexanes/EtOAc = 20/1 – 10/1) as colorless oil (inseparable diastereomers, 75% **yield**, 38.8 mg).

^1H NMR (400 MHz, CDCl_3) δ 7.97 – 7.91 (m, 2H), 7.28 (d, J = 8.0 Hz, 0.78H), 7.20 (d, J = 8.0 Hz, 1.21H), 5.61 (ddd, J = 17.2, 10.4, 7.2 Hz, 0.39H), 5.31 (ddd, J = 17.6, 10.4, 8.0 Hz, 0.62H), 4.92 – 4.76 (m, 2H), 3.88 (s, 3H), 3.80 – 3.74 (m, 6H), 3.48 (dt, J = 10.8, 7.6 Hz, 0.62H), 3.04 (p, J = 7.2 Hz, 0.63H), 2.92 (td, J = 11.2, 7.6 Hz, 0.41H), 2.81 – 2.53 (m, 3H), 2.41 – 2.32 (m, 1H), 2.22 – 2.13 (m, 0.39H).

¹³C NMR (101 MHz, CDCl₃) δ 173.1, 173.0, 172.9, 172.6, 167.1, 167.1, 147.1, 146.4, 138.4, 137.8, 129.9, 129.5, 128.7, 128.5, 128.3, 127.8, 116.1, 116.0, 59.1, 58.3, 53.1, 53.1, 53.0, 53.0, 52.1, 52.1, 51.5, 51.2, 48.2, 47.5, 42.2, 40.5, 39.1, 38.0.

Minor: **GC-MS** (EI, 70 eV) m/z (%) 346 (M⁺, 2), 315 (12), 286 (10), 227 (14), 179 (22), 167 (23), 152 (22), 145 (100), 141 (14), 128 (33), 115 (23), 103 (11), 91 (13), 77 (17), 59 (58). Major: **GC-MS** (EI, 70 eV) m/z (%) 346 (M⁺, 1), 286 (11), 227 (15), 179 (20), 167 (21), 152 (17), 145 (100), 141 (11), 128 (22), 115 (18), 103 (10), 77 (13), 59 (35).



3-phenyl-4-vinylspiro[cyclopentane-1,2'-indene]-1',3'-dione (14d)

(*cis:trans* = 70:30)

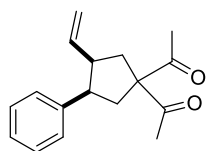
The titled compound was synthesized following **General Procedure C**: 2-vinylspiro[cyclopropane-1,2'-indene]-1',3'-dione (**12d**, 29.7 mg, 0.15 mmol, 1.0 equiv.), DBM (1.5 mL), CsPbBr₃ perovskite photocatalyst (1.0 mg) and styrene (**13a**, 34.4 μL, 0.30 mmol, 2.0 equiv.) were used. The product was purified by flash column chromatography on silica gel (Hexanes/EtOAc = 20/1 – 15/1) as colorless oil (inseparable diastereomers, 93% **yield**, 42.5 mg).

¹H NMR (400 MHz, CDCl₃) δ 8.03 – 7.98 (m, 2H), 7.89 – 7.85 (m, 2H), 7.36 – 7.30 (m, 4H), 7.23 – 7.18 (m, 1H), 5.76 – 5.60 (m, 1H), 4.96 – 4.86 (m, 2H), 3.88 – 3.82 (m, 0.70H), 3.38 – 3.31 (m, 0.70H), 3.27 – 3.10 (m, 0.61H), 2.52 (dd, *J* = 13.2, 10.0 Hz, 0.71H), 2.40 – 2.14 (m, 3H), 2.05 (dd, *J* = 13.2, 11.2 Hz, 0.33H).

¹³C NMR (101 MHz, CDCl₃) δ 204.7, 204.5, 204.4, 203.9, 141.9, 141.7, 141.6, 141.6, 141.3, 141.2, 138.7, 138.5, 135.9, 135.9, 135.9, 135.8, 128.6, 128.6, 128.2, 127.9, 126.8, 126.4, 123.7, 123.6, 123.6, 123.5, 116.0, 115.7, 59.1, 58.3, 52.7, 52.3, 49.5, 49.4, 42.8, 40.9, 39.8, 39.0.

Minor: **GC-MS** (EI, 70 eV) m/z (%) 302 (M⁺, 100), 287 (11), 273 (21), 248 (18), 231 (17), 202 (15), 197 (11), 191 (15), 165 (19), 159 (84), 144 (47), 129 (62), 115 (68), 104 (50), 91 (30), 76

(49), 65 (14). Major: **GC-MS** (EI, 70 eV) m/z (%) 302 (M^+ , 48), 273 (14), 248 (15), 231 (14), 202 (12), 191 (13), 165 (14), 159 (100), 144 (72), 133 (16), 129 (52), 115 (39), 104 (31), 91 (17), 77 (29).



1,1'-(3-phenyl-4-vinylcyclopentane-1,1-diyl)bis(ethan-1-one) (14e)

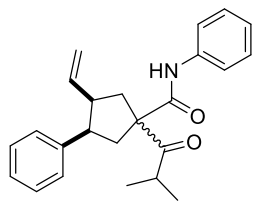
(*cis:trans* = 68:32)

The titled compound was synthesized following **General Procedure C**: 1,1'-(2-vinylcyclopropane-1,1-diyl)bis(ethan-1-one) (**12e**, 22.8 mg, 0.15 mmol, 1.0 equiv.), DBM (1.5 mL), CsPbBr₃ perovskite photocatalyst (1.0 mg) and styrene (**13a**, 34.4 μ L, 0.30 mmol, 2.0 equiv.) were used. The product was purified by flash column chromatography on silica gel (Hexanes/EtOAc = 50/1 – 20/1) as colorless oil (inseparable diastereomers, 51% **yield**, 19.6 mg).

¹H NMR (400 MHz, CDCl₃) δ 7.31 – 7.25 (m, 2H), 7.22 – 7.16 (m, 1.68H), 7.10 (d, J = 7.6 Hz, 1.36H), 5.61 (ddd, J = 17.2, 10.0, 7.2 Hz, 0.32H), 5.30 (ddd, J = 17.2, 10.4, 8.0 Hz, 0.68H), 4.91 – 4.80 (m, 2H), 3.29 – 3.23 (m, 0.68H), 2.96 – 2.89 (m, 0.68H), 2.83 (dd, J = 13.2, 7.2 Hz, 0.34H), 2.75 – 2.66 (m, 1.33H), 2.59 (ddd, J = 18.0, 10.8, 7.2 Hz, 0.37H), 2.51 – 2.32 (m, 2H), 2.17 – 2.13 (m, 6H), 2.07 (dd, J = 13.6, 11.6 Hz, 0.39H), 1.91 (dd, J = 13.6, 10.8 Hz, 0.33H).

¹³C NMR (101 MHz, CDCl₃) δ 205.1, 204.8, 204.7, 204.7, 141.5, 140.7, 138.8, 138.1, 128.6, 128.3, 128.2, 127.6, 126.8, 126.4, 115.8, 115.7, 74.5, 73.3, 51.4, 50.4, 47.9, 47.4, 39.4, 37.0, 35.6, 34.5, 27.2, 26.6, 26.6, 26.1, 26.0.

Minor: **GC-MS** (EI, 70 eV) m/z (%) 256 (M^+ , 1), 238 (30), 202 (20), 183 (12), 169 (10), 159 (11), 141 (21), 128 (41), 113 (100), 103 (11), 91 (51), 77 (22), 65 (16). Major: **GC-MS** (EI, 70 eV) m/z (%) 256 (M^+ , 2), 238 (42), 213 (11), 202 (19), 183 (17), 169 (13), 159 (12), 153 (12), 141 (24), 128 (45), 113 (100), 103 (13), 91 (46), 77 (21), 65 (12).



1-isobutyryl-*N*,3-diphenyl-4-vinylcyclopentane-1-carboxamide (14f)

(d.r. = 36:31:17:16, based upon ^{13}C NMR, structures of isomers could not be determined)

The titled compound was synthesized following **General Procedure C**: 1-isobutyryl-*N*-phenyl-2-vinylcyclopropane-1-carboxamide (**12f**, 38.6 mg, 0.15 mmol, 1.0 equiv.), DBM (1.5 mL), CsPbBr₃ perovskite photocatalyst (1.0 mg) and styrene (**13a**, 34.4 μL , 0.30 mmol, 2.0 equiv.) were used. The product was purified by flash column chromatography on silica gel (Hexanes/EtOAc = 20/1 – 15/1) as white solid (inseparable diastereomers, 15% **yield**, 8.1 mg).

^1H NMR (400 MHz, CDCl₃) δ 7.52 – 7.44 (m, 2H), 7.40 – 7.27 (m, 4H), 7.25 – 7.08 (m, 5H), 5.71 – 5.59 (m, 0.28H), 5.43 – 5.25 (m, 0.73H), 5.03 – 4.79 (m, 2H), 3.53 – 3.17 (m, 1H), 3.16 – 2.47 (m, 5H), 2.44 – 2.00 (m, 1H), 1.16 – 1.07 (m, 6H).

^{13}C NMR (101 MHz, CDCl₃) δ 215.4, 214.3, 214.2, 214.0, 168.9, 168.9, 168.7, 168.6, 141.7, 141.6, 140.9, 140.7, 138.9, 138.9, 138.2, 138.2, 137.6, 137.6, 137.5, 129.3, 129.3, 129.3, 128.6, 128.6, 128.5, 128.4, 128.3, 128.2, 127.7, 127.7, 126.8, 126.8, 126.5, 126.4, 124.9, 124.9, 124.9, 124.9, 120.1, 120.0, 120.0, 120.0, 115.9, 115.9, 115.8, 115.7, 68.3, 68.3, 67.4, 67.4, 51.7, 51.4, 50.8, 50.6, 48.2, 47.8, 47.6, 47.1, 40.8, 40.7, 38.5, 38.5, 37.9, 37.7, 37.4, 37.4, 36.8, 36.7, 36.2, 35.7, 20.6, 20.6, 20.6, 20.5, 20.4, 20.2, 20.2.

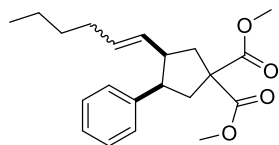
Diastereomer 1: **GC-MS** (EI, 70 eV) m/z (%) 361 (M^+ , 14), 290 (25), 218 (100), 187 (16), 171 (11), 161 (36), 153 (11), 141 (19), 128 (43), 115 (57), 104 (23), 91 (69), 77 (52), 71 (36), 65 (41).

Diastereomer 2: **GC-MS** (EI, 70 eV) m/z (%) 361 (M^+ , 8), 218 (100), 161 (16), 141 (11), 128 (24), 120 (10), 115 (32), 104 (11), 91 (46), 77 (30), 71 (24), 65 (22).

Diastereomer 3: **GC-MS** (EI, 70 eV) m/z (%) 361 (M^+ , 21), 291 (14), 218 (100), 215 (10), 187 (22), 169 (11), 161 (36), 153 (11), 141 (23), 128 (37), 120 (14), 115 (45), 104 (19), 91 (62), 77 (54), 71 (38), 65 (35).

4: **GC-MS** (EI, 70 eV) m/z (%) 361 (M^+ , 7), 218 (100), 141 (12), 128 (21), 115 (27), 104 (12), 91 (31), 77 (30), 71 (20), 65 (22).

HRMS (ESI⁺) (m/z): [$M+H$]⁺ calculated for C₂₄H₂₈NO₂, 362.2115; found, 362.2124.



dimethyl 3-(hex-1-en-1-yl)-4-phenylcyclopentane-1,1-dicarboxylate
(14g) (*cis:trans* = 65:35, E and Z are unassigned)

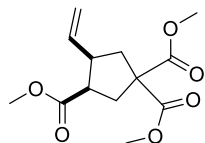
The titled compound was synthesized following **General Procedure C**:

dimethyl 2-(hex-1-en-1-yl)cyclopropane-1,1-dicarboxylate (**12g**, 36.0 mg, 0.15 mmol, 1.0 equiv.), DBM (1.5 mL), CsPbBr₃ perovskite photocatalyst (1.0 mg) and styrene (**13a**, 34.4 μ L, 0.30 mmol, 2.0 equiv.) were used. The product was purified by flash column chromatography on silica gel (Hexanes/EtOAc = 33/1 – 25/1) as colorless oil (inseparable diastereomers, 70% **yield**, 36.2 mg).

¹H NMR (400 MHz, CDCl₃) δ 7.32 – 7.09 (m, 5H), 5.34 – 5.11 (m, 1.33H), 5.01 – 4.87 (m, 0.68H), 3.83 – 3.71 (m, 6H), 3.45 – 3.26 (m, 0.75H), 3.04 – 2.89 (m, 0.65H), 2.87 – 2.51 (m, 3.30H), 2.43 – 2.18 (m, 1H), 2.17 – 2.01 (m, 0.35H), 1.95 – 1.62 (m, 2H), 1.24 – 0.97 (m, 4H), 0.93 – 0.65 (m, 3H).

¹³C NMR (101 MHz, CDCl₃) δ 173.4, 173.4, 173.3, 173.3, 173.2, 173.0, 141.9, 141.8, 141.2, 141.1, 132.3, 132.1, 131.8, 131.2, 130.3, 130.3, 129.8, 129.3, 128.6, 128.5, 128.4, 128.4, 128.0, 128.0, 127.8, 127.7, 126.6, 126.5, 126.3, 126.2, 59.3, 59.2, 58.6, 58.2, 53.0, 53.0, 53.0, 52.9, 52.9, 52.9, 52.3, 51.9, 50.2, 48.4, 48.3, 46.7, 45.9, 42.4, 42.1, 41.4, 41.3, 41.0, 40.9, 39.8, 38.3, 38.2, 32.2, 32.1, 31.8, 31.7, 31.6, 31.5, 27.5, 27.2, 22.4, 22.3, 22.0, 21.9, 14.1, 14.0, 14.0.

Inseparable: **GC-MS** (EI, 70 eV) m/z (%) 344 (M^+ , 9), 284 (27), 281 (10), 260 (17), 225 (18), 200 (27), 170 (26), 155 (13), 145 (100), 141 (19), 129 (18), 121 (21), 115 (34), 104 (15), 91 (36), 77 (12), 59 (13).



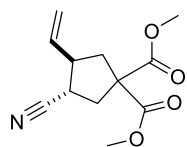
trimethyl 4-vinylcyclopentane-1,1,3-tricarboxylate (14h) (*cis:trans* = 75:25)

The titled compound was synthesized following **General Procedure C**: dimethyl 2-vinylcyclopropane-1,1-dicarboxylate (**12a**, 27.6 mg, 0.15 mmol, 1.0 equiv.), DBM (1.5 mL), CsPbBr₃ perovskite photocatalyst (1.0 mg) and methyl acrylate (**13h**, 27.2 μL, 0.30 mmol, 2.0 equiv.) were used. The product was purified by flash column chromatography on silica gel (Hexanes/EtOAc = 10/1 – 6/1) as colorless oil (inseparable diastereomers, 44% **yield**, 17.6 mg).

¹H NMR (400 MHz, CDCl₃) δ 5.77 – 5.65 (m, 1H), 5.09 – 5.01 (m, 2H), 3.75 – 3.62 (m, 9H), 3.10 – 3.05 (m, 0.75H), 3.02 – 2.84 (m, 1H), 2.71 – 2.35 (m, 4H), 1.98 (dd, *J* = 13.6, 10.4 Hz, 0.25H).

¹³C NMR (101 MHz, CDCl₃) δ 174.1, 173.7, 173.0, 172.5, 172.2, 172.0, 138.4, 136.8, 116.7, 116.0, 59.4, 58.8, 53.1, 53.1, 53.1, 53.0, 52.0, 51.6, 49.7, 48.1, 47.7, 46.0, 40.0, 38.7, 37.6, 36.1.

Minor: **GC-MS** (EI, 70 eV) *m/z* (%) 239 (M – 31, 13), 210 (41), 178 (47), 150 (100), 119 (25), 91 (68), 77 (16), 65 (16), 59 (48). Major: **GC-MS** (EI, 70 eV) *m/z* (%) 239 (M – 31, 12), 210 (39), 207 (14), 178 (46), 150 (100), 119 (29), 113 (11), 91 (68), 77 (18), 65 (17), 59 (47).



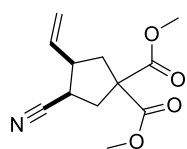
dimethyl 3-cyano-4-vinylcyclopentane-1,1-dicarboxylate (14i-*trans*) (*trans* = 53/100)

The titled compound was synthesized following **General Procedure C**: dimethyl 2-vinylcyclopropane-1,1-dicarboxylate (**12a**, 27.6 mg, 0.15 mmol, 1.0 equiv.), DBM (1.5 mL), CsPbBr₃ perovskite photocatalyst (1.0 mg) and acrylonitrile (**13i**, 19.7 μL, 0.30 mmol, 2.0 equiv.) were used. The product was purified by flash column chromatography on silica gel (Hexanes/EtOAc = 5/1) as colorless oil (19% **yield**, 6.7 mg).

¹H NMR (400 MHz, CDCl₃) δ 5.71 (ddd, *J* = 17.6, 10.4, 7.6 Hz, 1H), 5.29 – 5.18 (m, 2H), 3.77 (s, 3H), 3.75 (s, 3H), 2.90 – 2.81 (m, 2H), 2.71 – 2.60 (m, 2H), 2.47 (dd, *J* = 13.6, 10.4 Hz, 1H), 1.97 (dd, *J* = 14.0, 11.2 Hz, 1H).

¹³C NMR (101 MHz, CDCl₃) δ 171.8, 171.4, 135.8, 120.1, 118.3, 58.4, 53.4, 53.4, 48.7, 39.5, 37.7, 34.5.

GC-MS (EI, 70 eV) *m/z* (%) 237 (M⁺, 2), 206 (17), 177 (17), 150 (73), 145 (79), 124 (36), 118 (93), 113 (57), 96 (20), 91 (97), 79 (34), 71 (18), 65 (42), 59 (100).



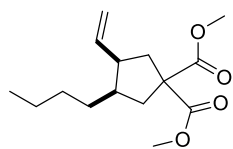
dimethyl 3-cyano-4-vinylcyclopentane-1,1-dicarboxylate (14i-cis) (*cis* = 47/100)

The product was purified by flash column chromatography on silica gel (Hexanes/EtOAc = 5/1) as colorless oil (17% **yield**, 5.9 mg).

¹H NMR (400 MHz, CDCl₃) δ 5.89 (dt, *J* = 17.2, 8.8 Hz, 1H), 5.25 – 5.21 (m, 2H), 3.78 (s, 3H), 3.76 (s, 3H), 3.12 (q, *J* = 6.8 Hz, 1H), 2.89 (p, *J* = 8.0 Hz, 1H), 2.72 – 2.63 (m, 2H), 2.52 (dd, *J* = 14.0, 6.8 Hz, 1H), 2.35 (dd, *J* = 14.0, 10.4 Hz, 1H).

¹³C NMR (101 MHz, CDCl₃) δ 172.1, 171.1, 135.4, 119.6, 118.7, 58.9, 53.4, 53.4, 45.5, 38.8, 37.6, 34.4.

GC-MS (EI, 70 eV) *m/z* (%) 237 (M⁺, 2), 206 (18), 177 (15), 150 (64), 145 (78), 124 (34), 118 (89), 113 (62), 96 (19), 91 (96), 79 (37), 71 (18), 65 (43), 59 (100).



dimethyl 3-butyl-4-vinylcyclopentane-1,1-dicarboxylate (14j) (*cis:trans* = 70:30)

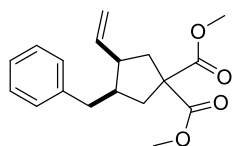
The titled compound was synthesized following **General Procedure C**: dimethyl 2-vinylcyclopropane-1,1-dicarboxylate (**12a**, 27.6 mg, 0.15 mmol, 1.0 equiv.), DBM (1.5 mL), CsPbBr₃ perovskite photocatalyst (1.0 mg) and 1-hexene (**13j**, 37.5 μL, 0.30 mmol, 2.0

equiv.) were used. The product was purified by flash column chromatography on silica gel (Hexanes/EtOAc = 33/1 – 25/1) as colorless oil (inseparable diastereomers, 35% **yield**, 14.1 mg).

¹H NMR (400 MHz, CDCl₃) δ 5.76 – 5.58 (m, 1H), 5.04 – 4.97 (m, 2H), 3.72 (apparent s, 6H), 2.71 – 2.66 (m, 0.73H), 2.59 – 2.45 (m, 1.41H), 2.42 – 2.33 (m, 0.76H), 2.21 – 1.94 (m, 3H), 1.78 (dd, *J* = 13.6, 10.8 Hz, 0.40H), 1.68 – 1.50 (m, 1H), 1.34 – 1.05 (m, 5H), 0.86 (t, *J* = 6.8 Hz, 3H).

¹³C NMR (101 MHz, CDCl₃) δ 173.5, 173.4, 173.3, 173.3, 140.5, 138.5, 115.5, 115.3, 59.1, 58.5, 52.9, 52.9, 50.6, 46.5, 45.4, 43.2, 40.8, 40.5, 39.4, 33.0, 30.5, 30.5, 30.2, 23.0, 23.0, 14.2, 14.2.

Minor: **GC-MS** (EI, 70 eV) *m/z* (%) 268 (M⁺, 0.5), 208 (95), 205 (19), 180 (43), 176 (10), 166 (13), 149 (50), 145 (100), 138 (66), 132 (25), 119 (23), 113 (65), 107 (39), 91 (87), 79 (73), 67 (36), 59 (75), 55 (41). Major: **GC-MS** (EI, 70 eV) *m/z* (%) 268 (M⁺, 0.3), 208 (78), 205 (15), 180 (23), 166 (11), 149 (45), 145 (100), 138 (41), 132 (21), 121 (19), 113 (62), 107 (32), 91 (69), 79 (60), 67 (28), 59 (58), 55 (33).



dimethyl 3-benzyl-4-vinylcyclopentane-1,1-dicarboxylate (14k) (*cis:trans*

= 69:31)

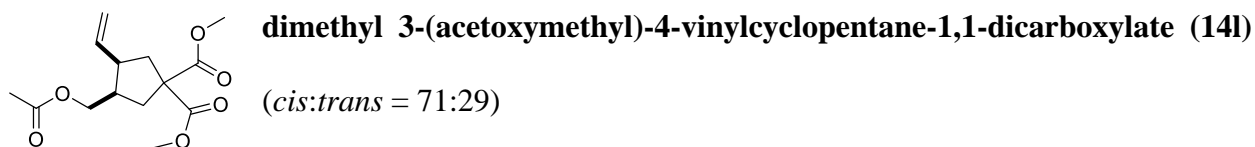
The titled compound was synthesized following **General Procedure C**:

dimethyl 2-vinylcyclopropane-1,1-dicarboxylate (**12a**, 27.6 mg, 0.15 mmol, 1.0 equiv.), DBM (1.5 mL), CsPbBr₃ perovskite photocatalyst (1.0 mg) and allylbenzene (**13k**, 39.7 μL, 0.30 mmol, 2.0 equiv.) were used. The product was purified by flash column chromatography on silica gel (Hexanes/EtOAc = 40/1 – 25/1) as colorless oil (inseparable diastereomers, 42% **yield**, 18.7 mg).

¹H NMR (400 MHz, CDCl₃) δ 7.28 – 7.24 (m, 2H), 7.19 – 7.13 (m, 3H), 5.84 (dd, *J* = 17.6, 10.8, 8.8 Hz, 0.69H), 5.68 (dd, *J* = 17.6, 10.0, 8.4 Hz, 0.31H), 5.11 – 5.01 (m, 2H), 3.73 – 3.67 (m, 6H), 2.92 (dd, *J* = 13.6, 3.6 Hz, 0.32H), 2.80 – 2.68 (m, 1.41H), 2.54 – 2.49 (m, 1H), 2.43 – 2.22 (m, 3.81H), 2.11 – 1.88 (m, 1.68H).

^{13}C NMR (101 MHz, CDCl_3) δ 173.3, 173.3, 173.2, 173.1, 141.2, 140.8, 140.0, 138.1, 129.0, 129.0, 128.4, 128.4, 126.0, 126.0, 116.1, 116.1, 58.8, 58.3, 52.9, 52.9, 52.9, 52.8, 50.2, 46.9, 46.7, 44.9, 40.6, 39.9, 39.4, 39.1, 38.6, 36.5.

Minor: **GC-MS** (EI, 70 eV) m/z (%) 302 (M^+ , 4), 242 (21), 211 (13), 183 (10), 151 (31), 143 (28), 128 (14), 115 (12), 91 (100), 77 (15), 65 (20), 59 (25). Major: **GC-MS** (EI, 70 eV) m/z (%) 302 (M^+ , 4), 242 (24), 215 (12), 183 (14), 151 (31), 143 (28), 128 (16), 115 (16), 104 (12), 91 (100), 77 (15), 65 (19), 59 (22).

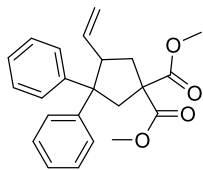


The titled compound was synthesized following **General Procedure C**: dimethyl 2-vinylcyclopropane-1,1-dicarboxylate (**12a**, 27.6 mg, 0.15 mmol, 1.0 equiv.), DBM (1.5 mL), CsPbBr_3 perovskite photocatalyst (1.0 mg) and allyl acetate (**13l**, 32.4 μL , 0.30 mmol, 2.0 equiv.) were used. The product was purified by flash column chromatography on silica gel (Hexanes/EtOAc = 40/1 – 8/1) as colorless oil (inseparable diastereomers, 28% **yield**, 11.8 mg).

^1H NMR (400 MHz, CDCl_3) δ 5.77 – 5.61 (m, 1H), 5.08 – 5.00 (m, 2H), 4.14 (dd, J = 11.2, 4.4 Hz, 0.29H), 4.05 (dd, J = 11.2, 6.0 Hz, 0.71H), 3.94 – 3.88 (m, 1H), 3.74 – 3.73 (m, 6H), 2.87 – 2.79 (m, 0.72H), 2.57 – 2.31 (m, 3H), 2.21 (dd, J = 13.6, 8.0 Hz, 0.74H), 2.16 – 1.99 (m, 4.80H).

^{13}C NMR (101 MHz, CDCl_3) δ 173.0, 172.8, 172.8, 172.7, 171.2, 171.1, 139.3, 137.0, 116.5, 116.2, 65.8, 65.1, 59.2, 58.6, 53.0, 53.0, 46.7, 45.0, 44.1, 41.4, 40.6, 39.2, 37.7, 36.8, 21.1, 21.0.

Minor: **GC-MS** (EI, 70 eV) m/z (%) 253 ($\text{M} - 31$, 1), 211 (14), 164 (57), 113 (10), 105 (100), 91 (39), 77 (20), 65 (11), 59 (31). Major: **GC-MS** (EI, 70 eV) m/z (%) 253 ($\text{M} - 31$, 0.2), 211 (23), 170 (10), 164 (61), 113 (11), 105 (100), 91 (35), 77 (20), 65 (11), 59 (25).



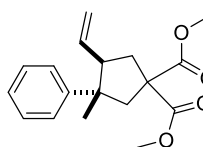
dimethyl 3,3-diphenyl-4-vinylcyclopentane-1,1-dicarboxylate (14m)

The titled compound was synthesized following **General Procedure C**: dimethyl 2-vinylcyclopropane-1,1-dicarboxylate (**12a**, 27.6 mg, 0.15 mmol, 1.0 equiv.), DBM (1.5 mL), CsPbBr₃ perovskite photocatalyst (1.0 mg) and 1,1-diphenylethylene (**13m**, 53.0 μ L, 0.30 mmol, 2.0 equiv.) were used. The product was purified by flash column chromatography on silica gel (Hexanes/EtOAc = 25/1 – 20/1) as colorless oil (22% **yield**, 12.0 mg).

¹H NMR (400 MHz, CDCl₃) δ 7.29 – 7.03 (m, 10H), 5.45 (ddd, J = 18.0, 10.4, 8.0 Hz, 1H), 5.11 (d, J = 17.2 Hz, 1H), 4.95 (d, J = 10.4 Hz, 1H), 3.78 (s, 3H), 3.64 (q, J = 8.0 Hz, 1H), 3.56 (s, 3H), 3.51 (d, J = 14.8 Hz, 1H), 2.97 (d, J = 14.8 Hz, 1H), 2.67 (dd, J = 14.0, 6.4 Hz, 1H), 2.22 (dd, J = 14.0, 9.2 Hz, 1H).

¹³C NMR (101 MHz, CDCl₃) δ 172.8, 172.7, 148.3, 145.0, 138.6, 129.1, 128.3, 127.7, 127.5, 126.2, 126.1, 116.2, 58.2, 58.0, 53.1, 53.0, 50.3, 46.6, 38.8.

GC-MS (EI, 70 eV) m/z (%) 364 (M⁺, 1), 332 (8), 304 (20), 278 (12), 250 (79), 246 (57), 232 (11), 218 (21), 205 (19), 191 (86), 184 (55), 178 (35), 165 (78), 152 (71), 145 (100), 141 (11), 124 (32), 115 (22), 91 (22), 77 (15), 59 (20).



dimethyl 3-methyl-3-phenyl-4-vinylcyclopentane-1,1-dicarboxylate (14n)

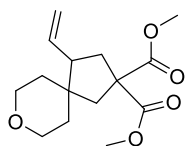
(*cis:trans* = 41:59)

The titled compound was synthesized following **General Procedure C**: dimethyl 2-vinylcyclopropane-1,1-dicarboxylate (**12a**, 27.6 mg, 0.15 mmol, 1.0 equiv.), DBM (1.5 mL), CsPbBr₃ perovskite photocatalyst (1.0 mg) and alpha-methylstyrene (**13n**, 39.0 μ L, 0.30 mmol, 2.0 equiv.) were used. The product was purified by flash column chromatography on silica gel (Hexanes/EtOAc = 33/1 – 25/1) as colorless oil (inseparable diastereomers, 83% **yield**, 37.6 mg).

¹H NMR (400 MHz, CDCl₃) δ 7.43 – 7.16 (m, 5H), 5.73 (ddd, *J* = 17.2, 10.4, 6.8 Hz, 0.59H), 5.19 (ddd, *J* = 17.6, 10.4, 8.8 Hz, 0.41H), 5.05 – 4.83 (m, 2H), 3.79 – 3.74 (m, 6H), 3.06 – 3.00 (m, 1H), 2.77 – 2.69 (m, 1H), 2.65 – 2.44 (m, 2.76H), 2.30 (dd, *J* = 13.6, 8.8 Hz, 0.4H), 1.42 (s, 1.21H), 1.22 (s, 1.83H).

¹³C NMR (101 MHz, CDCl₃) δ 173.6, 173.5, 173.2, 172.9, 147.8, 146.1, 138.7, 136.8, 128.3, 127.9, 127.5, 126.2, 126.1, 126.0, 116.7, 115.7, 58.8, 57.6, 55.1, 53.1, 53.1, 53.1, 53.0, 50.0, 49.6, 48.9, 45.9, 39.4, 38.5, 29.5, 21.9.

Minor: **GC-MS** (EI, 70 eV) *m/z* (%) 270 (M – 32, 24), 248 (16), 216 (16), 188 (83), 184 (100), 165 (17), 152 (23), 141 (24), 128 (72), 124 (13), 115 (39), 103 (23), 91 (34), 77 (39), 65 (13), 59 (58). Major: **GC-MS** (EI, 70 eV) *m/z* (%) 302 (M⁺, 2), 270 (18), 248 (26), 216 (18), 188 (82), 184 (100), 165 (17), 152 (25), 141 (23), 128 (77), 124 (12), 115 (41), 103 (31), 91 (42), 77 (38), 65 (15), 59 (63).



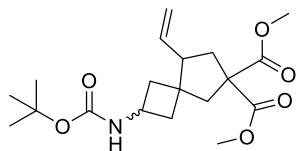
dimethyl 4-vinyl-8-oxaspiro[4.5]decane-2,2-dicarboxylate (14o)

The titled compound was synthesized following **General Procedure C**: dimethyl 2-vinylcyclopropane-1,1-dicarboxylate (**12a**, 27.6 mg, 0.15 mmol, 1.0 equiv.), DBM (1.5 mL), CsPbBr₃ perovskite photocatalyst (1.0 mg) and 4-methylenetetrahydro-2*H*-pyran (**13o**, 29.4 mg, 0.30 mmol, 2.0 equiv.) were used. The product was purified by flash column chromatography on silica gel (Hexanes/EtOAc = 10/1 – 5/1) as colorless oil (25% **yield**, 10.5 mg).

¹H NMR (400 MHz, CDCl₃) δ 5.70 (ddd, *J* = 17.6, 10.4, 7.6 Hz, 1H), 5.12 – 5.02 (m, 2H), 3.84 – 3.81 (m, 2H), 3.73 – 3.73 (m, 6H), 3.57 – 3.50 (m, 1H), 3.49 – 3.42 (m, 1H), 2.67 (d, *J* = 14.4 Hz, 1H), 2.49 (dd, *J* = 12.4, 5.6 Hz, 1H), 2.29 – 2.15 (m, 2H), 2.09 (d, *J* = 14.0 Hz, 1H), 1.78 (td, *J* = 13.2, 4.8 Hz, 1H), 1.52 (td, *J* = 12.8, 4.8 Hz, 1H), 1.20 – 1.14 (m, 2H).

^{13}C NMR (101 MHz, CDCl_3) δ 173.3, 173.2, 136.5, 117.3, 65.7, 64.5, 58.0, 54.0, 53.1, 53.0, 43.6, 42.5, 37.5, 37.0, 30.9.

GC-MS (EI, 70 eV) m/z (%) 282 (M^+ , 5), 253 (24), 238 (12), 228 (100), 222 (46), 219 (18), 194 (38), 186 (38), 178 (24), 164 (91), 150 (29), 145 (80), 132 (24), 119 (24), 113 (34), 105 (50), 96 (29), 91 (66), 83 (25), 79 (58), 65 (22), 59 (61).



dimethyl 2-((*tert*-butoxycarbonyl)amino)-8-vinylspiro[3.4]octane-6,6-dicarboxylate (14p) (d.r. = 61:39, amide)

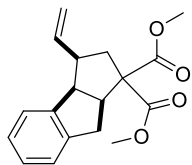
The titled compound was synthesized following **General Procedure C**: dimethyl 2-vinylcyclopropane-1,1-dicarboxylate (**12a**, 27.6 mg, 0.15 mmol, 1.0 equiv.), DBM (1.5 mL), CsPbBr_3 perovskite photocatalyst (1.0 mg) and *tert*-butyl (3-methylenecyclobutyl)carbamate (**13p**, 55.0 mg, 0.30 mmol, 2.0 equiv.) were used. The product was purified by flash column chromatography on silica gel (Hexanes/EtOAc = 10/1 – 5/1) as colorless oil (inseparable diastereomers, 58% **yield**, 31.6 mg).

^1H NMR (400 MHz, CDCl_3) δ 5.81 (ddd, J = 17.6, 10.4, 8.4 Hz, 0.61H), 5.66 (ddd, J = 17.6, 10.4, 8.4 Hz, 0.39H), 5.19 – 5.01 (m, 2H), 4.77 – 4.30 (m, 1H), 4.23 – 3.78 (m, 1H), 3.74 – 3.63 (m, 6H), 2.63 (d, J = 13.6 Hz, 0.39H), 2.50 – 2.12 (m, 5H), 2.07 – 1.93 (m, 1.4H), 1.88 (dd, J = 12.0, 8.4 Hz, 0.63H), 1.78 – 1.65 (m, 1H), 1.61 (dd, J = 12.0, 8.4 Hz, 0.65H), 1.40 (s, 9H).

^{13}C NMR (101 MHz, CDCl_3) δ 173.1, 173.0, 172.9, 172.8, 155.0, 137.7, 136.7, 117.6, 117.5, 79.4, 58.0, 57.6, 52.9, 52.9, 52.9, 51.6, 51.5, 48.2, 45.7, 43.2, 43.1, 41.5, 40.5, 39.5, 39.3, 38.5, 38.4, 38.0, 36.7, 28.5.

Inseparable: **GC-MS** (EI, 70 eV) m/z (%) 294 ($\text{M} - 73$, 4), 193 (11), 165 (21), 143 (13), 131 (20), 115 (16), 105 (47), 87 (23), 79 (14), 57 (100).

HRMS (ESI $^+$) (m/z): [$\text{M} + \text{Na}$] $^+$ calculated for $\text{C}_{19}\text{H}_{29}\text{NNaO}_6$, 390.1887; found, 390.1905.



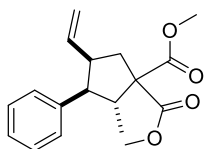
dimethyl 3-vinyl-3,3a,8,8a-tetrahydrocyclopenta[a]indene-1,1(2H)-dicarboxylate (14q) (*cis:trans* = 64:36)

The titled compound was synthesized following **General Procedure C**: dimethyl 2-vinylcyclopropane-1,1-dicarboxylate (**12a**, 27.6 mg, 0.15 mmol, 1.0 equiv.), DBM (1.5 mL), CsPbBr₃ perovskite photocatalyst (1.0 mg) and indene (**13q**, 35.0 μL, 0.30 mmol, 2.0 equiv.) were used. The product was purified by flash column chromatography on silica gel (Hexanes/EtOAc = 20/1 – 15/1) as colorless oil (inseparable diastereomers, 74% **yield**, 33.3 mg).

¹H NMR (400 MHz, CDCl₃) δ 7.16 – 7.07 (m, 4H), 5.90 – 5.81 (m, 0.36H), 5.35 (ddd, *J* = 17.2, 10.0, 8.8 Hz, 0.64H), 5.06 – 4.94 (m, 2H), 3.97 – 3.92 (m, 0.67H), 3.88 – 3.66 (m, 7H), 3.51 – 3.47 (m, 0.36H), 3.12 – 3.03 (m, 1H), 2.88 – 2.72 (m, 1.77H), 2.62 (dd, *J* = 16.8, 7.2 Hz, 0.64H), 2.21 (dd, *J* = 13.2, 6.4 Hz, 0.64H), 2.14 – 2.07 (m, 0.64H), 2.03 – 1.96 (m, 0.37H).

¹³C NMR (101 MHz, CDCl₃) δ 172.9, 172.4, 171.3, 171.0, 145.3, 142.9, 142.1, 141.8, 140.8, 139.1, 127.0, 127.0, 127.0, 126.8, 126.0, 124.5, 124.2, 123.9, 115.3, 114.8, 64.2, 63.0, 56.6, 53.0, 53.0, 52.9, 52.6, 52.4, 50.3, 50.1, 47.9, 45.6, 41.9, 38.0, 36.0, 35.0.

Minor: **GC-MS** (EI, 70 eV) *m/z* (%) 300 (M⁺, 26), 240 (20), 214 (58), 209 (29), 181 (72), 165 (50), 155 (39), 145 (100), 141 (34), 128 (57), 115 (91), 89 (14), 77 (11), 65 (12), 59 (36). Major: **GC-MS** (EI, 70 eV) *m/z* (%) 300 (M⁺, 25), 240 (20), 214 (55), 209 (33), 181 (62), 165 (35), 155 (34), 145 (100), 141 (26), 128 (43), 115 (69), 89 (11), 59 (21).



dimethyl 2-methyl-3-phenyl-4-vinylcyclopentane-1,1-dicarboxylate (14r)
(d.r. = 74:26)

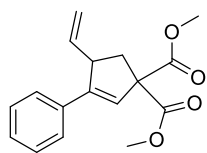
The titled compound was synthesized following **General Procedure C**: dimethyl 2-vinylcyclopropane-1,1-dicarboxylate (**12a**, 27.6 mg, 0.15 mmol, 1.0 equiv.), DBM (1.5 mL), CsPbBr₃ perovskite photocatalyst (1.0 mg) and *trans*-beta-methylstyrene (**13r**, 38.9 μL, 0.30

mmol, 2.0 equiv.) were used. The product was purified by flash column chromatography on silica gel (Hexanes/EtOAc = 33/1 – 25/1) as colorless oil (inseparable diastereomers, 45% **yield**, 20.1 mg).

¹H NMR (400 MHz, CDCl₃) δ 7.32 – 7.26 (m, 2H), 7.32 – 7.26 (m, 1.59H), 7.13 (d, *J* = 7.2 Hz, 1.49H), 5.68 (ddd, *J* = 17.2, 10.4, 7.2 Hz, 0.26H), 5.44 (ddd, *J* = 17.6, 10.4, 7.6 Hz, 0.74H), 4.87 – 4.69 (m, 2H), 3.80 – 3.74 (m, 6H), 3.18 – 3.00 (m, 2.26H), 2.96 – 2.86 (m, 0.29H), 2.83 (dd, *J* = 14.0, 7.6 Hz, 0.74H), 2.65 – 2.41 (m, 1H), 2.17 (dd, *J* = 14.0, 4.4 Hz, 0.75H), 0.95 (d, *J* = 6.4 Hz, 2.22H), 0.88 (d, *J* = 6.8 Hz, 0.82H).

¹³C NMR (101 MHz, CDCl₃) δ 173.3, 173.1, 172.5, 172.3, 141.0, 139.6, 139.4, 139.4, 129.1, 128.6, 128.2, 126.8, 126.5, 115.3, 114.8, 62.6, 62.3, 58.8, 55.1, 52.8, 52.7, 52.4, 50.0, 47.6, 46.4, 43.4, 39.5, 39.3, 14.7, 14.5.

Minor: **GC-MS** (EI, 70 eV) *m/z* (%) 302 (M⁺, 2), 184 (22), 152 (11), 145 (100), 141 (12), 129 (37), 121 (19), 115 (30), 91 (34), 77 (14), 59 (32). Major: **GC-MS** (EI, 70 eV) *m/z* (%) 302 (M⁺, 1), 184 (18), 165 (11), 152 (10), 145 (100), 141 (14), 129 (35), 121 (14), 115 (29), 91 (35), 77 (14), 59 (26).



dimethyl 3-phenyl-4-vinylcyclopent-2-ene-1,1-dicarboxylate (14s)

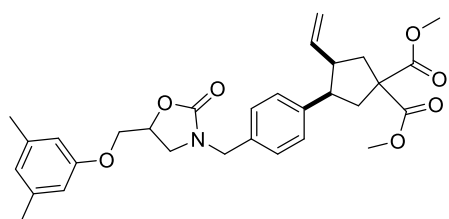
The titled compound was synthesized following **General Procedure C**: dimethyl 2-vinylcyclopropane-1,1-dicarboxylate (**12a**, 27.6 mg, 0.15 mmol, 1.0 equiv.), DBM (1.5 mL), CsPbBr₃ perovskite photocatalyst (1.0 mg) and phenylacetylene (**13s**, 32.9 μL, 0.30 mmol, 2.0 equiv.) were used. The product was purified by flash column chromatography on silica gel (Hexanes/EtOAc = 30/1 – 20/1) as colorless oil (44% **yield**, 18.9 mg).

¹H NMR (400 MHz, CDCl₃) δ 7.50 – 7.43 (m, 2H), 7.38 – 7.26 (m, 3H), 6.20 (s, 1H), 5.74 (ddd, *J* = 16.8, 10.4, 8.4 Hz, 1H), 5.13 (d, *J* = 16.8 Hz, 1H), 5.02 (d, *J* = 10.4 Hz, 1H), 3.95 (td, *J* = 8.4,

5.2 Hz, 1H), 3.77 (s, 3H), 3.74 (s, 3H), 2.94 (dd, $J = 13.6, 8.4$ Hz, 1H), 2.39 (dd, $J = 13.6, 5.2$ Hz, 1H).

^{13}C NMR (101 MHz, CDCl_3) δ 171.7, 171.5, 148.8, 140.4, 134.7, 128.4, 128.2, 127.1, 124.6, 116.3, 65.4, 53.0, 53.0, 49.4, 39.2.

GC-MS (EI, 70 eV) m/z (%) 286 (M^+ , 2), 226 (36), 195 (30), 167 (100), 152 (36), 141 (12), 128 (11), 115 (19), 91 (19), 59 (23).



dimethyl 3-(4-((5-((3,5-dimethylphenoxy)methyl)-2-oxooxazolidin-3-yl)methyl)phenyl)-4-vinylcyclopentane-1,1-dicarboxylate (14t) (*cis:trans* = 66:34)

The titled compound was synthesized following **General Procedure C**: dimethyl 2-vinylcyclopropane-1,1-dicarboxylate (**12a**, 27.6 mg, 0.15 mmol, 1.0 equiv.), DBM (1.5 mL), CsPbBr_3 perovskite photocatalyst (1.0 mg) and 5-((3,5-dimethylphenoxy)methyl)-3-(4-vinylbenzyl)oxazolidin-2-one (**13t**, 101.2 mg, 0.30 mmol, 2.0 equiv.) were used. The product was purified by flash column chromatography on silica gel (DCM – 1% MeOH/DCM with 1% triethylamine as additive) as colorless oil (inseparable diastereomers, 39% **yield**, 30.4 mg).

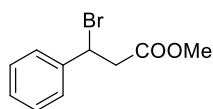
^1H NMR (400 MHz, CDCl_3) δ 7.25 – 7.18 (m, 2.69H), 7.13 (d, $J = 8.0$ Hz, 1.31H), 6.62 (s, 1H), 6.49 (s, 2H), 5.62 (ddd, $J = 17.2, 10.4, 6.8$ Hz, 0.33H), 5.40 – 5.25 (m, 0.66H), 4.92 – 4.74 (m, 3H), 4.42 (s, 1H), 4.11 – 3.99 (m, 2H), 3.80 – 3.73 (m, 6H), 3.57 – 3.50 (m, 1H), 3.47 – 3.36 (m, 1.77H), 3.00 (p, $J = 7.2$ Hz, 0.63H), 2.87 (td, $J = 11.2, 7.6$ Hz, 0.40H), 2.80 – 2.51 (m, 3H), 2.44 – 2.31 (m, 1H), 2.27 (s, 6H), 2.19 – 2.12 (m, 0.40H).

^{13}C NMR (101 MHz, CDCl_3) δ 173.2, 173.1, 173.0, 172.8, 158.3, 157.8, 141.5, 140.8, 139.5, 138.7, 138.1, 134.0, 133.6, 128.9, 128.3, 128.2, 128.0, 123.5, 115.9, 115.7, 112.4, 71.0, 68.1, 59.1, 58.2, 53.1, 53.0, 51.2, 51.0, 48.1, 47.9, 47.5, 46.4, 46.3, 42.5, 40.4, 39.1, 38.2, 21.5.

Minor: **GC-MS** (EI, 70 eV) m/z (%) 521 (M⁺, 19), 362 (14), 356 (22), 310 (56), 300 (59), 269 (29), 266 (10), 240 (100), 234 (11), 215 (14), 209 (21), 181 (62), 161 (35), 156 (65), 152 (21), 147 (35), 141 (37), 135 (24), 128 (45), 122 (54), 117 (67), 105 (52), 94 (16), 91 (80), 77 (36), 65 (11), 59 (34). Major: **GC-MS** (EI, 70 eV) m/z (%) 521 (M⁺, 9), 356 (11), 310 (25), 300 (64), 269 (23), 240 (100), 234 (11), 215 (11), 209 (17), 181 (56), 161 (25), 156 (60), 152 (17), 147 (26), 141 (33), 135 (20), 128 (40), 122 (41), 117 (55), 105 (44), 94 (13), 91 (62), 77 (29), 65 (10), 59 (30).

HRMS (ESI⁺) (m/z): [M+H]⁺ calculated for C₃₀H₃₆NO₇, 522.2486; found, 522.2509.

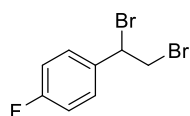
Photocatalytic Synthesis of Other Products



methyl 3-bromo-3-phenylpropanoate (15a)

The titled compound was synthesized following **General Procedure D**: methyl 3-phenylpropanoate (24.6 mg, 0.15 mmol, 1.0 equiv.), DBM (1.5 mL, 0.1 M) and CsPbBr₃ perovskite photocatalyst (1.0 mg) were used to react for 24h. The product was purified by flash column chromatography on silica gel (Hexanes/EtOAc = 40/1) as colorless oil (54% **yield**, 19.6 mg). The analytical data is in good agreement with the reported data.⁴⁵

¹H NMR (400 MHz, CDCl₃) δ 7.43 (d, *J* = 8.0 Hz, 2H), 7.39 – 7.27 (m, 3H), 5.41 (dd, *J* = 9.2, 6.0 Hz, 1H), 3.70 (s, 3H), 3.36 (dd, *J* = 16.0, 9.2 Hz, 1H), 3.22 (dd, *J* = 16.0, 6.0 Hz, 1H).

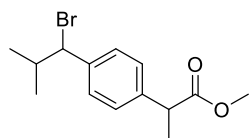


1-(1,2-dibromoethyl)-4-fluorobenzene (15b)

The titled compound was synthesized following **General Procedure D**: 1-(2-bromoethyl)-4-fluorobenzene (21.0 μL, 0.15 mmol, 1.0 equiv.), DBM (1.5 mL, 0.1 M) and CsPbBr₃ perovskite photocatalyst (1.0 mg) were used to react for 24h. The product was purified by flash column chromatography on silica gel (Hexanes) as white solid (24% **yield**, 10.2 mg). The analytical data is in good agreement with the reported data.⁴⁶

¹H NMR (400 MHz, CDCl₃) δ 7.43 – 7.36 (m, 2H), 7.11 – 7.04 (m, 2H), 5.13 (dd, *J* = 10.8, 5.2 Hz, 1H), 4.07 (dd, *J* = 10.4, 5.2 Hz, 1H), 3.97 (apparent t, *J* = 10.8 Hz, 1H).

¹⁹F NMR (376 MHz, CDCl₃) δ -111.74.



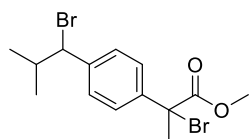
methyl 2-(4-(1-bromo-2-methylpropyl)phenyl)propanoate (15c-mono)

The titled compound was synthesized following **General Procedure D**: methyl 2-(4-isobutylphenyl)propanoate (33.0 mg, 0.15 mmol, 1.0 equiv.), DBM (1.5 mL, 0.1 M) and CsPbBr₃ perovskite photocatalyst (1.0 mg) were used to react for 24h. The product was purified by flash column chromatography on silica gel (Hexanes/EtOAc = 75/1) as colorless oil (28% **yield**, 12.7 mg).

¹H NMR (400 MHz, CDCl₃) δ 7.31 (d, *J* = 8.0 Hz, 2H), 7.25 (d, *J* = 8.0 Hz, 2H), 4.71 (d, *J* = 8.4 Hz, 1H), 3.72 (q, *J* = 7.2 Hz, 1H), 3.67 (s, 3H), 2.37 – 2.23 (m, 1H), 1.49 (d, *J* = 7.2 Hz, 3H), 1.18 (d, *J* = 6.8 Hz, 3H), 0.86 (d, *J* = 6.8 Hz, 3H).

¹³C NMR (101 MHz, CDCl₃) δ 175.0, 174.9, 140.6, 140.4, 140.3, 128.2, 127.7, 64.1, 52.2, 45.2, 36.7, 21.6, 20.7, 18.7.

GC-MS (EI, 70 eV) *m/z* (%) 298 (M⁺, 0.4), 255 (2), 239 (7), 219 (100), 191 (8), 177 (30), 159 (52), 145 (21), 128 (11), 117 (27), 105 (6), 91 (11).



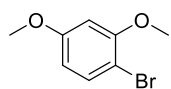
methyl 2-bromo-2-(4-(1-bromo-2-methylpropyl)phenyl)propanoate

(15c-di)

The product was purified by flash column chromatography on silica gel (Hexanes/EtOAc = 75/1) as colorless oil (11% **yield**, 6.0 mg).

¹H NMR (400 MHz, CDCl₃) δ 7.50 (d, *J* = 8.0 Hz, 2H), 7.34 (d, *J* = 8.0 Hz, 2H), 4.71 (d, *J* = 8.4 Hz, 1H), 3.80 (s, 3H), 2.35 – 2.22 (m, 4H), 1.17 (d, *J* = 6.4 Hz, 3H), 0.87 (d, *J* = 6.8 Hz, 3H).

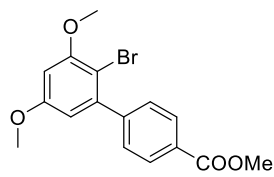
^{13}C NMR (101 MHz, CDCl_3) δ 171.5, 141.9, 140.7, 128.0, 127.1, 63.3, 63.3, 61.3, 61.3, 53.8, 36.6, 31.4, 31.4, 21.5, 20.7.



1-bromo-2,4-dimethoxybenzene (16a)

The titled compound was synthesized following **General Procedure D**: 1,3-dimethoxybenzene (19.6 μL , 0.15 mmol, 1.0 equiv.), DBM (1.5 mL, 0.1 M) and CsPbBr_3 perovskite photocatalyst (1.0 mg) were used to react for 48h. The product was purified by flash column chromatography on silica gel (Hexanes/EtOAc = 50/1) as colorless oil (45% **yield**, 14.6 mg). The analytical data is in good agreement with the reported data. ⁴⁷

^1H NMR (400 MHz, CDCl_3) δ 7.41 (d, J = 8.4 Hz, 1H), 6.49 (d, J = 2.8 Hz, 1H), 6.40 (dd, J = 8.4, 2.8 Hz, 1H), 3.87 (s, 3H), 3.80 (s, 3H).



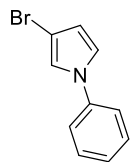
methyl 2'-bromo-3',5'-dimethoxy-[1,1'-biphenyl]-4-carboxylate (16b)

The titled compound was synthesized following **General Procedure D**: methyl 3',5'-dimethoxy-[1,1'-biphenyl]-4-carboxylate (40.8 mg, 0.15 mmol, 1.0 equiv.), DBM (1.5 mL, 0.1 M) and CsPbBr_3 perovskite photocatalyst (1.0 mg) were used to react for 48h. The product was purified by flash column chromatography on silica gel (Hexanes/EtOAc = 20/1 – 10/1) as white solid (34% **yield**, 17.7 mg).

^1H NMR (400 MHz, CDCl_3) δ 8.09 (d, J = 8.0 Hz, 2H), 7.46 (d, J = 8.0 Hz, 2H), 6.52 (d, J = 2.8 Hz, 1H), 6.47 (d, J = 2.8 Hz, 1H), 3.94 (s, 3H), 3.92 (s, 3H), 3.82 (s, 3H).

^{13}C NMR (101 MHz, CDCl_3) δ 167.0, 159.7, 157.2, 146.2, 143.6, 129.6, 129.5, 129.4, 107.4, 103.2, 99.3, 56.6, 55.8, 52.3.

GC-MS (EI, 70 eV) m/z (%) 350 (M^+ , 100), 319 (81), 307 (11), 289 (9), 261 (9), 241 (17), 226 (13), 212 (40), 197 (38), 182 (25), 169 (37), 161 (32), 154 (24), 139 (37), 126 (43), 115 (13).

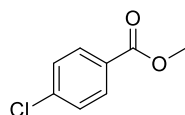


3-bromo-1-phenyl-1H-pyrrole (16c)

The titled compound was synthesized following **General Procedure D**: 1-phenylpyrrole (21.5 mg, 0.15 mmol, 1.0 equiv.), DBM (1.5 mL, 0.1 M) and CsPbBr₃ perovskite photocatalyst (1.0 mg) were used to react for 24h. The product was purified by flash column chromatography on silica gel (Hexanes – 0.83% EtOAc/Hexanes) as pale yellow solid (56% **yield**, 18.7 mg). The analytical data is in good agreement with the reported data.⁴⁸

¹H NMR (400 MHz, CDCl₃) δ 7.44 (t, *J* = 7.6 Hz, 2H), 7.34 (d, *J* = 8.0 Hz, 2H), 7.28 (t, *J* = 7.6 Hz, 1H), 7.11 – 7.05 (m, 1H), 7.01 – 6.95 (m, 1H), 6.38 – 6.31 (m, 1H).

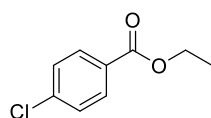
¹³C NMR (101 MHz, CDCl₃) δ 140.2, 129.8, 126.4, 120.6, 120.1, 119.2, 113.1, 98.3.



methyl 4-chlorobenzoate (17a)

The titled compound was synthesized following **General Procedure D**: 1-chloro-4-(dimethoxymethyl)benzene (28.0 mg, 0.15 mmol, 1.0 equiv.), DBM (1.5 mL, 0.1 M) and CsPbBr₃ perovskite photocatalyst (1.0 mg) were used to react for 24h. The product was purified by flash column chromatography on silica gel (Hexanes/EtOAc = 50/1 – 40/1) as white solid (53% **yield**, 13.6 mg). The analytical data is in good agreement with the reported data.⁴⁹

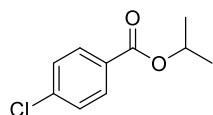
¹H NMR (400 MHz, CDCl₃) δ 7.97 (d, *J* = 8.4 Hz, 2H), 7.41 (d, *J* = 8.4 Hz, 2H), 3.91 (s, 3H).



ethyl 4-chlorobenzoate (17b)

The titled compound was synthesized following **General Procedure D**: 1-chloro-4-(diethoxymethyl)benzene (32.2 mg, 0.15 mmol, 1.0 equiv.), DBM (1.5 mL, 0.1 M) and CsPbBr₃ perovskite photocatalyst (1.0 mg) were used to react for 24h. The product was purified by flash column chromatography on silica gel (Hexanes/EtOAc = 50/1 – 40/1) as colorless oil (60% **yield**, 16.6 mg). The analytical data is in good agreement with the reported data.⁵⁰

¹H NMR (400 MHz, CDCl₃) δ 7.98 (d, *J* = 8.4 Hz, 2H), 7.41 (d, *J* = 8.4 Hz, 2H), 4.37 (q, *J* = 7.2 Hz, 2H), 1.39 (t, *J* = 7.2 Hz, 3H).

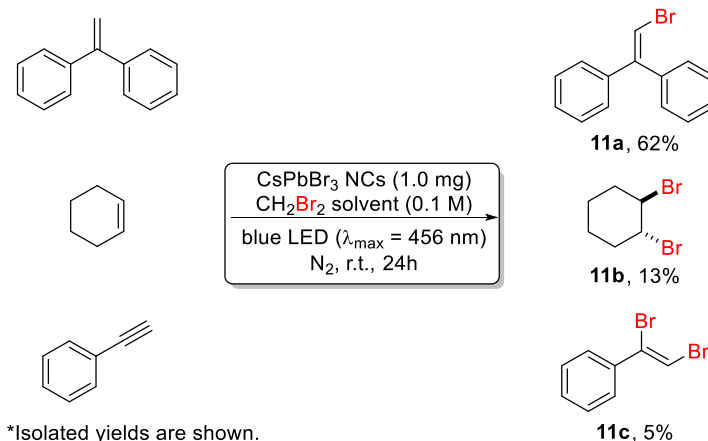


isopropyl 4-chlorobenzoate (17c)

The titled compound was synthesized following **General Procedure D**: 1-chloro-4-(diisopropoxymethyl)benzene (36.4 mg, 0.15 mmol, 1.0 equiv.), DBM (1.5 mL, 0.1 M) and CsPbBr₃ perovskite photocatalyst (1.0 mg) were used to react for 24h. The product was purified by flash column chromatography on silica gel (Hexanes/EtOAc = 50/1 – 40/1) as colorless oil (44% **yield**, 13.2 mg). The analytical data is in good agreement with the reported data.⁵¹

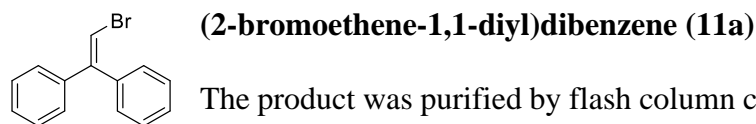
¹H NMR (400 MHz, CDCl₃) δ 7.97 (d, *J* = 8.4 Hz, 2H), 7.40 (d, *J* = 8.4 Hz, 2H), 5.23 (hept, *J* = 6.4 Hz, 1H), 1.36 (d, *J* = 6.4 Hz, 6H).

4.5.6 Bromine Radical Trapping Experiment



Bromine radical trapping experiments were performed according to the following procedure: To a 1-dram vial with a magnetic stirring bar was added bromine radical acceptor (0.15 mmol, 1.0 equiv.), DBM (1.5 mL, 0.1 M) and CsPbBr₃ perovskite photocatalyst (1.0 mg). The resulting mixture was degassed with N₂ for 20 min and sealed with parafilm. It was allowed to react at room temperature under blue LED (Kessil®, 40 W, λ_{max} = 456 nm) irradiation for 24h. Upon completion, the reaction mixture was first analyzed by GC-MS. Then the trapping product

was purified by flash column chromatography on silica gel using hexanes as eluent. Their ^1H NMR spectra were obtained and in good agreement with the reported data.



The product was purified by flash column chromatography on silica gel (Hexanes) as colorless oil (62% **yield**, 24.0 mg). The analytical data is in good agreement with the reported data.⁵²

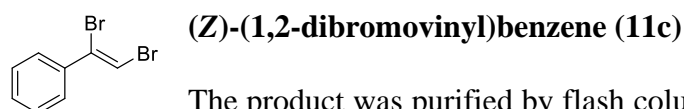
^1H NMR (400 MHz, CDCl_3) δ 7.46 – 7.35 (m, 3H), 7.35 – 7.27 (m, 5H), 7.25 – 7.19 (m, 2H), 6.79 (s, 1H).



The product was purified by flash column chromatography on silica gel (Hexanes) as colorless oil (13% **yield**, 4.7 mg). The analytical data is in good agreement with the reported data.

53

^1H NMR (400 MHz, CDCl_3) δ 4.45 (br s, 2H), 2.53 – 2.40 (m, 2H), 1.96 – 1.77 (m, 4H), 1.53 – 1.46 (m, 2H).

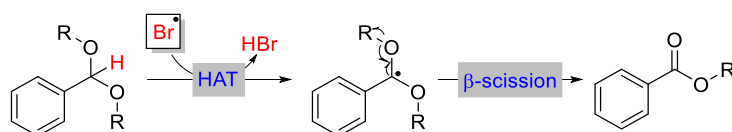


The product was purified by flash column chromatography on silica gel (Hexanes) as colorless oil (5% **yield**, 2.0 mg). The analytical data is in good agreement with the reported data.

54

^1H NMR (400 MHz, CDCl_3) δ 7.54 – 7.48 (m, 2H), 7.39 – 7.34 (m, 3H), 7.06 (s, 1H).

4.5.7 Proposed Mechanism for the Hydrogen Atom Transfer

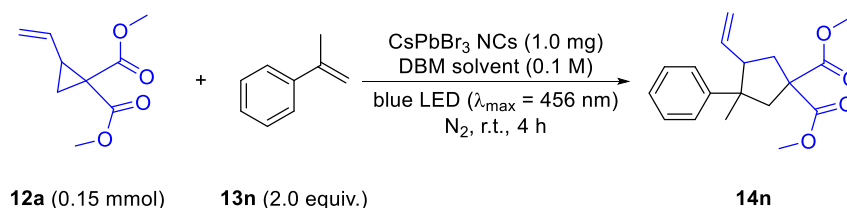


Scheme 4.7 The mechanism for the hydrogen atom transfer of benzaldehyde acetal by bromine radical studied by Doyle group.³⁷

4.5.8 CsPbBr₃ Nanocrystals Catalyst Recycling Experiment

To a 1-dram vial with a magnetic stirring bar was added dimethyl 2-vinylcyclopropane-1,1-dicarboxylate **12a** (27.6 mg, 0.15 mmol, 1.0 equiv.), DBM (1.5 mL, 0.1 M), CsPbBr₃ perovskite photocatalyst (1.0 mg) and alpha-methylstyrene **13n** (38.96 μ L, 0.3 mmol, 2.0 equiv.). The resulting mixture was degassed with N₂ for 20 min and sealed with parafilm. It was allowed to react at room temperature under blue LED (Kessil®, 40 W, $\lambda_{\text{max}} = 456$ nm) irradiation for 4h. Upon completion, the CsPbBr₃ NCs was collected by centrifugation at 10k rpm in a 1.5-mL micro centrifuge tube. The CsPbBr₃ NCs was washed by DBM (~0.5 mL). The CsPbBr₃ NCs was then transferred back to a 1-dram vial for use in another catalytic cycle. The combined DBM solution containing the reaction mixture was first subject to *vacuo* to remove solvent. Then the yield of the crude mixture was analyzed by ¹H NMR spectroscopy relative to 3,4,5-trichloropyridine (9.1 mg, 0.05 mmol) as an internal standard.

Table 4.4 NCs Catalyst Recycling experiments.



Cycle	Yield, %
1	90
2	84
3	90

CsPbBr₃ NCs catalyst shows no significant change in reactivity for [3+2] cycloaddition of **12a** and **13n** across three successive experimental cycles reusing the same catalyst.

4.5.9 Gram-scale Synthesis of Benzyl Bromide from Toluene

To a 1-dram vial with a magnetic stirring bar was added Toluene (1.3 mL, 12.23 mmol, 1.0 equiv.), DBM (212.8 μ L, 3.06 mmol, 0.25 equiv.), CsPbBr₃ perovskite photocatalyst (1.0 mg). The resulting mixture was degassed with N₂ for 20 min and sealed with black electric tape. It was allowed to react at room temperature under blue LED (Kessil®, 40 W, $\lambda_{\text{max}} = 456$ nm) irradiation. A 10- μ L aliquot of the reaction mixture was taken periodically using a Hamilton® microliter syringe through the PTFE septa and tested by ¹H NMR spectroscopy to analyze the product formation.

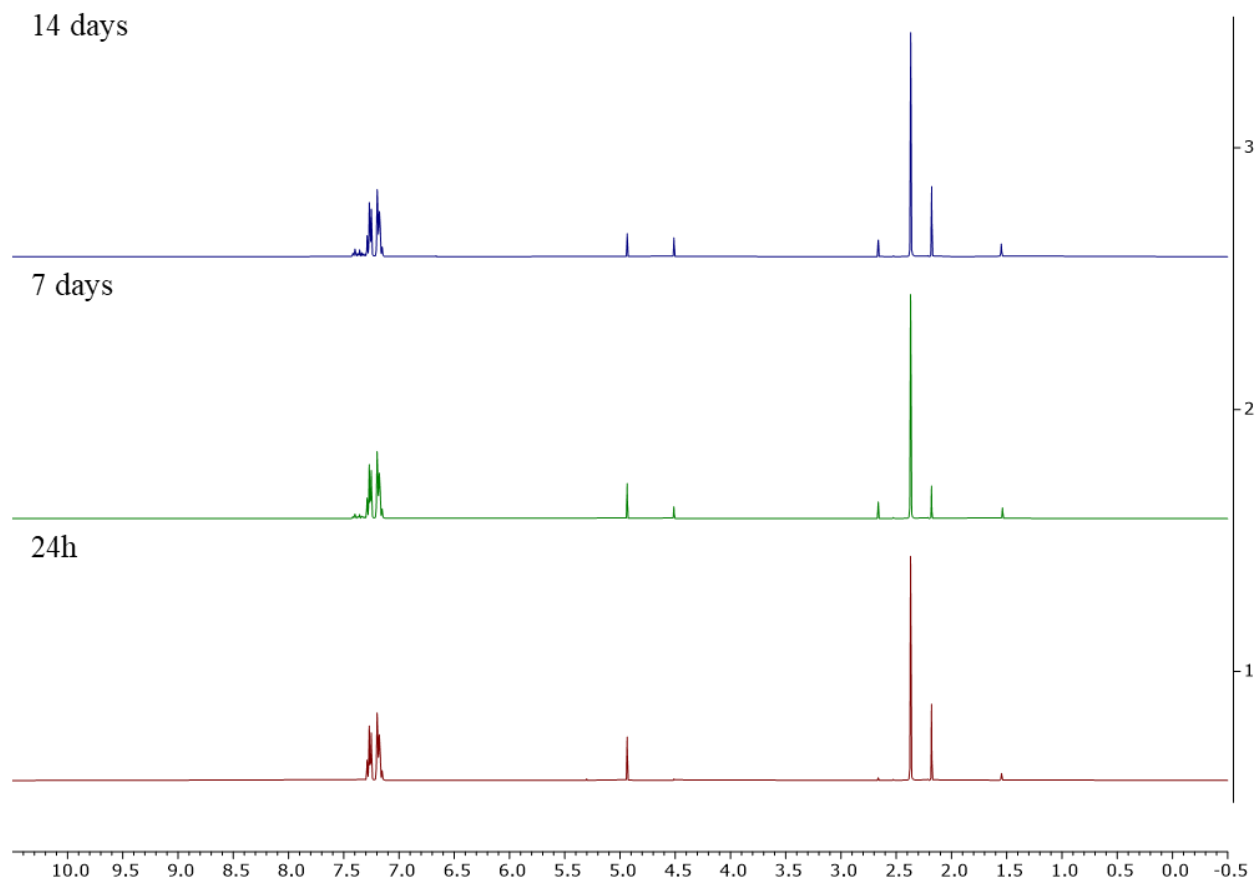


Figure 4.3 ¹H NMR analysis of the aliquots taken from the reaction mixture at different reaction time (24h/7 days/14 days) as indicated by the timestamp on top left of the stacked spectra showing the progressing benzyl bromide production.

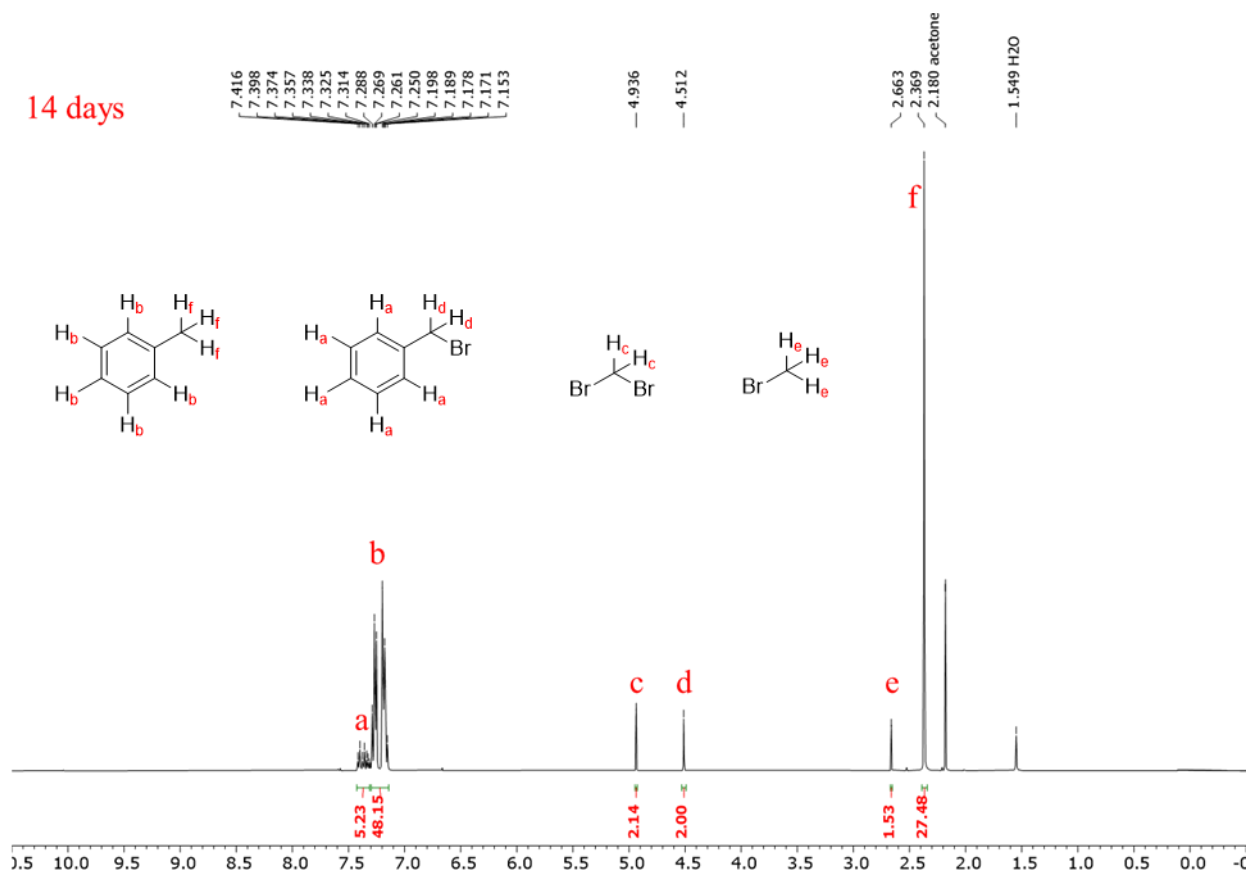
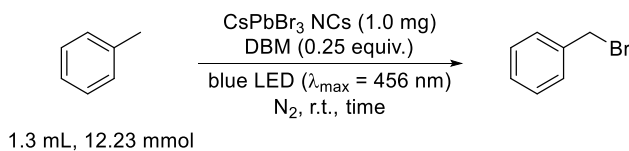


Figure 4.4 The structural assignments of the crude reaction mixture (14 days) by ¹H NMR spectroscopy showing high selectivity to benzyl bromide.

Table 4.5 Benzylic bromination of toluene.



Reaction time	Ratio of toluene vs. benzyl bromide
24h	106: 1
7 days	15: 1
14 days	9: 1

CsPbBr₃ NCs catalysts can continuously generate bromine radical from DBM under blue LED irradiation as indicated by the benzylic bromination of toluene over 14 days.

4.5.10 Analysis of Side Products from [3+2] Cycloaddition

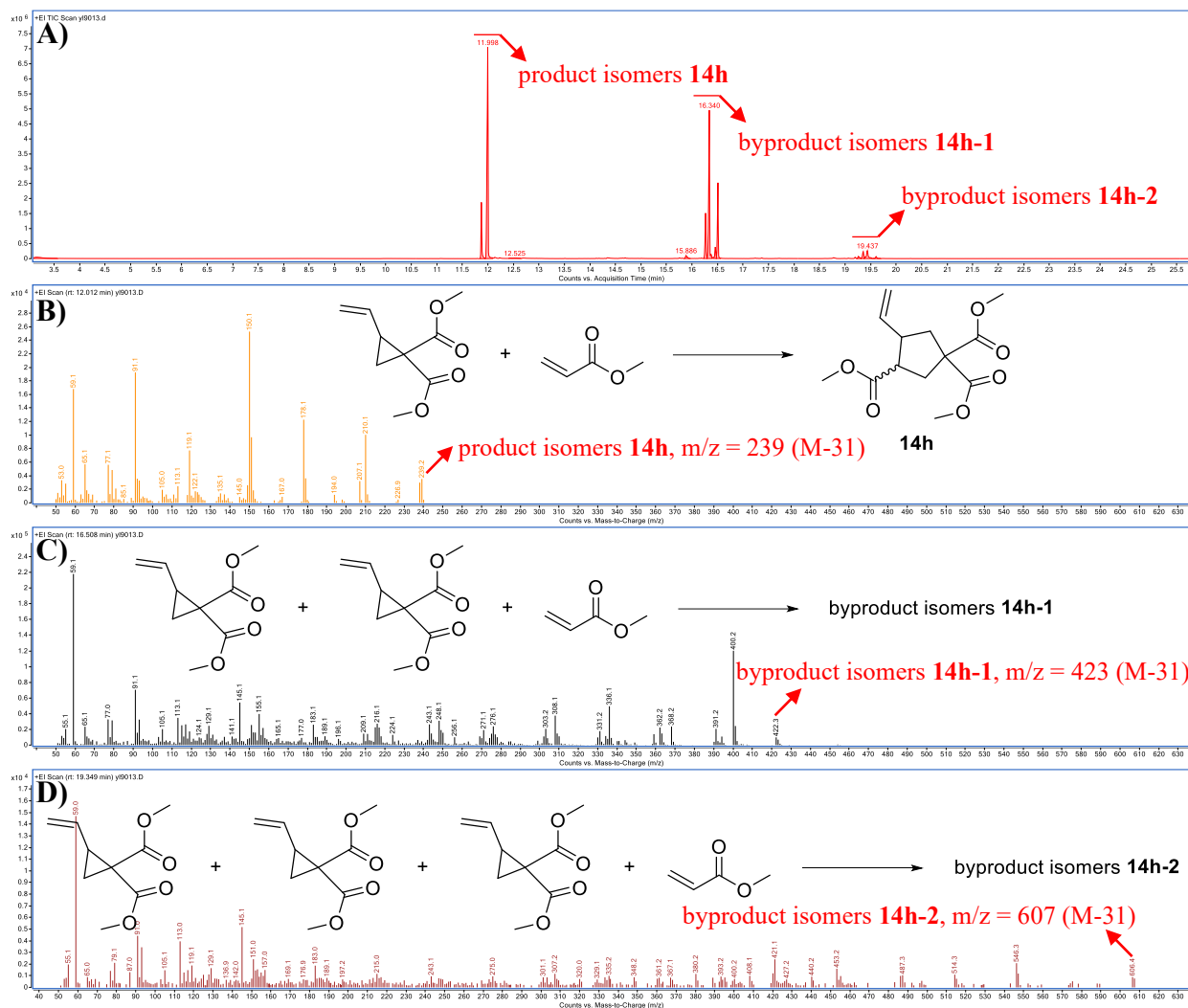


Figure 4.5 GC-MS analysis of the crude reaction mixture from **14h** reveals groups of oligomer side products based on vinylcyclopropane, which is likely the result of ring-opening polymerization.²⁵ Polymers of higher mass are not seen here because of detection limit. **A)** GC chromatogram of the crude reaction mixture. **B-D)** Mass spectra of selected groups of compounds and their formation routes.

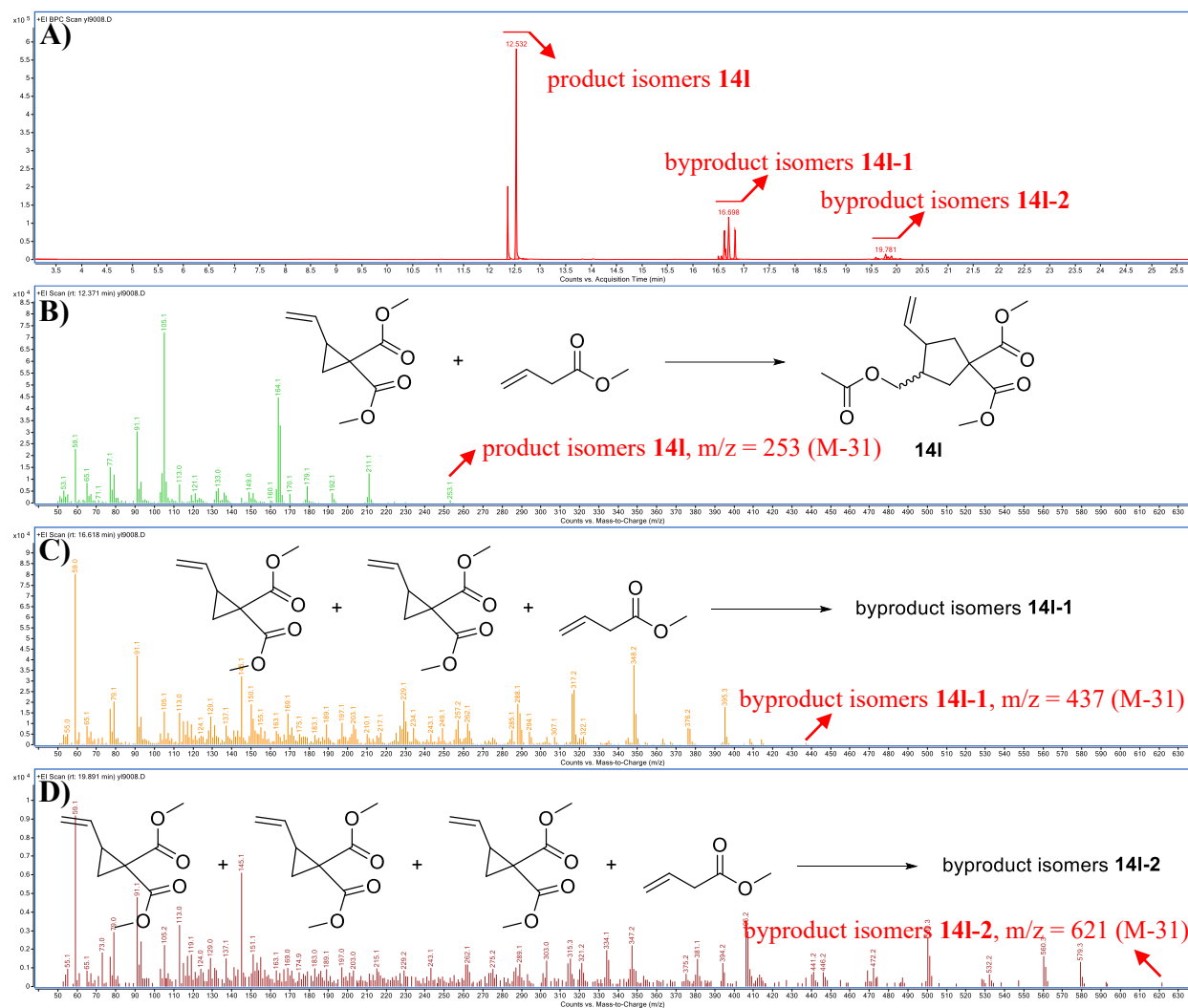


Figure 4.6 GC-MS analysis of the crude reaction mixture from **14I** reveals groups of oligomer side products based on vinylcyclopropane, which is likely the result of ring-opening polymerization.²⁵ Polymers of higher mass are not seen here because of detection limit. **A)** GC chromatogram of the crude reaction mixture. **B-D)** Mass spectra of selected groups of compounds and their formation routes.

4.5.11 Photoluminescence (PL) Measurements of CsPbBr₃ NCs in DBM

Steady-state emission spectra of CsPbBr₃ perovskite NCs in DBM were acquired using a HORIBA Fluoromax-3 spectrofluorometer. The sample was prepared by using CsPbBr₃ NCs (1.3 mg) and DBM (2.0 mL) and the resulting colloidal solution was degassed with N₂ for 20 min and sealed with parafilm. The PL emission spectra of the sample was collected at an excitation wavelength of 365 nm before and after blue LED irradiation for 1h.

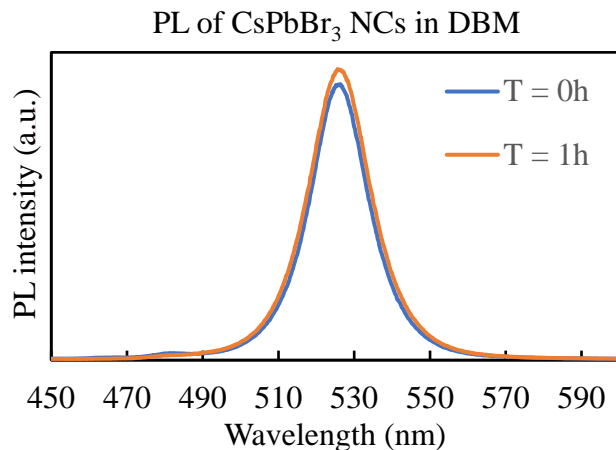


Figure 4.7 PL emission spectra of CsPbBr₃ NCs in DBM before and after blue LED (40 W, $\lambda_{\text{max}} = 456$ nm) irradiation (1h) showing slight increase in PL intensity, in line with previous reported bromide anion exchange of CsPbBr₃ perovskite NCs in DBM under visible light irradiation.

4.5.12 Cyclic Voltammetry Data

Cyclic voltammetry (CV) measurement was performed using a CH Instruments CHI660E Electrochemical Analyzer, a glassy carbon working electrode, a platinum wire counter electrode, and a saturated calomel reference electrode. The sample was prepared with 0.1 M tetrabutylammonium hexafluorophosphate in **CH₂Br₂**: CH₃CN = 1: 1 (10 mL) and sparged with N₂ for 20 minutes. Data was collected with a scan rate of 0.1 V/s.

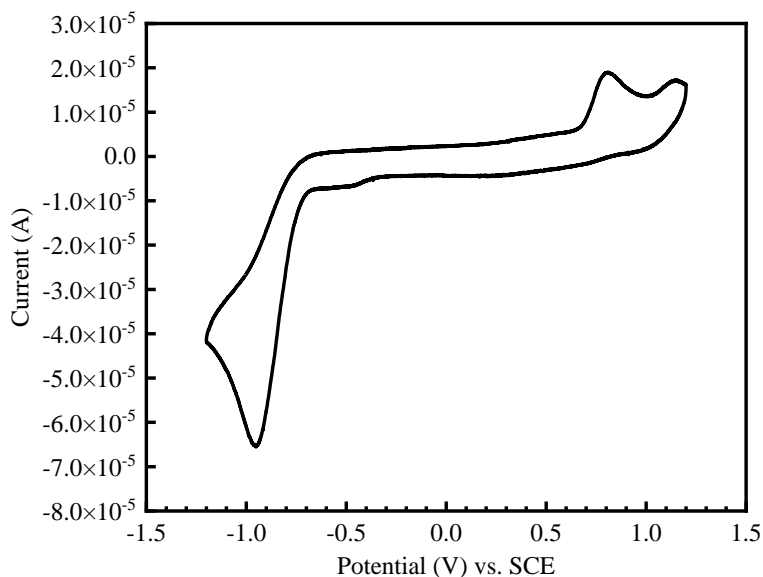


Figure 4.8 Cyclic voltammetry of CH₂Br₂.

4.6 Acknowledgements

Chapter 4, in full, is a reprint of the material as it appears in *ChemSusChem* **2023**, e202301060. **Lin, Y.**; Yan, Y. The dissertation author was the primary investigator and author of this paper.

I initiated the studies and produced all the data presented in the above-mentioned publication. I wrote the first draft of the manuscript.

4.7 Reference

1. Akkerman, Q. A.; D’Innocenzo, V.; Accornero, S.; Scarpellini, A.; Petrozza, A.; Prato, M.; Manna, L., Tuning the Optical Properties of Cesium Lead Halide Perovskite Nanocrystals by Anion Exchange Reactions. *J. Am. Chem. Soc.* **2015**, *137* (32), 10276-10281.
2. Jang, D. M.; Park, K.; Kim, D. H.; Park, J.; Shojaei, F.; Kang, H. S.; Ahn, J.-P.; Lee, J. W.; Song, J. K., Reversible Halide Exchange Reaction of Organometal Trihalide Perovskite Colloidal Nanocrystals for Full-Range Band Gap Tuning. *Nano Lett.* **2015**, *15* (8), 5191-5199.
3. Nedelcu, G.; Protesescu, L.; Yakunin, S.; Bodnarchuk, M. I.; Grotevent, M. J.; Kovalenko, M. V., Fast Anion-Exchange in Highly Luminescent Nanocrystals of Cesium Lead Halide Perovskites (CsPbX₃, X = Cl, Br, I). *Nano Lett.* **2015**, *15* (8), 5635-5640.
4. Parobek, D.; Dong, Y.; Qiao, T.; Rossi, D.; Son, D. H., Photoinduced Anion Exchange in Cesium Lead Halide Perovskite Nanocrystals. *J. Am. Chem. Soc.* **2017**, *139* (12), 4358-4361.
5. Zhu, X.; Lin, Y.; San Martin, J.; Sun, Y.; Zhu, D.; Yan, Y., Lead Halide Perovskites for Photocatalytic Organic Synthesis. *Nat. Commun.* **2019**, *10* (1), 2843.
6. Wong, Y.-C.; Wu, W.-B.; Wang, T.; Ng, J. D. A.; Khoo, K. H.; Wu, J.; Tan, Z.-K., Color Patterning of Luminescent Perovskites via Light-Mediated Halide Exchange with Haloalkanes. *Adv. Mater.* **2019**, *31* (24), 1901247.
7. Li, Y.; Wang, T.; Wang, Y.; Deng, Z.; Zhang, L.; Zhu, A.; Huang, Y.; Zhang, C.; Yuan, M.; Xie, W., Tunable Photocatalytic Two-Electron Shuttle between Paired Redox Sites on Halide Perovskite Nanocrystals. *ACS Catal.* **2022**, *12* (10), 5903-5910.
8. Jia, P.; Li, Q.; Poh, W. C.; Jiang, H.; Liu, H.; Deng, H.; Wu, J., Light-Promoted Bromine-Radical-Mediated Selective Alkylation and Amination of Unactivated C(sp³)-H Bonds. *Chem* **2020**, *6* (7), 1766-1776.
9. Wang, H.; Liu, H.; Wang, M.; Huang, M.; Shi, X.; Wang, T.; Cong, X.; Yan, J.; Wu, J., Bromine Radical as a Visible-Light-Mediated Polarity-Reversal Catalyst. *iScience* **2021**, *24* (6), 102693.

10. Tanko, J. M.; Sadeghipour, M., Functionalization of Hydrocarbons by a New Free Radical Based Condensation Reaction. *Angew. Chem. Intl. Ed.* **1999**, *38* (1-2), 159-161.
11. Dongbang, S.; Doyle, A. G., Ni/Photoredox-Catalyzed C(sp³)-C(sp³) Coupling between Aziridines and Acetals as Alcohol-Derived Alkyl Radical Precursors. *J. Am. Chem. Soc.* **2022**, *144* (43), 20067-20077.
12. Saikia, I.; Borah, A. J.; Phukan, P., Use of Bromine and Bromo-Organic Compounds in Organic Synthesis. *Chem. Rev.* **2016**, *116* (12), 6837-7042.
13. Kippo, T.; Hamaoka, K.; Ryu, I., Bromine Radical-Mediated Sequential Radical Rearrangement and Addition Reaction of Alkylidenecyclopropanes. *J. Am. Chem. Soc.* **2013**, *135* (2), 632-635.
14. Bemis, G. W.; Murcko, M. A., The Properties of Known Drugs. 1. Molecular Frameworks. *J. Med. Chem.* **1996**, *39* (15), 2887-2893.
15. Miura, K.; Fugami, K.; Oshima, K.; Utimoto, K., Synthesis of Vinylcyclopentanes from Vinylcyclopropanes and Alkenes Promoted by Benzenethiyl Radical. *Tetrahedron Lett.* **1988**, *29* (40), 5135-5138.
16. Feldman, K. S.; Berven, H. M.; Weinreb, P. H., 2,2-Dihalovinylcyclopropanes as Highly Diastereoselective Three-Atom Addends in Phenylthio Radical Mediated Vinylcyclopentane Synthesis. *J. Am. Chem. Soc.* **1993**, *115* (24), 11364-11369.
17. Hashimoto, T.; Kawamata, Y.; Maruoka, K., An Organic Thiyl Radical Catalyst for Enantioselective Cyclization. *Nat. Chem.* **2014**, *6* (8), 702-705.
18. Zhang, H.; Curran, D. P., A Short Total Synthesis of (±)-Epimeloscine and (±)-Meloscine Enabled by a Cascade Radical Annulation of a Divinylcyclopropane. *J. Am. Chem. Soc.* **2011**, *133* (27), 10376-10378.
19. Chen, D.-F.; Chrisman, C. H.; Miyake, G. M., Bromine Radical Catalysis by Energy Transfer Photosensitization. *ACS Catal.* **2020**, *10* (4), 2609-2614.
20. Archer, G.; Cavalère, P.; Médebielle, M.; Merad, J., Photoredox Generation of Isothiouronyl Radical Cations: A New Platform in Covalent Radical Catalysis. *Angew. Chem. Intl. Ed.* **2022**, *61* (32), e202205596.
21. Studer, A.; Curran, D. P., Catalysis of Radical Reactions: A Radical Chemistry Perspective. *Angew. Chem. Intl. Ed.* **2016**, *55* (1), 58-102.
22. Cismesia, M. A.; Yoon, T. P., Characterizing Chain Processes in Visible Light Photoredox Catalysis. *Chem. Sci.* **2015**, *6* (10), 5426-5434.
23. Lin, Y.; Avvacumova, M.; Zhao, R.; Chen, X.; Beard, M. C.; Yan, Y., Triplet Energy Transfer from Lead Halide Perovskite for Highly Selective Photocatalytic 2 + 2 Cycloaddition. *ACS Appl. Mater. Interfaces* **2022**, *14* (22), 25357-25365.

24. Wong, Y.-C.; De Andrew Ng, J.; Tan, Z.-K., Perovskite-Initiated Photopolymerization for Singly Dispersed Luminescent Nanocomposites. *Adv. Mater.* **2018**, *30* (21), 1800774.
25. Chen, D.-F.; Boyle, B. M.; McCarthy, B. G.; Lim, C.-H.; Miyake, G. M., Controlling Polymer Composition in Organocatalyzed Photoredox Radical Ring-Opening Polymerization of Vinylcyclopropanes. *J. Am. Chem. Soc.* **2019**, *141* (33), 13268-13277.
26. Zhang, P.; Le, C. C.; MacMillan, D. W. C., Silyl Radical Activation of Alkyl Halides in Metallaphotoredox Catalysis: A Unique Pathway for Cross-Electrophile Coupling. *J. Am. Chem. Soc.* **2016**, *138* (26), 8084-8087.
27. This transformation favors a conformation that can minimize the 1,3-diaxial interaction in the chair-like transition state III-a/b. The bulkiness of a carbon-centered substituent usually follows the trend: $C(sp^3) > C(sp^2) > C(sp)$. For compound **14n**, since the methyl is bulkier than the phenyl group, this compound favors a *trans*-conformation where the methyl and the vinyl group are on the same side. For compound **14i**, since the nitrile group (sp hybridization) is linear, the 1,3-diaxial interaction is weak, the d.r. value of it is nearly 1: 1.
28. Ravi, V. K.; Markad, G. B.; Nag, A., Band Edge Energies and Excitonic Transition Probabilities of Colloidal CsPbX₃ (X = Cl, Br, I) Perovskite Nanocrystals. *ACS Energy Lett.* **2016**, *1* (4), 665-671.
29. Prier, C. K.; Rankic, D. A.; MacMillan, D. W. C., Visible Light Photoredox Catalysis with Transition Metal Complexes: Applications in Organic Synthesis. *Chem. Rev.* **2013**, *113* (7), 5322-5363.
30. Romero, N. A.; Nicewicz, D. A., Organic Photoredox Catalysis. *Chem. Rev.* **2016**, *116* (17), 10075-10166.
31. Uoyama, H.; Goushi, K.; Shizu, K.; Nomura, H.; Adachi, C., Highly Efficient Organic Light-Emitting Diodes from Delayed Fluorescence. *Nature* **2012**, *492* (7428), 234-238.
32. Neumann, M.; Fuldner, S.; König, B.; Zeitler, K., Metal-Free, Cooperative Asymmetric Organophotoredox Catalysis with Visible Light. *Angew. Chem. Intl. Ed.* **2011**, *50* (4), 951-954.
33. Wei, S.; Yang, Y.; Kang, X.; Wang, L.; Huang, L.; Pan, D., Room-Temperature and Gram-Scale Synthesis of CsPbX₃ (X = Cl, Br, I) Perovskite Nanocrystals with 50–85% Photoluminescence Quantum Yields. *Chem. Commun.* **2016**, *52* (45), 7265-7268.
34. ten Brinck, S.; Infante, I., Surface Termination, Morphology, and Bright Photoluminescence of Cesium Lead Halide Perovskite Nanocrystals. *ACS Energy Lett.* **2016**, *1* (6), 1266-1272.
35. The CsPbBr₃ NCs first reduce the DCM solvent ($E_{red} = -1.04$ V vs. SCE) to the respective chloromethyl radical and chloride anion, then oxidize the bromide anion from its own surface to Br radical. Meanwhile, the chloride anion compensates for the loss of halide from perovskite, making it towards CsPbCl₃. However, since the Br· generation here is very minimum and is not

sustainable, only a trace amount of [3+2] cycloaddition product was detected. The Br in this case can only come from the NCs itself.

36. Argyle, M. D.; Bartholomew, C. H., Heterogeneous Catalyst Deactivation and Regeneration: A Review. *Catalysts* **2015**, *5* (1), 145-269.
37. Kariofillis, S. K.; Jiang, S.; Żurański, A. M.; Gandhi, S. S.; Martinez Alvarado, J. I.; Doyle, A. G., Using Data Science To Guide Aryl Bromide Substrate Scope Analysis in a Ni/Photoredox-Catalyzed Cross-Coupling with Acetals as Alcohol-Derived Radical Sources. *J. Am. Chem. Soc.* **2022**, *144* (2), 1045-1055.
38. Huang, H.; Zhao, F.; Liu, L.; Zhang, F.; Wu, X.-g.; Shi, L.; Zou, B.; Pei, Q.; Zhong, H., Emulsion Synthesis of Size-Tunable CH₃NH₃PbBr₃ Quantum Dots: An Alternative Route toward Efficient Light-Emitting Diodes. *ACS Appl. Mater. Interfaces* **2015**, *7* (51), 28128-28133.
39. Bowman, R. K.; Johnson, J. S., Nickel-Catalyzed Rearrangement of 1-Acyl-2-vinylcyclopropanes. A Mild Synthesis of Substituted Dihydrofurans. *Org. Lett.* **2006**, *8* (4), 573-576.
40. Wei, F.; Ren, C.-L.; Wang, D.; Liu, L., Highly Enantioselective [3+2] Cycloaddition of Vinylcyclopropane with Nitroalkenes Catalyzed by Palladium(0) with a Chiral Bis(tert-amine) Ligand. *Chem. Eur. J.* **2015**, *21* (6), 2335-2338.
41. Wang, D.; Cao, F.-R.; Lu, G.; Ren, J.; Zeng, B.-B., Practical Acetalization and Transacetalization of Carbonyl Compounds Catalyzed by Recyclable PVP-I. *Tetrahedron* **2021**, *92*, 132250.
42. Kotke, M.; Schreiner, P. R., Acid-Free, Organocatalytic Acetalization. *Tetrahedron* **2006**, *62* (2), 434-439.
43. Bogdan, A. R.; Poe, S. L.; Kubis, D. C.; Broadwater, S. J.; McQuade, D. T., The Continuous-Flow Synthesis of Ibuprofen. *Angew. Chem. Intl. Ed.* **2009**, *48* (45), 8547-8550.
44. Rosen, B. M.; Huang, C.; Percec, V., Sequential Ni-Catalyzed Borylation and Cross-Coupling of Aryl Halides via in Situ Prepared Neopentylglycolborane. *Org. Lett.* **2008**, *10* (12), 2597-2600.
45. Canestrari, D.; Cioffi, C.; Biancofiore, I.; Lancianesi, S.; Ghisu, L.; Ruether, M.; O'Brien, J.; Adamo, M. F. A.; Ibrahim, H., Sulphide as a Leaving Group: Highly Stereoselective Bromination of Alkyl Phenyl Sulphides. *Chem. Sci.* **2019**, *10* (39), 9042-9050.
46. Wilson, K. L.; Murray, J.; Jamieson, C.; Watson, A. J. B., Cyrene as a Bio-Based Solvent for the Suzuki–Miyaura Cross-Coupling. *Synlett* **2018**, *29* (05), 650-654.
47. Song, S.; Sun, X.; Li, X.; Yuan, Y.; Jiao, N., Efficient and Practical Oxidative Bromination and Iodination of Arenes and Heteroarenes with DMSO and Hydrogen Halide: A Mild Protocol for Late-Stage Functionalization. *Org. Lett.* **2015**, *17* (12), 2886-2889.

48. Bellesia, F.; Ghelfi, F.; Grandi, R.; Pagnoni, U. M.; Pinetti, A., The Reaction of Pyrroles with Trimethylhalosilanes-Dialkyl Sulfoxides. *J. Heterocyclic Chem.* **1993**, *30* (3), 617-621.
49. Molander, G. A.; Cavalcanti, L. N., Metal-Free Chlorodeboronation of Organotrifluoroborates. *J. Org. Chem.* **2011**, *76* (17), 7195-7203.
50. Feng, Y.; Luo, H.; Zheng, W.; Matsunaga, S.; Lin, L., Light-Promoted Nickel-Catalyzed Aromatic Halogen Exchange. *ACS Catal.* **2022**, *12* (18), 11089-11096.
51. Liu, Q.; Li, G.; He, J.; Liu, J.; Li, P.; Lei, A., Palladium-Catalyzed Aerobic Oxidative Carbonylation of Arylboronate Esters under Mild Conditions. *Angew. Chem. Intl. Ed.* **2010**, *49* (19), 3371-3374.
52. Song, X.; Meng, S.; Zhang, H.; Jiang, Y.; Chan, A. S. C.; Zou, Y., Dibrominated Addition and Substitution of Alkenes Catalyzed by $Mn_2(CO)_{10}$. *Chem. Commun.* **2021**, *57* (98), 13385-13388.
53. Ryu, I.; Matsubara, H.; Yasuda, S.; Nakamura, H.; Curran, D. P., Phase-Vanishing Reactions that Use Fluorous Media as a Phase Screen. Facile, Controlled Bromination of Alkenes by Dibromine and Dealkylation of Aromatic Ethers by Boron Tribromide. *J. Am. Chem. Soc.* **2002**, *124* (44), 12946-12947.
54. Yao, M.-L.; Reddy, M. S.; Yong, L.; Walfish, I.; Blevins, D. W.; Kabalka, G. W., Chemoselective Bromodeboronation of Organotrifluoroborates Using Tetrabutylammonium Tribromide: Application in (Z)-Dibromoalkene Syntheses. *Org. Lett.* **2010**, *12* (4), 700-703.

Chapter 5 Summary and Outlook

5.1 Dissertation Summary

This dissertation leverages the unique photophysical and photochemical properties of lead-halide perovskite photovoltaic material into the field of visible-light photocatalysis. Specifically, this dissertation describes the application of heterogeneous semiconductor-based lead-halide perovskite nanocrystals as efficient photocatalysts for three types of visible-light-driven ring-forming reactions: 1) Redox-neutral N-heterocyclization for the syntheses of pyrroles and pyrazoles; 2) Triplet-energy-transfer-mediated surface-templated [2+2] cycloaddition for the synthesis of HH-*syn*-cyclobutanes; 3) Br radical-mediated ring-opening [3+2] cycloaddition for the synthesis of vinylcyclopentanes.

The first project detailed in **Chapter 2** extended our initial work on LHP for photocatalytic α -alkylation of aldehydes. A key intermediate for the Hantzsch pyrrole synthesis can be formed through radical addition of the electron-transfer-generated α -ketone radical to a stable enamine, thus a mild radical-based methodology for pyrrole synthesis can be achieved photocatalytically by LHP NCs. The key radical intermediates were verified via radical trapping experiments in support of our proposed mechanism. Furthermore, the reaction partner was further extended from the stable enamine radical acceptor to a hydrazone in this photocatalytic system which successfully led to the production of another important pharmaceutical ingredient, *i.e.*, a pyrazole scaffold. The substrate scopes for both N-heterocyclization reactions were explored systematically, paving the road for potential application of this strategy in drug discovery.

The second project detailed in **Chapter 3** harnessed the triplet energy of LHP NCs for the first time for photocatalytic organic synthesis, namely, triplet-energy-transfer-mediated [2+2] cycloaddition of 4-vinylbenzoic acid derivatives. The carboxyl group on the substrates was found

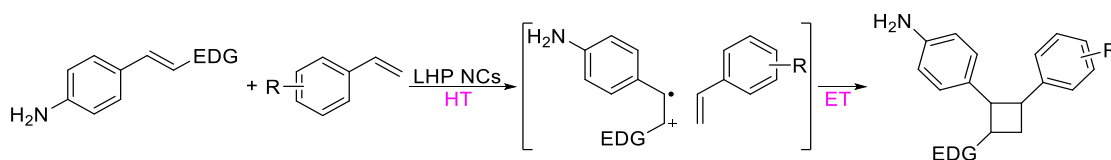
to be responsible for an efficient triplet energy transfer event via surface anchoring on the perovskite NCs, which was corroborated by IR qualitative analysis and ^1H NMR quantitative analysis. An array of highly selective HH-*syn*-cyclobutanes were produced in synthetically useful yields as a result of the surface-templated catalysis. Our approach demonstrates a distinct reaction pathway by using a heterogeneous solid photocatalyst as opposed to the commonly studied homogeneous molecular photocatalysts. Furthermore, collaborating with NREL, a triplet-energy-transfer rate of ~ 110 ps and a moderate fraction of *ca.* 13-20% NCs undergoing such triplet energy transfer process were demonstrated for representative substrates by ultra-fast transient absorption spectroscopy. The origin of the diastereoselectivity was also illustrated by DFT calculations where the *syn*-binding mode showed noticeable stabilization enthalpy compared to the *anti*-binding mode throughout the cycloaddition process.

The third project detailed in **Chapter 4** discovered a continuous generation of Br radicals from the underexplored hole transfer process in the visible-light-induced halide exchange between CsPbBr_3 perovskite NCs and alkyl bromide organic solvents, rendering an easy-to-handle Br radical reservoir. Br radical produced in such a mild photoredox pathway was employed for a Br-mediated ring-opening [3+2] cycloaddition of vinylcyclopropanes and alkenes for the synthesis of a library of $\text{C}(\text{sp}^3)$ -enriched vinylcyclopentanes (20 distinctive examples). The CsPbBr_3 NCs photocatalysts maintained high catalytic performance during catalyst recycling experiments, hence were highly recyclable probably due to the surface defect healing resulting from the bromide exchange. The versatility of the Br radicals generated by this method was further demonstrated by successful aromatic bromination, benzylic bromination, and hydrogen atom transfer of structurally diverse substrates respectively.

5.2 Future Directions and Outlook

5.2.1 Charge-Transfer-Based [2+2] Cycloaddition

As discussed in **Chapter 2**, amino-containing substrate **9** and **10** failed to undergo TET-mediated [2+2] cycloaddition even though strong quenching constants were shown. We reasoned that the hole transfer (HT) process was dominant between these substrates and LHP NCs. In fact, charge-transfer-based [2+2] cycloadditions were reported in many other photocatalytic systems with focus on 4-vinylaniline substrates.¹ Here, I propose that an electron rich 4-vinylaniline derivative can undergo single electron oxidation by hole transfer from LHP NCs, hence attaining an oxidative [2+2] cycloaddition with another styrene molecule. Such strategy may provide a complementary substrate scope to the carboxyl group (electron deficient) limiting TET-based [2+2] cycloaddition. Additionally, amines are known to be good surface ligands to LHP NCs, this charge-transfer-based [2+2] cycloaddition may also proceed through a surface-templated mechanism thus provide products with high selectivity.

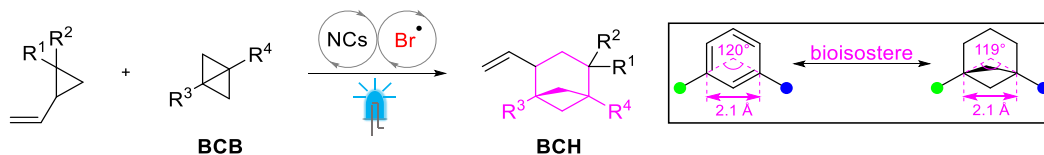


Scheme 5.1 Proposed hole-transfer-initiated [2+2] cycloaddition of 4-vinylaniline derivatives photocatalyzed by LHP NCs. EDG: electron-donating group. HT: hole transfer. ET: electron transfer.

5.2.2 Synthesis of Bioisosteres of *meta*-Substituted Benzenes via Br Radical-Mediated Ring-Opening [3+2] Cycloaddition

The replacement of benzene in drug candidates with saturated bioisosteres generally improves their pharmacokinetics without affecting the biological activity.^{2, 3} Strained, rigid scaffold such as bicyclo[3.1.1]heptane (BCH) provides a close geometric match to *meta*-substituted benzenes.⁴ To date, the facile preparative method for BCH is still limited. I hypothesize that our established Br radical-mediated ring opening [3+2] cycloaddition can be leveraged for the

construction of BCH by changing the alkene coupling partner to bicyclo[1.1.0]butane (BCB). The weak central C-C bond of BCB was reported to resemble a π -bond and its reactivity has been harnessed in concerted cycloaddition.⁵ Here, under visible light irradiation, LHP NCs can generate Br radicals in alkylbromide solvent. Upon Br radical addition, the vinylcyclopropane may undergo ring opening and rapid [3+2] cycloaddition with BCB to afford BCH.



Scheme 5.2 Proposed pathway for construction of BCH via LHP NCs-photocatalyzed Br radical-mediated ring-opening [3+2] cycloaddition of vinylcyclopropane and BCB.

5.2.3 Outlook

In this dissertation, I first showed that the fundamental photoinduced charge transfer capability of LHP NCs could be utilized for a redox-neutral radical-based Hantzsch-type cyclization. Then, I took advantage of the surface binding interaction of LHP NCs with carboxyl-containing substrates to enable a highly selective triplet-energy-transfer-mediated [2+2] cycloaddition. In the last project, I showed that the photoinduced dynamic bromide-exchange of CsPbBr₃ NCs with bromoalkane solvent generates Br radicals, which can be further utilized for a Br radical-mediated ring-opening [3+2] cycloaddition. The works presented here not only show that the homogeneous noble metal-based photocatalysts could be replaced by recyclable heterogeneous LHP NCs photocatalysts, but also highlight the distinctive photochemical selectivity and reactivity achieved by leveraging the unique properties (e.g., surface binding, bromide-exchange) of LHP NCs.

In addition to the binding interaction and halide component of LHP NCs, one may logically consider to exploit the ligand and/or A-site component of LHP NCs to achieve other interesting LHP NCs-photocatalyzed ring-forming reactions. Whilst exploring new methodologies for

syntheses of pharmaceutically important cyclic scaffolds is indispensable, in a practical perspective, an LHP NCs photocatalytic reaction on a large preparative scale has yet to be achieved. Developing a suitable continuous flow protocol would be an appealing solution to this while leveraging the heterogeneous nature of LHP NCs photocatalysts, e.g., immobilizing the photocatalysts in the reactor. We believe that this dissertation will inspire and facilitate more exciting design and development of heterogeneous visible-light-driven ring-forming reactions and beyond through lead-halide perovskite photocatalysis.

5.3 Reference

1. Ischay, M. A.; Lu, Z.; Yoon, T. P., [2+2] Cycloadditions by Oxidative Visible Light Photocatalysis. *J. Am. Chem. Soc.* **2010**, *132* (25), 8572-8574.
2. Subbaiah, M. A. M.; Meanwell, N. A., Bioisosteres of the Phenyl Ring: Recent Strategic Applications in Lead Optimization and Drug Design. *J. Med. Chem.* **2021**, *64* (19), 14046-14128.
3. Mykhailiuk, P. K., Saturated Bioisosteres of Benzene: Where to Go Next? *Org. Biomol. Chem.* **2019**, *17* (11), 2839-2849.
4. Iida, T.; Kanazawa, J.; Matsunaga, T.; Miyamoto, K.; Hirano, K.; Uchiyama, M., Practical and Facile Access to Bicyclo[3.1.1]heptanes: Potent Bioisosteres of meta-Substituted Benzenes. *J. Am. Chem. Soc.* **2022**, *144* (48), 21848-21852.
5. Golfmann, M.; Walker, J. C. L., Bicyclobutanes as Unusual Building Blocks for Complexity Generation in Organic Synthesis. *Commun. Chem.* **2023**, *6* (1), 9.

Appendix A. DFT Geometries

Cartesian coordinates for structures of computation shown in **Section 3.5.13**:

	NC		
Pb	-5.05017400	3.13168000	-0.93890200
Pb	-8.18181100	-1.91842900	-0.93890200
Pb	-0.00006500	0.00004300	-0.93890200
Pb	-3.13170200	-5.05006600	-0.93890200
Br	-0.00006500	0.00004300	2.03224100
Br	-5.05017400	3.13168000	2.03224100
Br	-2.52511900	1.56586200	-0.93890200
Br	-3.13170200	-5.05006600	2.03224100
Br	-8.18181100	-1.91842900	2.03224100
Br	-5.65675700	-3.48424800	-0.93890200
Br	-1.56588300	-2.52501200	-0.93890200
Br	-6.61599300	0.60662600	-0.93890200
Cs	-4.09093800	-0.95919300	2.03224100
Cs	0.95917100	-4.09083000	2.03224100
Pb	5.05703400	-3.13600500	-0.93890200
Pb	1.91840700	-8.18170300	-0.93890200
Br	5.05004400	-3.13159400	2.03224100
Br	1.91840700	-8.18170300	2.03224100
Br	3.47098900	-5.64839200	-0.93890200
Br	2.52499000	-1.56577600	-0.93890200
Br	-0.60664700	-6.61588500	-0.93890200
Pb	8.18168200	1.91851500	-0.93890200
Pb	3.13157200	5.05015200	-0.93890200
Pb	-1.91853700	8.18178900	-0.93890200
Br	0.60651800	6.61597100	-0.93890200
Br	-3.48435500	5.65673500	-0.93890200
Br	5.65662700	3.48433400	-0.93890200
Br	6.61586300	-0.60654000	-0.93890200
Br	1.56575400	2.52509800	-0.93890200
Cs	4.09080800	0.95927900	2.03224100
Cs	-0.95930100	4.09091600	2.03224100
Br	8.18168200	1.91851500	2.03224100
Br	3.13157100	5.05015300	2.03224100
Br	-1.91853600	8.18178900	2.03224100
Br	-4.44358973	9.74760559	-0.93890200
Br	-7.57522673	4.69749659	-0.93890200
Br	-10.70686301	-0.35261124	-0.93890200

Br	-9.74762759	-4.44348173	-0.93890200
Br	-4.69751976	-7.57511801	-0.93890200
Br	0.36586920	-10.71494189	-0.93890200
Br	4.44345945	-9.74752004	-0.93890200
Br	7.58205232	-4.70187708	-0.93890200
Br	10.70673428	0.35269768	-0.93890200
Br	9.74749932	4.44356728	-0.93890200
Br	4.69738904	7.57520445	-0.93890200
Br	-0.35271996	10.70684145	-0.93890200
Cs	-9.14105124	2.17244663	2.03224100
Cs	-6.00941424	7.22255563	2.03224100
Cs	9.14092124	-2.17236063	2.03224100
Cs	6.00928424	-7.22246963	2.03224100
Cs	-2.17246863	-9.14094324	2.03224100
Cs	-7.22257763	-6.00930624	2.03224100
Cs	2.17233863	9.14102924	2.03224100
Cs	7.22244763	6.00939224	2.03224100
Cs	12.27256086	2.87775261	2.03224100
Cs	-2.87777461	12.27266886	2.03224100
Cs	-12.27269086	-2.87766661	2.03224100
Cs	2.87764461	-12.27258286	2.03224100

NC- <i>syn</i> -7a+7a			
Pb	5.92214100	0.35347900	-1.85843200
Pb	5.61195800	6.28728200	-1.79115400
Pb	-0.01201500	0.04310800	-1.84349500
Pb	-0.32219800	5.97691100	-1.77621600
Br	-0.00279900	0.00990500	1.12744900
Br	5.93135500	0.32027600	1.11251200
Br	2.95506200	0.19829300	-1.85096300
Br	-0.31298200	5.94370800	1.19472700
Br	5.62117300	6.25407900	1.17979000
Br	2.64488000	6.13209700	-1.78368600
Br	-0.16710700	3.01000900	-1.80985600
Br	5.76705000	3.32038000	-1.82479200
Cs	2.80918700	3.13199200	1.15362000
Cs	-3.12496900	2.82162200	1.16855700
Pb	-5.95442800	-0.26762900	-1.82853600
Pb	-6.25635300	5.66654000	-1.76127800
Br	-5.93695500	-0.30046600	1.14238700
Br	-6.24713800	5.63333700	1.20966400

Br	-6.08568100	2.70041300	-1.79495800
Br	-2.97909400	-0.11207700	-1.83602600
Br	-3.28927700	5.82172600	-1.76874800
Pb	-5.63598800	-6.20106600	-1.89583400
Pb	0.29816800	-5.89069500	-1.91077300
Pb	6.23232400	-5.58032500	-1.92571000
Br	3.26524600	-5.73551000	-1.91824000
Br	6.07723200	-2.61342300	-1.89207000
Br	-2.66891000	-6.04588100	-1.90330400
Br	-5.79107900	-3.23416300	-1.86219600
Br	0.14307700	-2.92379400	-1.87713400
Cs	-2.81478700	-3.11218200	1.10127900
Cs	3.11937000	-2.80181100	1.08634200
Br	-5.62677300	-6.23426900	1.07510900
Br	0.30738400	-5.92389800	1.06017100
Br	6.24153800	-5.61352700	1.04523400
Br	9.19939900	-5.42513800	-1.93317800
Br	8.88921600	0.50866500	-1.86590000
Br	8.57903300	6.44246600	-1.79862200
Br	5.45686600	9.25418100	-1.75751500
Br	-0.47728800	8.94381000	-1.74257800
Br	-6.42702100	8.63258300	-1.72760100
Br	-9.22342900	5.51135500	-1.75381000
Br	-8.92150600	-0.42275000	-1.82106600
Br	-8.60306300	-6.35625100	-1.88836600
Br	-5.48089700	-9.16796600	-1.92947400
Br	0.45325900	-8.85759400	-1.94441100
Br	6.38741500	-8.54722300	-1.95934800
Cs	8.74334700	3.44236300	1.13868200
Cs	9.05353000	-2.49144000	1.07140400
Cs	-8.74894700	-3.42255300	1.11621700
Cs	-9.05913000	2.51125000	1.18349400
Cs	-3.43515200	8.75543000	1.23583500
Cs	2.49900300	9.06580000	1.22089700
Cs	3.42955200	-8.73561900	1.01906300
Cs	-2.50460300	-9.04599000	1.03400200
Cs	-8.43876400	-9.35636100	1.04893900
Cs	9.36371400	-8.42524800	1.00412500
Cs	8.43316400	9.37617100	1.20596000
Cs	-9.36931200	8.44505800	1.25077200
C	1.58507000	1.18805100	6.16917100

C	1.66354400	0.00237700	5.42588700
C	1.77126400	-1.21912800	6.11375700
C	1.80006200	-1.25945700	7.50131800
C	1.72136900	-0.06713300	8.26046100
C	1.61323000	1.15665800	7.56013100
H	1.50234200	2.11626500	5.59912400
H	1.82975400	-2.11818900	5.49580200
H	1.88434600	-2.22079500	8.01600800
H	1.55166000	2.08544600	8.13717800
C	1.74647400	-0.04527000	9.70945200
H	1.67823900	0.94353800	10.17921200
C	1.84360800	-1.08825400	10.57386400
H	1.91696700	-2.11741500	10.21124100
O	1.77832300	0.22303400	12.55912400
C	1.82058800	0.12701200	3.88052400
O	1.96294900	-0.96041100	3.28246300
O	1.78339400	1.29641300	3.44471100
C	1.85410200	-0.87726500	12.02917300
C	1.96783100	-2.13788200	12.87902100
H	2.59233400	-2.89026800	12.36844000
H	0.97393100	-2.59347500	13.02522100
H	2.40883300	-1.88941600	13.85343500
C	-1.63850200	0.99757400	6.14785300
C	-1.56002800	-0.18810000	5.40456900
C	-1.45230800	-1.40960500	6.09243900
C	-1.42351000	-1.44993400	7.48000000
C	-1.50220300	-0.25761000	8.23914300
C	-1.61034200	0.96618100	7.53881300
H	-1.72123000	1.92578800	5.57780700
H	-1.39381900	-2.30866600	5.47448400
H	-1.33922600	-2.41127200	7.99469000
H	-1.67191200	1.89496800	8.11586000
C	-1.47709800	-0.23574800	9.68813500
H	-1.54533300	0.75306100	10.15789500
C	-1.37996400	-1.27873100	10.55254700
H	-1.30660500	-2.30789200	10.18992300
O	-1.44524900	0.03255700	12.53780700
C	-1.81655600	-0.13266100	3.86851500
O	-1.81206800	-1.24476300	3.29962000
O	-1.99253600	1.01512900	3.40979400
C	-1.36947000	-1.06774300	12.00785600

C	-1.25574100	-2.32835900	12.85770400
H	-0.63570300	-3.08278400	12.34469500
H	-2.25033100	-2.78095800	13.00843600
H	-0.80974400	-2.08081800	13.83007800

NC- <i>anti-7a+7a</i>			
Pb	5.72661000	1.55296000	-1.85782600
Pb	4.17929500	7.29024500	-1.84610400
Pb	-0.01066400	0.00562000	-1.84442300
Pb	-1.55798000	5.74290400	-1.83270100
Br	-0.00266700	0.00170700	1.12670700
Br	5.73460600	1.54904700	1.11330400
Br	2.85797300	0.77928900	-1.85112400
Br	-1.54998200	5.73899100	1.13842900
Br	4.18729100	7.28633100	1.12502500
Br	1.31065800	6.51657400	-1.83940400
Br	-0.78432200	2.87426200	-1.83856200
Br	4.95295300	4.42160200	-1.85196500
Cs	2.09231300	3.64401900	1.12586700
Cs	-3.64496300	2.09667900	1.13927000
Pb	-5.75593600	-1.54380900	-1.83100000
Pb	-7.29525400	4.19556400	-1.81929700
Br	-5.73994100	-1.54563400	1.14011200
Br	-7.28725700	4.19165100	1.15183200
Br	-6.50652300	1.33094500	-1.82519400
Br	-2.87930200	-0.76805000	-1.83772100
Br	-4.42661800	4.96923400	-1.82600000
Pb	-4.20062400	-7.27900500	-1.84274000
Pb	1.53665200	-5.73166500	-1.85614400
Pb	7.27392600	-4.18432500	-1.86954700
Br	4.40528800	-4.95799600	-1.86284400
Br	6.50026800	-1.31568300	-1.86368600
Br	-1.33198600	-6.50533500	-1.84944200
Br	-4.97428100	-4.41036200	-1.83688000
Br	0.76299500	-2.86302300	-1.85028400
Cs	-2.09764800	-3.64060600	1.12754900
Cs	3.63962800	-2.09326600	1.11414600
Br	-4.19262700	-7.28291900	1.12839000
Br	1.54464900	-5.73557800	1.11498600
Br	7.28192100	-4.18823900	1.10158300
Br	10.14256000	-3.41065500	-1.87624900

Br	8.59524500	2.32663000	-1.86452700
Br	7.04792900	8.06391300	-1.85280600
Br	3.40563800	10.15888400	-1.84024400
Br	-2.33163500	8.61154400	-1.82684100
Br	-8.08396200	7.06010200	-1.81340200
Br	-10.16388800	3.42189500	-1.81259500
Br	-8.62458600	-2.31741700	-1.82429900
Br	-7.06925800	-8.05267500	-1.83603800
Br	-3.42696600	-10.14764600	-1.84860100
Br	2.31030700	-8.60030500	-1.86200400
Br	8.04758300	-7.05296500	-1.87540700
Cs	7.82959100	5.19136100	1.11246300
Cs	9.37690600	-0.54592500	1.10074200
Cs	-7.83492600	-5.18794800	1.14095300
Cs	-9.38224100	0.54933800	1.15267300
Cs	-5.19227900	7.83396900	1.15099200
Cs	0.54499500	9.38130800	1.13758700
Cs	5.18694400	-7.83055600	1.10242400
Cs	-0.55033000	-9.37789500	1.11582800
Cs	-6.28761000	-10.92523600	1.12923100
Cs	10.92422400	-6.28321400	1.08902000
Cs	6.28227500	10.92864900	1.12418400
Cs	-10.92955700	6.28662700	1.16439500
C	1.28942400	1.53167200	6.15840900
C	1.61669000	0.38218400	5.42627100
C	1.97622300	-0.78338300	6.12557900
C	2.00911100	-0.80434500	7.51347700
C	1.68019300	0.35174100	8.26141100
C	1.31980500	1.51934400	7.54962200
H	1.01549200	2.41677300	5.57967200
H	2.22353200	-1.65570500	5.51607700
H	2.29165600	-1.72200200	8.03717000
H	1.06336200	2.41971800	8.11793800
C	1.69626900	0.39136200	9.71015500
H	1.42101500	1.34806300	10.17062400
C	2.00755500	-0.60029500	10.58432600
H	2.29599000	-1.59441500	10.23136800
O	1.66352000	0.68590300	12.55722400
C	1.74826600	0.52312000	3.87993000
O	2.11701500	-0.51560900	3.29214000
O	1.46793800	1.65478700	3.43320600

C	1.96968200	-0.37876400	12.03761100
C	2.34285400	-1.57986200	12.89926000
H	3.11256500	-2.18915400	12.39618200
H	1.46614800	-2.23236000	13.04895900
H	2.71935800	-1.23574700	13.87164400
C	-1.82253300	0.66946700	6.13646300
C	-1.49526700	-0.48002000	5.40432500
C	-1.13573400	-1.64558700	6.10363400
C	-1.10284600	-1.66654900	7.49153100
C	-1.43176300	-0.51046400	8.23946600
C	-1.79215100	0.65714000	7.52767600
H	-2.09646400	1.55456800	5.55772700
H	-0.88842500	-2.51790900	5.49413200
H	-0.82030100	-2.58420600	8.01522500
H	-2.04859400	1.55751300	8.09599300
C	-1.41568800	-0.47084200	9.68820900
H	-1.11735800	-1.44993000	10.08249100
C	-1.67798600	0.47328900	10.62856800
H	-1.98362800	1.48410300	10.34416200
O	-1.22989300	-0.91386400	12.51006000
C	-1.75359300	-0.49335500	3.86762900
O	-1.51455800	-1.58485600	3.30913100
O	-2.16503100	0.58788100	3.39809600
C	-1.56212200	0.17609300	12.06411600
C	-1.88659700	1.32994500	13.00628100
H	-2.67765200	1.96671100	12.57553500
H	-1.00062200	1.97190300	13.14669200
H	-2.21579400	0.93487900	13.97646200

NC+ <i>syn</i> -7aa			
Pb	5.92934700	0.31885500	-1.82884000
Pb	5.56587900	6.24964900	-1.89464100
Pb	-0.00170500	-0.04514900	-1.82099400
Pb	-0.36527900	5.88624600	-1.88680200
Br	-0.00072700	-0.01059800	1.14630900
Br	5.93124700	0.35193400	1.14211800
Br	2.96376000	0.13726800	-1.82492300
Br	-0.36337800	5.91932400	1.08415700
Br	5.56777900	6.28272700	1.07631800
Br	2.60030000	6.06794700	-1.89072300
Br	-0.18360600	2.92084500	-1.85390100

Br	5.74761400	3.28425100	-1.86174000
Cs	2.78469400	3.13470200	1.11429400
Cs	-3.14751700	2.77139100	1.12194000
Pb	-5.94123900	-0.40841600	-1.81315100
Pb	-6.29643600	5.52284300	-1.87896200
Br	-5.93096400	-0.37476800	1.15774100
Br	-6.29453600	5.55592100	1.09199100
Br	-6.09913700	2.55835500	-1.84608600
Br	-2.96739000	-0.22626000	-1.81708100
Br	-3.33085900	5.70454500	-1.88288300
Pb	-5.56950200	-6.33874500	-1.74736000
Pb	0.36165700	-5.97534300	-1.75520000
Pb	6.29281400	-5.61194000	-1.76303900
Br	3.32723500	-5.79364100	-1.75911900
Br	6.11108000	-2.64654200	-1.79594000
Br	-2.60392200	-6.15704500	-1.75128000
Br	-5.75123100	-3.37334600	-1.78026200
Br	0.17999200	-3.00994200	-1.78810100
Cs	-2.78406600	-3.15792900	1.18768500
Cs	3.14789800	-2.79446400	1.17958600
Br	-5.56760200	-6.30566800	1.22359700
Br	0.36355800	-5.94226300	1.21575800
Br	6.29471400	-5.57886100	1.20791900
Br	9.25839100	-5.43023700	-1.76695900
Br	8.89492400	0.50055700	-1.83276000
Br	8.53145500	6.43134900	-1.89856100
Br	5.38414500	9.21504300	-1.92754200
Br	-0.54701200	8.85164000	-1.91970300
Br	-6.49373900	8.48724200	-1.91184200
Br	-9.26201500	5.34113800	-1.87504500
Br	-8.90680800	-0.59003600	-1.80922600
Br	-8.53508000	-6.52044500	-1.74344200
Br	-5.38776800	-9.30414100	-1.71446000
Br	0.54339000	-8.94073600	-1.72230000
Br	6.47454800	-8.57733400	-1.73013900
Cs	8.71509700	3.49903300	1.10529700
Cs	9.07856500	-2.43176200	1.17109800
Cs	-8.71491600	-3.52197400	1.19462700
Cs	-9.07840300	2.40880400	1.12884400
Cs	-3.51069100	8.70302600	1.05517700
Cs	2.42046600	9.06642800	1.04733600

Cs	3.51087000	-8.72596500	1.24473900
Cs	-2.42028800	-9.08936700	1.25257900
Cs	-8.35145000	-9.45277100	1.26041900
Cs	9.44203300	-8.36256100	1.23690000
Cs	8.35162900	9.42983100	1.03949700
Cs	-9.44185400	8.33962200	1.06301600
C	-2.49712500	-1.17411900	6.22477500
C	-2.46239500	-0.10073400	5.32474100
C	-1.87290100	1.09703100	5.74451800
C	-1.31034500	1.21299800	7.01553900
C	-1.34627100	0.14342400	7.92232400
C	-1.96472800	-1.04793100	7.50813800
H	-2.94426000	-2.10969900	5.88234400
H	-1.84758200	1.92703000	5.03666600
H	-0.81462400	2.14731200	7.28783600
H	-1.99928900	-1.89558200	8.20098600
C	-0.65351500	0.18728600	9.25141600
H	-1.17226500	-0.45403700	9.97894100
C	-0.29533500	1.53599600	9.92473700
H	-0.12013400	2.29541900	9.14609700
O	-0.89691400	2.50769200	12.02277900
C	-3.03364700	-0.23050100	3.90474100
O	-3.23022500	-1.40369100	3.49948100
O	-3.23729000	0.84985900	3.29985600
C	-1.25101700	2.14062500	10.91864300
C	-2.68431800	2.26588900	10.44808600
H	-3.11849100	1.25836900	10.33903300
H	-2.73053800	2.72237300	9.44705200
H	-3.26970700	2.84639600	11.17341000
C	2.13754500	-1.06708200	5.86727600
C	2.59185500	0.15648100	5.35781800
C	2.56175000	1.27462300	6.19811000
C	2.08113000	1.17924500	7.50688600
C	1.59749800	-0.03812600	8.00938600
C	1.64211700	-1.16024800	7.16555600
H	2.16593400	-1.93381000	5.20482100
H	2.90713600	2.22574900	5.78757000
H	2.06056900	2.07800200	8.12989600
H	1.25145400	-2.11424000	7.53232600
C	0.88994400	-0.17691200	9.32874800
H	1.04885900	-1.18096500	9.74501800

C	1.07354400	0.95551500	10.38190900
H	1.92953600	1.62577400	10.22704600
O	0.40241700	-0.52593500	12.13820800
C	3.07994500	0.26348800	3.90452600
O	3.27053000	-0.82654400	3.31314200
O	3.22859600	1.43015200	3.46090600
C	1.06317100	0.44005800	11.81356600
C	1.92778700	1.18654600	12.80464100
H	1.83680900	0.73234500	13.80017100
H	1.59024400	2.23355400	12.83631300
H	2.98093200	1.17634600	12.47720500

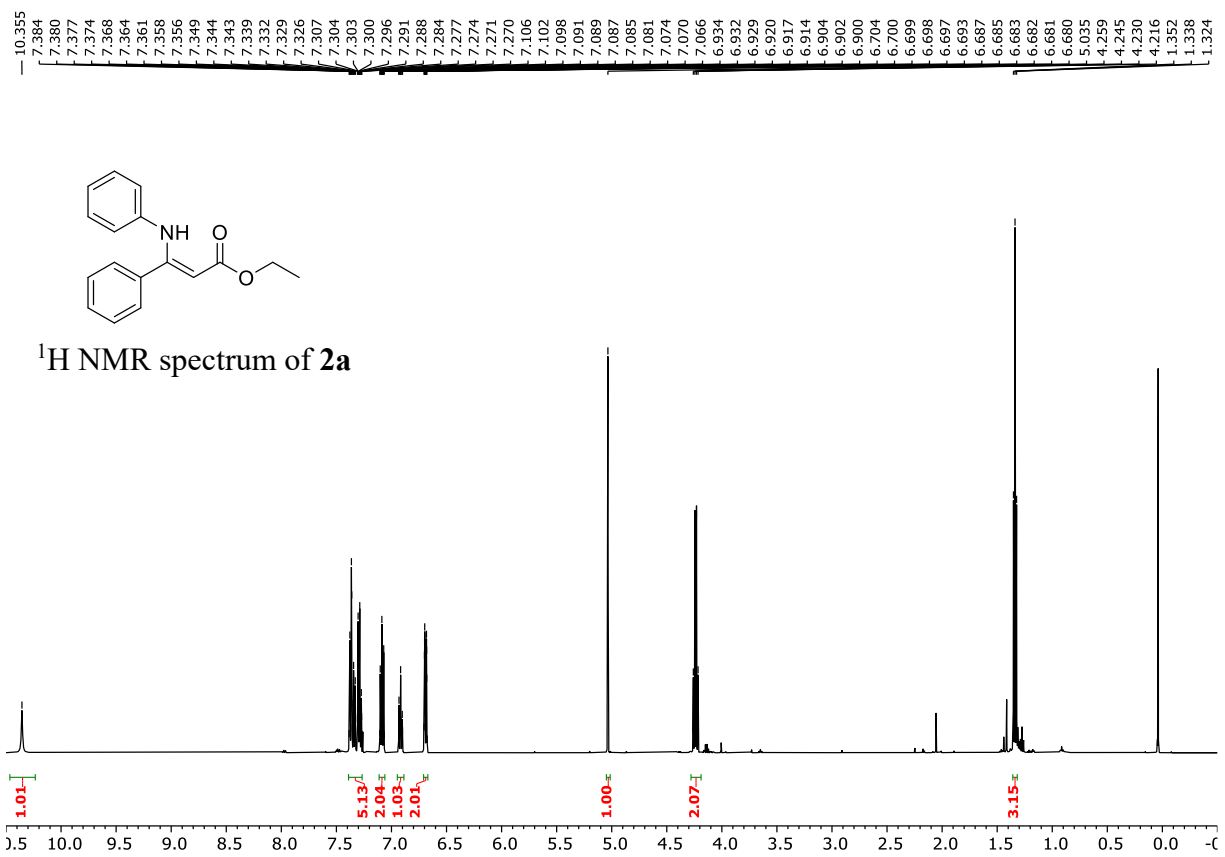
NC+ <i>anti-7aa</i>			
Pb	5.87163000	-0.91639200	-1.81783000
Pb	6.78796900	4.95483900	-1.81780100
Pb	0.00038900	-0.00062900	-1.81784500
Pb	0.91676200	5.87118700	-1.81781400
Br	-0.00019500	0.00103300	1.14965900
Br	5.87153800	-0.91626200	1.15327900
Br	2.93603500	-0.45807600	-1.81783700
Br	0.91675300	5.87117300	1.15332800
Br	6.78795800	4.95482600	1.15333900
Br	3.85236500	5.41301200	-1.81780900
Br	0.45852800	2.93559200	-1.81783000
Br	6.32980200	2.01923100	-1.81781800
Cs	3.39474500	2.47626700	1.15449200
Cs	-2.47751100	3.39300500	1.15426300
Pb	-5.87898300	0.91769500	-1.81785900
Pb	-4.95444400	6.78753500	-1.81782900
Br	-5.87056000	0.91620300	1.15314000
Br	-4.95445400	6.78752000	1.15330600
Br	-5.39721200	3.84948100	-1.81785000
Br	-2.93519100	0.45813800	-1.81785200
Br	-2.01884300	6.32936100	-1.81782200
Pb	-6.78714100	-4.95487800	-1.81788800
Pb	-0.91593200	-5.87122600	-1.81787500
Pb	4.95527200	-6.78757400	-1.81786100
Br	2.01966900	-6.32940100	-1.81786700
Br	5.41344200	-3.85196900	-1.81784600
Br	-3.85153700	-5.41305300	-1.81788100
Br	-6.32897400	-2.01926500	-1.81788000

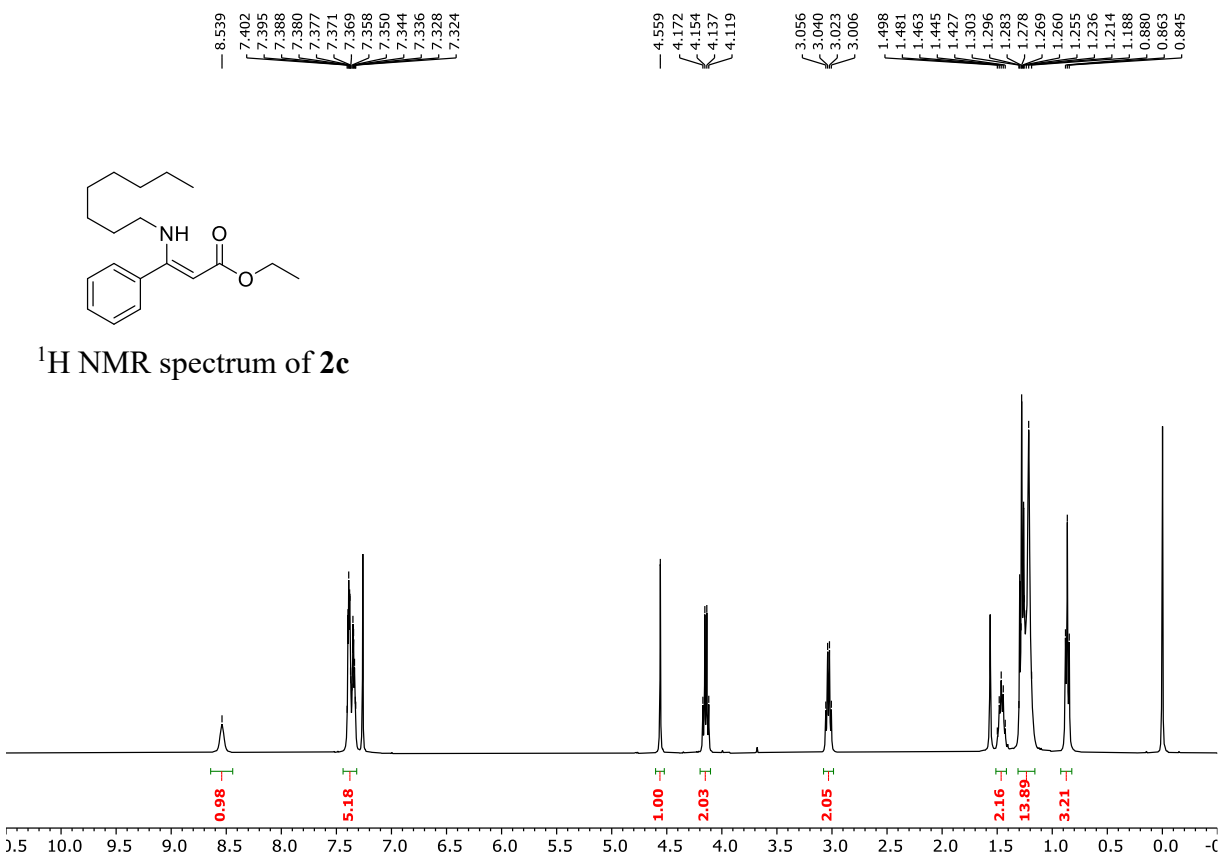
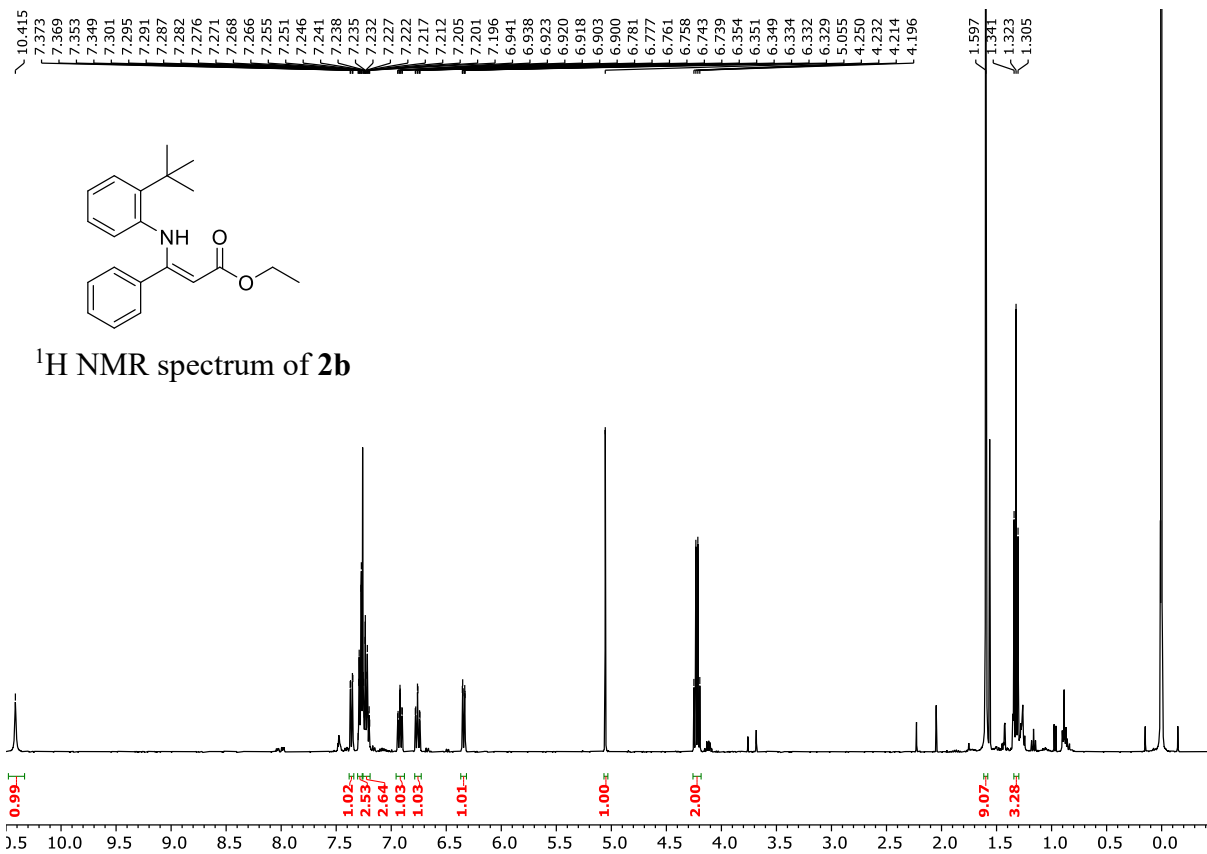
Br	-0.45769100	-2.93563400	-1.81786100
Cs	-3.39357600	-2.47669700	1.15424800
Cs	2.47847600	-3.39325600	1.15394200
Br	-6.78715000	-4.95489200	1.15324600
Br	-0.91594200	-5.87123900	1.15326800
Br	4.95526300	-6.78758700	1.15328200
Br	7.89087400	-7.24574500	-1.81785300
Br	8.80722500	-1.37454900	-1.81782000
Br	9.72356900	4.49666400	-1.81779600
Br	7.24614100	7.89044000	-1.81778600
Br	1.37493600	8.80678800	-1.81780100
Br	-4.51169100	9.72550100	-1.81781400
Br	-7.89004900	7.24570400	-1.81783900
Br	-8.81455200	1.37591300	-1.81785100
Br	-9.72274500	-4.49670000	-1.81790000
Br	-7.24531400	-7.89048000	-1.81790400
Br	-1.37410800	-8.80682500	-1.81788900
Br	4.49709900	-9.72317400	-1.81787500
Cs	9.26540300	1.56103600	1.15335000
Cs	8.34904700	-4.31015700	1.15330800
Cs	-9.26459800	-1.56109400	1.15330300
Cs	-8.34826000	4.31007400	1.15333100
Cs	-1.56067500	9.26495600	1.15333700
Cs	4.31053000	8.34860800	1.15335000
Cs	1.56148500	-9.26502200	1.15326100
Cs	-4.30972100	-8.34867400	1.15324800
Cs	-10.18093200	-7.43232500	1.15323400
Cs	7.43269700	-10.18136900	1.15327500
Cs	10.18174200	7.43225900	1.15336400
Cs	-7.43188600	10.18130400	1.15332300
C	-2.48355700	-1.00001100	5.75352100
C	-2.82175600	0.30050800	5.36425300
C	-2.63151500	1.34233000	6.28392600
C	-2.04806900	1.10229700	7.52907600
C	-1.61508700	-0.18829000	7.87914100
C	-1.87856400	-1.23855200	6.98564700
H	-2.64519300	-1.80241900	5.03214100
H	-2.89869100	2.35290200	5.96752000
H	-1.85677800	1.94011700	8.20751900
H	-1.53021500	-2.24580200	7.23474000
C	-0.64154400	-0.43551200	8.98887700

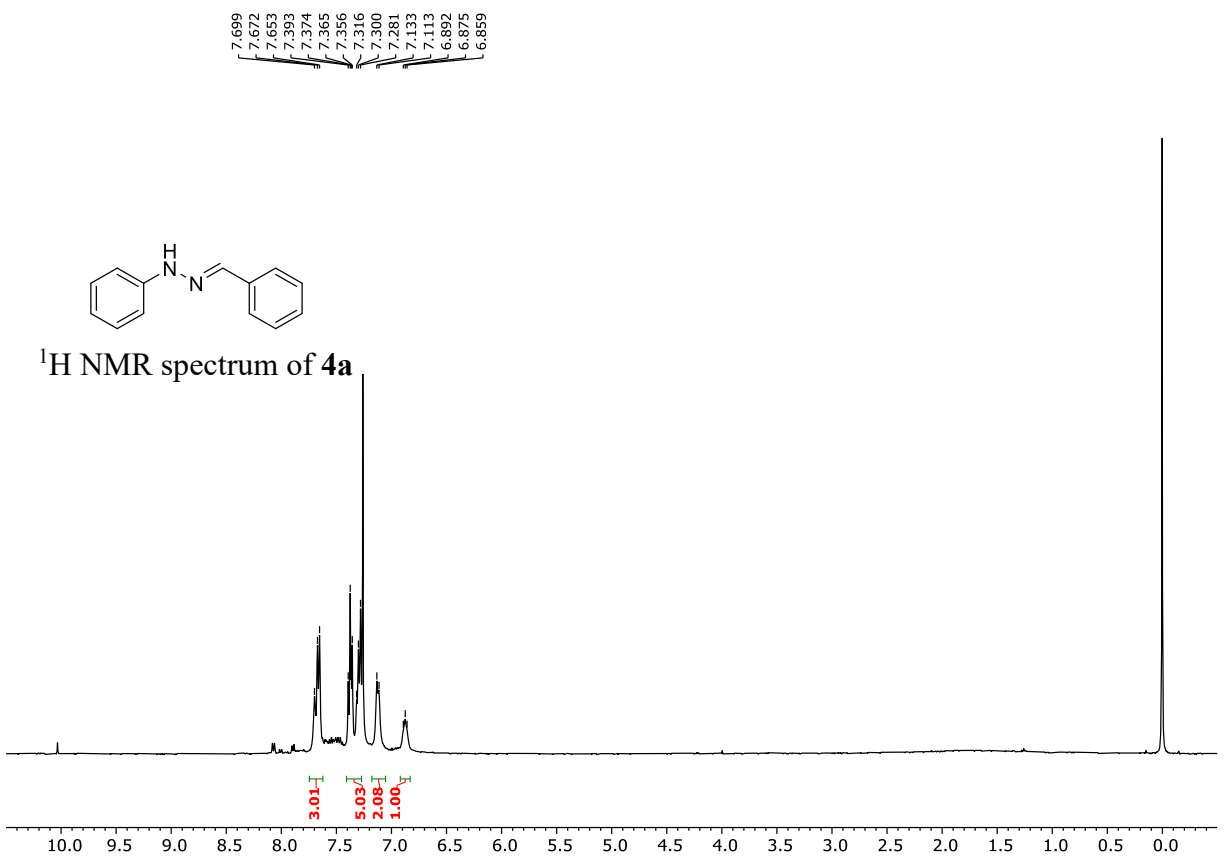
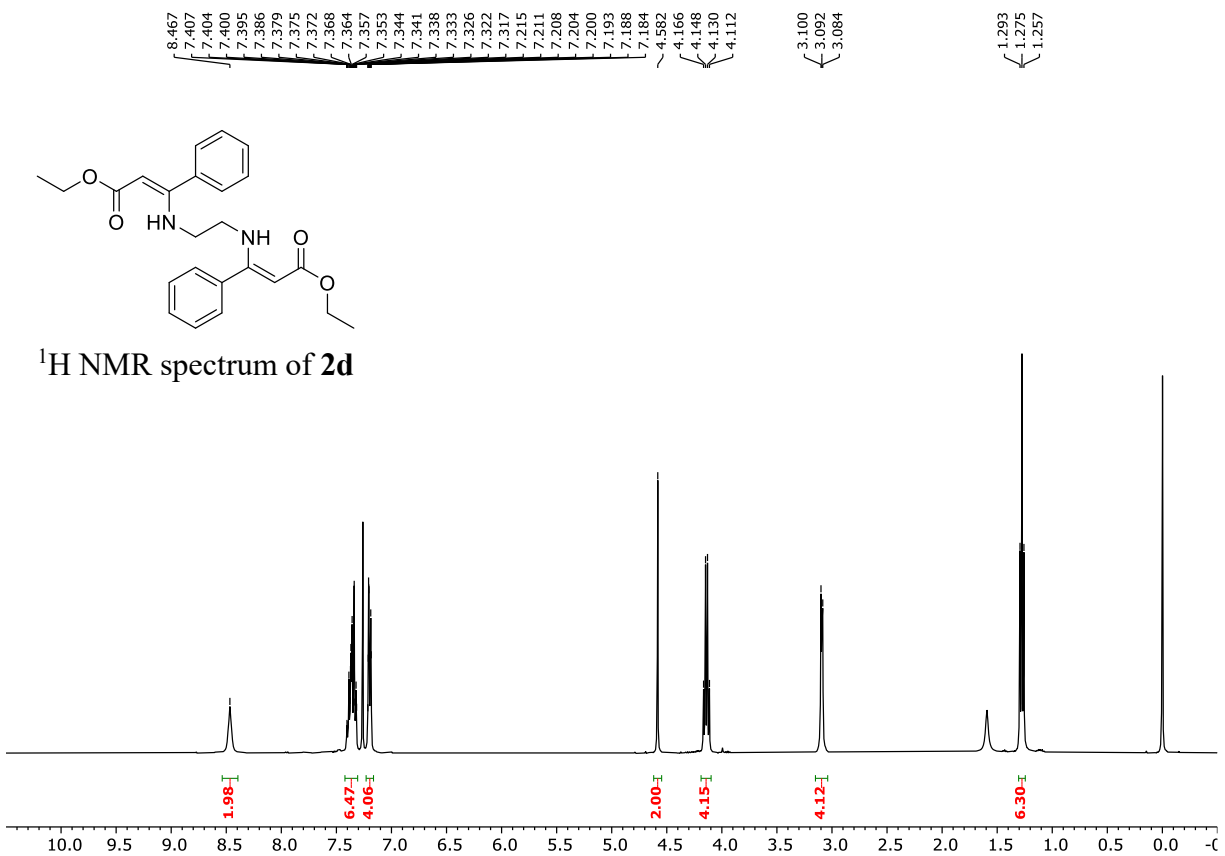
H	-0.31794100	-1.48635100	8.92603700
C	-0.76063300	-0.12113700	10.52151600
H	-1.30521200	0.81968100	10.69376800
O	-0.62842400	-2.00737500	11.98003200
C	-3.26971100	0.56744200	3.91654600
O	-3.54437800	-0.45424600	3.24282300
O	-3.27174500	1.77082900	3.55506100
C	-1.32949500	-1.23994800	11.35083700
C	-2.83524900	-1.39257900	11.27825700
H	-3.15203900	-1.44859800	10.22303100
H	-3.32263100	-0.50094000	11.70627100
H	-3.15426200	-2.29113800	11.82298200
C	2.62994900	-1.34270000	6.28412000
C	2.81970500	-0.30104000	5.36415800
C	2.48110600	0.99946000	5.75313900
C	1.87623300	1.23810800	6.98530200
C	1.61327000	0.18798300	7.87910900
C	2.04661700	-1.10255000	7.52930300
H	2.89743600	-2.35325800	5.96793300
H	2.64234300	1.80173700	5.03152700
H	1.52758900	2.24530400	7.23419400
H	1.85572400	-1.94025500	8.20800300
C	0.63979300	0.43518900	8.98890800
H	0.31619700	1.48603100	8.92612000
C	0.75885400	0.12077300	10.52151900
H	1.30339000	-0.82006900	10.69379000
O	0.62671300	2.00671500	11.98043200
C	3.26758000	-0.56814200	3.91646900
O	3.26984100	-1.77161400	3.55521200
O	3.54195000	0.45345700	3.24253000
C	1.32774500	1.23953400	11.35089900
C	2.83345200	1.39244600	11.27791500
H	3.15250400	2.29072600	11.82307700
H	3.14984500	1.44919800	10.22260700
H	3.32115300	0.50061300	11.70515000

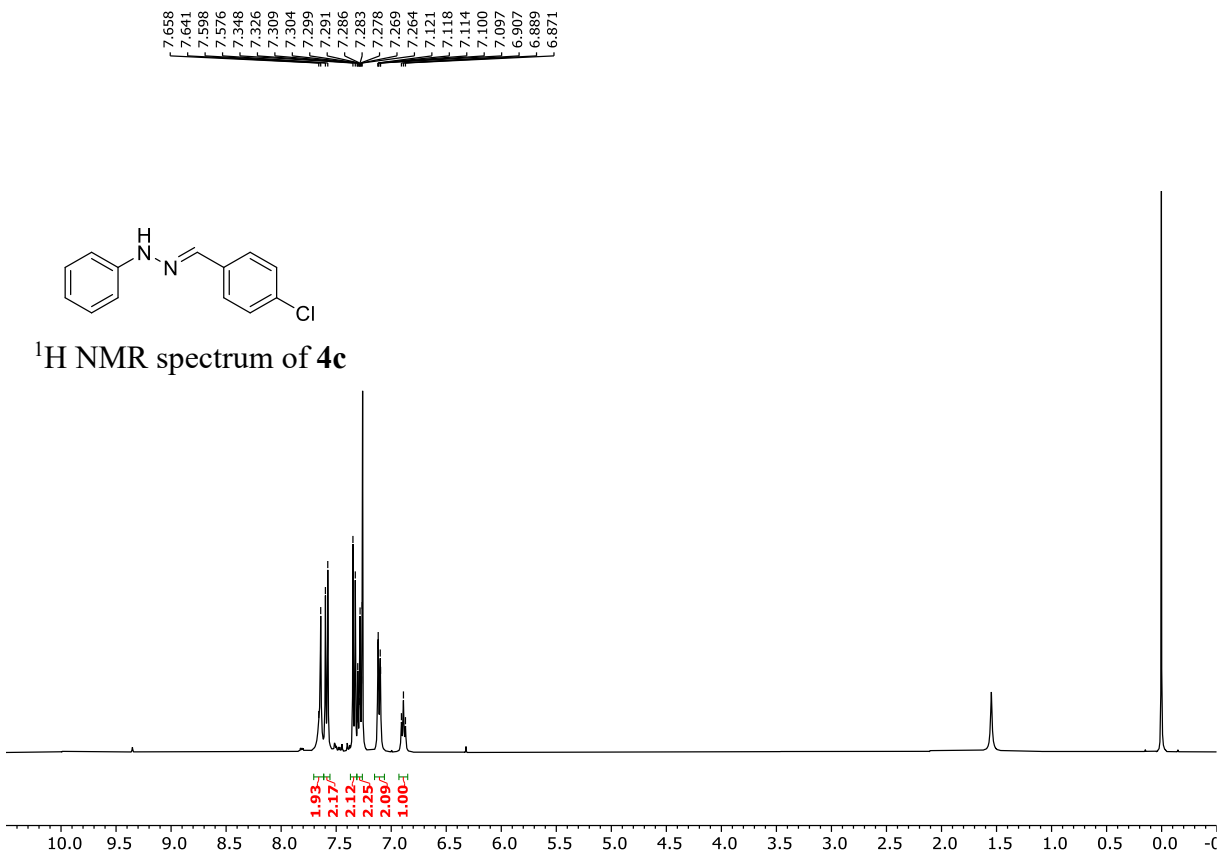
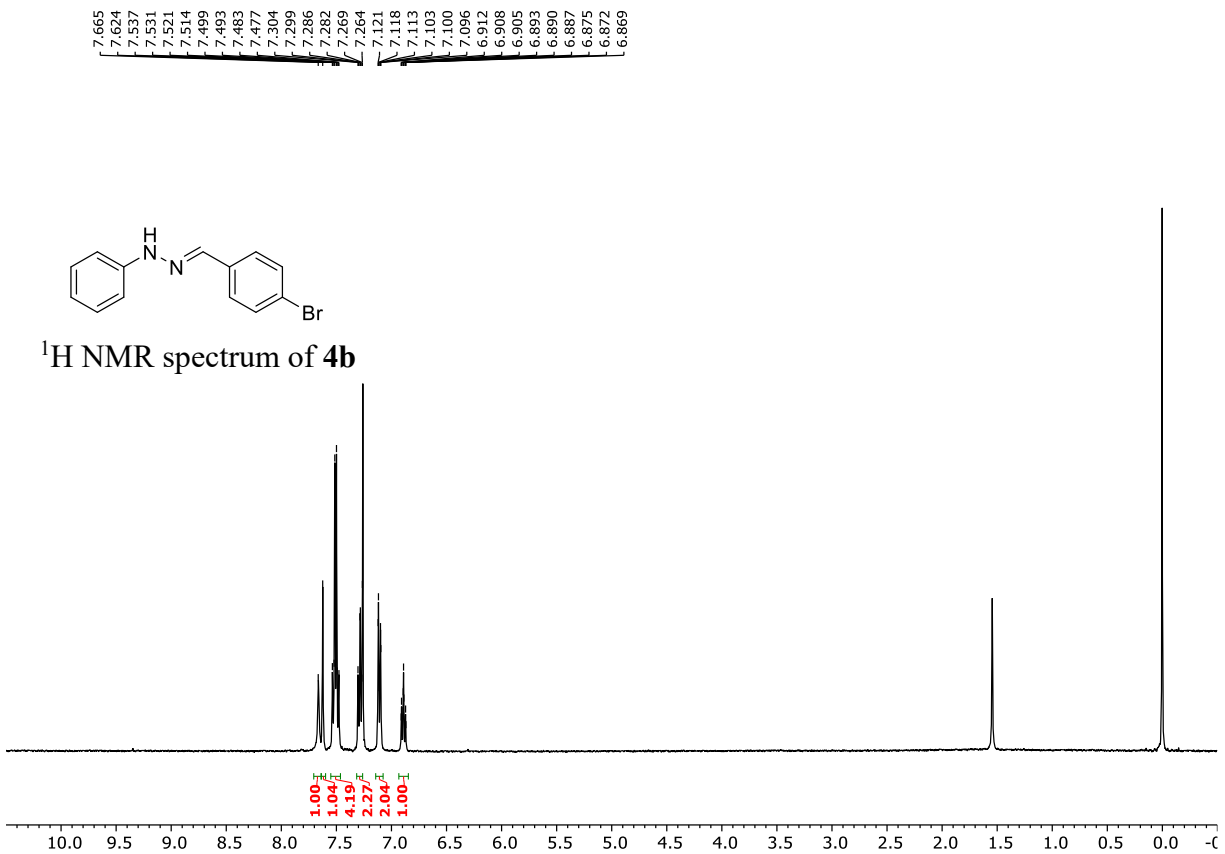
Appendix B. NMR Spectra

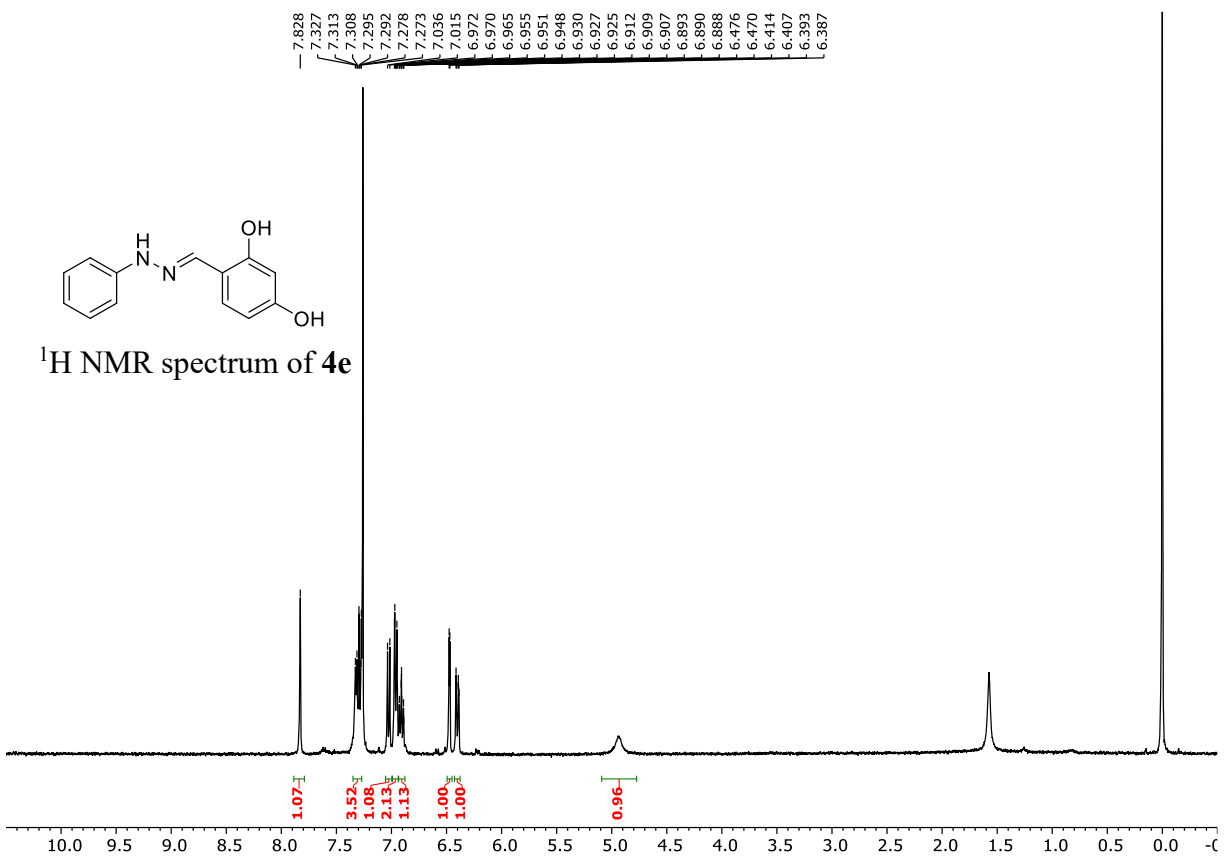
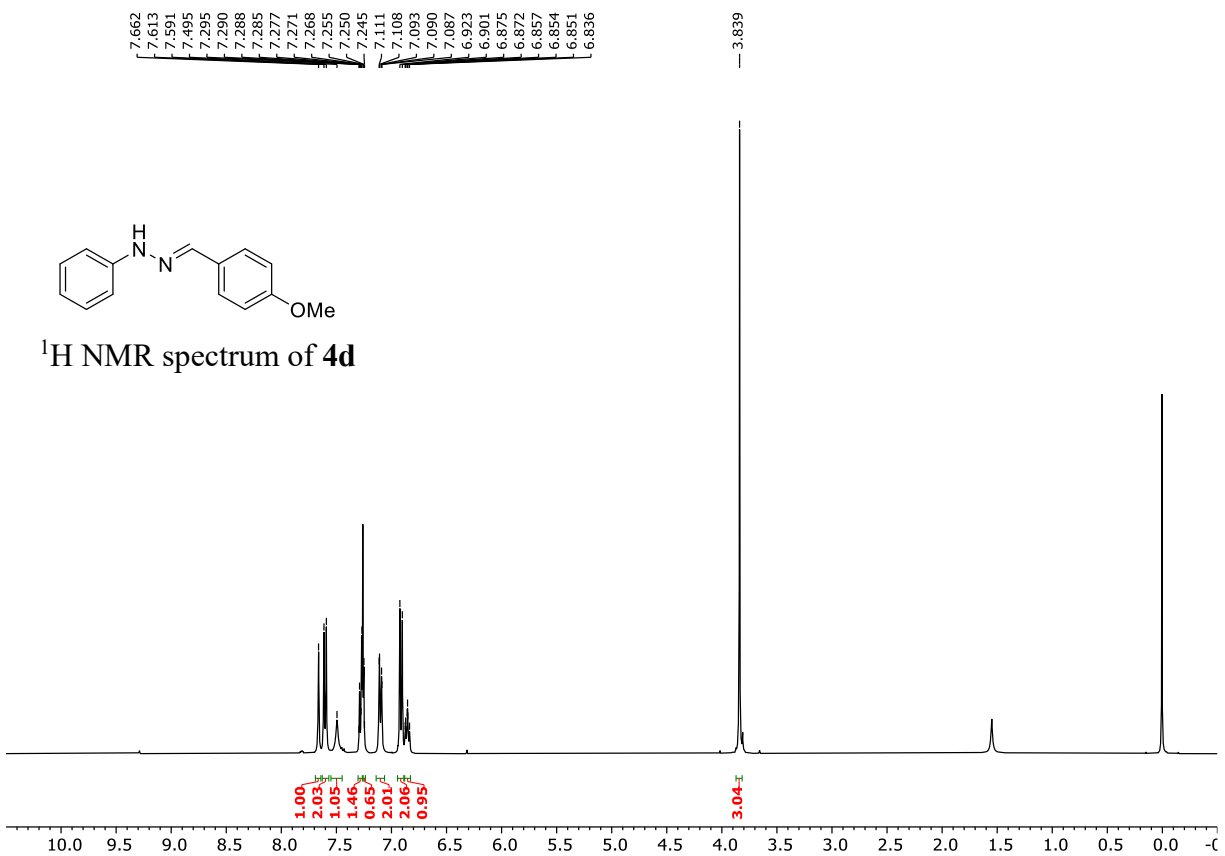
NMR spectra for compounds in **Chapter 2**:

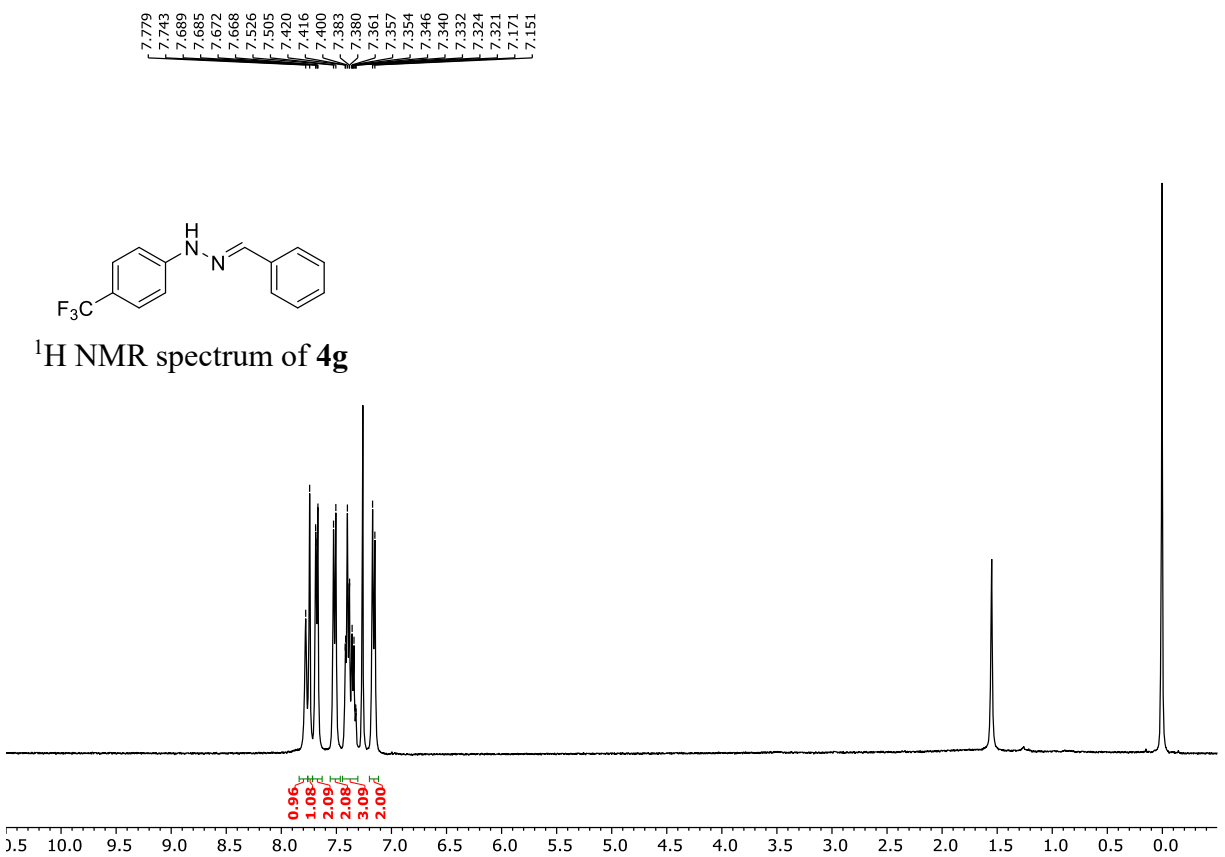
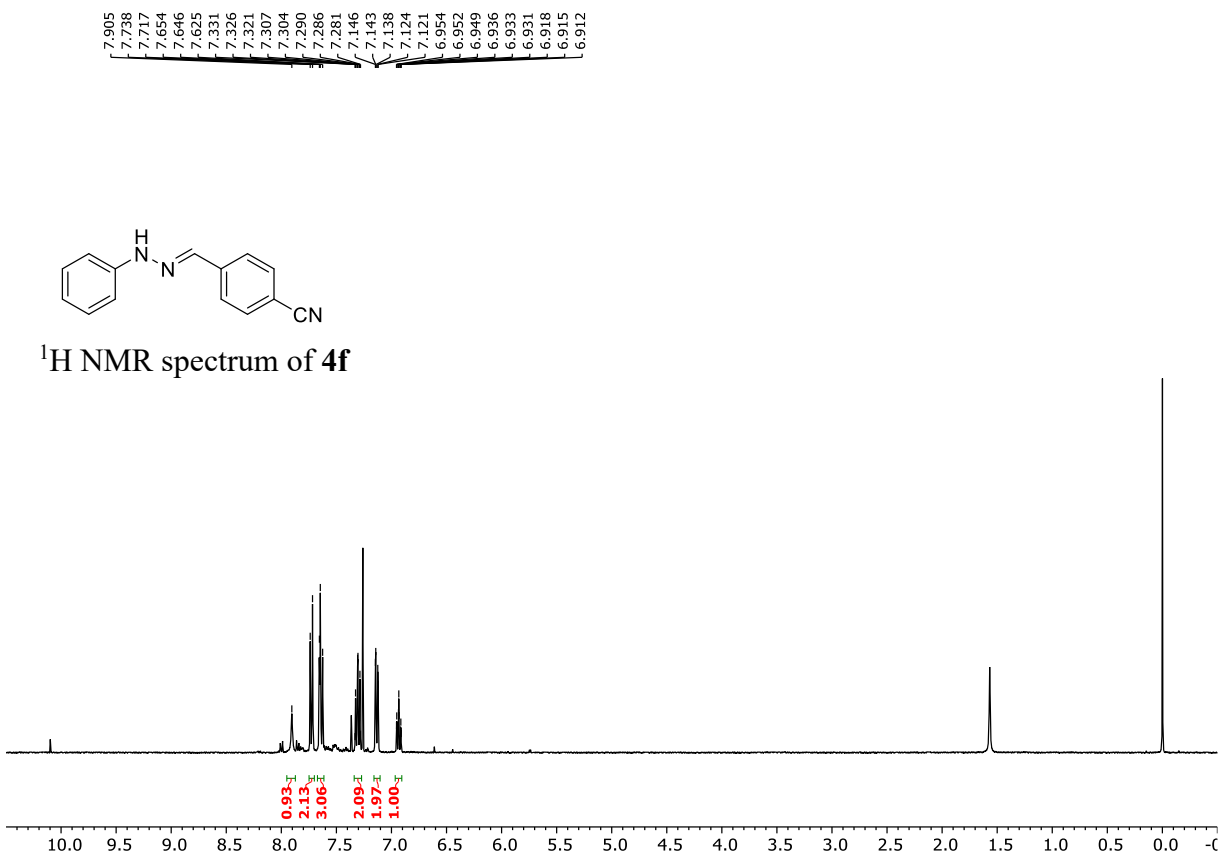


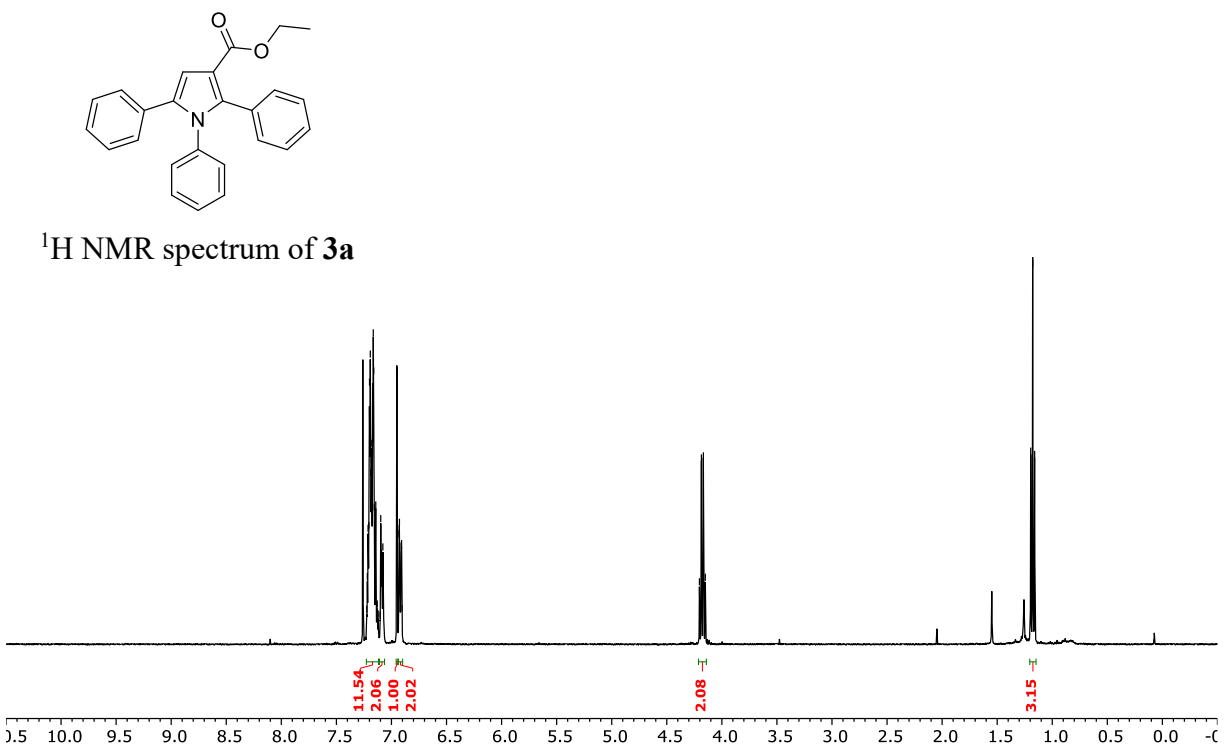
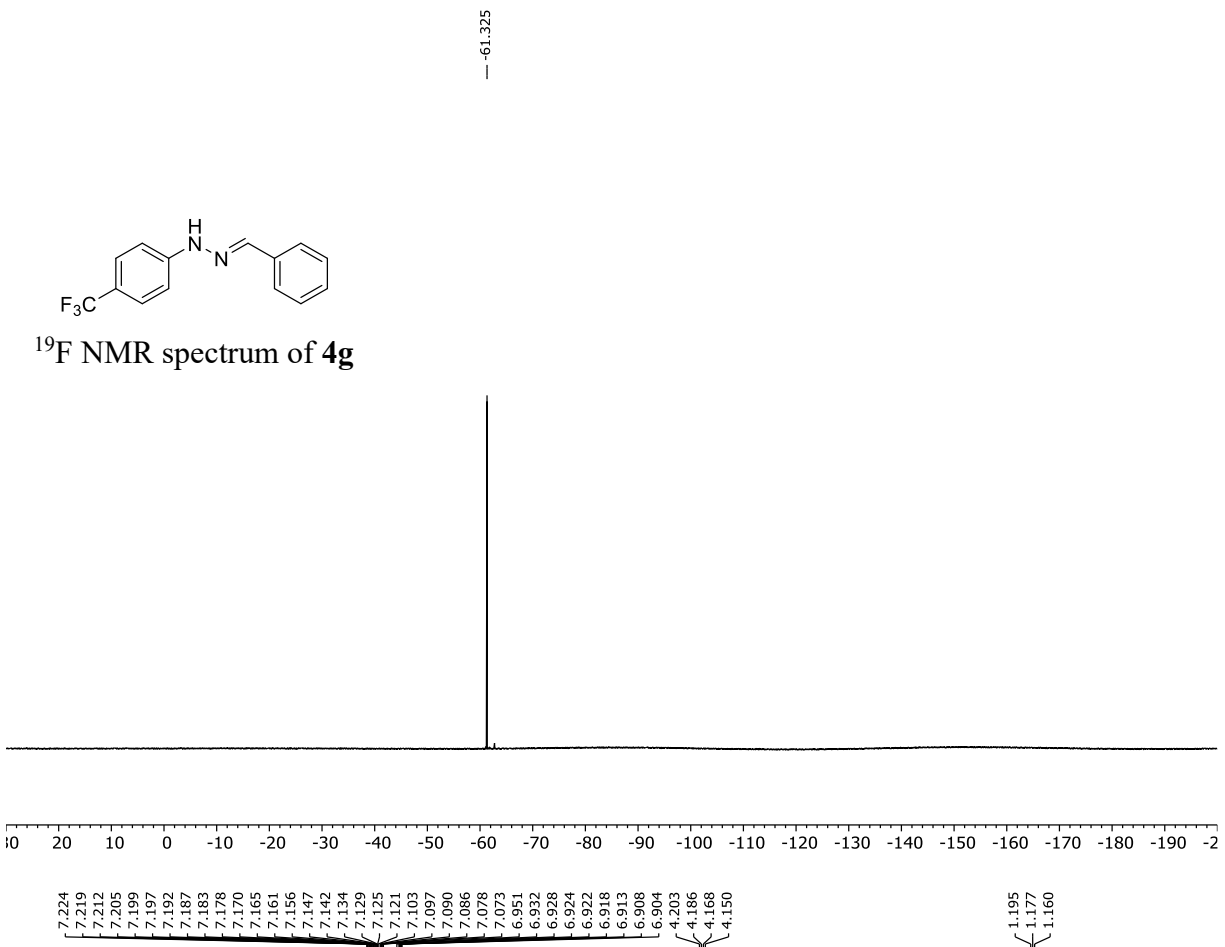


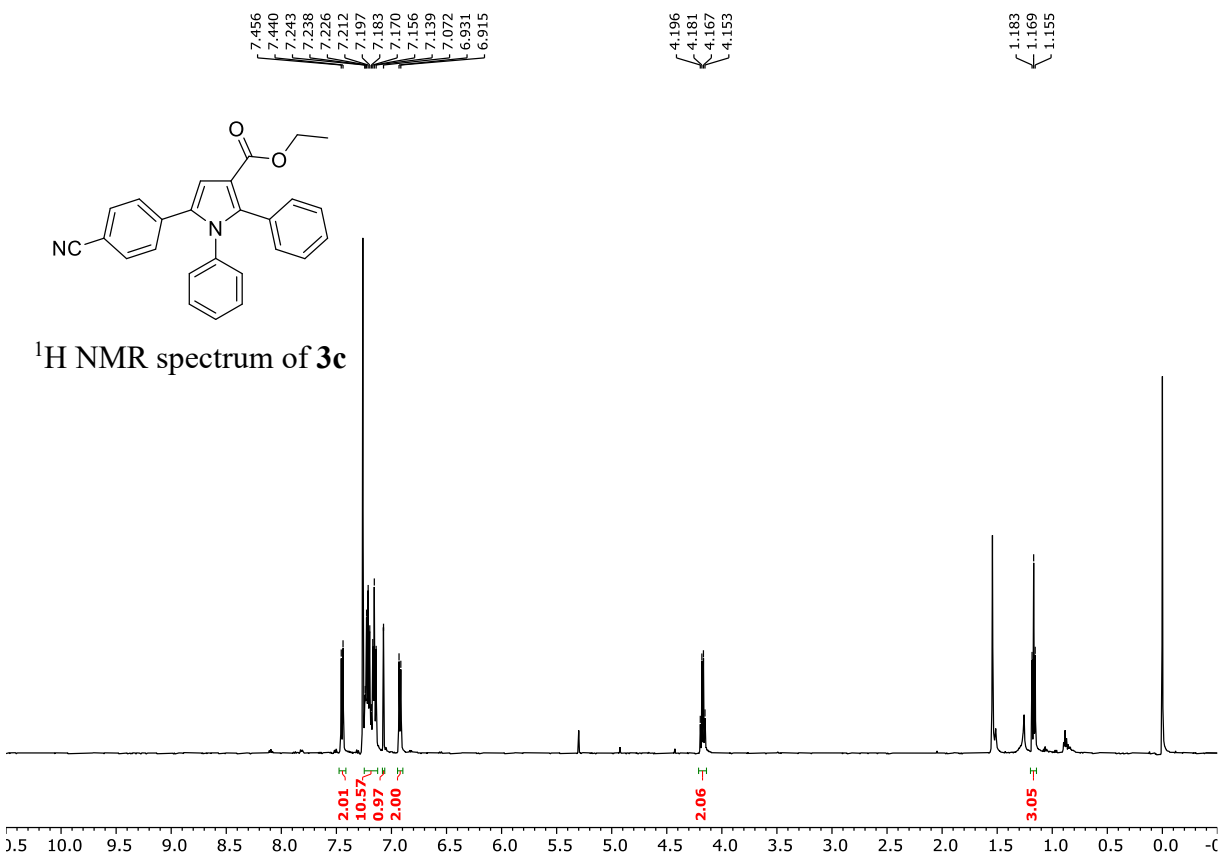
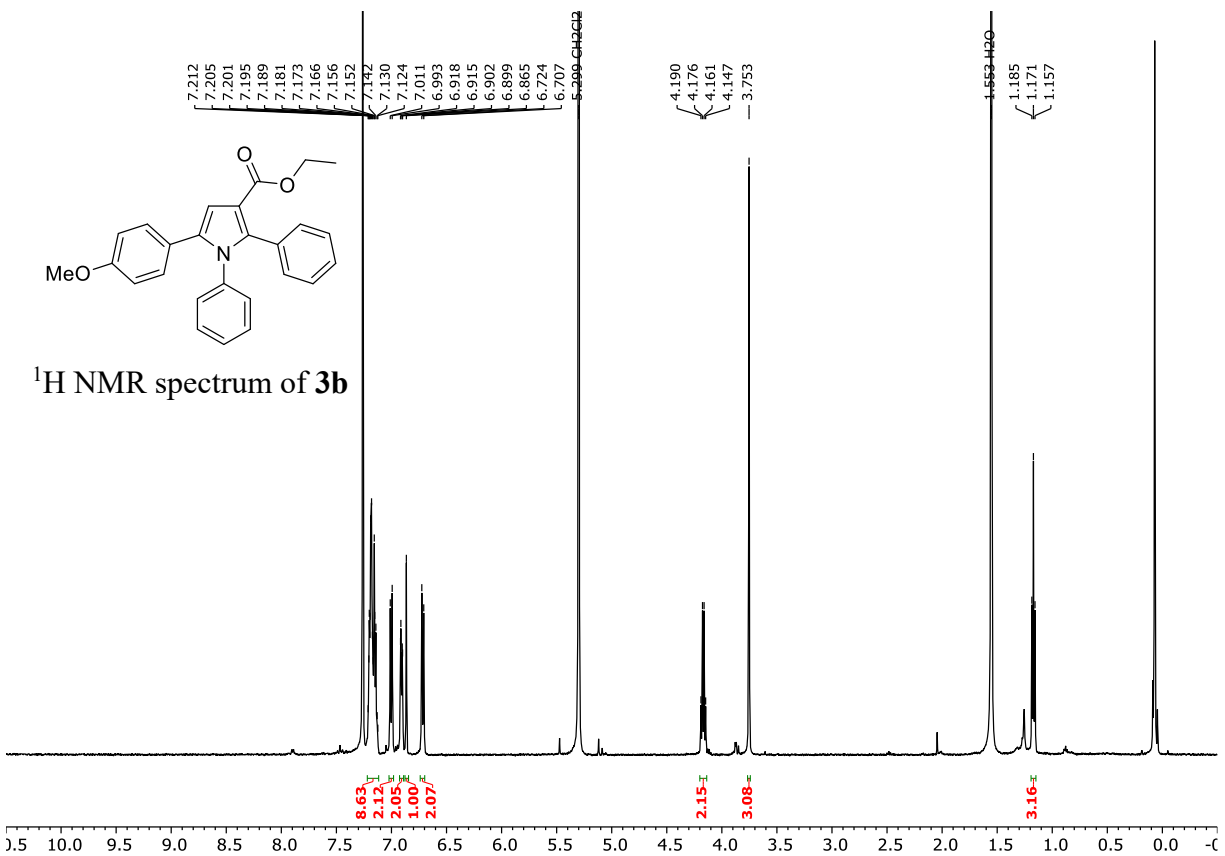


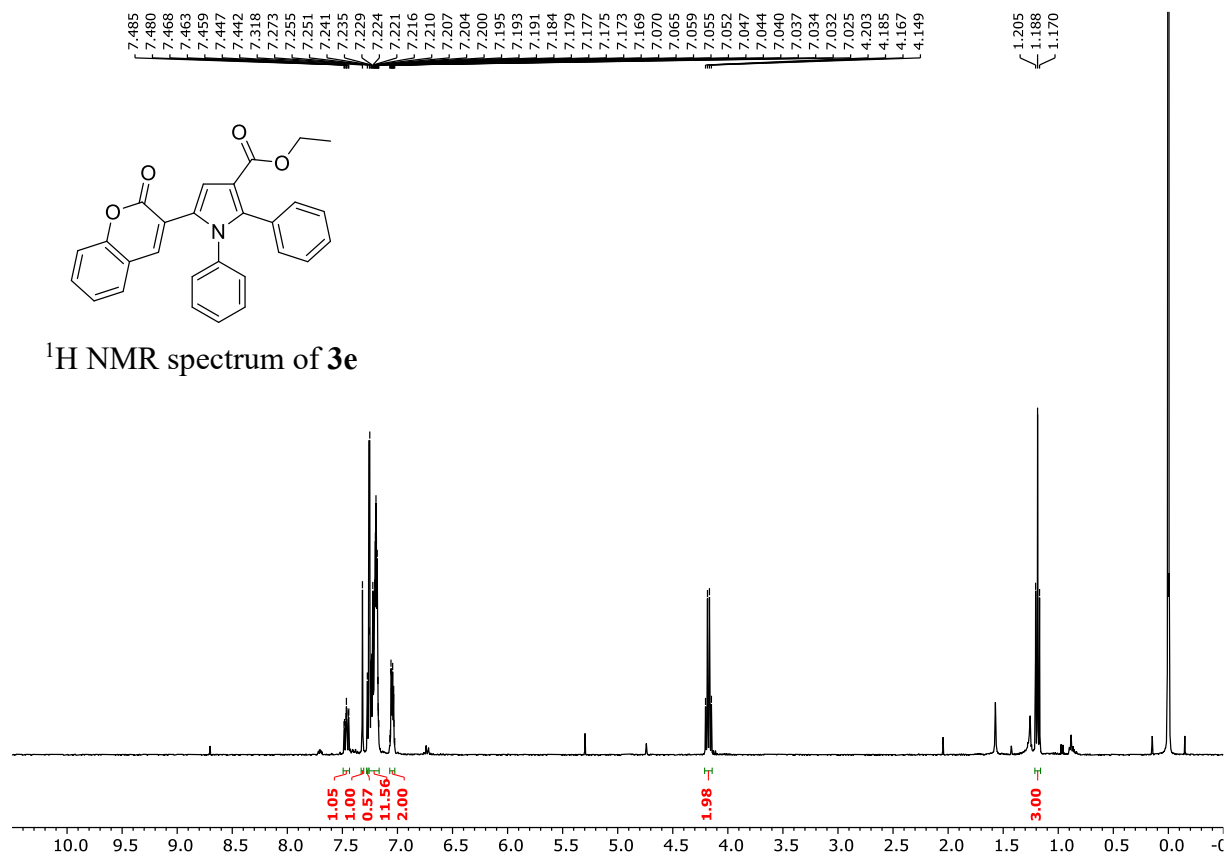
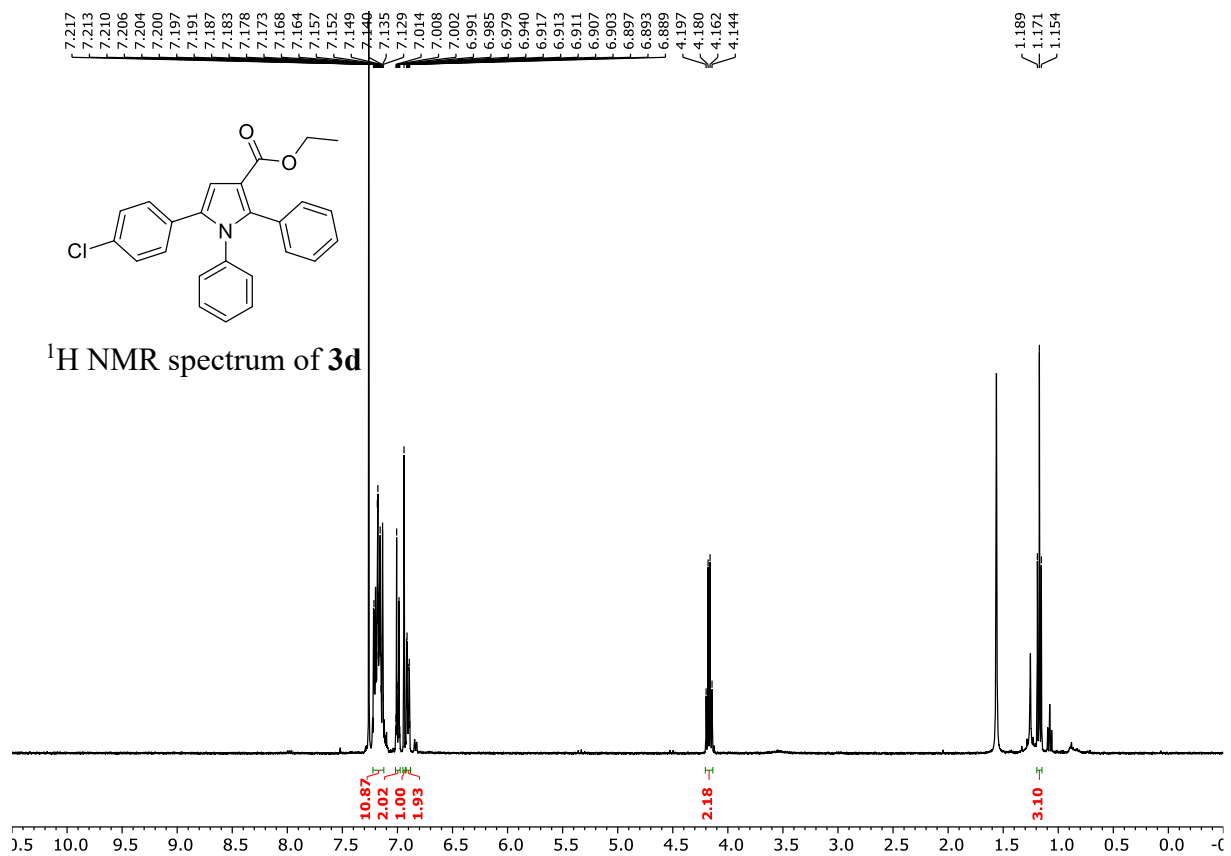


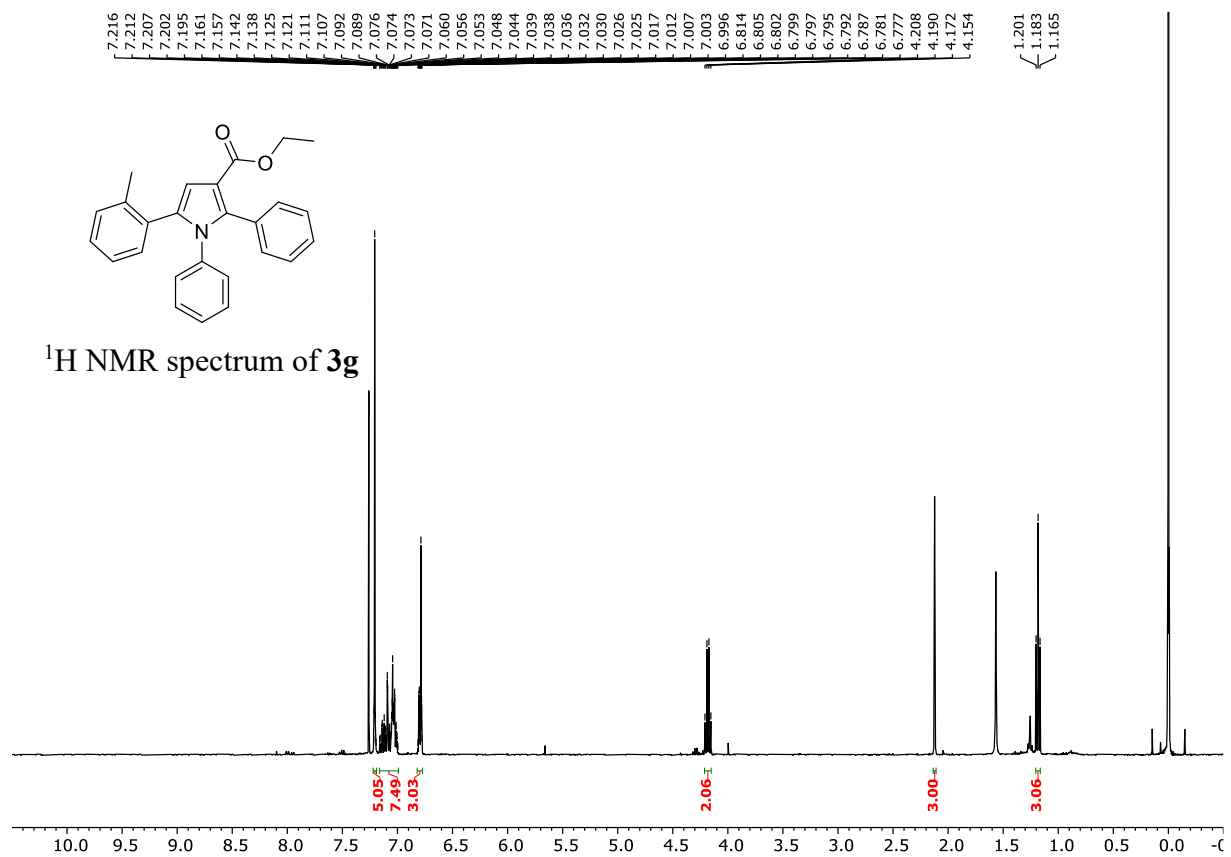
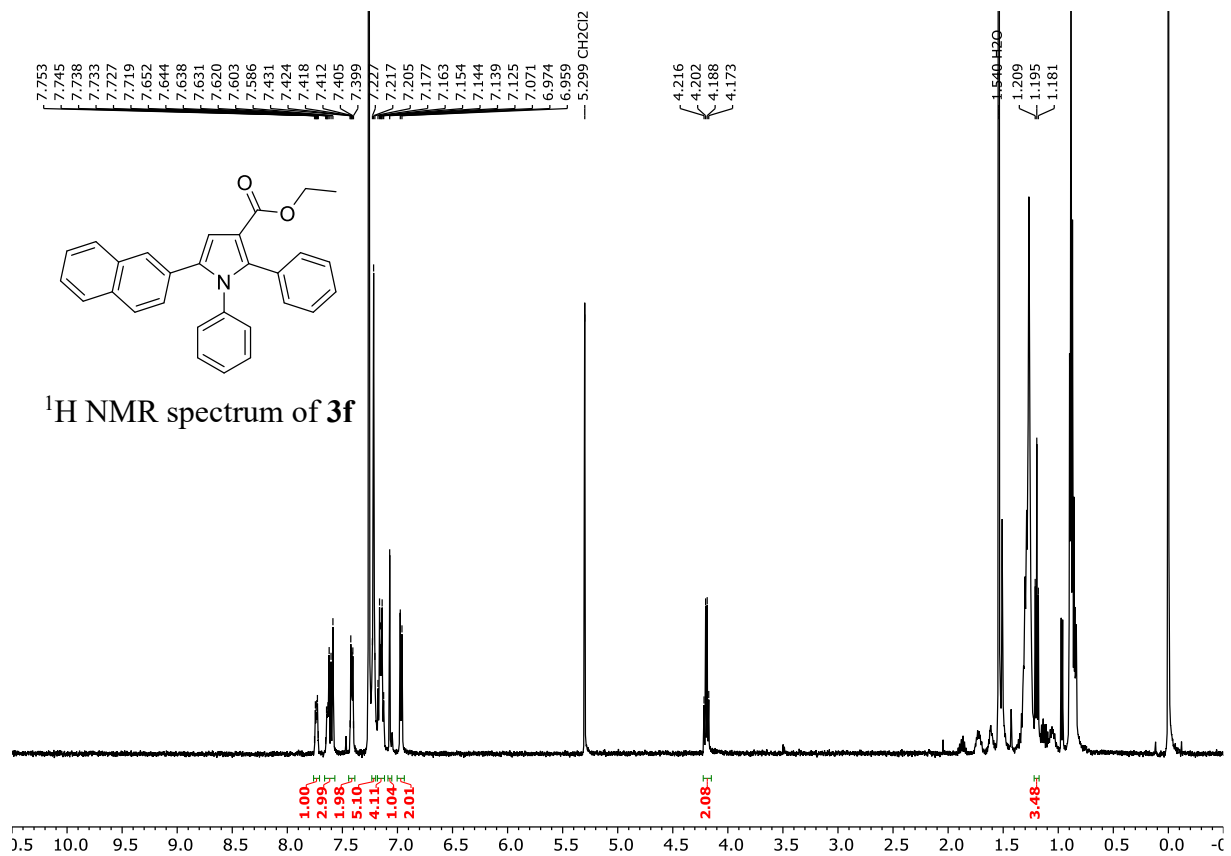


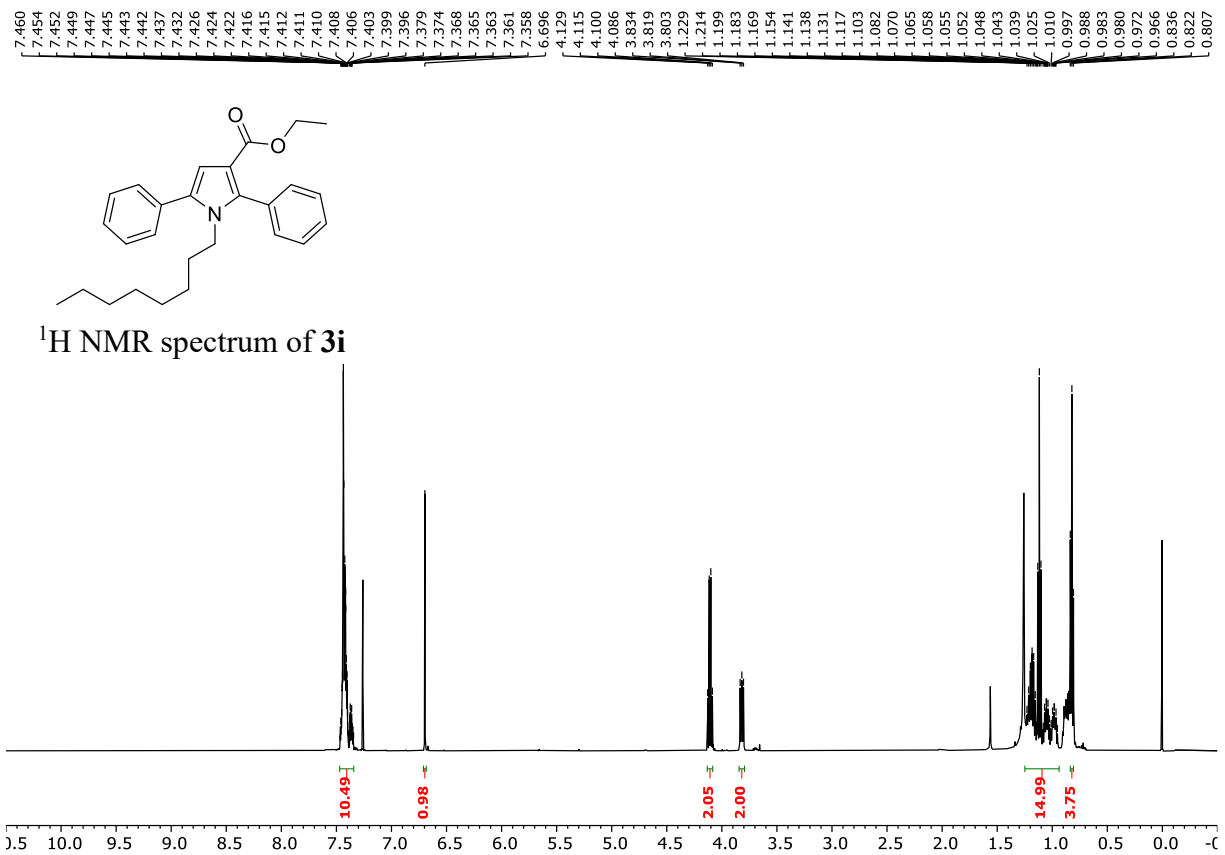
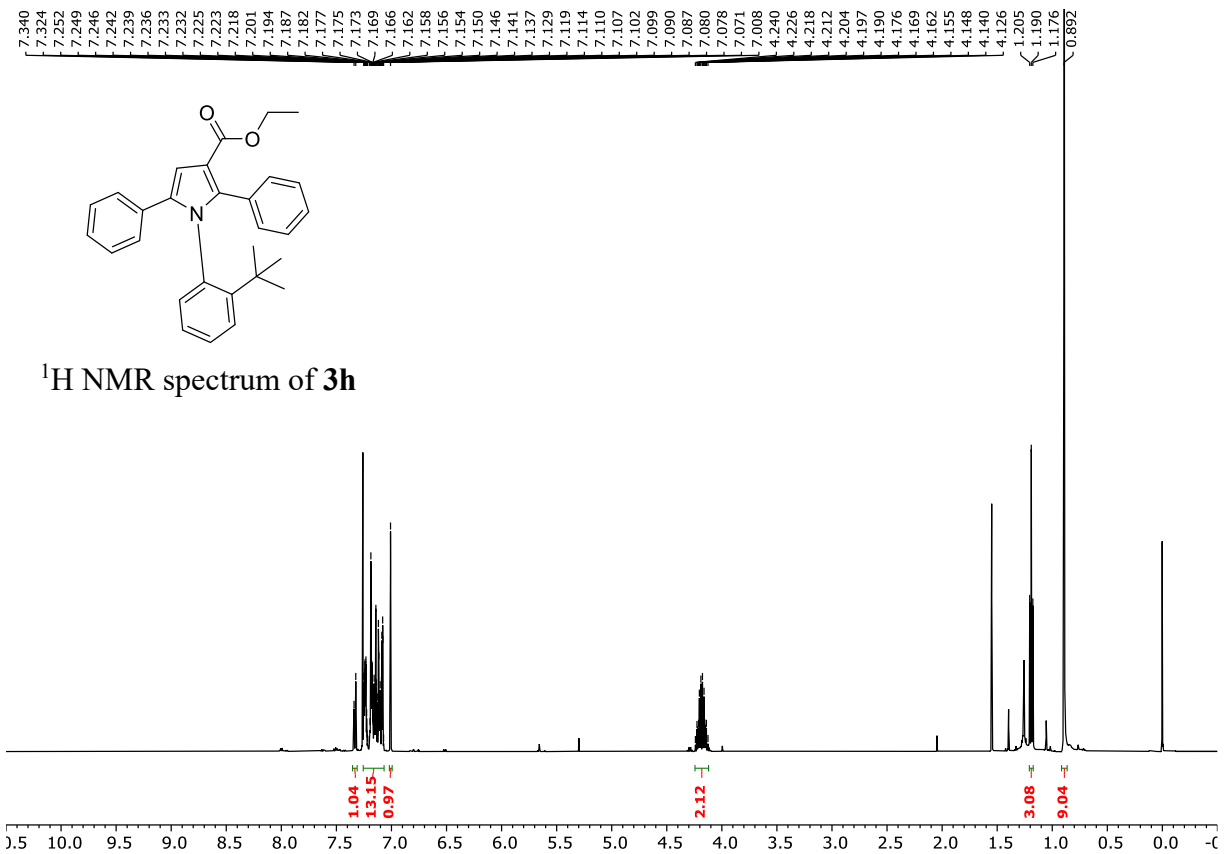


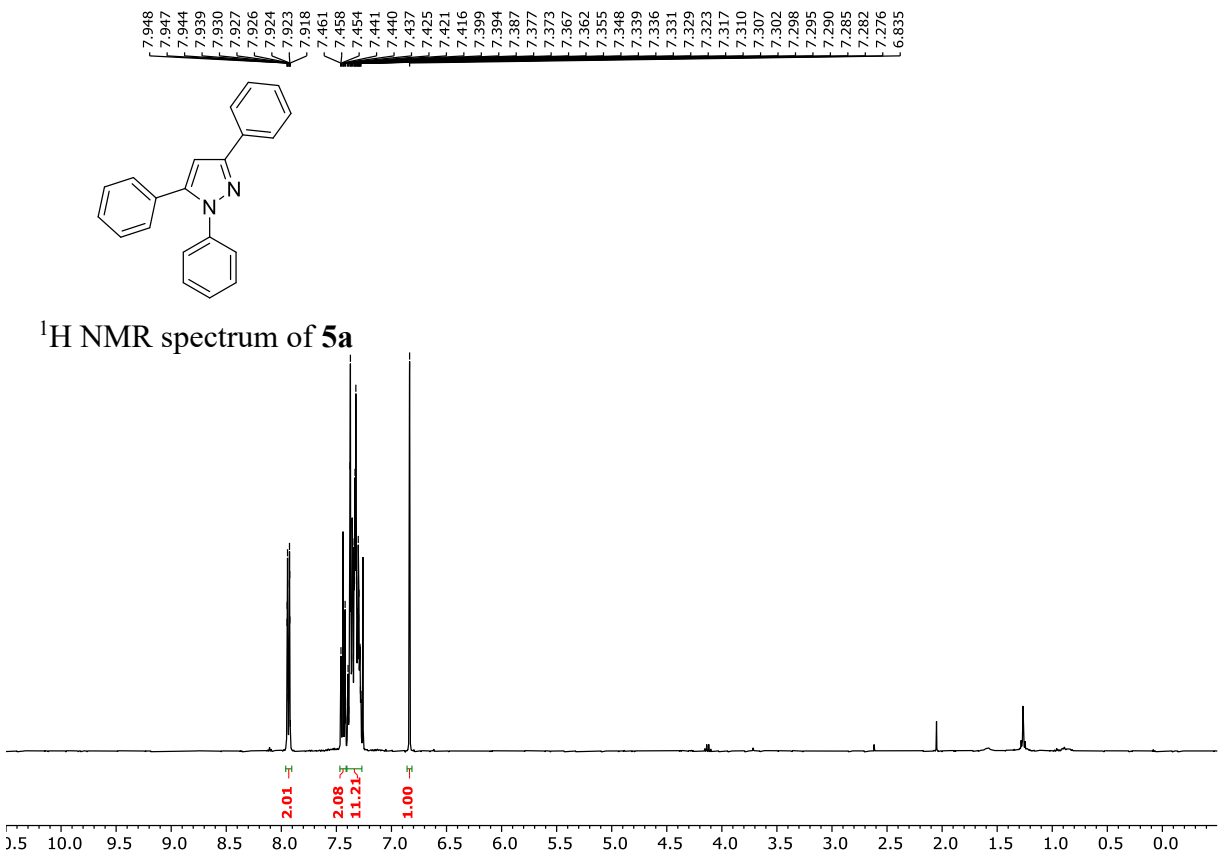
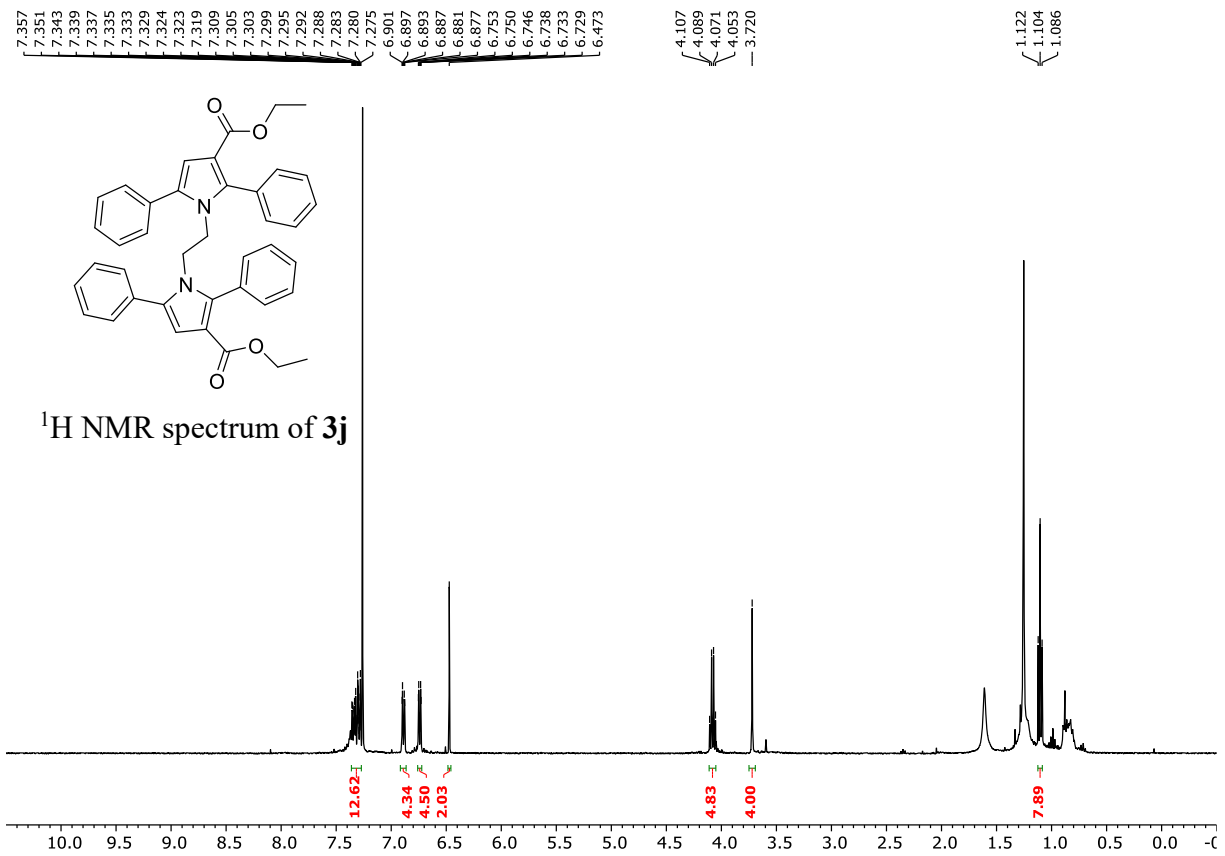


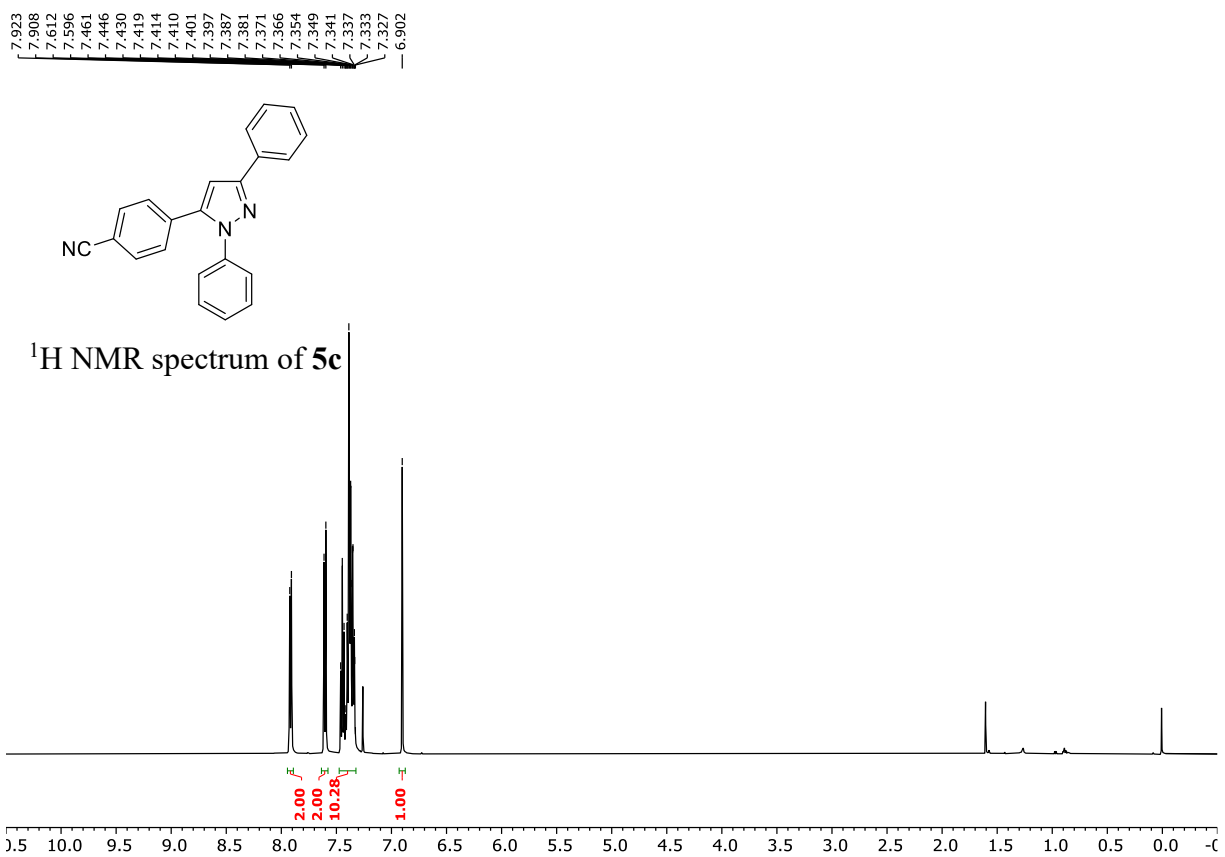
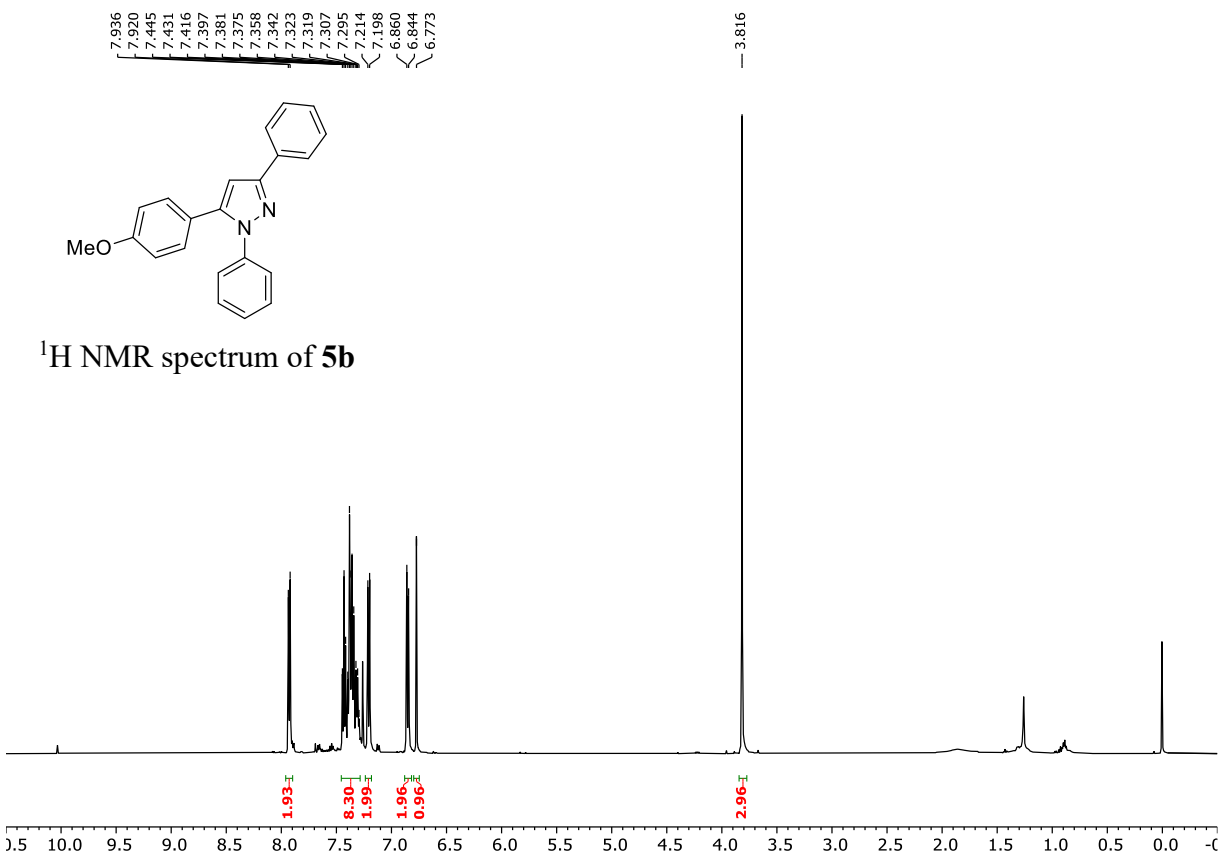




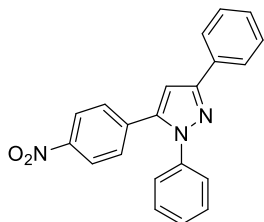




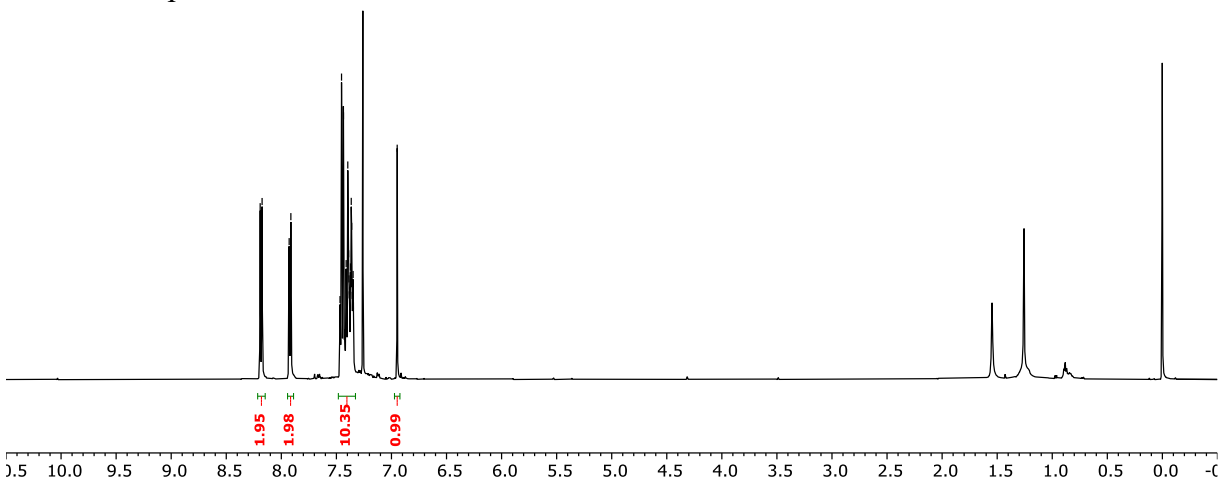




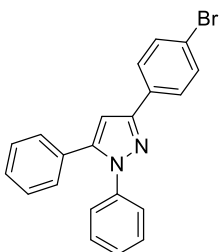
8.192
8.175
7.929
7.913
7.467
7.453
7.436
7.424
7.411
7.407
7.397
7.389
7.386
7.383
7.381
7.372
7.365
7.361
7.356
7.348
7.345
6.948



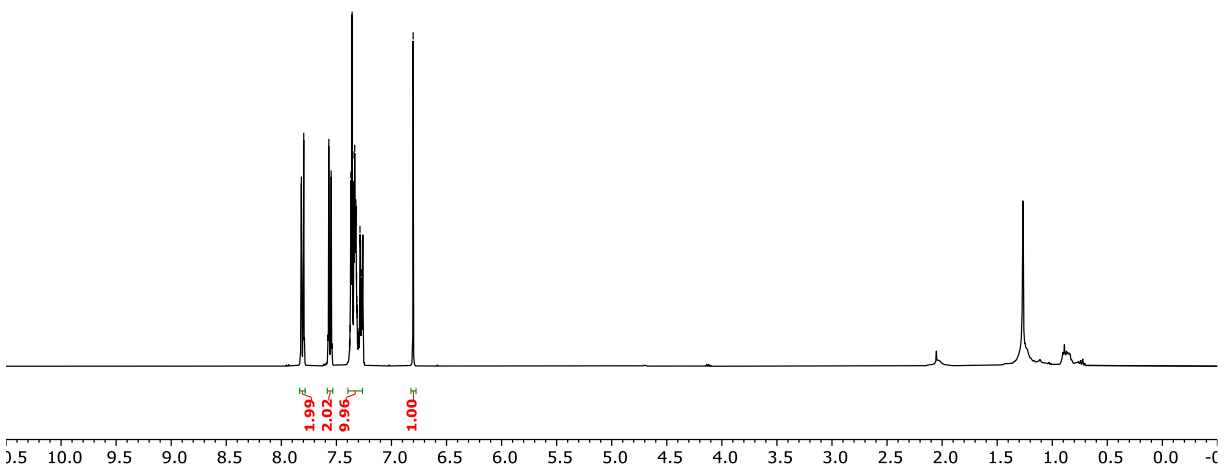
^1H NMR spectrum of **5d**

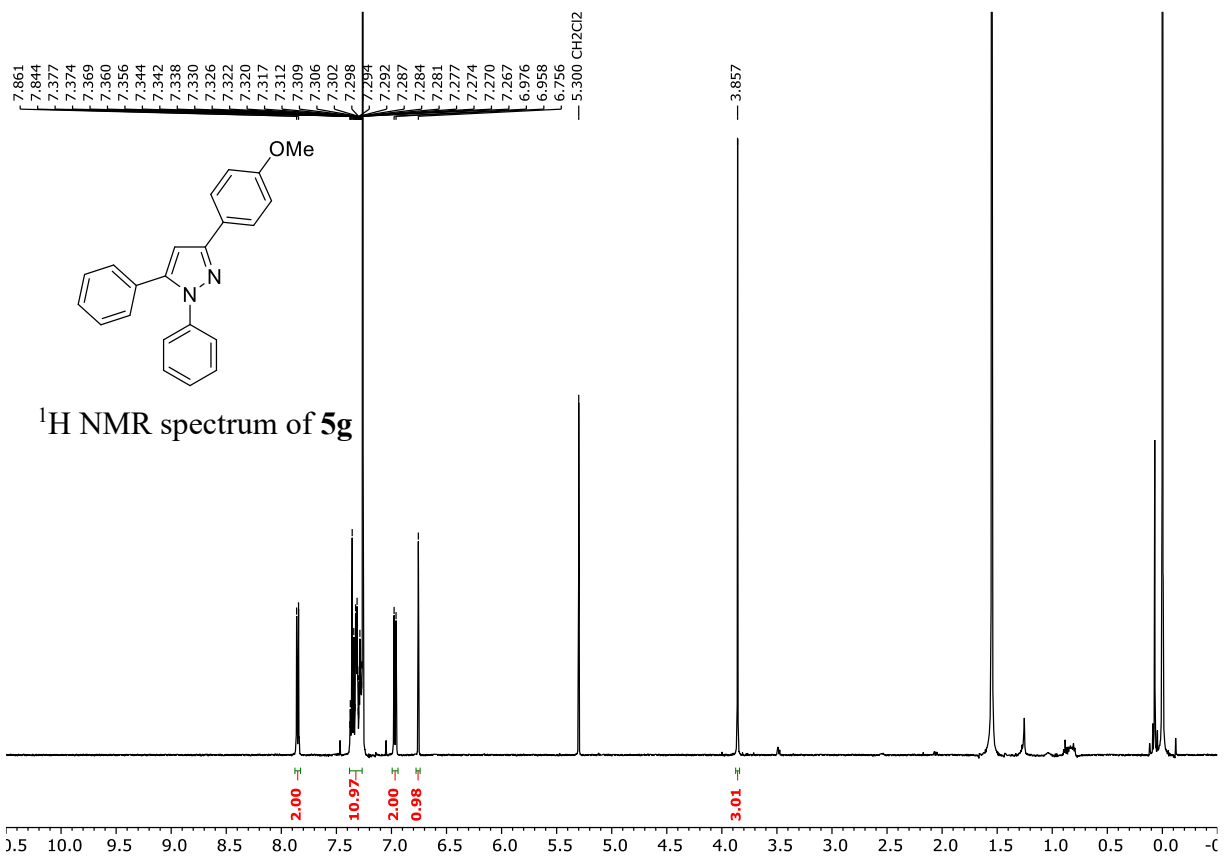
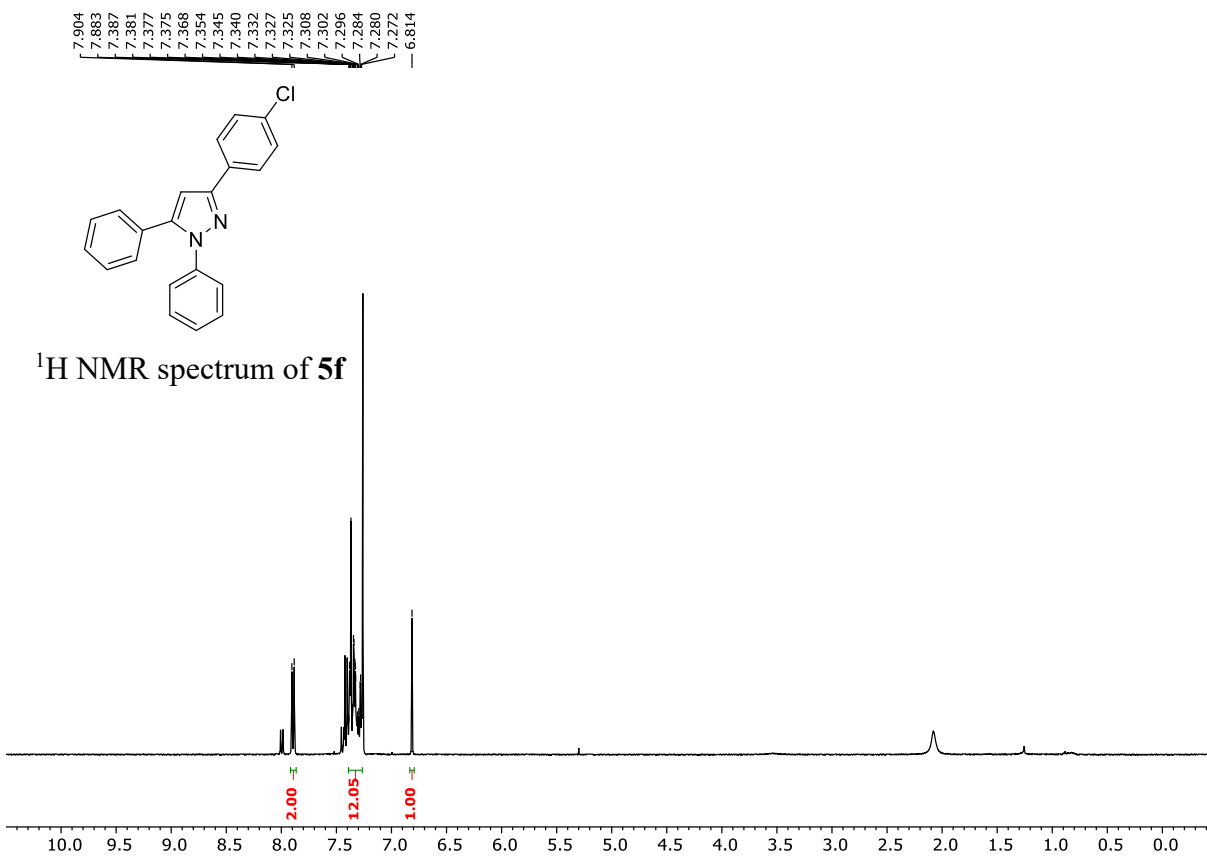


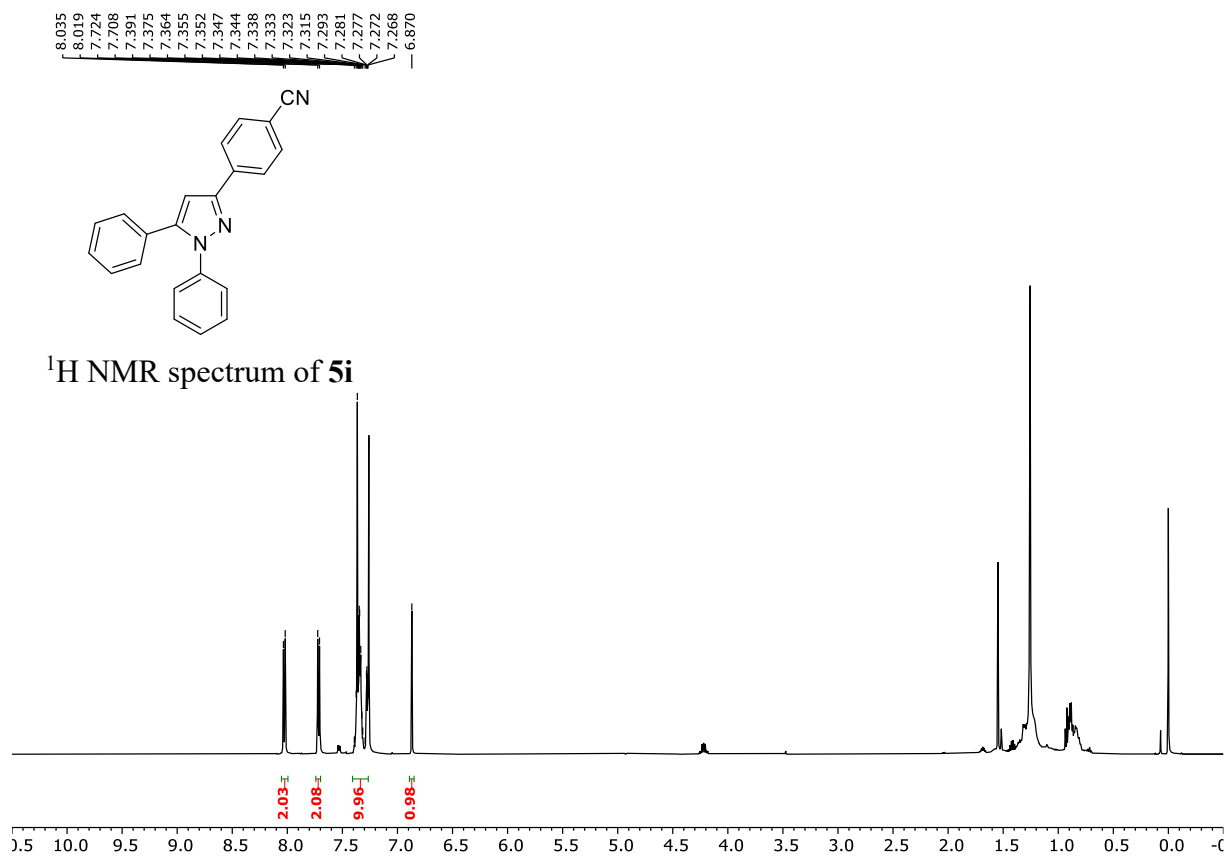
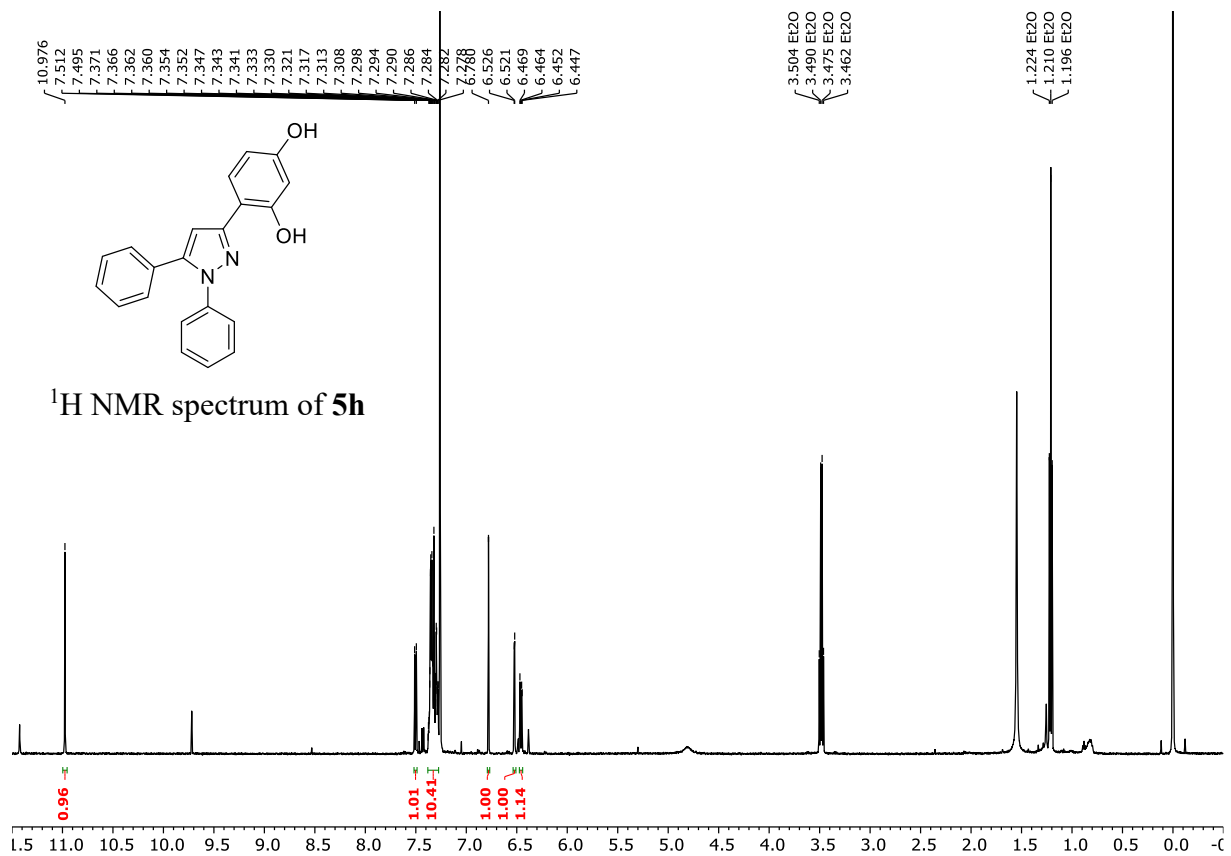
7.818
7.797
7.569
7.547
7.381
7.377
7.375
7.371
7.368
7.366
7.360
7.357
7.356
7.349
7.348
7.345
7.339
7.334
7.328
7.325
7.323
7.321
7.317
7.314
7.311
7.308
7.305
7.302
7.298
7.296
7.294
7.286
7.280
7.277
7.272
7.269
7.267
7.264
6.803



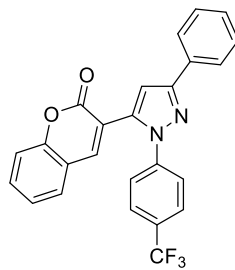
^1H NMR spectrum of **5e**



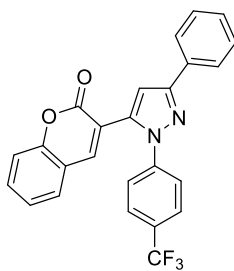
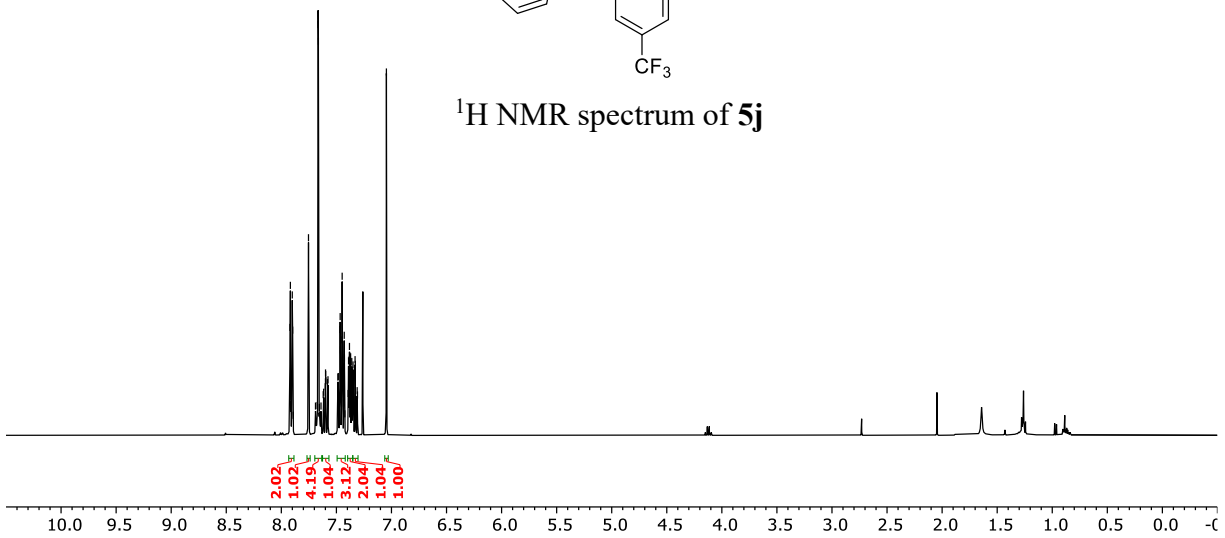




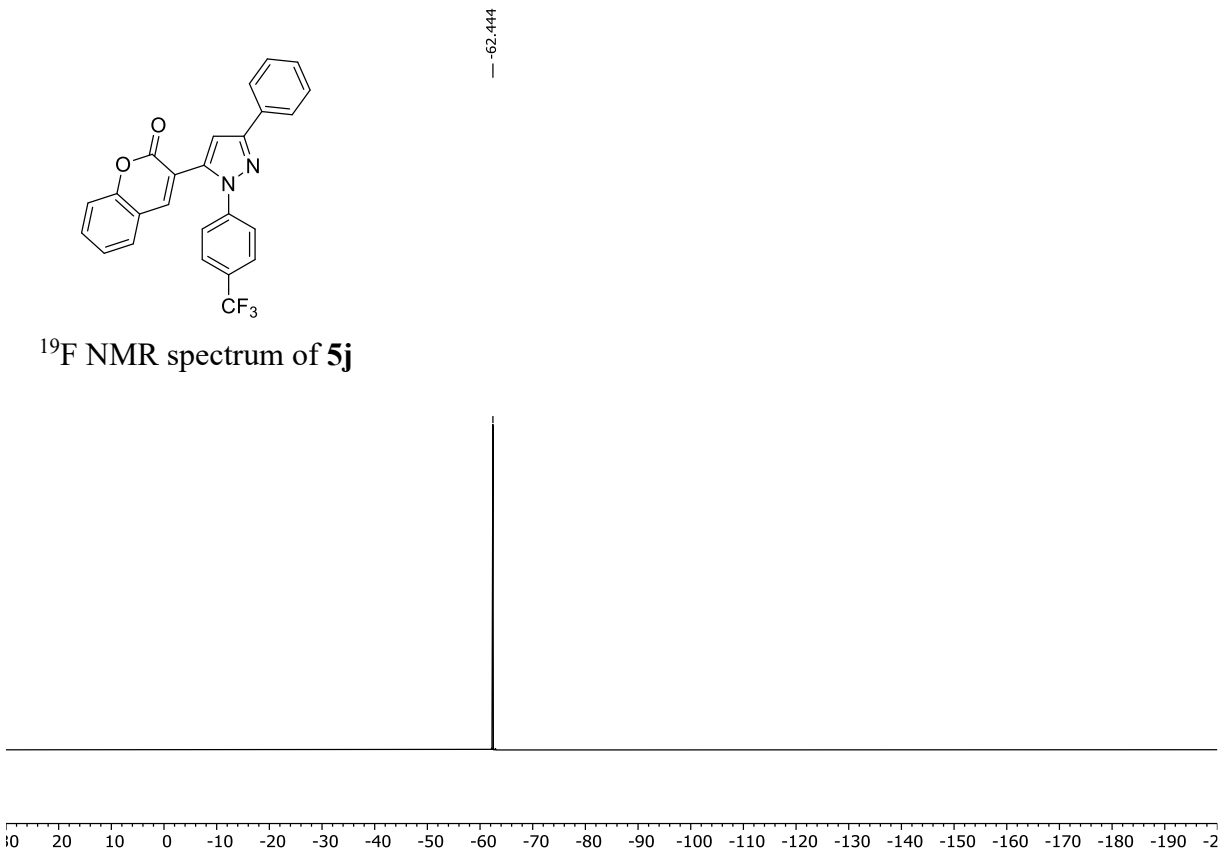
7.922
7.918
7.913
7.904
7.901
7.897
7.892
7.753
7.690
7.675
7.666
7.663
7.655
7.640
7.620
7.616
7.601
7.599
7.597
7.595
7.580
7.576
7.487
7.483
7.467
7.466
7.463
7.453
7.449
7.448
7.444
7.432
7.429
7.427
7.423
7.393
7.390
7.386
7.383
7.381
7.380
7.377
7.372
7.371
7.365
7.362
7.360
7.359
7.356
7.353
7.349
7.346
7.330
7.328
7.311
7.309
7.046

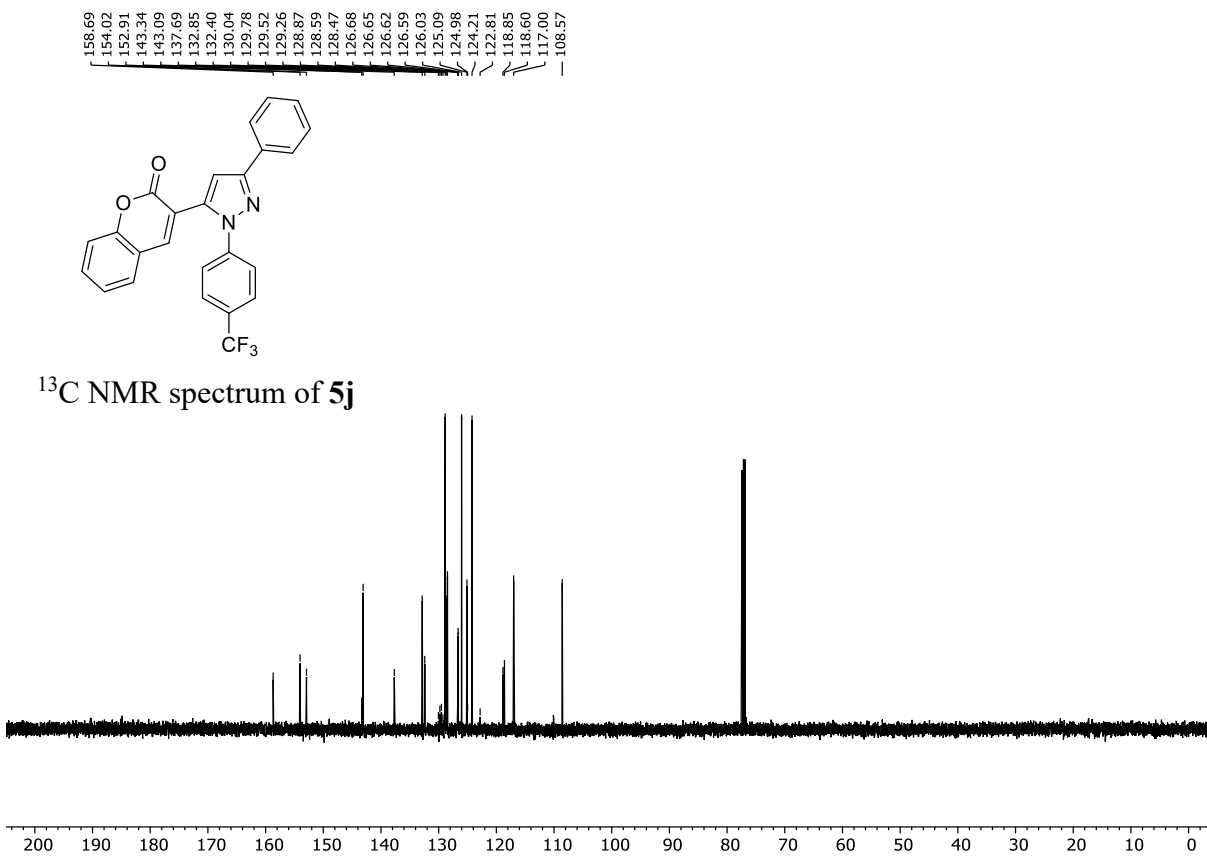


¹H NMR spectrum of **5j**

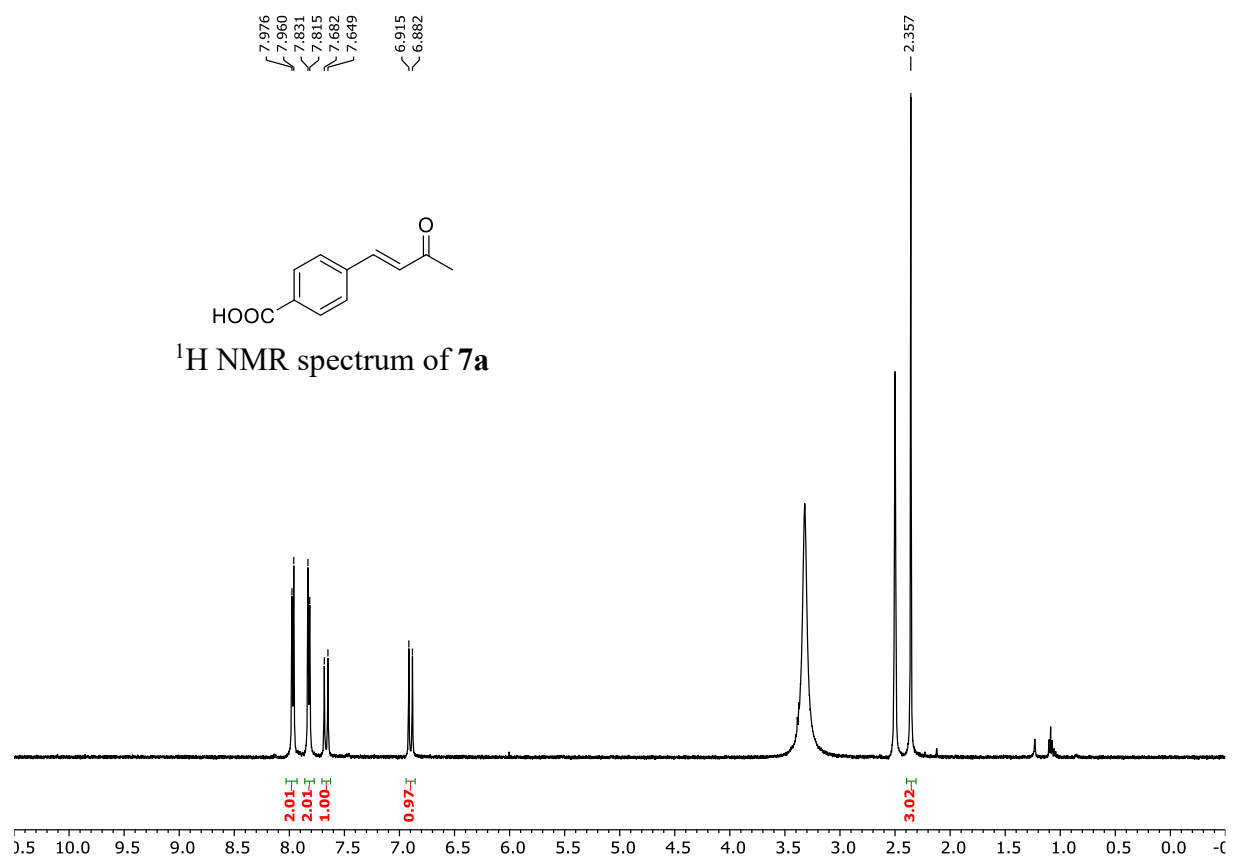


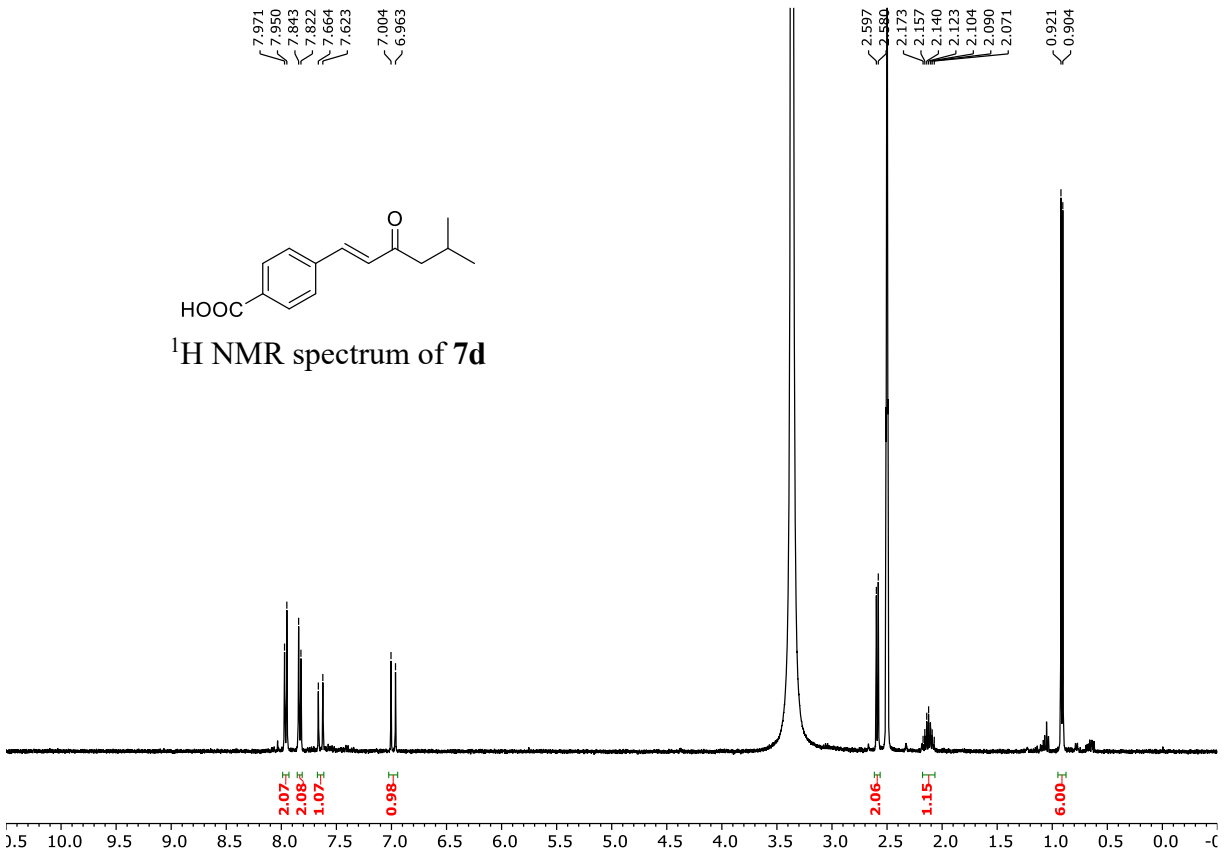
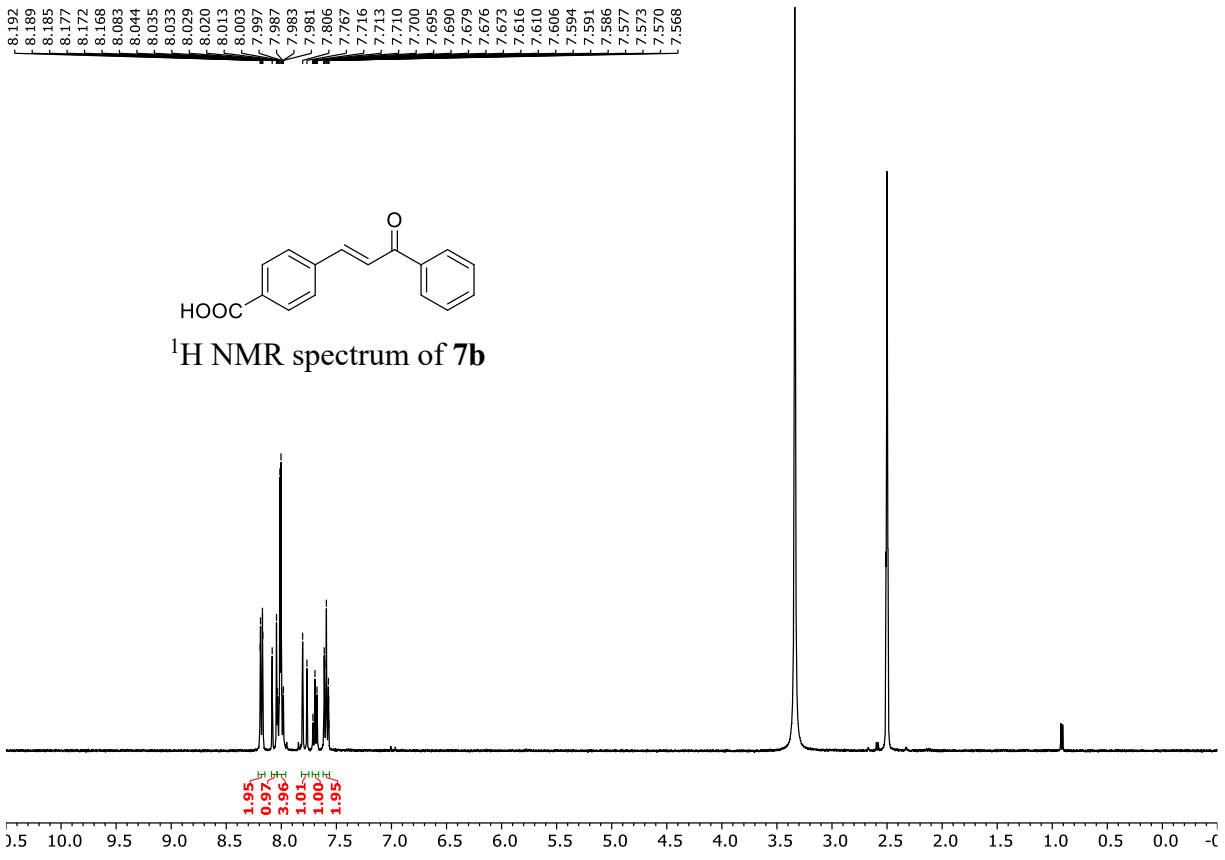
¹⁹F NMR spectrum of **5j**

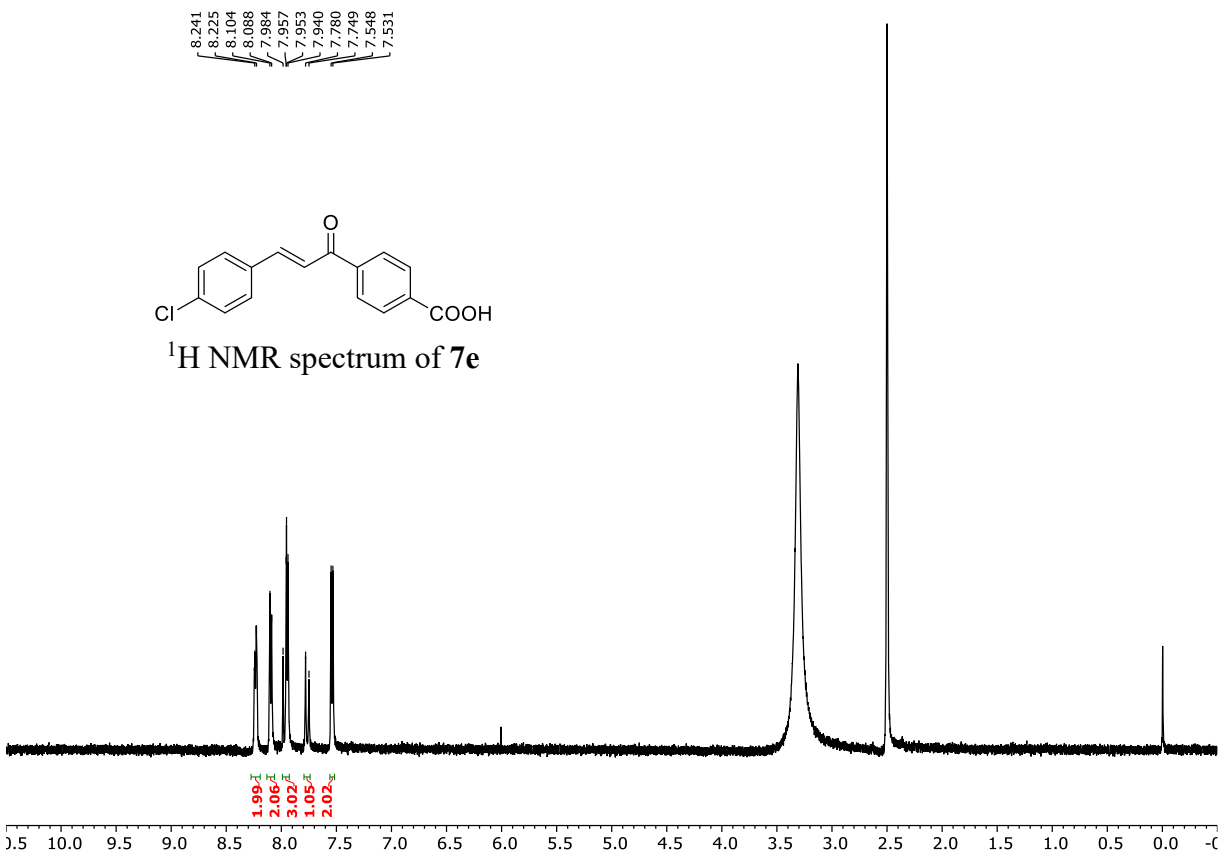
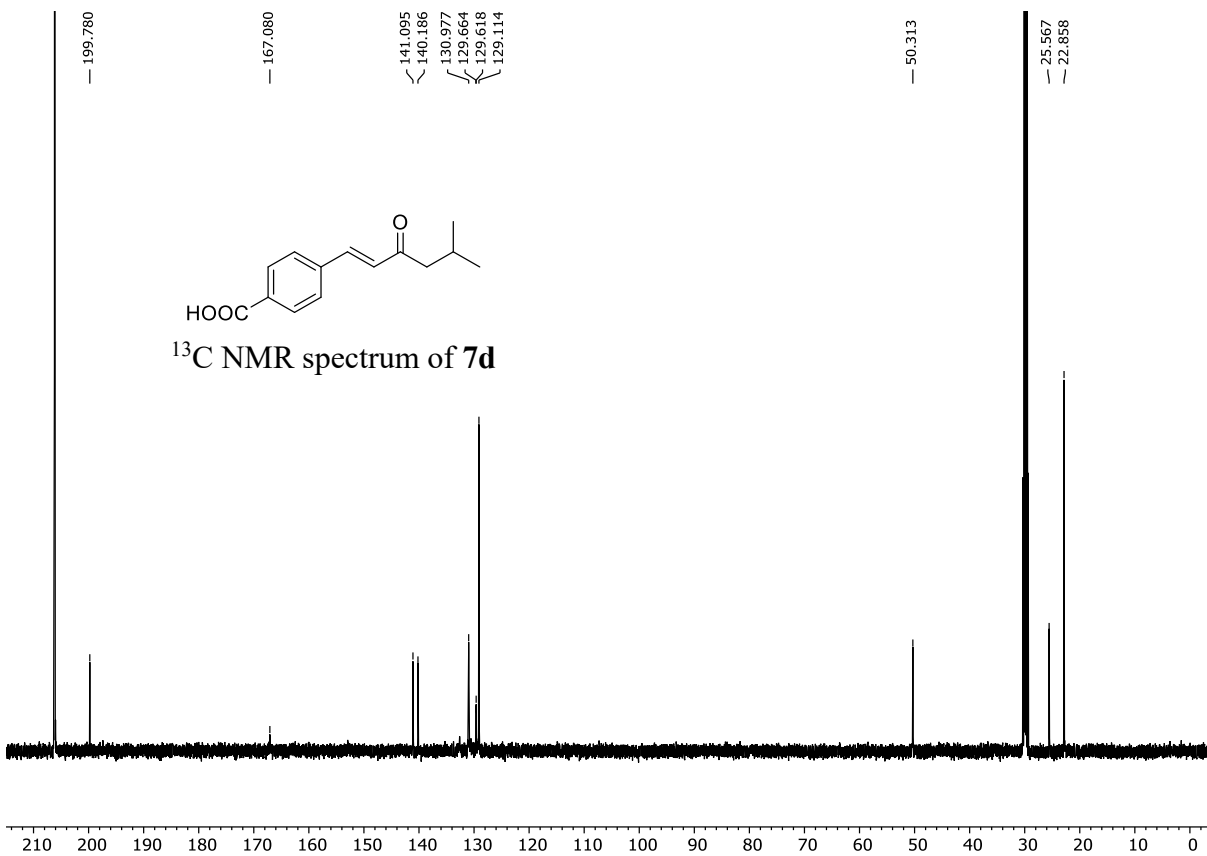


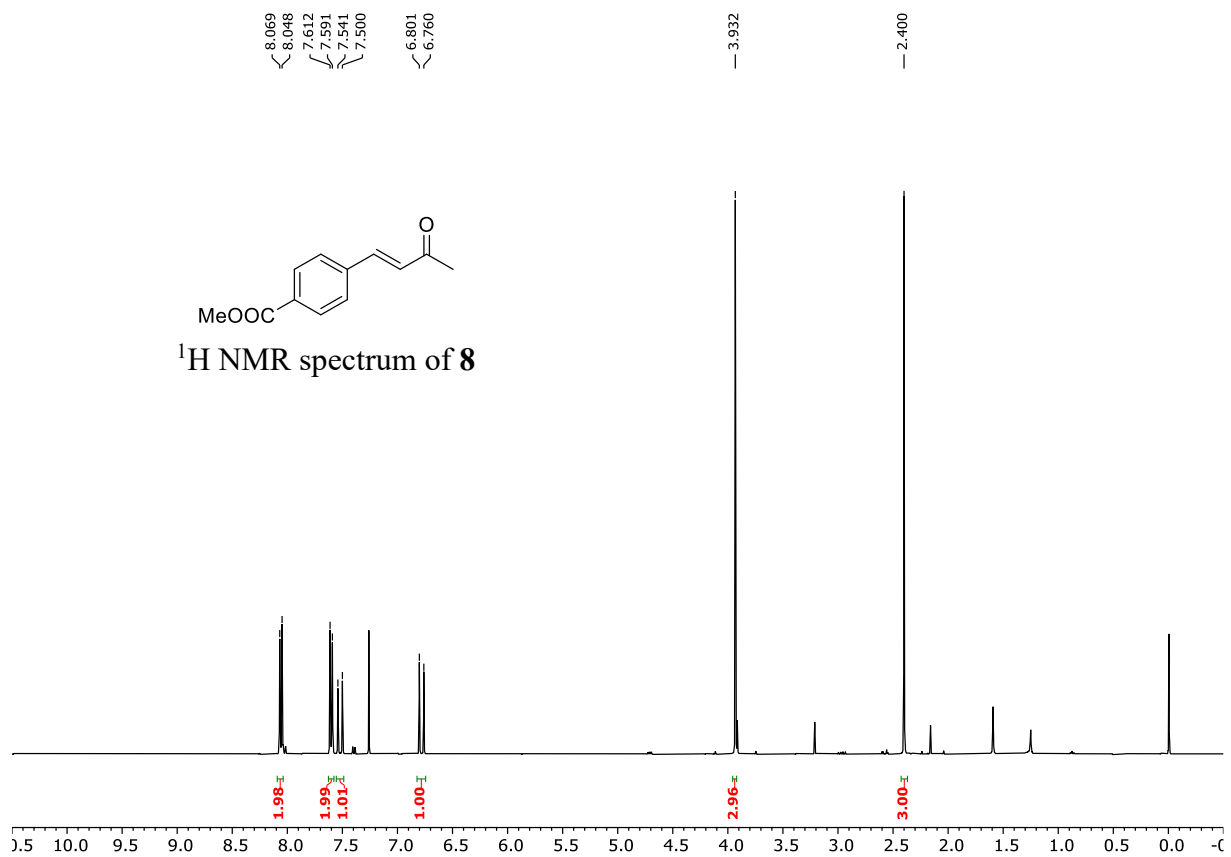
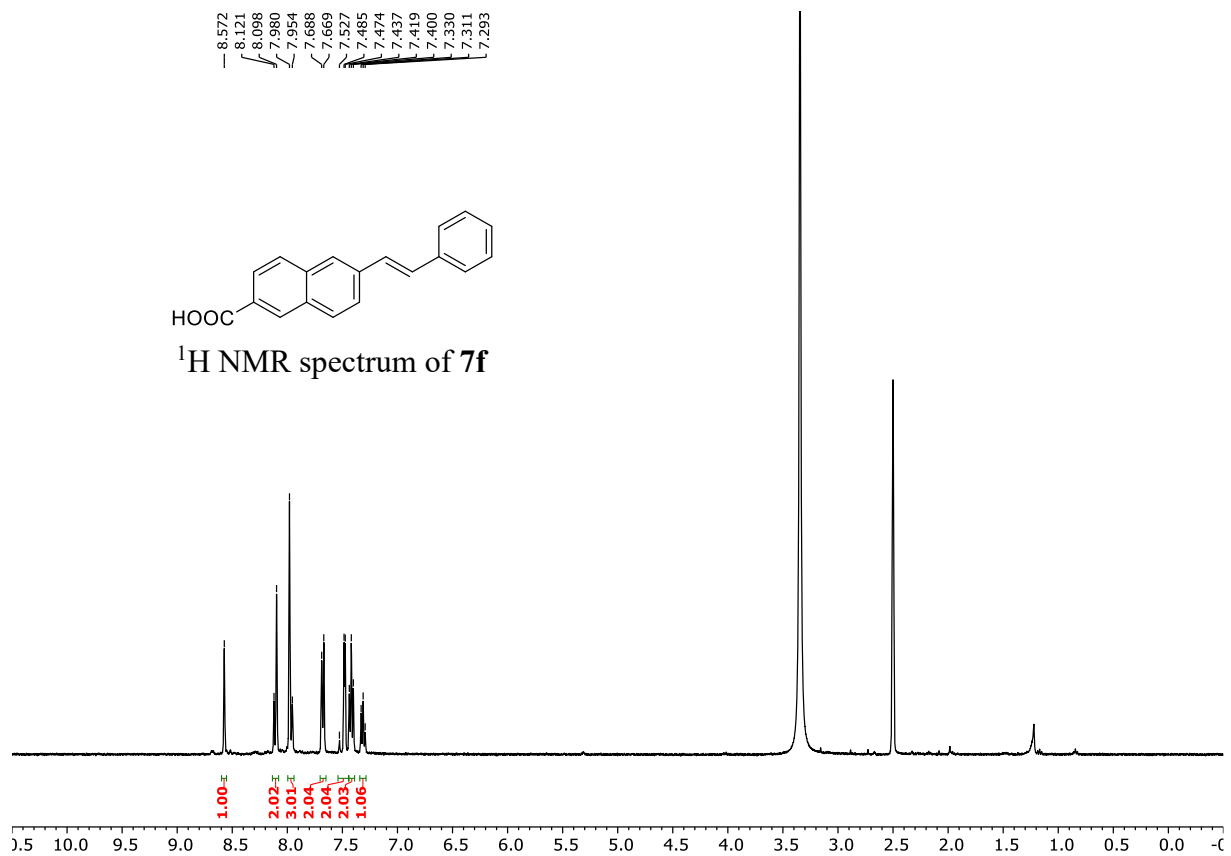


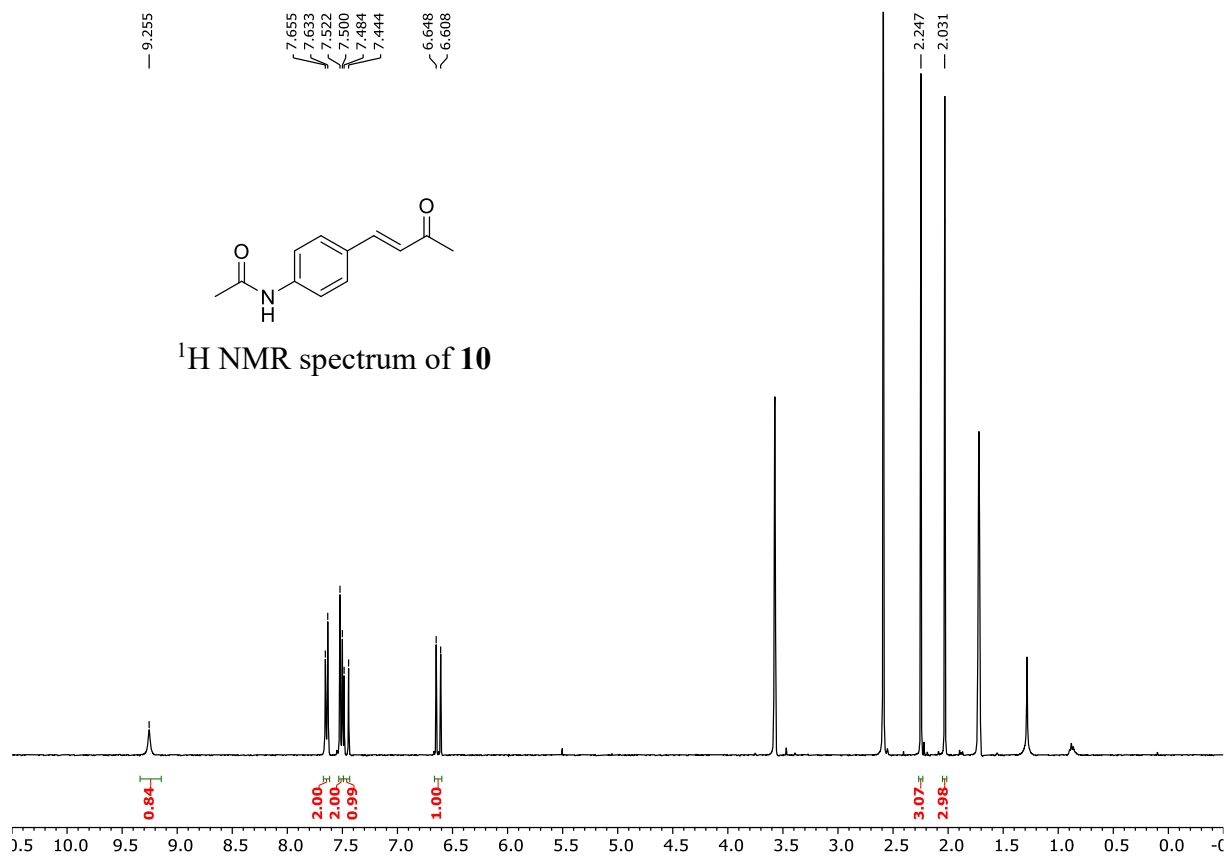
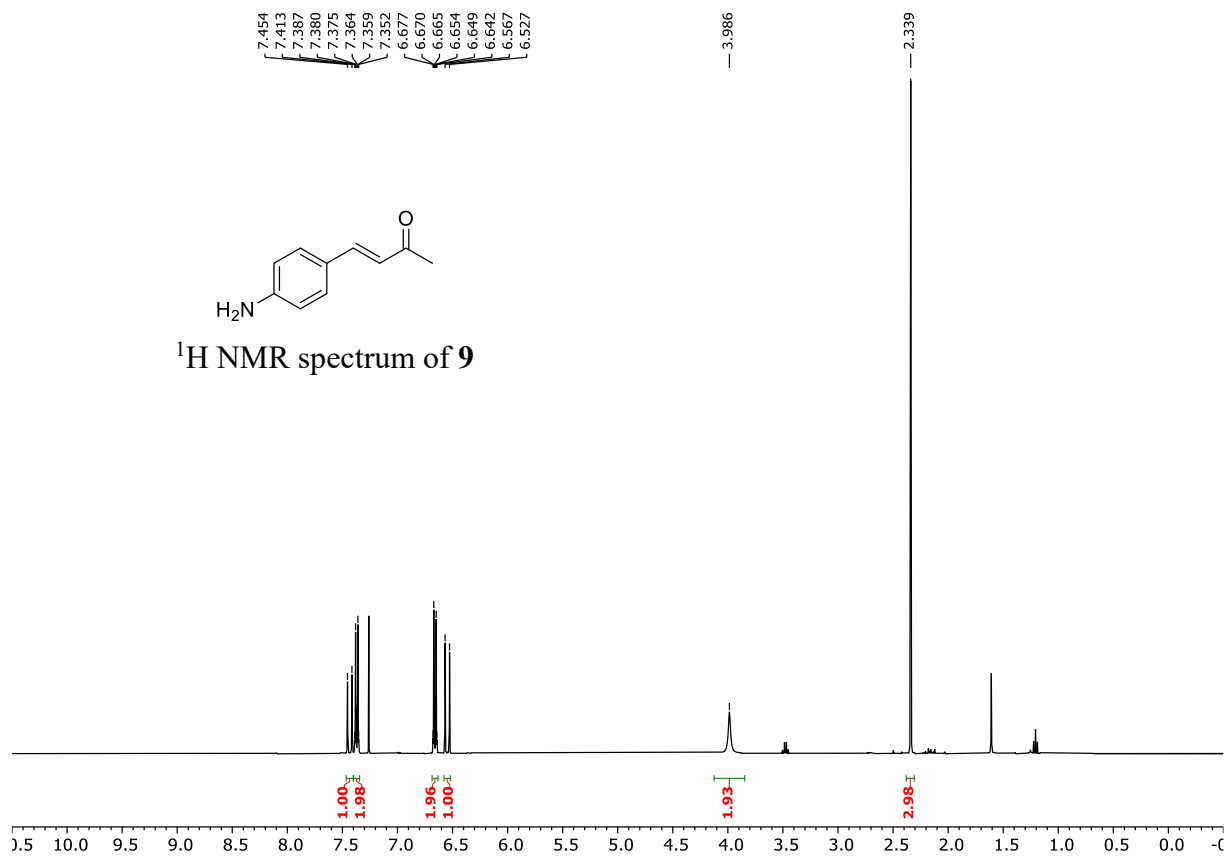
NMR spectra for compounds in Chapter 3:

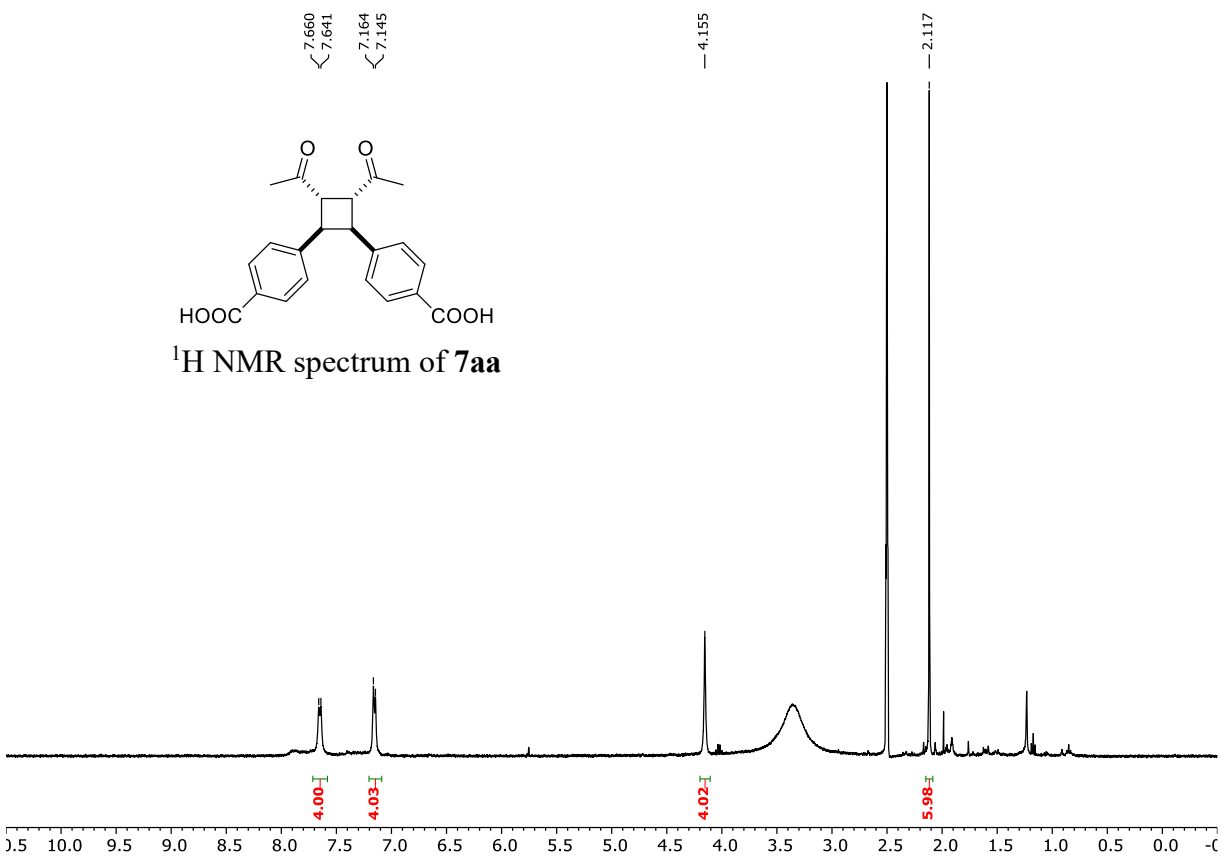
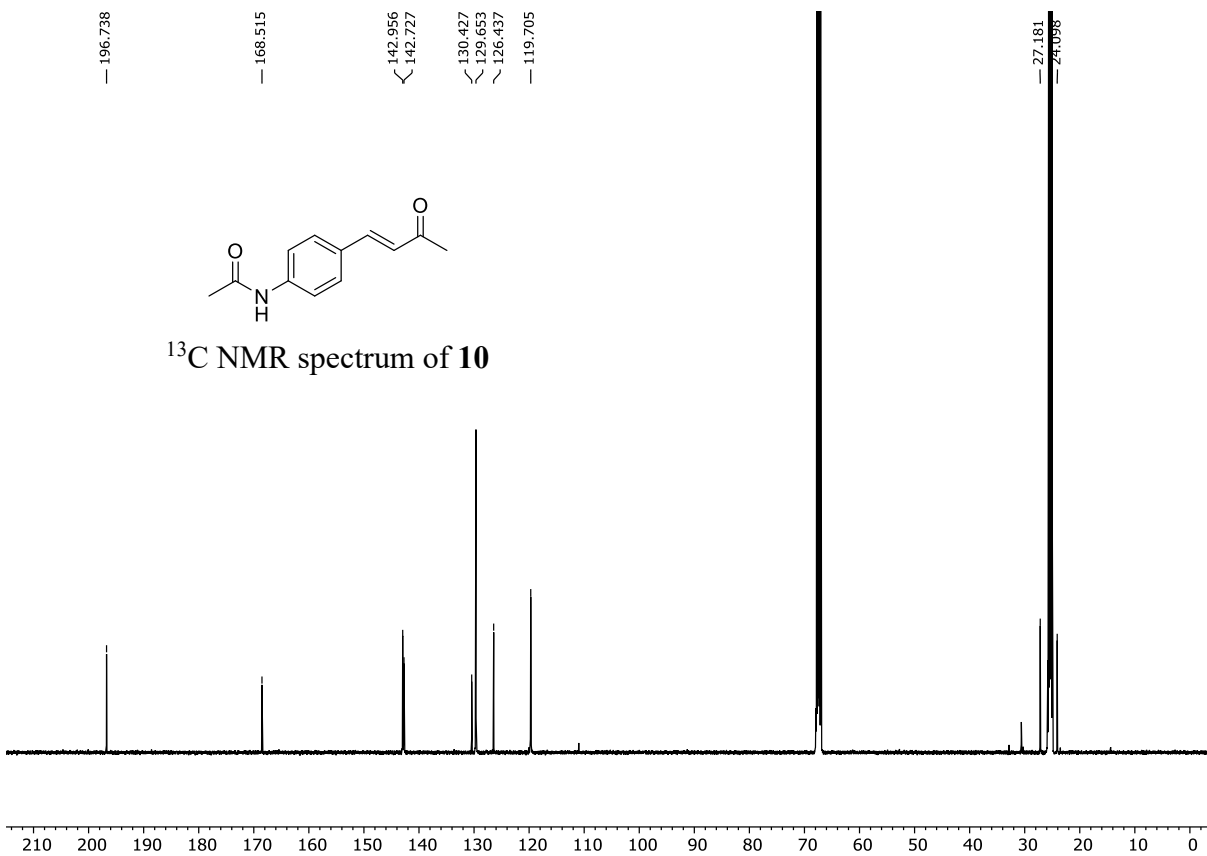


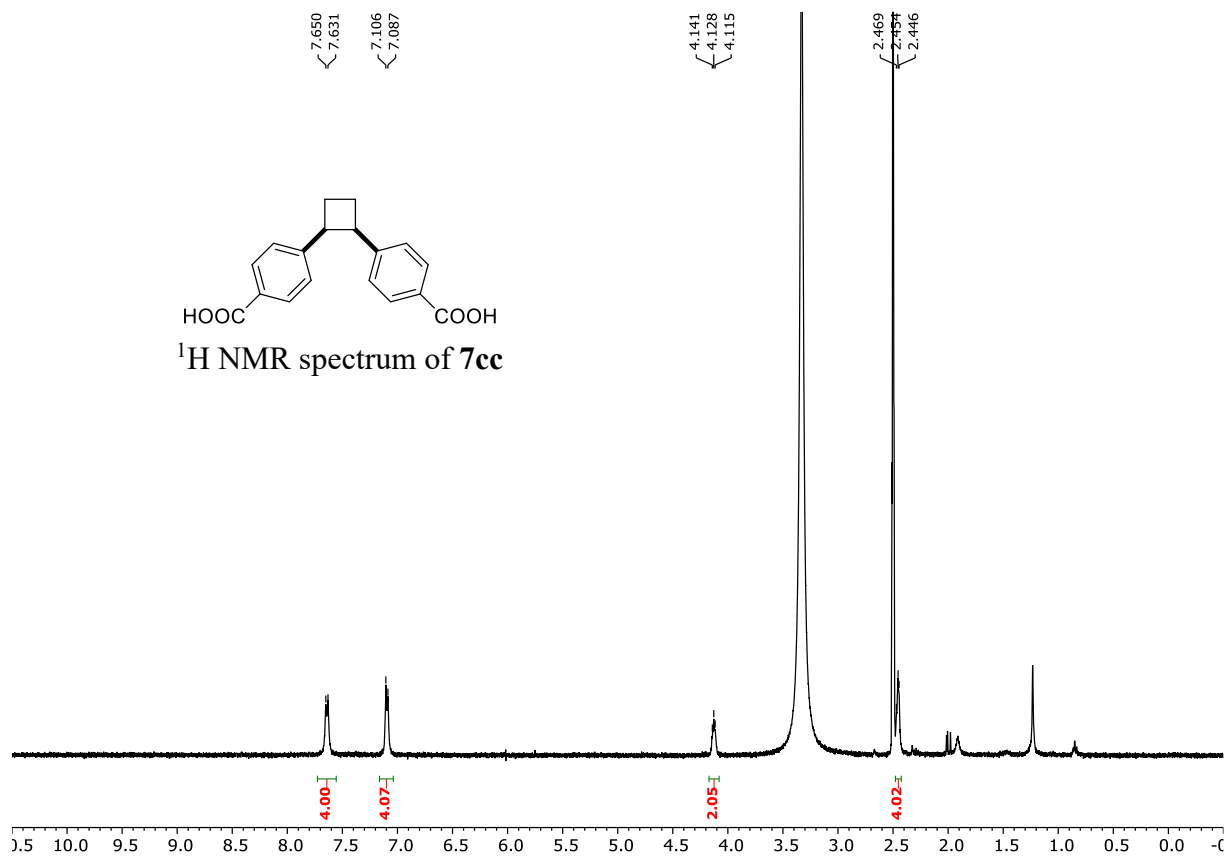
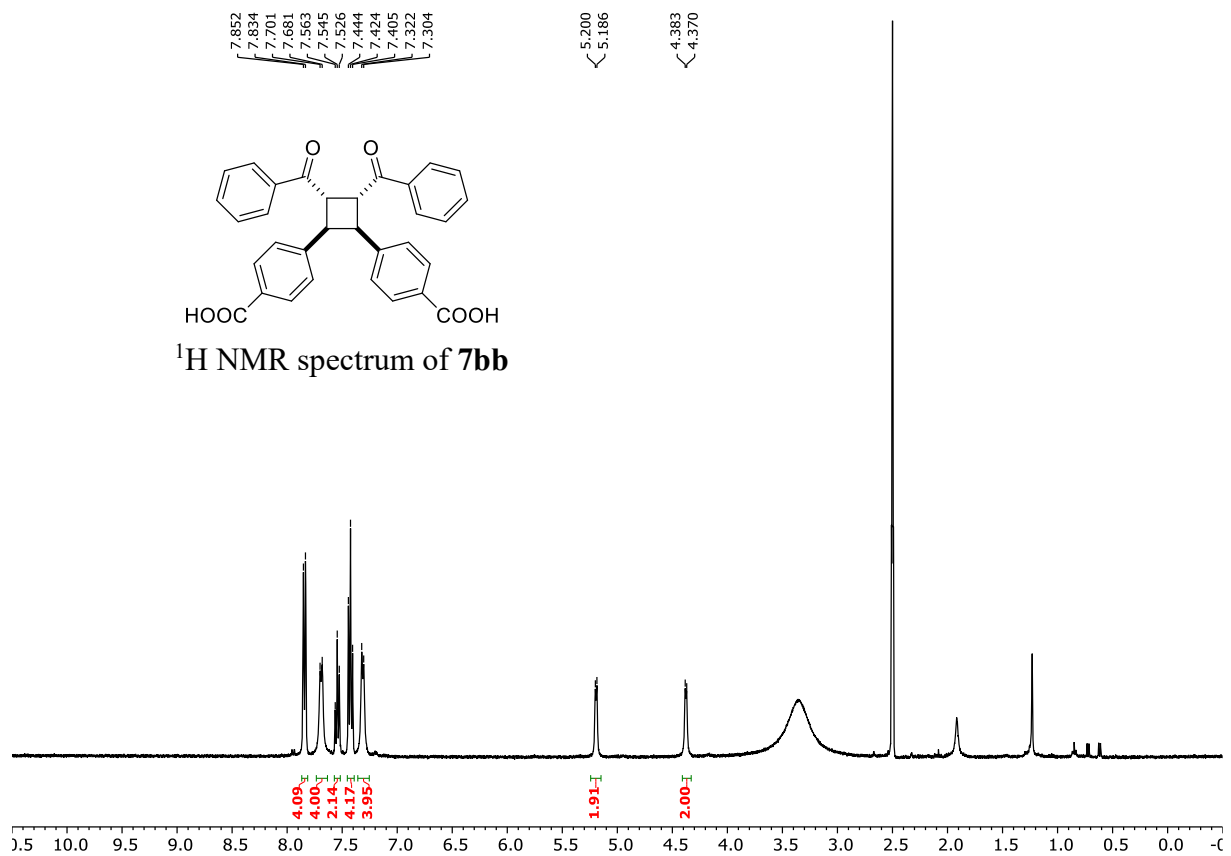


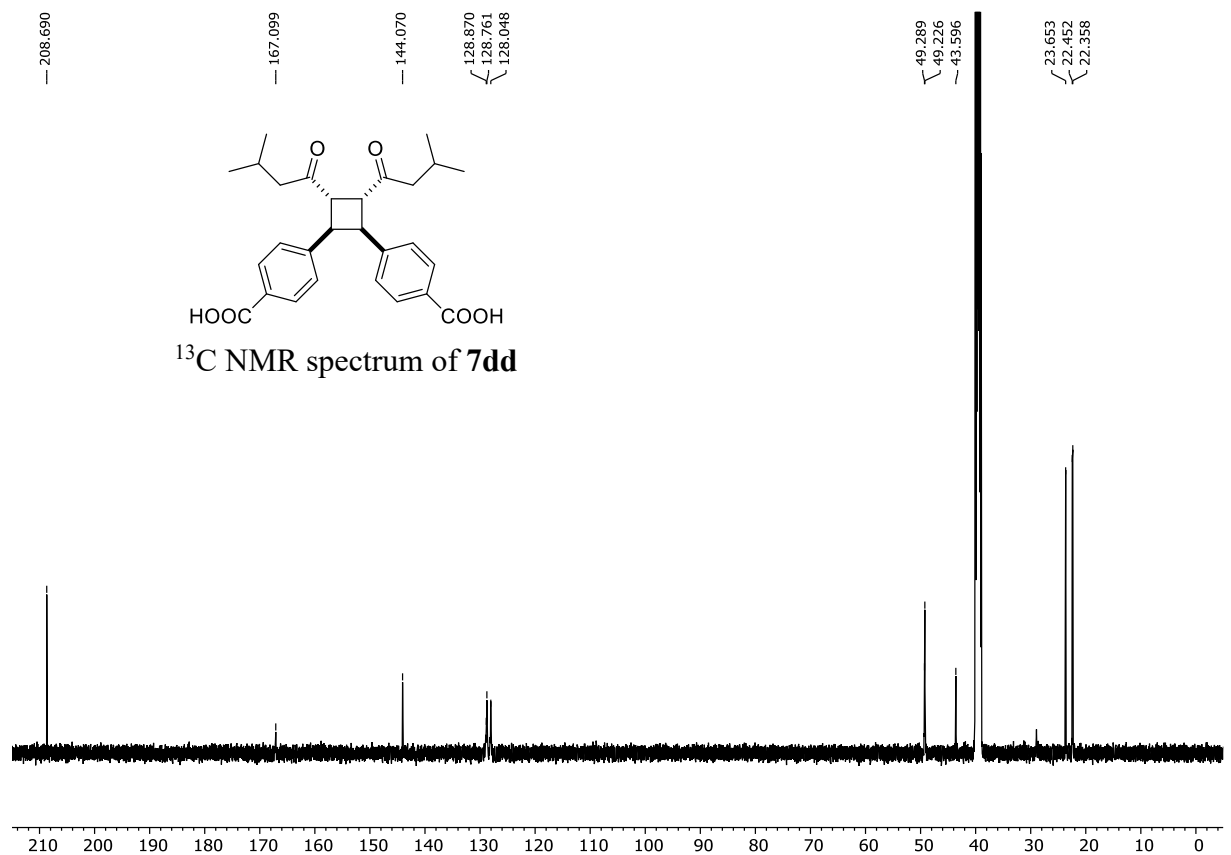
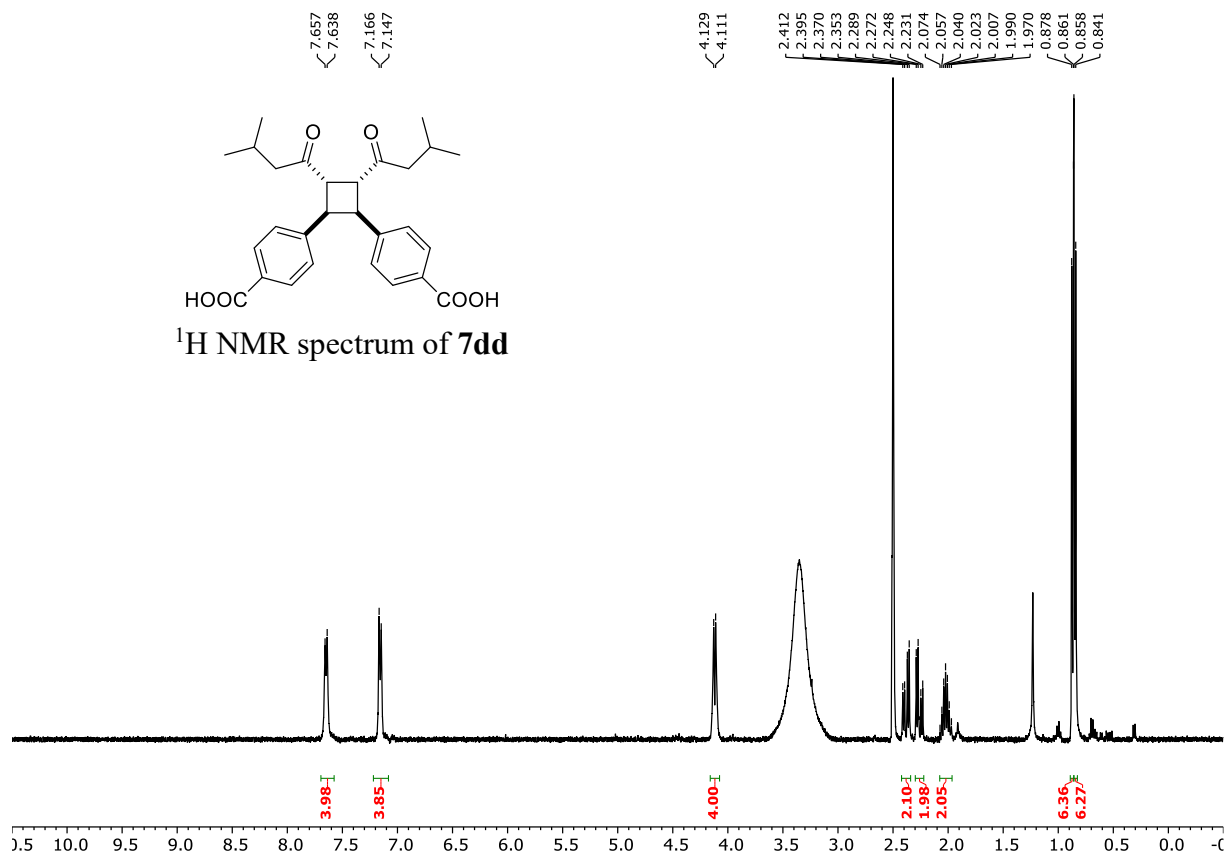


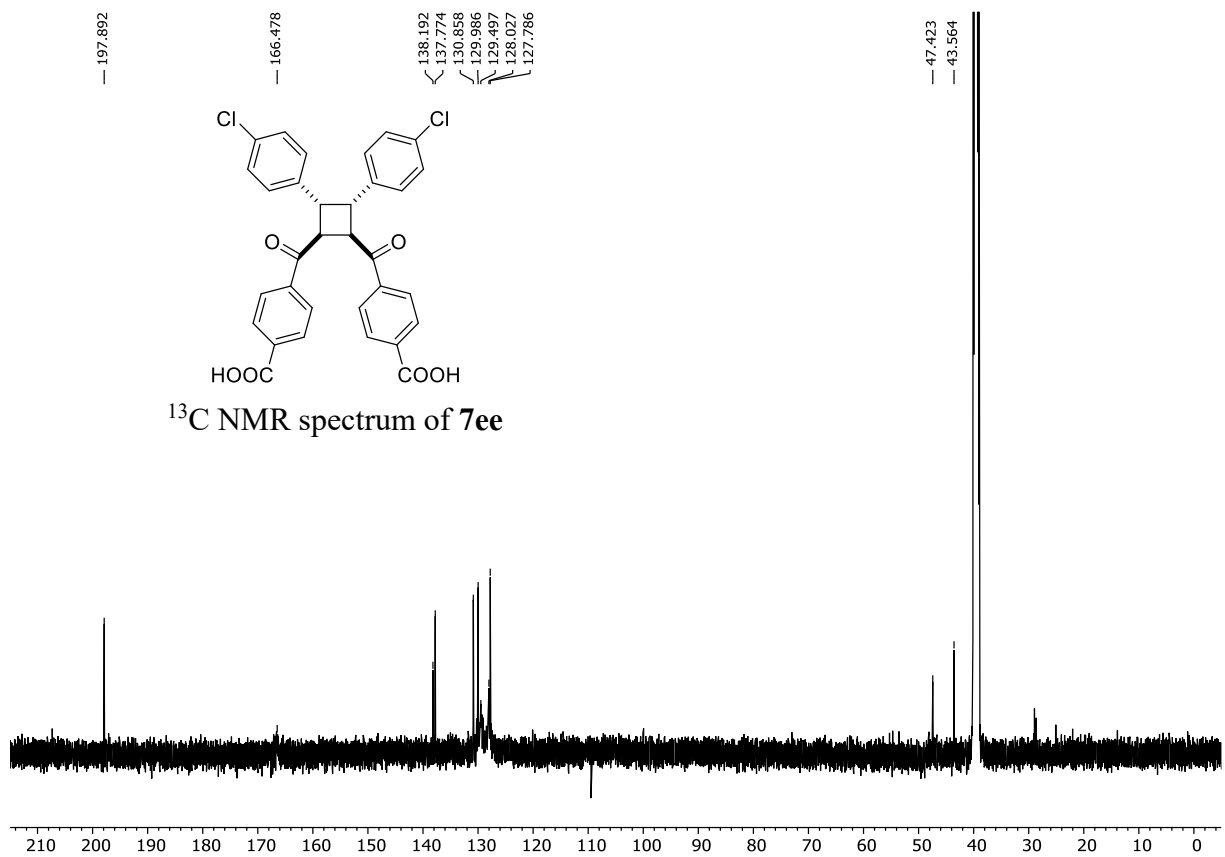
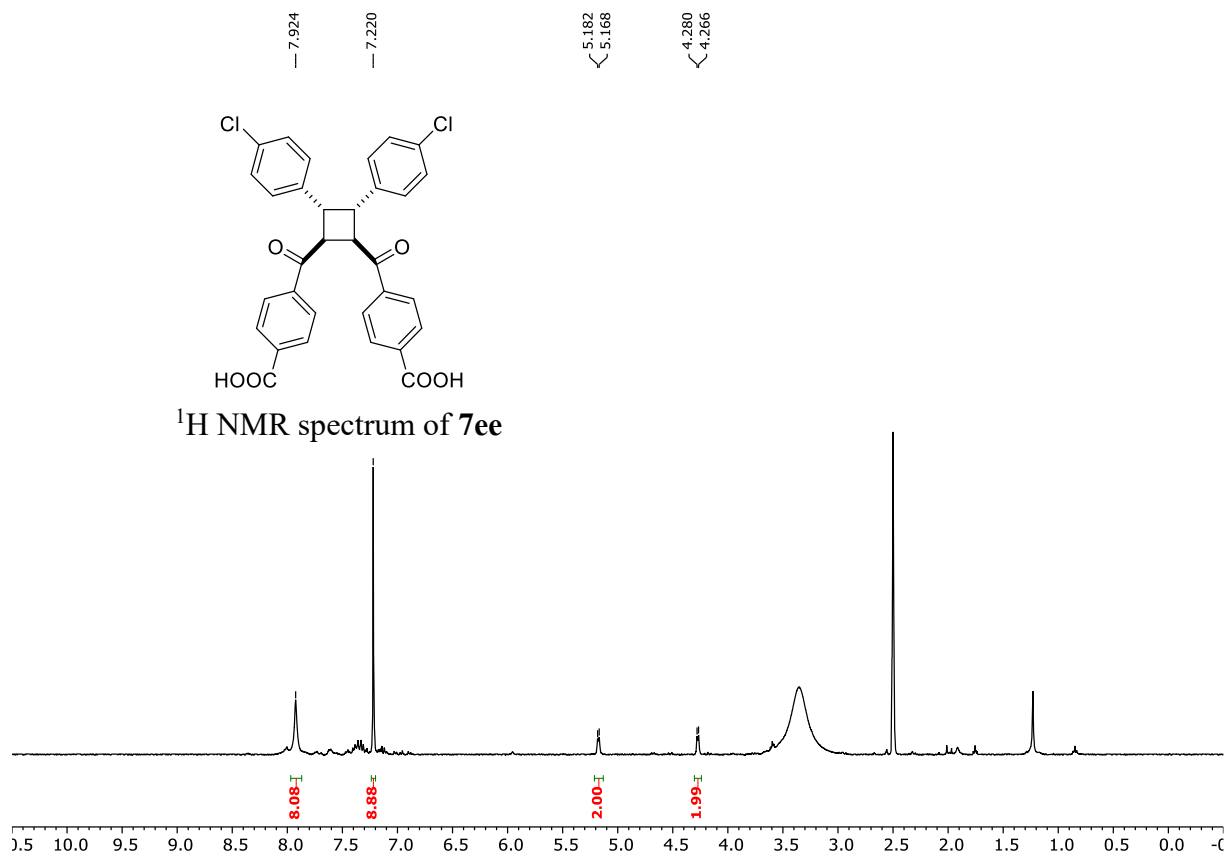


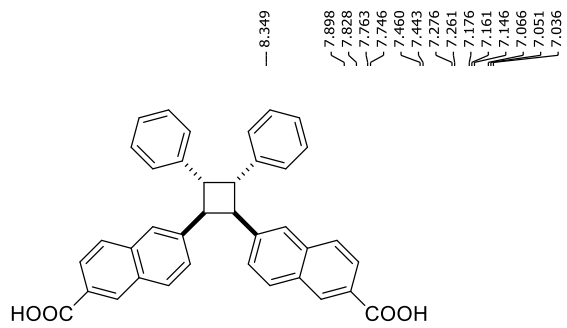




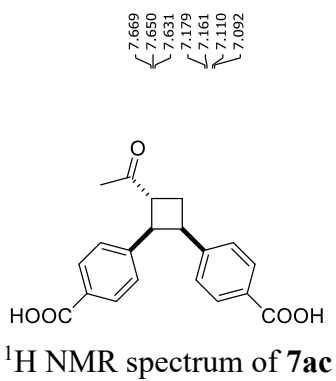
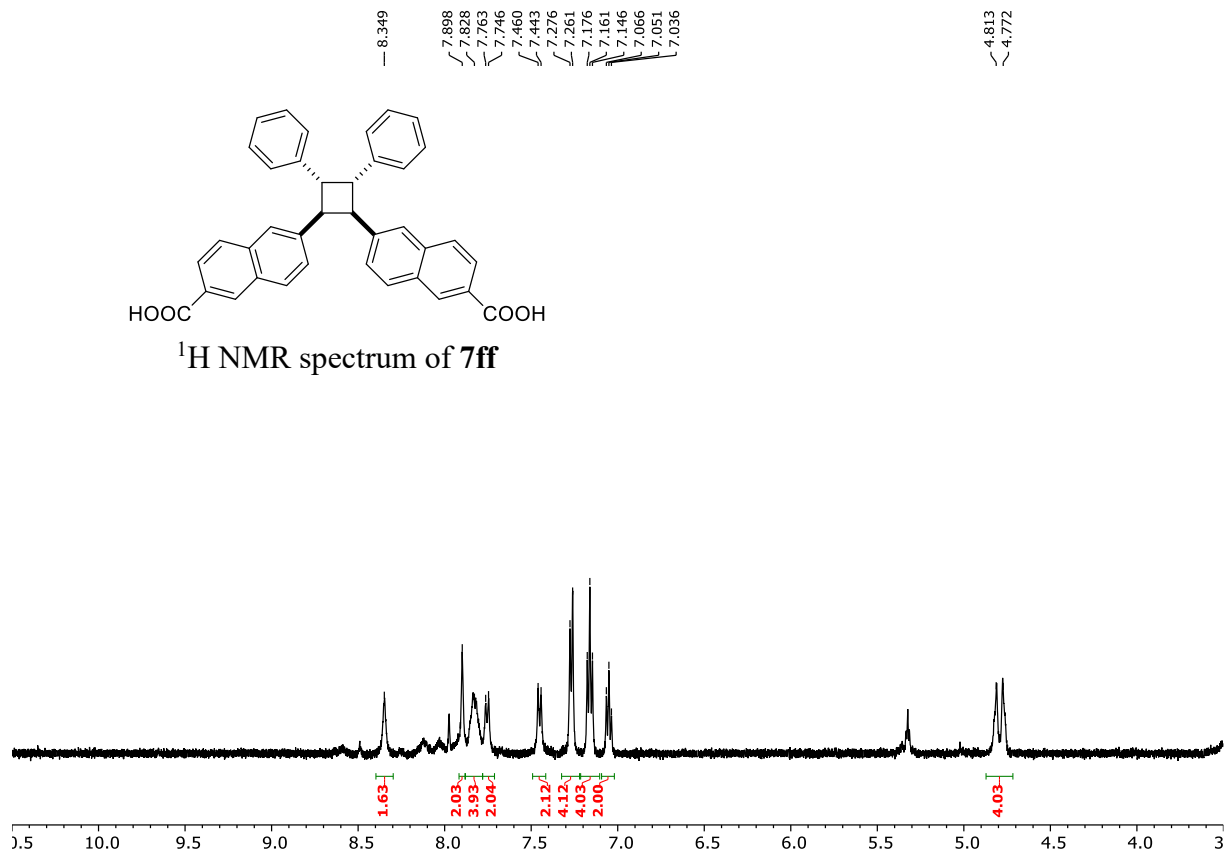




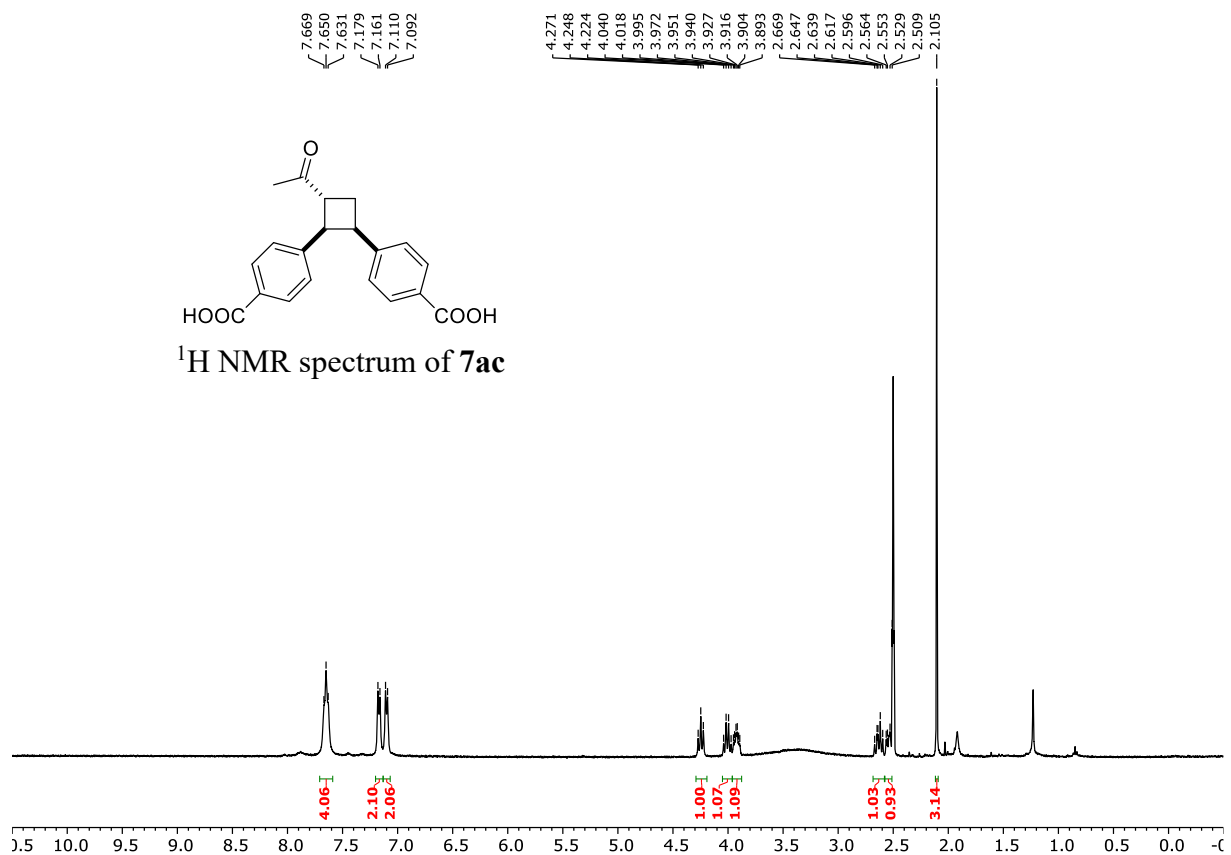


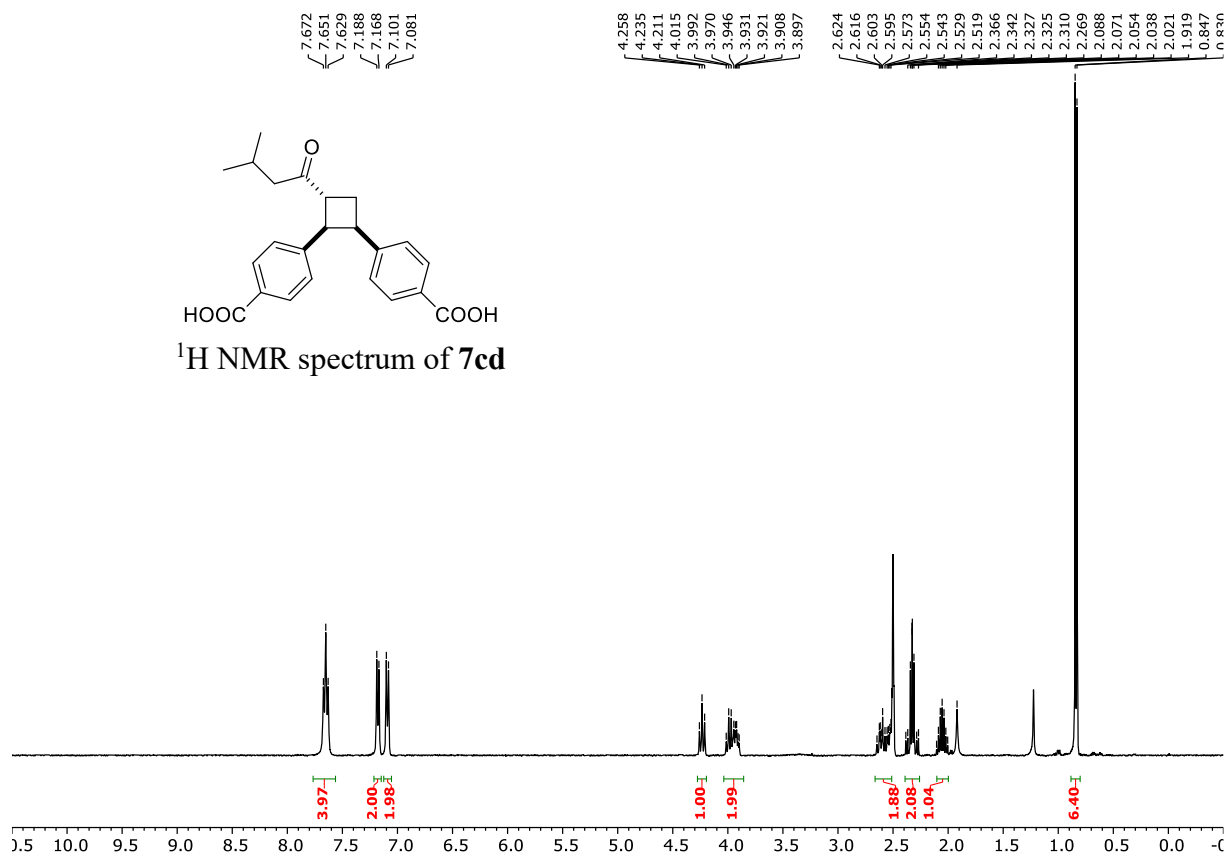
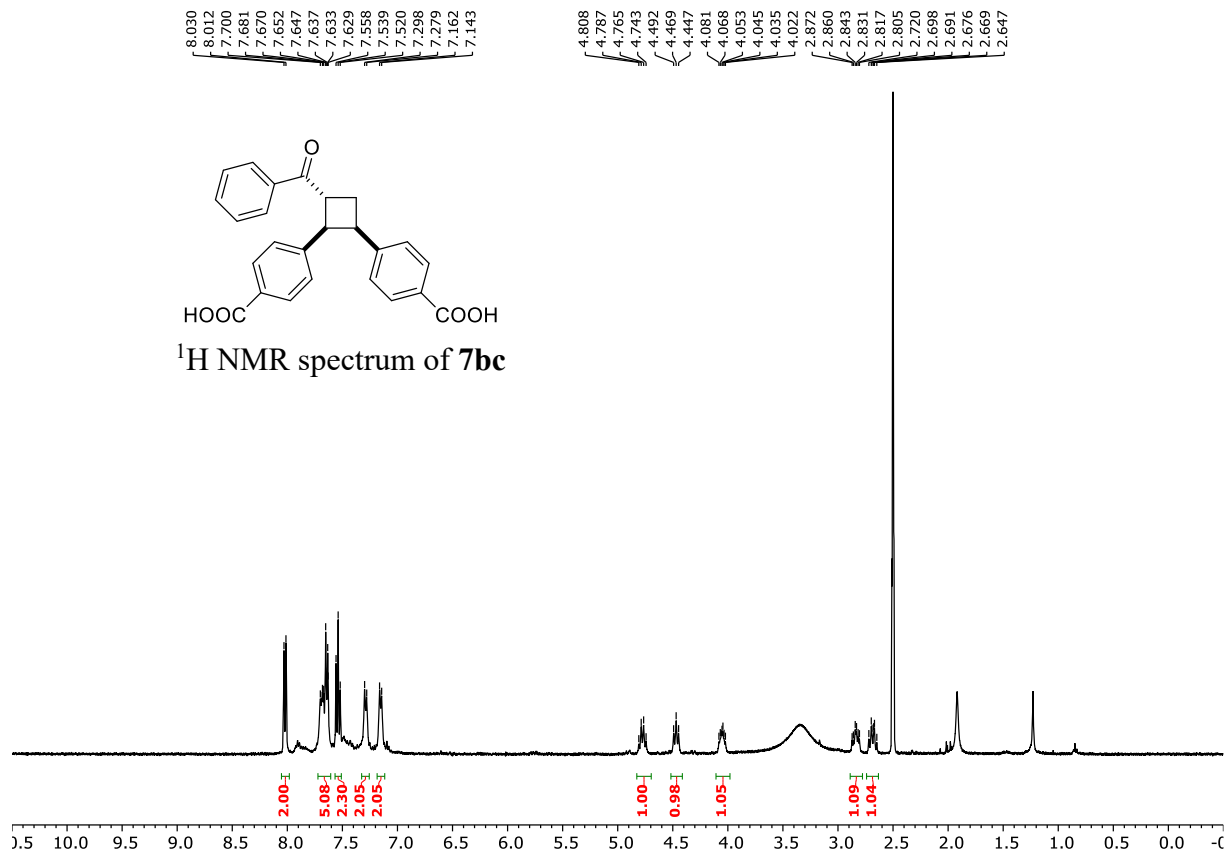


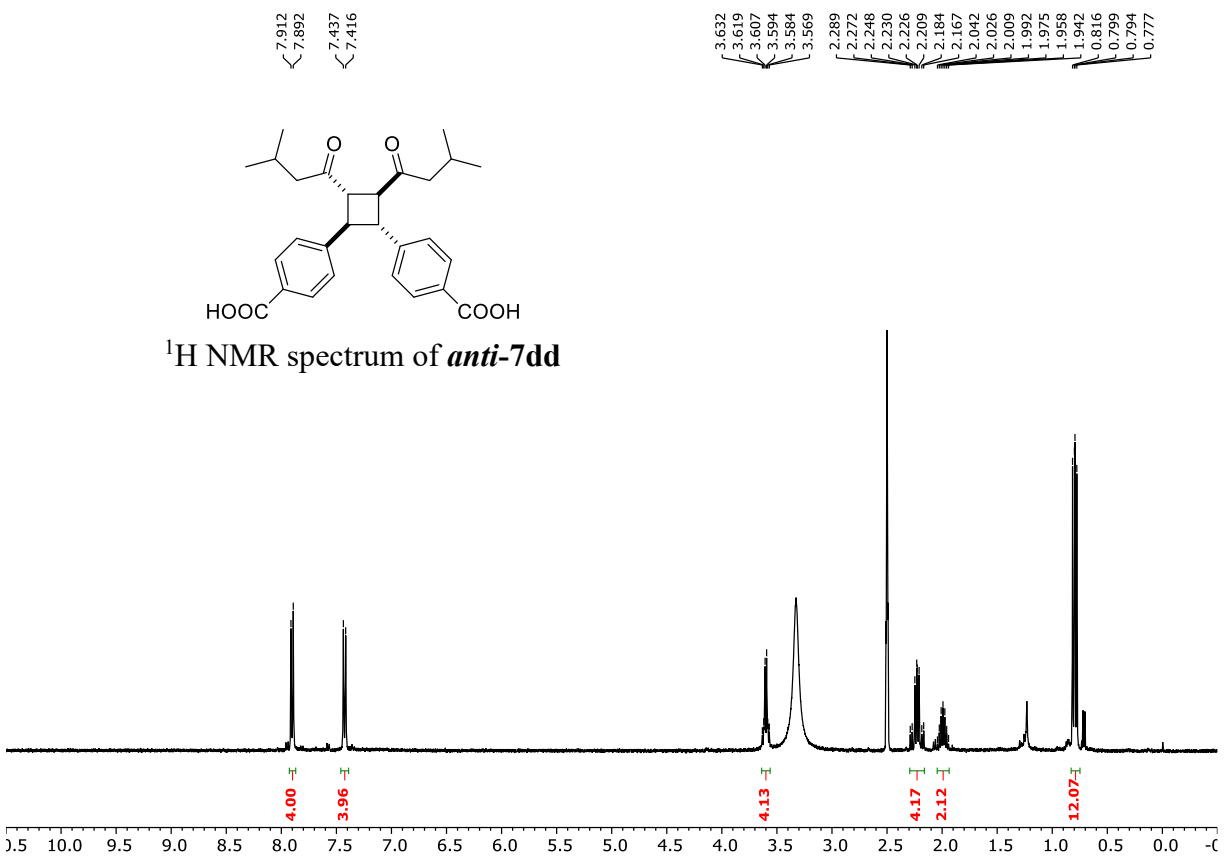
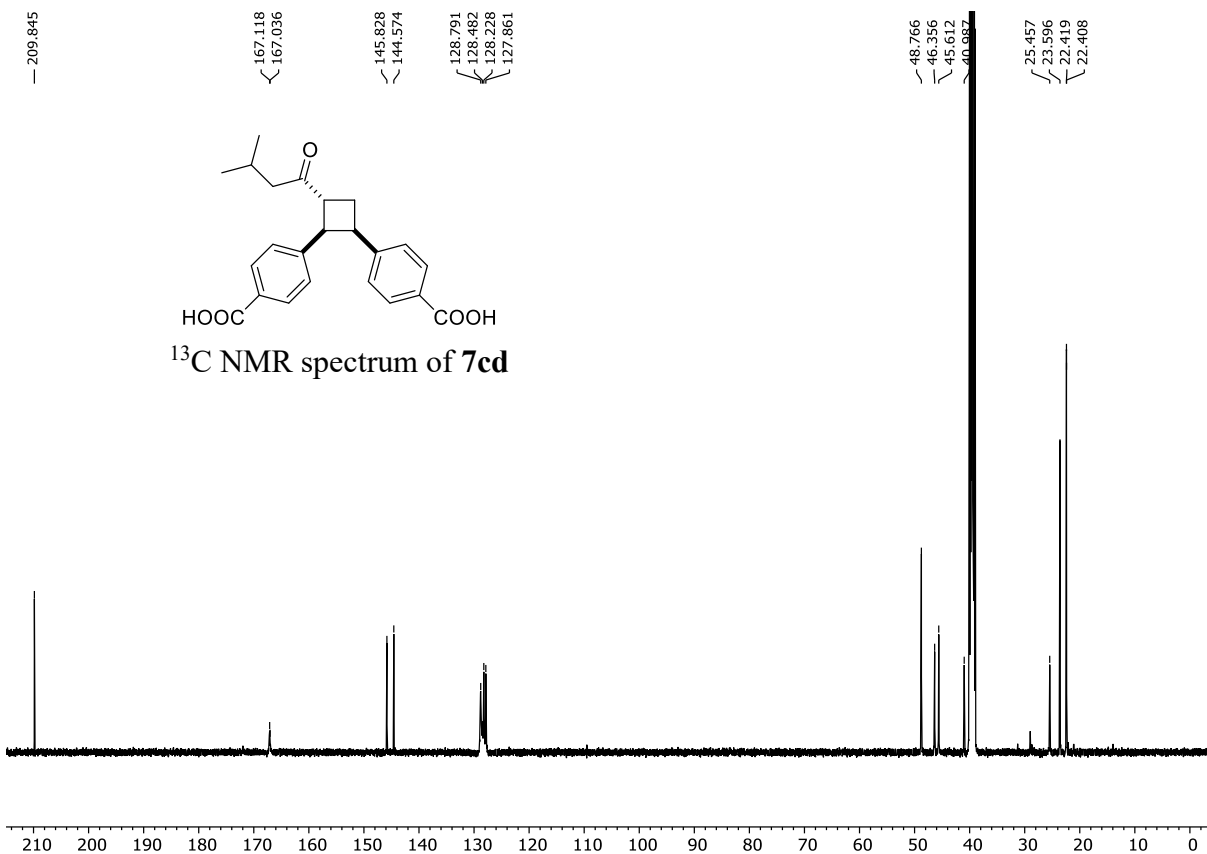
¹H NMR spectrum of **7ff**

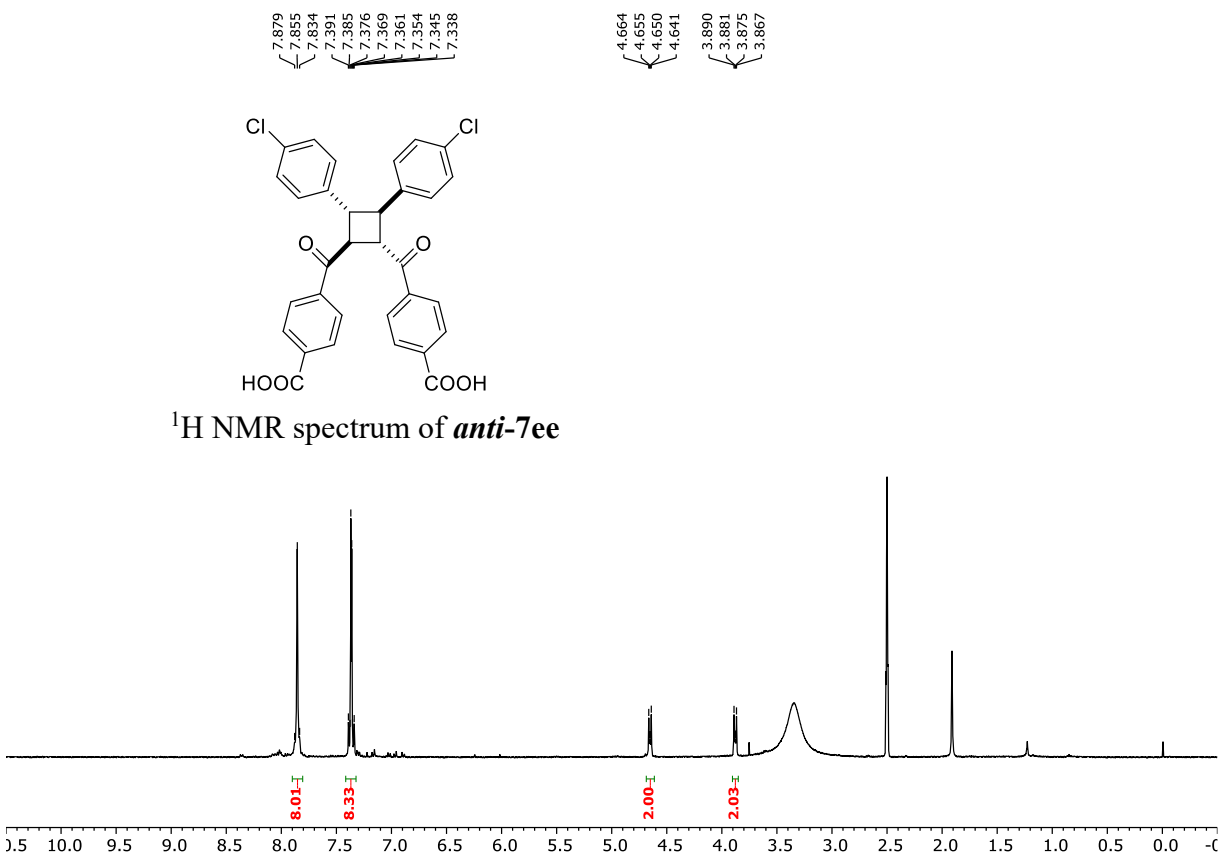
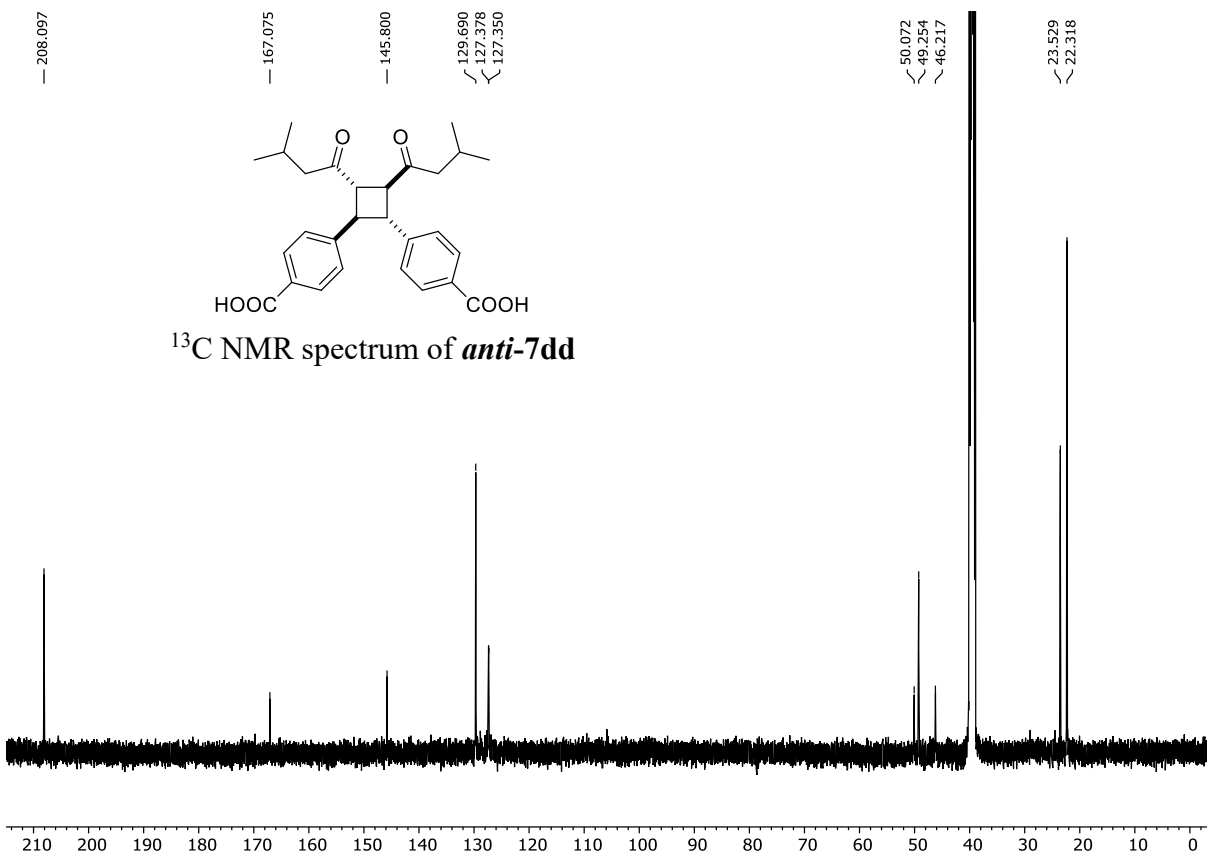


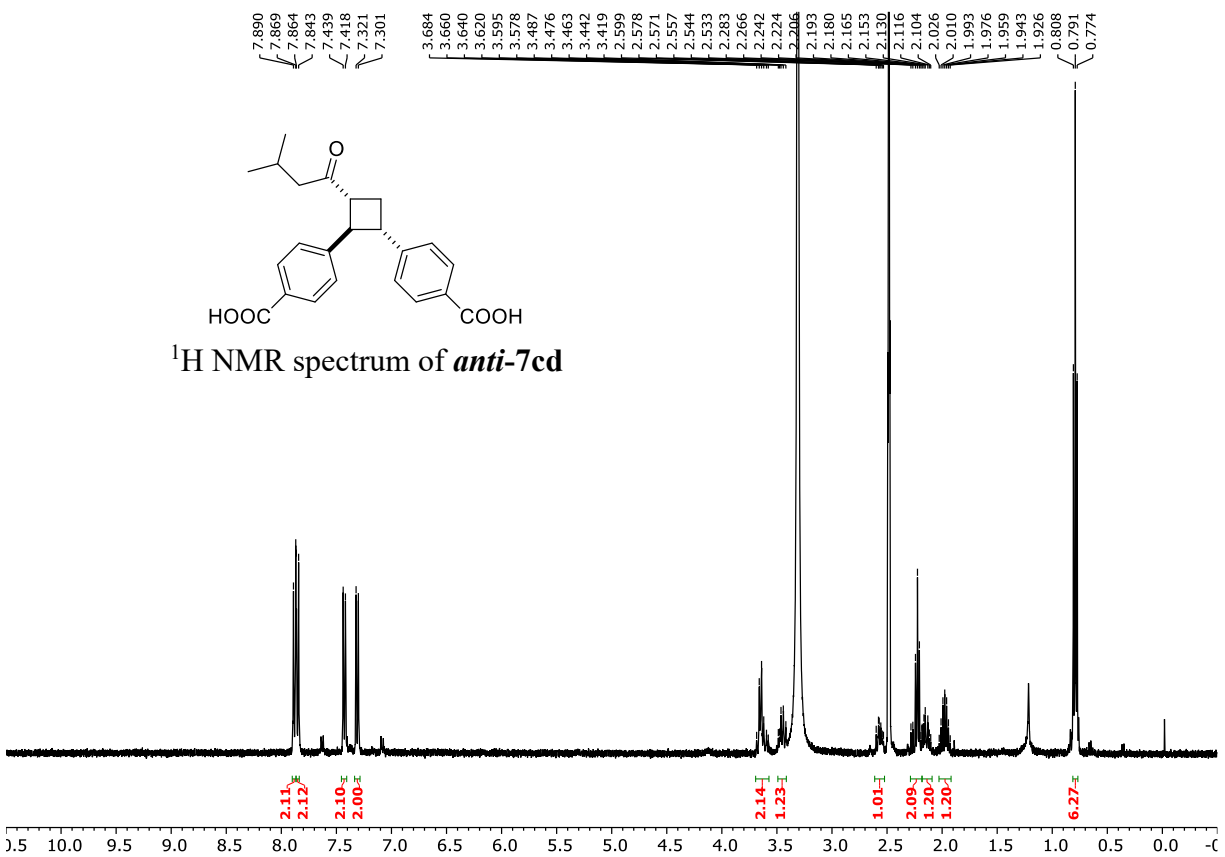
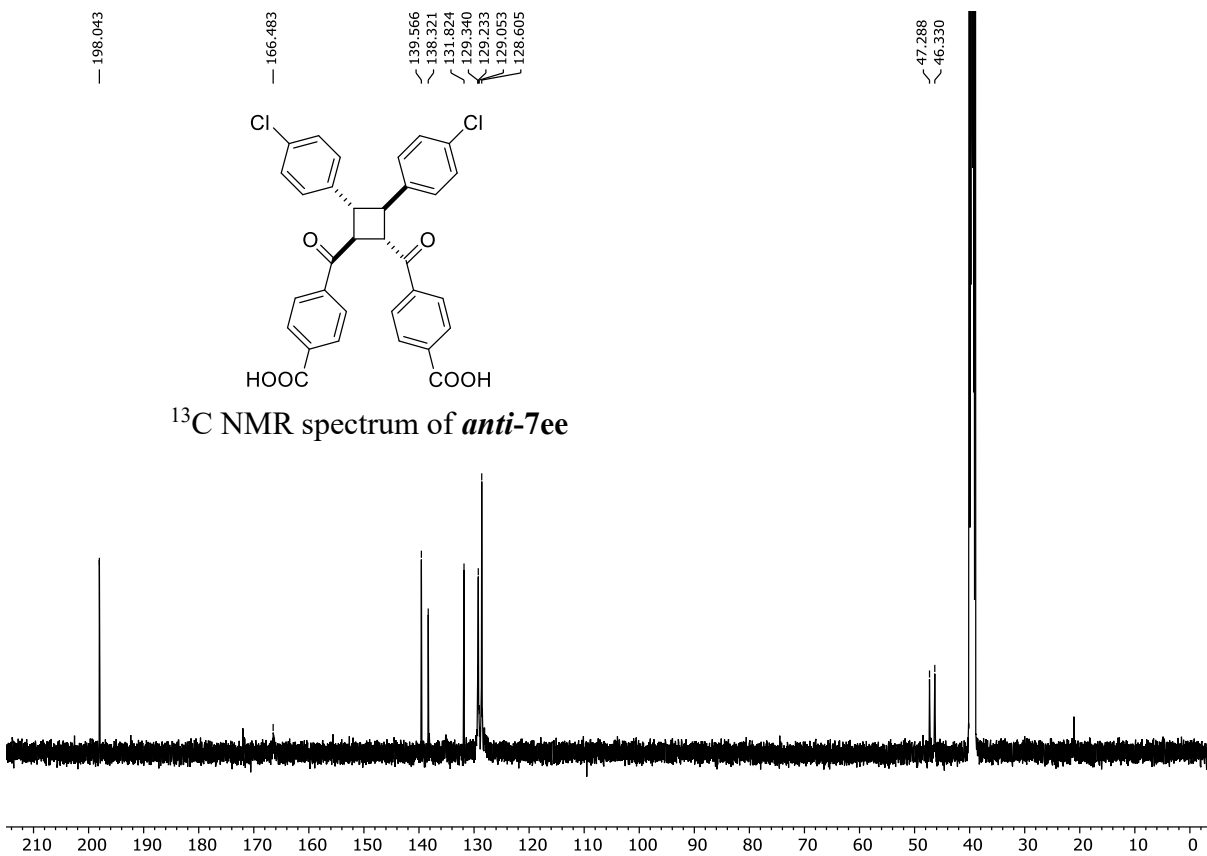
¹H NMR spectrum of **7ac**

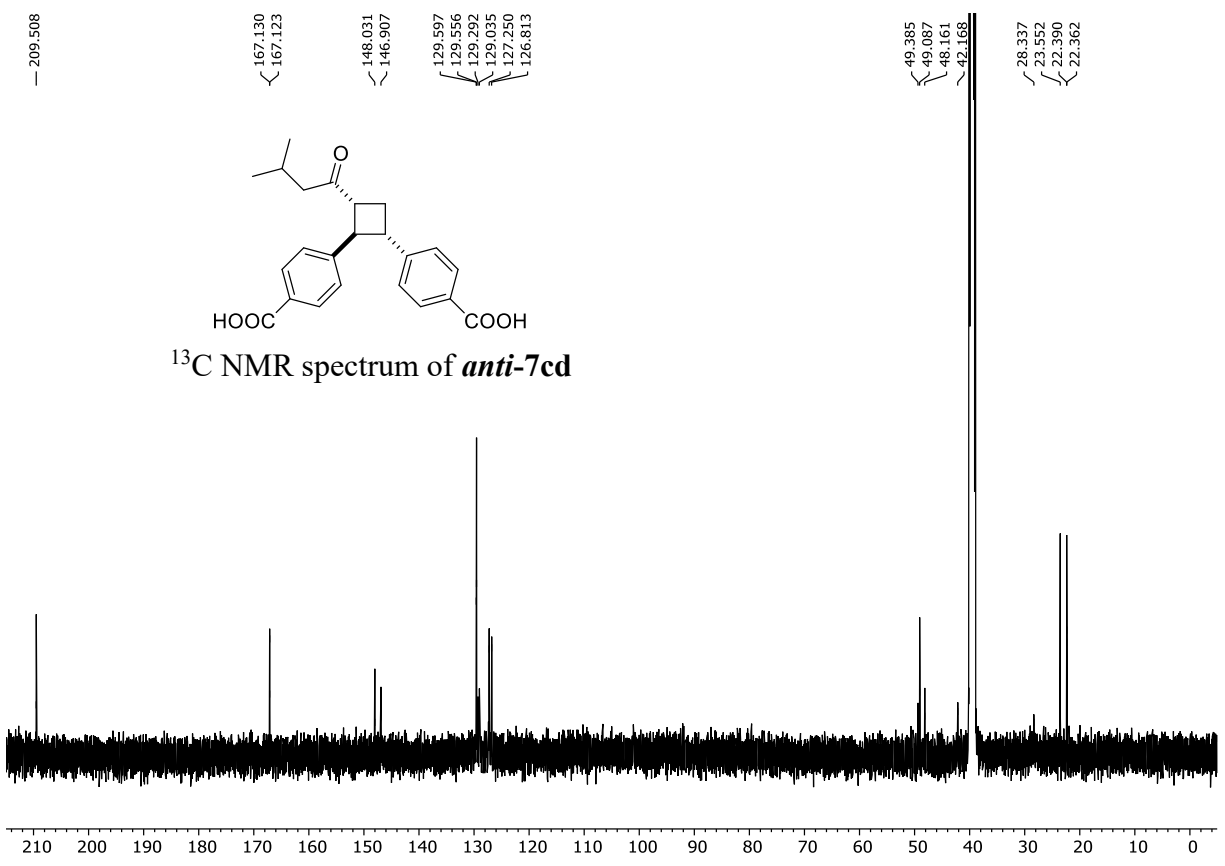




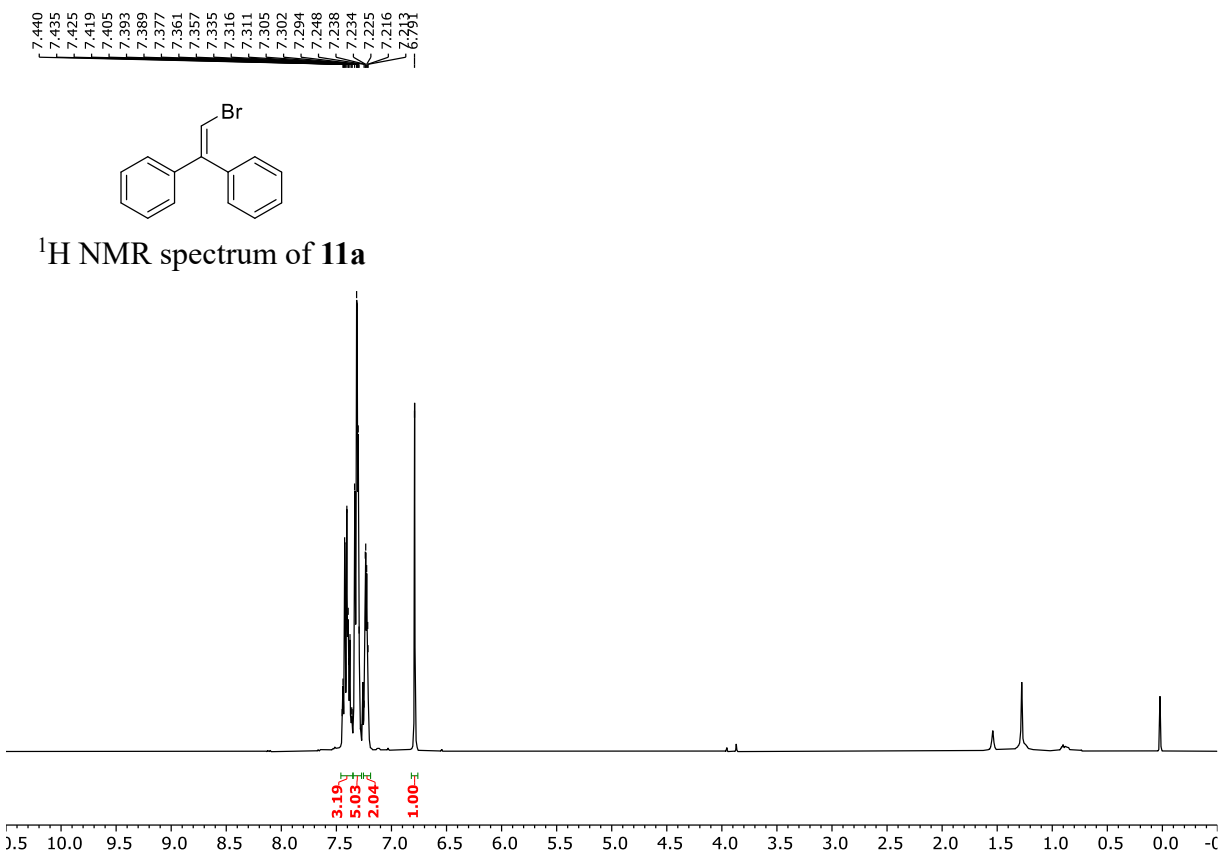


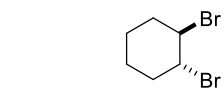




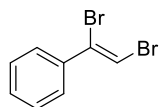
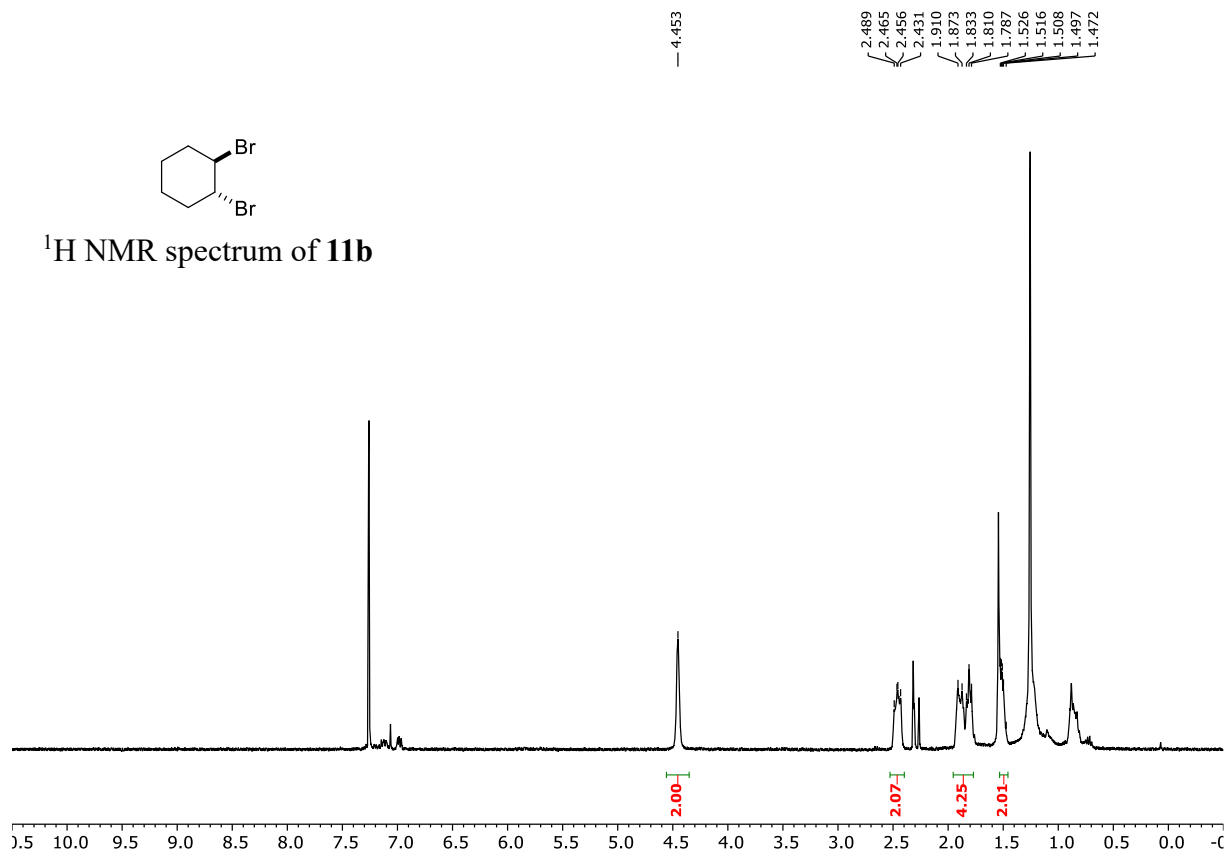


NMR spectra for compounds in Chapter 4:

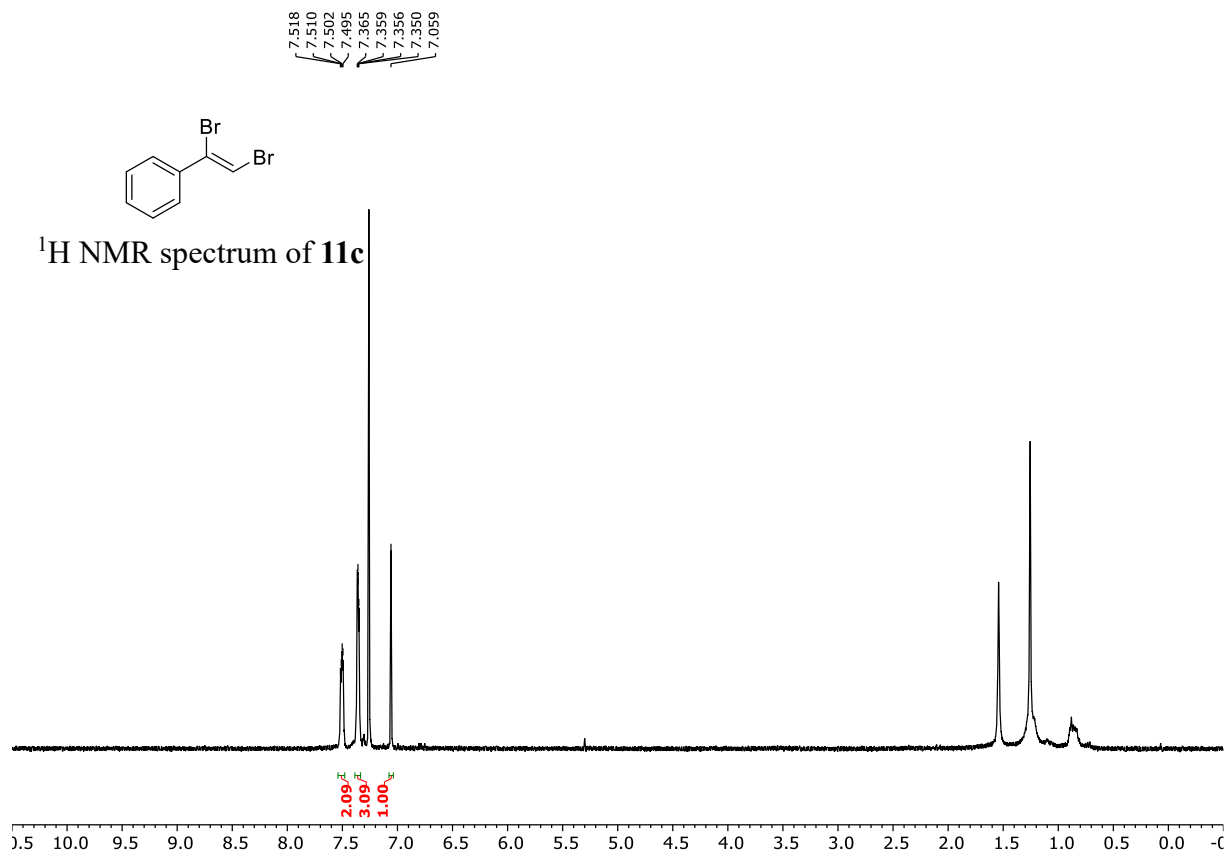




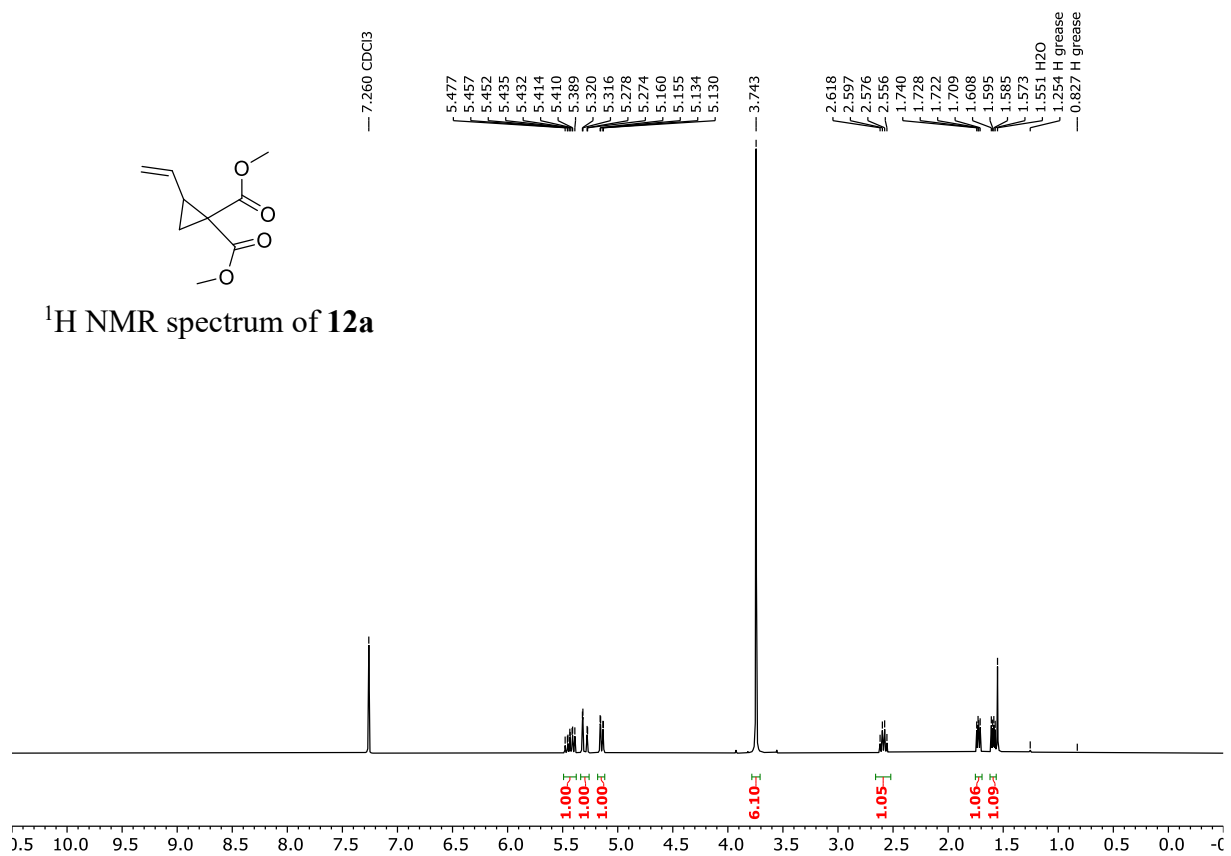
^1H NMR spectrum of **11b**



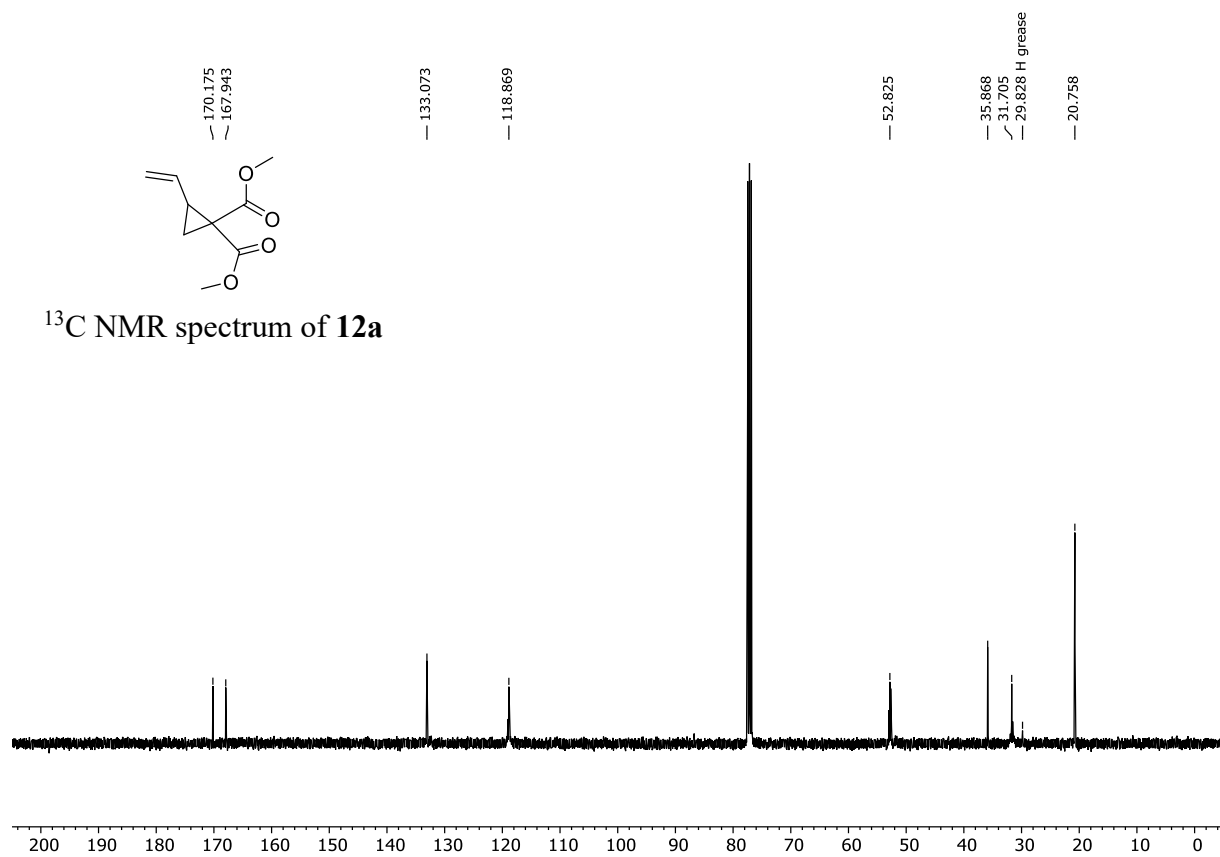
^1H NMR spectrum of **11c**

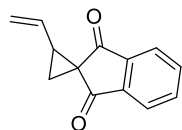


¹H NMR spectrum of **12a**

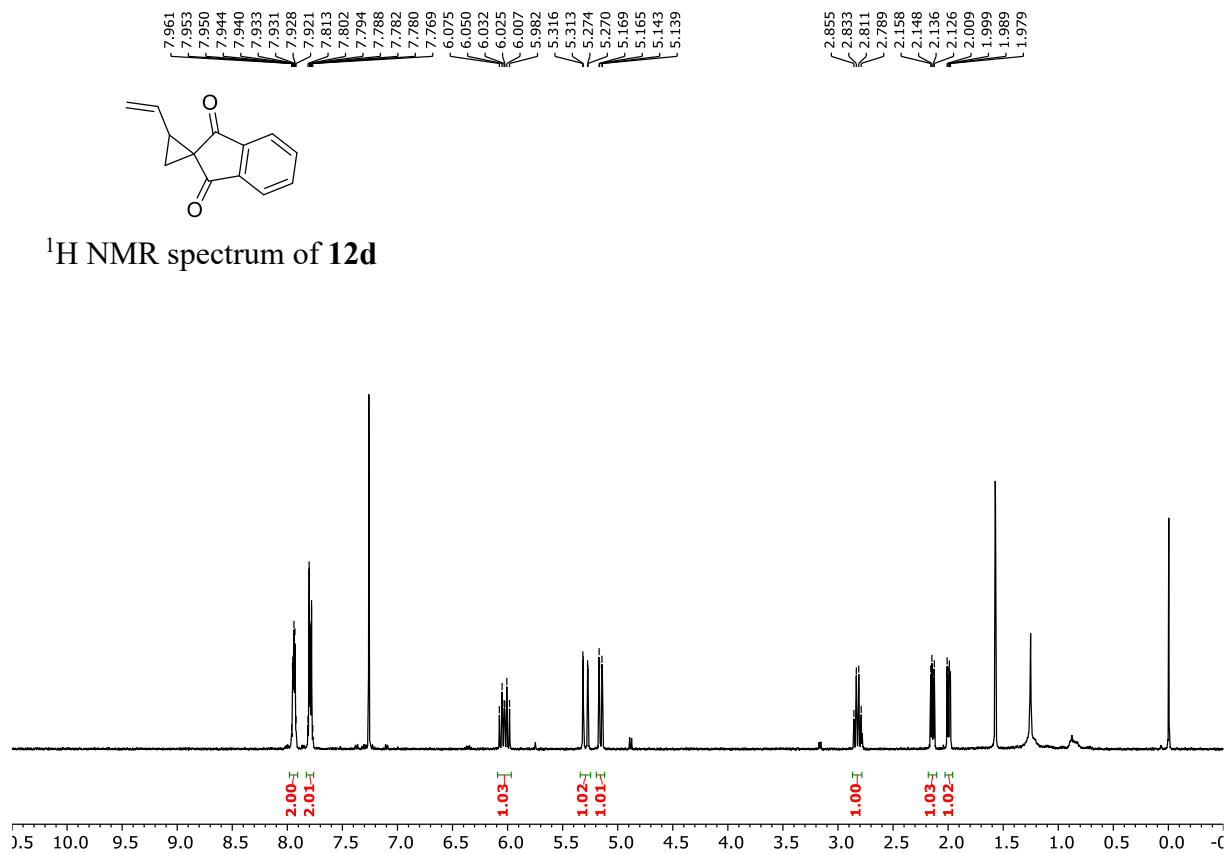


¹³C NMR spectrum of **12a**

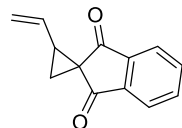




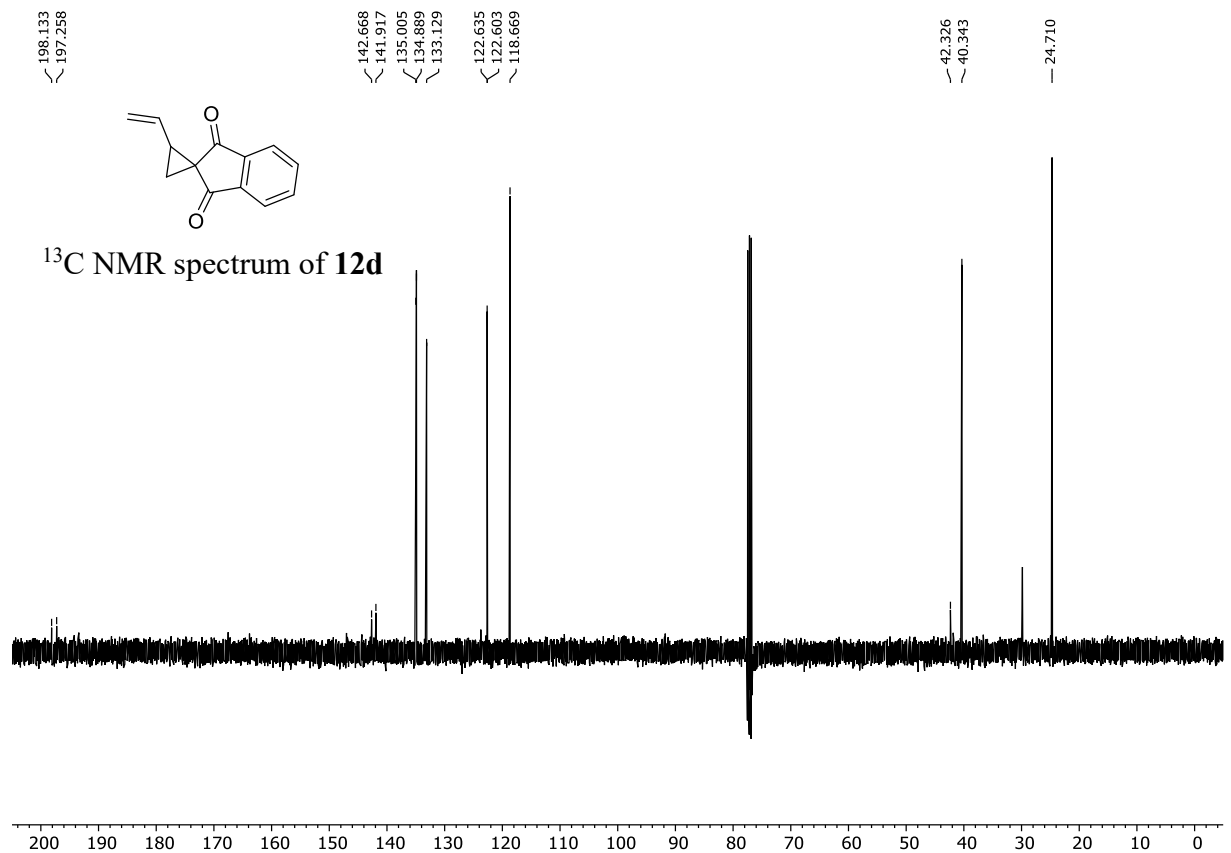
^1H NMR spectrum of **12d**

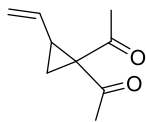


198.133
197.258

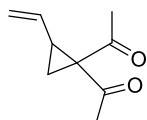
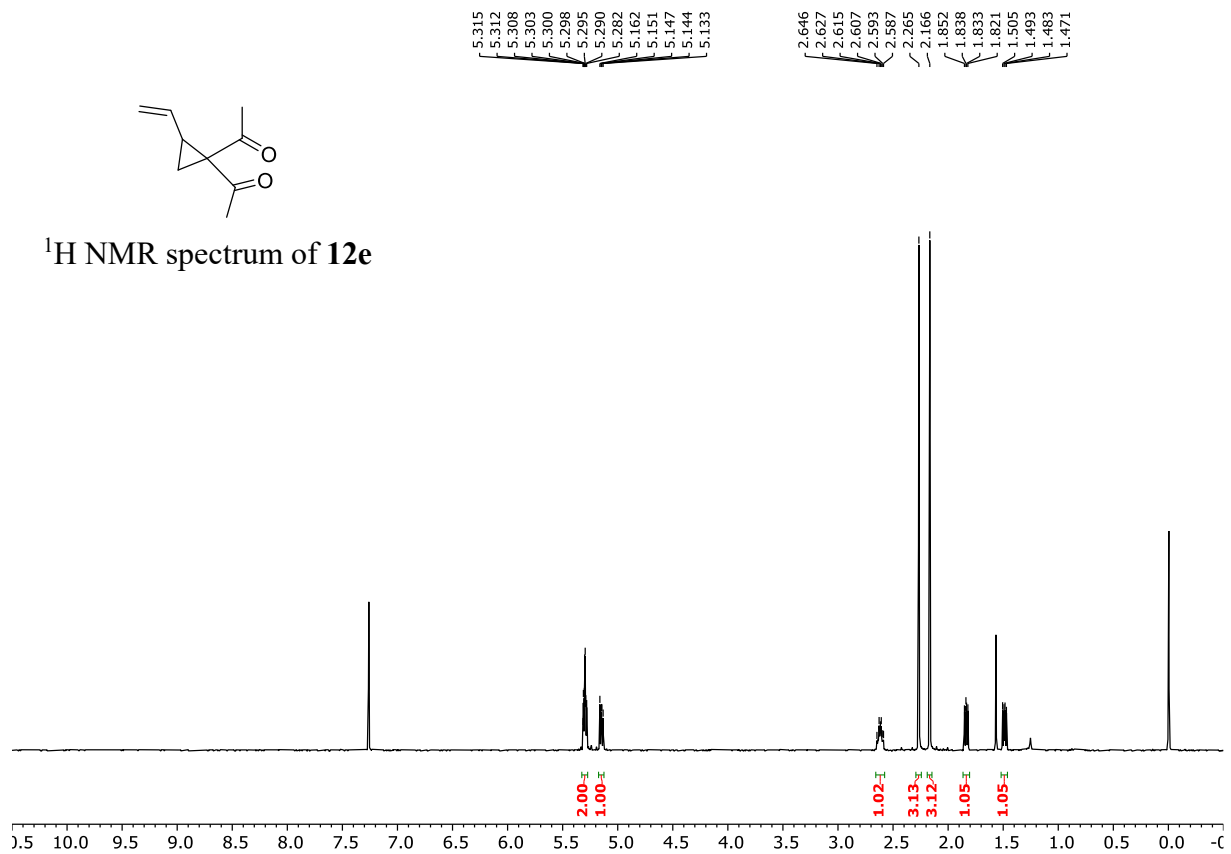


^{13}C NMR spectrum of **12d**

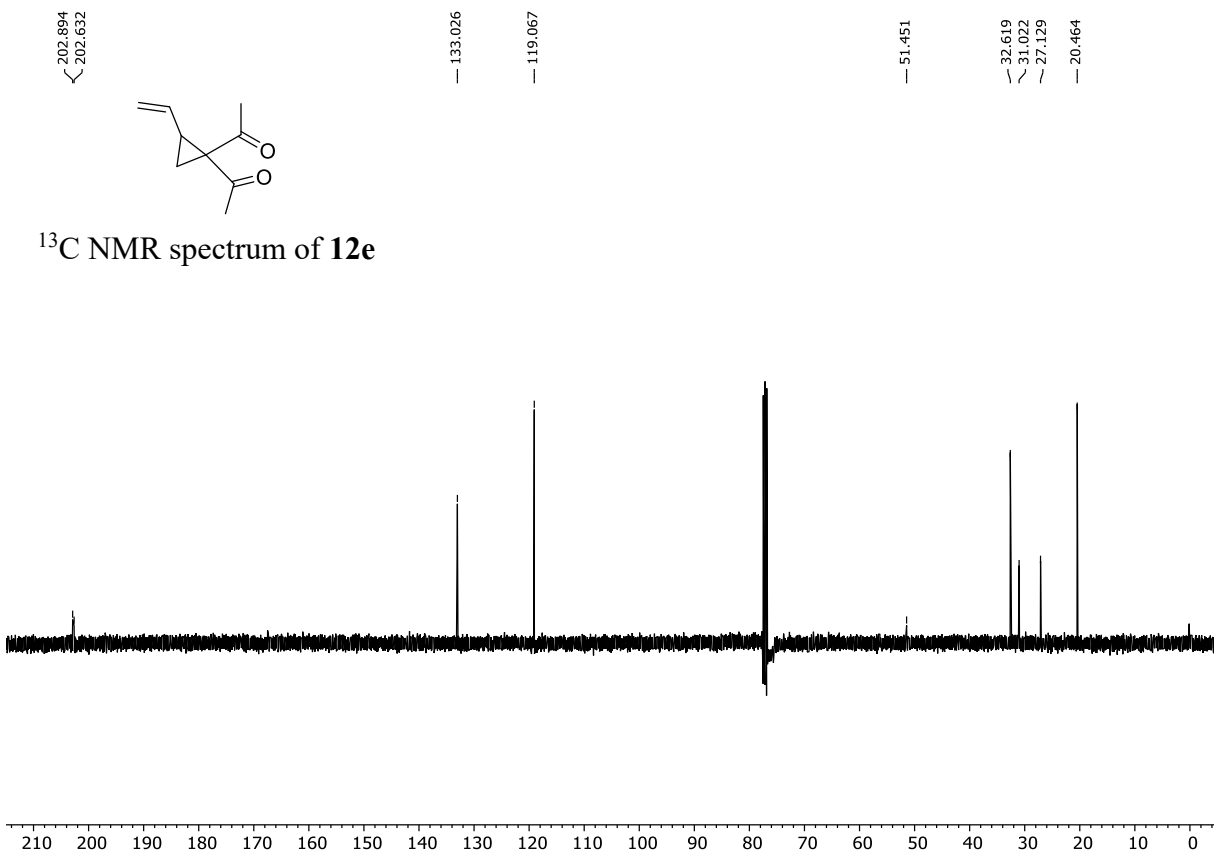


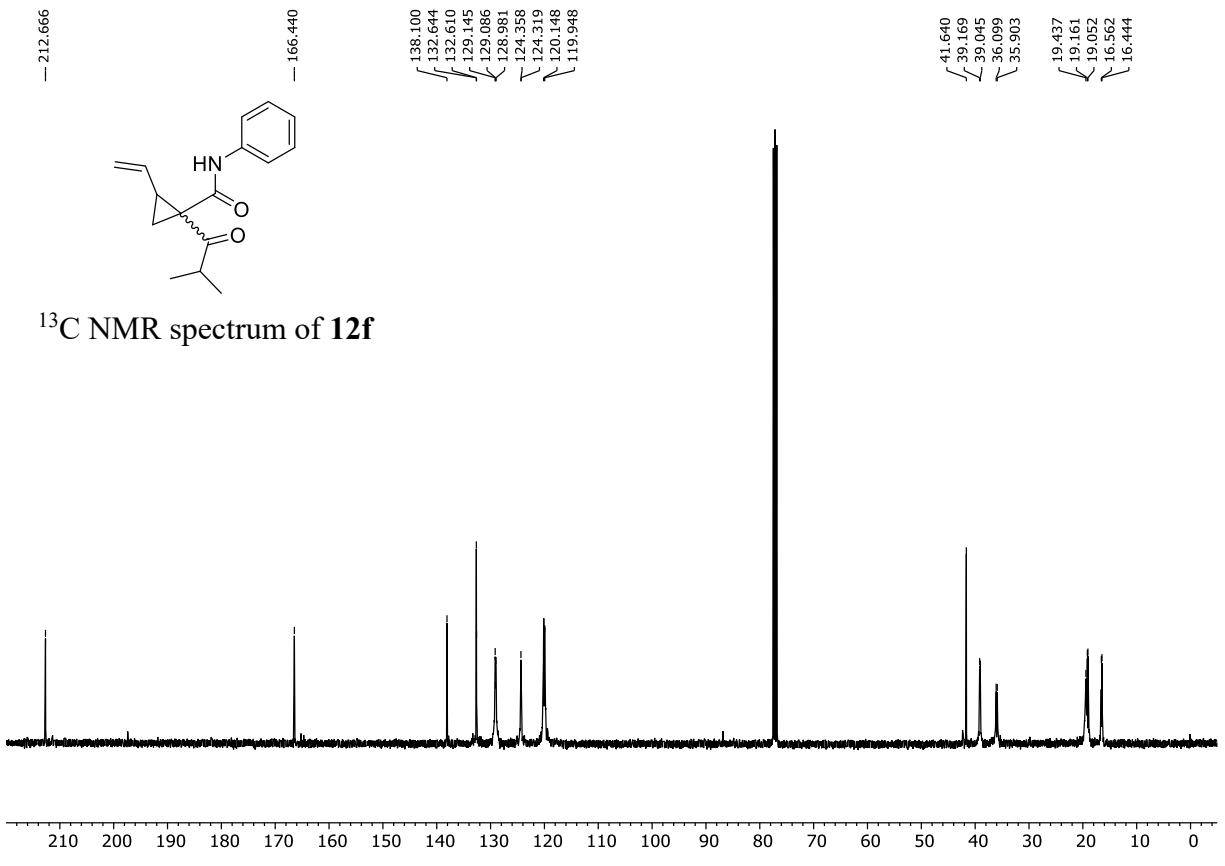
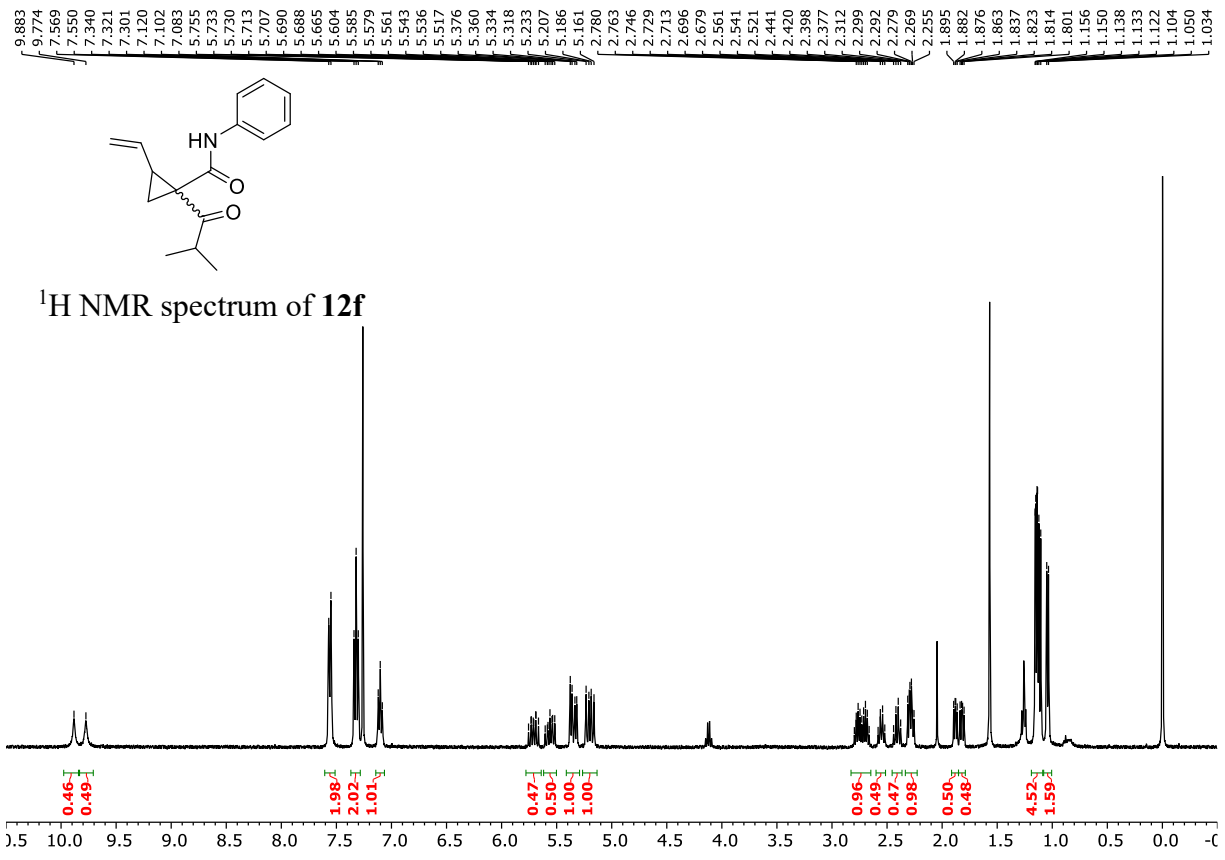


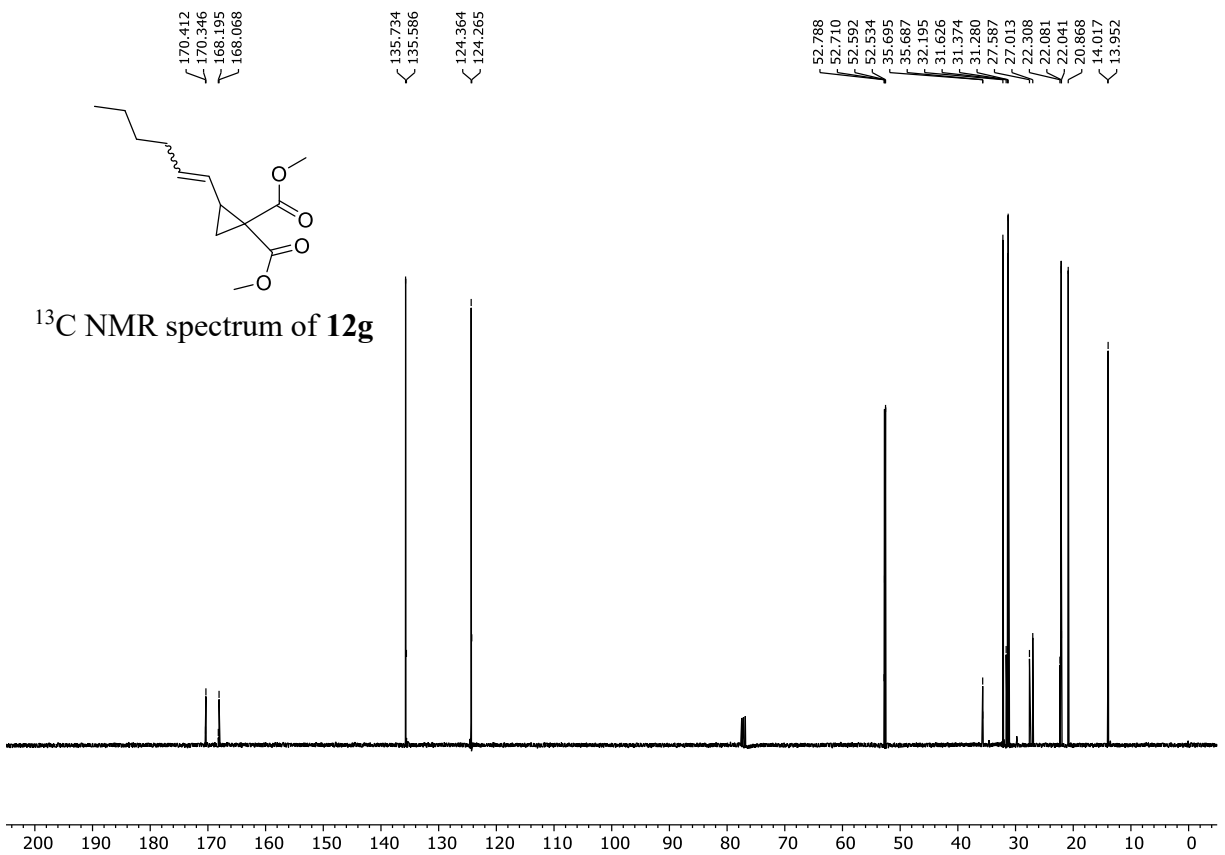
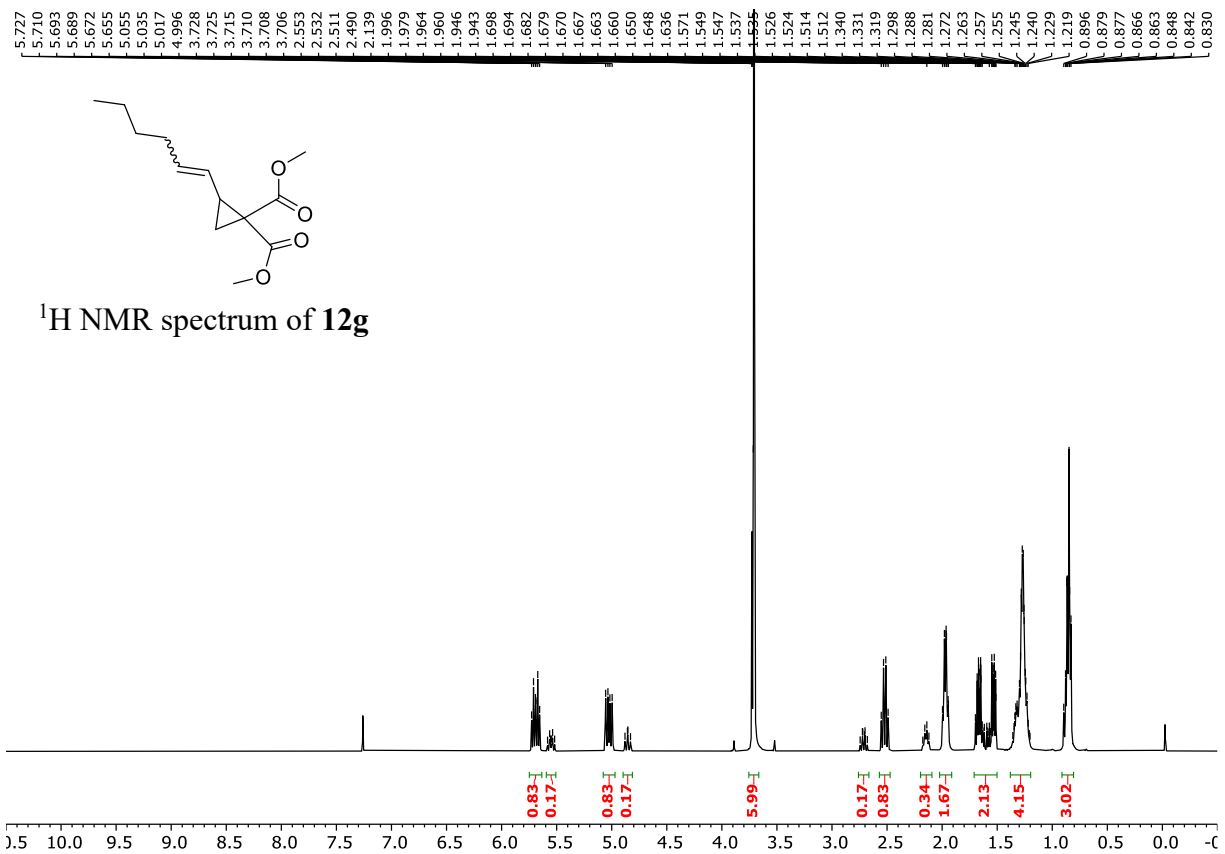
^1H NMR spectrum of **12e**

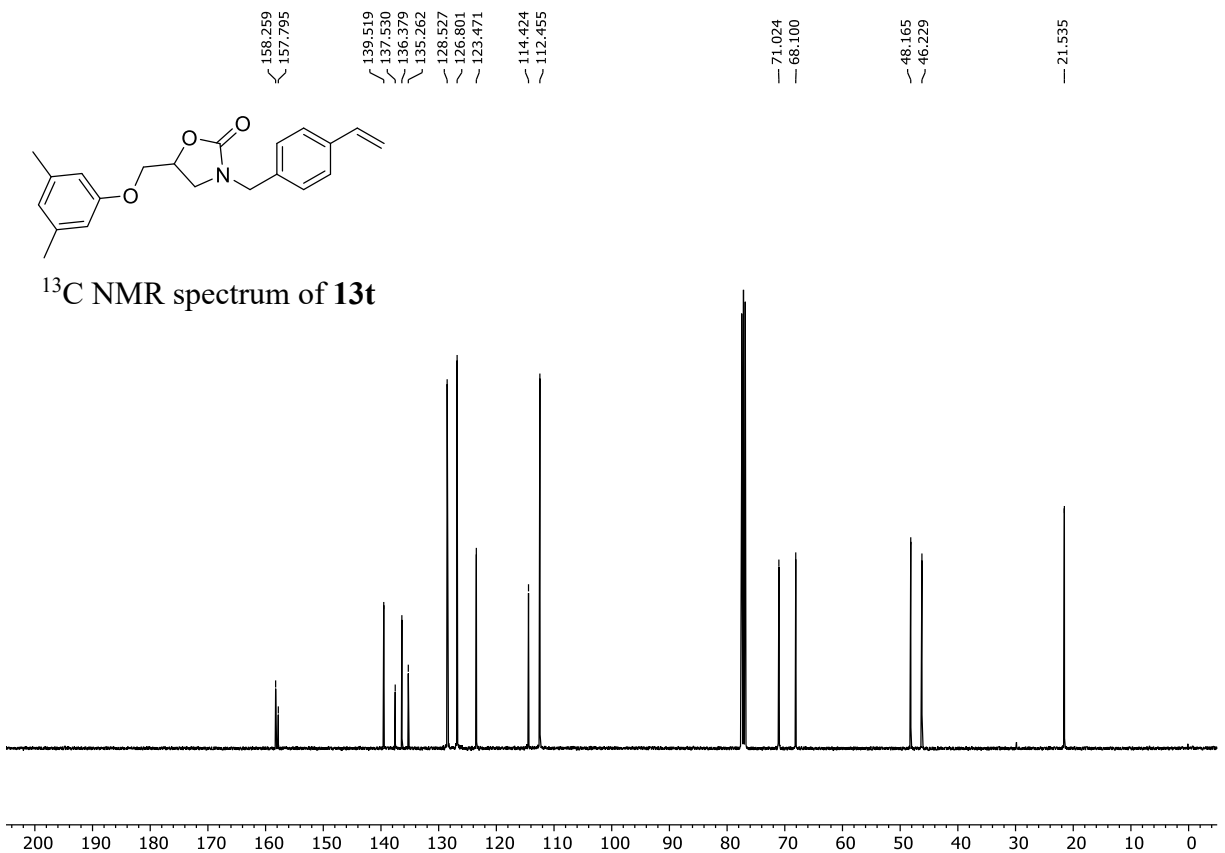
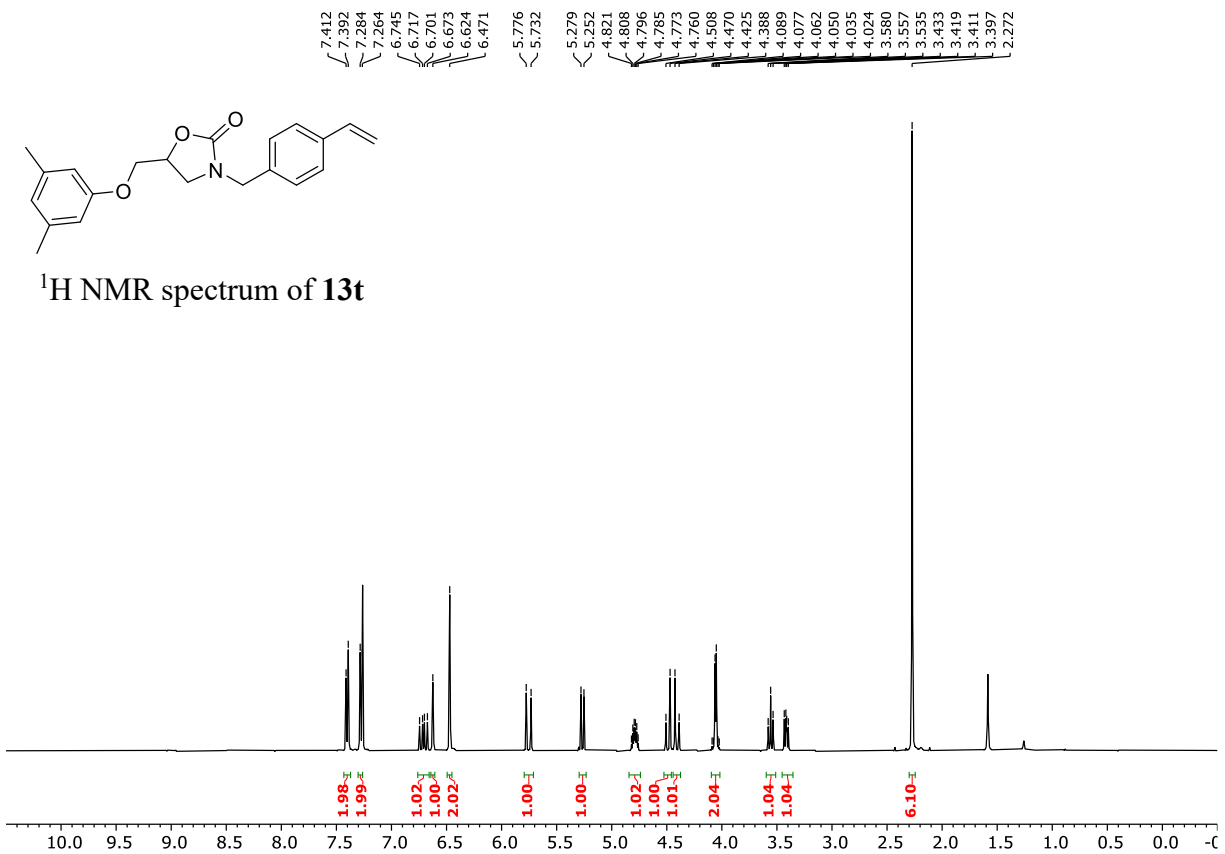


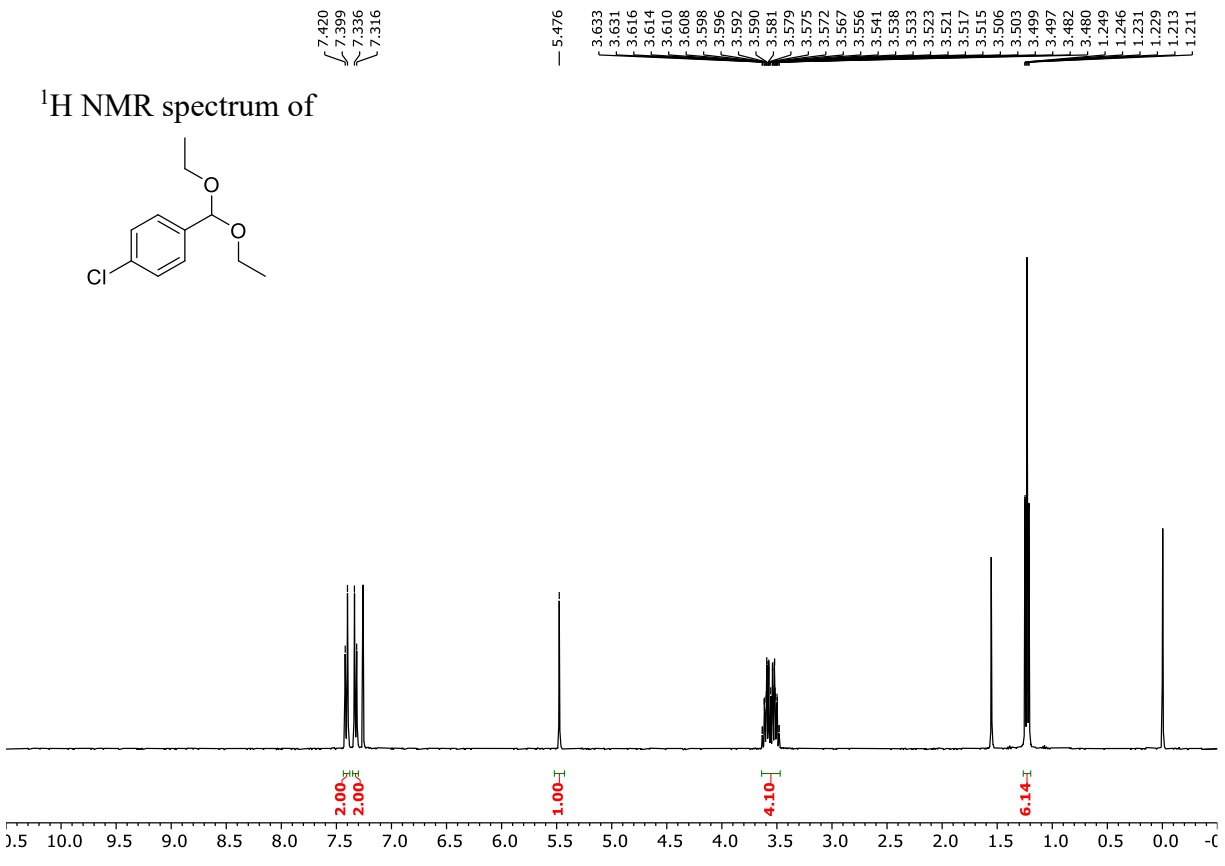
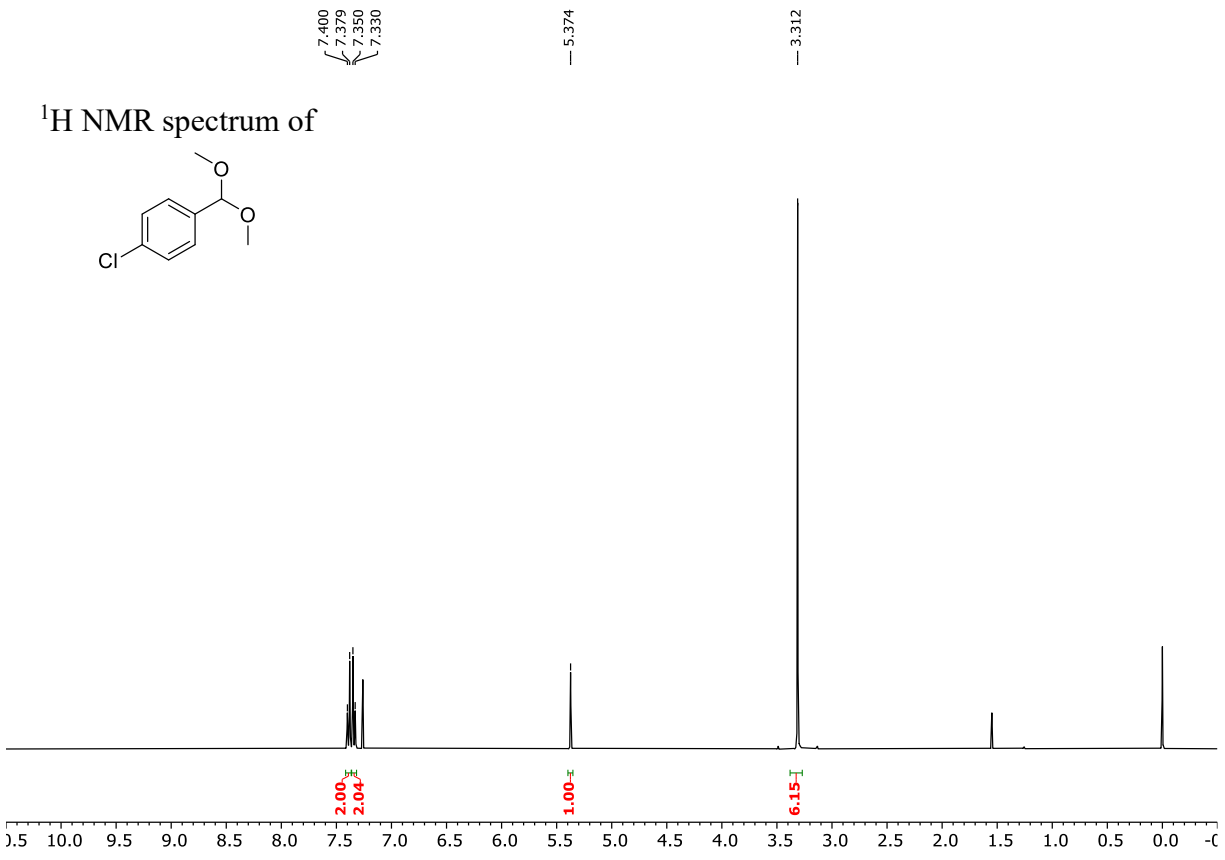
^{13}C NMR spectrum of **12e**

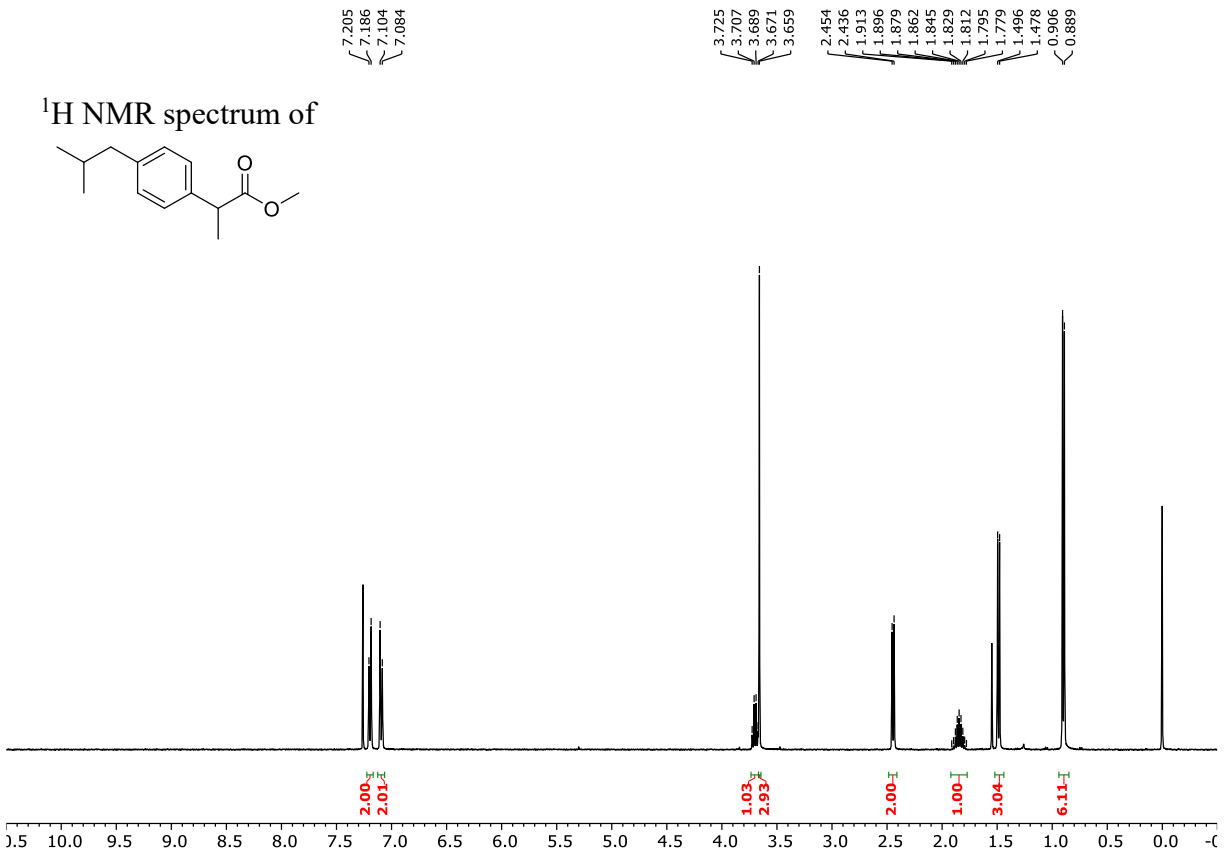
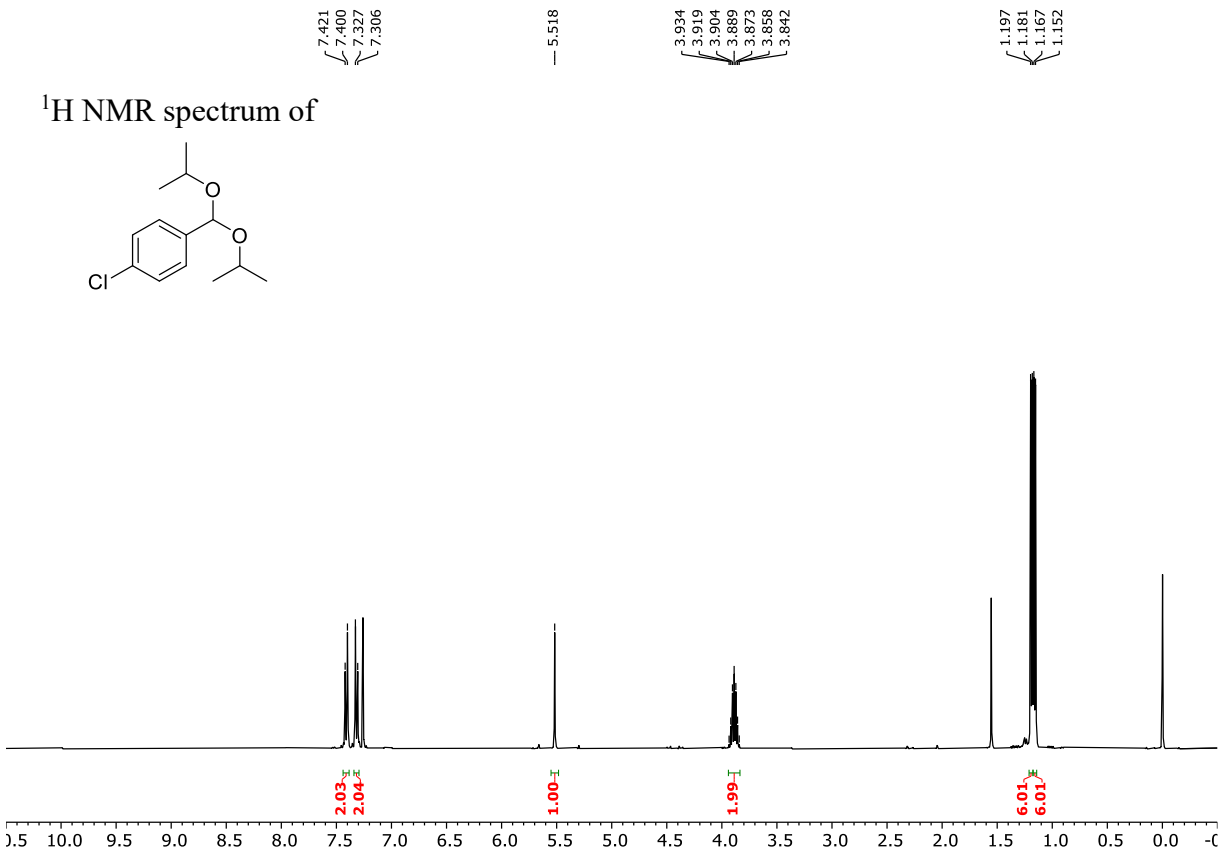


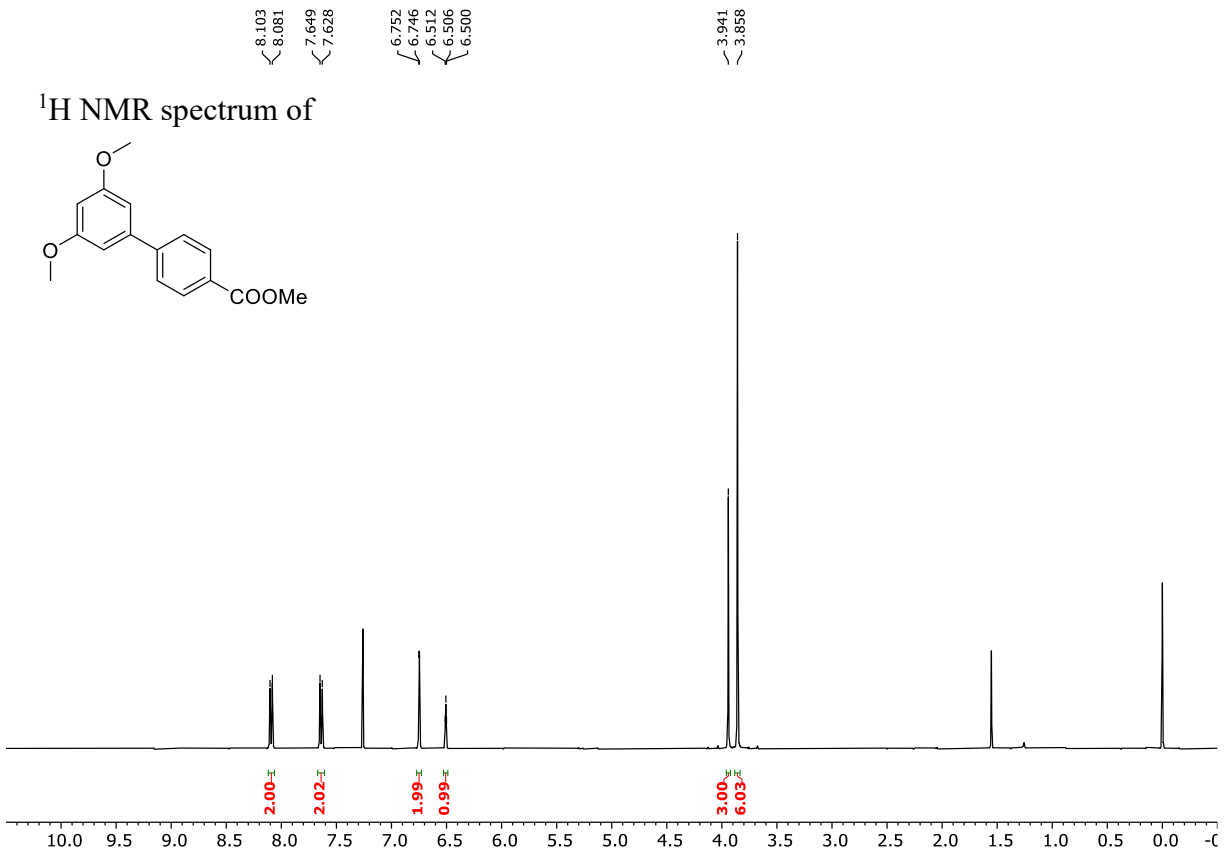


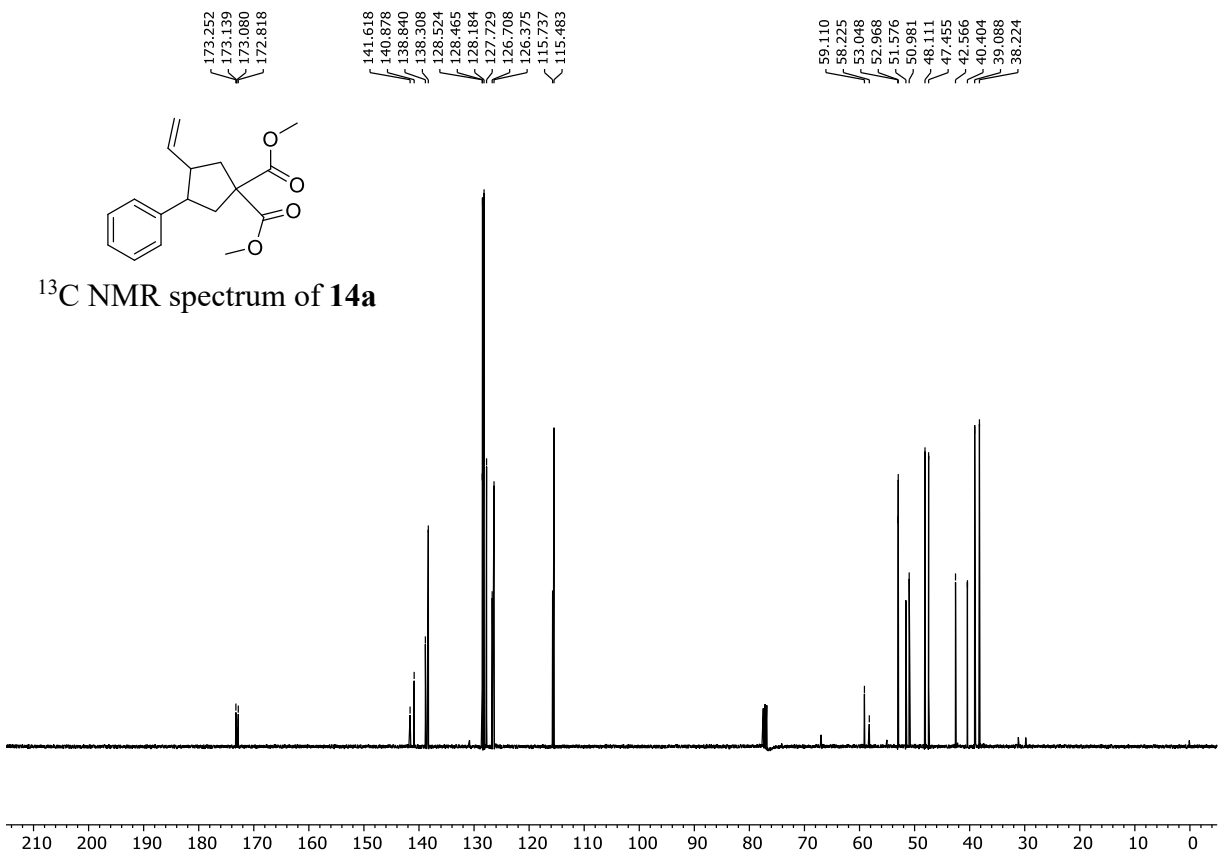
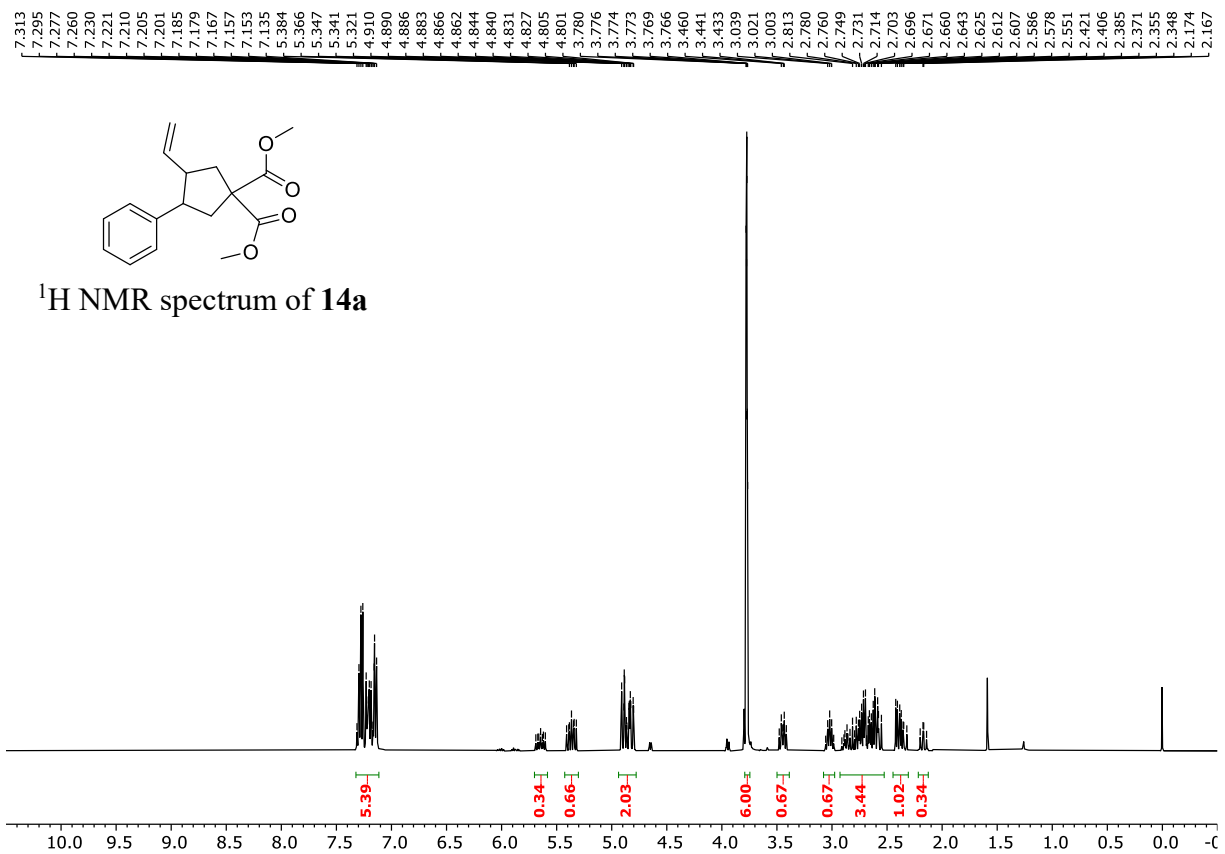




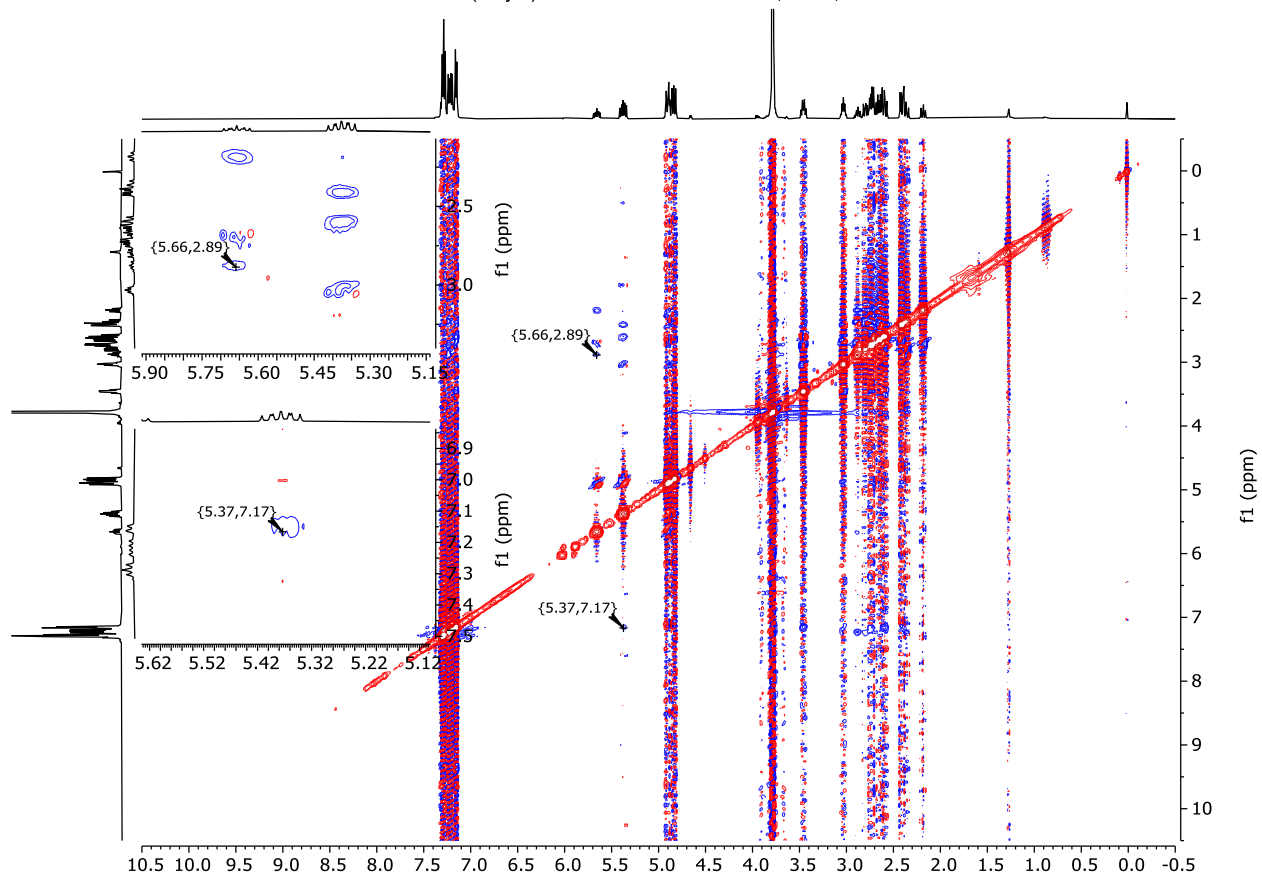
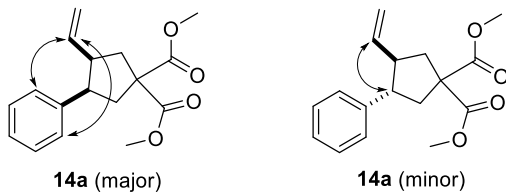


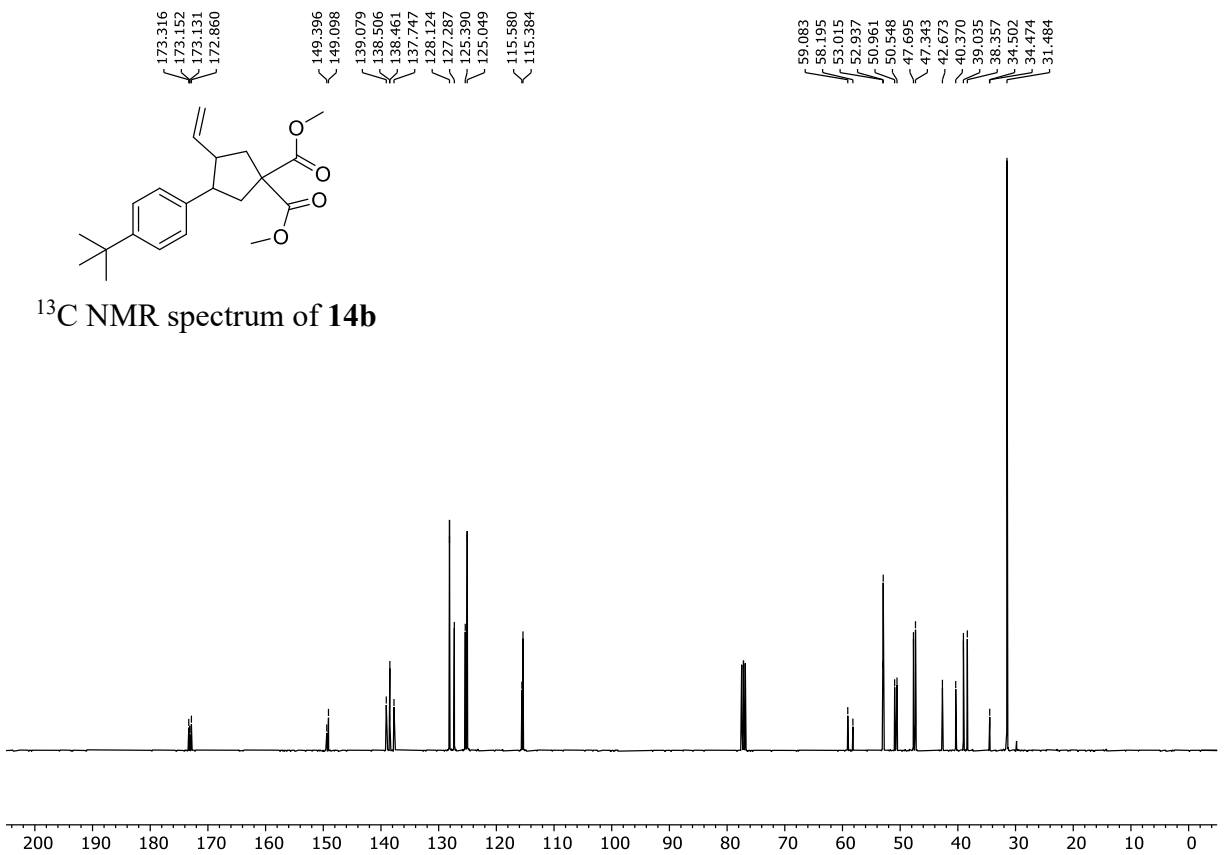
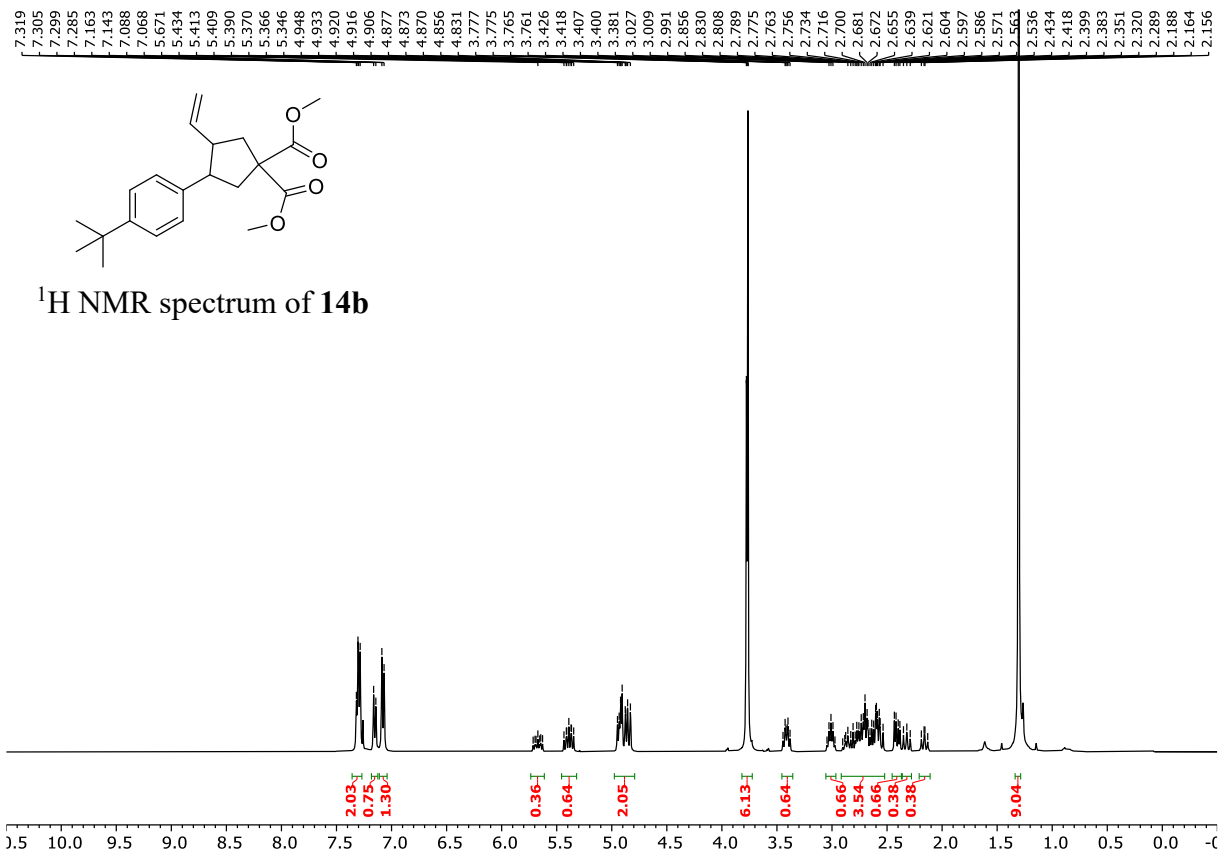


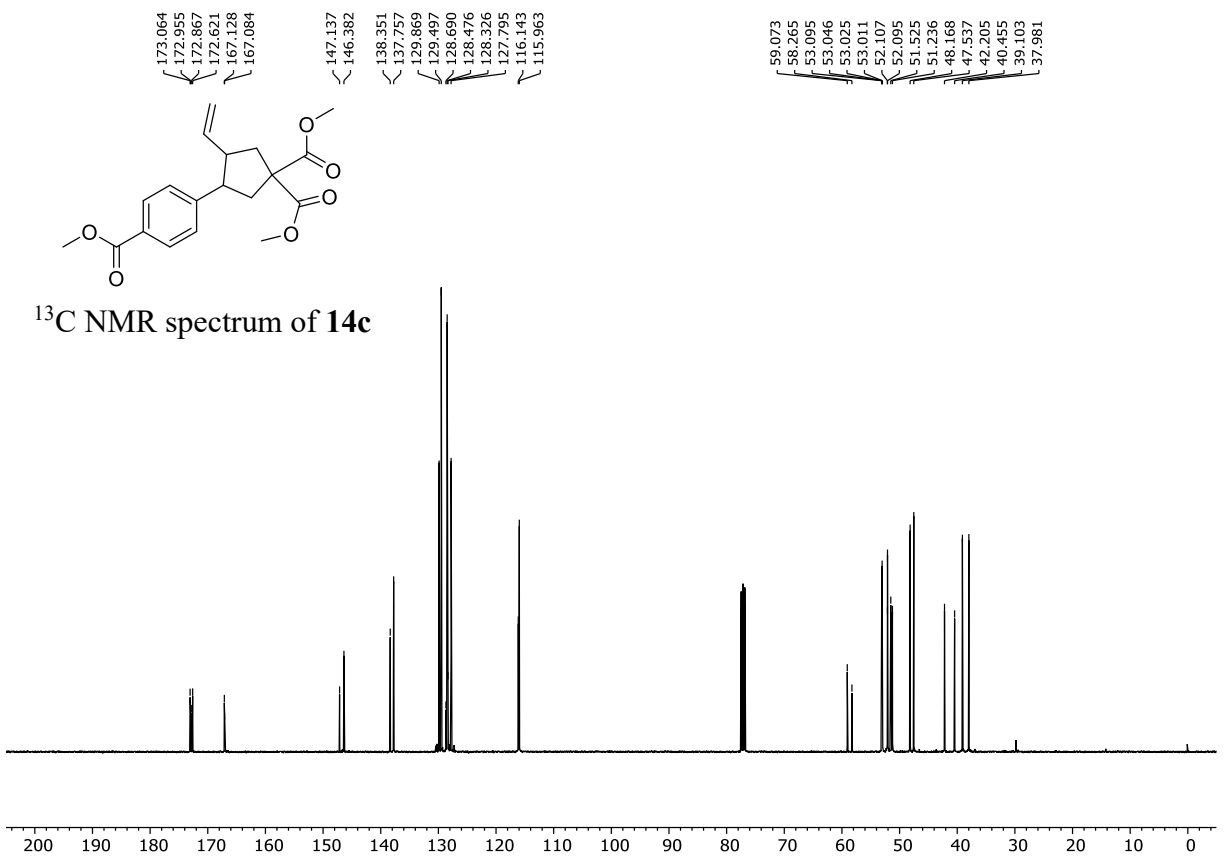
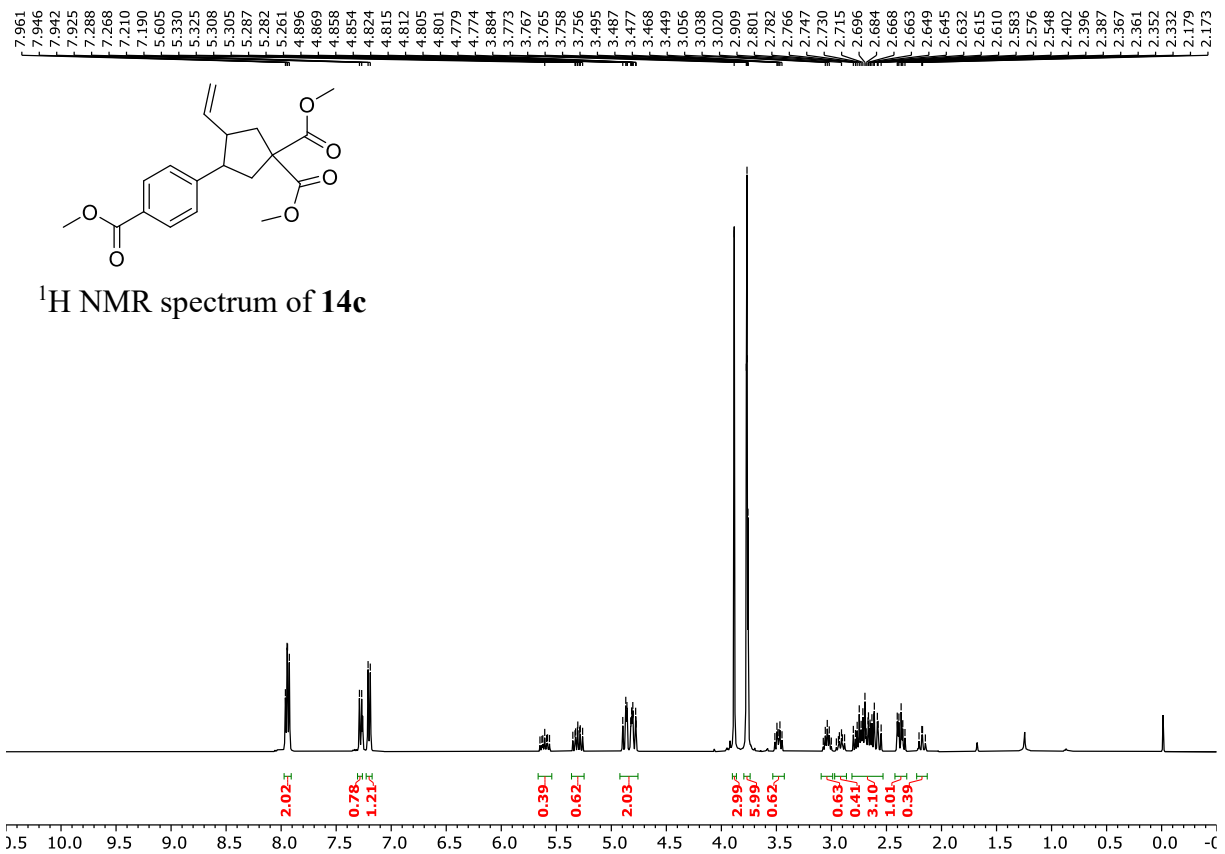


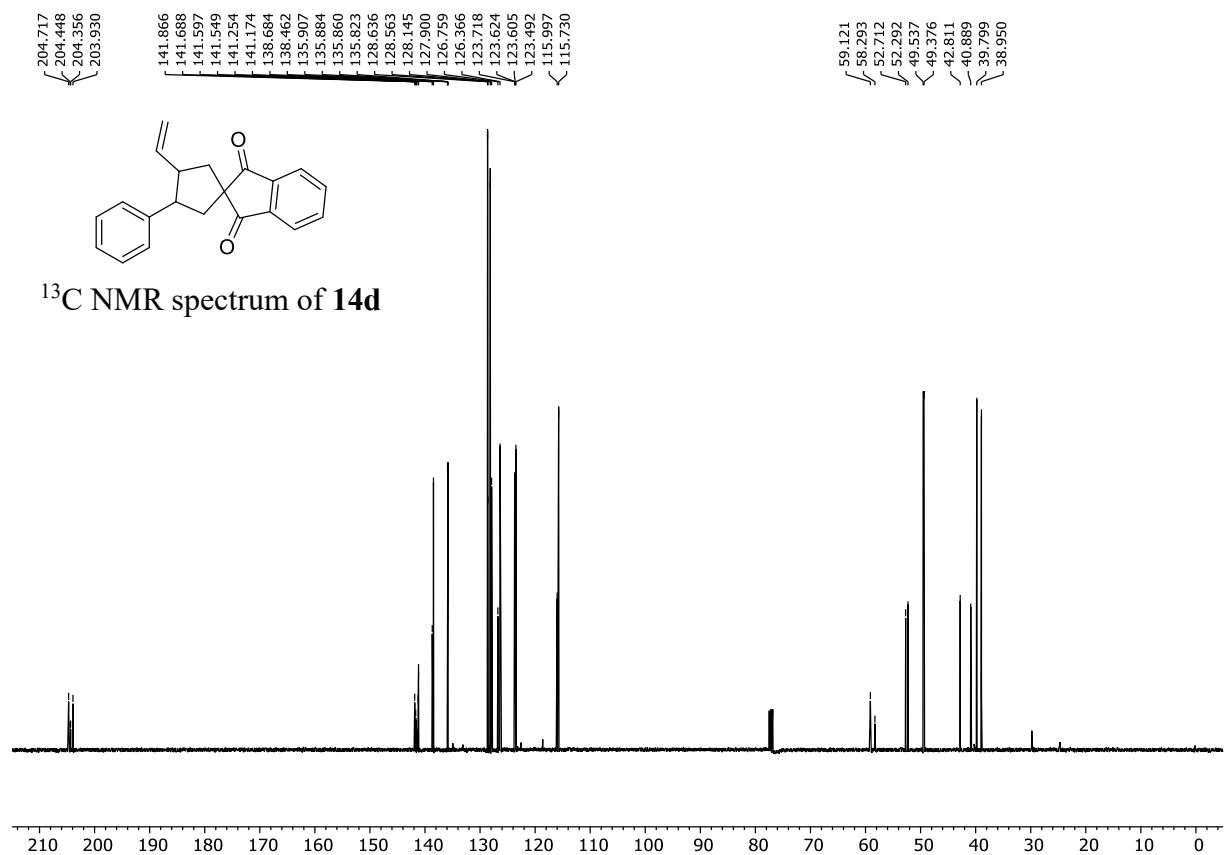
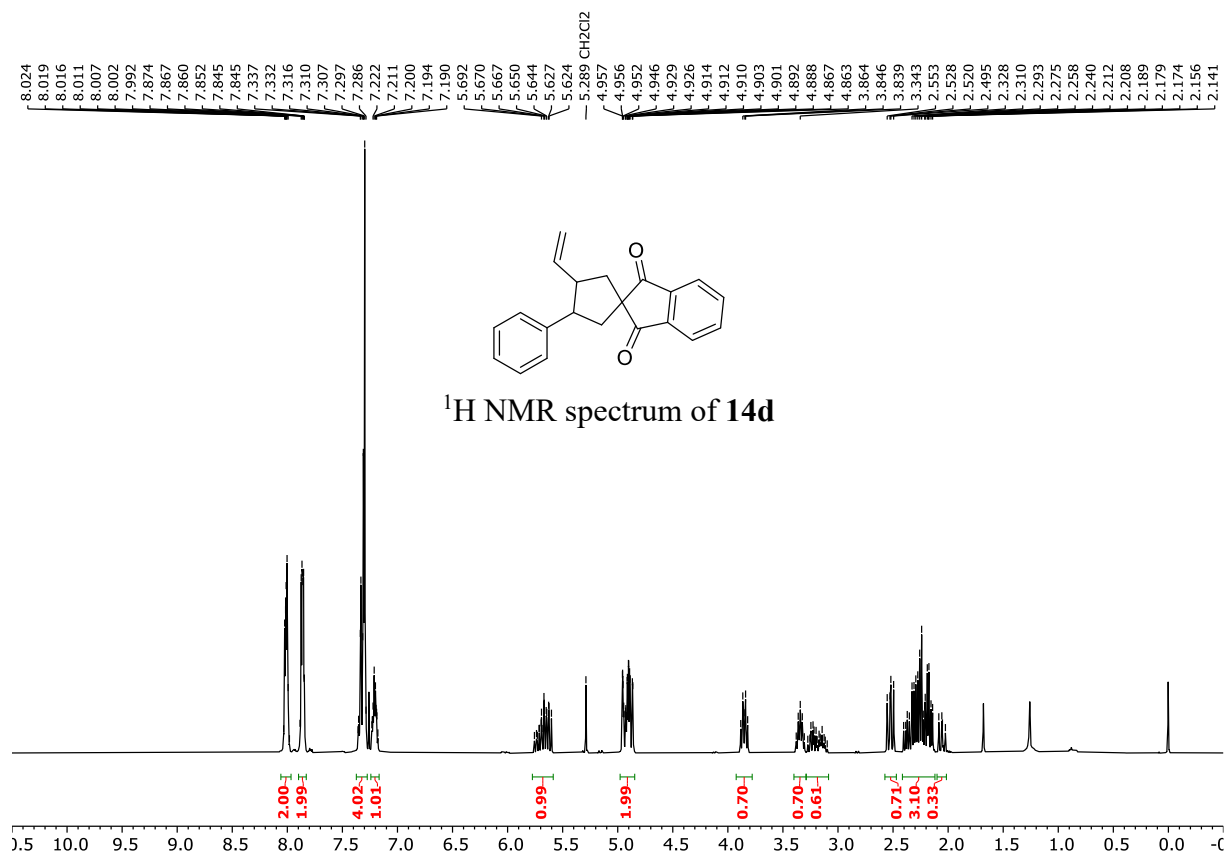


NOESY spectrum of 14a

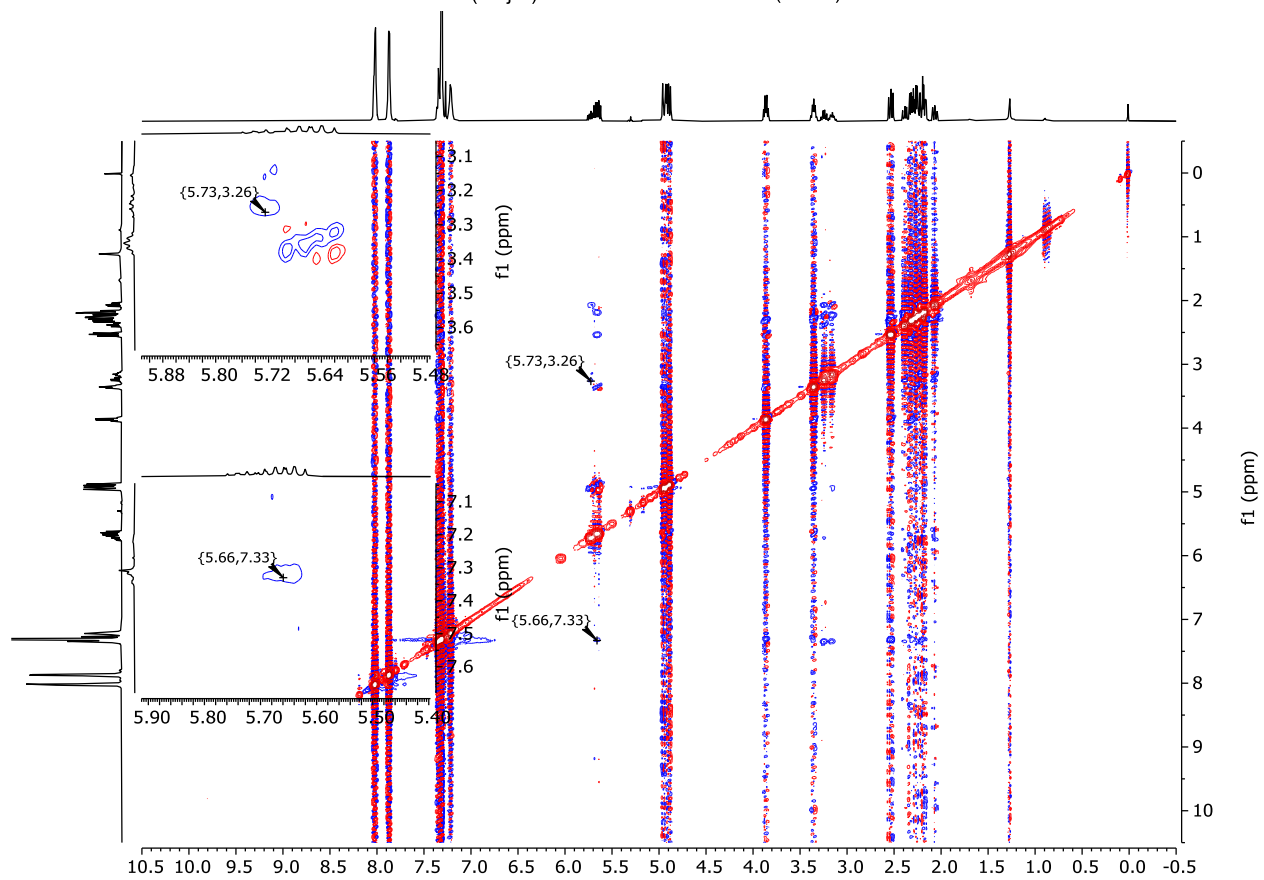
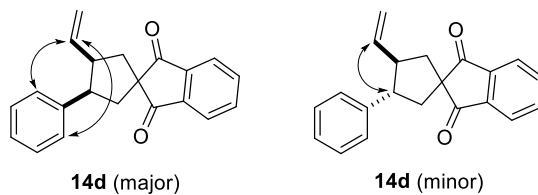


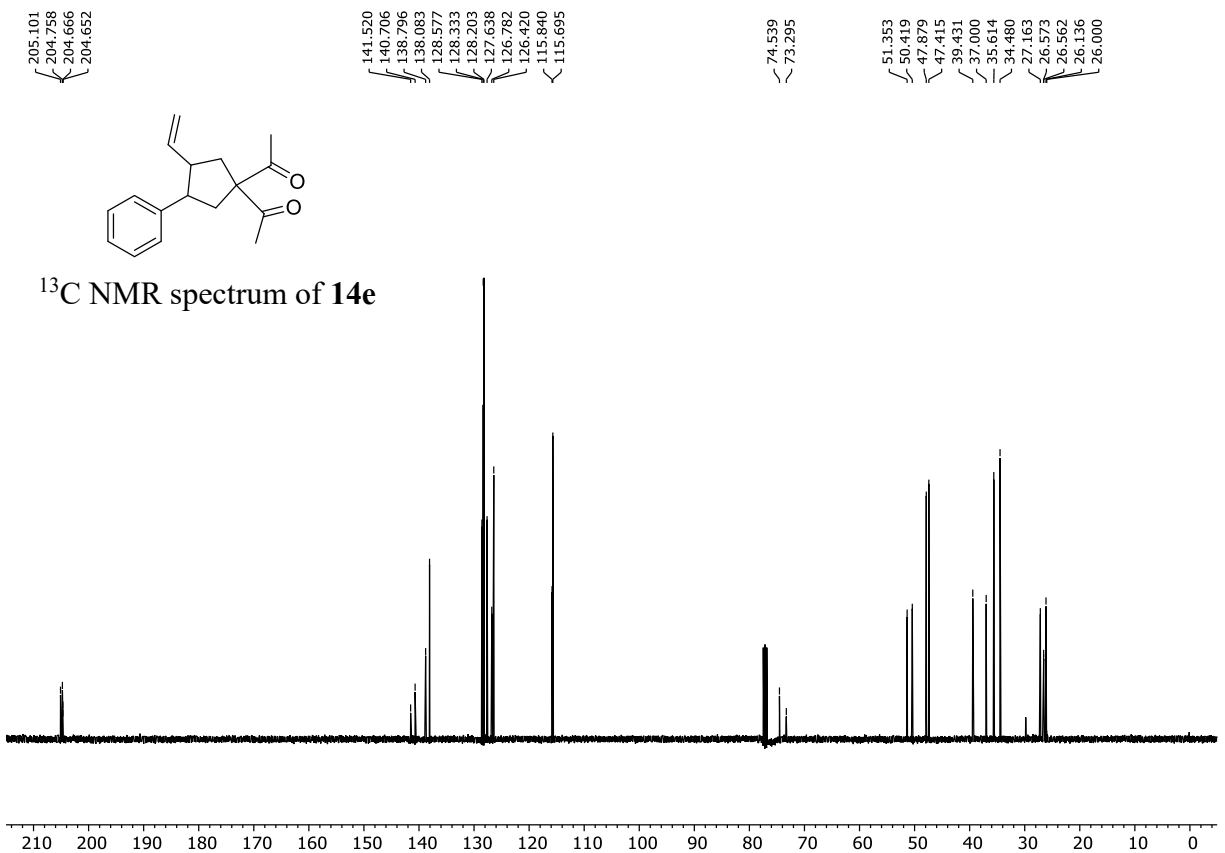
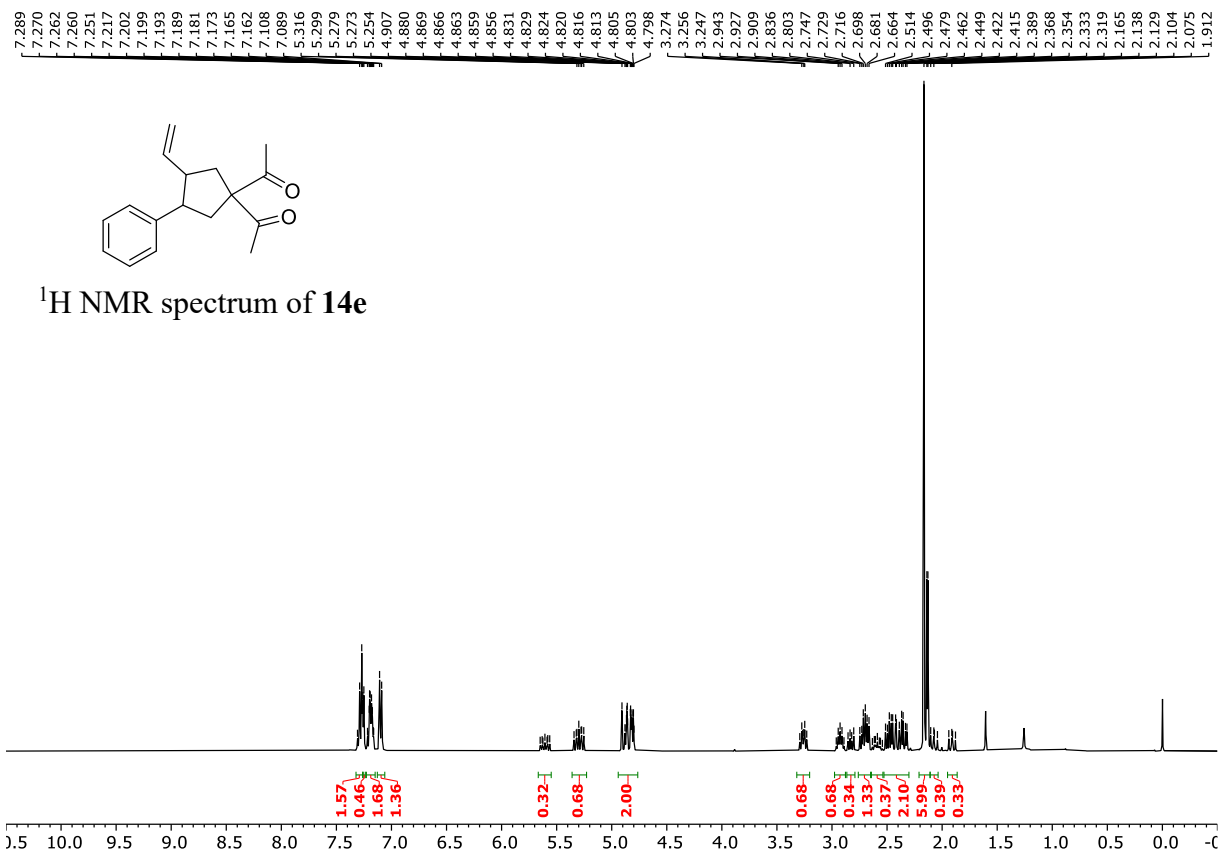


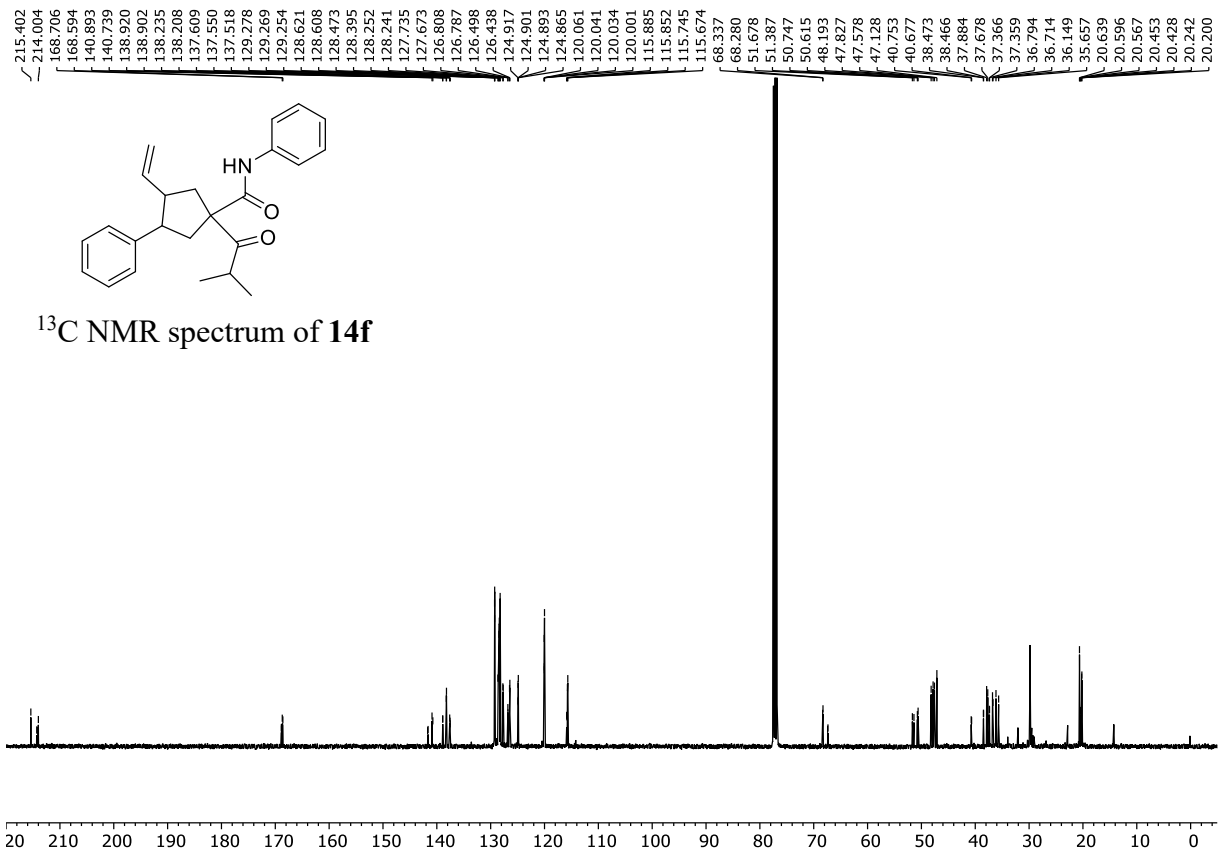
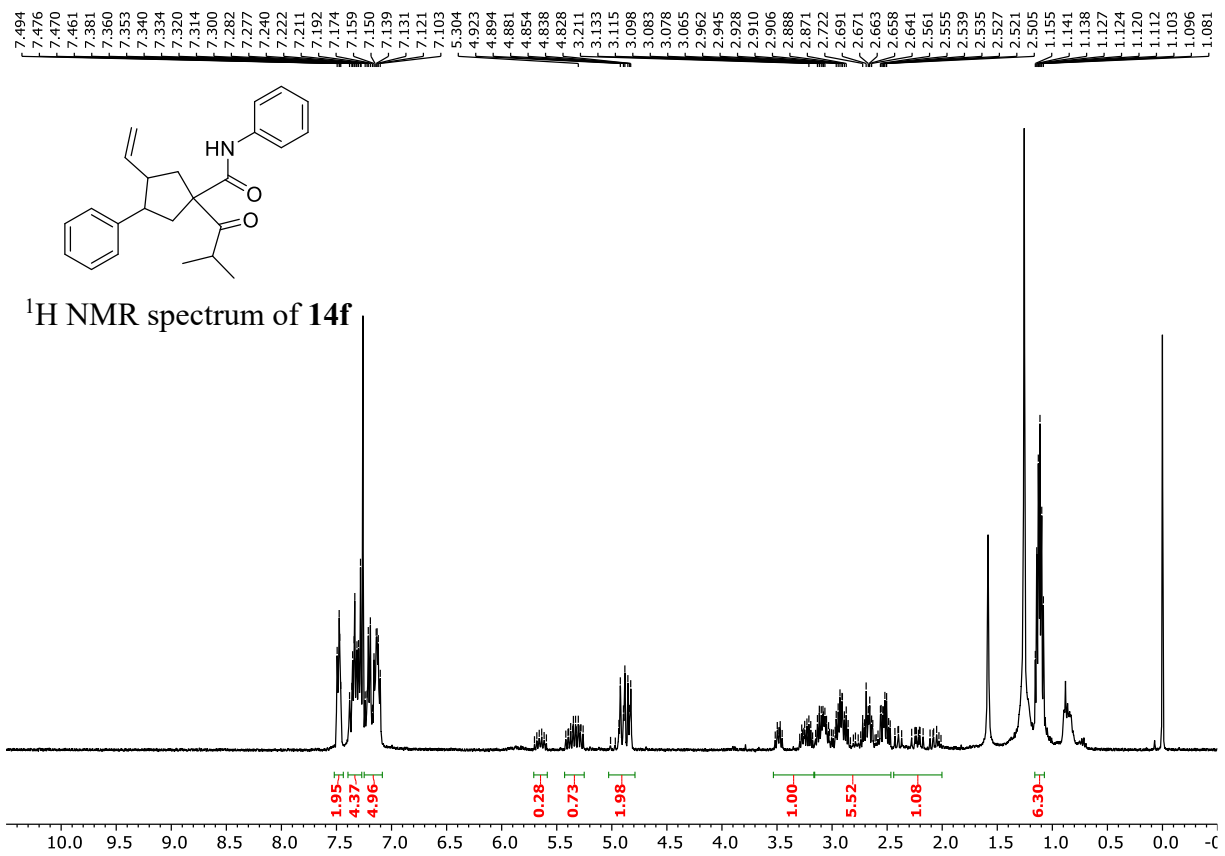


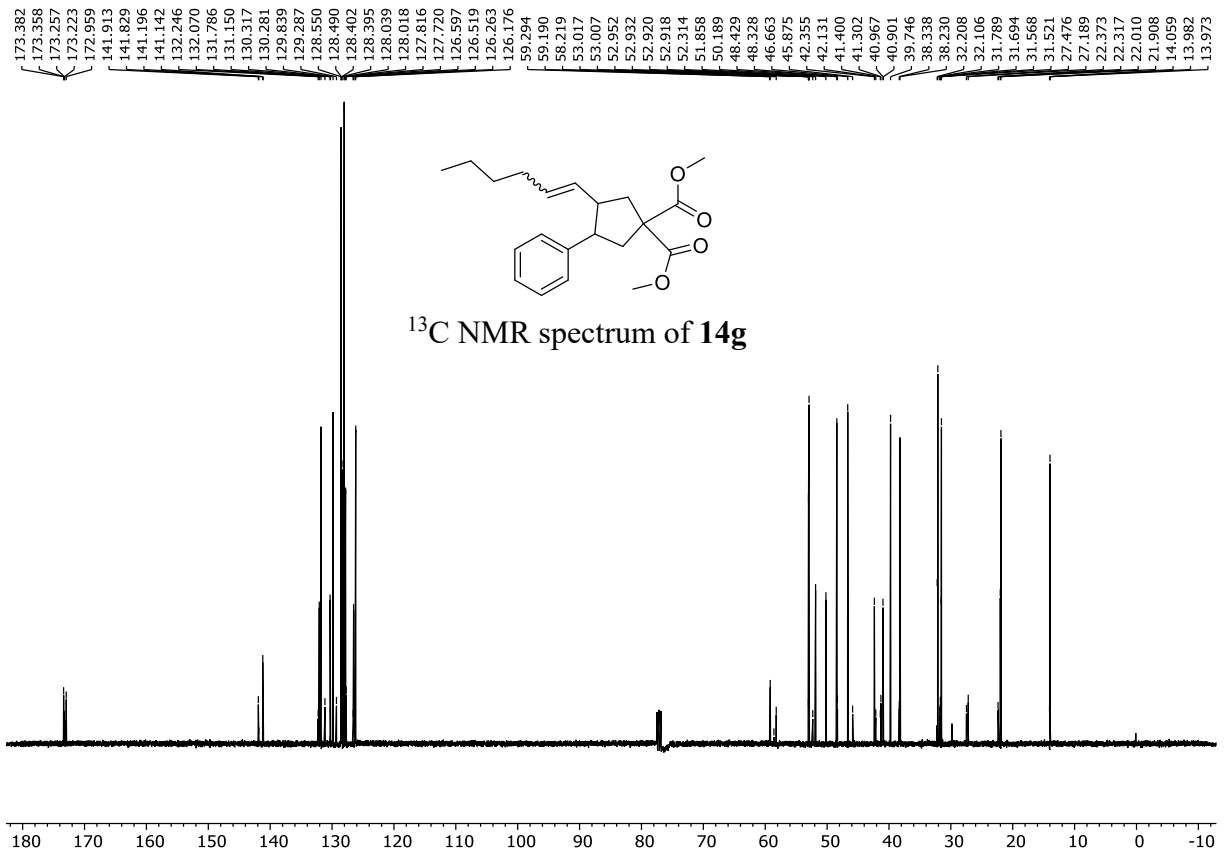
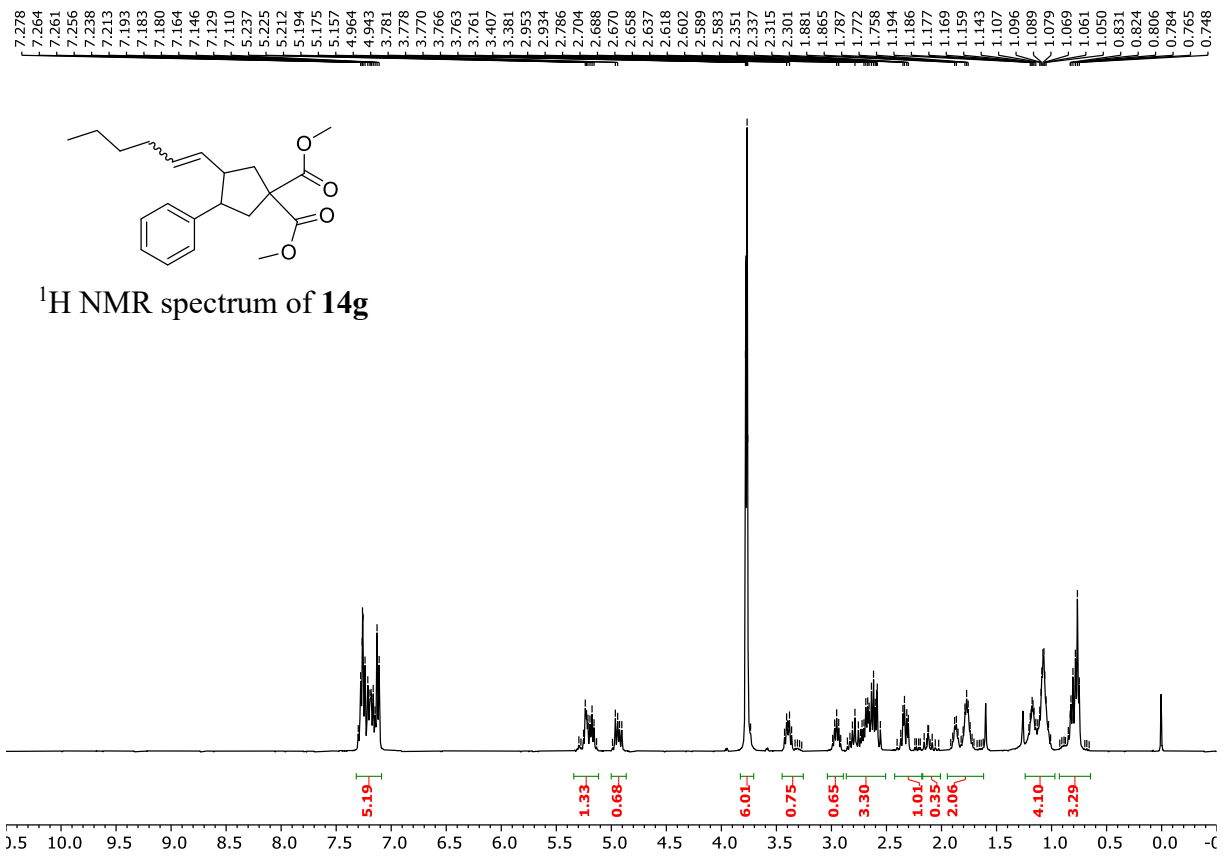


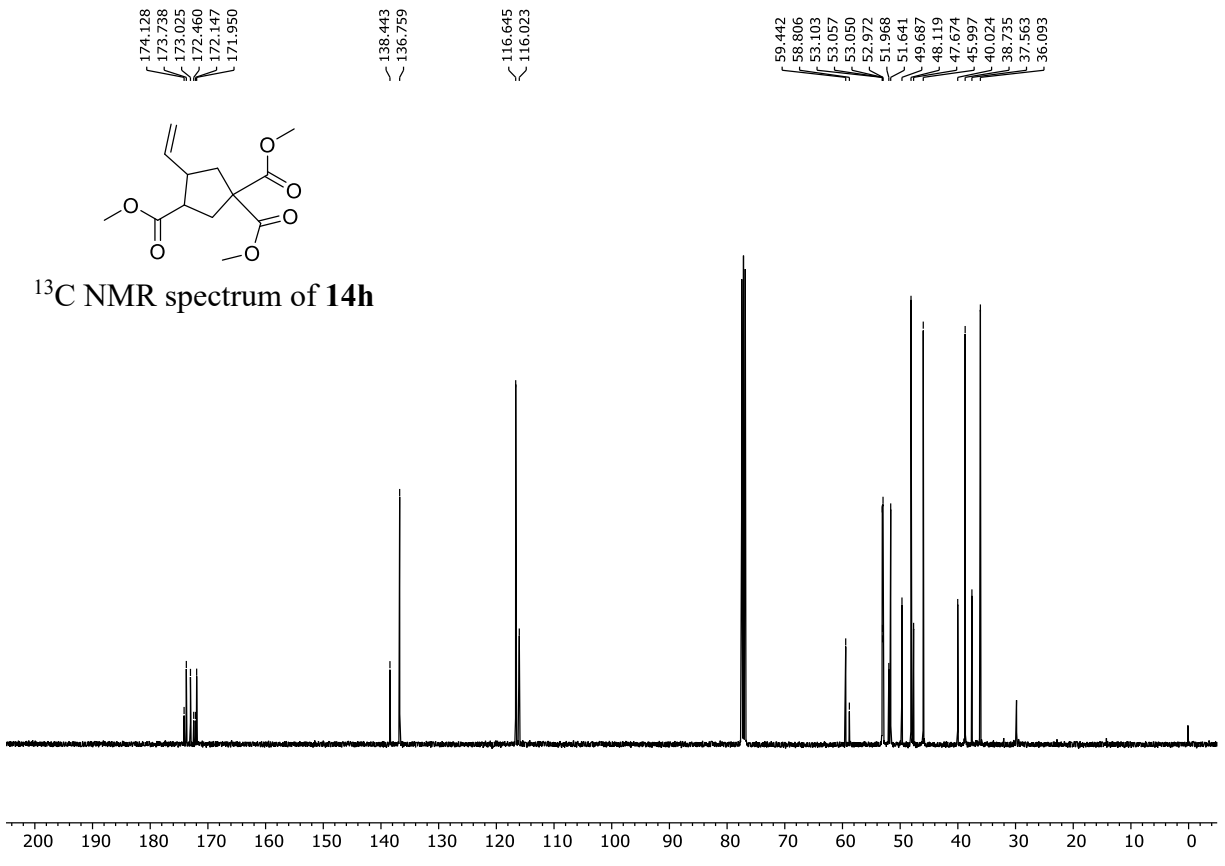
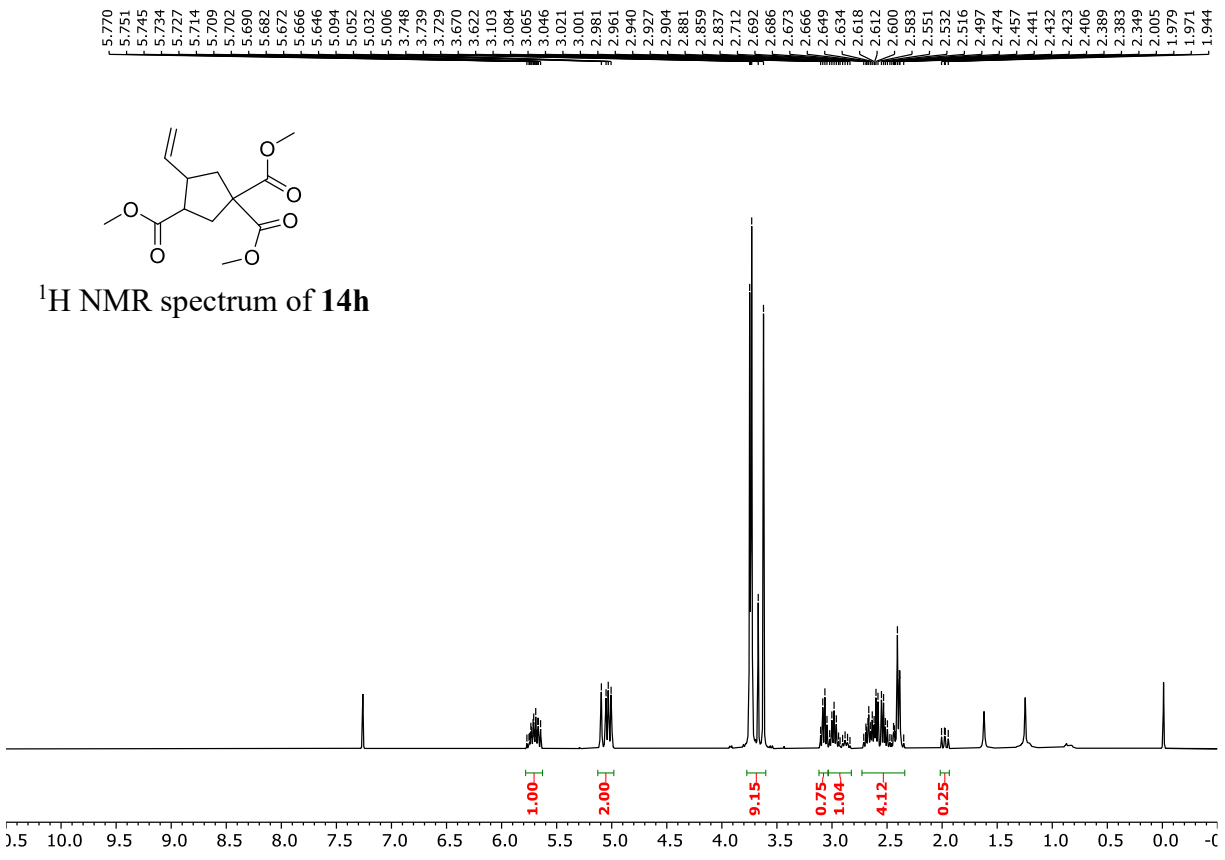
NOESY spectrum of **14d**



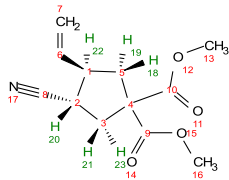




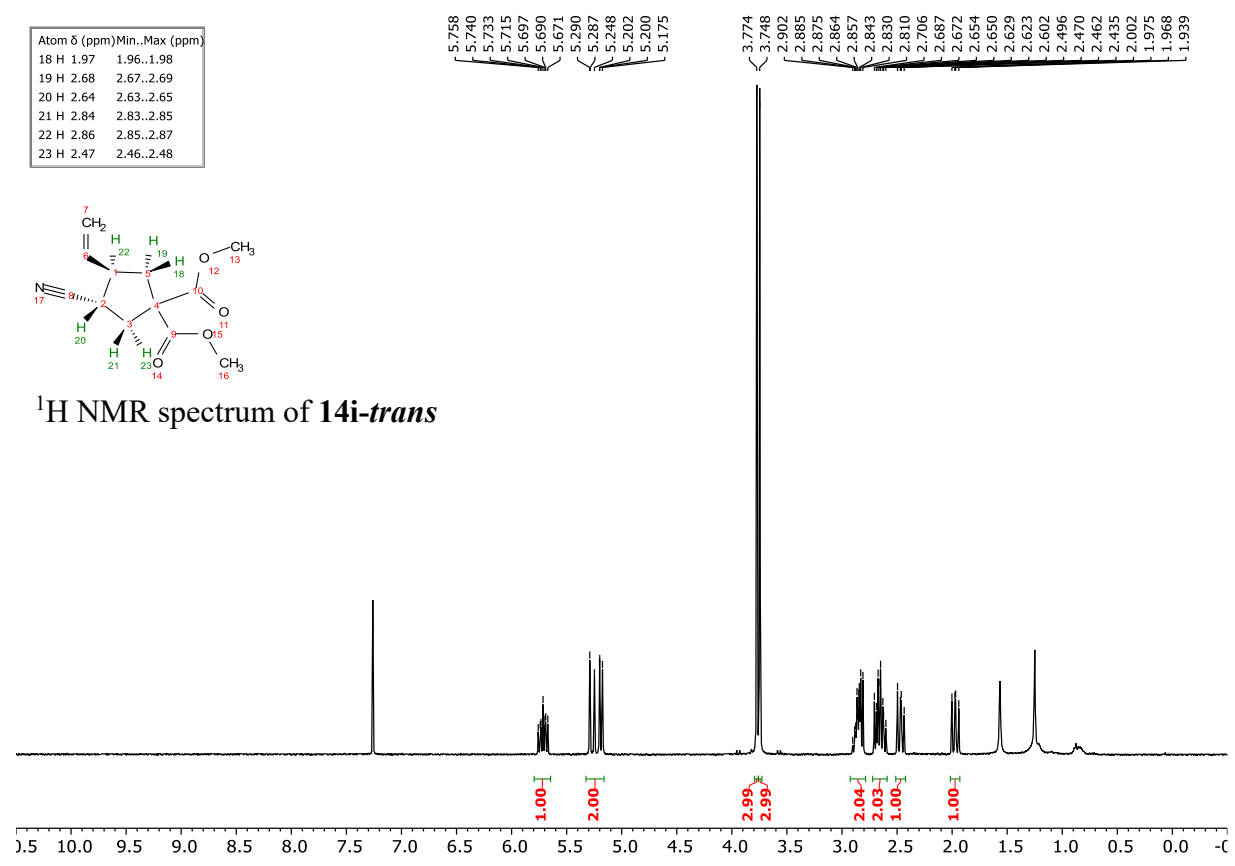




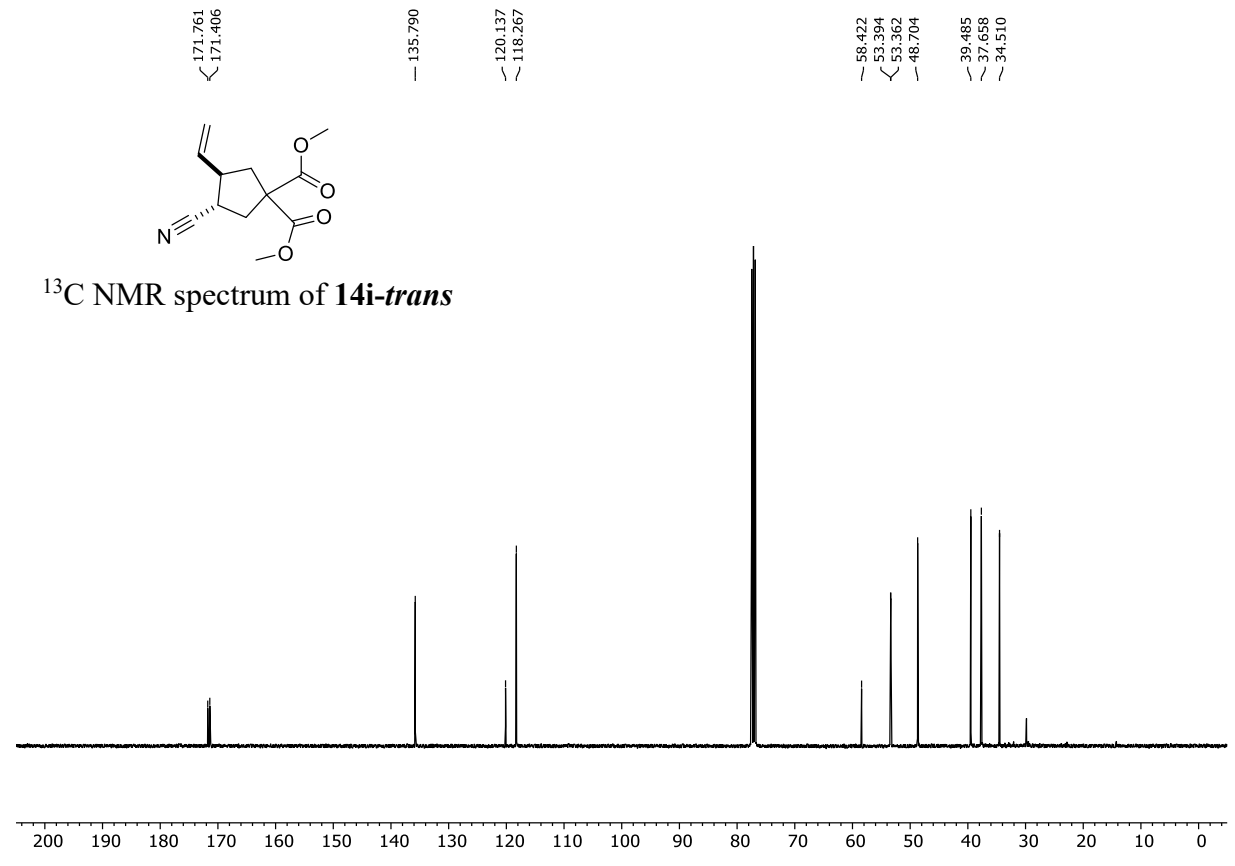
Atom δ (ppm)	Min. (ppm)	Max. (ppm)
18 H	1.97	1.96..1.98
19 H	2.68	2.67..2.69
20 H	2.64	2.63..2.65
21 H	2.84	2.83..2.85
22 H	2.86	2.85..2.87
23 H	2.47	2.46..2.48



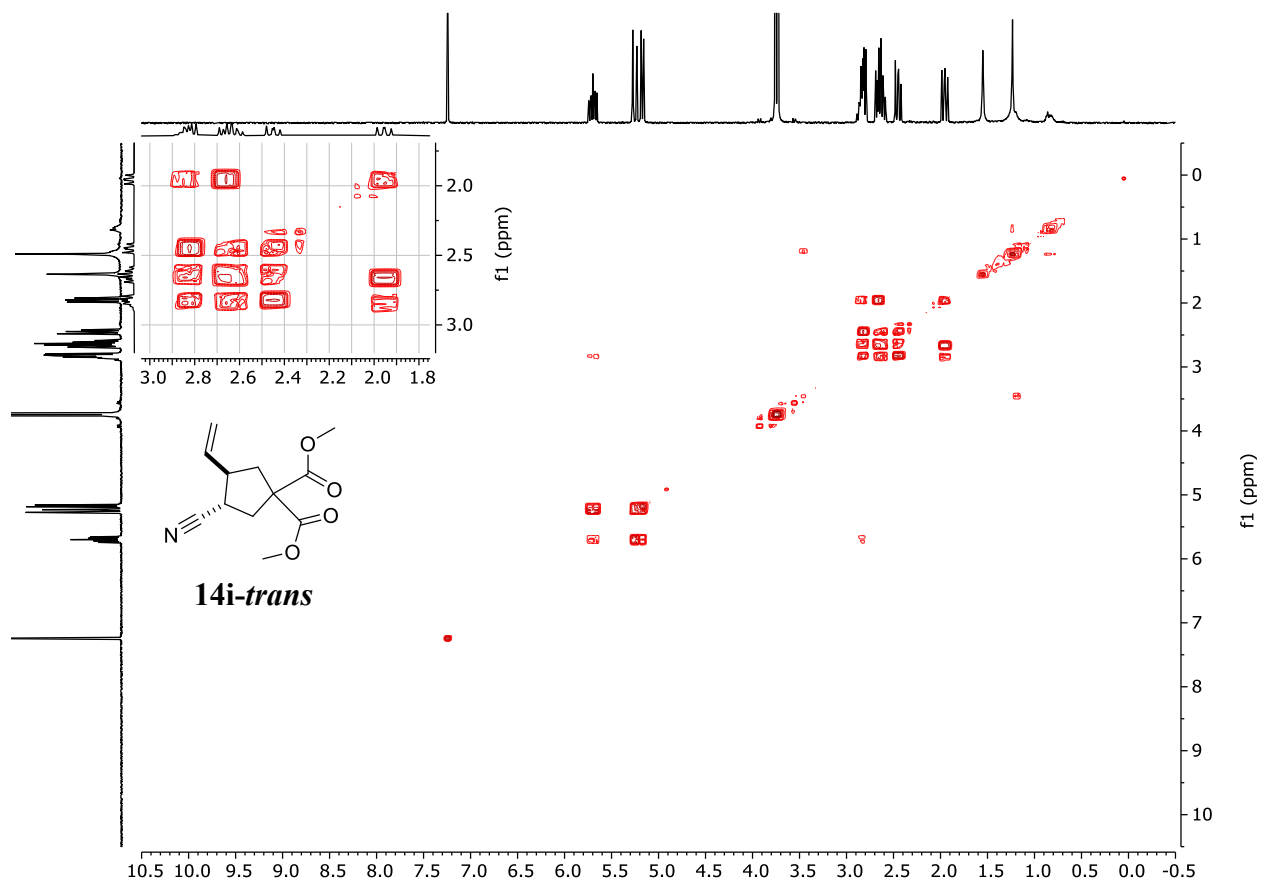
^1H NMR spectrum of **14i-trans**



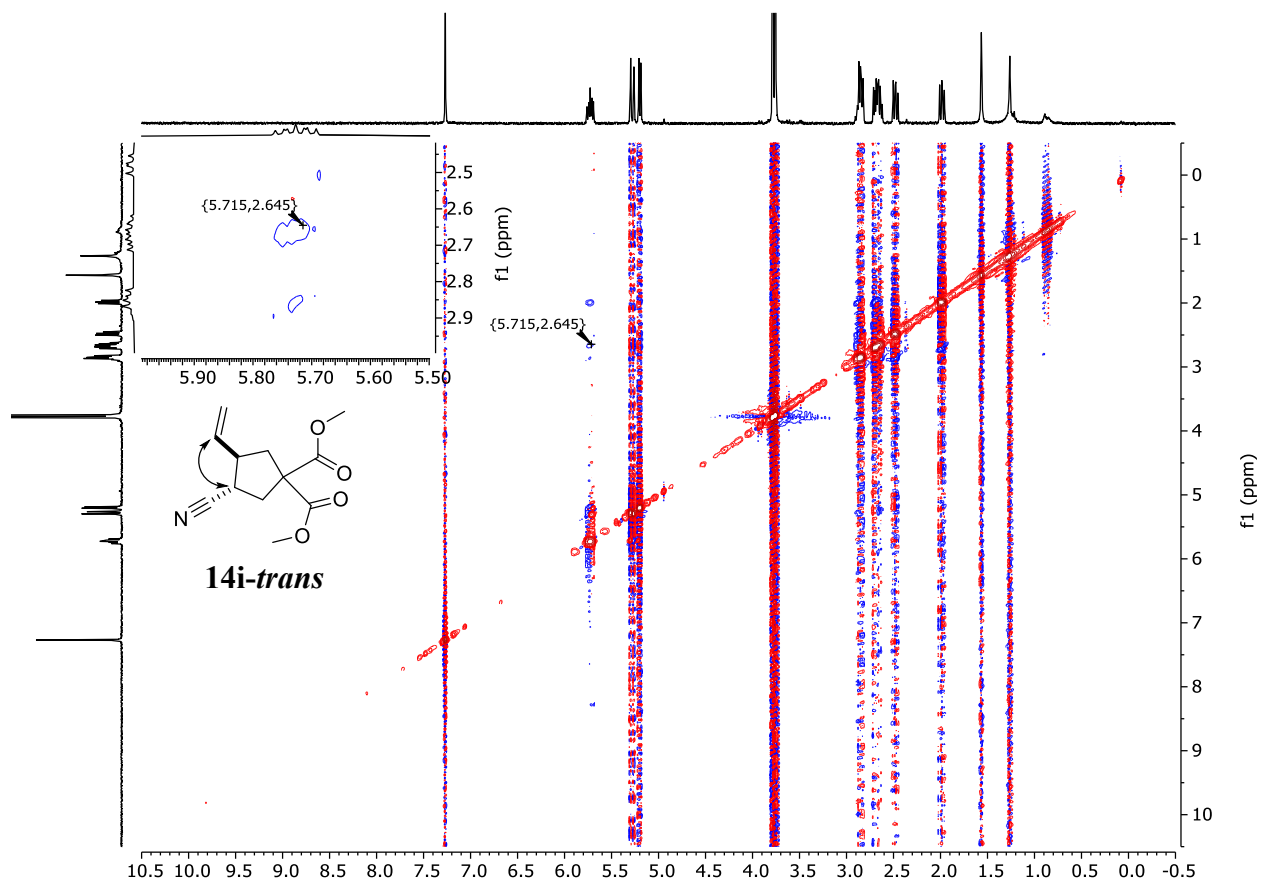
^{13}C NMR spectrum of **14i-trans**

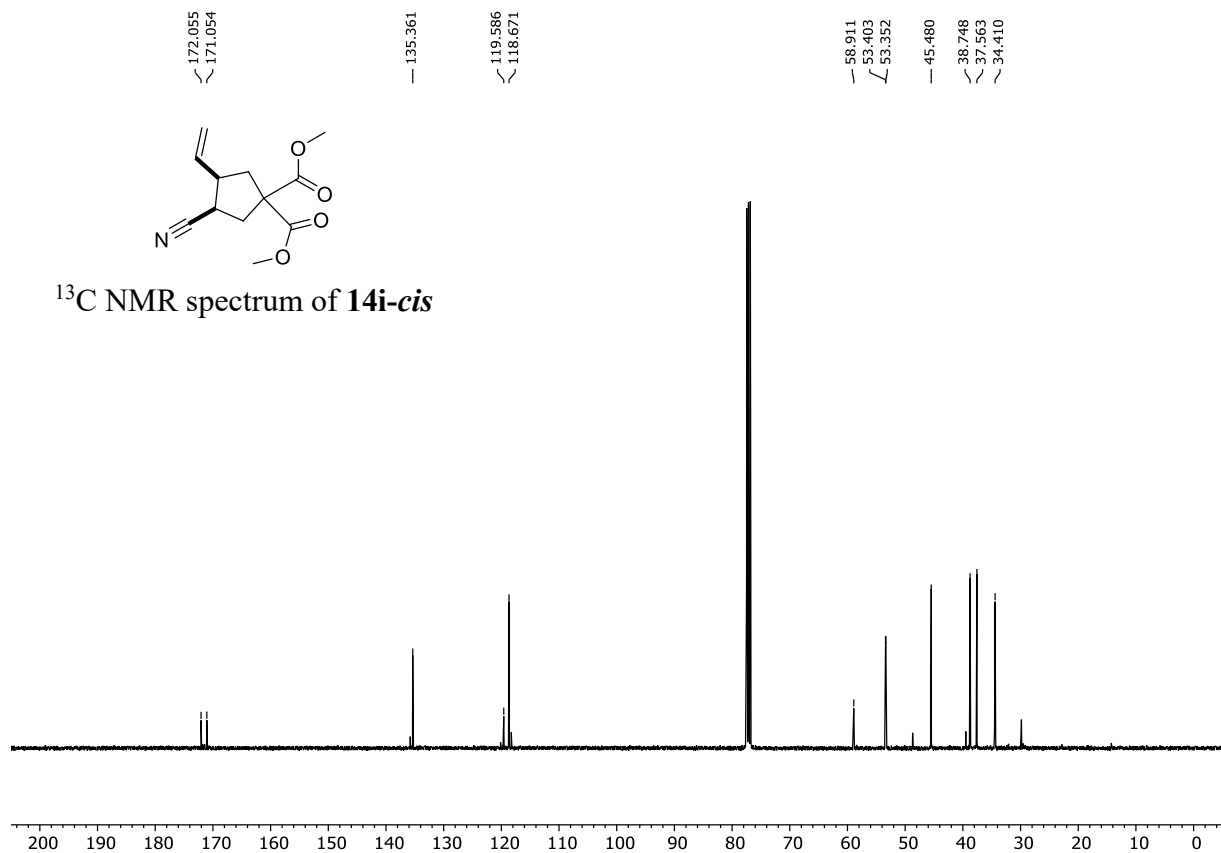
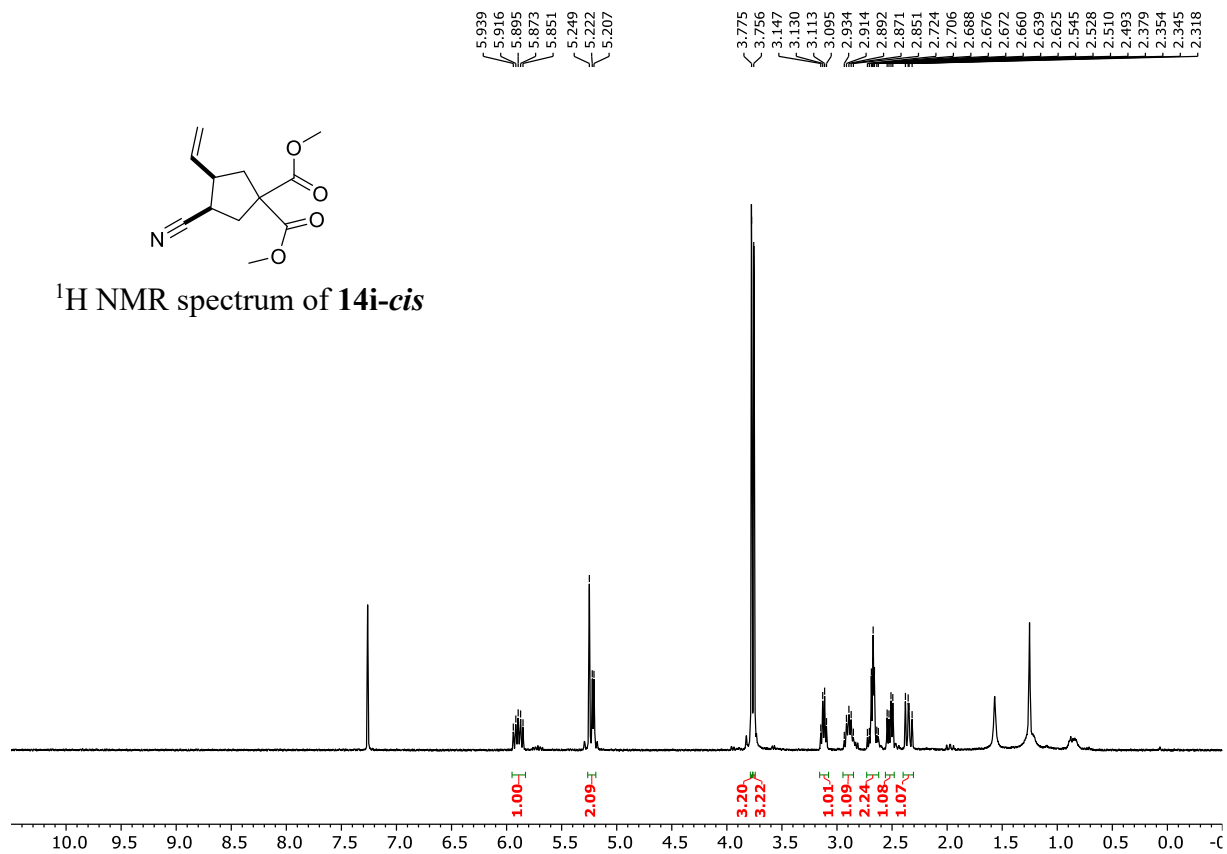


COSY spectrum of **14i-trans**

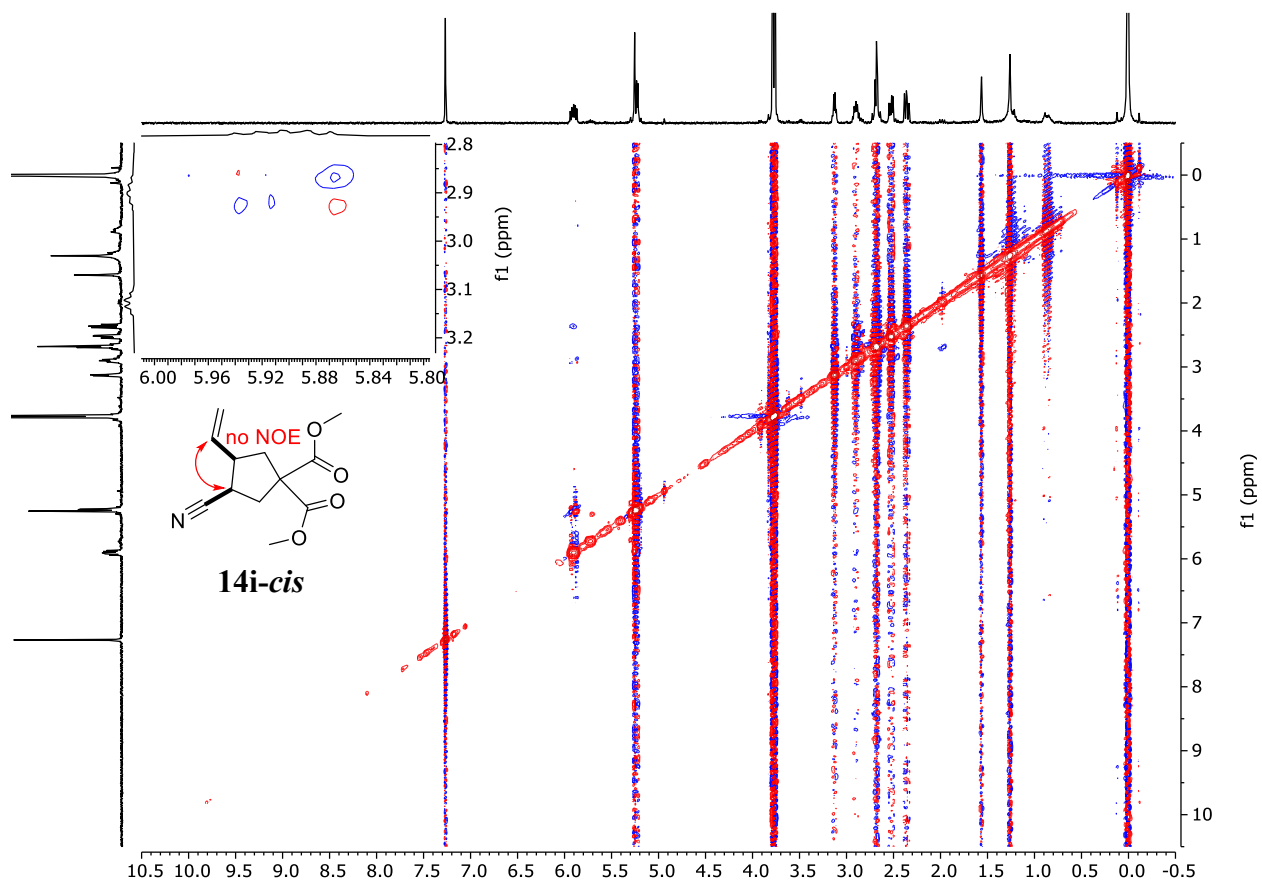


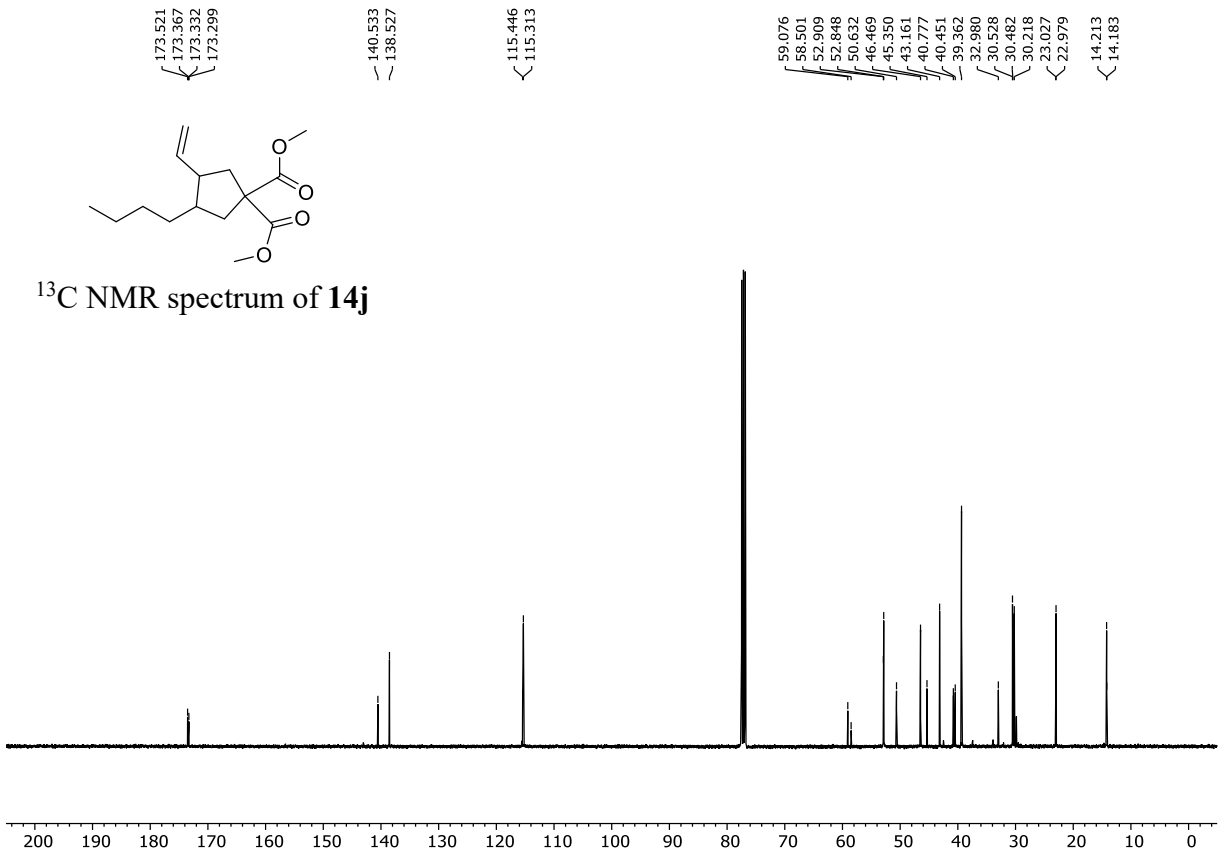
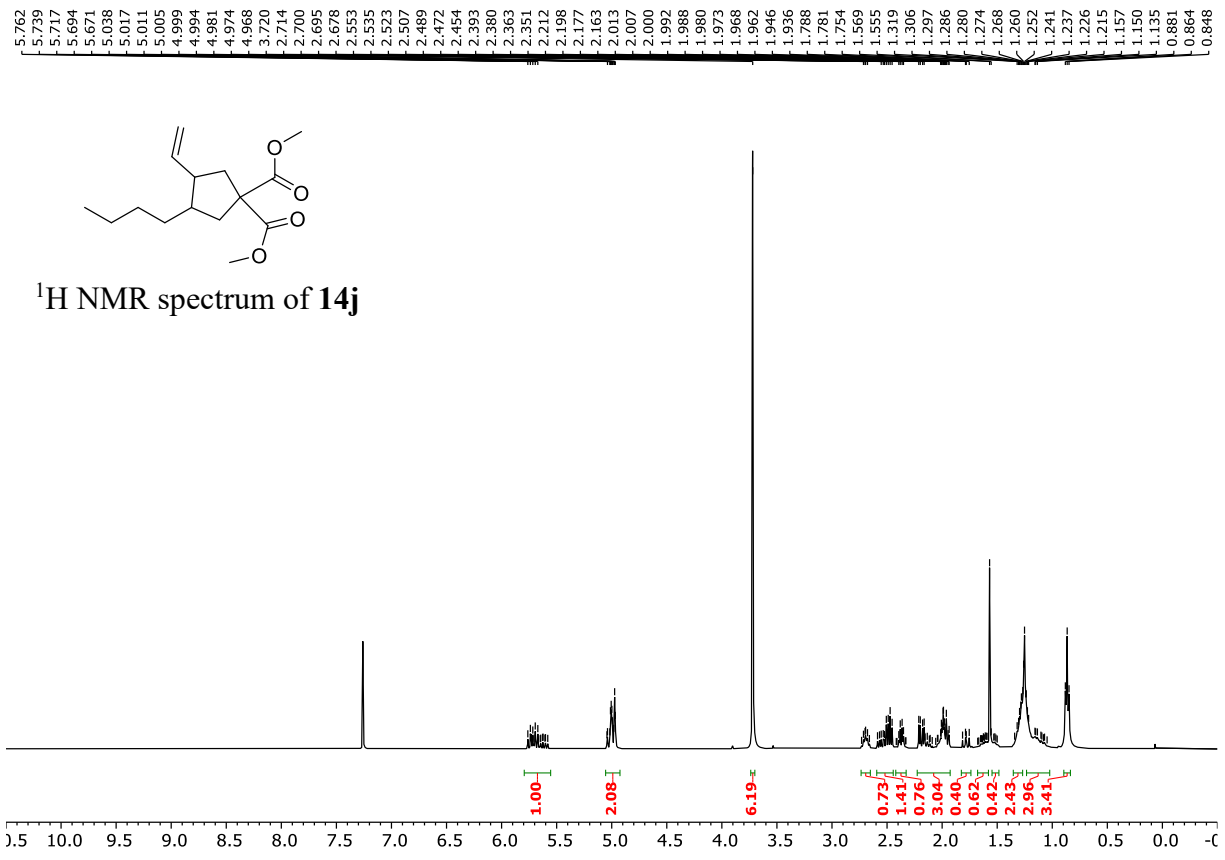
NOESY spectrum of **14i-trans**

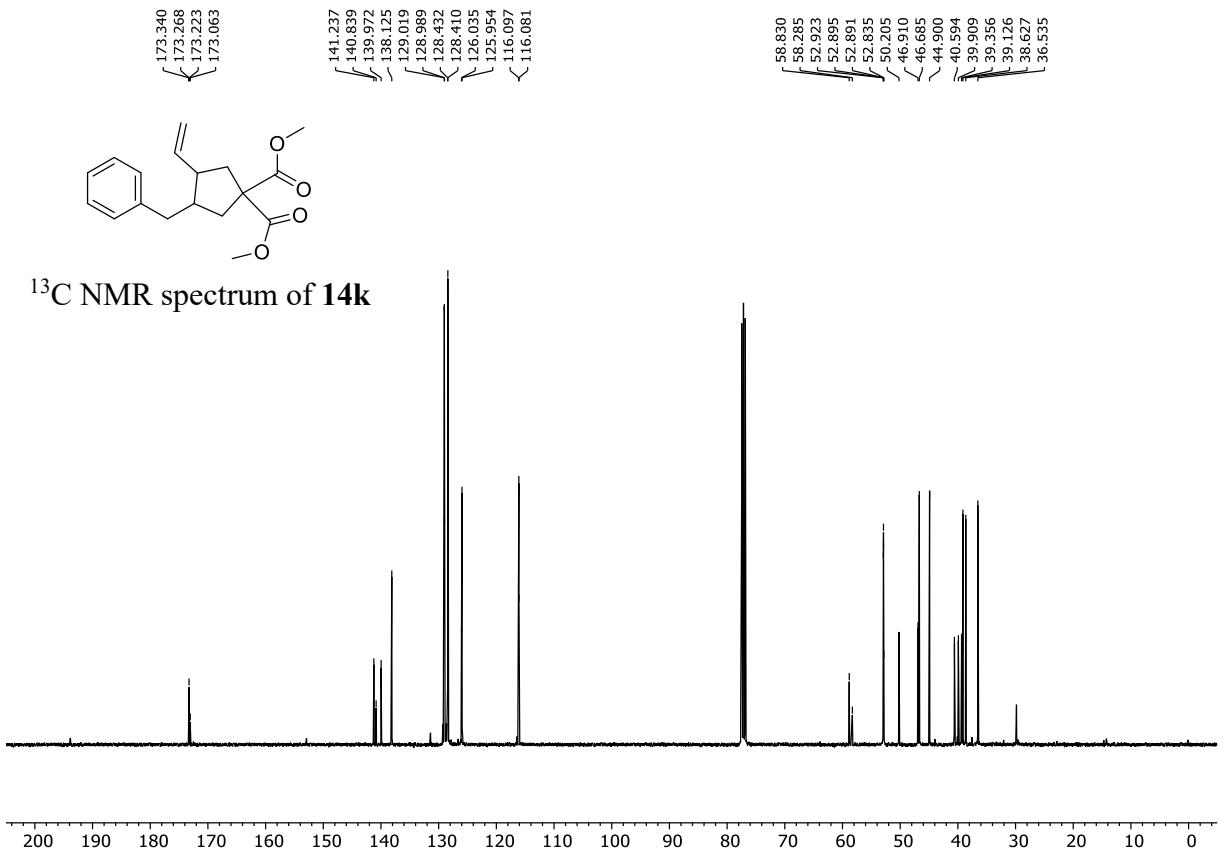
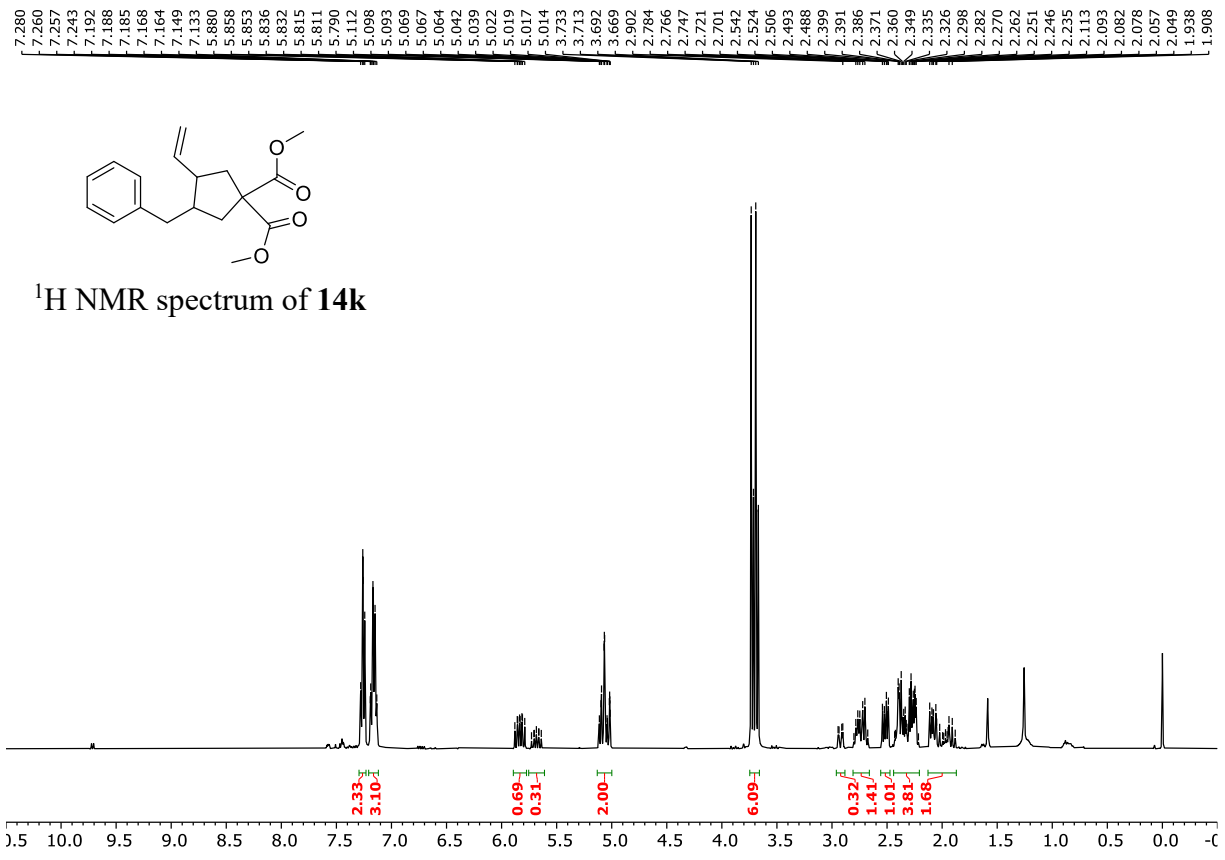




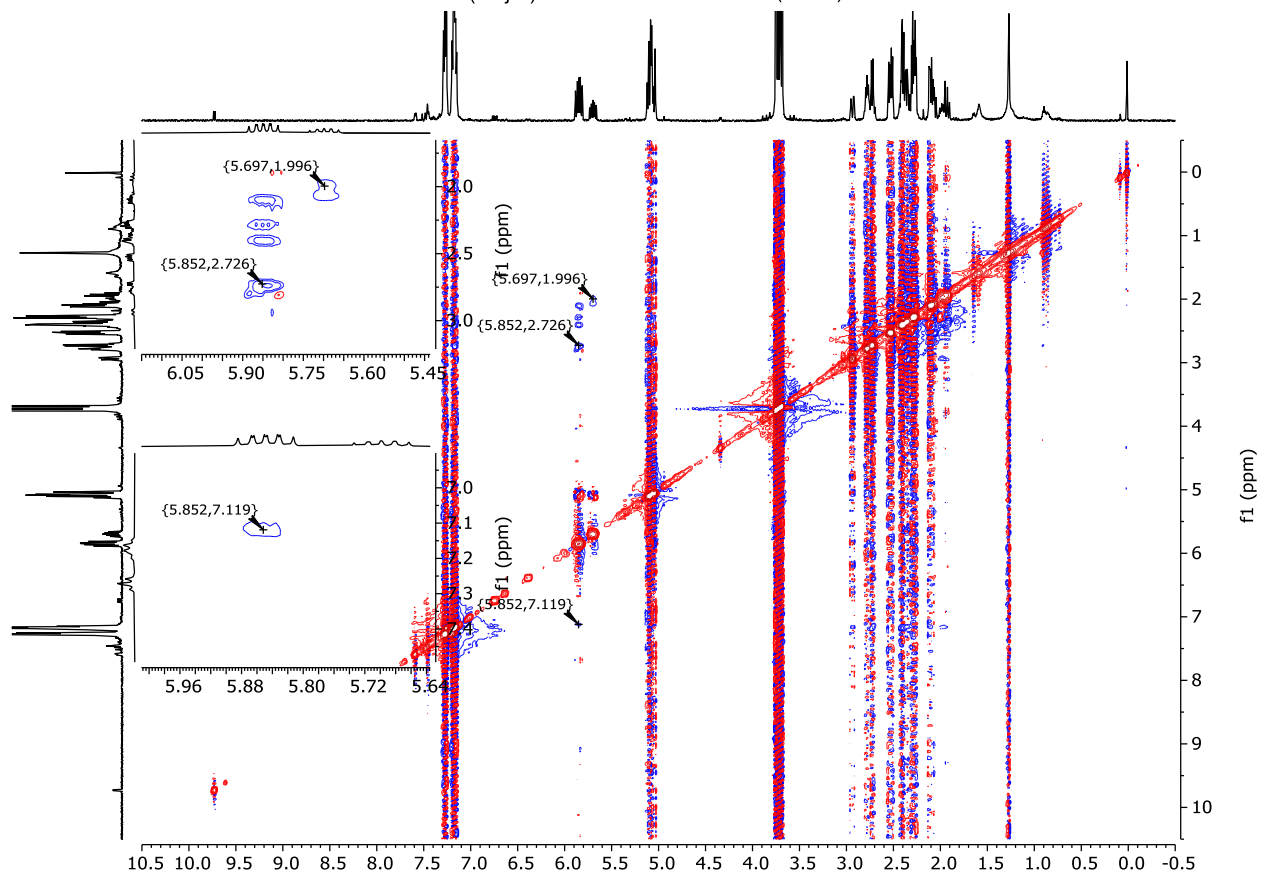
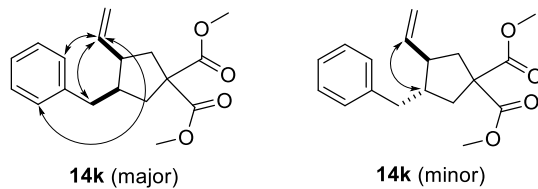
NOESY spectrum of **14i-cis**

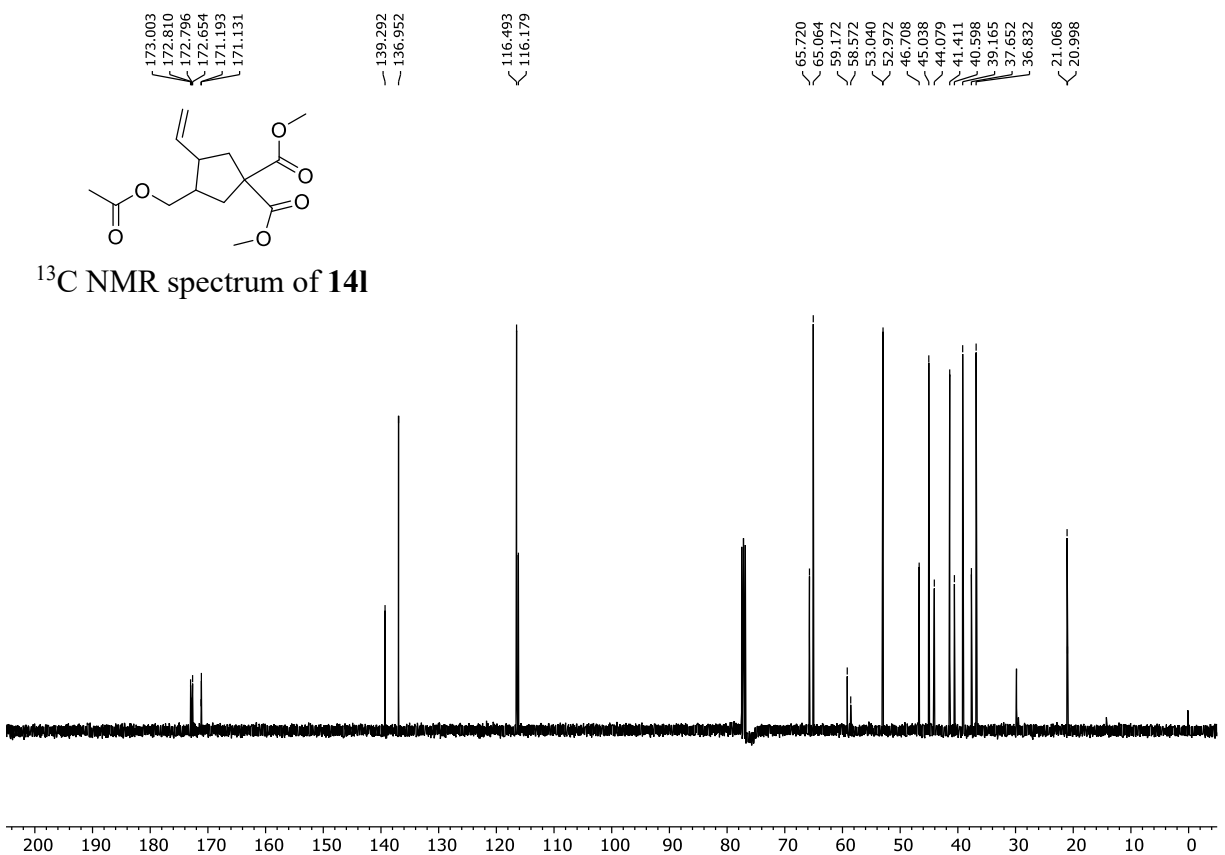
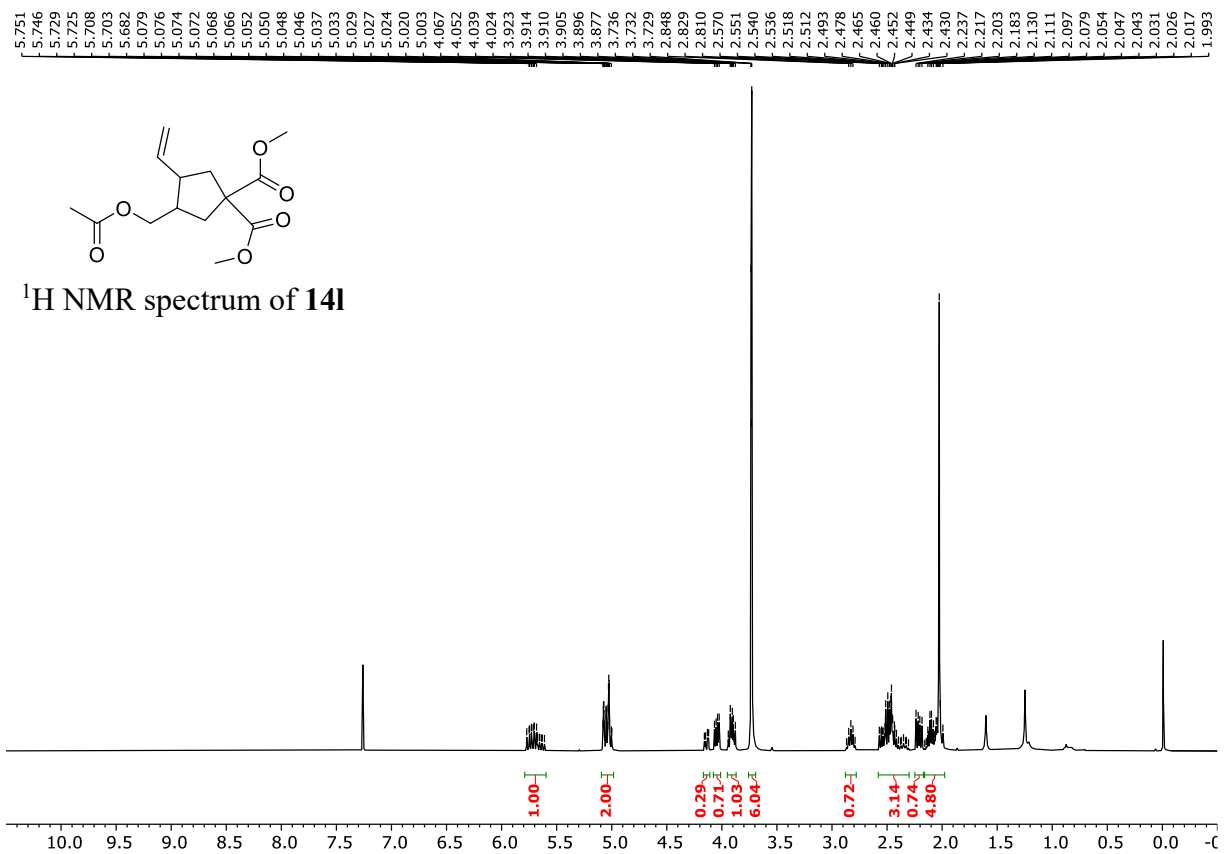




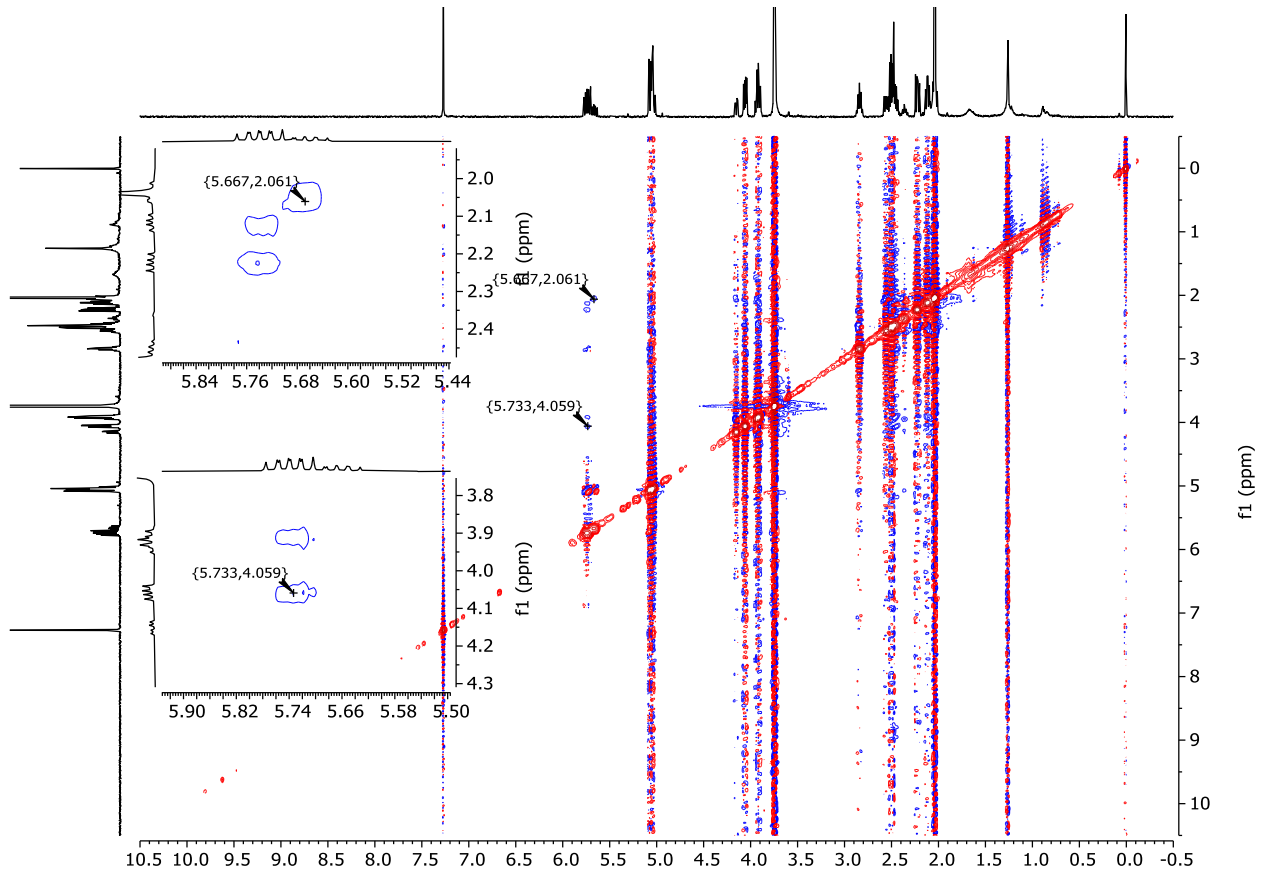
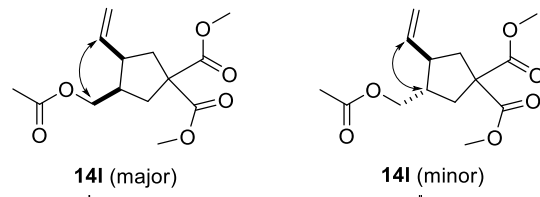


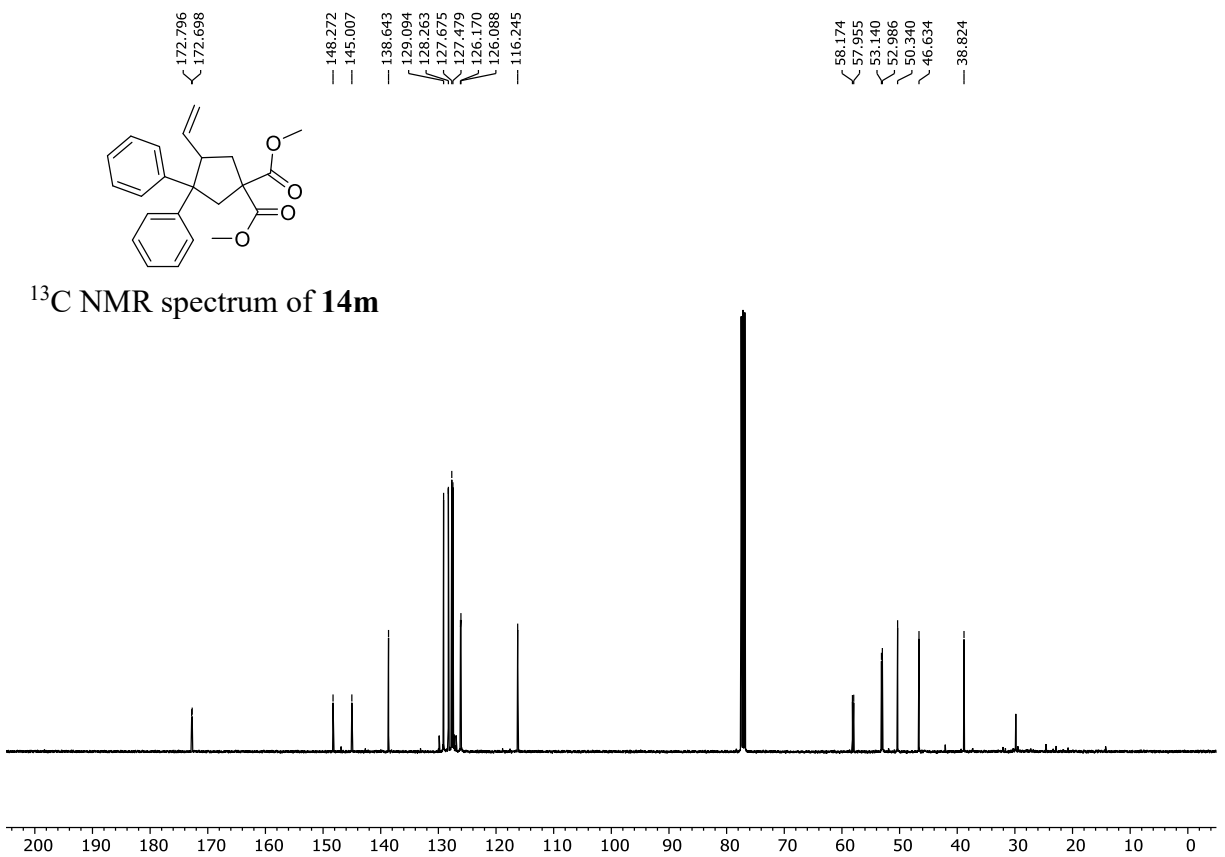
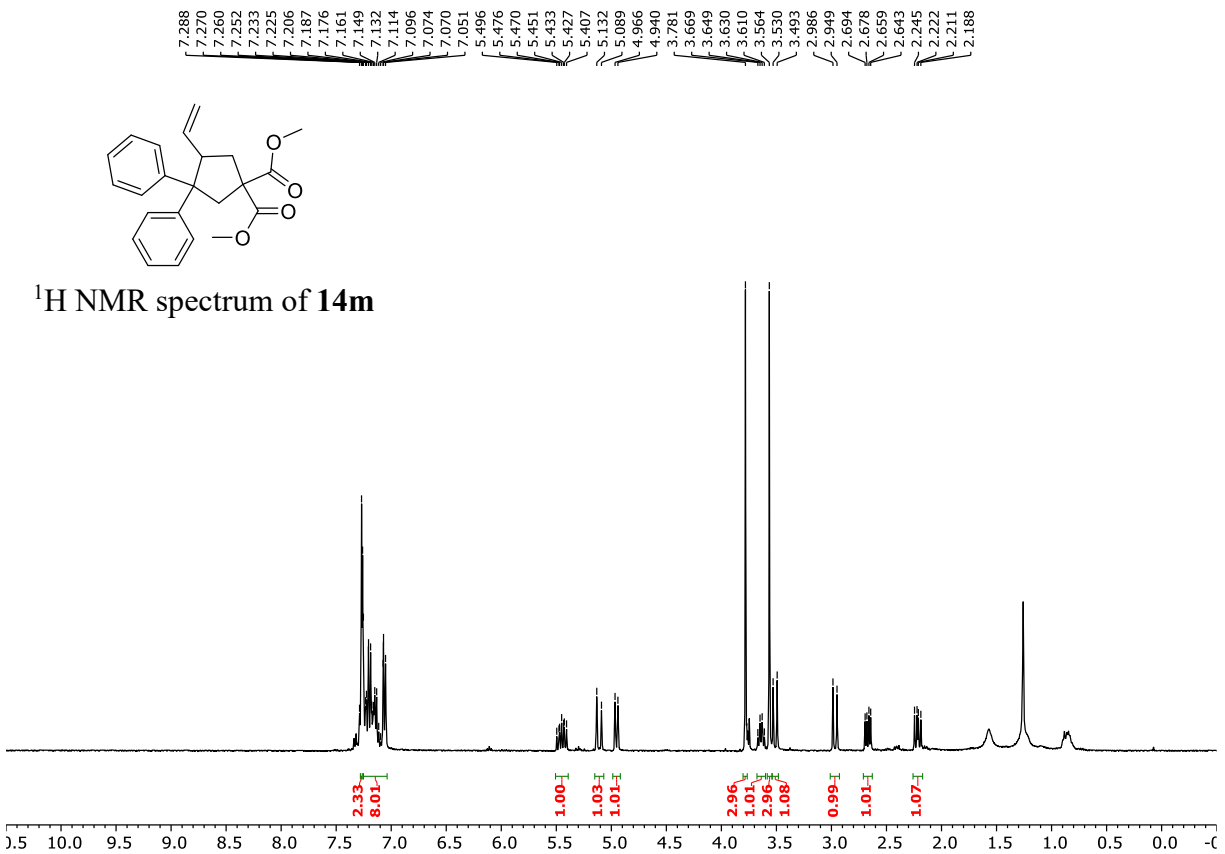
NOESY spectrum of 14k

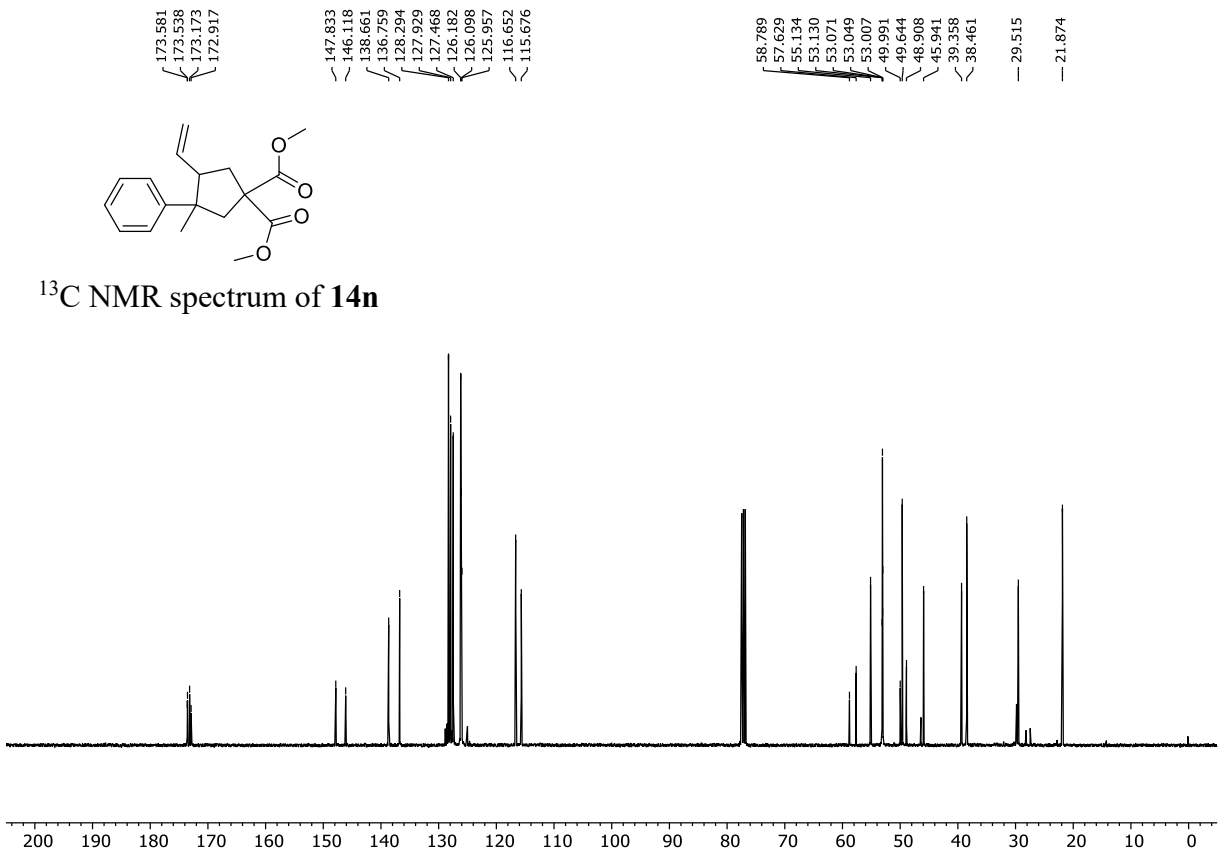
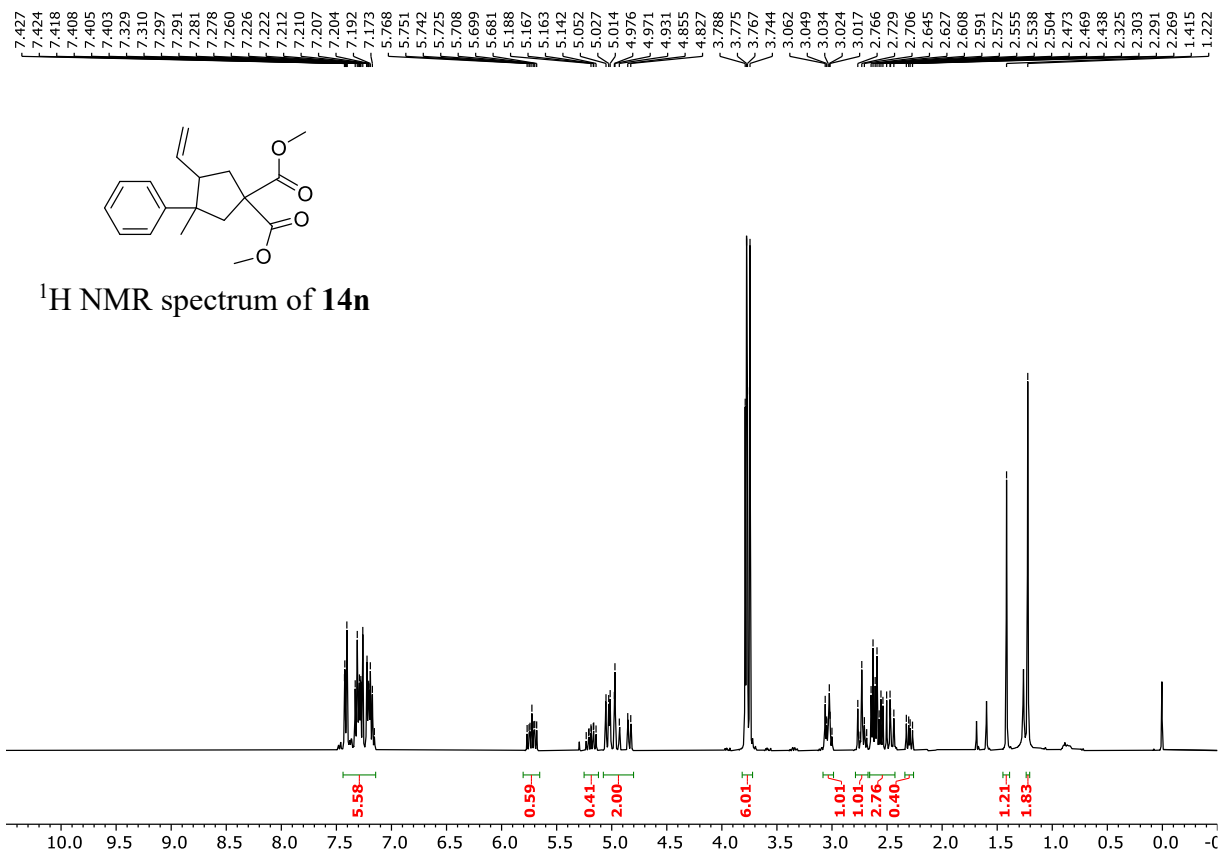




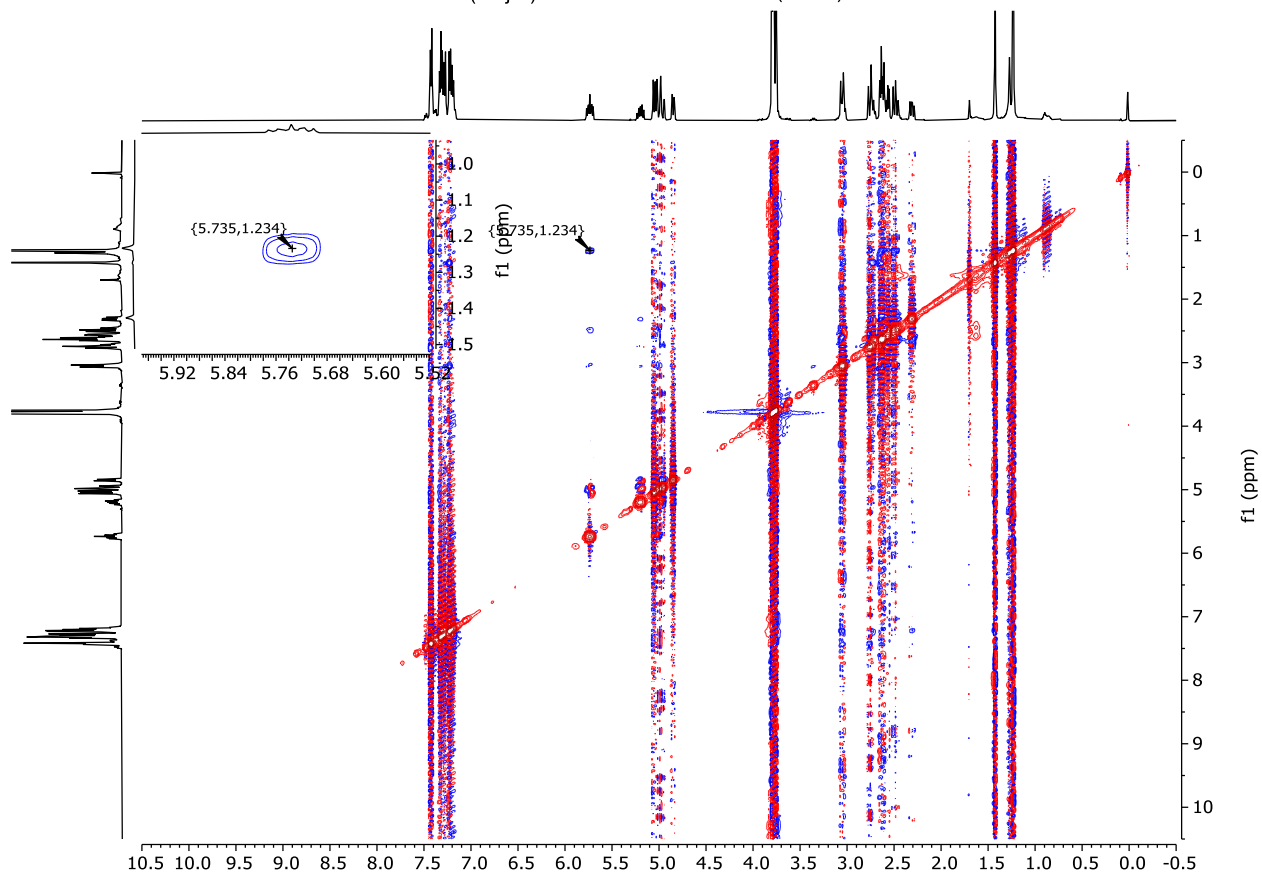
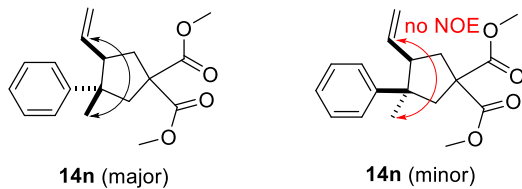
NOESY spectrum of **14l**

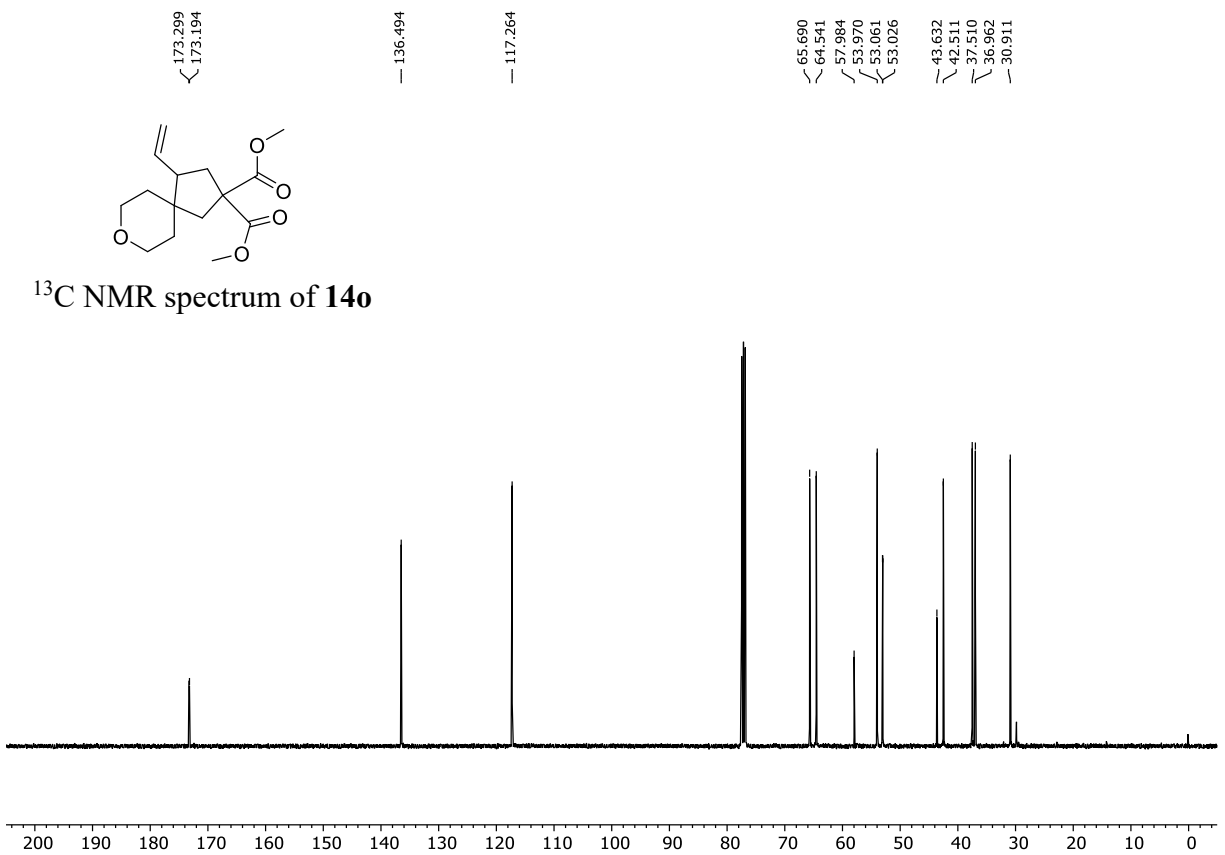
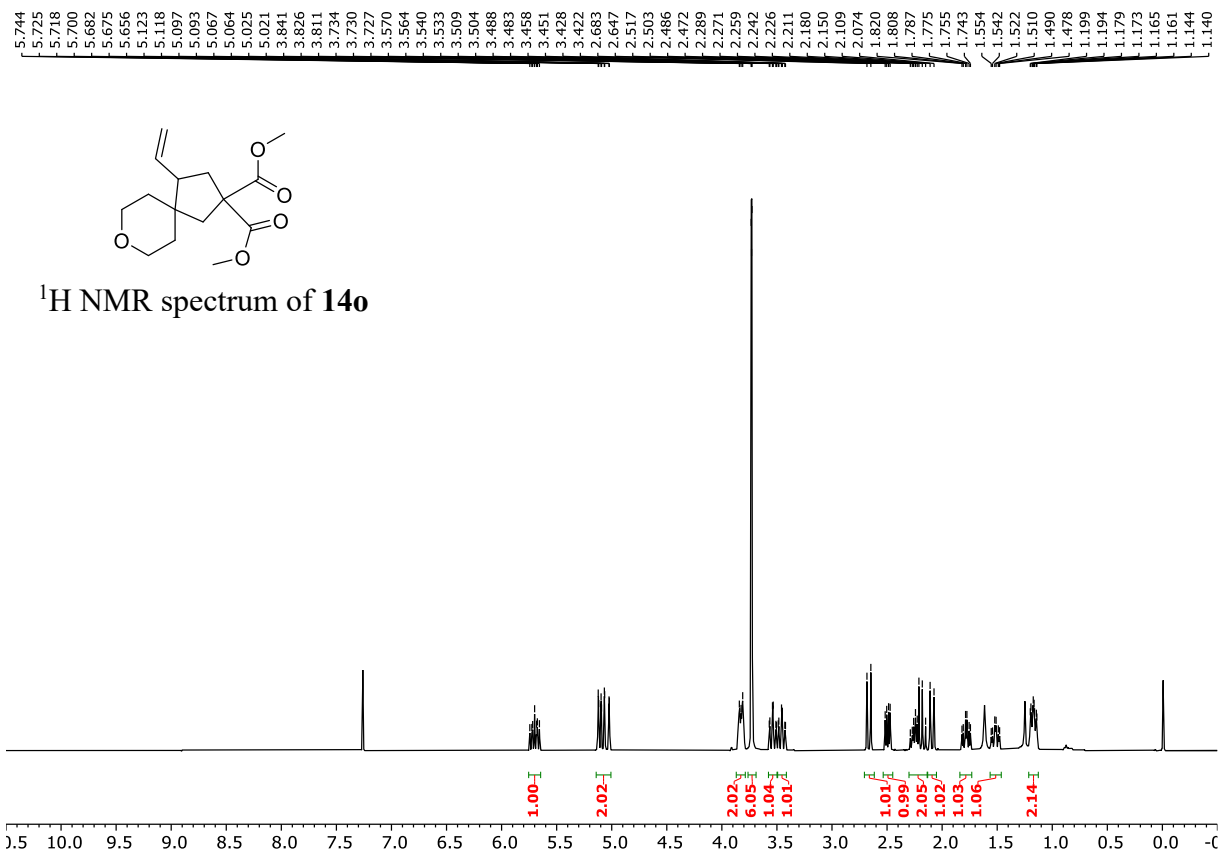


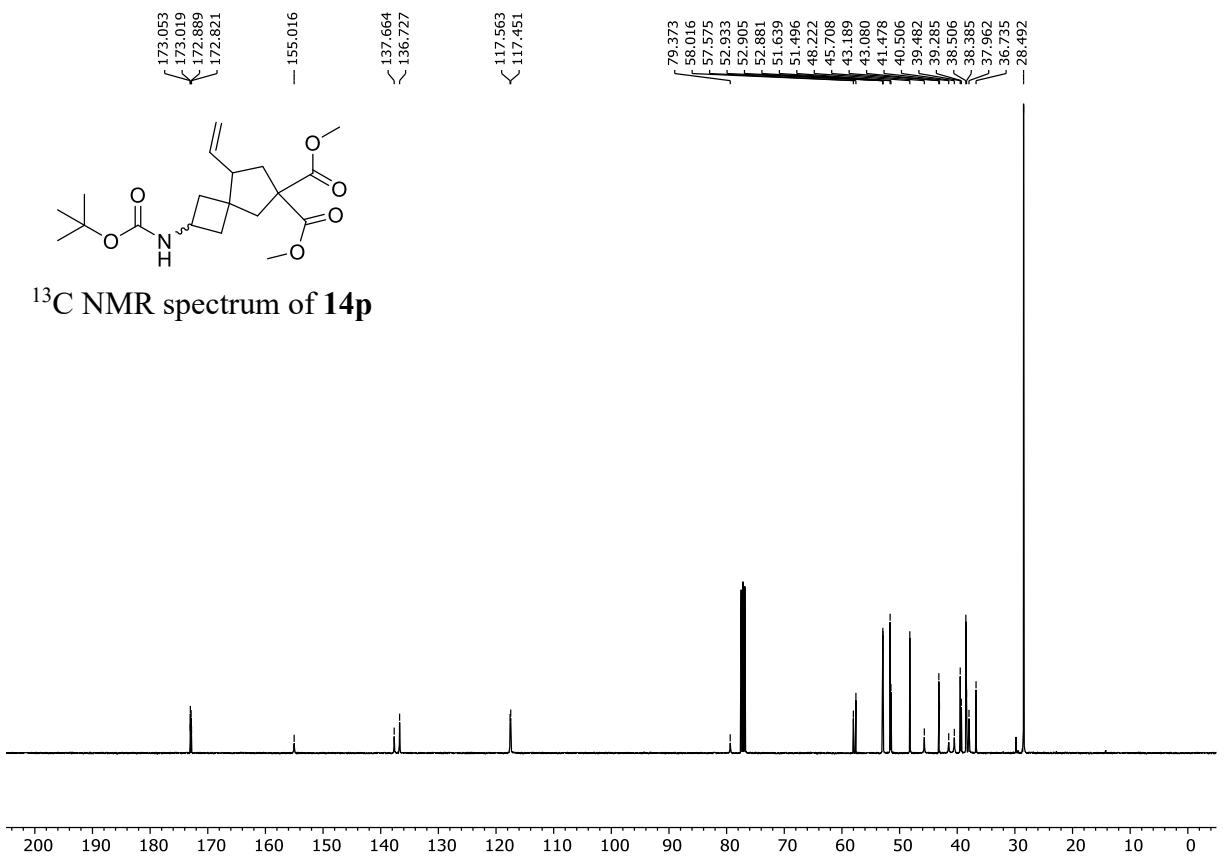
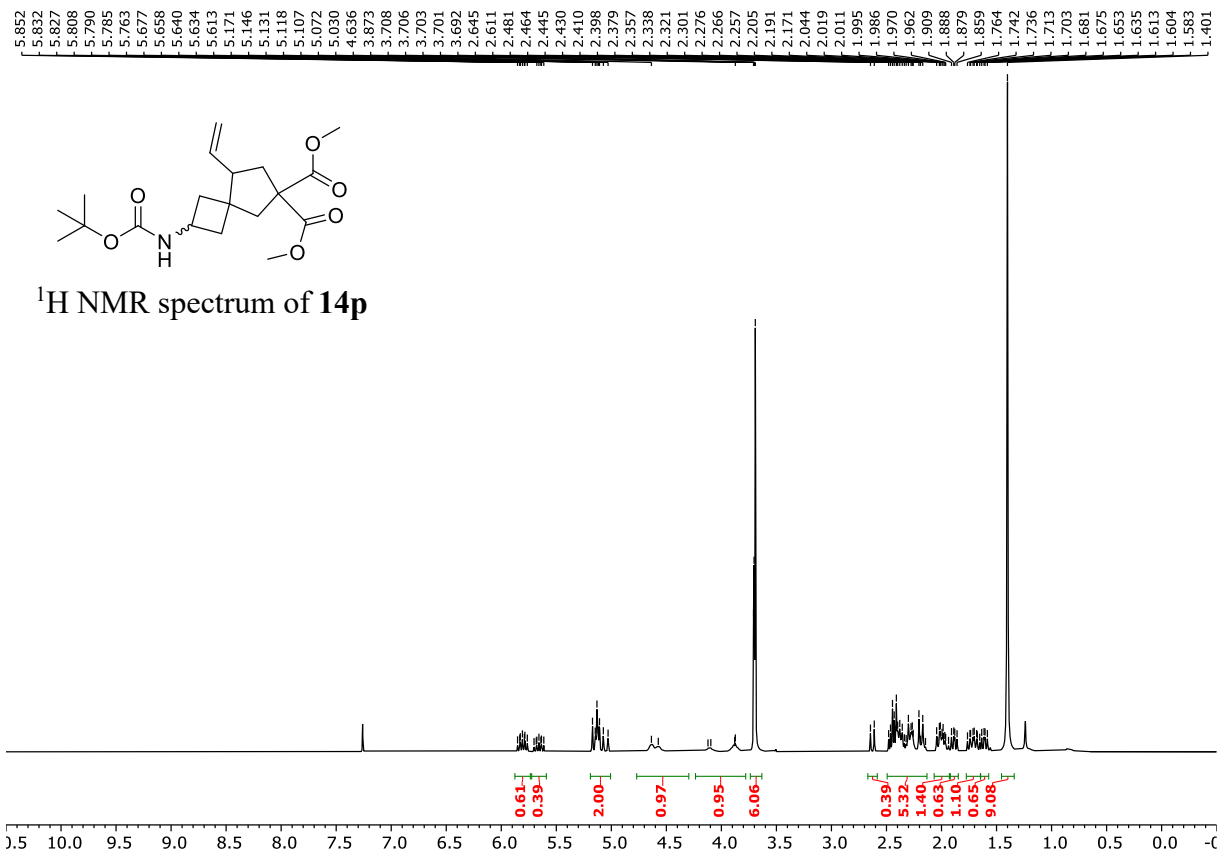


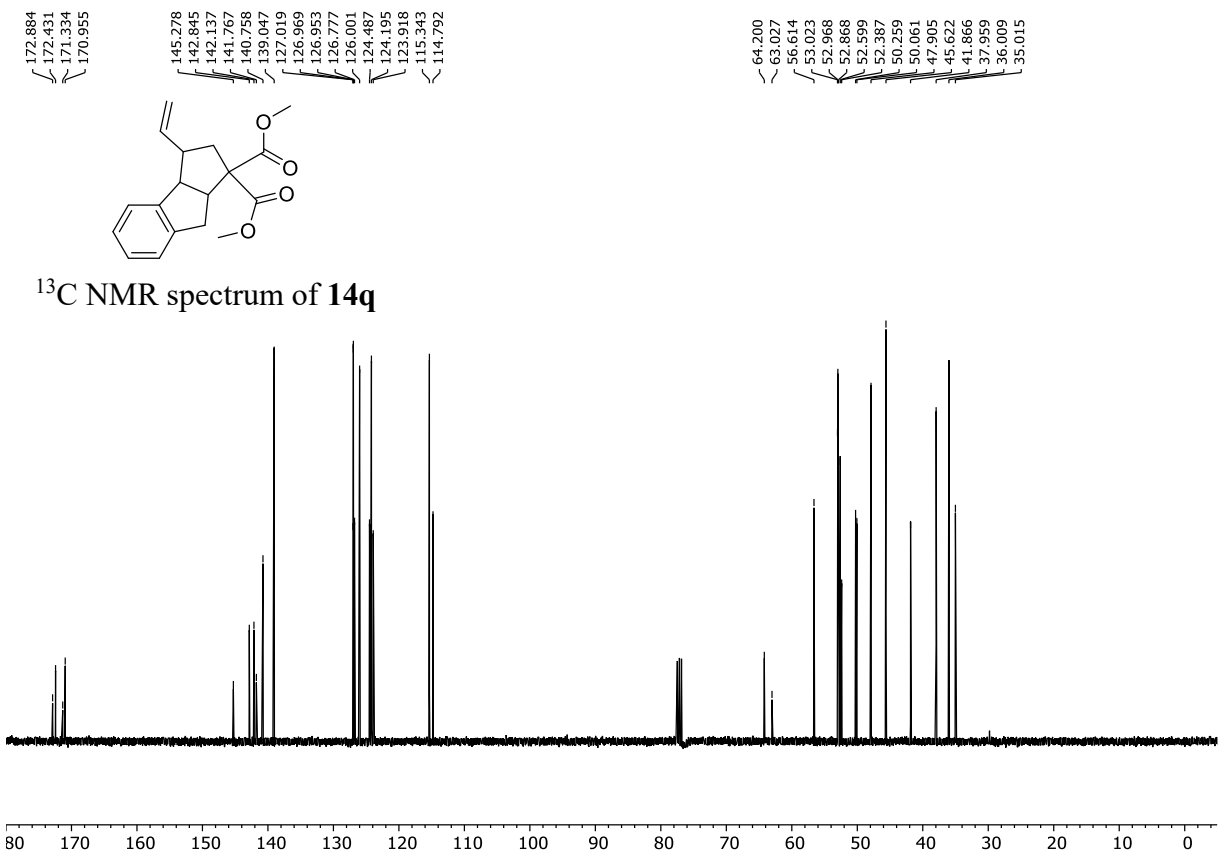
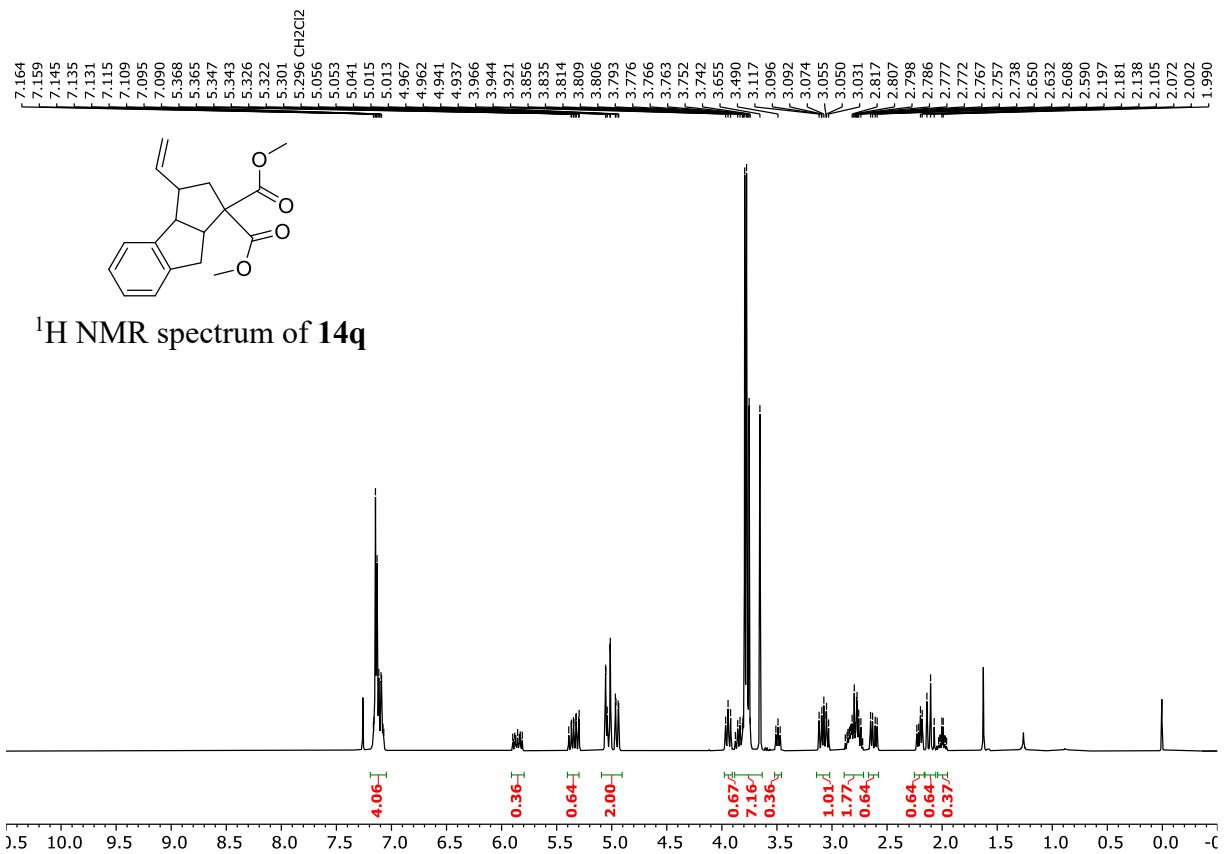


NOESY spectrum of **14n**

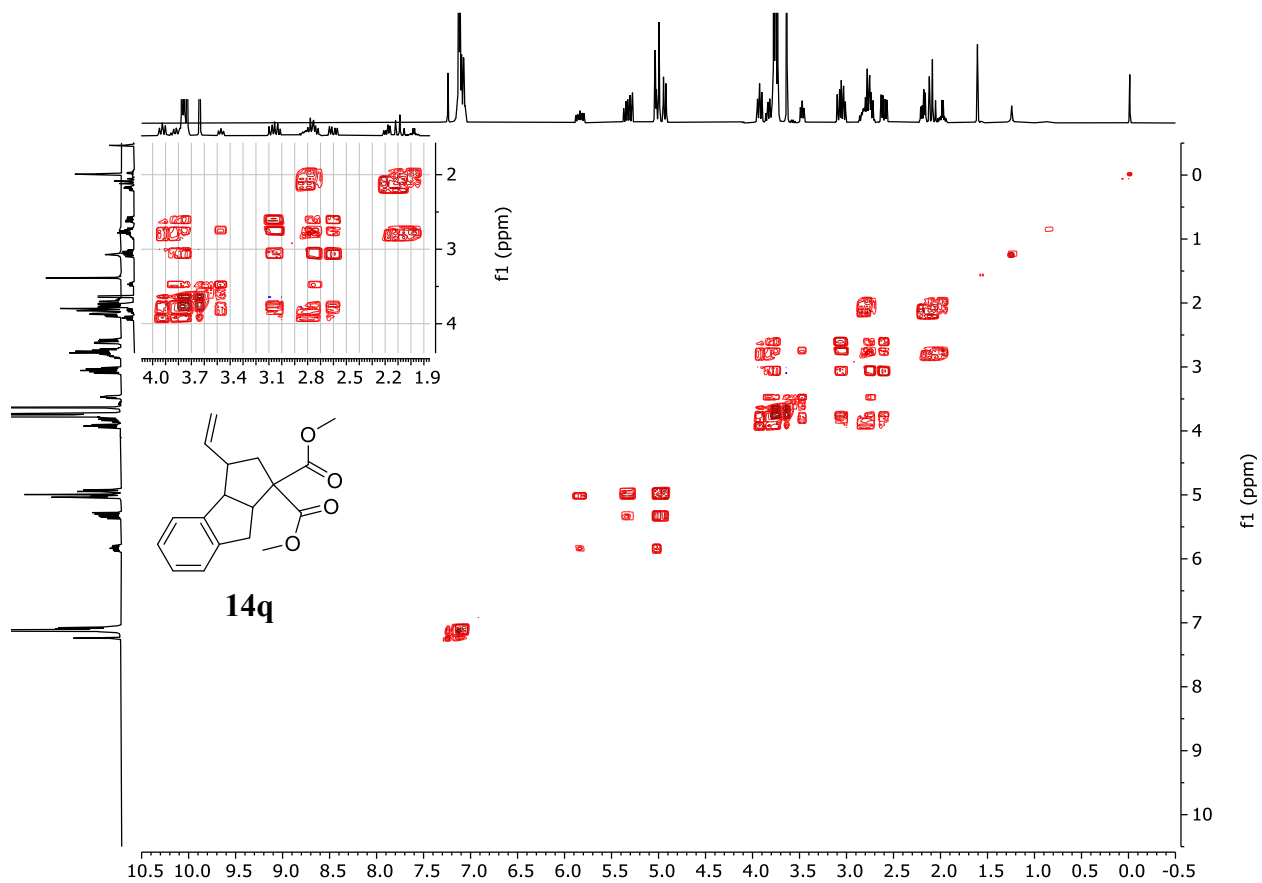




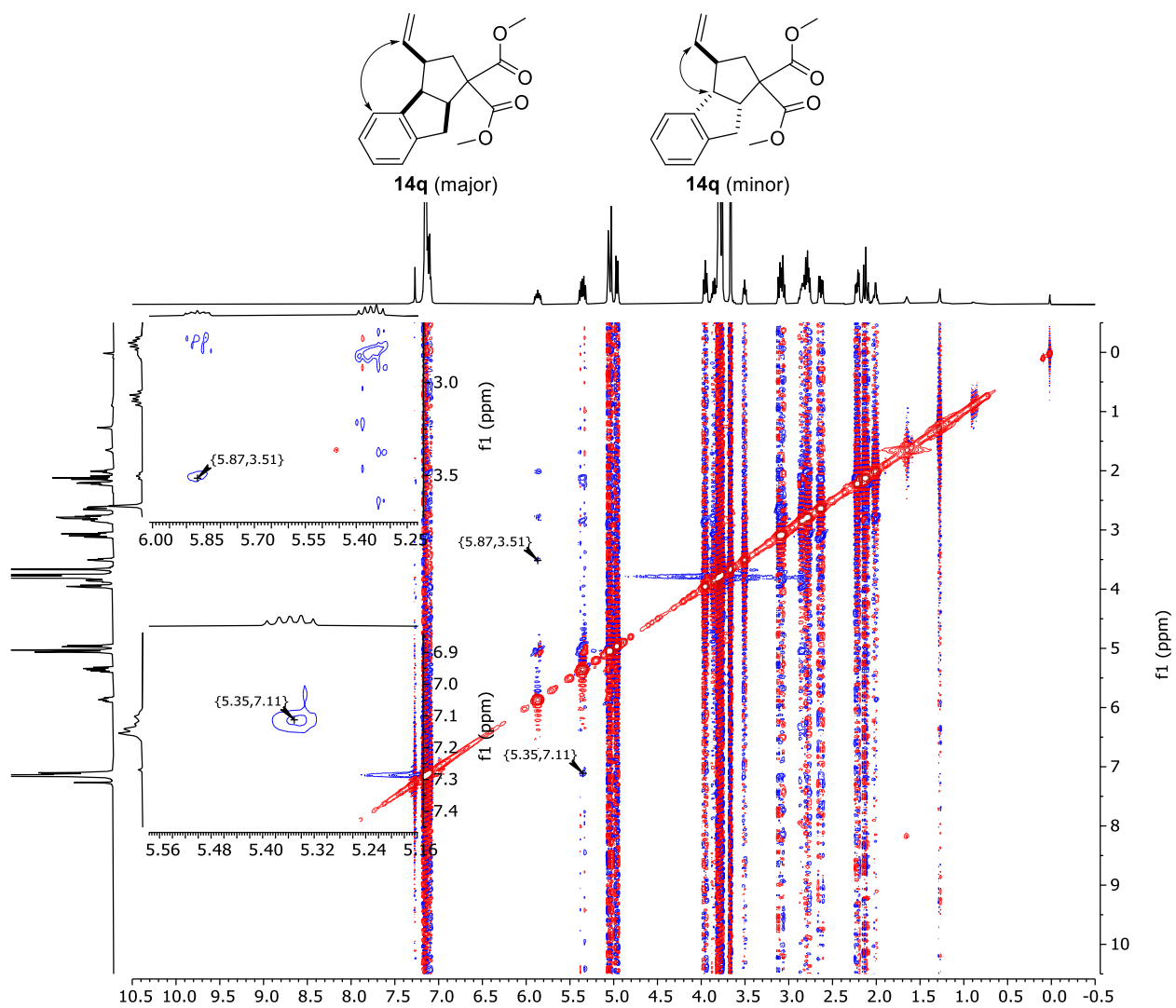


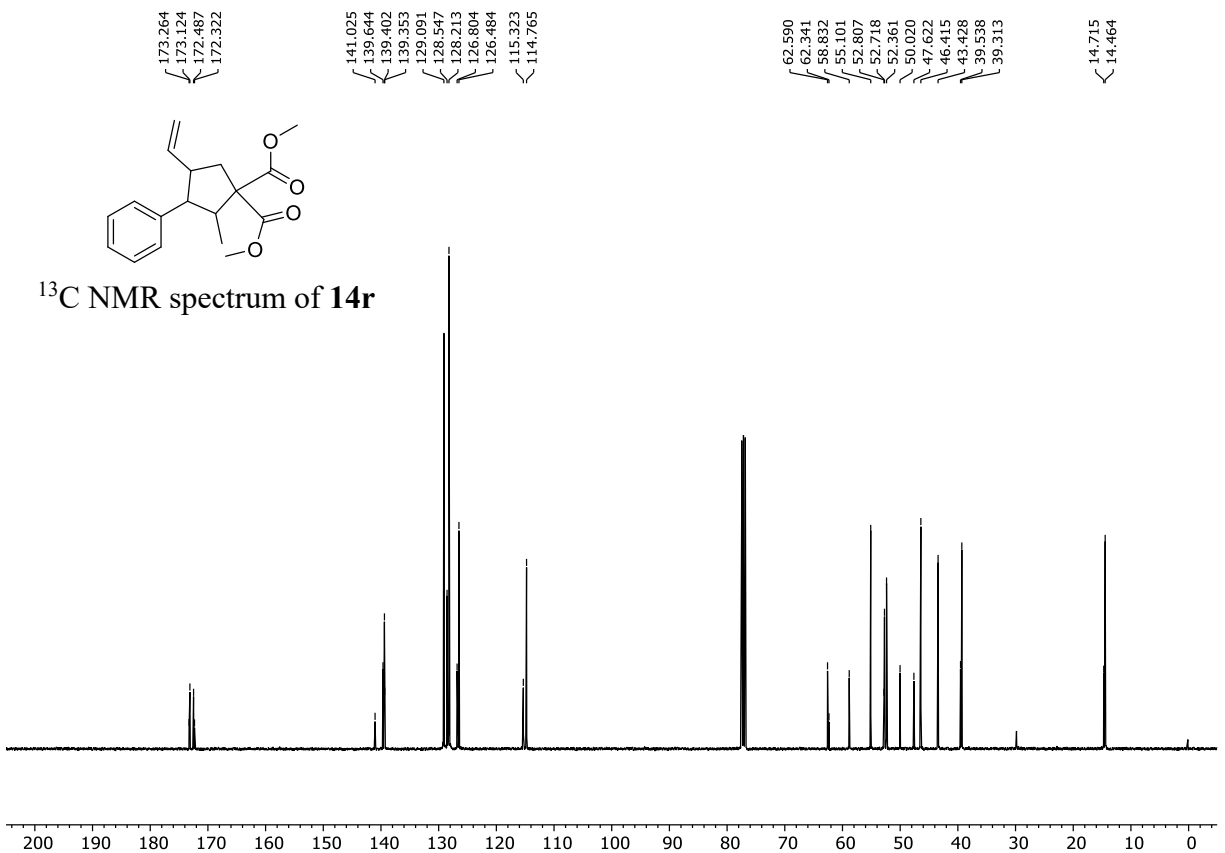
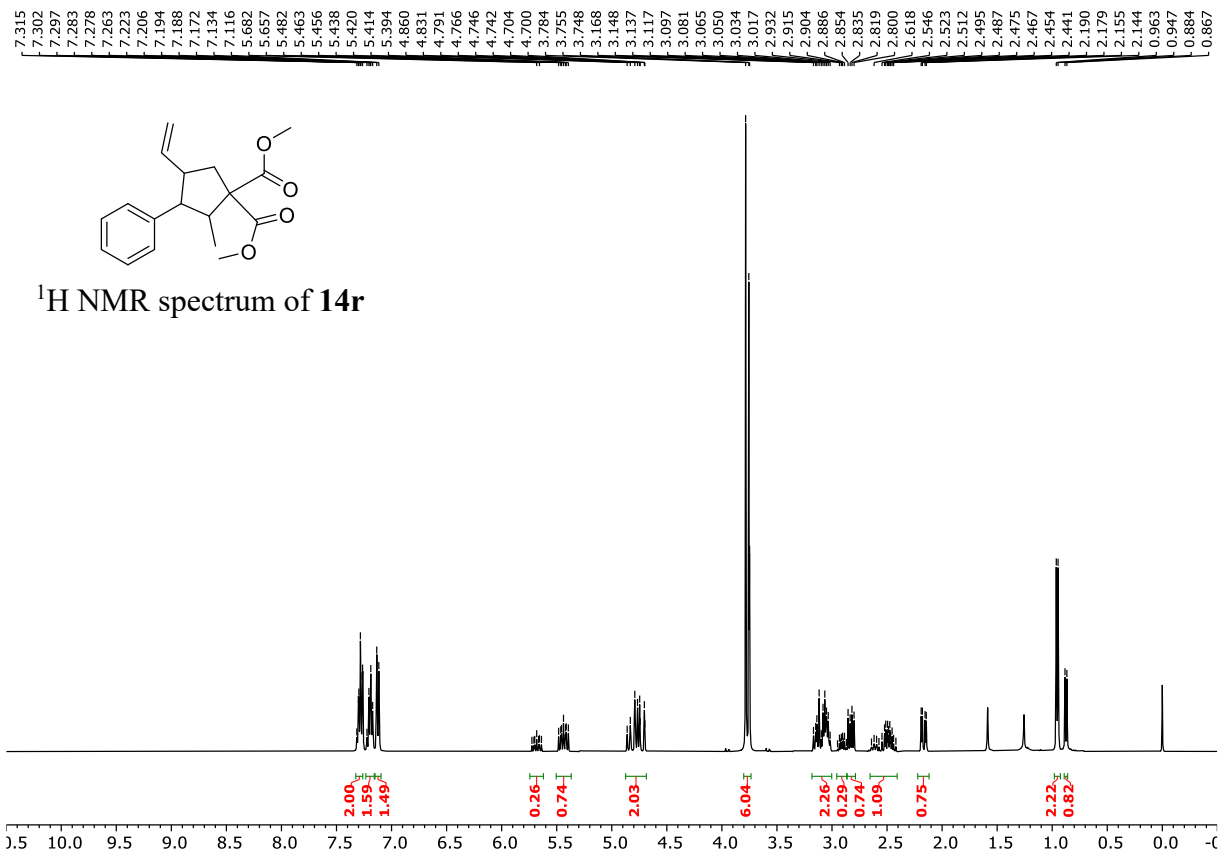


COSY spectrum of **14q**

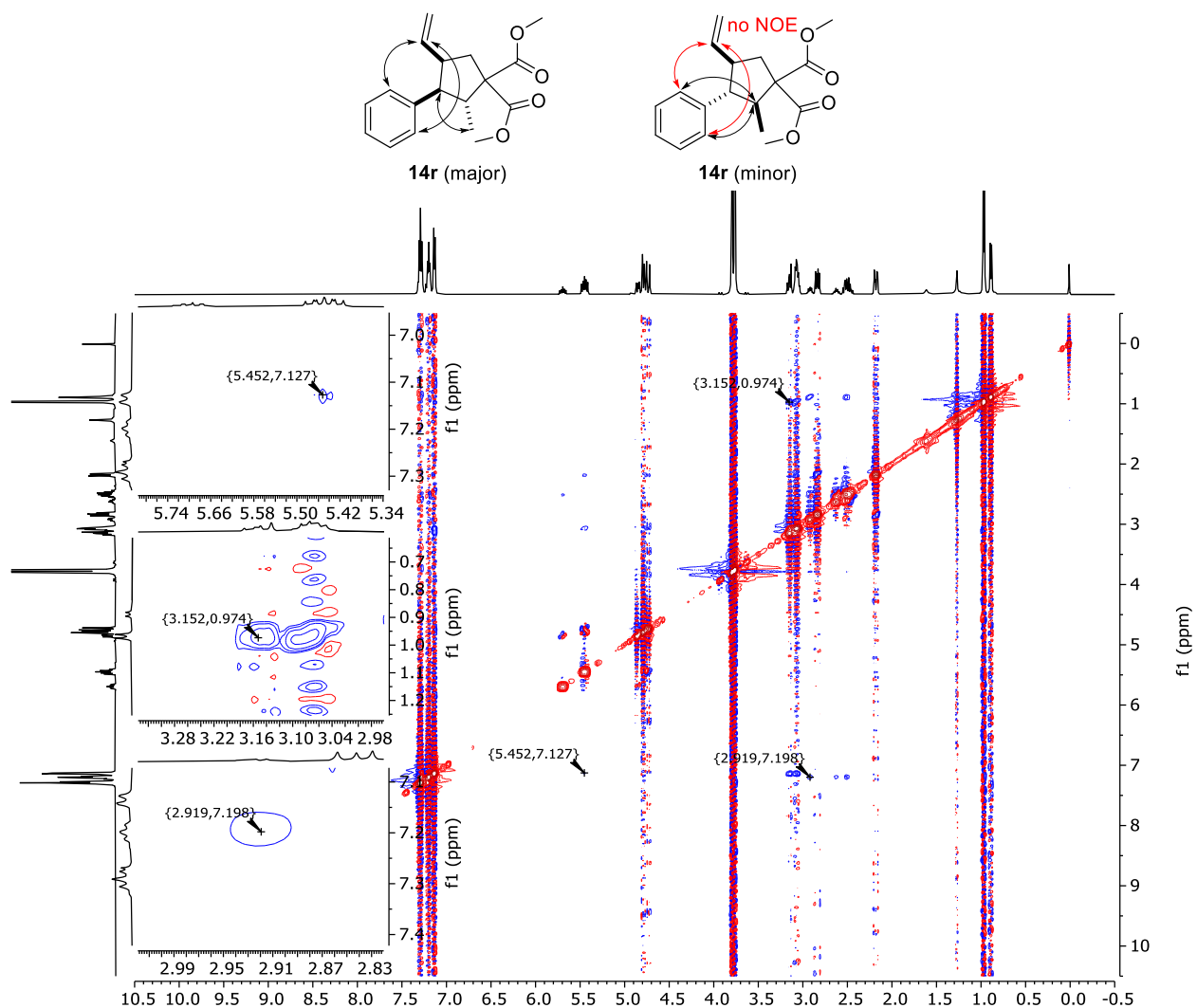


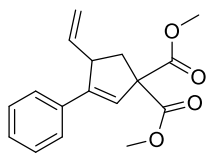
NOESY spectrum of **14q**



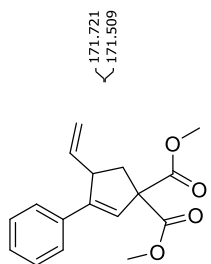
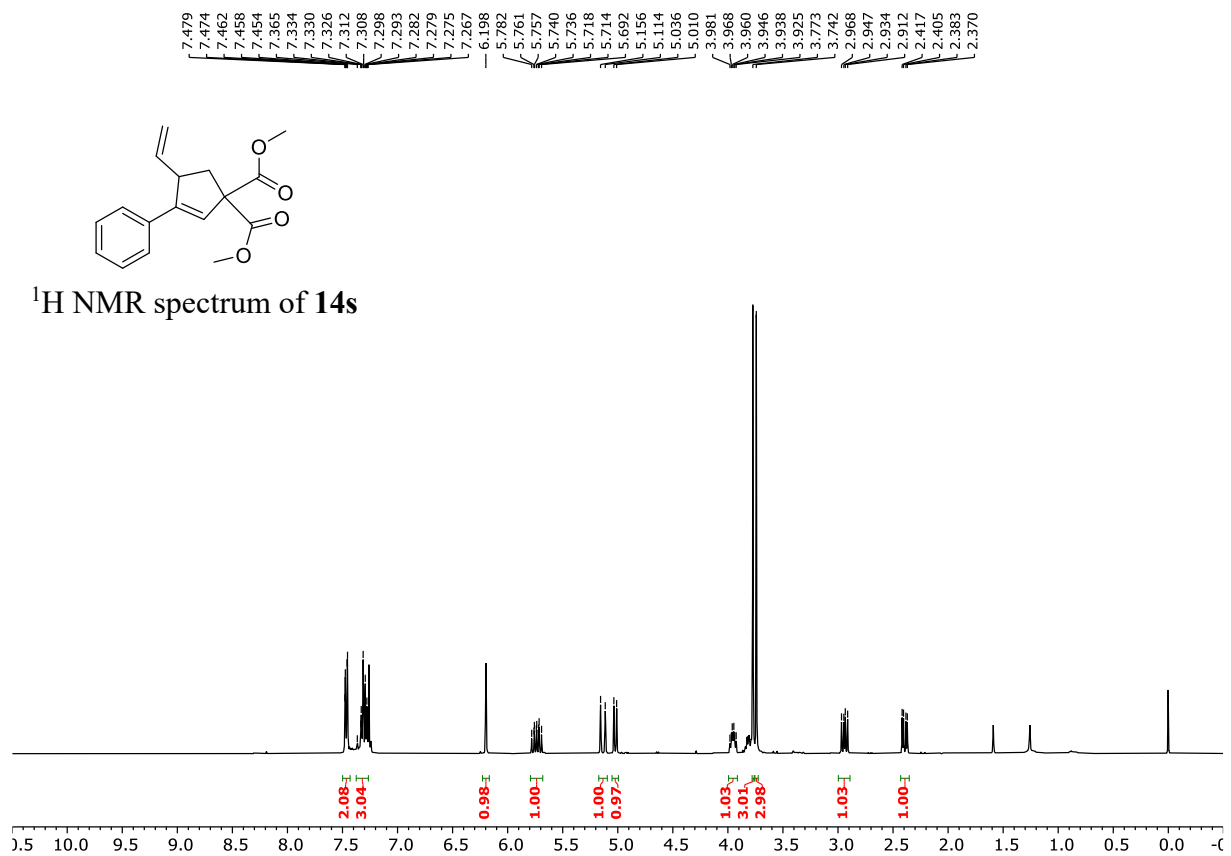


NOESY spectrum of **14r**

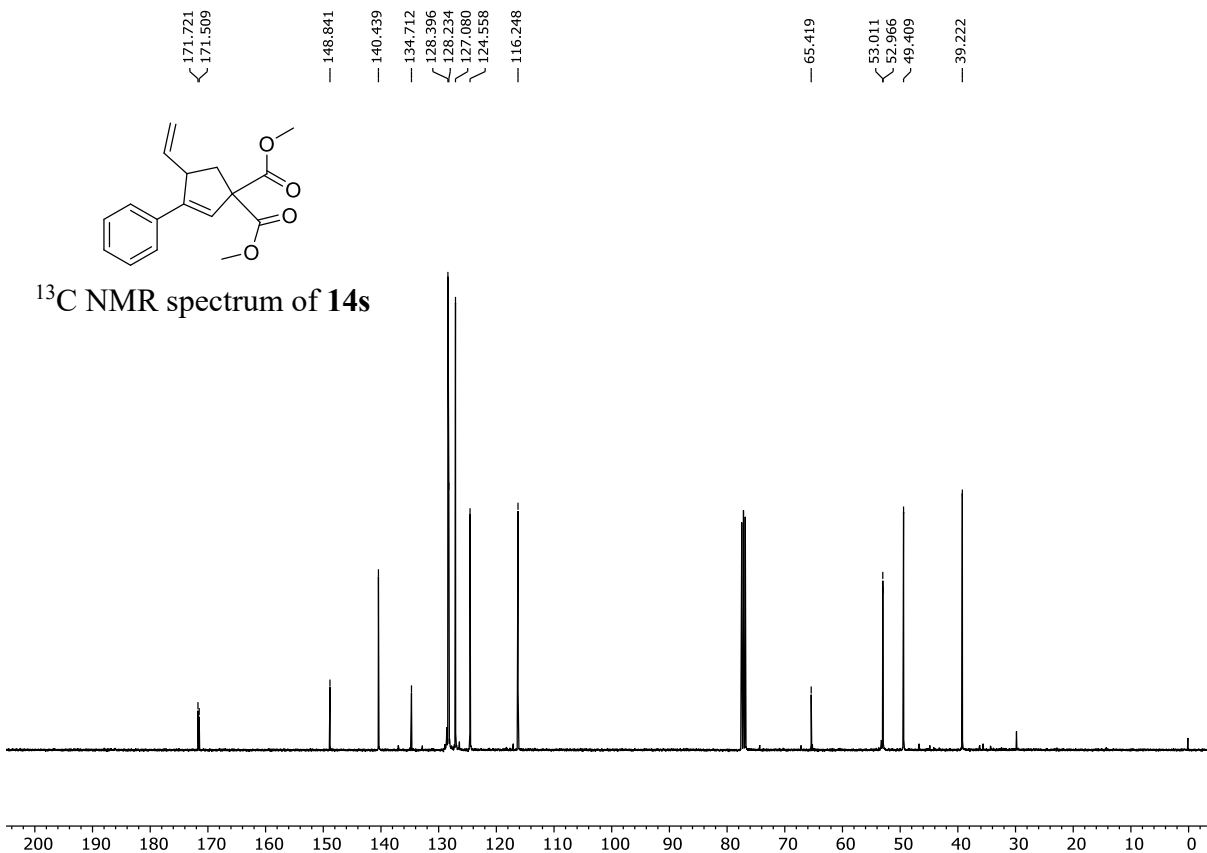


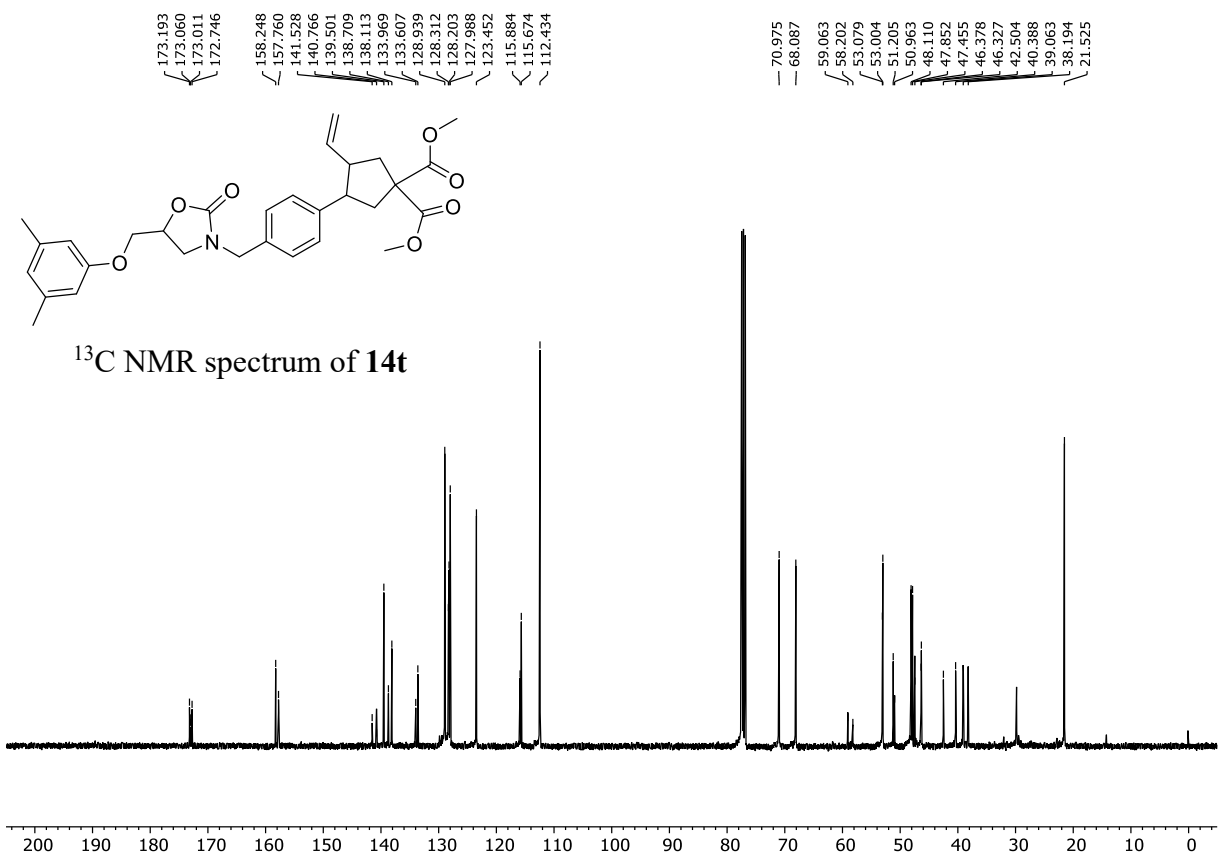
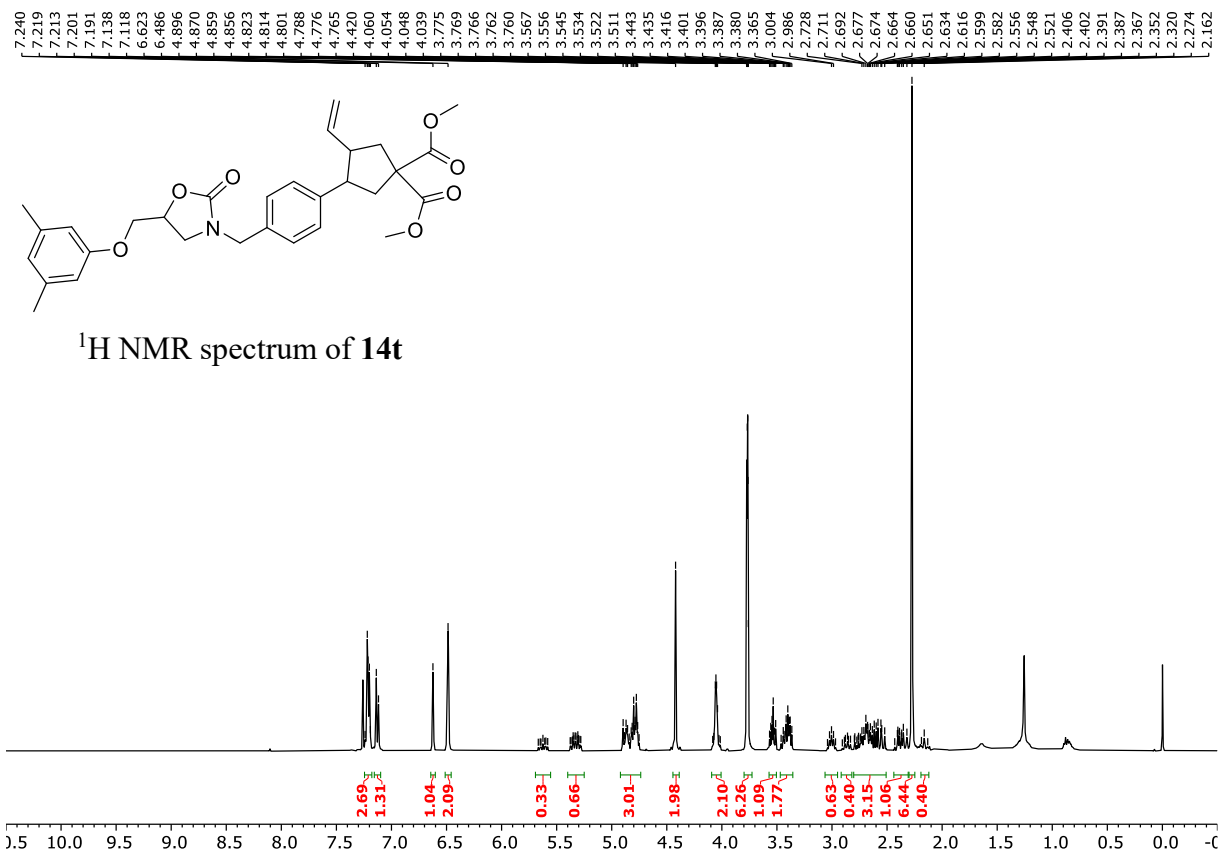


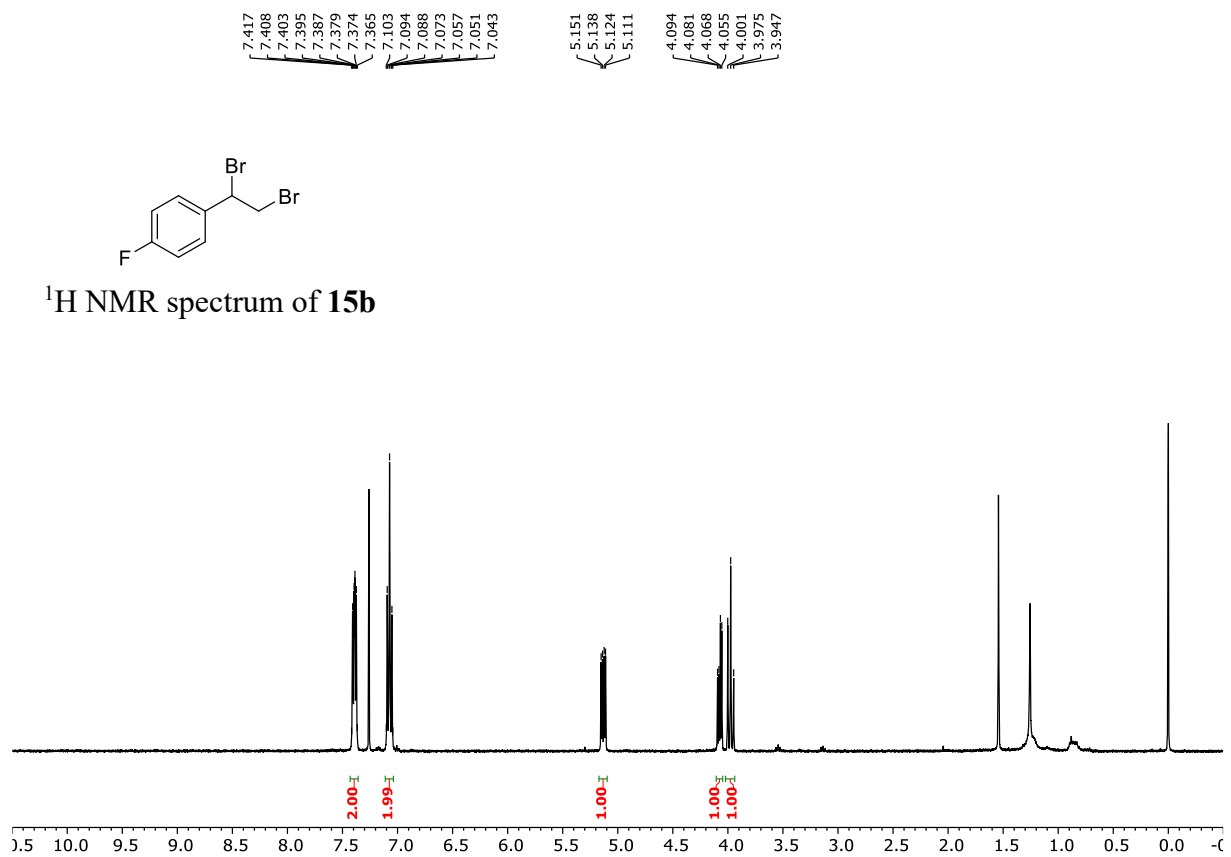
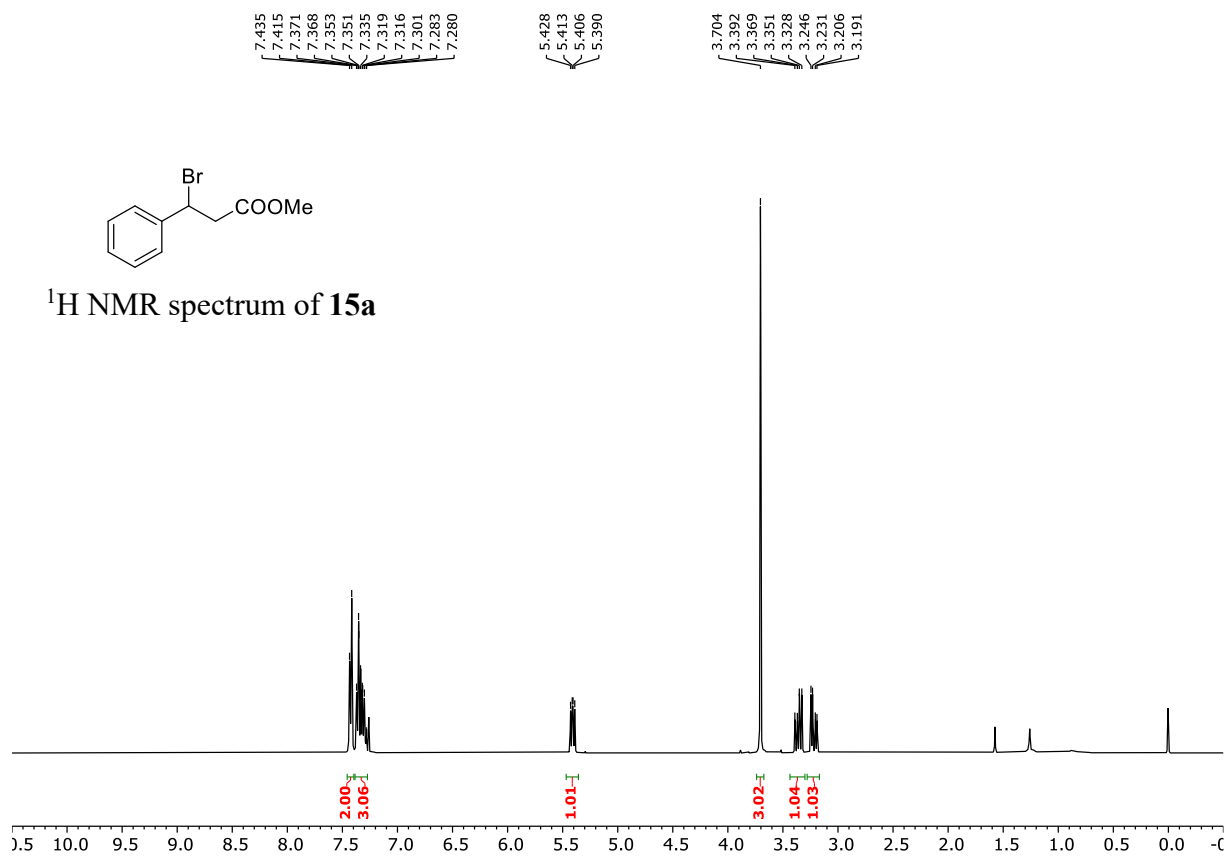
^1H NMR spectrum of **14s**

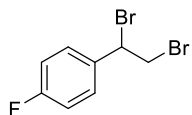


^{13}C NMR spectrum of **14s**

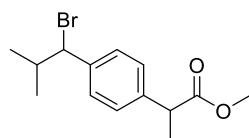
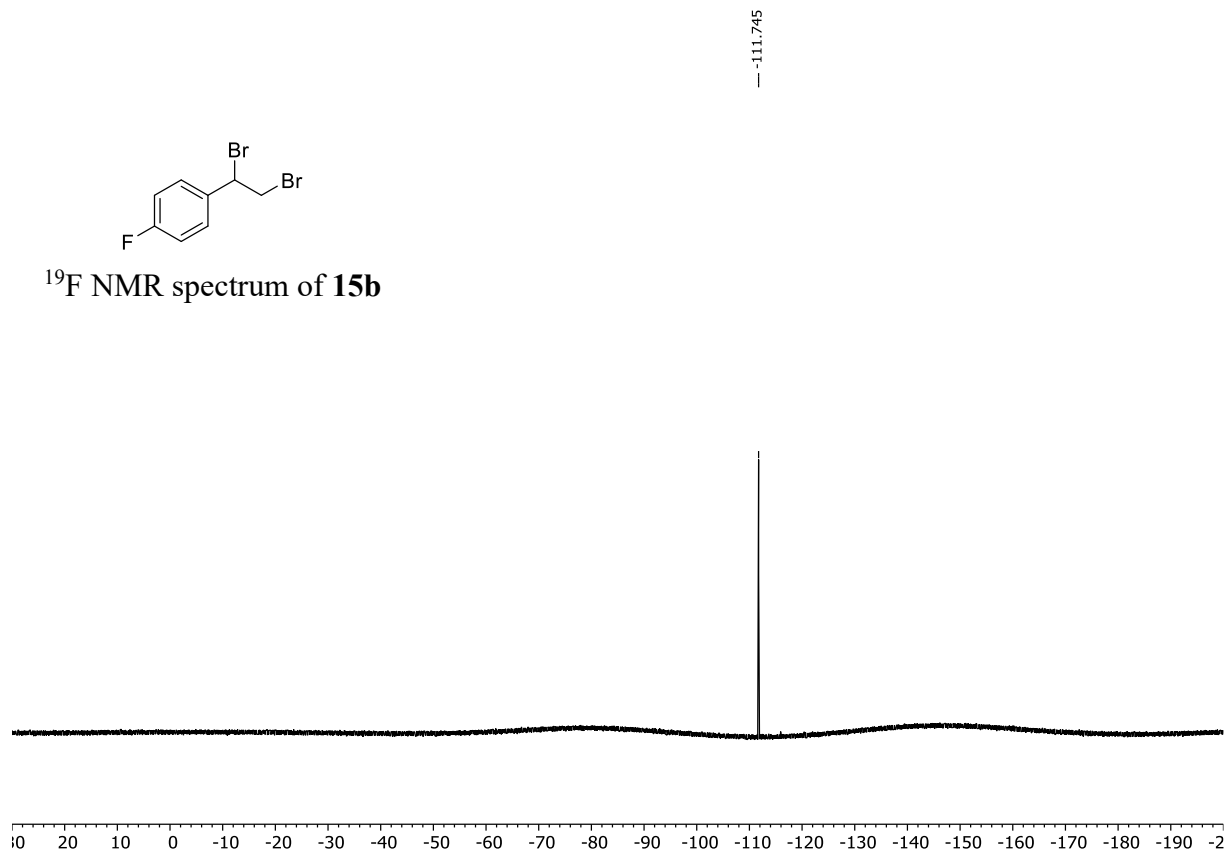




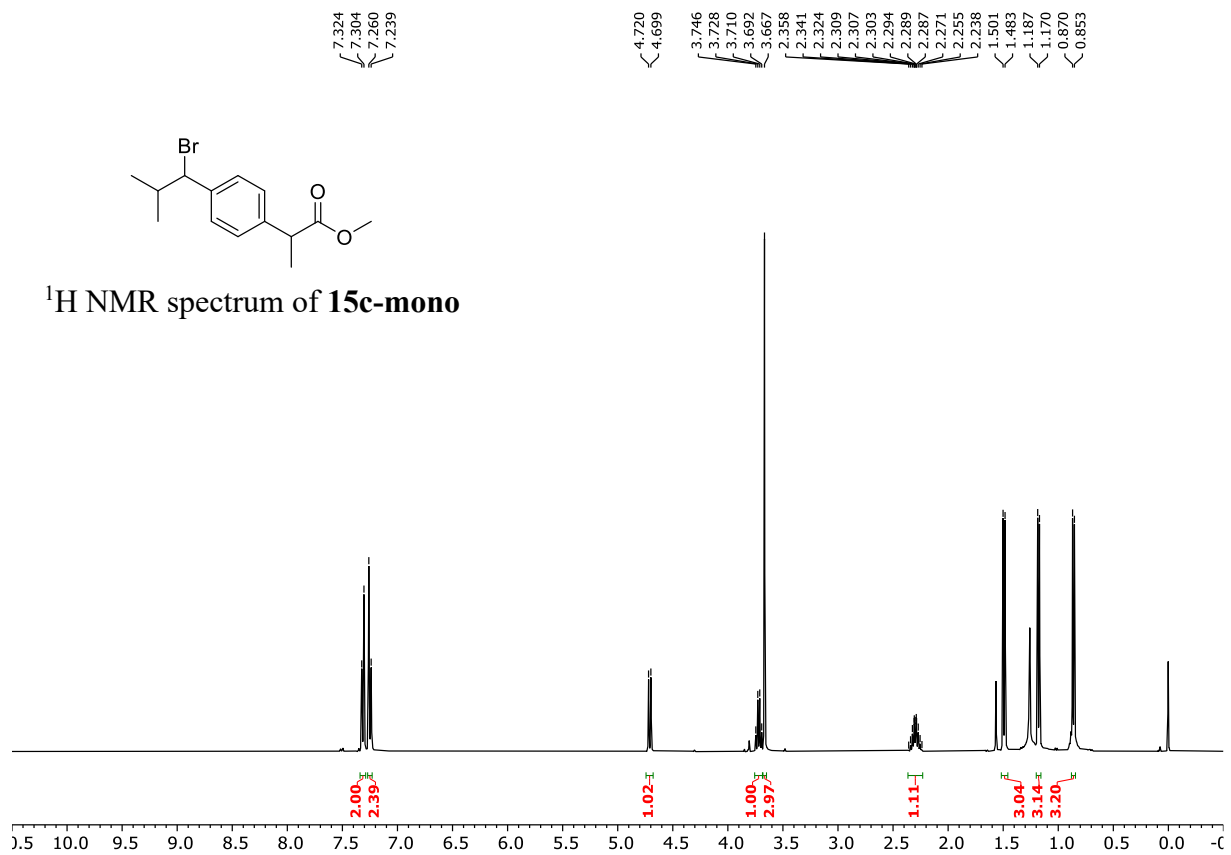


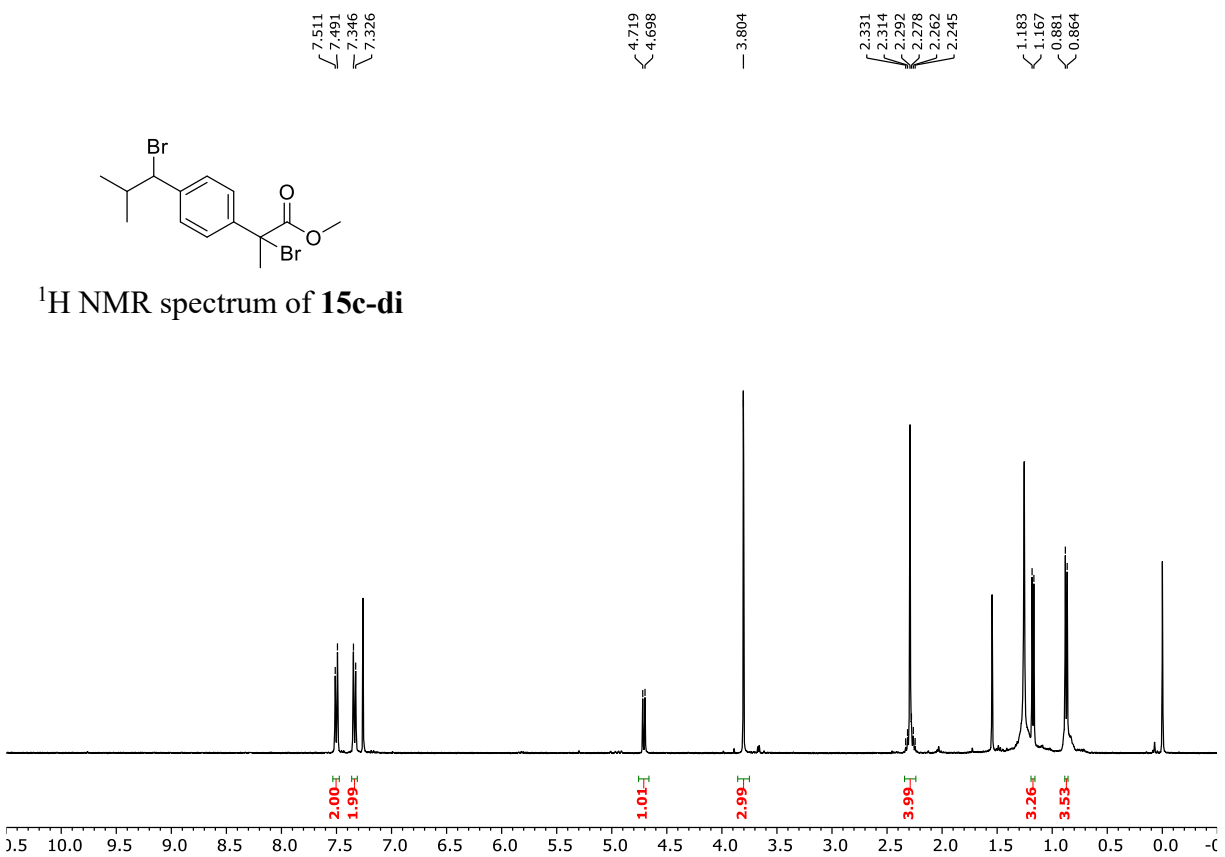
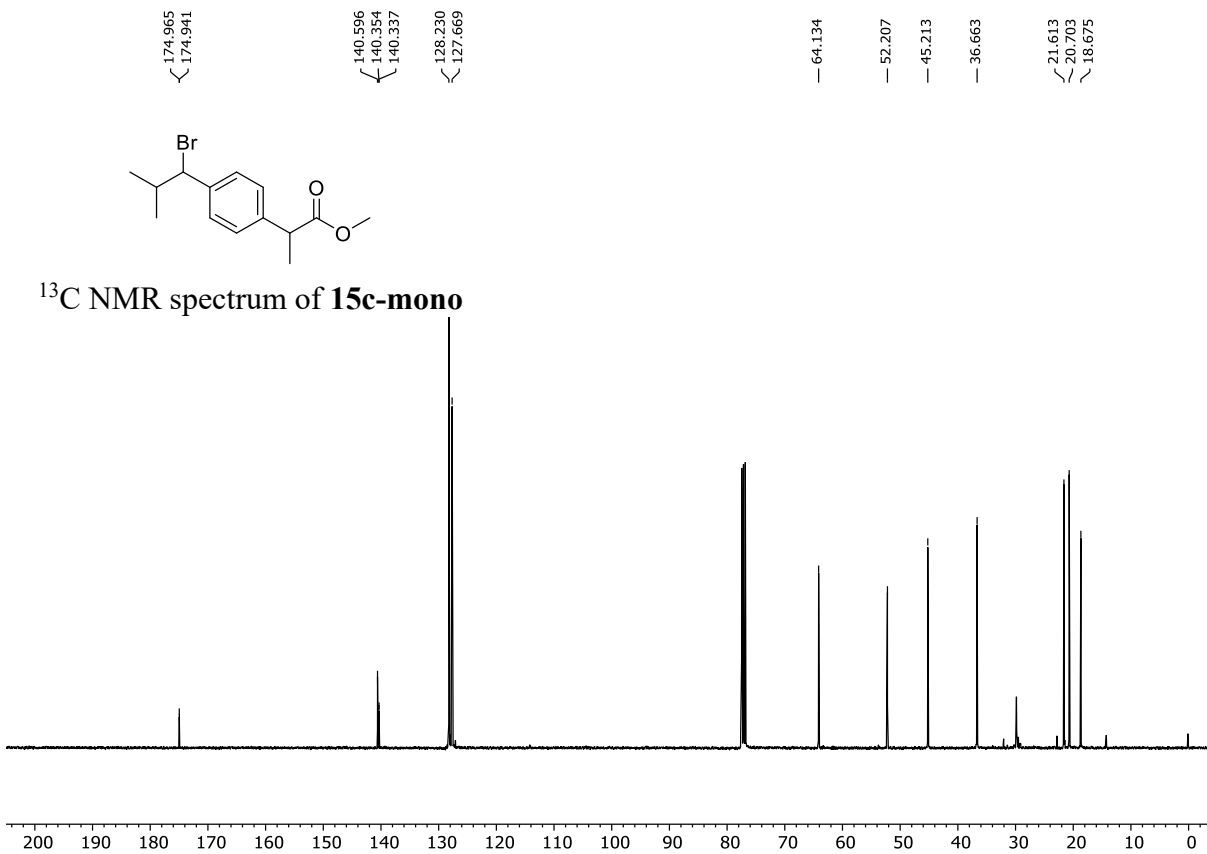


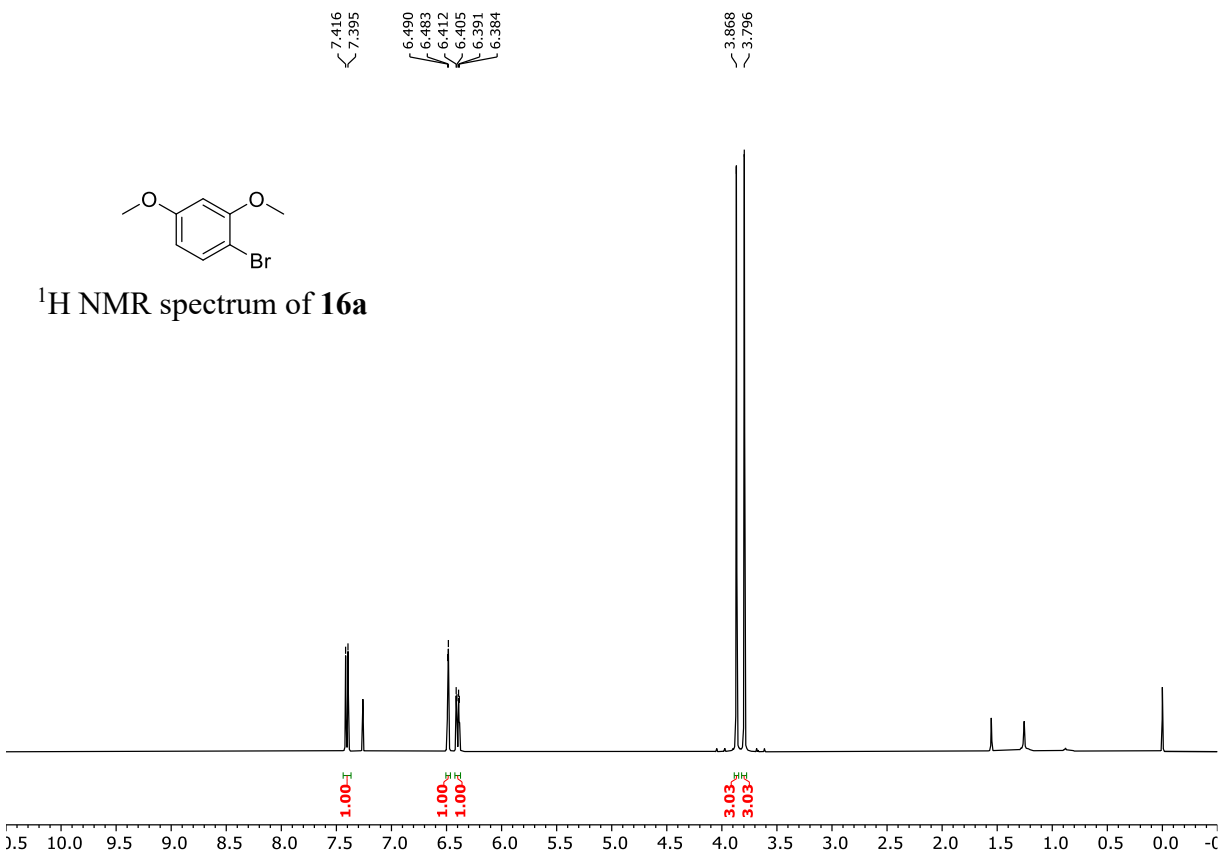
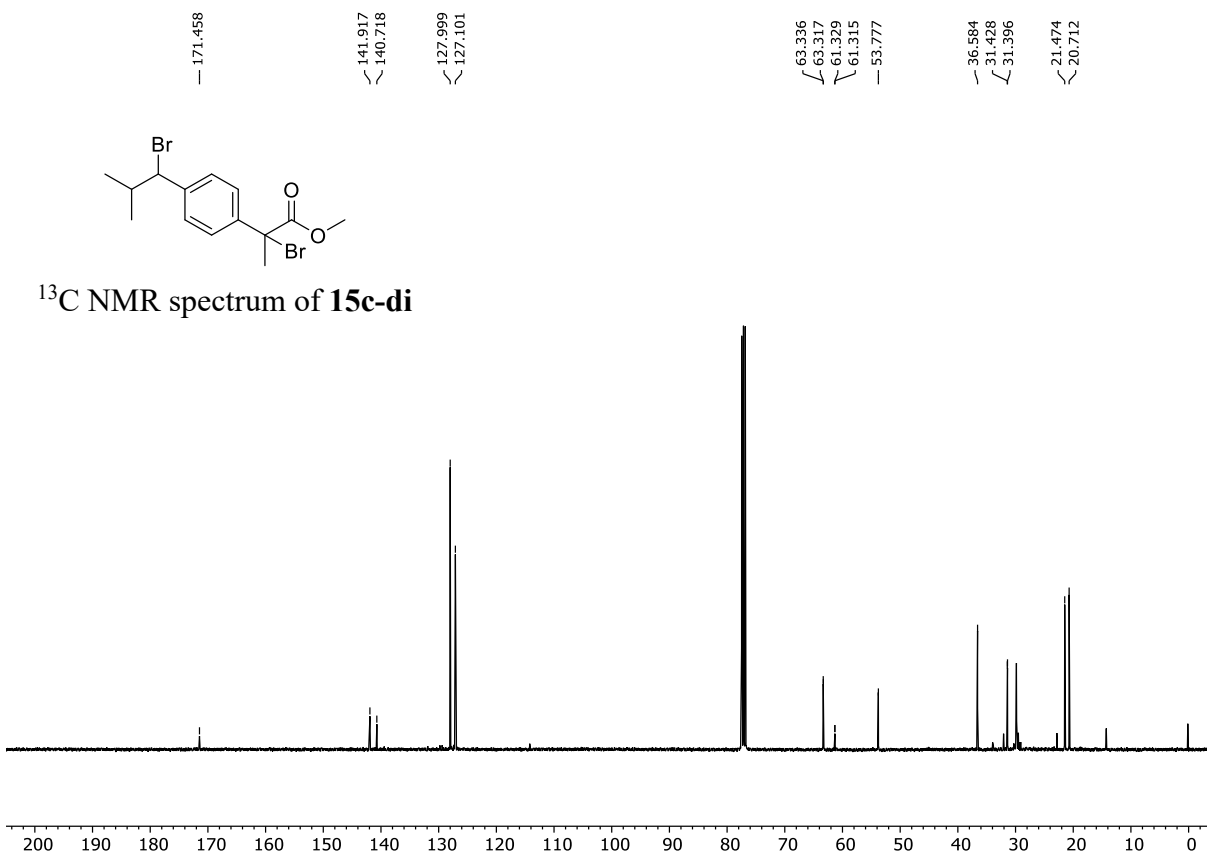
^{19}F NMR spectrum of **15b**

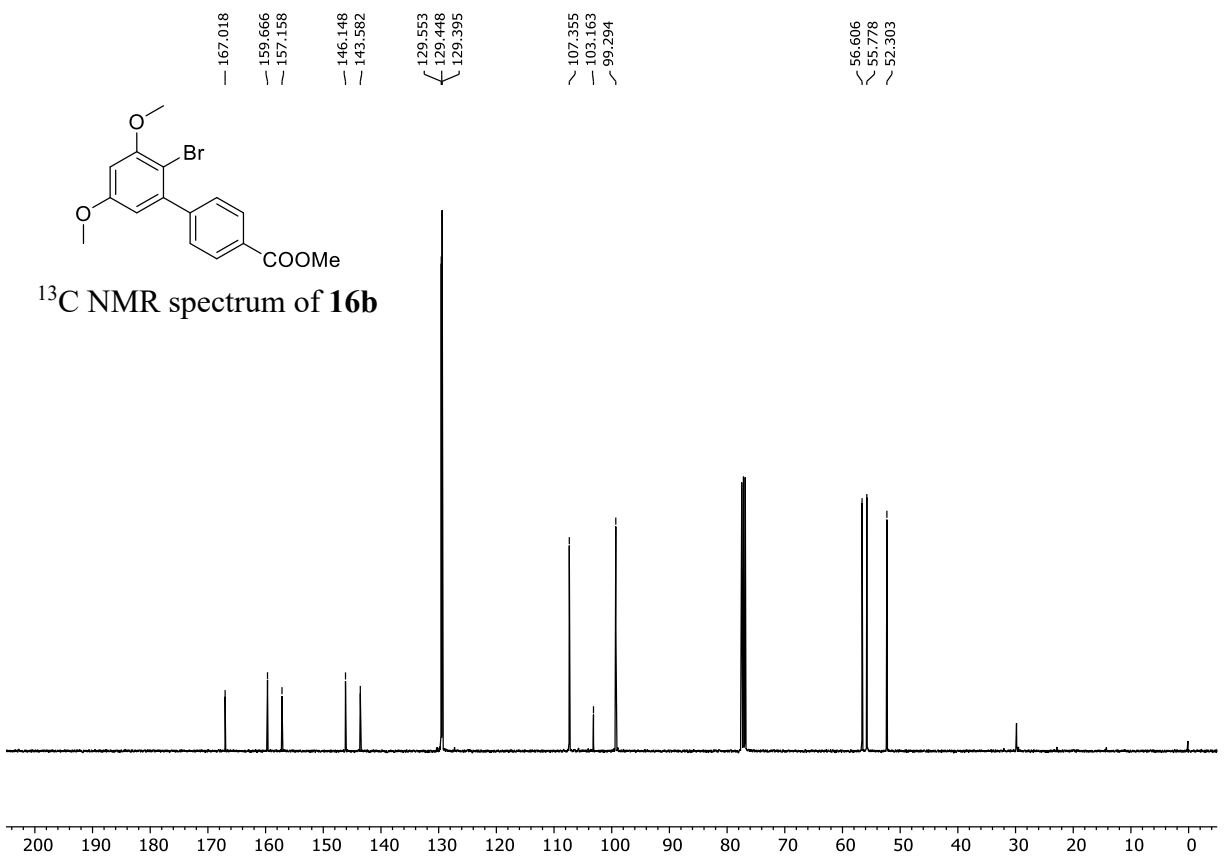
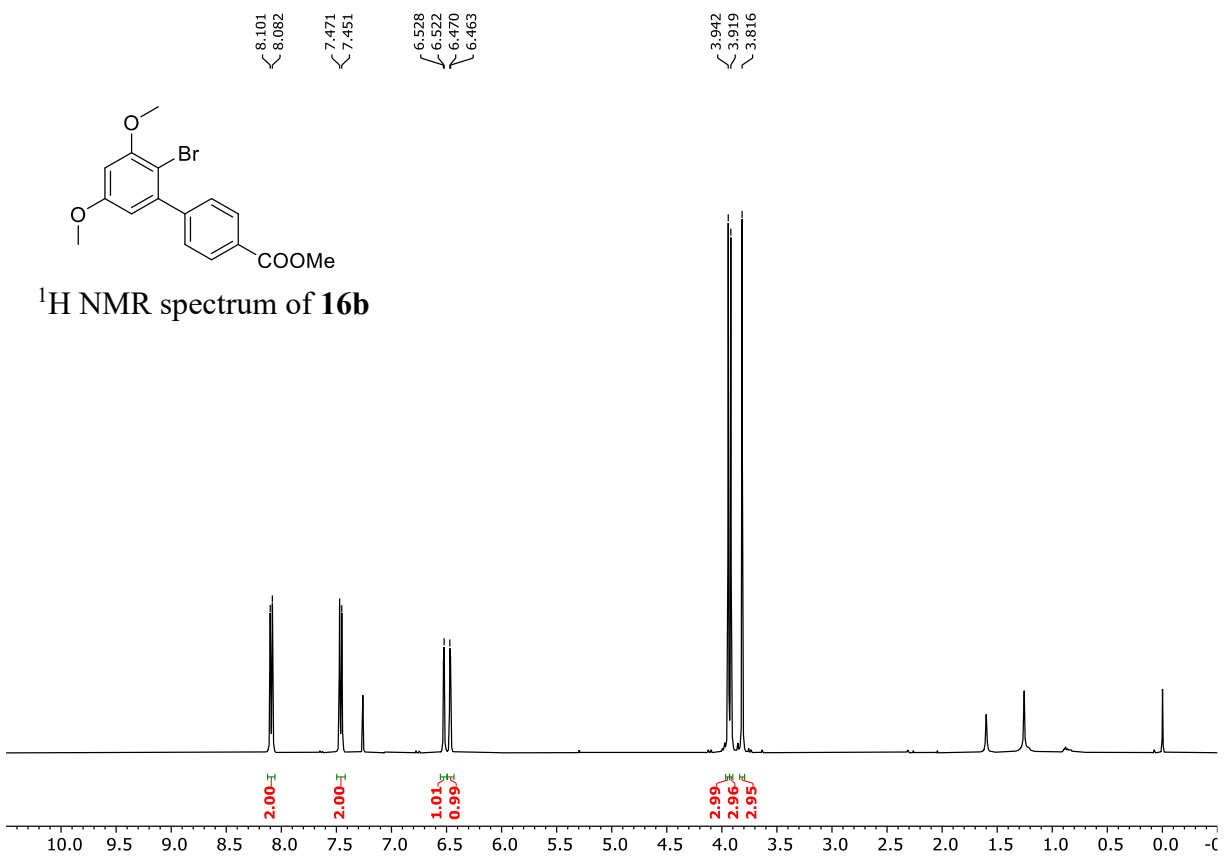


^1H NMR spectrum of **15c-mono**

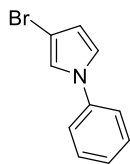




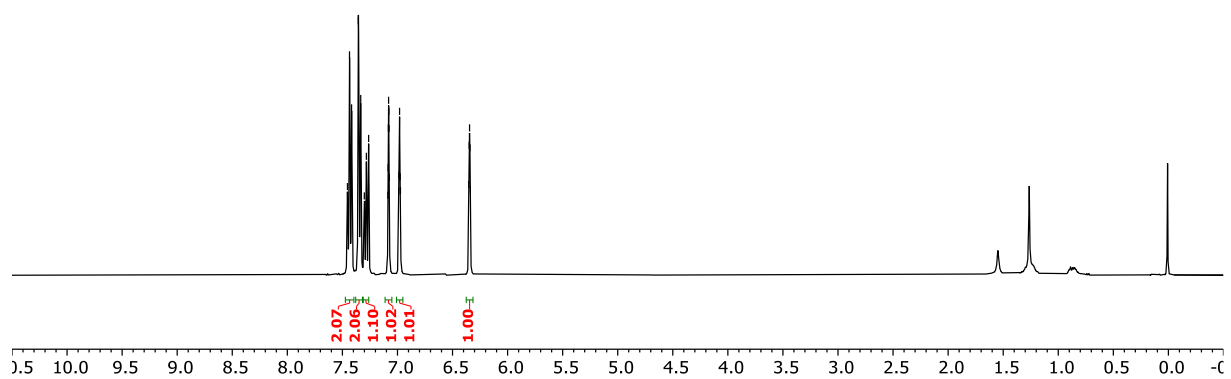




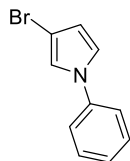
7.454
7.435
7.417
7.355
7.334
7.301
7.282
7.262
7.087
7.085
7.063
7.080
7.078
7.077
7.074
6.989
6.987
6.981
6.975
6.973
6.352
6.349
6.345
6.341
6.338



^1H NMR spectrum of **16c**



140.203
129.832
126.413
120.595
120.048
119.202
113.116
98.304



^{13}C NMR spectrum of **16c**

